Berichte
zur Polar-
und Meeresforschung

573
2008

Reports
on Polar and Marine Research

Reactions on surfaces of frozen water: Importance of surface reactions for the distribution of reactive compounds in the atmosphere

Reaktionen an gefrorenem Wasser: Bedeutung von Oberflächenreaktionen für die Verteilung von reaktiven Verbindungen in der Atmosphäre

Hans-Werner Jacobi

HELMHOLTZ GEMEINSCHAFT

ALFRED-WEGENER-INSTITUT FÜR
POLAR- UND MEERESFORSCHUNG
In der Helmholtz-Gemeinschaft
D-27570 BREMERHAVEN
Bundesrepublik Deutschland

ISSN 1866-3192

Hinweis

Die Berichte zur Polar- und Meeresforschung werden vom Alfred-Wegener-Institut für Polar-und Meeresforschung in Bremerhaven* in unregelmäßiger Abfolge herausgegeben.

Sie enthalten Beschreibungen und Ergebnisse der vom Institut (AWI) oder mit seiner Unterstützung durchgeführten Forschungsarbeiten in den Polargebieten und in den Meeren.

Es werden veröffentlicht:

- Expeditionsberichte (inkl. Stationslisten und Routenkarten)
- Expeditionsergebnisse (inkl. Dissertationen)
- wissenschaftliche Ergebnisse der Antarktis-Stationen und anderer Forschungs-Stationen des AWI
- Berichte wissenschaftlicher Tagungen

Die Beiträge geben nicht notwendigerweise die Auffassung des Instituts wieder.

Notice

The Reports on Polar and Marine Research are issued by the Alfred Wegener Institute for Polar and Marine Research in Bremerhaven*, Federal Republic of Germany. They appear in irregular intervals.

They contain descriptions and results of investigations in polar regions and in the seas either conducted by the Institute (AWI) or with its support.

The following items are published:

- expedition reports (incl. station lists and route maps)
- expedition results (incl. Ph.D. theses)
- scientific results of the Antarctic stations and of other AWI research stations
- reports on scientific meetings

The papers contained in the Reports do not necessarily reflect the opinion of the Institute.

The „Berichte zur Polar- und Meeresforschung” continue the former „Berichte zur Polarforschung”

* Anschrift / Address
Alfred-Wegener-Institut
Für Polar- und Meeresforschung
D-27570 Bremerhaven
Germany
www.awi.de

Editor in charge:
Dr. Franz Riemann

Die "Berichte zur Polar- und Meeresforschung" (ISSN 1866-3192) werden ab 2008 ausschließlich als Open-Access-Publikation herausgegeben (URL: http://epic.awi.de).

Since 2008 the "Reports on Polar and Marine Research" (ISSN 1866-3192) are only available as web based open-access-publications (URL: http://epic.awi.de)

Reactions on surfaces of frozen water: Importance of surface reactions for the distribution of reactive compounds in the atmosphere

Reaktionen an gefrorenem Wasser: Bedeutung von Oberflächenreaktionen für die Verteilung von reaktiven Verbindungen in der Atmosphäre

---

Hans-Werner Jacobi

ISSN 1866-3192

Dr. Hans-Werner Jacobi
Alfred Wegener Institute for Polar and Marine Research
Am Handelshafen 12
27570 Bremerhaven
Germany

Die vorliegende Arbeit ist die inhaltlich unveränderte Fassung einer Habilitationsschrift, die im August 2006 dem Fachbereich Biologie & Chemie der Universität Bremen vorgelegt wurde

Table of contents

Summary

This Habilitation thesis compiles 19 publications and manuscripts dealing with photochemical and physical processes at frozen water surfaces and the influence of these processes on concentrations of reactive trace compounds in the atmosphere mainly in the higher latitudes of Northern and Southern Hemispheres of the Earth. Frozen water is ubiquitous in the global environment: snow at high latitudes or high elevations, solid cloud particles in the upper troposphere or in the stratosphere, sea ice in both polar regions. Although solid water ice crystals dominate these structures, variable amounts of impurities are incorporated. Due to the specific properties of water, only small fractions of the impurities are included in the ice crystal. Significant fractions are located at the surfaces enhancing the formation of a quasi-liquid surface layer with interesting and specific properties. Due to the large enrichment of the impurities in the surface layer high concentrations of ionic and organic compounds are possible. Under the influence of the solar radiation remarkable photochemical reactions can occur in the surface layer, which are not commonly observed in the atmosphere. These reactions can lead to the formation of highly reactive compounds, which influence the composition of the atmosphere if they are released to the gas phase. This thesis contributes to a comprehensive understanding of these processes with an impact on environmental issues. It provides information about several field and laboratory investigations. These studies examined the nature of the surface layer, the distribution and reactions of selected impurities, and the exchange of the impurities between the condensed phase and the gas phase.

Photochemical and physical processes in the top layer of a snow pack (surface snow) contribute to the transformation of deposited trace compounds in the snow into more reactive species, the exchange of trace compounds between the snow and the interstitial air of the surface snow (firn air), and further to the exchange of compounds between the snow and the lower layer of the atmosphere. Field studies demonstrated that water soluble compounds like hydrogen peroxide and formaldehyde are exchanged between the atmosphere and the snow driven by temperature-dependent snow-air equilibria: while during daytime the warmer snow releases hydrogen peroxide and formaldehyde, both compounds are deposited to the colder snow during the night and in the early morning hours. However, in addition to such physical equilibria these compounds can also undergo photochemical reactions as demonstrated in laboratory experiments performed with artificial snow samples. The slow photolysis of formaldehyde is probably unimportant under natural conditions, while the photochemical decomposition of hydrogen peroxide needs to be taken into account for the formation of highly reactive compounds like hydroxy radicals in the snow and the interpretation of hydrogen peroxide profiles in firn and ice cores. In contrast, the photolysis of nitrate in snow initiates a series of reactions, which can be described only by a comprehensive reaction mechanism. Such a mechanism is presented using available data from laboratory and field experiments. An extremely important compound in this mechanism is the hydroxyl radical, whose sinks in the snow are currently not well described. A preliminary budget of the OH radical in the snow including reactions with organic compounds is presented.

Chemical processes at the surface of newly formed sea ice are responsible for the activation of reactive halogens from the non-reactive sea salt halides. This is mainly expressed in the depletion of ozone in the atmospheric boundary layer to non-detectable levels, which is catalyzed by several reaction cycles involving reactive halogen species. Several observations indicate that under stable atmospheric conditions ozone is regularly removed in the marginal ice zone of the Arctic and Antarctic Oceans.

However, field measurements in regions, where new sea ice is formed, are currently too limited to determine the active sites responsible for the transformation of the halides.

1 Introduction

One of the major goals in atmospheric chemistry is the understanding of the distribution of reactive trace compounds in the atmosphere on a global scale. Field and laboratory measurements to specify and quantify different processes and reactions at the surface of snow and ice with the aim of improving our understanding for the influence of these processes on the composition of the atmosphere has been the main focus of the investigations presented here. This compilation submitted for my Habilitation at the Fachbereich *Biologie & Chemie*, University Bremen, comprises 19 publications and manuscripts, which have been published since 1999. The status of these contributions is as follows: 17 publications have already appeared in international journals or proceedings and two are currently in press. Of the 19 manuscripts, 10 were produced as a leading author, two contain a major scientific contribution reflected by co-authorship in the second or third place, and the remaining seven have substantially benefited from support by collection of samples, analyses of data sets, contributions to discussions, and participation in manuscript writing.

Parts of the scientific results presented in this thesis were obtained within projects funded by the German Research Foundation (DFG) and the German Academic Exchange Service (DAAD). The project *Investigations of the transfer of reactive trace compounds between the troposphere and ice in polar regions* (in German) funded by the DFG supported investigations at the Department of Hydrology at the University of Arizona dealing mainly with the exchange of reactive trace compounds between the atmospheric boundary layer and the surface snow at the Summit Station in Greenland. A second DFG project *Photochemical and physical processes at the surface snow* (in German) funded the development of the laboratory experiments regarding processes in artificial snow and further field measurements regarding the importance of processes at the surfaces of sea ice. The project *Photochemical Experiment at Neumayer 1999* involving groups from the Alfred Wegener Institute and the British Antarctic Survey was supported by the DAAD.

All investigations carried out during the last years have substantially benefited from the excellent and constructive cooperation between the various groups at the Fachbereich *Climate Sciences* at the Alfred Wegener Institute for Polar and Marine Research and at the *Department of Hydrology* at the University of Arizona in Tucson (Arizona). Further studies have been performed in collaboration with Anna Jones, Phil Anderson, and Eric Wolff (British Antarctic Survey, Cambridge, United Kingdom), Thomas Blunier and Gregoire Floch (University Bern, Switzerland), and Lars Kaleschke, Andreas Richter, and John Burrows (University Bremen).

Photochemical processes in snow are now a well-established research topic in atmospheric research. For example, such processes are the focus of two international projects entitled AICI (Air ice chemical interaction) and OASIS (Ocean-Atmosphere-Sea Ice-Snowpack), which are endorsed by the IGAC (International Global Atmospheric Chemistry) and the SOLAS (Surface Ocean Lower Atmosphere Study) projects.

In the following synthesis the results of the various publications are summarized and put into a general context – grouped under the three topics mentioned above. The appendix collecting the publications on the different topics is subdivided into four sections to account for the global distribtution of trace compounds and the field and laboratory studies concerning the investigations of the photochemical processes in snow and sea ice.

2 Synthesis of Publications

2.1 Impact of long-range transport on the global distribution of trace compounds

The global distribution of many trace compounds in the atmosphere is influenced by long-range transport. This parameter is especially important for polar regions, where direct sources of trace compounds are limited. However, the role of the atmospheric transport strongly depends on the atmospheric lifetime of each compound compared to the transport times in the atmosphere. The atmospheric lifetime is determined by the degradation due to chemical reactions as well as the removal by wet and dry deposition. Only if the atmospheric lifetime is comparable or longer than the transport times, the atmospheric transport can distribute trace compounds on a larger spatial scale. Typical times for the transport of molecules in the troposphere range from 1 to 2 months for the mixing within the Northern or Southern Hemisphere to approximately 1 year for the interhemispheric exchange [Seinfeld and Pandis, 1998]. Thus, only compounds with atmospheric lifetimes larger than 2 months can for example be transported from continental emission sources to the polar regions.

Important reactive species in the atmosphere are the nitrogen oxides (NO_x = NO + NO_2). They control the photochemical formation of tropospheric ozone (O_3), thus influencing the oxidation capacity of the atmosphere [Carroll and Thompson, 1995]. Increased interest in the global distribution is due to the fact that human activities caused increased concentrations in large regions of the Earth leading also to higher photochemical O_3 production rates [Carroll and Thompson, 1995]. The atmospheric lifetime of the nitrogen oxides is determined by the oxidation by hydroxyl radicals (OH) leading to a typical lifetime of less than 1 day [Seinfeld and Pandis, 1998]. The primary NO_x sources (fossil fuel combustion, biomass burning, microbial activity in soils, lightning) are all restricted to continental regions. As a result the direct transport of NO_x to the polar regions from these continental source regions is negligible.

Further chemical reactions in the atmosphere can lead to the formation of NO_x reservoir species, which can be transported over larger distances. For example, NO_2 can react with peroxyacetyl radicals, which are formed during the oxidation of organic compounds in the atmosphere. This reaction generates peroxyacetyl nitrate (PAN), which can have a significantly longer lifetime in the atmosphere. The main chemical sink of PAN is the thermal dissociation back into the peroxyacetyl radical and NO_2, which is strongly temperature dependent: the dissociation rate decreases from 4.6×10^{-4} s^{-1} to 1.1×10^{-6} s^{-1} if the temperature drops from 298 K to 263 K [Bridier et al., 1991]. According to this behavior a latitudinal distribution of PAN inversely correlated to the air temperature can be expected.

The data presented in the publications 3.1.1 to 3.1.3 are used to construct a latitudinal PAN profile over the Atlantic Ocean covering 80 °N to 70 °S. The measured PAN concentrations were averaged for bins of 1 degree of latitude for the measurements performed over Atlantic. For each 1° bin, the PAN value is plotted versus latitude as shown in Fig. 1. Averaged concentrations observed in the Arctic [Publ. 3.1.2] and Antarctic [Publ. 3.1.3] are also shown. In general, the profile is in agreement with the previous deliberations: lowest concentrations were encountered in the tropics with increasing concentrations to the north and south. However, the observed concentrations are also modified by the chemical production of PAN. Air masses recently influenced

by continental emissions exhibit the highest concentrations encountered [Publ. 3.1.2]. It is further obvious that over the South Atlantic at latitudes higher than 40° S PAN values start to decrease again due to the increasing distance from continental source regions [Publ. 3.1.1].

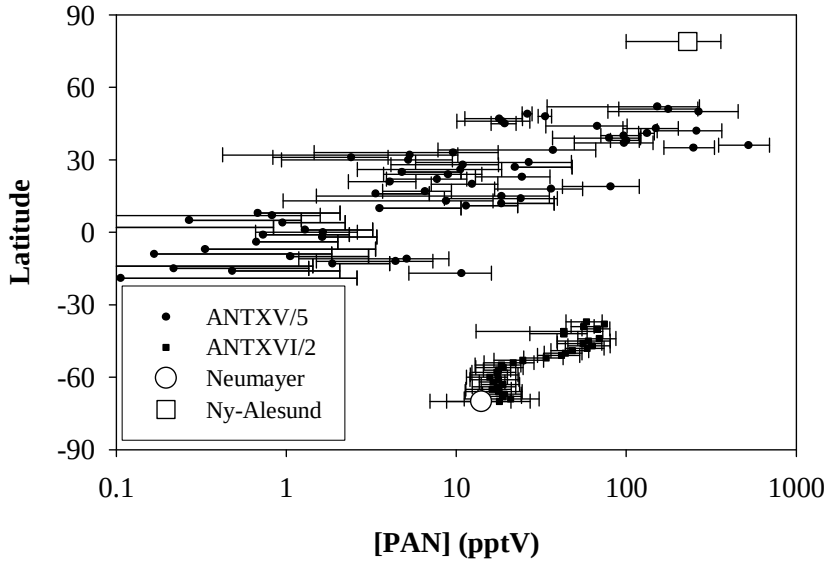

Figure 1: Latitudinal distribution of PAN concentrations as observed during two Polarstern cruises: ANTXV/5 (26 May to 21 June 1998, Cape Town to Bremerhaven) and ANTXVI/2 (1 to 16 March 1999, Neumayer station to Cape Town). PAN concentrations were averaged for bins of 1° of latitude. The error bars represent one standard deviations calculated for the bins. Also shown are average PAN concentrations observed at Ny-Alesund (Svalbard, March 1998) and Neumayer station (Antarctica, February / March 1999).

Since the dissociation of PAN leads to the formation of NO_2 it must also be considered as a direct source of NO_x in the atmosphere. This role becomes unimportant in areas where other larger sources of NO_x are present. However, in polar regions PAN can potentially constitute an appreciable direct NO_x source. Fig. 2 presents times series of PAN concentrations, air temperatures, and calculated thermal PAN decay rates as observed at the Arctic and Antarctic locations [Publ. 3.1.2 and 3.1.3]. Publ. 3.1.2 demonstrates that in spring PAN concentrations as well as air temperatures in the Arctic in Ny-Alesund (Svalbard) are sufficiently high to lead to significant local NO_x production with calculated rates in the range from 0.2 to 10 pptV hr^{-1}. However, the measurements in Ny-Alesund are possibly only representative for coastal locations or locations at lower altitudes. Ford et al. [2002] reported PAN measurements made at Summit Station on top of the Greenland ice sheet at an altitude of more than 3000 m. They found that at this location the thermal decay of PAN is a negligible source of NO_x.

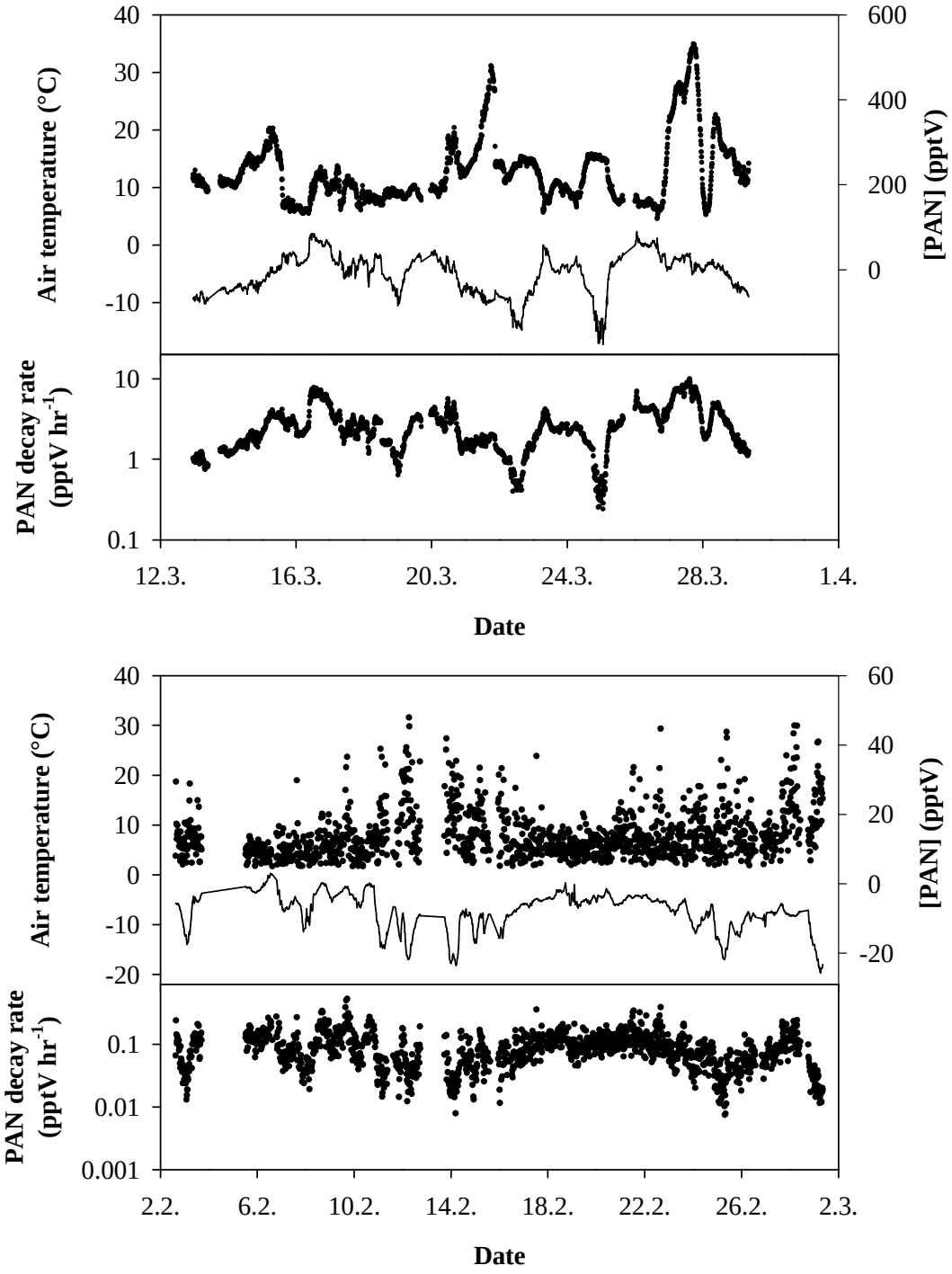

Figure 2: Air temperatures and PAN concentrations observed in March 1998 in Ny-Alesund (Svalbard) (top) and in February / March 1999 at Neumayer station (Antarctica) (bottom). The lower panels in the top and bottom section of the figures show calculated PAN decay rates using temperature dependent rate constants for the thermal PAN dissociation.

On the Antarctic continent conditions seem to be comparable to the results reported by Ford et al. [2002] from central Greenland. In Publ. 3.1.3 we demonstrate that in the late summer air temperatures are comparable to the temperatures observed in spring in Ny-Alesund. However, due to the significantly lower PAN concentrations the NO_x production rates were in the range from 0.01 to 0.2 pptV hr^{-1} and, thus, much smaller compared to the Arctic.

Organic nitrates are another class of stable N-containing compounds, which may release NO_x upon degradation in the atmosphere [Roberts, 1990]. Interestingly, organic nitrates are released by marine sources [Blake et al., 1999, 2003; Talbot et al., 2000] exhibiting fairly high concentrations at higher latitudes of the Southern Hemisphere, where they can constitute a large fraction of the sum of reactive N-containing compounds [Talbot et al., 2000]. The measurements of alkyl nitrates on the Antarctic continent presented in Publ. 3.1.4 and 3.1.5 confirm a non-biogenic marine source. This is most obvious for methyl nitrate, which was encountered at relatively high concentrations. Higher organic nitrates are probably much less influenced by marine emissions. The high methyl nitrate levels are probably not caused by local emission, but are rather induced by uniform marine emissions throughout the Southern Hemisphere [Publ. 3.1.5].

In summary, the transformation of organic nitrates including PAN in the atmosphere does not constitute a significant source of NO_x in the lower troposphere over the Antarctic continent. The relatively high NO_x levels are sustained by emissions from the snow surface, which are caused by photochemical processes within the snow. These findings point to the important role of photochemical production in the surface snow leading to the higher than expected NO_x concentrations in snow covered areas in both polar regions [e.g. Publ. 3.2.1 and 3.2.2; Honrath et al., 1999, 2002; Ridley et al., 2000; Davis et al., 2001, 2004; Beine et al., 2002].

2.2 Photochemical transformation of trace compounds in snow

A wealth of information about photochemical processes in snow has been obtained from a wide range of field and laboratory measurements [Publ. 3.2.1, 3.2.2, 3.2.5, 3.2.6, 3.2.7, 3.3.1, 3.3.2, 3.3.3, 3.3.4; Honrath et al., 1999, 2000a, 2000b, 2002; Sumner and Shepson, 1999; Couch et al., 2000; Klán et al., 2000, 2001, 2003; Ridley et al., 2000; Davis et al., 2001, 2004; Dubowski et al., 2001, 2002; Peterson and Honrath, 2001; Zhou et al., 2001; Beine et al., 2002a, 2002b, 2003, 2005; Boudries et al., 2002; Dassau et al., 2002; 2004; Dibb and Arsenault, 2002; Dibb et al., 2002, 2004; Dominé and Shepson, 2002; Ford et al., 2002; Grannas et al., 2002, 2004; Guimbaud et al., 2002; Houdier et al., 2002; Ianniello et al., 2002; Perrier et al., 2002; Slusher et al., 2002; Sumner et al., 2002; Swanson et al., 2002, 2003, 2005; Qiu et al., 2002; Boxe et al., 2003, 2005, 2006; Chu and Anastasio, 2003, 2005; Cotter et al., 2003; Klánová et al., 2003a, 2003b; Anastasio and Jordan, 2004; Holoubek et al., 2004; Oncley et al., 2004; Riedel et al., 2005; Amoroso et al., 2006; Liao et al., 2006]. Currently the best-investigated process is the photochemical production of NO_x in surface snow induced by UV and visible irradiation. Field measurements using snow blocks [Publ. 3.2.1], snow piles [Beine et al., 2002b], and snow chambers [Honrath et al., 1999; Beine et al., 2002b] have indicated that snow produces larger amounts of NO_x under the influence of the solar radiation leading to significantly higher NO_x concentrations in the interstitial air of the surface snow (= firn air) [Publ. 3.2.7; Honrath et al., 1999]. Upward fluxes of

NO_x from the snow surface to the atmosphere observed at several polar and mid-latitude locations [Publ. 3.2.2; Honrath et al., 2000a, 2002; Beine et al., 2002a; Oncley et al., 2004] indicate that the produced NO_x are subsequently released to the atmosphere. In addition, higher firn air concentrations and emissions from the snow surface have also been observed for nitrous acid (HONO) [Publ. 3.2.7; Zhou et al., 2001; Honrath et al., 2002; Dibb et al., 2002, 2004]. The mechanism controlling the NO_x and HONO production in the snow has been the subject of a range of laboratory studies indicating that the primary step is the photolysis of nitrate (NO_3^-) [Honrath et al., 1999], which is ubiquitous in natural snow samples [e.g. Legrand and Mayewski, 1997]. The studies have been used to extract information about the decomposition of NO_3^- under the influence of UV and visible radiation [Publ. 3.3.3, 3.3.4], the absorption coefficients and quantum yields of NO_3^- in ice as a function of wavelength [Chu and Anastasio, 2003], the formation of products like OH [Dubowski et al., 2002; Chu and Anastasio, 2003] and nitrite (NO_2^-) in the condensed phase [Publ. 3.3.3; Dubowski et al., 2001, 2002], and the release of NO_x from the condensed to the gas phase [Honrath et al, 2000; Dubowski et al., 2001; Cotter et al., 2003; Boxe et al., 2003, 2005, 2006]. We reported the so far only study regarding the kinetic isotope effect for the photolysis of NO_3^- in snow [Publ. 3.3.2]. Such information can deliver useful information for the interpretation of isotope ratios measured in NO_3^- present in snow samples.

Most of the experiments described in the literature were performed using thin ice films or natural snow samples. In contrast, we performed laboratory experiments using artificial snow samples, which were produced by spraying solutions of purified water containing a single impurity into liquid nitrogen [Publ. 3.3.1, 3.3.3, 3.3.4]. Such experiments offer the possibility to investigate single reactions under controlled conditions and to quantify important photolysis reactions in the snow. Our results demonstrated that under the applied experimental conditions NO_2^- was produced during the NO_3^- photolysis. However, the photolysis of NO_2^- also led to the formation of significant amounts of NO_3^-. In Publ. 3.3.4 we developed a reaction mechanism for the transformation of NO_3^- and NO_2^- in snow using several series of laboratory experiments investigating the photolysis of NO_3^- and NO_2^- in the artificial snow samples. Using the experimental data, rate constants were determined for the involved photolysis reactions of NO_3^- and NO_2^- and the transfer of both compounds from the snow to the gas phase for the applied experimental conditions. The calculations were performed with the assumptions that all of the impurities were located in the so-called quasi-liquid layer (QLL) [e.g. Petrenko and Whitworth, 1999] at the surface of the snow crystals and that the reactions occur in this liquid-like medium. Subsequently, the obtained photolysis rate constants were adjusted for Arctic summer conditions as observed on the Greenland ice sheet. Further calculations with the adjusted rate constants demonstrated that under natural conditions the formation of nitrogen oxides in the snow is dominated by NO_2, which is either generated directly by the photolysis of NO_3^- or by the reaction of NO_2^- with the hydroxyl radical (OH). Due to the quick transformation of NO_2^- to NO_2 the NO_2^- concentrations remain low. Consequently, a direct formation of nitrous acid (HONO) in the QLL is probably negligible independent of the pH of the QLL.

Investigations of further photochemical reactions of reactive species in snow include studies on the photolysis of hydrogen peroxide (H_2O_2) [Publ. 3.3.1, 3.3.3; Chu and Anastasio, 2005], which delivered for example absorption coefficients of H_2O_2 in ice. Product studies also indicated the formation of OH radicals [Chu and Anastasio, 2005] confirming results from previous experiments performed at significantly lower temperatures [Ingram et al., 1955; Smith and Wyard, 1960; Kroh et al., 1961, 1962;

Gurman et al., 1967]. Investigations regarding the photolytic decomposition of further reactive compounds with a potential relevance for photochemical processes in surface snow are limited to our studies, in which the photolysis of HCHO has been examined [Publ. 3.3.1, 3.3.3].

The full and simplified mechanisms for the transformation of NO_3^- and NO_2^- and the production of NO_x in snow presented in Publ. 3.3.4 take into account reactions of N-containing compounds. However, the importance of the role of the OH radical for the reactions in the so-called quasi-liquid layer (QLL) at the surface of the snow crystals is also discussed. The laboratory studies presented by Chu and Anastasio [2005] indicated that the photolysis of H_2O_2 is probably the most important OH source in the snow. Thus, a comprehensive reaction mechanism needs to consider a full set of OH sources and sinks.

Table 1: Reported concentrations of organic components in snow samples from Summit Station collected in June 2000 [Publ. 3.2.6].

Compound or class of compounds	**Concentration**	
	μg L^{-1}	**μM**
Total organic carbon (TOC)	1850	3.7 [a]
Inorganic Carbon	1080	17.7 [b]
Formaldehyde	35.7	1.19
Acetate	21.8	0.369
Propionate	5.9	0.080
Formate	3.9	0.087
Methanesulfonate	0.6	0.006
Lactate	0.4	0.004

[a] Since Grannas et al. [2004] reported that the molecular mass of the organic carbon in snow can reach values of higher than 1 kDa, we used an estimated average molecular mass of 500 Da to translate the measured TOC concentration into μM.

[b] Assuming that the inorganic carbon is dominated by carbonate.

The importance of the OH radical for the chemical reactions in the QLL becomes obvious if the calculated QLL concentrations are compared to levels calculated for tropospheric cloud droplets. For example, Herrmann et al. [2000] demonstrated that OH levels in the tropospheric aqueous phase reach maximum values between 1 and $2 \cdot 10^{-12}$ M depending mainly on the concentrations of organic compounds. In contrast, the OH levels in the calculations presented in Publ. 3.3.4 increase to levels on the order of $1 \cdot 10^{-9}$ M in the QLL for conditions at Summit Station. This number is possibly an upper limit for the OH concentrations since a rage of reactions, which are known to be significant OH sinks in the tropospheric aqueous phase [Herrmann et al., 200], were not included in the mechanism. Among these reactions are mainly reactions with organic

compounds. However, knowledge about concentrations of single organic compounds in the snow is still very limited [e.g. Publ. 3.2.6]. Currently, only formaldehyde concentrations in snow have been investigated in detail at several polar locations [Staffelbach et al., 1991; Sumner and Shepson, 1999; Gillett et al., 2000; Houdier et al., 2000; Hutterli et al., 2002; Publ. 3.2.6]. The reported concentrations range from 0.05 to $1.2 \cdot 10^{-6}$ M. A more comprehensive characterization of the organic content is available for Summit Station. Measurements of total organic carbon and several individual components were performed using surface snow samples collected in June 2000 [Publ. 3.2.6]. The reported concentrations are summarized in Table 1.

Table 2 summarizes an updated reaction mechanism with additional reactions and estimated rate coefficient adjusted to conditions encountered at Summit Station in Greenland in June 2000. Assuming that the conditions at Summit are typical summer conditions for both polar regions it can be suggested to use these reactions together with the recommended rates as a basis for further modeling studies of photochemical processes in surface snow. In addition, Table 3 summarizes typical concentrations of NO_3^-, H_2O_2, and HCHO in surface snow at Summit, which are also recommended to initialize modeling calculations if specific measurements are not available.

The reaction rate for the photolysis rate of H_2O_2 (R8) was calculated using Publ. 3.3.3 and 3.3.4. Publ. 3.3.3 describes photolysis experiments of NO_3^- and H_2O_2 in artificial snow for comparable experimental conditions. Therefore, the obtained experimental rate constant of 0.48 hr^{-1} for the H_2O_2 photolysis was divided by a factor of 400 similar to the procedure for the photolysis rate of NO_3^- as described in Publ. 3.3.4. The photolysis of HCHO in snow was also investigated [Publ. 3.3.3]. However, a HCHO decrease was only observed for concentrations much higher than encountered in natural snow samples. Moreover, the photolysis rate was significantly smaller compared to the photolysis of H_2O_2 and NO_3^-. Therefore, the HCHO photolysis reaction in snow is probably negligible under natural conditions and is not included in the recommended reaction mechanism.

According to modeling studies regarding the tropospheric aqueous phase, the reaction of hydrated formaldehyde with OH represents an important OH sink [e.g. Herrmann et al., 2000]. Using temperature dependent kinetic data [Herrmann et al., 2000] for this reaction, an extrapolated rate constant of $5.4 \cdot 10^8$ M^{-1} s^{-1} is obtained for a temperature of –20 °C. Since the used kinetic data was measured in bulk aqueous solutions, the reaction (R9) involves the attack of the OH radical on the hydrated formaldehyde $CH_2(OH)_2$. Grannas et al. [2002] suggested that formaldehyde in snow is mainly present in the non-hydrated form. Nevertheless, I recommend using the aqueous phase rate constant since it seems likely that the hydration of the HCHO molecules can occur in the QLL of the snow crystals. Due to the presence of the high concentration of organic compounds in the snow as demonstrated in Publ. 3.2.5 the reaction of these compounds with OH needs to be included because it probably also establishes an efficient sink for OH. Since most of the individual organic compounds are not identified, reactions with single organic reactants cannot be included. I rather suggest including the general reaction (R10) with an estimated rate constant for this reaction on the order of $1 \cdot 10^8$ M^{-1} s^{-1}. This rate constant represents a reduced average for the reaction of the OH radical with several organic compounds in the aqueous phase [Herrmann et al., 2000] taking into account the low temperatures in the snow.

Table 2: Recommended reactions with rates estimated for -20 °C for a comprehensive mechanism for reactions occurring in natural surface snow layers.

No.	Reaction			Rate constant	Reference
(R1)	NO_3^- (+ H^+)	$\xrightarrow{h\nu}$	NO_2 + OH	$8.3 \cdot 10^{-7}$ s^{-1}	Publ. 3.3.4
(R2)	NO_3^-	$\xrightarrow{h\nu}$	NO_2^- + O	$1.7 \cdot 10^{-7}$ s^{-1}	Publ. 3.3.4
(R3)	NO_3^- + O	$\rightarrow$	NO_2^- + O_2	$2 \cdot 10^8$ M^{-1} s^{-1}	Publ. 3.3.4
(R4)	O (+ O_2)	$\rightarrow$	O_3	$1.2 \cdot 10^6$ s^{-1}	Publ. 3.3.4
(R5)	NO_2^- + OH	$\rightarrow$	NO_2 + OH	$1 \cdot 10^{10}$ M^{-1} s^{-1}	Publ. 3.3.4
(R6)	NO_2 + OH	$\rightarrow$	H^+ + NO_3^-	$5 \cdot 10^9$ M^{-1} s^{-1}	Publ. 3.3.4
(R7)	NO_2	$\rightarrow$	NO_2 (gas)	9.7 s^{-1}	Publ. 3.3.4
(R8)	H_2O_2	$\xrightarrow{h\nu}$	2 OH	$3.3 \cdot 10^{-7}$ s^{-1} [a]	See text
(R9)	$CH_2(OH)_2$ + OH	$\rightarrow$	prod.	$5.4 \cdot 10^8$ M^{-1} s^{-1}	Herrmann et al., 2000
(R10)	ORG + OH	$\rightarrow$	prod.	$1 \cdot 10^8$ M^{-1} s^{-1}	See text

[a] The photolysis rate is extrapolated relative to the total NO_3^- photolysis rate using the ratio of the experimental photolysis rates reported in Publ. 3.3.3 and 3.3.4.

According to modeling studies regarding the tropospheric aqueous phase, the reaction of hydrated formaldehyde with OH represents an important OH sink [e.g. Herrmann et al., 2000]. Using temperature dependent kinetic data [Herrmann et al., 2000] for this reaction, an extrapolated rate constant of $5.4 \cdot 10^8$ M^{-1} s^{-1} is obtained for a temperature of –20 °C. Since the used kinetic data was measured in bulk aqueous solutions, the reaction (R9) involves the attack of the OH radical on the hydrated formaldehyde $CH_2(OH)_2$. Grannas et al. [2002] suggested that formaldehyde in snow is mainly present in the non-hydrated form. Nevertheless, I recommend using the aqueous phase rate constant since it seems likely that the hydration of the HCHO molecules can occur in the QLL of the snow crystals. Due to the presence of the high concentration of organic compounds in the snow as demonstrated in Publ. 3.2.5 the reaction of these compounds with OH needs to be included because it probably also establishes an efficient sink for OH. Since most of the individual organic compounds are not identified, reactions with single organic reactants cannot be included. I rather suggest including the general reaction (R10) with an estimated rate constant for this reaction on the order of $1 \cdot 10^8$ M^{-1} s^{-1}. This rate constant represents a reduced average for the reaction of the OH radical with several organic compounds in the aqueous phase [Herrmann et al., 2000] taking into account the low temperatures in the snow.

To start simulations of reactions in surface snow initial concentrations of the involved stable species are also needed. Table 3 gives a summary of concentrations of NO_3^-, H_2O_2, HCHO, and organic compounds (ORG) observed in surface snow samples collected at Summit Station in the summer of the year 2000. Assuming that all photochemical reactions take place in the QLL these reported concentrations must be translated into QLL concentrations. As described in Publ. 3.3.4 the impurities are confined to the very small volume of the QLL leading to significantly higher concentrations. In Publ. 3.3.4 such an enrichment factor representing the summer conditions at Summit was used to obtain the initial NO_3^- concentration in the QLL for the simulation of processes in natural snow. Applying the same factor of $1.94 \cdot 10^{-5}$

representing the ratio of the QLL to the total volume, the QLL concentrations for the further compounds was estimated (Table 3). In the case of H_2O_2 this value possibly represents only an upper limit. Previous studies have shown that a significant fraction of H_2O_2 can be located within the snow crystal [Publ. 3.2.5].

Table 3: Concentrations of stable compounds included in the reaction mechanism as observed in the snow at Summit Station in the summer of the year 2000.

Compound	Observed Concentration μM	QLL concentration mM	Reference
NO_3^-	4.4	230	Publ. 3.3.4
NO_2^-	0	0	Publ. 3.3.4
H_2O_2	18	930	Publ. 3.2.3
HCHO	1.19	61	Publ. 3.2.5
ORG	2.5 [a]	130	Publ. 3.2.5

[a] The concentration for the sum of organic compounds ORG are calculated as the difference of the total organic content and the HCHO measurements shown in Table 1.

I performed additional simulations for the QLL with the photochemical mechanism described in Table 2 using the commercial FACSIMILE software. Calculations were started with initial concentrations as shown in Table 3. Initial concentrations of all further compounds were set to zero. Results of the calculations are shown in Figure 3. The presented numbers were calculated after a simulation period of 100 min. Although concentrations of the stable compounds H_2O_2, NO_3^-, HCHO, and ORG steadily decrease due to the photolysis reactions or the reactions with OH calculated concentrations remain rather constant over a longer periods. Therefore, the presented numbers are representative for typical conditions in surface snow. The calculations clearly demonstrate the strong impact of the organic compounds on the OH levels in the QLL. The reactions of OH with HCHO and ORG clearly dominate the OH sinks. The additional OH production due to the photolysis of H_2O_2 cannot outweigh this OH sink. As a result the OH concentrations are significantly lower as compared to the calculations with the N-containing compounds alone [Publ. 3.3.4]. Nevertheless, the production of OH in the QLL is dominated by the photolysis of H_2O_2. The OH source strength is more than a factor of three higher than the OH production due to the NO_3^- photolysis. This is in agreement with the results presented by Chu and Anastasio [2005].

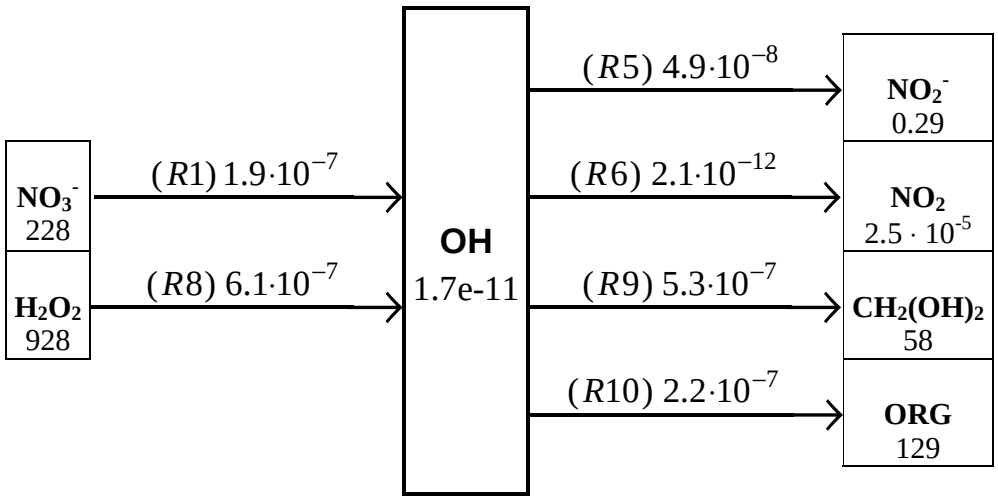

Figure 3: Sources and sinks of OH in the QLL. Numbers are calculated after a simulation period of 100 minutes. Numbers below molecules represent concentrations in mM, numbers above arrows represent fluxes in M s^{-1}. Numbers in brackets refer to the reaction numbers as shown in Table 2.

The experiments and model calculations regarding photochemical processes in surface snow clearly demonstrate that photochemical transformations in the snow are very diverse. The OH radical plays a critical role for these transformations comparable to the atmospheric gas and liquid phase. However, the sinks of this radical are not well defined. The reactions with organic compounds are probably the most important OH destruction reactions. However, due to the limited information of the concentrations of single organic compounds in snow it is currently impossible to assemble a detailed mechanism for snow chemistry. Therefore, a class of compounds representing organic material as a sum parameter was introduced. Further investigations of organic components in snow can be used to refine the mechanism.

Processes at the interface of the surface snow and the atmospheric boundary layer can be described in detail in one-dimensional models [McConnell et al., 1997a, 1997b, 1998; Hutterli et al., 1999, 2002, 2003; Albert et al., 2002]. These models have been used to develop so-called transfer functions relating atmospheric and snow concentrations of species like H_2O_2 and HCHO. Such transfer functions can possibly be applied to reconstruct past atmospheric concentrations of these two compounds using firn and ice core concentrations profiles, which are available for several locations [Sigg and Neftel, 1988, 1991; Staffelbach et al., 1991; Kamiyama et al., 1992; Fuhrer et al., 1993; Jacob and Klockow, 1993; Van Ommen and Morgan, 1996; Anklin and Bales, 1997; Gillett et al., 2000; Sommer et al., 2000; Hutterli et al., 2002; Largiuni et al., 2003]. However, simple transfer functions cannot be developed since H_2O_2 and HCHO concentrations in the snow are both influenced by bi-directional fluxes between the snow and the atmosphere [e.g. Publ. 3.2.3, 3.2.5, 3.2.7]. Therefore, the snow concentrations depend on a range of physical and meteorological parameters like snow temperature, snow accumulation and timing of snow accumulation events [McConnell et al., 1997a, 1997b, 1998; Hutterli et al., 1999, 2002, 2003]. In addition, as

demonstrated in the laboratory experiments photochemical processes need to be taken into account at least in the case of H_2O_2.

A further improvement of one-dimensional models for the atmosphere – snow pack system is the inclusion of photochemical processes in surface snow. The mechanism presented in Table 2 comprises a still limited number of reactions. It seems feasible to include this mechanism in one-dimensional models. Since the transformations are driven by photolysis reactions, radiation levels as a function of snow depth are also needed as input parameters. Such measurements have been reported for several polar locations [King and Simpson, 2001; Lee-Taylor and Madronich, 2002; Peterson et al., 2002; Simpson et al., 2002] demonstrating that in general the intensities decrease exponentially with depth. In summary, sufficient knowledge and data are available for all relevant physical and chemical processes occurring in natural snow surfaces, so that the development of a full one-dimensional model seems possible.

Such models are necessary to investigate the impact of the exchange of reactive trace compounds on the composition of the atmospheric boundary layer in snow-covered regions. It has been demonstrates that the observed emissions of the NO_x and HONO can strongly influence the OH budget under these conditions [e.g. Publ. 3.2.4]. These effects are most obvious for the conditions at South Pole. Due to the regularly observed limited height of the stable atmospheric boundary layer at this location NO_x emission have a pronounced effect on the observed atmospheric concentrations [Davis et al., 2001, 2004; Oncley et al. 2004]. In addition HONO, H_2O_2, and HCHO, which are also emitted by the snow surface, contribute to the formation of OH and hydroperoxyl radicals (HO_2) in the boundary layer [Publ. 3.2.4].

2.3 Impact of sea ice formation on atmospheric trace compounds

A very different kind of a frozen surface also encountered in polar regions is sea ice. While snow is generated in the atmosphere by condensation and nucleation of water vapor, sea ice forms by freezing of ocean water at low air temperatures. The freezing of ocean water involves several physical and thermodynamical processes since the ocean water contains sea salt at relatively high concentrations. The main sea salt components are chloride (Cl^-), sodium (Na^+), and sulfate (SO_4^{2-}) with average concentrations of 1.94, 1.0, and 0.27 g per kg of ocean water [Millero, 2006]. These three ions contribute 94 % of the total sea salt. While the sea salt can easily be dissolved in the liquid ocean water, much smaller amounts of salt ions can be incorporated in the sea ice crystals [Thomas and Diekmann, 2003]. Therefore, the sea salt ions are rejected from the ice lattice during the freezing process. The ions remain dissolved in a liquid forming a salty brine, which is collected in microscopic brine inclusions in the sea ice. Eventually these inclusions form an entire network of pores making the vertical transport of the brine into the ocean water or to the top of the sea ice possible [Eicken et al., 2000]. Therefore, new sea ice is covered with the brine with salt concentrations significantly higher than encountered in the ocean water. Due to the high salt concentrations of the brine, it remains liquid even at temperatures well below the freezing point of water.

Figure 4: Photographs of frost flowers on the Arctic Ocean. The photographs were taken on 25 March 2003 (75.9° N, 27.0° E).

An additional feature of new sea ice is the generation of dendritic ice crystals, which form in the polar regions under calm wind conditions [Perovich and Richter-Menge, 1994]. These so-called frost flowers (Figure 4) appear upon condensation of water vapor from a supersaturated layer above the sea ice surface on solid irregularities [Perovich and Richter-Menge, 1994; Martin et al., 1995]. Depending on the temperature gradient between the relatively warm sea ice surface and the colder air temperatures, the frost flowers can quickly cover large fractions of newly formed sea ice. Laboratory experiments demonstrated that at T = –30 °C the growth rate can be as large as 10 % area coverage per hour [Martin et al., 1996]. Interestingly, frost flowers also contain high concentrations of sea salt [Drinkwater and Crocker, 1988; Perovich and Richter-Menge, 1994; Martin et al., 1995; Rankin et al., 2002], although they are initially formed by the condensation of water vapor. The observations have demonstrated that the overall salinity of the frost flowers can be a factor of almost 5 higher than the salinity of the ocean water [Drinkwater and Crocker, 1988].

The transport of the sea salt ions into the frost flowers is only possible within the QLL of the single crystals. Within this liquid layer the ions can migrate from the brine layer on the sea ice surface into the frost flower crystals. The driving force of this migration is the so-called thermomolecular pressure gradient, which induces a transport of liquid water and the ions from warmer to colder regions within the frost flowers [Wettlaufer and Worster, 1995]. Since the temperature gradient in the air above the sea ice is also imprinted in the frost flowers (Figure 5), the coldest portion of the frost flower crystals are the highest tips with the largest distance from the warm sea ice surface [Martin et al., 1996].

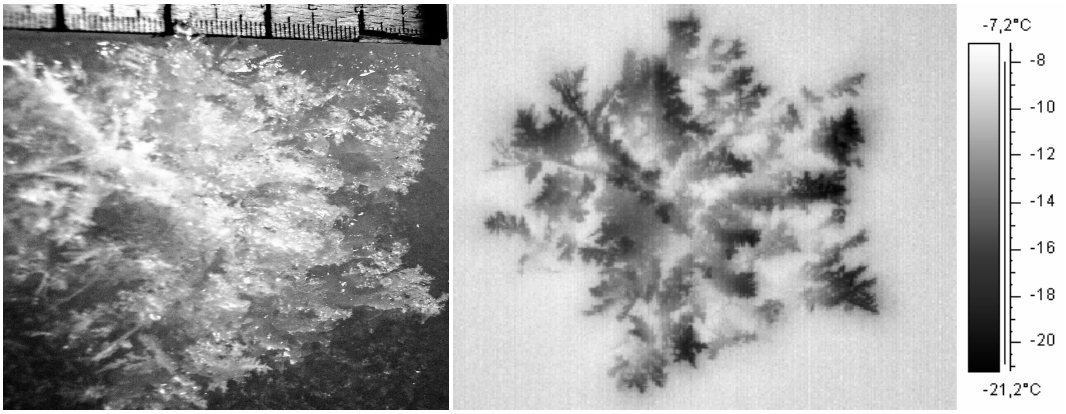

Figure 5: Photographs of an artificial frost flower grown in the laboratory at air temperatures between –25 and –30 °C (left regular digital picture, right IR picture). The horizontal dimension of the frost flower is on the order of 10 cm. The same structures can be recognized in both pictures. In the IR picture the strong temperature difference between the warmer sea ice surface (–9 °C) and the cold frost flower (temperature at tips between –14 and –20 °C) can be observed.

The observations of Rankin et al. [2002] demonstrated that in general the enrichment of the single sea salt components in the frost flowers were comparable to the enrichment of the salinity. The main exception was SO_4^{2-}, which showed much lower enrichment factors. This change in composition was attributed to the formation of mirabilite ($Na_2SO_4 \cdot 10\ H_2O$), which precipitates at a temperature of –8 °C [Untersteiner, 1986]. Due to the higher amount of Na^+ available in the brine compared to SO_4^{2-}, the precipitation has a stronger effect on the SO_4^{2-} concentration compared to the Na^+ concentration.

It is well known that halides like chloride and bromide can be converted to reactive halogen compounds due to heterogeneous reactions [McConnell et al., 1992; Fan and Jacob, 1992; Vogt et al., 1996]. Crucial reactions in the case of bromide (Br^-) are the formation of hypobromous acid (HOBr) in the gas phase, which is readily absorbed at surfaces, and the oxidation of the corresponding hypobromite anion (BrO^-) to molecular bromine (Br_2) in the presence of Br^- and sufficient acidity. The solubility of Br_2 is rather low leading to a release of this compound back to the gas phase. In the gas phase, Br_2 is quickly photolyzed by UV and visible radiation producing bromine atoms (Br). A similar mechanism is also feasible for chloride (Cl^-). Such a mechanism can occur on any environmental surface with the appropriate properties. However, new sea ice covered with frost flowers seems to offer ideal conditions for this mechanism: the brine as well as the frost flowers contain high concentrations of sea salt including Cl^- and Br^- and the specific surface area is drastically increased due to the prickly structure of the single crystals (Figure 4). For example, measurements of the specific surface areas of frost flowers resulted in a value of 200 $cm^2\ g^{-1}$ [Domine et al., 2005].

The relation between sea ice formation and release of reactive halogens to the atmosphere was explored in Publ. 3.4.2 using remote sensing data. If a Br atom reacts with O_3 bromine monoxide (BrO) is formed. This molecule can be detected using satellite observations [Richter et al., 1998; Wagner and Platt, 1998]. Enhanced BrO

concentrations are regularly observed over the frozen Arctic and Antarctic Oceans during springtime [Richter et al., 1998; Wagner and Platt, 1998]. In Publ. 3.4.2 a thermodynamic model was presented to derive potential frost flower areas. This model utilizes several further remote sensing data like calculated open water areas or assimilated global data sets of the air temperature. The spatial agreement of open water areas with low air temperatures are a prerequisite for frost flower formation and are expressed as potential frost flower areas. In several case studies it was demonstrated that large potential frost flower areas are strongly related to air masses containing elevated BrO levels if the transport is taken into account using trajectories [Publ. 3.4.2].

A further indication that new sea ice is connected with the halogen activation process is the occurrence of tropospheric ozone depletion events. Such events were first observed almost 20 years ago [Barrie et al., 1988] in the Arctic. It is now well known that such events occur regularly in springtime in both hemispheres [e.g. Tarasick and Bottenheim, 2002; Wessel et al., 1998] and that they are related to the elevated tropospheric BrO concentrations observed by remote sensing techniques [Richter et al., 1998; Wagner and Platt, 1998]. The O_3 destruction is caused by several catalytic cycles involving the reactive halogen compounds [Platt and Hönninger, 2003; Publ. 3.4.3]. Therefore, the depletion of ozone can be regarded as an indicator of vigorous halogen activation processes. In Publ. 3.4.1 we presented a time series of O_3 concentrations measured in springtime in the marginal ice zone of the Arctic Ocean. Low O_3 concentrations were encountered during numerous periods lasting for several days. Further analysis of the conditions during the onset of the longest O_3 depletion event indicated that the O_3 decrease was not caused by a change in air mass transport [Publ. 3.4.3]. It was demonstrated that the observed O_3 decrease was a local phenomenon probably initiated by the local release of reactive halogens in the marginal ice zone. Further analysis indicated that larger areas with newly formed sea ice characterized the ice edge region at the time of the O_3 measurements [Publ. 3.4.3]. Since air temperatures remained very low, the formation of frost flowers on the newly formed sea ice was very likely. Nevertheless, all these observations do not reveal, which of the specific surfaces formed through the freezing of ocean water (e.g. brine, frost flowers) are responsible for the halogen activation. It has also been suggested that aerosols generated in the new sea ice areas and subsequently deposited on adjacent snow surfaces could be the active sites for the halogen release mechanism [Avallone et al., 2003; Simpson et al., 2005]. Currently, the observations are too limited to resolve this question. Even if the specific source of the reactive halogen species is unknown, the observed O_3 decrease can be used to estimate concentrations of halogen atoms [Publ. 3.4.3]. These induced concentrations are extremely high in agreement with the observed rapid O_3 decrease.

2.4 Outlook and future perspectives

The presented measurements indicate that in the polar regions of the Earth the atmospheric concentrations of a range of reactive trace gases are influenced by interactions with underlying frozen surfaces. The effects can be immense. The most drastic example is the complete destruction of O_3 in the atmospheric boundary caused by the activation of reactive halogen compounds over the frozen polar oceans. In the recent years our knowledge about the mechanisms and processes responsible for the interactions with snow and sea ice has advanced considerably.

In the field of snow photochemistry, we have developed a simplified reaction mechanism, which is able to reproduce field observation like the NO_x release to the atmosphere. This mechanism was adjusted to conditions at Summit Station in Greenland, but can probably be applied to further locations too. Such a mechanism now allows a range of further systematic investigation looking for example at the influence of NO_3^- snow concentrations or the snow pH on NO_x production rates in the snow. Including this mechanism into one-dimensional models of the snow pack – atmosphere system would further allow exploring NO_x emission rates from the surface snow as a function of latitude and season. These numbers finally could be included into regional or global models describing transport and chemistry of reactive trace compounds. Such simulations would probably result in much better agreement of calculated and actually measured trace gas concentrations in both polar regions. In a further step, simulations that take into account interactions with the snow could even analyse the influence of a change in snow cover extent either in the past or in the future due to a changing climate. For example, in the last glacial maximum much larger areas were covered with snow and ice [e.g. Peltier, 1994], which could have had a profound effect on the concentrations of several trace gases like the NO_x.

Nevertheless, the here presented reaction mechanism for snow photochemistry can only represent an initial step. A full representation of the sinks and sources of the OH radical in the QLL will be needed in the future to increase the performance of the mechanism. Since the organic compounds are crucial for the OH budget, improvements in the measurements or organics in snow are clearly needed. First, the speciation of the organic matter in the snow needs to be analyzed and representative concentrations of the main components are required as input parameters. Second, rate constants for the reactions of the OH radical with the identified organic compounds for the conditions in the QLL must be determined. A combination of field and laboratory measurements can help elucidating these topics.

Our mechanistic understanding of chemical processes at the surface of new sea ice is much more limited. This is probably due to more difficult field measurements. First, in contrast to snow-covered regions areas covered with new sea ice including frost flower are extremely difficult to access. Only the most modern research icebreakers are able to operate in springtime in the ice-covered polar oceans with the highest probability of chemical activity. Second, the reactive halogens generated at the new sea ice surfaces only reach low concentrations, so that for most of these species detectors for field measurements are unavailable. Therefore, a direct observation of the emission of halogen species in the field will remain unlikely for the near future. A more promising approach is possibly to perform laboratory experiments with frost flowers to investigate the halogen release. The generation of artificial frost flowers in laboratory experiments has been described in the literature [Martin et al. 1995, 1996; Ngheim et al., 1997]. However, additional field measurements will also be needed to verify results of laboratory experiments with artificial frost flowers.

For the reactions in the snow as well as at the surface of sea ice the properties of the disordered layer at the surface of the snow or ice crystals is crucial. Nevertheless, information about this layer is still rather limited. Neither the thickness of the layer on pure water, nor the influence of impurities is well characterized. Several theoretical models exist [Chen and Crutzen, 1994; Wettlaufer, 1999; Cho et al., 2002; Henson et al., 2005; Voss et al., 2005], which have been used to calculate the thickness of the QLL. However, the available measurements are too variable to validate or even improve the different models. A better experimental characterization of the QLL is clearly

needed. Such investigations seem to be feasible since improved techniques for the analysis of surface properties have become available [e.g. Bluhm et al., 2002; Cho et al., 2002; Wei et al., 2002; Ewing, 2004]. Further information can be expected from molecular dynamics simulations [Girardet and Toubin, 2001]. Such calculations have for example been used to investigate the freezing process of water with and without impurities [Vrbka and Jungwirth, 2005; Carignano et al., 2005; Ikeda-Fukazawa and Kawamura, 2006]. MD simulations can possibly also help identifying where impurities are located: within the QLL or at the interface of the condensed and gas phase. This can have important implications since reaction rates and products can be very different depending on the environment of the reactive specie. For example, similar calculations for the interface of the liquid water with the gas phase have demonstrated that the halides Cl^- and Br^- are preferably located at the interface, where they are readily available for heterogeneous reactions [Jungwirth and Tobias, 2001, 2002].

2.5 References

Albert, M.R., A.M. Grannas, J. Bottenheim, P.B. Shepson, and F.E. Perron, Processes and properties of snow-air transfer in the high Arctic with application to interstitial ozone at Alert, Canada, *Atmos.Environ.* 36, 2779-2787, 2002.

Amoroso, A., H.J. Beine, R. Sparapani, M. Nardino, and I. Allegrini, Observation of coinciding arctic boundary layer ozone depletion and snow surface emissions of nitrous acid, *Atmos.Environ.* 40, 1949-1956, 2006.

Anastasio, C., and A.L. Jordan, Photoformation of hydroxyl radical and hydrogen peroxide in aerosol particles from Alert, Nunavut: Implications for aerosol and snowpack chemistry in the Arctic, *Atmos.Environ.* 38, 1153-1166, 2004.

Anklin, M., and R.C. Bales, Recent increases in H_2O_2 concentration at Summit, Greenland, *J.Geophys.Res.* 102, 19099-19104, 1997.

Avallone, L.M., D.W. Toohey, T.J. Fortin, K.A. McKinney, and J.D. Fuentes, In situ measurements of bromine oxide at two high-latitude boundary layer sites: Implications of variability, *J.Geophys.Res.* 108 (D3), 4089, doi: 10.1029/2002JD002843, 2003.

Barrie, L.A., J.W. Bottenheim, R.C. Schnell, P.J. Crutzen, and R.A. Rasmussen, Ozone destruction and photochemical reactions at polar sunrise in the lower Arctic atmosphere, *Nature* 334, 138-141, 1988.

Beine, H.J., R.E. Honrath, F. Dominé, W.R. Simpson, and J.D. Fuentes, NO_x during background and ozone depletion periods at Alert: Fluxes above the snow surface, *J.Geophys.Res.* 107 (D21), 4584, doi: 10.1029/2002JD002082, 2002a.

Beine, H.J., F. Dominé, W.R. Simpson, R.E. Honrath, R. Sparapani, X. Zhou, and M. King, Snow-pile and chamber experiments during the Polar Sunrise Experiment 'Alert 2000': Exploration of nitrogen chemistry, *Atmos.Environ.* 36, 27007-2719, 2002b.

Beine, H.J., F. Dominé, A. Ianniello, M. Nardino, I. Allegrini, K. Teinilä, and R. Hillamo, Fluxes of nitrate between snow surfaces and the atmosphere in the European high Arctic, *Atmos.Chem.Phys.* 3, 335-346, 2003.

Beine, H.J., A. Amoroso, G. Esposito, R. Sparapani, A. Ianniello, T. Georgiadis, M. Nardino, P. Bonasoni, P. Cristofanelli, and F. Dominé, Deposition of atmospheric nitrous acid on alkaline snow surfaces, *Geophys.Res.Lett.* 32, L10808, doi: 10.1029/2005GL022589, 2005.

Blake, N.J., D.R. Blake, O.W. Wingenter, B.C. Sive, C.H. Kang, D.C. Thornton, A.R. Bandy, E. Atlas, F. Flocke, J.M. Harris, and F.S. Rowland, Aircraft measurements of the latitudinal, vertical, and seasonal variations of NMHCs, methyl nitrate, methyl halides, and DMS during the First Aerosol Characterization Experiment (ACE 1), *J.Geophys.Res.* 104, 21803-21817, 1999.

Blake, N.J., D.R. Blake, A.L. Swanson, E. Atlas, F. Flocke, and F.S. Rowland, Latitudinal, vertical, and seasonal variations of C_1-C_4 alkyl nitrates in the troposphere over the Pacific Ocean during PEM-Tropics A and B: Oceanic and continental sources, *J.Geophys.Res.* 108 (D2), 8242, doi: 10.1029/2001JD001444, 2003.

Bluhm, H., D.F. Ogletree, C.S. Fadley, Z. Hussain, and M. Salmeron, The premelting of ice studied with photoelectron spectroscopy, *J.Phys.Condens.Matter* 14, L227-L233, 2002.

Boudries, H., J.W. Bottenheim, C. Guimbaud, A.M. Grannas, P.B. Shepson, S. Houdier, S. Perrier, and F. Dominé, Distribution and trends of oxygenated hydrocarbons in the

high arctic derived from measurements in the atmospheric boundary layer and interstitial snow air during the ALERT2000 field campaign, *Atmos.Environ.* 36, 2573-2583, 2002.

Boxe, C.S., A.J. Colussi, M.R. Hoffmann, D. Tan, J. Mastromarino, A.T. Case, S.T. Sandholm, and D.D. Davis, Multiscale ice fluidity in NO_x photodesorption from frozen nitrate solutions, *J.Phys.Chem.A* 107, 11409-11413, 2003.

Boxe, C.S., A.J. Colussi, M.R. Hoffmann, J.G. Murphy, P.J. Wooldridge, T.H. Bertram, and R.C. Cohen, Photochemical production and release of gaseous NO_2 from nitrate-doped water ice, *J.Phys.Chem.A* 109, 8520-8525, 2005.

Boxe, C.S., A.J. Colussi, M.R. Hoffmann, I.M. Perez, J.G. Murphy, and R.C. Cohen, Kinetics of NO and NO_2 evolution from illuminated frozen nitrate solutions, *J.Phys.Chem.A* 110, 3578-3583, 2006.

Bridier, I., F. Caralp, H. Loirat, R. Lesclaux, B. Veyret, K.H. Becker, A. Reimer, and F. Zabel, Kinetic and theoretical studies of the reactions $CH_3C(O)O_2 + NO_2 + M \leftrightarrow CH_3C(O)O_2NO_2 + M$ between 248 and 393 K and between 30 and 760 Torr, *J.Phys.Chem.* 95, 3594-3600, 1991.

Carignano, M.A., P.B. Shepson, and I. Szleifer, Molecular dynamics simulations of ice growth from supercooled water, *Mol.Phys.* 103, 2957-2967, 2005.

Carroll, M.A., and A.M. Thompson, NO_x in the non-urban troposphere, in J.R. Barker (ed.), *Progress and problems in atmospheric chemistry*, World Scientific, Singapore, 198-255, 1995.

Chen, J.-P., and P.J. Crutzen, Solute effects on the evaporation of ice articles, *J.Geophys.Res.* 99, 18847-18859, 1994.

Cho, H., P.B. Shepson, L.A. Barrie, J.P. Cowin, and R. Zaveri, NMR investigation of the quasi-brine layer in ice/brine mixtures, *J.Phys.Chem.B* 106, 11226-11232, 2002.

Chu, L., and C. Anastasio, Quantum yields of hydroxyl radical and nitrogen dioxide from the photolysis of nitrate on ice, *J.Phys.Chem.A* 107, 9594-9602, 2003.

Chu, L., and C. Anastasio, Formation of hydroxyl radical from the photolysis of frozen hydrogen peroxide, *J.Phys.Chem.A* 109, 6264-6271, 2005.

Cotter, E.S.N., A.E. Jones, E.W. Wolff, and S.J.-B. Baugitte, What controls photochemical NO and NO_2 production from Antarctic snow? Laboratory investigation assessing the wavelength and temperature dependence, *J.Geophys.Res.* 108 (D4), 4147, doi: 10.1029/2002JD002602, 2003.

Couch, T.L., A.L. Sumner, T.M. Dassau, P.B. Shepson, and R.E. Honrath, An investigation of the interaction of carbonyl compounds with the snowpack, *Geophys.Res.Lett.* 27, 2241-2244, 2000.

Dassau, T.M., A.L. Sumner, S.L. Koeniger, P.B. Shepson, J. Yang, R.E. Honrath, N.J. Cullen, K. Steffen, H.-W. Jacobi, M. Frey, and R.C. Bales, Investigation of the role of the snowpack on atmospheric formaldehyde chemistry at Summit, Greenland, *J.Geophys.Res.* 107 (D19), 4394, doi: 10.1029/2002JD002182, 2002.

Dassau, T.M., P.B. Shepson, J.W. Bottenheim, and K.M. Ford, Peroxyacetyl nitrate photochemistry and interactions with the Arctic surface, *J.Geophys.Res.* 109, D18302, doi: 10.1029/2004JD004562, 2004.

Davis, D., J.B. Nowak, G. Chen, M. Buhr, R. Arimoto, A. Hogan, F. Eisele, L. Mauldin, D. Tanner, R. Shetter, B. Lefer, and P. McMurry, Unexpected high levels of NO observed at South Pole, *Geophys.Res.Lett.* 28, 3625-3628, 2001.

Davis, D., G. Chen, M. Buhr, J. Crawford, D. Lenschow, B. Lefer, R. Shetter, F. Eisele, L. Mauldin, and A. Hogan, South Pole NO_x chemistry: An assessment of factors controlling variability and absolute levels, *Atmos.Environ.* 38, 5375-5388, 2004.

Dibb, J.E., and M. Arsenault, Should not snowpacks be a source of monocarboxylic acids? *Atmos.Environ.* 36, 2513-2522, 2002.

Dibb, J.E., M. Arsenault, M.C. Peterson, and R.E. Honrath, Fast nitrogen oxide photochemistry in Summit, Greenland snow, *Atmos.Environ.* 36, 2501-2511, 2002.

Dibb, J.E., L.G. Huey, D.L. Slusher, and D.J. Tanner, Soluble reactive nitrogen oxides at South Pole during ISCAT 2000, *Atmos.Environ.* 38, 5399-5409, 2004.

Dominé, F., and P.B. Shepson, Air-snow interactions and atmospheric chemistry, *Science* 297, 1506-1510, 2002.

Domine, F., A.S. Taillandier, W.R. Simpson, and K. Severin, Specific surface area, density and microstructure of frost flowers, *Geophys.Res.Lett.* 32, L13502, doi:10.1029/2005GL023245, 2005.

Drinkwater, M.R., and G.B. Crocker, Modelling changes in the dielectric and scattering properties of young snow-covered sea ice at GHz frequencies, *J.Glaciol.* 34, 274-282, 1988.

Dubowski, Y., A.J. Colussi, and M.R. Hoffmann, Nitrogen dioxide release in the 302 nm band photolysis of spray-frozen aqueous nitrate solutions. Atmospheric implications, *J.Phys.Chem.A* 105, 4928-4932, 2001.

Dubowski, Y., A.J. Colussi, C. Boxe, and M.R. Hoffmann, Monotonic increase of nitrite yields in the photolysis of nitrate in ice and water between 238 and 294 K, *J.Phys.Chem.A* 106, 6967-6971, 2002.

Eicken, H., C. Bock, R. Wittig, H. Miller, and H.-O. Pörtner, Magnetic resonance imaging of sea-ice pore fluids: Methods and thermal evolution of pore microstructure, *Cold Reg.Sci.Technol.* 31, 207-225, 2000.

Ewing, G.E., Thin film water, *J.Phys.Chem.B* 108, 15953-15961, 2004.

Fan, S.-M., and D.J. Jacob, Surface ozone depletion in Arctic spring sustained by bromine reactions on aerosols, *Nature* 359, 522-524, 1992.

Ford, K.M., B.M. Campbell, P.B. Shepson, S.B. Bertman, R.E. Honrath, M. Peterson, and J.E. Dibb, Studies of peroxyacetyl nitrate (PAN) and its interaction with the snowpack at Summit, Greenland, *J.Geophys.Res.* 107 (D10), 10.1029/2001JD000547, 2002.

Fuhrer, K., A. Neftel, M. Anklin, and V. Maggi, Continuous measurements of hydrogen peroxide, formaldehyde, calcium and ammonium concentrations along the new GRIP ice core from Summit, central Greenland, *Atmos.Environ.* 27, 1873-80, 1993.

Gillett, R.W., T.D. van Ommen, A.V. Jackson, and G.P. Ayers, Formaldehyde and peroxide concentrations in Law Dome (Antarctica) firn and ice cores, *J.Glaciol.* 46, 15–19, 2000.

Grannas, A.M., P.B. Shepson, C. Guimbaud, A.L. Sumner, M. Albert, W. Simpson, F. Domine, H. Boudries, J. Bottenheim, H.J. Beine, R. Honrath, and X. Zhou, A study of photochemical and physical processes affecting carbonyl compounds in the Arctic atmospheric boundary layer, *Atmos.Environ.* 36, 2733-2742, 2002.

Grannas, A.M., P.B. Shepson, and T.R. Filley, Photochemistry and nature of organic matter in Arctic and Antarctic snow, *Global Biogeochem.Cycles* 18 (GB1006), doi: 10.1029/2003GB002133, 2004.

Guimbaud, C., A.M. Grannas, P.B. Shepson, J.D. Fuentes, H. Boudries, J.W. Bottenheim, F. Dominé, S. Houdier, S. Perrier, T.B. Bisenthal, and B.G. Splawn, Snowpack processing of acetaldehyde and acetone in the arctic atmospheric boundary layer, *Atmos.Environ.* 36, 2743-2752, 2002.

Gurman, V.S., V.A. Batyuk, and G.B. Sergeev, Photolysis of frozen dilute solutions of H_2O_2 in water (Translated), *Kin.Kat.* 8, 527-531, 1967.

Henson, B.F., L.F. Voss, K.R. Wilson, and J.M. Robinson, Thermodynamic model of quasiliquid formation on H_2O ice: Comparison with experiment, *J.Chem.Phys.* 123, 144707, doi: 10.1063/1.2056541, 2005.

Herrmann, H., B. Ervens, H.-W. Jacobi, R. Wolke, P. Nowacki, and R. Zellner, CAPRAM2.3: A chemical aqueous phase radical mechanism for tropospheric chemistry, *J.Atmos.Chem.* 36, 231-284, 2000.

Holoubek, I., P. Klán, A. Ansorgová, and D. del Favero, Photochemistry of PBT compounds in ice: A new potential source of ice contamination? *Organohalogen Compd.* 46, 228-231, 2000.

Honrath, R.E., M.C. Peterson, S. Guo, J.E. Dibb, P.B. Shepson, and B. Campbell, Evidence of NO_x production within or upon ice particles in the Greenland snowpack, *Geophys.Res.Lett.* 26, 695-698, 1999.

Honrath, R.E., M.C. Peterson, M.P. Dziobak, J.E. Dibb, M.A. Arsenault, and S.A. Green, Release of NO_x from sunlight-irradiated midlatitude snow, *Geophys.Res.Lett.* 27, 2237-2240, 2000a.

Honrath, R.E., S. Guo, M.C. Peterson, M.P. Dziobak, J.E. Dibb, and M.A. Arsenault, Photochemical production of gas phase NO_x from ice crystal NO_3^-, *J.Geophys.Res.* 105, 24183-24190, 2000b.

Honrath, R.E., Y. Lu, M.C. Peterson, J.E. Dibb, M.A. Arsenault, N.J. Cullen, and K. Steffen, Vertical fluxes of NO_x, HONO, and HNO_3 above the snowpack at Summit, Greenland, *Atmos.Environ.* 36, 2629-2640, 2002.

Houdier, S., S. Perrier, E. Defrancq, and M. Legrand, A new fluorescent probe for sensitive detection of carbonyl compounds: Sensitivity improvement and application to environmental water samples, *Anal.Chim.Acta* 412, 221-233, 2000.

Houdier, S., S. Perrier, F. Dominé, A. Cabanes, L. Legagneux, A.M. Grannas, C. Guimbaud, P.B. Shepson, H. Boudries, and J.W. Bottenheim, Acetaldehyde and acetone in the Arctic snowpack during the ALERT2000 campaign. Snowpack composition, incorporation processes and atmospheric impact, *Atmos.Environ.* 36, 2609-2618, 2002.

Hutterli, M.A., R. Röthlisberger, and R.C. Bales, Atmosphere-to-snow-to-firn transfer studies of HCHO at Summit, Greenland, *Geophys.Res.Lett.* 26, 1691-1694, 1999.

Hutterli, M.A., R.C. Bales, J.R. McConnell, and R.W. Stewart, HCHO in Antarctic snow: Preservation in ice cores and air-snow exchange, *Geophys.Res.Lett.* 29 (8), doi: 10.1029/2001GL014256, 2002.

Hutterli, M.A., J.R. McConnell, R.C. Bales, and R.W. Stewart, Sensitivity of hydrogen peroxide (H_2O_2) and formaldehyde (HCHO) preservation in snow to changing environmental conditions: Implications for ice core records, *J.Geophys.Res.* 108 (D1), 4023, doi: 10.1029/2002JD002528, 2003.

Ianniello, A., H.J. Beine, R. Sparapani, F. Di Bari, I. Allegrini, and J.D. Fuentes, Denuder measurements of gas and aerosol species above Arctic snow surfaces at Alert 2000, *Atmos.Environ.* 36, 5299-5309, 2002.

Ingram, D.J.E., W.G. Hodgson, C.A. Parker, and W.T. Rees, Detection of labile photochemical free radicals by paramagnetic resonance, *Nature* 176, 1227-1228, 1955.

Jacob, P., and D. Klockow, Measurements of hydrogen peroxide in Antarctic ambient air, snow and firn cores, *Fresenius J.Anal.Chem.* 346, 429-434, 1993.

Jungwirth, P., and D.J. Tobias, Molecular structure of salt solutions: A new view of the interface with implications for heterogeneous atmospheric chemistry, *J.Phys.Chem.B* 105, 10468-10472, 2001.

Jungwirth, P., and D.J. Tobias, Ions at the air/water interface, *J.Phys.Chem.B* 106, 6361-6373, 2002.

Kamiyama, K., O. Watanabe, and E. Nakayama, Atmospheric conditions reflected in chemical components in snow over East Queen Maud Land, Antarctica, *Proc. NIPR Symp.Polar Meteorol.Glaciol.* 6, 88-98, 1992.

King, M.D., and W.R. Simpson, The extinction of UV radiation in Arctic snow at Alert, Canada (82ºN), *J.Geophys.Res.* 106, 12499-12507, 2001.

Klán, P., A. Ansorgová, D. Del Favero, and I. Holoubek, Photochemistry of chlorobenzene in ice, *Tetrahed.Lett.* 41, 7785-7789, 2000.

Klán, P., D. Del Favero, A. Ansorgová, J. Klánová, and I. Holoubek, Photodegradation of halobenzenes in water ice, *Environ.Sci.Poll.Res.* 8, 195-200, 2001.

Klán, P., J. Klánová, I. Holoubek, and P. Čupr, Photochemical activity of organic compounds in ice induced by sunlight irradiation: The Svalbard project, *Geophys.Res.Lett.* 30 (6), 1313, doi: 10.1029/2002GL016385, 2003.

Klánová, J., P. Klán, J. Nosek, and I. Holoubek, Environmental ice photochemistry: Monochlorphenols, *Environ.Sci.Technol.* 37, 1568-1574, 2003a.

Klánová, J., P. Klán, D. Heger, and I. Holoubek, Comparison of the effects of UV, H_2O_2/UV and γ-irradiation on frozen and liquid water solutions of monochlorphenols, *Photochem.Photobiol.Sci.* 2, 1023-1031, 2003b.

Kroh, J., B.C. Green, and J.W.T. Spinks, Electron paramagnetic resonance studies on the production of free radicals in hydrogen peroxide at liquid nitrogen temperature, *J.Am.Chem.Soc.* 83, 2201-2202, 1961.

Kroh, J., B.C. Green, and J.W.T. Spinks, Electron paramagnetic resonance studies on free radicals produced by Tβ-particles in frozen H_2O and D_2O media at liquid nitrogen temperature, *Can.J.Chem.* 40, 413-425, 1962.

Largiuni, O., R. Udisti, S. Becagli, R. Traversi, V. Maggi, E. Bolzacchini, P. Casati, C. Uglietti, and S. Borghi, Formaldehyde record from Lys glacier firn core, Monte Rosa massif (Italy), *Atmos.Environ.* 37, 3849-3860, 2003.

Lee-Taylor, J., and S. Madronich, Calculation of actinic fluxes with a coupled atmosphere–snow radiative transfer model, *J.Geophys.Res.* 107 (D24), 4796, doi: 10.1029/2002JD002084, 2002.

Legrand, M., and P. Mayewski, Glaciochemistry of polar ice cores: A review, *Rev.Geophys.* 35, 219-243, 1997.

Liao, W., A.T. Case, J. Mastromarino, D. Tan, and J.E. Dibb, Observations of HONO by laser-induced fluorescence at the South Pole during ANTCI 2003, *Geophys.Res.Lett.* 33, L09810, doi: 10.1029/2005GL025470, 2006.

McConnell, J.C., G.S. Henderson, L. Barrie, J. Bottenheim, H. Niki, C.H. Langford, and E.M.J. Templeton, Photochemical bromine production implicated in Arctic boundary-layer ozone depletion, *Nature* 355, 150-152, 1992.

McConnell, J.R., J.R. Winterle, R.C. Bales, A.M. Thompson, and R.W. Stewart, Physically based inversion of surface snow concentrations of H_2O_2 to atmospheric concentrations at South Pole, *Geophys.Res.Lett.* 24, 441-444, 1997a.

McConnell, J.R., R.C. Bales, J.R. Winterle, H. Kuhns, and C.R. Stearns, A lumped parameter model for the atmosphere-to-snow transfer function for hydrogen peroxide, *J.Geophys.Res.* 102, 26809-26818, 1997b.

McConnell, J.R., R.C. Bales, R.W. Stewart, A.M. Thompson, M.R. Albert, and R. Ramos, Physically based modeling of atmosphere-to-snow-to-firn transfer of H_2O_2 at South Pole, *J.Geophys.Res.* 103, 10561-10570, 1998.

Martin, S., R. Drucker, and M. Fort, A laboratory study of frost flower growth on the surface of young sea ice, *J.Geophys.Res.* 100, 7027-7036, 1995.

Martin, S., Y. Yu, and R. Drucker, The temperature dependence of frost flower growth on laboratory sea ice and the effect of the flowers on infrared observations of the surface, *J.Geophys.Res.* 101, 12111-12125, 1996.

Millero, F.J., *Chemical Oceanography*, 3. ed., Taylor & Francis, Boca Raton, Florida, 2006.

Nghiem, S.V., S. Martin, D.K. Perovich, R. Kwok, R. Drucker, and A.J. Gow, A laboratory study of the effect of frost flowers on C band radar backscatter from sea ice, *J.Geophys.Res.* 102, 3357-3370, 1997.

Oncley, S.P., M. Buhr, D.H. Lenschow, D. Davis, and S.R. Semmer, Observations of summerime NO fluxes and boundary-layer height at the South Pole during ISCAT 2000 using scalar similarity, *Atmos.Environ.* 38, 5389-5398, 2004.

Peltier, W.R., Ice age paleotopography, *Science* 265, 195-201, 1994.

Perovich, D.K., and J.A. Richter-Menge, Surface characteristics of lead ice, *J.Geophys.Res.* 99, 16341-16350, 1994.

Perrier, S., S. Houdier, F. Dominé, A. Cabanes, L. Legagneux, A.L. Sumner, and P.B. Shepson, Formaldehyde in Arctic snow. Incorporation into ice particles and evolution in the snowpack, *Atmos.Environ.* 36, 2695-2705, 2002.

Peterson, M.C., and R.E. Honrath, Observations of rapid photochemical destruction of ozone in snowpack interstitial air, *Geophys.Res.Lett.* 28, 511-514, 2001.

Peterson, M., D. Barber, and S. Green, Monte Carlo modeling and measurements of actinic flux levels in Summit, Greenland snowpack, *Atmos.Environ.* 36, 2545-2551, 2002.

Petrenko, V.F., and R.W. Whitworth, *Physics of ice*, Oxford University Press, Oxford, U.K., 1999.

Platt, U., and G. Hönninger, The role of halogen species in the troposphere, *Chemosphere* 52, 325-338, 2003.

Qiu, R., S.A. Green, R.E. Honrath, M.C. Peterson, Y. Lu, and M. Dziobak, Measurements of J_{NO3^-} in snow by nitrate-based actinometry, *Atmos.Environ.* 36, 2563-2571, 2002.

Rankin, A.M., E.W. Wolff, and S. Martin, Frost flowers: Implications for tropospheric chemistry and ice core interpretation, *J.Geophys.Res.* 107 (D23), 4683, doi: 10.1029/2002JD002492, 2002.

Richter, A., F. Wittrock, M. Eisinger, and J. P. Burrows (1998), GOME observations of tropospheric BrO in Northern Hemispheric spring and summer 1997, *Geophys.Res.Lett.*, 25, 2683-2686.

Ridley, B., J. Walega, D. Montzka, F. Grahek, E. Atlas, F. Flocke, V. Stroud, J. Deary, A. Gallant, H. Boudries, J. Bottenheim, K. Anlauf, D. Worthy, A.L. Sumner, B. Splawn, and P. Shepson, Is the Arctic surface layer a source and sink of NO_x in winter / spring? *J.Atmos.Chem.* 36, 1-22, 2000.

Riedel, K., W. Allan, R. Weller, and O. Schrems, Discrepancies between formaldehyde measurements and methane oxidation model predictions in the Antarctic troposphere: An assessment of other possible formaldehyde sources, *J.Geophys.Res.* 110, D15308, doi: 10.1029/2005JD005859, 2005.

Roberts, J.M., The atmospheric chemistry of organic nitrates, *Atmos.Environ.* 24A, 243-287, 1990.

Seinfeld, J.H., and S.N. Pandis, *Atmospheric chemistry and physics*, Wiley, New York, 1998.

Sigg, A., and A. Neftel, Seasonal variations in hydrogen peroxide in polar ice cores, *Ann.Glaciol.* 10, 157-162, 1988.

Sigg, A., and A. Neftel, Evidence for a 50 % increase in H_2O_2 over the past 200 years from a Greenland ice core, *Nature* 351, 557-559, 1991.

Simpson, W.R., M.D. King, H.J. Beine, R.E. Honrath, and X. Zhou, Radiation-modeling of snow-pack photochemical processes during ALERT2000, *Atmos.Environ.* 36, 2663-2670, 2002.

Simpson, W.R., L. Alvarez-Aviles, T.A. Douglas, M. Sturm, and F. Domine, Halogens in the coastal snow pack near Barrow, Alaska: Evidence for active bromine air-snow chemistry during springtime, *Geophys.Res.Lett.* 32, L04811, doi: 10.1029/2004GL021748, 2005.

Slusher, D.L., L.G. Huey, D.J. Tanner, G. Chen, D.D. Davis, M. Buhr, J.B. Nowak, F.L. Eisele, E. Kosciuch, R.L. Mauldin, B.L. Lefer, R.E. Shetter, and J.E. Dibb, Measurements of pernitric acid at the South Pole during ISCAT 2000, *Geophys.Res.Lett.* 29 (21), 2011, doi: 10.1029/2002GL015703, 2002.

Smith, R.C., and S.J. Wyard, Electron spin resonance in hydrogen peroxide – water solutions at 90 K irradiated with ultra-violet light, *Nature* 186, 226-228, 1960.

Sommer, S., C. Appenzeller, R. Röthlisberger, M.A. Hutterli, B. Stauffer, D. Wagenbach, H. Oerter, F. Wilhelms, H. Miller, and R. Mulvaney, Glacio-chemical study spanning the past 2 kyr on three ice cores from Dronning Maud Land, Antarctica. 1. Annually resolved accumulation rates, *J.Geophys.Res.* 105, 29411-29421, 2000.

Staffelbach, T., A. Neftel, B. Stauffer, and D. Jacob, A record of atmospheric methane sink from formaldehyde in polar ice cores, *Nature* 349, 603-605, 1991.

Sumner, A.L. and P.B. Shepson, Snowpack production of formaldehyde and its effect on the Arctic troposphere, *Nature* 398, 230-233, 1999.

Sumner, A.L., P.B. Shepson, A.M. Grannas, J.W. Bottenheim, K.G. Anlauf, D. Worthy, W.H. Schroeder, A. Steffen, F. Domine, S. Perrier, and S. Houdier, Atmospheric chemistry of formaldehyde in the Arctic troposphere at polar sunrise, and the influence of the snowpack, *Atmos.Environ.* 36, 2553-2562, 2002.

Swanson, A.L., N.J. Blake, J.E. Dibb, M.R. Albert, D.R. Blake, and F.S. Rowland, Photochemically induced production of CH_3Br, CH_3I, C_2H_5I, ethene, and propene within surface snow at Summit, Greenland, *Atmos.Environ.* 36, 2671-2682, 2002.

Swanson, A.L., N.J. Blake, E. Atlas, F. Flocke, D.R. Blake, and F.S. Rowland, Seasonal variations of C_2-C_4 nonmethane hydrocarbons and C_1-C_4 alkyl nitrates at the Summit research station in Greenland, *J.Geophys.Res.* 108 (D2), 4065, doi: 10.1029/2001JD001445, 2003.

Swanson, A.L., B.L. Lefer, V. Stroud, and E. Atlas, Trace gas emissions through a winter snowpack in the subalpine ecosystem at Niwot Ridge, Colorado, *Geophys.Res.Lett.* 32, L03805, doi: 10.1029/2004GL021809, 2005.

Talbot, R.W., J.E. Dibb, E.M. Scheuer, J.D. Bradshaw, S.T. Sandholm, H.B. Singh, D.R. Blake, N.J. Blake, E. Atlas, and F. Flocke, Tropospheric reactive odd nitrogen over the South Pacific in austral springtime, *J.Geophys.Res.* 105, 6681-6694, 2000.

Tarasick, D.W., and J.W. Bottenheim, Surface ozone depletion episodes in the Arctic and Antarctic from historical ozonesonde records, *Atmos.Chem.Phys.* 2, 197-205, 2002.

Thomas, D.N., and G.S. Dieckmann, *Sea ice*, Blackwell Science Ltd., Oxford, UK, 2003.

Untersteiner, N. (ed.), *The geophysics of sea ice*, NATO ASI Series B, Physics, Vol. 146, Plenum Press, New York, 1986.

Van Ommen, T.D., and V. Morgan, Peroxide concentrations in the Dome Summit South ice core, Law Dome, Antarctica, *J.Geophys.Res.* 101, 15147-15152, 1996.

Vogt, R., P.J. Crutzen, and R. Sander, A mechanism for halogen release from sea-salt aerosol in the remote marine boundary layer, *Nature* 383, 327-330, 1996.

Voss, L.F., B.F. Henson, K.R. Wilson, and J.M. Robinson, Atmospheric impact of quasiliquid layers on ice surfaces, *Geophys.Res.Lett.* 32, L07807, doi: 10.1029/2004GL022010, 2005.

Wagner, T., and U. Platt, Satellite mapping of enhanced BrO concentrations in the troposphere, *Nature* 395, 486-488, 1998.

Wei, X., P.B. Miranda, C. Zhang, and Y.R. Shen, Sum-frequency spectroscopic studies of ice interfaces, *Phys.Rev.B* 66, 085401, 2002.

Wessel, S., S. Aoki, P. Winkler, R. Weller, A. Herber, H. Gernandt, and O. Schrems, Tropospheric ozone depletion in polar regions - A comparison of observations in the Arctic and Antarctic, *Tellus* 50B, 34-50, 1998.

Wettlaufer, J.S., Impurity effects in the premelting of ice, *Phys.Rev.Lett.* 82, 2516-2519, 1999.

Wettlaufer, J.S., and M.G. Worster, Dynamics of premelted films: Frost heave in a capillary, *Phys.Rev.E* 51, 4679-4689, 1995.

Zhou, X., H.J. Beine, R.E. Honrath, J.D. Fuentes, W. Simpson, P.B. Shepson, and J.W. Bottenheim, Snowpack photochemical production of HONO: A major source of OH in the arctic boundary layer in springtime, *Geophys.Res.Lett.* 28, 4087-4090, 2001.

2.6 Acknowledgments

I thank my advisors, Professor Otto Schrems and Roger Bales, for giving me the opportunity to work in their research groups and for their support.

I wish to express my gratitude to the Master and diploma students Bright Kwakye-Awuah, Thompson Annor, Emmanuel Quansah, Birgit Hilker, and Sandra Lehmann, who performed many of the laboratory experiments reported in this thesis.

I thank my colleagues of the research groups I worked with in the present and the past:

> Peter Beichert, Thaddäus Bluszcz, Andreas Herber, Thomas Max, Andreas Minikin, Michael Kriews, Nico Klassen, Christoph Kleefeld, Meike Liebehentschel, Heiko Reinhardt, Ilsetraut Stölting, Sieglinde Unverricht, Rolf Weller, Laura Wischniewski, Mareile Wolff, and Sigrid Wuttke at the Alfred Wegener Institute in Bremerhaven
>
> Deirdree Bell-Audry, Constance Brown, Jonny Burkhart, Markus Frey, and Manuel Hutterli at the Department of Hydrology of the University of Arizona.

I also enjoyed collaborative field work at Ny-Alesund, at the Summit Station in Greenland, at the Neumayer Station in Antarctica, and on board of the research icebreaker Polarstern with:

> Mary Albert, Matthew Arsenault, Gerit Birnbaum, James Boulter, Nicolas Cullen, Jack Dibb, Dorothee Dick, Mike Dziobak, Jörg Hartmann, Detlev Helmig, Richard Honrath, Anna Jones, Cathi Koehler, Yanyan Lu, Christof Lüpkes, Robin Pascal, Matthew Peterson, Edward Shultz, Konrad Steffen, Aaron Swanson, and Margret Yelland.

I gratefully acknowledge financial support by the German Research Foundation (DFG), the German Academic Exchange Service (DAAD), and the German Chemical Society (GDCh).

3.1 Appendix of Publications

3.1 Measurements of the global distribution of trace compounds

Publication 3.1.1

Jacobi, H.-W., and O. Schrems,
Peroxyacetyl nitrate (PAN) distribution over the South Atlantic Ocean,
Phys.Chem.Chem.Phys. **1**, 5517-5521, 1999.

PCCP

Peroxyacetyl nitrate (PAN) distribution over the South Atlantic Ocean

Hans-Werner Jacobi* and Otto Schrems

Alfred-Wegener-Institute for Polar and Marine Research, Am Handelshafen 12, D-27570 Bremerhaven, Germany. E-mail: hwjacobi@awi-bremerhaven.de

Received 1st July 1999, Accepted 20th August 1999

The atmospheric concentration of peroxyacetyl nitrate (PAN) was measured over the South Atlantic Ocean in the range between 37° and 70 °S in March 1999 in order to investigate its latitudinal distribution and its role in the NO_y chemistry of the remote marine boundary layer (MBL) in the high latitudes of the southern hemisphere. The measurements were performed using an automatic gas chromatographic system aboard RV *Polarstern*. Mean mixing ratios of 62($\pm$21) pptv were obtained between 37° and 49 °S. South of 55 °S, PAN concentrations were very low with values of the order of 10–30 pptv. Pronounced diurnal cycles could not be observed. The concentrations over the South Atlantic were considerably lower compared with the North Atlantic where the MBL is influenced by continental air masses.

1 Introduction

Peroxyacetyl nitrate (PAN) is a by-product formed in the course of the atmospheric oxidation of selected non-methane hydrocarbons in the presence of nitrogen dioxide.[1] It constitutes a major contribution to the odd nitrogen budget in the troposphere and acts as a temporary reservoir of nitrogen oxides ($NO_x = NO + NO_2$).[2,3] On the other hand, nitrogen oxides are very important for tropospheric processes such as production and destruction of ozone and regulation of the concentration of hydroxy radicals and can therefore also indirectly affect the climate of the Earth.[4–8]

The only known pathway for the formation of PAN is the reaction of acetylperoxy radicals with NO_2 (R1). Precursors of the acetylperoxy radicals are specific hydrocarbons (*e.g.* acetone, acetaldehyde, methylglyoxal). These organic compounds have diffuse background and large anthropogenic sources confined to relatively small urban areas.[1] The main sink of PAN is thermal decomposition (R2) followed by the destruction of the acetylperoxy radical through reaction with NO (R3) or other peroxy radicals (R4).

$$CH_3C(O)OO + NO_2 \rightarrow CH_3C(O)OONO_2 \quad (R1)$$

$$CH_3C(O)OONO_2 \rightarrow CH_3C(O)OO + NO_2 \quad (R2)$$

$$CH_3C(O)OO + NO \rightarrow CH_3C(O)O + NO_2 \quad (R3)$$

$$CH_3C(O)OO + RO_2 \rightarrow \text{products} \quad (R4)$$

Thus, PAN mixing ratios are determined by temperature, ambient concentrations of the acetylperoxy radical and the relative rates of the competing reactions of the acetylperoxy radical with NO, NO_2 and RO_2. In the marine boundary layer (MBL) other sinks such as reaction with OH, photolysis or deposition are negligible.[1] Lower limits of tropospheric PAN lifetimes of 30 min at 298 K and 10 d at 263 K can be calculated from the decay rate of reaction (R2).[9] However, lifetimes can further increase due to low NO/NO_2 ratios and low concentrations of RO_2.

While several chemical transport models exist to describe the global distribution of PAN,[10–12] the coverage of observational data is sparse both in space and time.[12,13] However, to validate model simulations of the distribution of reactive nitrogen, reliable PAN measurements are badly needed. Here, we report the first shipborne measurements of PAN mixing ratios over the South Atlantic Ocean. The values are compared with results over the North Atlantic Ocean and a latitudinal distribution in the (MBL) is presented. The importance of NO_x release due to thermal decomposition of PAN in the MBL is investigated.

2. Methods and instrumentation

The field campaign was conducted aboard the German research vessel RV *Polarstern* (ANT XVI/2) in March, 1999. The cruise started at the German Antarctic research station Neumayer (70.6 °S, 8.3 °W) and its final destination was Cape Town, South Africa (33.9 °S, 18.4 °E). The itinerary of the cruise is shown in Fig. 1. Standard meteorological parameters were routinely monitored aboard at the meteorological station and stored in the database POLDAT.

The PAN gas chromatograph was installed in an air-

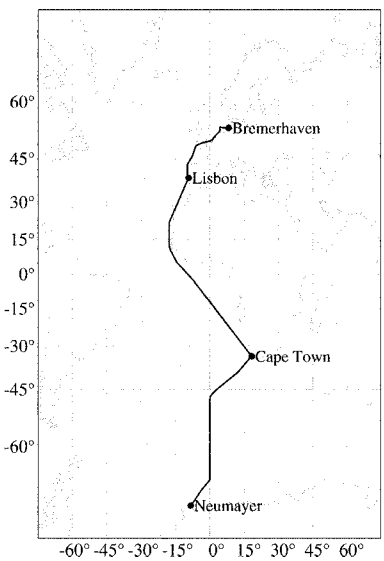

Fig. 1 Map of the cruise tracks ANT XV/5 (Cape Town–Bremerhaven; 25 May–21 June, 1998) and ANT XVI/2 (Neumayer–Cape Town; 1–16 March, 1999) of the RV *Polarstern*.

conditioned laboratory container placed on the compass deck of the ship. The inlet line (10 m of 0.4 cm id PFA tubing) was mounted on the compass deck rail approximately 22 m above sea level. The outboard end of the line was equipped with a spray deflector to avoid sea spray contamination which was controlled each day by visual inspection. Inside the laboratory container, the line was connected with a manifold and flushed with a flow rate of about 10 l min^{-1}, leading to a residence time of the air samples in the inlet lines of less than 1 s. From this manifold a pump sucked sample air into the O_3 and PAN analysers. Surface level O_3 mixing ratios were measured continuously by means of an UV spectrometer ($O_3$41MC, Environnement, Poissy, France).

PAN was measured with a commercial analyser (Meteorologie Consult, Glashütten, Germany) based on the electron capture gas chromatographic technique which has been described earlier.[14] In short, PAN was enriched for 7 min on a Peltier-cooled cryogenic sampling trap. For desorption, the temperature of the preconcentration loop was quickly heated and the gas mixture was transferred onto the pre-column using nitrogen as carrier gas. The separation was performed isothermally at 17 °C on the analytical columns. While the selected fraction of the pre-column eluate was passed onto the main column, the pre-column was back-flushed. The eluates were detected by electron capture detection (ECD) at 60 °C. PAN measurements were performed in 10 min analytical cycles. Calibration was based on the photochemical synthesis of PAN from NO-pre-mixtures in the presence of a large excess of acetone and synthetic air in a flow reactor which consisted of a glass chamber chamber (approx. 100 ml) equipped with a penray lamp (Meteorologie Consult). Calibrations were performed on board at the beginning and at the end of the cruise and showed good agreement. A detection limit of 5 pptv is defined as three times the standard deviation calculated from the noise of the output signal of the analyser when only purified air produced by a clean air generator (PAG 003, Eco Physics, Munich, Germany) was investigated. The overall error in the PAN measurements was estimated to be less than $\pm 15\%$.

Shipborne measurements can be disturbed by contamination due to the exhaust gases of the ship's engines. These gases are powerful local sources of numerous reactive compounds.[15,16] PAN concentrations measured during relative wind directions outside a $\pm 90°$ corridor with respect to the ship's heading could be affected by contamination originating from the exhaust plume. However, such cases were identified using the meteorological observations and these data were then discarded from the original data sets. The corrected data sets were used for further analysis.

3. Results

PAN and O_3 were measured within the latitudinal range 37°–71 °S. Within this region the cruise track followed mainly the prime meridian (see Fig. 1). The measured time series of PAN and O_3 are shown together with the air temperature in Fig. 2. From the PAN time series it can be clearly seen that during the cruise no pronounced diurnal variations could be observed. Instead, the values can be divided into three different groups having to some extent rather homogeneous concentrations (see Table 1). Until noon on 8 March, PAN values always remained below 40 pptv, resulting in an average concentration of approximately 18 pptv. On the following days the mixing ratios indicated a clearly rising tendency. Starting at noon on 10 March, PAN concentrations stabilised at a distinct, higher level. Maximum mixing ratios around 140 pptv occurred and the mean value increased to 62 pptv. Obviously, the rise of the PAN concentrations occurred mutually with the increase of the measured air temperature (see Fig. 2). After a first strong increase in the morning of 8 March the temperature was always above 0 °C. The jump of the air temperature indicated the position of an extensive system of cold and warm fronts during the cruise. Therefore, three different regions may be classified as south and north of the front system with PAN values around 18 and 60 pptv, respectively, and between a region, where the PAN mixing ratios constantly increased northward. The different regions may be characterised by different modes in the frequency distribution of the PAN concentration. Since atmospheric dilution of trace gases as well as their chemical degradation follow an exponential evolution with time, frequency distributions of observed mixing ratios often exhibit a log-normal distribution (see *e.g.* ref. 17). Fig. 3 shows the absolute frequency as a function of the natural logarithm of the PAN concentration. Two distinct modes can be identified which correspond to the areas north and south of the polar front. These modes are centred near their mean values of 18 and 62 pptv, whereas the frequency distribution of the transient region is not well defined.

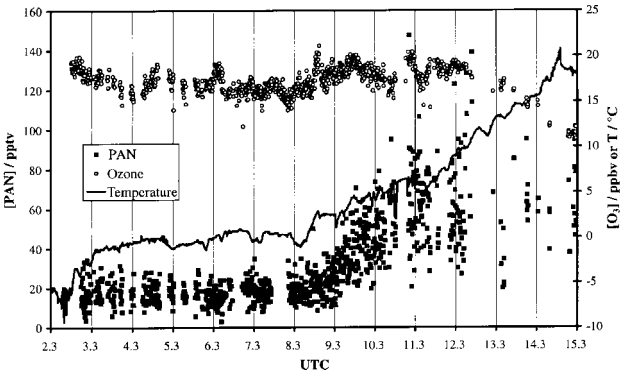

Fig. 2 Time series of PAN and O_3 concentrations measured during ANT XVI/2 on board the RV *Polarstern* in March, 1999. Also included are air temperature measurements.

Table 1 Overview of the measured PAN mixing ratios. Given are the number of PAN measurements per day, daily means, standard deviations (1σ) and the daily position of RV *Polarstern* at 12:00 UTC

Date	Number	Daily mean (pptv)	Standard deviation (pptv)	Ship's position at 12:00 UTC
2/3	36	17.6	7.3	70.1 °S; 7.1 °W
3/3	62	18.2	5.6	66.5 °S; 0 °E
4/3	72	17.6	5.1	63.9 °S; 0 °E
5/3	63	16.6	4.7	61.1 °S; 0 °E
6/3	85	17.5	5.3	59.1 °S; 0.1 °E
7/3	84	17.9	4.9	57.0 °S; 0.1 °E
8/3	137	20.9	7.0	54.4 °S; 0 °E
9/3	139	37.7	11.7	51.1 °S; 0 °E
10/3	78	54.8	19.4	48.1 °S; 0 °E
11/3	78	63.2	17.2	46.5 °S; 0.8 °E
12/3	36	64.4	27.7	43.7 °S; 5.3 °E
13/3	15	52.7	23.0	40.7 °S; 10.1 °E
14/3	14	58.6	13.1	38.2 °S; 14.1 °E

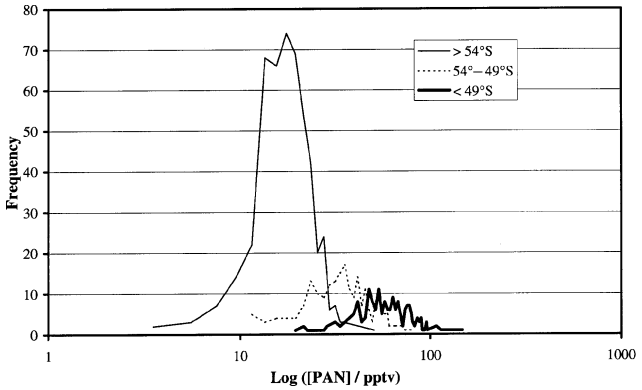

Fig. 3 Frequency distribution of the natural logarithm of the PAN concentrations in pptv measured throughout ANT XVI/2. The given absolute frequency is the number of observations for intervals of log ([PAN]/pptv) with a width of 2.

Comparable sections were not observed for the O_3 mixing ratios. An increase of the O_3 values was ascertainable on 8 and 9 March. However, the concentrations measured in the periods before and after did not differ significantly.

4. Discussion

The results obtained over the South Atlantic can be compared with data measured over the tropical and North Atlantic during another recent campaign performed also on board the RV *Polarstern* (ANT XV/5).[14] Fig. 4 shows calculated mean PAN concentrations from both campaigns averaged in 1°-latitude segments. Obviously, measured mixing ratios were considerably higher in the northern hemisphere. The highest values, about 1500 pptv, were found in the English Channel,

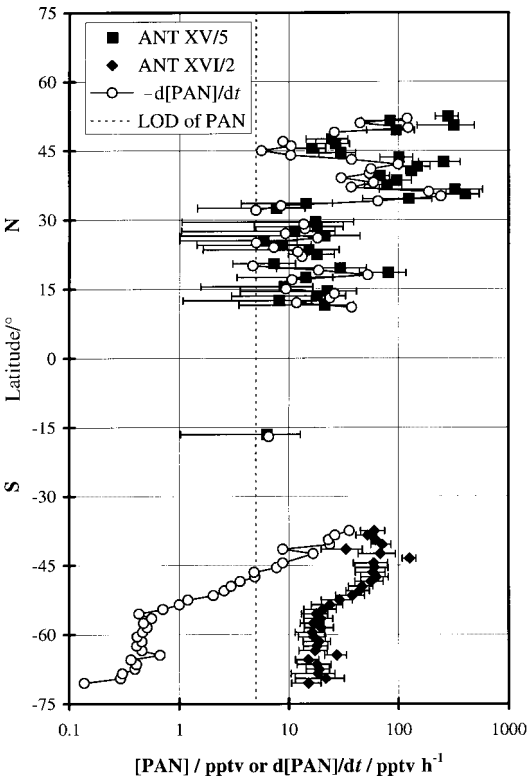

Fig. 4 Latitudinal distribution of PAN concentrations measured on board RV *Polarstern* during cruises ANT XV/5 (25 May–21 June, 1998) (ref. 14) and ANT XVI/2 (1–16 March, 1999). All 10-min means collected during the cruises regardless of time of day are included. The data points indicate the mean and its standard deviation for all averages in a 1°-latitude segment. For the same segments, averaged PAN decay rates solely due to thermal loss are also shown. The dotted line indicates the limit of detection (LOD) of 5 pptv of the PAN analyser.

while maxima in the southern hemisphere were an order of magnitude lower. In tropical latitudes between 11 °N and 16 °S, the values were generally below the limit of detection of the PAN analyser of 5 pptv. Low values in this latitudinal range are mainly due to the fast thermal decomposition of PAN at high air temperatures.[18]

Higher concentrations in the northern hemisphere can be attributed to various reasons. First, the campaigns were performed during different seasons. While the campaign on the North Atlantic took place at the end of spring 1998 (25 May–21 June), the results of this work were obtained at the end of the austral summer 1999 (1–16 March). In the northern as well as in the southern hemisphere PAN generally increases in remote areas during winter. Maximum values were achieved in early spring with a subsequent decrease until autumn.[1,11] The increase during winter is mainly due to the higher thermal stability of PAN at lower temperatures, whereas the faster thermal decay during summer can be compensated for in part by higher photochemical activity accompanied by higher formation rates of PAN. Therefore, it must be taken into account that the values measured over the South Atlantic at the end of the summer were probably lower compared with the annual mean, while the mixing ratios measured over the North Atlantic may be regarded as annual mean values.

However, more important for the measured differences in the northern and southern hemisphere is the influence of continental air masses. Jacobi *et al.*[14] have shown that the increase of PAN along the coasts of North Africa and Europe can mainly be attributed to horizontal advection of polluted air into the MBL of the North Atlantic. Moreover, several distinct diurnal variations suggest that even in the MBL *in situ* PAN formation can occur.[14] These diurnal variations also explain the much larger standard deviations of the averaged PAN mixing ratios in the latitudinal range of 15° to 50 °N shown in Fig. 4. In contrast to our results, Müller and Rudolph[19] obtained considerably lower PAN concentrations in the remote MBL of the North Atlantic. Along 30 °W, they found PAN mixing ratios around 10 pptv in the latitudinal range of 35° and 41 °N. Consequently, these values are sometimes lower than PAN concentrations over the South Atlantic reported in this work.

A direct influence due to horizontal transport of continental air masses to higher latitudes over the South Atlantic was not identifiable. Moreover, we did not observe diurnal variations in this area. Instead, rather homogeneous PAN concentrations were found, while at higher latitudes the standard deviation of the averaged PAN concentrations further decreases. The homogeneous distribution can probably be attributed to the long atmospheric lifetime of PAN. While the overall chemical lifetime of PAN in the MBL is confined by thermal decay (R2) and the destruction of the acetylperoxy radicals by reactions (R3) and (R4),[1,18] the lower limit is solely given by the thermal decay (R2). Therefore, a minimum lifetime of several days in the region south of 55 °S can be estimated as a consequence of the low air temperatures. A lifetime of this order of magnitude seems to be sufficient to establish homogeneous concentrations due to effective mixing and transport in the MBL.

Such homogeneous PAN distributions are also indicated by results of three-dimensional modelling studies with coupled global transport and chemistry models.[10,11,20] With these models, PAN concentrations in the planetary boundary layer (PBL) south of 60 °S of less than 50 pptv,[11] between 10 and 30 pptv[10] and less than 20 pptv,[20] respectively, have been calculated. The simulated results are partly in good agreement with measured data obtained in this study. However, the increase of PAN mixing ratios north of 55 °S is not reflected by global models. The area with calculated PAN values up to 50 pptv includes the whole South Atlantic and can also extend to

30 °N over the North Atlantic.[10,11,20] The models also show that the MBL close to the continents is influenced by horizontal transport of PAN-rich air masses. This is in good agreement with our results in the northern hemisphere, where we have measured enhanced PAN concentrations while the cruise track crossed regions influenced by polluted continental air masses.[14]

PAN mixing ratios of approximately 60 pptv in the MBL over the South Atlantic in the latitudinal range 40°–50 °S have not been reproduced by recent modelling studies.[10,11,20] A global comparison shows that observed PAN concentrations in the lower layers of the troposphere are frequently underestimated by global models, while calculated values in the upper troposphere are generally too high.[12]

Hauglustaine *et al.*[20] also report higher PAN mixing ratios in the free troposphere of the southern hemisphere. They calculate PAN concentrations for January at 500 mbar in the range of 20–60 pptv over the South Atlantic between 30° and 50 °S. The results of Moxim *et al.*[11] show that the region with PAN up to 50 pptv at 500 mbar extends to 47 °S in April. It may be suggested that strong vertical mixing can lead to enhanced PAN values in the MBL of this region. The synoptical observations made during the cruise showed a cold front around 50 °S accompanied by sleet showers, indicating strong advection which makes effective vertical transport possible. In higher southern latitudes, PAN mixing ratios in the free and upper troposphere are probably too low (<20 pptv), so that advection may not lead to enhanced PAN mixing ratios in the lower troposphere.[11,20]

The possible role of PAN acting as a reservoir species for NO_x has been discussed for many years (see *e.g.* ref. 21). Several field campaigns and modelling studies have shown that the thermal decay of PAN in the remote MBL is sufficient to establish observed NO_x concentrations.[8,22] To investigate the impact of PAN decomposition on ambient NO_x mixing ratios in the MBL over the Atlantic, the decay rates were calculated using observed PAN mixing ratios and air temperatures. The rates averaged in a 1°-latitude segment are shown in Fig. 4. The calculated PAN loss rates in the northern hemisphere can be divided into two different regimes. North of 35 °N, decay rates are between 10 and 100 pptv h^{-1}, while in temperate latitudes between 35° and 15 °N they are around 10 pptv h^{-1}. Mainly due to the very low PAN concentrations in tropical latitudes between 15 °N and 20 °S, decomposition rates are less than 10 pptv h^{-1} and partly even less than 1 pptv h^{-1}. In the southern hemisphere, the rates increase at first until they reach their maximum value of 10 pptv h^{-1} at 40 °S. However, the loss strongly decreases towards higher latitudes. South of 55 °S, the maximum PAN decay is much less than 1 pptv h^{-1} which is mainly due to the high thermal stability at the low ambient air temperatures in that region (see Fig. 2).

The thermal decay of PAN corresponds to the maximum NO_x production because the decomposition of one PAN molecule leads to the release of one NO_2 molecule (R2). However, the overall NO_x formation also depends on other variables such as concentration ratios of NO_2, NO and RO_2. The maximum NO_x formation only occurs if the likewise produced acetylperoxy radical reacts with NO (R3) or RO_2 (R4) and hence will not be available for the back reaction (R1). If NO_2 is high compared with NO and/or RO_2, the back reaction (R1) is strongly favoured, leading to considerably longer PAN lifetimes and corresponding lower NO_x production rates. The ratio of the rate constants of the competing reactions with NO_2 (R1) and NO (R3) accounts for $k_1/k_3 \approx 0.6$ in a temperature range of −20 to +25 °C. If organic peroxy radicals are not taken into account, a concentration ratio of $[NO]/[NO_2] \approx 0.6$ is already sufficient to ensure that half of the produced acetylperoxy radicals react back with NO_2 to form PAN again. Unfortunately, no NO_x measurements were performed during cruise ANT XVI/2. Concentration ratios of $[NO]/[NO_2]$ in the range 0.2–0.7 were derived from recent field campaigns performed in the MBL over the Pacific and Atlantic Ocean in temperate and tropical latitudes, respectively.[23–26] These averaged ratios were obtained during the daytime with solar angles higher than 70°. At noon the ratios are higher due to increased solar radiation, while during night-time NO concentrations are negligible, so that then the reaction (R1) dominates.

In consideration of these approximations it can be suggested that the calculated PAN decomposition rates only reflect the magnitude of the NO_x production during daytime. Modelling studies concerning NO_x and NO_y balances in the MBL of the tropical South Pacific[8] or South Atlantic,[22] respectively, show that NO_x production rates of less than 1 pptv h^{-1} are sufficient to replenish the MBL by 10 pptv of NO_x. Therefore, it can be concluded that even at low temperatures prevailing at high southern latitudes the PAN decay can contribute significantly to NO_x formation in this area, establishing NO_x mixing ratios of the magnitude of a few pptv.

5. Conclusions

The first measurements of PAN in the MBL of the South Atlantic in higher latitudes showed a rather homogeneous distribution. Two regions with different concentration regimes could be identified. South of 55 °S, mean PAN mixing ratios were around 18 pptv, while north of 50 °S, averaged values of 62 pptv were measured. These observations are partly in contrast to results of recent three-dimensional modelling studies which indicate PAN mixing ratios of less than 50 pptv in the MBL both in higher and temperate latitudes over the South Atlantic.[10,11,20]

The homogeneous distribution is probably due to the long lifetimes of PAN at the prevailing low temperatures. The strong differences in the mixing ratios north and south of 50 °S can be influenced by strong vertical mixing with air masses originating from the upper troposphere. A comparison of the concentrations with observations in the northern hemisphere shows that the values over the South Atlantic in the range 37°–50 °S can be higher than mixing ratios obtained in the remote MBL over the North Atlantic.[19] On the other hand, the MBL over the North Atlantic can also be influenced by advection of continental air masses, leading to PAN concentrations more than one order of magnitude higher than over the South Atlantic (see *e.g.* ref. 14).

The role of PAN in NO_x formation in the remote MBL of the South Atlantic due to thermal decomposition was investigated. It was found that even at the prevailing low temperatures and hence slow decomposition, PAN can contribute significantly to the production of NO_x in higher southern latitudes.

Acknowledgements

We thank the crew of the RV *Polarstern* for their co-operation and technical assistance and H. Weiland (German Weather Service DWD) for helpful discussions. This paper is contribution No. 1646 of the Alfred-Wegener-Institute for Polar and Marine Research.

References

1 J. M. Roberts, *Atmos. Environ.*, 1990, **24A**, 243.
2 H. B. Singh, D. Herlth, R. Kolyer, L. Salas, J. D. Bradshaw, S. T. Sandholm, D. D. Davis, J. Crawford, Y. Kondo, M. Koike, R. Talbot, G. L. Gregory, G. W. Sachse, E. Browell, D. R. Blake, F. S. Rowland, R. Newell, J. Merrill, B. Heikes, S. C. Liu, P. J. Crutzen and M. Kanakidou, *J. Geophys. Res.*, 1996, **101**, 1793.
3 S. Solberg, T. Krognes, F. Stordal, O. Hov, H. J. Beine, D. A.

Jaffe, K. C. Clemintshaw and S. A. Penkett, *J. Atmos. Chem.*, 1997, **28**, 209.
4 A. J. Haagen-Smit, *Ind. Eng. Chem.*, 1952, **44**, 1342.
5 P. J. Crutzen, *Annu. Rev. Earth Planet. Sci.*, 1979, **7**, 443.
6 J. A. Logan, *J. Geophys. Res.*, 1994, **99**, 25553.
7 J. S. Fuglestvedt, T. K. Berntsen, I. S. A. Isaksen, H. Mao, X.-Z. Liang and W.-C. Wang, *Atmos. Environ.*, 1999, **33**, 961.
8 M. G. Schultz, D. J. Jacob, Y. Wang, J. A. Logan, E. T. Atlas, D. R. Blake, N. J. Blake, J. D. Bradshaw, E. V. Browell, M. A. Fenn, F. Flocke, G. L. Gregory, B. G. Heikes, G. W. Sachse, S. T. Sandholm, R. E. Shetter, H. B. Singh and R. W. Talbot, *J. Geophys. Res.*, 1999, **104**, 5829.
9 I. Bridier, F. Caralp, H. Loirat, R. Lesclaux, B. Veyret, K. H. Becker, A. Reimer and F. Zabel, *J. Phys. Chem.*, 1991, **95**, 3594.
10 D. A. Jaffe, T. K. Berntsen and I. S. A. Isaksen, *J. Geophys. Res.*, 1997, **102**, 21281.
11 W. J. Moxim, H. Levy II and P. S. Kasibhatla, *J. Geophys. Res.*, 1996, **101**, 12621.
12 A. N. Thakur, H. B. Singh, P. Mariani, Y. Chen, Y. Wang, D. J. Jacob, G. Brasseur, J.-F. Müller and M. Lawrence, *Atmos. Environ.*, 1999, **33**, 1403.
13 L. K. Emmons, M. A. Carroll, D. A. Hauglustaine, G. P. Brasseur, C. Atherton, J. Penner, S. Sillman, H. Levy II, F. Rohrer, W. M. F. Wauben, P. F. J. Van Velthoven, Y. Wang, D. Jacob, P. Bakwin, R. Dickerson, B. Doddridge, C. Gerbig, R. Honrath, G. Hübler, D. Jaffe, Y. Kondo, J. W. Munger, A. Torres and A. Volz-Thomas, *Atmos. Environ.*, 1997, **31**, 1851.
14 H.-W. Jacobi, R. Weller, T. Bluszcz and O. Schrems, *J. Geophys. Res.*, in the press.
15 R. Weller, R. Lilischkis, O. Schrems, R. Neuber and S. Wessel, *J. Geophys. Res.*, 1996, **101**, 1387.
16 R. Weller and O. Schrems, *J. Geophys. Res.*, 1996, **101**, 9139.
17 J. W. Bottenheim, A. Sirois, K. A. Brice and A. J. Gallant, *J. Geophys. Res.*, 1994, **99**, 5333.
18 T. E. Kleindienst, *Res. Chem. Intermed.*, 1994, **20**, 335.
19 K. P. Müller and J. Rudolph, *J. Atmos. Chem.*, 1992, **15**, 361.
20 D. A. Hauglustaine, G. P. Brasseur, S. Walters, P. J. Rasch, J.-F. Müller, L. K. Emmons and M. A. Carroll, *J. Geophys. Res.*, 1998, **103**, 28291.
21 H. B. Singh and P. L. Hanst, *Geophys. Res. Lett.*, 1981, **8**, 941.
22 B. Heikes, M. Lee, D. Jacob, R. Talbot, J. Bradshaw, H. Singh, D. Blake, B. Anderson, H. Fuelberg and A. M. Thompson, *J. Geophys. Res.*, 1996, **101**, 24221.
23 M. A. Carroll, D. R. Hastie, B. A. Ridley, M. O. Rodgers, A. L. Torres, D. D. Davis, J. D. Bradshaw, S. T. Sandholm, H. I. Schiff, D. R. Karecki, G. W. Harris, G. I. Mackay, G. L. Gregory, E. P. Condon, M. Trainer, G. Hübler, D. D. Montzka, S. Madronich, D. L. Albritton, H. B. Singh, S. M. Beck, M. C. Shipham and A. S. Bachmeier, *J. Geophys. Res.*, 1990, **95**, 10205.
24 R. Weller, O. Schrems, A. Boddenberg and S. Gäb, in *Proceedings of EUROTRAC Symposium '98, Vol. 1*, ed. P. M. Borrell and P. Borrell, WIT Press, Southampton, 1999, p. 370.
25 D. D. Davis, G. Chen, W. Chameides, J. Bradshaw, S. Sandholm, M. Rodgers, J. Schendal, S. Madronich, G. Sachse, G. Gregory, B. Anderson, J. Barrick, M. Shipham, J. Collins, L. Wade and D. Blake, *J. Geophys. Res.*, 1993, **98**, 23501.
26 Y. Kondo, H. Ziereis, M. Koike, S. Kawakami, G. L. Gregory, G. W. Sachse, H. B. Singh, D. D. Davis and J. T. Merrill, *J. Geophys. Res.*, 1996, **101**, 1809.

Paper 9/05290I

Publication 3.1.2

Jacobi, H.-W., R. Weller, T. Bluszcz, and O. Schrems,

Latitudinal distribution of peroxyacetyl nitrate (PAN) over the Atlantic Ocean,

J.Geophys.Res. **104**, 26901-26912, 1999.

JOURNAL OF GEOPHYSICAL RESEARCH, VOL. 104, NO. D21, PAGES 26,901–26,912, NOVEMBER 20, 1999

Latitudinal distribution of peroxyacetyl nitrate (PAN) over the Atlantic Ocean

H.-W. Jacobi, R. Weller, T. Bluszcz, and O. Schrems

Alfred-Wegener-Institute for Polar and Marine Research, Bremerhaven, Germany

Abstract. Atmospheric concentrations of peroxyacetyl nitrate (PAN) were measured during a cruise of RV *Polarstern* from Cape Town (South Africa) to Bremerhaven (Germany) in May/June 1998 and at Ny-Ålesund, Svalbard, in March 1998. The continuous in-situ measurements were using electron capture gas chromatography combined with a cryogenic preconcentration technique. The time resolution of the measurements was 10 min with a detection limit of 5 parts per trillion by volume (pptv). The mixing ratios of PAN exhibited a maximum of 1100 pptv in the English Channel and values less than 5 pptv in tropical latitudes between 10°N and 10°S. The latitudinal distribution of PAN showed significantly higher concentrations in the northern hemisphere compared to the southern hemisphere. North of 10°N, daily maximum PAN concentrations normally exceeded 100 pptv. Mean mixing ratios decreased from 244 pptv between 50°N and 54°N to 13 pptv between 20°N and 30°N. Enhanced concentrations were detected in continentally influenced air masses identified by trajectory analysis and simultaneous measurements of black carbon and ozone. Intrusions of air masses from the upper troposphere could not be inferred from trajectory analysis. In temperate northern latitudes, enhanced PAN mixing ratios can be used as an indicator of long-range transport of photochemically active pollutants.

1. Introduction

Peroxyacetyl nitrate (PAN) has long been recognized as a minor product of the photochemical oxidation of nonmethane hydrocarbons in the presence of nitrogen oxides [*Stephens*, 1969]. PAN is formed in the reaction of acetylperoxy radicals with NO_2:

(R1) $CH_3C(O)OO + NO_2 \rightarrow CH_3C(O)OONO_2$

Although the rate coefficient for this reaction ($k_1 = 9.6 \times 10^{-12}$ cm^{-3} s^{-1} at 298 K [*Bridier et al.*, 1991]) is large, PAN concentrations are limited owing to the thermal decomposition of PAN:

(R2) $CH_3C(O)OONO_2 \rightarrow CH_3C(O)OO + NO_2$

Thus atmospheric PAN concentrations are strongly dependent on temperature because the rate coefficient for the decomposition reaction (R2) decreases at lower temperatures ($k_2 = 4.6 \times 10^{-4}$ s^{-1} at 298 K; 1.1×10^{-6} s^{-1} at 263 K [*Bridier et al.*, 1991]). In addition, PAN formation is limited by the competing reaction of $CH_3C(O)OO$ with NO:

(R3) $CH_3C(O)OO + NO \rightarrow CH_3C(O)O + NO_2$

Reaction (R3) proceeds with a rate constant of $k_3 = 1.8 \times 10^{-11}$ cm^{-3} s^{-1} at 298 K [*DeMore et al.*, 1997] and leads to the final decomposition of the organic peroxy radical.

Therefore the net loss rate of PAN mainly depends on the temperature and the NO/NO_2 ratio. Lower limits of PAN lifetimes are 30 min at 298 K and 10 days at 263 K which can be calculated from the decay rate of reaction (R2). However, reaction sequence (R1) and (R2) also allows an increase of the effective lifetime of PAN at higher temperatures if reactions of the acetylperoxy radicals with NO (R3) or peroxy radicals RO_2 are suppressed due to high concentrations of NO_2 and/or low concentrations of NO and RO_2. A detailed review of the atmospheric chemistry of organic nitrates given by *Roberts* [1990] showed that other chemical loss processes like photolysis or reaction with OH radicals become important under conditions with PAN lifetimes larger than 100 days. However, such conditions only exist in the upper troposphere.

Precursors of the acetylperoxy radicals are specific hydrocarbons and aldehydes (e.g., propene, butene, pentene, acetaldehyde). These organic compounds have diffuse background sources as well as large anthropogenic sources confined to relatively small urban areas [*Roberts*, 1990]. Several experimental and theoretical studies have demonstrated that PAN is transported from polluted continental sites into the upper troposphere and relatively clean marine environments [e.g., *Singh et al.*, 1996; *Jaffe et al.*, 1997] where it can constitute a major component of reactive nitrogen compounds (NO_y). Thus PAN can be used as a specific indicator of anthropogenic photochemical air pollution in remote air masses. Furthermore, PAN can act as a reservoir for odd nitrogen during the transport into remote areas, especially when the transport is directed from colder parts of the troposphere (e.g., upper troposphere and polar regions) to warmer regions. Increasing PAN decomposition at higher temperatures can release NO_2 in remote areas. This can effect the NO_x balance of these regions in the troposphere which are not directly influenced by long-range transport of NO_x from continental sources due to the short chemical lifetime of NO_x of 1-2 days under typical tropospheric conditions [*Liu et al.*, 1987]. In this case, PAN would act as a temporary reservoir for NO_x

Paper number 1999JD900462.
0148-0227/99/1999JD900462$09.00

[*Singh et al.*, 1992] influencing not only NO_x concentrations in remote areas but also the chemical production of ozone, which is usually limited by NO_x in the remote troposphere [e.g., *Carroll and Thompson*, 1995].

This paper reports measurements of PAN performed during two field campaigns in the marine boundary layer (MBL) and at an Arctic site. The latitudinal distribution of PAN is analyzed on the basis of ground-level trajectories. Simultaneous measurements of ozone and black carbon (BC) are also employed in a discussion of PAN mixing ratios in the MBL. The measurements are compared with results of modeling studies of the global distribution of PAN.

2. Methods and Instrumentation

One of the field campaigns was performed aboard the RV *Polarstern* (ANT XV/5). The cruise track started at Cape Town, South Africa (34°S), on May 26, 1998, and ended in Bremerhaven, Germany (54°N), on June 21, 1998. The cruise included an intermediate stay of 2 days in Lisbon, Portugal (June 13-15). The itinerary of the cruise and ground-level 3-day back trajectories are shown in Figure 1.

The gas chromatograph for the detection of PAN and the BC monitor were installed in an air-conditioned laboratory container placed on the compass deck of the ship. The inlet lines were mounted on the compass deck rail approximately 22 m above sea level. The inlet line of the PAN analyzer was 3.7 m of 0.8 cm ID perfluoroalkoxy (PFA) tubing. The outboard end of the line was equipped with a spray deflector to avoid sea spray contamination which was controlled daily by visual inspection. Inside the laboratory container, the line was connected with a manifold and flushed with a flow rate of about 20 L min^{-1} leading to a residence time of the air samples in the inlet line and the manifold of less than 1 s. From the manifold a pump sucked sample air into the analyzer.

Measurements of PAN were also made during spring 1998 at the Koldewey-Station of the Alfred-Wegener-Institute in Ny-Ålesund, Svalbard, at 79°N and 12°E (Figure 2). Ny-Ålesund is a small settlement situated on the southern shore of the Kongsfjord on the west coast of Spitsbergen. The campaign was conducted from March 11-29, 1998. The PAN analyzer was installed inside the chemistry laboratory building located on the east border of the village. The inlet line, mounted approximately 4 m above ground, was the same type as used in the shipborne measurements.

Continuous measurements of meteorological quantities (temperature, pressure, wind speed, wind direction, relative humidity) were routinely performed on board the RV *Polarstern* as well as on Koldewey Station. Shipborne measurements are generally disturbed by possible contamination due to the exhaust of the ship's engines because they are powerful local BC and NO_x sources. O_3, PAN, and BC concentrations measured during relative wind directions outside a ±80° corridor with respect to the ship's heading could be affected by contamination originating from the exhaust plume. In such cases the data were discarded from the original data sets. Only corrected data sets were used for further analysis. Trajectory calculations were used to investigate the effects of large-scale atmospheric flow patterns on the measured concentrations during both field experiments. Trajectories were provided by the German Weather Service (DWD) and were calculated using a global spectral numerical weather prediction model derived from the global model of the European Centre for Medium-Range Weather Forecasts

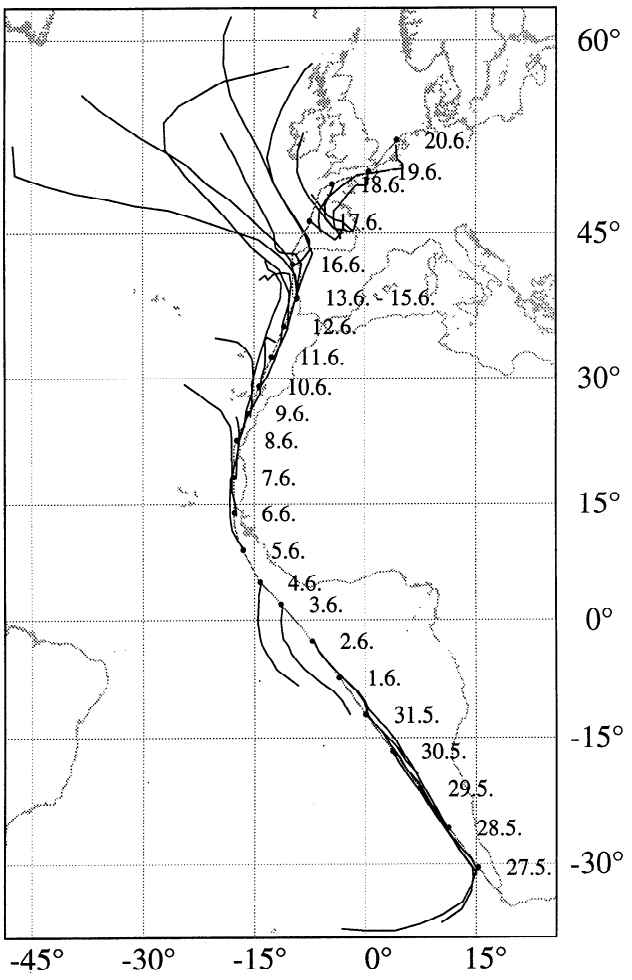

Figure 1. Map of the cruise track of the RV *Polarstern* (ANT XV/5). Also shown are ground-level 3-day back trajectories (arrival time 1200 UTC) provided by the German Weather Service (DWD). Dots indicate the ship's position each day at 1200 UTC.

[*Kottmeier and Fay*, 1998]. Three-day ground-level back trajectories ending at Ny-Ålesund or at the ship's position at 1200 UTC each day were used to classify the synoptic flow patterns.

2.1. Ozone Analyzer

Measurements of ozone concentrations were routinely performed on board the RV *Polarstern*. Data were obtained by using an electrochemical concentration cell (ECC) based on the iodide-ozone reaction [*Winkler*, 1988]. The analyzer consisted of a small pump that bubbled ambient air into a cell containing a 2% potassium iodide solution. A flowmeter was installed to control the air volumes which were sampled with a PTFE tube without a filter as the air intake. The current generated by the reaction in the cell is proportional to the ozone concentration in the sample air. Data were continuously recorded and stored together with the meteorological quantities in the database POLDAT. Ten minute averages were extracted and used for further evaluations. On previous cruises, intercomparisons were made with UV photometric analyzers which gave good agreement within a range of ±1 ppbv [*Weller and Schrems*, 1996; *Weller et al.*, 1996]. Disturbances due to NO_x and SO_2 seem to be negligible over the ocean [*Winkler*, 1988].

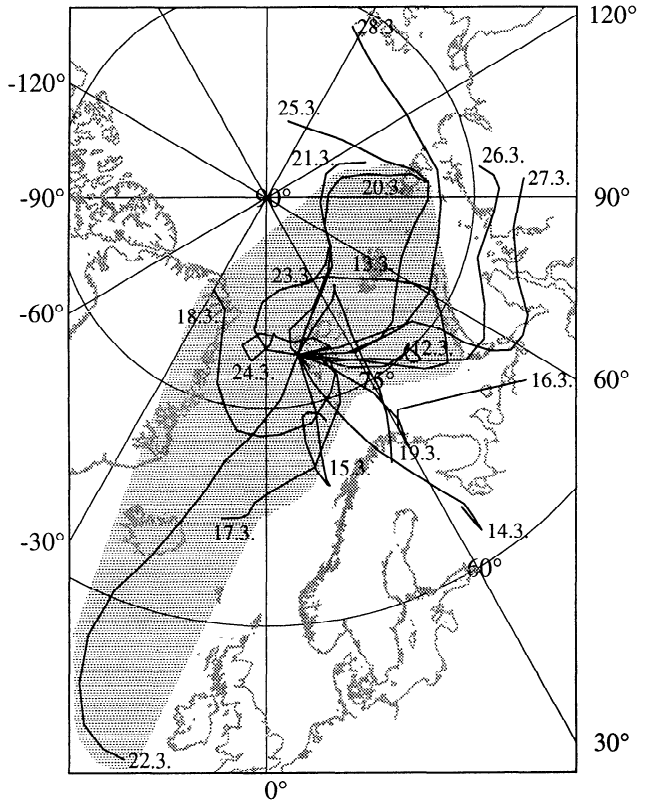

Figure 2. Map of Svalbard with calculated ground-level 3-day back trajectories (arrival time 1200 UTC) provided by the German Weather Service (DWD). A "background" production rate of 1-2 pptv PAN h^{-1} is assumed for the shaded area (see text).

2.2. PAN Analyzer

A commercial PAN analyzer was used which was based on chromatographic separation with subsequent electron capture detection (Meteorologie Consult GmbH, Glashütten, Germany). A schematic drawing of the instrument is shown in Figure 3. Ambient air was continuously drawn from the inlet line with a flow rate of about 10 mL min^{-1}. PAN was enriched at 3°C on a cryogenic sampling trap which consisted of a Peltier-cooled column filled with solid absorption material. For the enrichment the sampling trap was flushed with air for 7 min. This period was sufficient to establish an equilibrium between the gas phase concentration of PAN and the amount of absorbed PAN. The calibration procedure showed that absorbed amounts of PAN were constant in mass at constant gas phase concentration and enrichment temperature due to the established equilibrium. Higher gas phase concentrations were linearly correlated with higher amounts of absorbed PAN and vice versa. For desorption the temperature of the preconcentration loop was quickly raised with ballistic electrical heating and switched off when a temperature of 27°C was reached. By means of a 10-way valve the gas mixture was transferred onto the precolumn using nitrogen as a carrier gas. The carrier gas was moistened by a cartridge containing hydrated copper sulfate (Meteorologie Consult GmbH, Glashütten, Germany) that was located in the gas supply in order to ensure constant carrier gas humidity. Both precolumn and main column were wide bore capillary columns [*Müller and Rudolph*, 1992] which were mounted in a thermostatically controlled oven cooled by Peltier elements. Temperature fluctuations were less than 1°C. The separation was performed isothermally at 17°C on the analytical columns. While the selected fraction of the precolumn eluate was passed onto the main column, the precolumn was back-flushed to prevent column contamination and to decrease analysis running time. The eluates were detected by electron capture detection (ECD) at 60°C. The signal was evaluated by integration of the PAN peak. Chromatograms and calculated areas were recorded and saved for further analysis. PAN measurements were performed in 10 min analytical cycles.

The calibration was based on the photochemical synthesis of PAN from NO premixtures in the presence of a large excess of acetone and synthetic air in a flow reactor which consisted of a glass chamber (~100 mL) equipped with a penray lamp (Meteorologie Consult GmbH, Glashütten, Germany). The UV

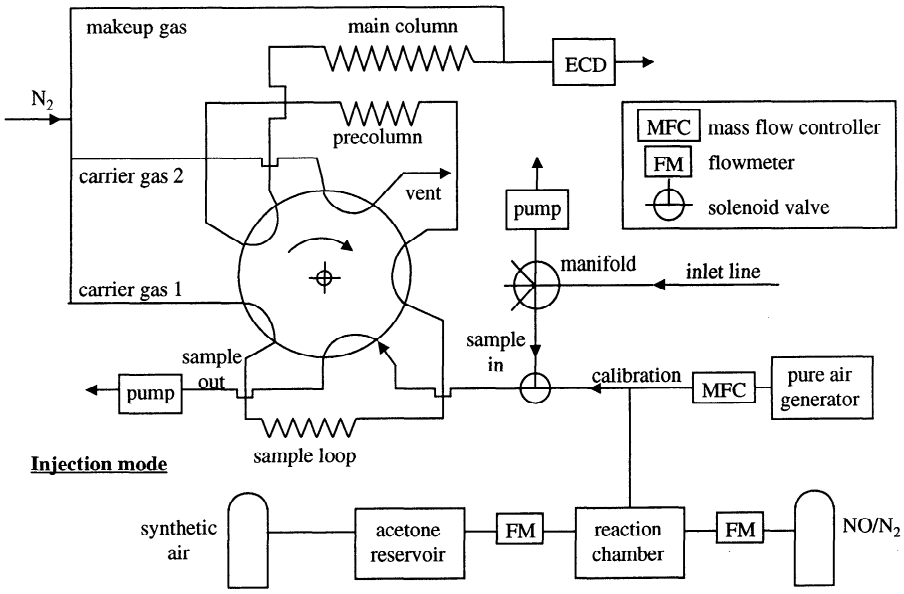

Figure 3. Schematic drawing of the experimental setup of the PAN analyzer.

radiation emitted by the lamp led to the photolytic-induced oxidation of a small amount of acetone. During this oxidation process, acetylperoxy radicals were produced which transformed the employed NO to NO_2 (R3). NO_2 reacted further with excess acetylperoxy radicals leading to the formation of PAN (R1). Within the reaction chamber of the system, reactant flows and photon fluxes were such that complete conversion of NO to PAN is maintained within a wide range of NO and acetone concentrations in the premixtures. A conversion factor of 0.90±0.05 for the employed NO was obtained by using two other analytical techniques for the determination of PAN [*Volz-Thomas et al.*, 1998]. Purified ambient air produced by a clean air generator (PAG 003, Eco Physics GmbH, Munich, Germany) was used for subsequent dynamic dilution to concentrations of 100 parts per trillion by volume (pptv) to 2 ppbv PAN. The procedure required only the determination of the NO calibration gas flow. The calibration of the analyzer was performed on board during the intermediate stay in Lisbon (June 14 and 15). Differences in the operating conditions whether the ship was moving under power or in port were negligible because the complete setup including the power supply was the same during the whole cruise. Moreover, laboratory experiments showed that variations in instrument sensitivity were less than 2% during a period of 3 weeks.

The detection limit of 5 pptv is defined as 3 times the standard deviation calculated from the noise of the output signal of the analyzer when PAN was not present in ambient air samples (June 1-4). The overall error in the PAN measurements was estimated to be less than ±15%.

2.3. Black Carbon Analyzer

Black carbon (BC) measurements were based on the optical attenuation method described by *Hansen et al.* [1988] and *Hansen and McMurry* [1990]. A commercial aethalometer (AE 10, Magee Scientific, Berkeley, California) was used. The aerosol was accumulated on a circular spot with a reduced area of 35 ± 1 mm^2. This area was obtained by a modification of the sampling mimic in order to enhance the sensitivity of the instrument. For the calculation of the accumulated BC quantities, an attenuation cross section on the filter material (Pallflex, type T60A20) of σ = 14 $m^2 g^{-1}$ was used.

The detection limit is derived from the noise level of the output signal of the aethalometer in cases where black carbon was absent in ambient air samples (June 11). The detection limit of 50 ng m^{-3} was defined to be 3 times the standard deviation of this noise level. The overall error was estimated to be less than 15 %. Owing to problems with the automatic data storage procedure, 10 min means were recorded before June 2 and after June 8.

3. Results

3.1. PAN Concentrations in the MBL

The time series of PAN, ozone, and black carbon measured aboard the RV *Polarstern* during the cruise ANT XV/5 are presented in Figure 4. In the southern hemisphere, PAN mixing ratios above the detection limit of 5 pptv were measured only during 2 days. The highest PAN concentration of about 19 pptv over the South Atlantic was observed at 17°S. In tropical latitudes between 10°N and 10°S, the output of the PAN analyzer showed fluctuations around zero. Apparently, a sufficient amount of measurable PAN was absent in the ambient air during this period. Therefore data obtained between June 1 and 4 were used to calculate a detection limit of 5 pptv.

In the northern hemisphere, PAN was present at higher concentrations. The averages and the range of the mixing ratios calculated for several latitudinal ranges are summarized in Table 1. In the region north of the Cape Verde Islands, PAN concentrations increased strongly. PAN mixing ratios up to about 150 pptv during daytime were found along the west coast of Africa. Close to the European continent, even higher values were observed. The maximum concentration of about 1100 pptv was measured in the English Channel. The high time resolution of the PAN analyzer was very useful in following the strong fluctuations of PAN mixing ratios in the ambient air, but only on

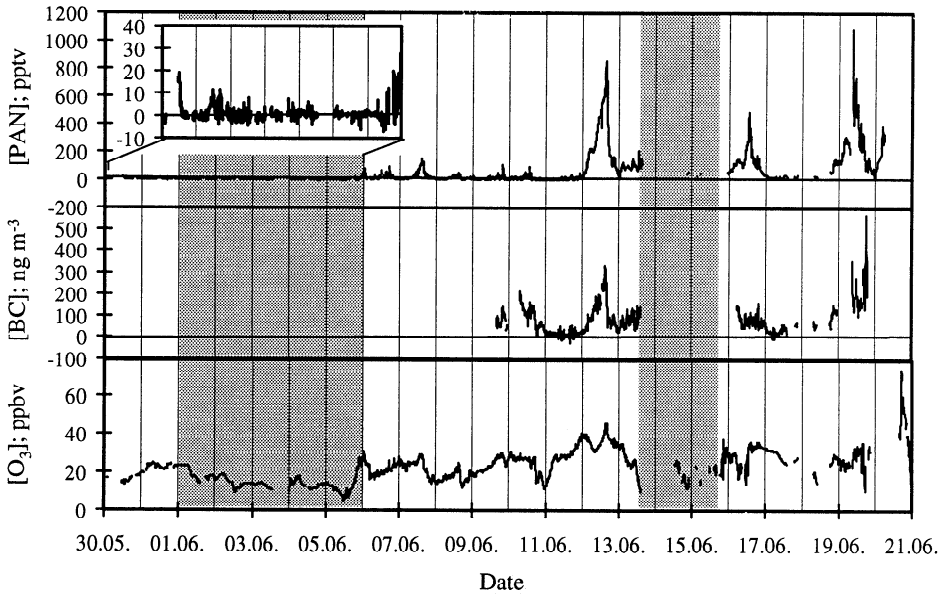

Figure 4. Time series of PAN, black carbon, and ozone concentrations measured on board the RV *Polarstern* (ANT XV/5). The shaded areas represent the latitudinal range between 10°S and 10°N and the intermediate stay in Lisbon, respectively.

Table 1. Measurements of PAN During the RV *Polarstern* Cruise ANT XV/5 From May 29 to June 20, 1998, and a Comparison With Other Studies in the MBL

Region	Period	Height	Mean, pptv	Range, pptv	Reference
Pacific cruise	Nov./Dec. 1984	sea level			1
48°N-25°N				30-80	
25°N-0°				5-40	
0°-48°S				~5	
Atlantic cruise	Aug./Sept. 1988	sea level			2
7°N-64°N				<1-40	
Atlantic cruise	Sept./Oct. 1988	sea level			3
35°N-54°N				2-2000	
30°S-30°N				<1	
31°S				10-100	
Atlantic flights	Sept./Oct. 1992	160-320 m			4
34°S-0°			3	1-7	
Atlantic cruise	May/June 1998	sea level			5
24°S-10°S			<5	<5-19	
10°S-0°			<5	<5-8	
0°-10°N			<5	<5-12	
10°N–20°N			22	<5-147	
20°N–30°N			13	<5-108	
30°N–40°N			121	<5-850	
40°N–50°N			98	8-483	
50°N–54°N			244	23-1088	

References are 1, *Singh et al.* [1986]; 2, *Gallagher et al.* [1990]; 3, *Müller and Rudolph* [1992]; 4, *Singh et al.* [1996]; 5, this study.

particular days were distinct diurnal variations of PAN observed (e.g., June 7, 8, and 12). During these days, PAN values increased in the morning, and maximum concentrations were observed in the early afternoon. After the maximum was reached, mixing ratios strongly decreased to low nighttime values (Figure 5).

The meridional distribution of BC measured during the RV *Polarstern* transect differs from the distribution of PAN mixing ratios. Nevertheless, it is possible to identify several episodes with enhanced BC concentrations in the range of 100 to 600 ng m^{-3} coinciding with enhanced PAN concentrations (Figure 4). The ozone concentrations measured on board the RV *Polarstern* were always less than 50 ppbv with mixing ratios below 25 ppbv in the latitudinal range between 25°S and 10°N (Figure 4). Only when the ship reached the Northern Sea were concentrations up to 75 ppbv observed. The calculated daily means were in the range of 12 to 36 ppbv with lower concentrations in the southern hemisphere. These values are in the same range as the calculated latitudinal distribution of surface ozone over the Atlantic presented by *Winkler* [1988]. Although diurnal O_3 variations were absent during the main part of the cruise, they could be observed in combination with the diurnal cycles of the PAN mixing ratios. In these cases, the diurnal O_3 cycles were similar to those typical in continental air masses with the lowest mixing ratios occurring before sunrise and maxima occurring in the early afternoon.

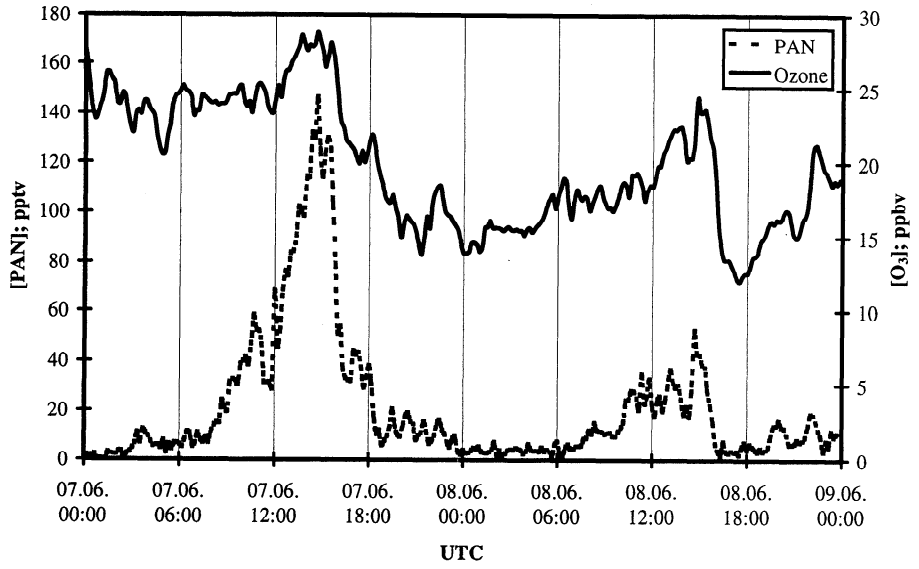

Figure 5. Time series of PAN and of ozone measured on board the RV *Polarstern* (ANT XV/5) on June 7 and 8.

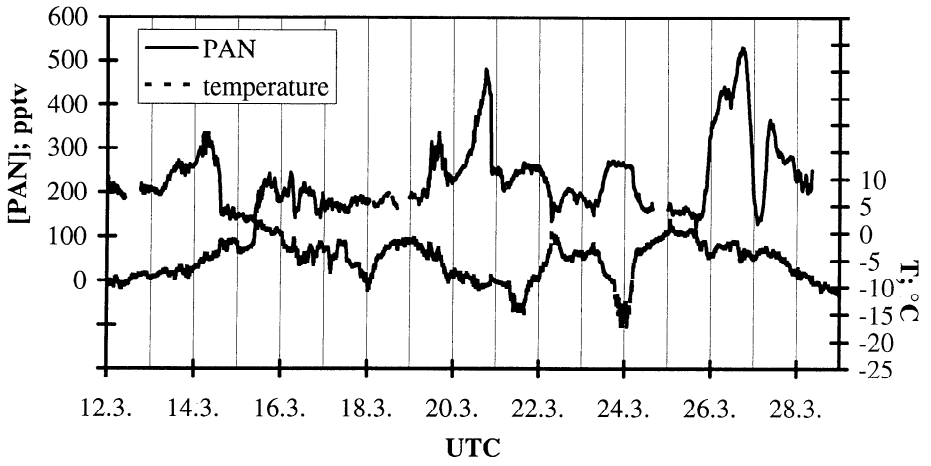

Figure 6. Time series of PAN and temperature measured at Ny-Ålesund, Svalbard (79°N, 12°E).

3.2. PAN Concentrations at Ny-Ålesund

The measured PAN mixing ratios at Ny-Ålesund were in a narrow range from 100 to 420 pptv. A distinct diurnal cycle could not be observed. On the other hand, a temporary relationship between PAN and air temperature was obtained. Figure 6 shows the time series of PAN mixing ratios and temperature during the measuring period. Several short-time episodes can be identified (e.g., March 22 and 24) during which temperature and PAN concentrations were anti-correlated. This anti-correlation may correspond in part to the faster decomposition with increasing temperatures due to reaction (R2). However, the investigation of the relationship between PAN and temperature was inherently hampered by advection of different air masses to the measuring site.

4. Discussion

4.1. PAN Concentrations in the MBL

Since no direct emissions of PAN or PAN precursors occur in the marine or Arctic troposphere, it can only be present in the remote boundary layer if PAN or its precursors are either horizontally or vertically transported from regions with higher concentrations. On a global scale, the continents and the upper troposphere can in general be characterized as regions with enhanced PAN concentrations [*Singh and Hanst*, 1981; *Sandholm et al.*, 1992; *Seinfeld and Pandis*, 1998]. This is due either to faster formation rates in the presence of high precursor concentrations or to slower decomposition at low temperatures. Moreover, the continents are the most important source regions of PAN precursors. In order to identify source regions of PAN or its precursors, the data set was interpreted by utilizing the obtained BC and ozone concentrations together with calculated 3-day back trajectories.

BC represents a minor part of carbonaceous aerosol in the troposphere. Carbonaceous aerosol has several sources such as emissions of volatile organic compounds from vegetation, combustion of fossil fuels, and biomass burning [*Wolff and Cachier*, 1998]. The global budget is dominated by biomass burning in tropical regions and industrial combustion in the temperate latitudes of the northern hemisphere. Owing to its resistance to chemical or physical transformation and its ability to be transported over large distances, BC can be used as tracer for combustion processes and therefore for continentally influenced air masses. Like PAN, tropospheric ozone is produced from NO_x and reactive hydrocarbons [e.g., *Logan*, 1985]. It can be demonstrated that in polluted air masses a linear relationship between PAN and O_3 concentrations can be expected regardless of atmospheric dilution rates [*Schmidt et al.*, 1998]. *Parrish et al.* [1993] also showed that ozone can be used as an indicator of continental influence for air transported off North America to the North Atlantic Ocean. In contrast to BC, ozone has an additional strong natural source in the stratosphere. *Law and Pyle* [1993] calculated a stratospheric ozone flux of 692 Tg y^{-1} compared to a net chemical production of 2074 Tg y^{-1} on a global scale. Therefore enhanced ozone concentrations are not an unequivocal indicator of continentally influenced air masses.

In order to identify the impact of horizontally or vertically transported air masses, the relations between PAN, BC, and ozone were investigated. Figure 7 shows a plot of observed PAN concentrations versus BC concentrations. A linear fit to the data resulted in a regression line with a correlation coefficient of R^2 = 0.32. Although higher BC concentrations at lower PAN concentrations occurred, Figure 7 indicates that increased PAN mixing ratios were generally accompanied by enhanced BC concentrations. From these results, it may be concluded that downward vertical transport of PAN from the upper troposphere, which would be accompanied by low BC concentrations, was negligible during the cruise. This is supported by trajectory analysis of the advected air masses, which showed no impact from the upper troposphere or even the stratosphere.

On the other hand, the relation between PAN and ozone was not very pronounced. A linear regression of PAN concentrations versus O_3 concentrations (not shown) resulted in a correlation coefficient of R^2 = 0.17. However, the relationship of PAN and O_3 in the MBL is not only dependent on photochemical production or emission but also on the different atmospheric lifetimes of these species. *Hov* [1984] showed that at elevated temperatures the persistence of PAN over the sea is lower compared to that of ozone due to the thermal decomposition of PAN. Moreover, surface removal affects ozone, but loss of PAN by wet or dry deposition is thought to be negligible in the MBL [*Roberts et al.*, 1996]. While ozone appears to be a good indicator for polluted continental air masses where fossil fuel combustion is a dominant source [*Parrish et al.*, 1993], this correlation is likely to be disturbed by various mixing processes

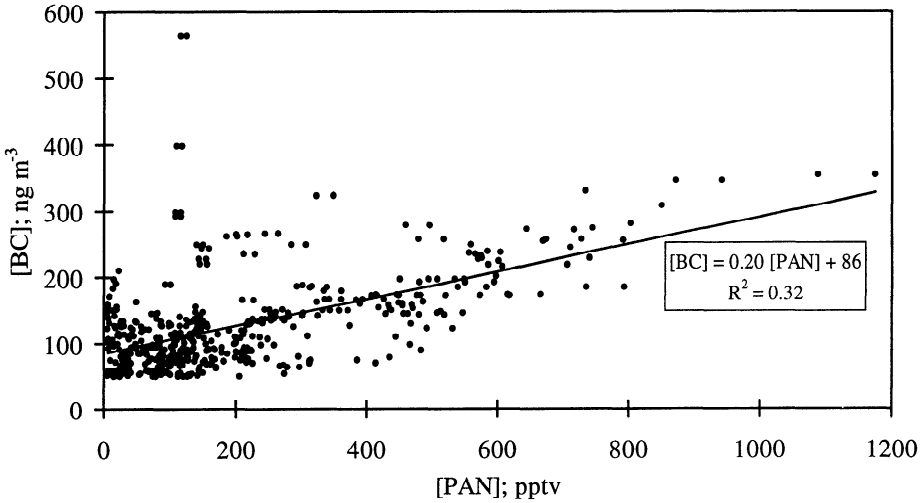

Figure 7. Relation between PAN and BC measured during cruise ANT XV/5. Each dot indicates a 10-min average. Also given is the fit obtained by a linear regression analyses.

and a multiplicity of sources [*Singh et al.*, 1996] which is most probably the case along the African and European coast. These different influences may explain the scatter in the correlation between PAN and O_3 concentrations.

However, several days could be identified with distinct diurnal variations of PAN and O_3 (e.g., June 7, 8, and 12). Both diurnal cycles exhibited an increase of the mixing ratios during daytime with coincident maximum concentrations in the early afternoon (Figure 5). These cycles indicate that photochemical production of ozone and PAN can also occur in the MBL. In this case the precursors of ozone and PAN (hydrocarbons and NO_x) must be transported from their continental source regions into the MBL. The calculated trajectories for these specific days show that the air masses investigated on June 7 and 8 traveled along the coast of West Africa within the last 18 hours, while the air mass sampled on June 12 even crossed Spain and Portugal within the same period. Thus precursors which have tropospheric lifetimes within the range of 1-2 days may have been transported to the cruise track of ANT XV/5. Estimated tropospheric lifetimes of organic compounds which can act as precursors for PAN as well as for O_3 (e.g., acetaldehayde, acetone) are in that range [*Seinfeld and Pandis*, 1998]. Under typical tropospheric conditions, the estimated chemical lifetime of NO_x is also 1-2 days [*Liu et al.*, 1987]. Therefore it is likely that these pollutants can be transported several hundred kilometers from the West African or European coast into the MBL of the North Atlantic Ocean. In such cases, photochemistry in this marine region is comparable to aged continental air masses leading to the formation of secondary pollutants like PAN and ozone.

In contrast to the northern hemisphere, PAN mixing ratios in the latitude range 10°N to 10°S were always below the detection limit of 5 pptv. Because in this region air temperatures at sea level were generally around 26°C, PAN lifetimes were less than half an hour due to thermal decomposition [*Bridier et al.*, 1991]. The lifetime is not only influenced by the temperature but also by the NO/NO_2 ratio. Measurements of NO and NO_2 performed during the cruise ANT XIV/1 of the RV *Polarstern* showed mean ratios of $[NO] / [NO_2] \approx 0.45$ during daytime in the latitudinal range of 10°N to 2°S [*Weller et al.*, 1999]. This ratio is comparable to results obtained during several airborne campaigns over the Atlantic and Pacific Ocean [e.g., *Carroll et al.*, 1990; *Davis et al.*, 1993; *Kondo et al.*, 1996]. At NO/NO_2 ratios higher than 0.5, acetylperoxy radicals formed in reaction (R2) will mainly react with NO. Only at much lower NO/NO_2 ratios does the lifetime of PAN significantly increase due to the steady state maintained by reactions (R1) and (R2). *Müller and Rudolph* [1992] estimated an upper limit of 0.2 to 0.7 pptv for the steady state concentration of PAN at tropical latitudes in the MBL. Under such conditions, PAN cannot serve as an indicator for long-range transport of continentally influenced air masses because any effect on PAN mixing ratios at temperatures higher than 20°C can only be observed if the transport occurs at timescales of less than a few hours.

Measurements of PAN concentrations in the remote MBL have previously been performed during two cruises on the Atlantic Ocean (Table 1). *Gallagher et al.* [1990] found the highest PAN concentrations of up to 40 pptv at high latitudes, whereas at lower latitudes PAN was usually below 10 pptv. They described a number of episodes with elevated PAN mixing ratios and attributed these higher PAN levels to air masses with terrestrial influence or to enhanced stability of PAN at cooler temperatures in the sub-Arctic region. They observed discernible diurnal cycles with maximum PAN concentrations at or near local noon, similar to diurnal cycles in continental air masses. *Gallagher et al.* [1990] attributed the noontime maxima to local photochemical processes, contrary to diurnal cycles in continental air masses which are also strongly influenced by nonchemical parameters like surface deposition and nocturnal inversions.

Müller and Rudolph [1992] measured PAN mixing ratios aboard the RV *Polarstern* during cruise ANT VII/1 on the Atlantic Ocean during September/October 1988. They found PAN mixing ratios between 2 and 2000 pptv in the latitude range 54°N to 35°N with the highest values in the English Channel. South of 35°N, PAN mixing ratios never exceeded the detection limit of 0.4 pptv. At 31°S, PAN concentrations between 10 and 100 pptv were detected in continentally influenced air masses.

Measurements of PAN mixing ratios above the Pacific Ocean in November/December 1984 have been reported by *Singh et al.* [1986]. In the northern hemisphere, they found highly variable PAN mixing ratios between <10 pptv and about 80 pptv. The

concentrations sharply decreased toward the equator with mean mixing ratios of 5 pptv. *Singh et al.* [1986] also concluded that high PAN concentrations can be attributed to air masses of continental origin.

The most recent PAN measurements have been performed during the Transport and Atmospheric Chemistry Near the Equator-Atlantic (TRACE-A) campaign [*Singh et al.*, 1996]. This airborne study was conducted in September/October 1992 to investigate the impact of biomass burning on the atmosphere above the southern tropical Atlantic Ocean. Distinct biomass burning plumes were identified at higher altitudes, but the MBL remained relatively clean. In the boundary layer, low PAN concentrations in the range from 1 to 7 pptv were obtained. This is in the same order of magnitude as our observations.

The interhemispheric PAN distribution of these former studies is comparable to our results, especially for the higher northern latitudes. Moreover, in all studies very low PAN mixing ratios have been obtained in the latitudinal region between 10°N and 10°S. However, north of 10°N only during two days did PAN concentrations remain below 100 pptv, whereas the PAN mixing ratios reported by *Gallagher et al.* [1990] and *Müller and Rudolph* [1992] never exceeded this value. *Müller and Rudolph* [1992] found the highest values, up to 2000 pptv, in the English Channel only in air masses influenced by continental emissions. These differences are most likely due to different cruise tracks and seasons. Whereas cruise ANT VII/1 was mainly performed along 30°W [*Müller and Rudolph*, 1992], and *Gallagher et al.* [1990] obtained their results between 20°W and 50°W in late summer, our measurements were performed in late spring in the vicinity of the western coast of Africa and Europe between 20°W and 15°E. North of 10°N, the cruise track had a maximum distance of 500 km from the coast line. The elevated PAN concentrations in this region of the Atlantic Ocean indicate that this part of the MBL is strongly influenced by continental emissions.

4.2. PAN Concentrations in the Arctic (Ny-Ålesund)

Several short- and long-term measurements of PAN at Arctic sites have been performed (Table 2). Peaks in mixing ratios of PAN are usually observed in spring due to wintertime accumulation of oxidant precursors followed by the increase of actinic radiation and temperature [*Beine et al.*, 1997; *Solberg et al.*, 1997]. Mean PAN concentrations during March between 85 pptv at Poker Flat, Alaska [*Beine et al.*, 1997], and around 300 pptv at Alert, Canada [*Bottenheim et al.*, 1993], and Ny-Ålesund, Svalbard [*Solberg et al.*, 1997], have been reported. These values are comparable to the mean PAN mixing ratio of 232 pptv measured in this study. Strong fluctuations in the time series due to short-term episodes have also been observed in former studies. Only *Bottenheim et al.* [1986] found nearly constant PAN concentrations at 210 pptv during a period of 2 weeks at Alert.

Unfortunately, no measurements of other trace compounds like BC and ozone were performed during the field experiment in Ny-Ålesund. Therefore only the calculated 3-day back trajectories (Figure 2) can be used for analysis of the obtained PAN concentrations.

In order to evaluate the influence of continental sources on PAN mixing ratios, the data set was divided into two bins depending on the age of the air masses. Within these two sets, air masses which remained for less than 3 days over the ocean since having passed over any landmass except Greenland were classified as continental air masses. Any other air masses remaining 3 days over the ocean or Greenland were defined as marine. Although the four days with the highest averaged concentrations (March 20, 21, 26, and 27) coincided with trajectories originating from northern Russia; the mean PAN concentration of around 260 pptv in continental air masses was only slightly higher compared to marine air masses with a mean mixing ratio of about 195 pptv. These results are in agreement with the conclusions of *Beine et al.* [1997] and *Solberg et al.* [1997]. However, the standard deviations of 70 and 20 pptv,

Table 2. Measurements of PAN at Arctic Stations

Location	Period	Height	Mean, pptv	Range, pptv	Reference
Alert, Canada	March 1985	surface			1
82°N			210	180-290	
Alert, Canada	April 1986	surface			2
82°N			439	370-590	
Alert, Canada	March/April 1988	surface			3
82°N			303	136-505	
Alert, Canada	Jan./April 1992	surface			4
82°N				100-900	
Poker Flat, Alaska	March/May 1993	501 m			5
65°N			132.1	27-371	
Ny-Ålesund, Svalbard	March/May 1994	474 m			6
79°N			255.3	69-729	
Poker Flat, Alaska	March/May 1995	470 m			
65°N			85.4	2-910	
Ny-Ålesund, Svalbard		474 m			7
79°N	Feb. 1994		156	100-350	
	March 1994		304	150-800	
	April 1994		290	100-700	
	May 1994		164	50-300	
Ny-Ålesund, Svalbard	March 1998	surface			8
79°N			232	100-420	

References are 1, *Bottenheim et al.* [1986]; 2, *Barrie et al.* [1989]; 3, *Bottenheim et al.* [1993]; 4, *Muthuramu et al.* [1994]; 5, *Beine et al.* [1996]; 6, *Beine et al.* [1997]; 7, *Solberg et al.* [1997]; 8, this study.

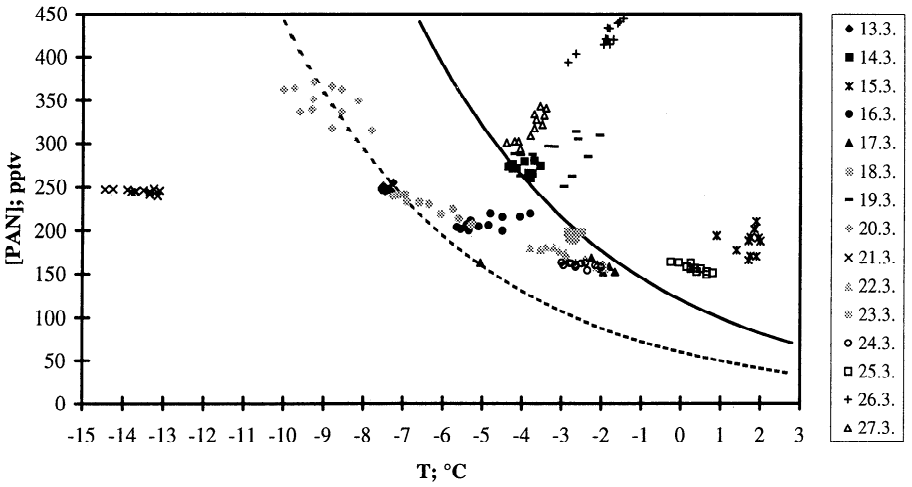

Figure 8. Relationship between PAN and temperature at Ny-Ålesund. Shown are all PAN values measured daily between 1100 and 1300 UTC and calculated PAN concentrations assuming equal rates for thermal loss and photochemical PAN production of 1 pptv h^{-1} (dashed curve) and 2 pptv h^{-1} (solid curve).

respectively, show that this difference is not significant and is probably due to the much shorter time series of our study compared to previous field studies. An additional source of uncertainty is the air temperature which leads to different loss rates. These two factors influencing local PAN concentrations in Ny-Ålesund are illustrated in Figure 8. PAN mixing ratios measured daily between 1100 and 1300 UTC are plotted versus air temperature. These data are shown because the calculated trajectories at 1200 UTC allow the identification of the origin of the measured air masses. *Solberg et al.* [1997] showed that a local in situ photochemical production P_{chem} of 1-2 pptv PAN h^{-1} can occur, which is in the same order of magnitude as the thermal loss rate. PAN concentrations can be calculated assuming equal rates for photochemical production and thermal decomposition described by k_2.

$$P_{chem} = k_2 \times [PAN] \quad (1)$$

This equation neglects the influence of other parameters such as local meteorology, dry deposition, or NO to NO_2 ratios. Figure 8 shows the calculated range of PAN concentrations as a function of temperature using 1 and 2 pptv h^{-1} for the upper and lower limit of P_{chem} [*Solberg et al.*, 1997]. Because most of the measured concentrations were found in this range, one may conclude that an estimated production rate in the range of 1-2 pptv PAN h^{-1} is not only valid for Ny-Ålesund but can be regarded as the "background" production rate within large parts of the Arctic region as indicated by the shaded area in Figure 2. The observed PAN mixing ratios in air masses with origins in this region seem to be mainly determined by thermal loss rates and thus by ambient air temperatures.

Nevertheless, considerably higher and lower PAN concentrations compared to the calculated range shown in Figure 8 were also measured. Higher concentrations were probably due to horizontal and vertical long-range transport of air masses with enhanced PAN mixing ratios. However, calculated trajectories indicate no significant vertical intrusions of air masses during the measuring period. The origins of the air masses with elevated PAN mixing ratios can be identified to be Russia (e.g., March 26 and 27) and western Europe (e.g., March 14 and 19). *Beine et al.* [1997] also reported peak PAN concentrations for periods with trajectories originating from Russia. *Solberg et al.* [1997] defined four different types of air masses: Arctic, Russian, western European, and North Atlantic. Their results indicate that Arctic air masses exhibit substantially enhanced PAN mixing ratios compared to marine air, but the highest average mixing ratios were obtained during airflow from Russia and Europe. *Barrie et al.* [1989] observed correlated concentrations of PAN, sulfate, and potassium. They proposed an anthropogenic origin for all of these compounds. Thus, at Ny-Ålesund, continentally influenced air masses can easily be identified by enhanced PAN mixing ratios at relatively high air temperatures.

Only values measured on March 21 were much lower than the range of PAN concentrations calculated using equation (1). These mixing ratios were due to either lower production rates or additional loss processes. The trajectory indicates that during this day Arctic air masses arrived at Ny-Ålesund which traveled across the Polar Sea. Because PAN deposition in this area was probably not enhanced compared to other Arctic regions, it is most likely that concentrations of PAN precursors in this part of the Arctic were very low.

4.3. Latitudinal Distribution of PAN and Comparison With Modeling Studies

Recent studies with three-dimensional global chemical transport models [*Jaffe et al.*, 1997; *Moxim et al.*, 1996] show different PAN distribution patterns in the northern and southern hemisphere. In the southern hemisphere, higher PAN concentrations have been found above South America and Africa, while PAN remains low in marine regions. Only at higher altitudes does long-range transport of PAN from continental source regions to the oceans occur, especially within biomass burning plumes [*Singh et al.*, 1996]. In the northern hemisphere, PAN is more uniformly distributed. Differences between continental and marine regions are less pronounced and become negligible at higher altitudes during winter and spring. These results are in agreement with our studies showing that PAN is effectively transported to remote areas in temperate northern

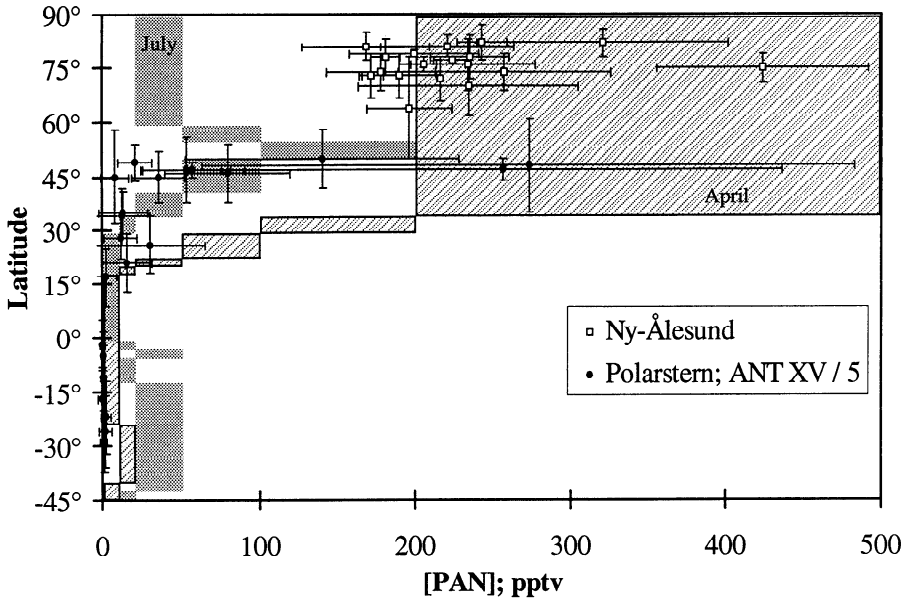

Figure 9. Latitudinal profile of surface PAN concentrations. PAN data obtained from measurements aboard the RV *Polarstern* and at the Koldewey-Station, Ny-Ålesund. Horizontal error bars indicate the standard deviation of daily means of PAN, and vertical error bars indicate the latitude range of the trajectories for the same days. Hatches and shaded boxes represent simulated zonal mean PAN mixing ratios at 990 mbar for April and July, respectively, calculated with a three-dimensional global model [*Moxim et al.*, 1996].

latitudes, whereas PAN mixing ratios in remote marine regions in the southern hemisphere remain low.

The direct comparison of the results of both field experiments of this study is difficult, mainly because the campaigns were performed in different seasons. Particularly in Arctic and sub-Arctic regions, PAN concentrations show a distinct seasonal pattern with the highest mixing ratios in March [*Beine et al.*, 1997, *Bottenheim et al.*, 1994]. This seasonal cycle is less pronounced in temperate northern latitudes and is completely absent in the tropics [*Moxim et al.*, 1996].

Figure 9 shows calculated daily mean PAN mixing ratios as a function of the latitudinal range covered by the ground-level 3-day back trajectories. This latitudinal distribution can only represent a rough estimate because it is calculated from individual measurements in a restricted longitudinal range (9°W-18°E). However, there is evidence that the measured PAN concentrations during both experiments were strongly influenced by long-range transport indicating that different kinds of air masses (e.g., marine, Arctic, continental) were investigated. Because of the different origins of the trajectories, these values may be considered as latitudinal averages. Moreover, *Moxim et al.* [1996] showed that in the northern hemisphere PAN is uniformly distributed. During winter and spring, PAN lifetimes are long enough that PAN is effectively transported from continental source regions to remote areas.

Figure 9 also shows a comparison between the observed data and simulated zonal mean PAN mixing ratios at ground level reported by *Moxim et al.* [1996]. Their study indicates higher PAN concentrations in the northern compared to the southern hemisphere. Highest concentrations are calculated for the northern extratropical troposphere during winter and spring. Concentrations decrease strongly during summer with increasing temperatures. Only in the latitudinal range with the highest NO_x emissions do the PAN concentrations remain high. In the tropics, the concentrations are always very low, while the southern hemisphere also has maximum PAN mixing ratios during austral winter and spring.

The latitudinal distribution of the observed PAN mixing ratios near the surface exhibits a similar pattern as simulated zonal means. Nevertheless, the calculated values are significantly higher than the measurements and are only comparable to the upper limits of the observed mixing ratios. There are several reasons which can cause discrepancies between surface observations and modeled concentrations. The simulated values are calculated for April or July, whereas the measurements were performed during March and May/June. Other measurements on Arctic sites show that the observed PAN mixing ratios usually peak in April [e.g., *Beine et al.*, 1997]. In northern polar regions, slightly higher PAN concentrations during April compared to March can be expected. Moreover, calculated mean zonal mixing ratios include continental, marine, and remote regions on a global scale, whereas the investigated air masses cover only a restricted geographical region. Calculated PAN mixing ratios are also sensitive to the concentrations of nonmethane hydrocarbons (NMHC) which act as PAN precursors. In their calculations, *Moxim et al.* [1996] increased NMHC concentrations between 30°N and 65°N to reproduce observed PAN levels at three sites in North America. South of 30°N, NMHC concentrations over land have been adjusted to continental NMHC concentrations during summer between 30°N and 65°N. These assumed NMHC concentration levels may lead to an overestimation of PAN concentrations in the model.

5. Conclusions

PAN measurements with a time resolution of 10 min were performed during two field campaigns. Shipborne measurements on the Atlantic and observations at an Arctic site, encompassing

nearly 95° of latitude, were carried out. Observed PAN mixing ratios were enhanced in the northern hemisphere as compared to the southern hemisphere. In the latitudinal range between 10°N and 10°S, PAN concentrations were below the detection limit of 5 pptv. Higher PAN mixing ratios of up to 1100 pptv were found in regions influenced by the advection of continental air masses. These air masses were identified by higher concentrations of other indicators of continental pollution like black carbon and ozone. These results are consistent with previous field experiments and also with the results of modeling studies. However, the latter are only comparable to the upper limit of observed values.

It may be concluded that in temperate northern latitudes, PAN can serve as a useful indicator of photochemical air pollution caused by long-range transport. This has already been confirmed by a former modeling study [*Hov*, 1984]. However, in tropical and Arctic regions, PAN concentrations are also influenced by air temperature. Simultaneous measurements of PAN and NO_x in the MBL are required to estimate PAN lifetimes and to explore the long-range transport of photochemical pollutants to the South Atlantic Ocean. Such experiments in temperate northern latitudes could also be useful to further investigate the observed diurnal cycles of PAN in the MBL and intrusions from the upper troposphere.

Acknowledgments. We would like to thank the crew of the RV *Polarstern* and the staff of the Koldewey-Station for their cooperation and assistance. The trajectories have been provided by the German Weather Service (DWD). We thank the two anonymous reviewers for their helpful comments on the manuscript. This paper is contribution 1606 of the Alfred-Wegener-Institute for Polar and Marine Research.

References

Barrie, L.A., G. den Hartog, J.W. Bottenheim, and S. Landsberger, Anthropogenic aerosols and gases in the lower troposphere at Alert, Canada in April 1986, *J. Atmos. Chem., 9*, 101-127, 1989.

Beine, H.J., D.A. Jaffe, D.R. Blake, E. Atlas, and J. Harris, Measurements of PAN, alkyl nitrates, ozone, and hydrocarbons during spring in interior Alaska, *J. Geophys. Res., 101*, 12,613-12,619, 1996.

Beine, H.J., D.A. Jaffe, J.A. Herring, J.A. Kelley, T. Krognes, and F. Stordal, High-latitude springtime photochemistry, I, NO_x, PAN and ozone relationships, *J. Atmos. Chem., 27*, 127-153, 1997.

Bottenheim, J.W., A.G. Gallant, and K.A. Brice, Measurements of NO_y species and O_3 at 82°N latitude, *Geophys. Res. Lett., 13*, 113-116, 1986.

Bottenheim, J.W., L.A. Barrie, and E. Atlas, The partitioning of nitrogen oxides in the lower Arctic troposphere during spring 1988, *J. Atmos. Chem., 17*, 15-27, 1993.

Bottenheim, J.W., A. Sirois, K.A. Brice, and A.J. Gallant, Five years of continuous observations of PAN and ozone at a rural location in eastern Canada, *J. Geophys. Res., 99*, 5333-5352, 1994.

Bridier, I., F. Caralp, H. Loirat, R. Lesclaux, B. Veyret, K.H. Becker, A. Reimer, and F. Zabel, Kinetic and theoretical studies of the reactions $CH_3C(O)O_2 + NO_2 + M \leftrightarrow CH_3C(O)O_2NO_2 + M$ between 248 and 393 K and between 30 and 760 torr, *J. Phys. Chem., 95*, 3594-3600, 1991.

Carroll, M.A., and A.M. Thompson, NO_x in the non-urban troposphere, in *Progress and Problems in Atmospheric Chemistry*, edited by J.R. Barker, pp. 198-255, World Sci., River Edge, N.J., 1995.

Carroll, M.A., et al., Aircraft measurements of NO_x over the eastern Pacific and continental United States and implications for ozone production, *J. Geophys. Res., 95*, 10,205-10,233, 1990.

Davis, D.D., et al., A photostationary state analysis of the NO_2-NO system based on airborne observations from the subtropical/tropical North and South Atlantic, *J. Geophys. Res., 98*, 23,501-23,523, 1993.

DeMore, W.B., S.P. Sander, D.M. Golden, R.F. Hampson, M.J. Kurylo, C.J. Howard, A.R. Ravishankara, C.E. Kolb, and M.J. Molina, Chemical kinetics and photochemical data for use in stratospheric modeling, *Eval. 12*, 278 pp., Jet Propul. Lab., Pasadena, Calif., 1997.

Gallagher, M.S., T.P. Carsey, and M.L. Farmer, Peroxyacetyl nitrate in the North Atlantic marine boundary layer, *Global Biogeochem. Cycles, 4*, 297-308, 1990.

Hansen, A.D.A., and P.H. McMurry, An intercomparison of measurements of aerosol elemental carbon during the 1986 carbonaceous species method comparison study, *J. Air Waste Manage. Assoc., 40*, 894-895, 1990.

Hansen, A.D.A., B.A. Bodhaine, E.G. Dutton, and R.C. Schnell, Aerosol black carbon measurements at the South Pole: Initial results, 1986-1987, *Geophys. Res. Lett., 15*, 1193-1196, 1988.

Hov, Ø., Modeling of the long-range transport of peroxyacetylnitrate to Scandinavia, *J. Atmos. Chem., 1*, 187-202, 1984.

Jaffe, D.A., T.K. Berntsen, and I.S.A. Isaksen, A global three-dimensional chemical transport model, 2, Nitrogen oxides and nonmethane hydrocarbon results, *J. Geophys. Res.*, 102, 21,281-21,296, 1997.

Kondo, Y., H. Ziereis, M. Koike, S. Kawakami, G.L. Gregory, G.W. Sachse, H.B. Singh, D.D. Davis, and J.T. Merrill, Reactive nitrogen over the Pacific Ocean during PEM-West A, *J. Geophys. Res., 101*, 1809-1828, 1996.

Kottmeier, C., and B. Fay, Trajectories in the Antarctic lower troposphere, *J. Geophys. Res., 103*, 10,947-10,959, 1998.

Law, K.S., and J.A. Pyle, Modeling trace gas budgets in the troposphere, 1, Ozone and odd nitrogen, *J. Geophys. Res., 98*, 18,377-18,400, 1993.

Liu, S.C., M. Trainer, F.C. Fehsenfeld, D.D. Parish, E.J. Williams, D.W. Fahey, G. Hübler, and P.C. Murphy, Ozone production in the rural troposphere and the implications for regional and global ozone distributions, *J. Geophys. Res., 92*, 4191-4207, 1987.

Logan, J., Tropospheric ozone: Seasonal behavior, trends, and anthropogenic influence, *J. Geophys. Res., 90*, 10,403-10,482, 1985.

Moxim, W.J., H. Levy II, and P.S. Kasibhatla, Simulated global tropospheric PAN: Its transport and impact on NO_x, *J. Geophys. Res., 101*, 12,621-12,638, 1996.

Müller, K.P., and J. Rudolph, Measurements of peroxyacetylnitrate in the marine boundary layer over the Atlantic, *J. Atmos. Chem., 15*, 361-367, 1992.

Muthuramu, K., P.B. Shepson, J.W. Bottenheim, B.T. Jobson, H. Niki, and K.G. Anlauf, Relationships between organic nitrates and surface ozone destruction during Polar Sunrise Experiment 1992, *J. Geophys. Res., 99*, 25,369-25,378, 1994.

Parrish, D.D., J.S. Holloway, M. Trainer, P.C. Murphy, G.L. Frobes, and F.C. Fehsenfeld, Export of North American ozone pollution to the North Atlantic Ocean, *Science, 259*, 1436-1439, 1993.

Roberts, J.M., The atmospheric chemistry of organic nitrates, *Atmos. Environ., Part A, 24*, 243-287, 1990.

Roberts, J.M., et al., Episodic removal of NO_y species from the marine boundary layer over the North Atlantic, *J. Geophys. Res., 101*, 28,947-28,960, 1996.

Sandholm, S.T., et al., Summertime tropospheric observations related to N_xO_y distributions and partitioning over Alaska: Arctic Boundary Layer Expedition 3A, *J. Geophys. Res., 97*, 16,481-16,509, 1992.

Schmidt, R.W.H., F. Slemr, and U. Schurath, Airborne peroxyacetyl nitrate (PAN) and peroxypropionyl nitrate (PPN) measurements during TRACT 1992, *Atmos. Environ., 32*, 1203-1227, 1998.

Seinfeld, J.H., and S.N. Pandis, *Atmospheric Chemistry and Physics*, 1326 pp., John Wiley, New York, 1998.

Singh, H.B., and P.L. Hanst, Peroxyacetyl nitrate (PAN) in the unpolluted atmosphere: An important reservoir for nitrogen oxides, *Geophys. Res. Lett., 8*, 941-944, 1981.

Singh, H.B., L.J. Salas, and W. Viezee, Global distribution of peroxyacetyl nitrate, *Nature, 321*, 588-591, 1986.

Singh, H.B., D. Herlth, D. O'Hara, K. Zahnle, J.D. Bradshaw, S.T. Sandholm, R. Talbot, P.J. Crutzen, and M Kanakidou, Relationship of peroxyacetyl nitrate to active and total odd nitrogen at northern high latitudes: Influence of reservoir species on NO_x and O_3, *J. Geophys. Res., 97*, 16,523-16,530, 1992.

Singh, H.B., et al., Impact of biomass burning emissions on the composition of the South Atlantic troposphere: Reactive nitrogen and ozone, *J. Geophys. Res., 101*, 24,203-24,219, 1996.

Solberg, S., T. Krognes, F. Stordal, Ø. Hov, H.J. Beine, D.A. Jaffe, K.C. Clemitshaw, and S.A. Penkett, Reactive nitrogen compounds at Spitsbergen in the Norwegian Arctic, *J. Atmos. Chem., 28*, 209-255, 1997.

Stephens, E.R., The formation, reactions, and properties of peroxyacetyl

nitrates (PAN) in photochemical air pollution, *Adv. Environ. Sci. Technol., 1*, 119-146, 1969.

Volz-Thomas, A., N. Houben, A. Lerner, and W. Pätz, Charakterisierung der dynamischen PAN-Kalibriereinheit der Meteorologie Consult GmbH, *Rep. 07 TFS QS 2/4*, 10 pp., Forsch. Jülich, Jülich, Germany, 1998.

Weller, R., and O. Schrems, Photooxidants in the marine Arctic troposphere in summer, *J. Geophys. Res., 101*, 9139-9147, 1996.

Weller, R., R. Lilischkis, O. Schrems, R. Neuber, and S. Wessel, Vertical ozone distribution in the marine atmosphere over the central Atlantic Ocean (56°S-50°N), *J. Geophys. Res., 101*, 1387-1399, 1996.

Weller, R., O. Schrems, A. Boddenberg, and S. Gäb, Hydroperoxides, formaldehyde and NO/NO_2 measurements in the marine boundary layer of the Atlantic Ocean (48°N-35°S), in *Proceedings of EUROTRAC Symposium '98, Vol. 1*, edited by P.M. Borrell and P. Borrell, pp. 370-374, WIT Press, Southampton, England, U.K., 1999.

Winkler, P., Surface ozone over the Atlantic Ocean, *J. Atmos. Chem., 7*, 73-91, 1988.

Wolff, E.W., and H. Cachier, Concentrations and seasonal cycle of black carbon in aerosol at a coastal Antarctic station, *J. Geophys. Res., 103*, 11,033-11,041, 1998.

T. Bluszcz, H.-W. Jacobi, O. Schrems, and R. Weller, Alfred-Wegener-Institute for Polar and Marine Research, Am Handelshafen 12, D-27570 Bremerhaven, Federal Republic of Germany.
(hwjacobi@awi-bremerhaven.de)

(Received November 24, 1998; revised June 22, 1999;
accepted June 23, 1999.)

Publication 3.1.3

Jacobi, H.-W., R. Weller, A.E. Jones, P.S. Anderson, and O. Schrems,

Peroxyacetyl nitrate (PAN) concentrations in the Antarctic troposphere measured during the Photochemical Experiment at Neumayer (PEAN'99),

Atmos.Environ. **34**, 5235-5247, 2000.

PERGAMON

Atmospheric Environment 34 (2000) 5235–5247

ATMOSPHERIC ENVIRONMENT

www.elsevier.com/locate/atmosenv

Peroxyacetyl nitrate (PAN) concentrations in the Antarctic troposphere measured during the photochemical experiment at Neumayer (PEAN'99)

H.-W. Jacobi[a,*], R. Weller[a], A.E. Jones[b], P.S. Anderson[b], O. Schrems[a]

[a]*Alfred Wegener Institute for Polar and Marine Research, Am Handelshafen 12, 27570 Bremerhaven, Germany*
[b]*British Antarctic Survey, Natural Environment Research Council, High Cross, Madingley Road, Cambridge CB3 0ET, UK*

Received 30 November 1999; received in revised form 15 March 2000; accepted 24 March 2000

Abstract

Because investigations of PAN at higher southern latitudes are very scarce, we measured surface PAN concentrations for the first time in Antarctica. During the Photochemical Experiment at Neumayer (PEAN'99) campaign mean surface PAN mixing ratios of 13 ± 7 pptv and maximum values of 48 pptv were found. When these PAN mixing ratios were compared to the sum of NO_x and inorganic nitrate they were found to be equal or higher. Low ambient air temperatures and low PAN concentrations caused a slow homogeneous PAN decomposition rate of approximately 5×10^{-2} pptv h^{-1}. These slow decay rates were not sufficient to firmly establish the simultaneously observed NO_x concentrations. In addition, low concentration ratios of $[HNO_3]/[NO_x]$ imply that the photochemical production of NO_x within the snow pack can influence surface NO_x mixing ratios in Antarctica. Alternate measurements of PAN mixing ratios at two different heights above the snow surface were performed to derive fluxes between the lower troposphere and the underlying snow pack using calculated friction velocities. Most of the concentration differences were below the precision of the measurements. Therefore, only an upper limit for the PAN flux of $\pm 1 \times 10^{13}$ molecules m^{-2} s^{-1} without a predominant direction can be estimated. However, PAN fluxes below this limit can still influence both the transfer of nitrogen compounds between atmosphere and ice, and the PAN budget in higher southern latitudes.

Keywords: Peroxyacetyl nitrate; Antarctica; Nitrogen oxides; Nitrogen budget; Air–surface exchange

1. Introduction

Peroxyacetyl nitrate (PAN) is an important compound within the class of reactive nitrogen oxides in the atmosphere. While it is mainly produced during the oxidation of organic compounds in the presence of nitrogen oxides, its destruction is dominated by thermal decompositon. Therefore, many field and modelling studies (e.g. Kleindienst, 1994; Moxim et al., 1996; Jaffe et al., 1997; Wang et al., 1998) have shown that high PAN concentrations not only occur in regions with strong sources of its precursors (e.g. highly polluted urban areas) but also at low temperatures in regions with no sources (e.g. Arctic, or middle and upper troposphere). Concurrent observations of PAN and the sum of reactive nitrogen (NO_y) have revealed that PAN can constitute up to 90% of the total NO_y budget at higher northern latitudes or higher altitudes (Bottenheim et al., 1986, 1993; Barrie et al., 1989; Bottenheim and Gallant, 1989; Muthuramu et al., 1994; Solberg et al., 1997; Sandholm et al., 1992; Singh et al., 1994, 1998; Bradshaw et al., 1998; Talbot et al., 1999). Despite lower PAN concentration at lower altitudes in remote marine areas, its decomposition has been found to be sufficient to maintain observed NO_x

* Corresponding author; Present address: Department of Hydrology and Water Resources, 1133 E. North Campus Dr., P.O. Box 210011, University of Arizona, Tucson, AZ 85721-0011, USA.

E-mail address: hwj@hwr.arizona.edu (H.-W. Jacobi).

1352-2310/00/$ - see front matter
PII: S1352-2310(00)00190-4

($= NO + NO_2$) mixing ratios (e.g. Heikes et al., 1996; Jacob et al., 1996; Schultz et al., 1999), thus demonstrating that PAN can act as a transport agent for NO_x from its continental sources to remote tropospheric regions. As a result, PAN influences the NO_x balance, which in turn critically controls photochemical production and destruction of ozone in many regions of the troposphere (e.g. Carroll and Thompson, 1995).

In addition to its role in tropospheric photochemistry, PAN is thought to be of great importance for the air–snow-transfer of nitrogen compounds in high northern latitudes. Because PAN constitutes a large fraction of the arctic NO_y budget, Munger et al. (1999) assume that it participates in the NO_y transfer and must be taken into account for the interpretation of nitrate concentrations in ice cores. Moreover, a recent investigation of NO_y gradients above the snowpack in Greenland indicate that NO_y fluxes can be of different size and direction compared to concurrently measured HNO_3 fluxes (Dibb et al., 1998). Due to PAN's high abundance in Greenland, it may be suggested that PAN contributes to the observed NO_y fluxes.

Despite its great impact at higher latitudes, no direct observations of PAN mixing ratios in Antarctica have been reported in the literature. Therefore, measurements of PAN concentrations were part of the Antarctica field campaign Photochemical Experiment at Neumayer (PEAN'99) performed at the German research station in the second half of the austral summer 1999. Besides this first experimental investigation of PAN mixing ratios in Antarctica, a wide range of chemical and physical variables were measured during this program, including NO, NO_2, HNO_3, and particulate nitrate (p-NO_3^-). This suite of measurements provides a unique opportunity to study the partitioning of odd nitrogen compounds in the lower troposphere over Antarctica. We further investigated gradients of PAN concentrations in the lower 2.5 m above the snow surface to resolve fluxes of PAN between the atmosphere and the underlying snow pack.

2. Methods and instrumentation

Measurements of PAN, NO, NO_2, HNO_3 and p-NO_3^- concentrations were performed within the frame of the Photochemical Experiment at Neumayer 1999 (PEAN'99) campaign which was conducted between 25th January and 28th February 1999 at the German research station Neumayer (70°39′N, 8°15′W). This station is located on the Ekström ice shelf, about 8 km from the Atka Bay. The analysers were installed in a specially equipped laboratory container located 1.5 km south of the main station near the permanent Air Chemistry Observatory. In this location prevailing wind directions are from east. Concentrations measured during wind directions from the north could be affected by contamination from emissions of the base. During the campaign this situation occurred only on 14 February between 20:30 and 22:30 UTC. These data were discarded from the original data sets which were then used for further analysis. Normally, air masses advected to Neumayer passed over the continent for two to three days, but originate generally from marine regions.

Three different inlet lines were used for collecting air samples for PAN measurements. For gradient measurements two inlet lines (each 9 m in length of 0.4 cm ID perfluoroalkoxy (PFA) tubing) were fixed at two vertical braces of a mast at 0.1 and 2.5 m height above the snow surface. At the beginning of the campaign the mast was erected approximately 5 m west of the container. Until the first gradient measurements the snow surface was completely renewed due to several days of strong snow drift. Inside the container both inlet lines were connected via a three-way Teflon valve with a manifold. The valve was switched every 10 min from the upper to the lower inlet line which were both flushed with a flow rate of about 7 l min^{-1} leading to a residence time of the air samples in the tubes and the manifold of less than 3 s. In addition, a third inlet line (10 m of 0.4 cm ID PFA) was fixed at a height of approximately 2.3 m and equipped with a spray deflector. This line was connected to the manifold during periods with strong snow drift. From the manifold air was sucked into the analyser using a second pump.

The method for the PAN measurements is based on electron capture gas chromatography with cryogenic pre-concentration technique (Schrimpf et al., 1995). Details of the commercial analyser (Meteorologie Consult GmbH, Glashütten, Germany) were recently described (Jacobi et al., 1999). After enrichment for 7 min on a Peltier-cooled cryogenic sampling trap at 0°C, desorption was maintained by quickly heating the pre-concentration loop. The gas mixture was transferred to the analytical column with nitrogen as carrier gas. The separation was performed within 10 min analytical cycles using pre- and main columns maintained at 12°C. Only a selected fraction including PAN was passed from the pre-column onto the main column. The eluates of the main column were analysed by electron capture detection (ECD) at 60°C. Calibration was based on photochemical synthesis of PAN using NO-premixtures in the presence of acetone and synthetic air (Warneck and Zerbach, 1992). A flow reactor equipped with a penray lamp (Meteorologie Consult GmbH, Glashütten, Germany) was used for the synthesis. The limit of detection (LOD) was derived from the noise of the output signal of the analyser when air produced by a clean air generator (PAG 003, Eco Physics GmbH, Munich, Germany) was analysed. A LOD of 5 pptv is obtained from two times the standard deviation of the noise. Multipoint calibrations were performed at the beginning and at the end of

the campaign and showed good agreement resulting in an estimated overall precision of $\pm 15\%$ or ± 3 ppt, whatever is higher.

NO was measured with a chemiluminescence detector (CLD 780 TR, Eco Physics GmbH, Munich, Germany) based on the conversion of ambient NO to excited NO_2^* in a flow reactor. A preceding reduction of NO_2 to NO using a photolytic converter (PLC 760, Eco Physics GmbH, Munich, Germany) allows the selective detection of NO_2 in a separate measurement cycle. The conversion efficiency of the photolytic converter was determined every 5–7 days to be in the range of 63–66% throughout the campaign. The calculated accuracies of the NO and NO_2 measurements were ± 2–3 and ± 3–4 pptv, respectively. LODs of 3 pptv for NO and 4 pptv for NO_2 were calculated. Samples for HNO_3 were collected in the Air Chemistry Observatory using a low volume three-stage Teflon/nylon/nylon filter combination described by Jones et al. (1999). The air intake height for the filter samples was approximately 7 m above the snow level. Local contamination by anthropogenic sources was prevented by a wind and condensation particle-controlled sampling procedure (Wagenbach et al., 1988). The collected filters were extracted using MilliQ water, the Teflon filters having first been wetting with < 200 μl isopropanol. The solution was then analysed with an ion chromatograph to determine the nitrate content. Regular blank determinations were used to estimate an overall error including the IC error and the error of the sample air volume. Errors of 21% for HNO_3 and 9% for p-NO_3^- were derived. The LOD calculated from twice the standard deviation of the blank values was found to be 1 pptv for both compounds.

In addition, continuous measurements of meteorological quantities (temperature, wind speed, wind direction, relative humidity) were routinely performed at Neumayer Station. All parameters except the PAN gradients were averaged to 20-min means. Because HNO_3 concentrations are averages for longer sample integration intervals the obtained values were used for all 20-min intervals within the several filter sampling periods.

3. Results and discussion

3.1. PAN time series

Fig. 1 shows the observed PAN time series during PEAN'99. Ambient concentrations were measured between 1 and 28 February 1999. The mixing ratios were in the range from < 5 pptv (LOD) to 48 pptv. The values exhibited a strong temporal variability without a distinct diurnal variation and an average of 13 ± 7 pptv for the entire campaign.

A comparison with PAN mixing ratios previously obtained in high northern latitudes (e.g. Bottenheim et al., 1994; Muthuramu et al., 1994; Beine et al., 1996; Jacobi et al., 1999) shows that the concentrations in the Antarctic

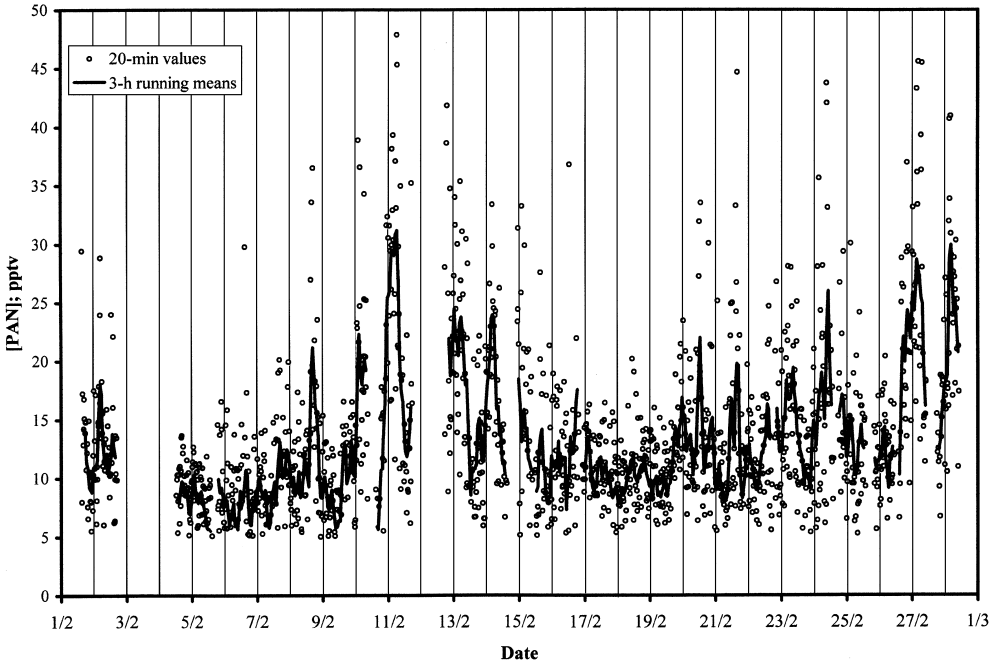

Fig. 1. Time series of PAN measured at Neumayer station during PEAN'99.

obtained during this campaign were approximately one order of magnitude lower. This difference is probably due to the fact that the Arctic is surrounded by continents which are strong sources of PAN precursors (Roberts, 1990). Trajectory analysis of PAN measurements at Ny-Ålesund, Svalbard, has demonstrated that air masses with origins over Europe or Asia were accompanied by higher PAN concentrations compared to air masses with marine or polar origins (Solberg et al., 1997; Jacobi et al., 1999). The larger distance from other continents makes the transport of PAN or its precursors to higher southern latitudes less effective. Therefore, several global modelling studies have demonstrated that surface PAN mixing ratios in Antarctica could be considerably lower than in the Arctic (e.g. Moxim et al., 1996; Jaffe et al., 1997; Wang et al., 1998). Moxim et al. (1996) and Wang et al. (1998) calculated mixing ratios below 10 pptv for Antarctica in January, while Jaffe et al. (1997) obtained concentrations between 10 and 30 pptv in April. The mean PAN concentration of 13 pptv observed during this study are in good agreement with the simulated results. However, they cannot explain our maximum values in the order of 40 pptv. These high concentrations can probably be explained by long-range transport of PAN-enriched air from lower latitudes or higher altitudes. Several airborne and ship-based field experiments have demonstrated that PAN mixing ratios are normally below 10 pptv in the MBL of the Southern Hemisphere (Singh et al., 1986, 1996, 1998; Rudolph et al., 1987; Müller and Rudolph, 1992; Schultz et al., 1999). In contrast, recent investigations onboard RV *Polarstern* showed that over the South Atlantic mean PAN concentrations of 60 pptv north of 49°S can occur (Jacobi and Schrems, 1999). Müller and Rudolph (1992) also found mixing ratios up to 100 pptv around 30°S in air masses influenced by continental emissions. In addition, high PAN concentrations up to 140 pptv were observed in the upper and middle troposphere of the southern hemisphere (Singh et al., 2000). For example, the global PAN distribution simulated by Moxim et al. (1996) shows concentrations in the range of 20–50 pptv at a height of 8 km at 60°S. In order to investigate the influence of air mass origin, daily ground-level 5-day back trajectories were analysed. Because PAN concentrations showed no systematic trends as a function of latitude or altitude of the initial points of the trajectories, an identification of the source region of air masses with enhanced PAN concentrations remains impossible.

Year-round measurements of PAN concentrations in higher northern latitudes have shown that PAN follows a distinct seasonal variation (Bottenheim et al., 1994). During summertime PAN concentrations decrease due to increased photochemical destruction of its organic precursors. If the same annual variation of PAN occurs in the high southern latitudes it may be concluded that the PAN concentrations obtained during PEAN'99 were probably lower than the annual mean because the campaign was performed in late austral summer.

3.2. PAN lifetimes

For further investigations of the PAN concentrations, we calculated PAN lifetimes which are mainly dependent on the ambient air temperature. The campaign may be divided due to the meteorological conditions into consecutive periods of several days with either low wind speeds and temperatures or high wind speeds and temperatures accompanied with strongly drifting snow. The different periods are indicated in Fig. 2. The highest PAN concentrations were observed during the two periods with low wind speed and temperature. Although the mean mixing ratio for these periods was slightly higher (17 pptv) compared to the rest of the campaign (11 pptv), the difference in the PAN mixing ratios was not statistically significant.

Reactions (R1)–(R4) demonstrate that PAN lifetimes are influenced by temperature as well as by concentration ratios of NO_2 to NO and NO_2 to organic peroxy radicals RO_2 (Seinfeld and Pandis, 1998).

$$CH_3C(O)OONO_2 \rightleftharpoons CH_3C(O)OO + NO_2, \qquad \text{(R1,R2)}$$

$$CH_3C(O)OO + NO \rightarrow CH_3 + CO_2 + NO_2, \qquad \text{(R3)}$$

$$CH_3C(O)OO + RO_2 \rightarrow \Pi. \qquad \text{(R4)}$$

We applied Eqs. (1) and (2) to calculate PAN decay rates during the campaign using reaction rate constants reported by Bridier et al. (1991) and DeMore et al. (1997) and measured NO_2 to NO ratios (Fig. 3).

$$-\frac{d[PAN]}{dt} = k_1[PAN], \qquad (1)$$

$$-\frac{d[PAN]}{dt} = k_1[PAN]\left(1 - \frac{k_2}{k_2 + k_3[NO]/[NO_2]}\right). \qquad (2)$$

While the upper limit of the decay rates is defined by Eq. (1), the rates obtained with Eq. (2) represent only the lower limits. Additional reactions of acetyl peroxy radicals with organic peroxy radicals (R4) or aerosols can further increase the PAN decay rate. However, the actual decay rate is restricted to the range of the calculated upper and lower limits. Obviously, the decay rates can be lowered by more than one order of magnitude at high ratios of $[NO_2]/[NO]$. Nevertheless, Fig. 3 shows that most of the calculated lower limits of the decay rate are similar to the upper limits defined by reaction (R1). While all calculated rates comprise a range of $< 10^{-3}$–0.4 pptv h^{-1}, most of them ($> 75\%$) were in the much narrower range of 10^{-2}–10^{-1} pptv h^{-1}. Assuming a mean rate of

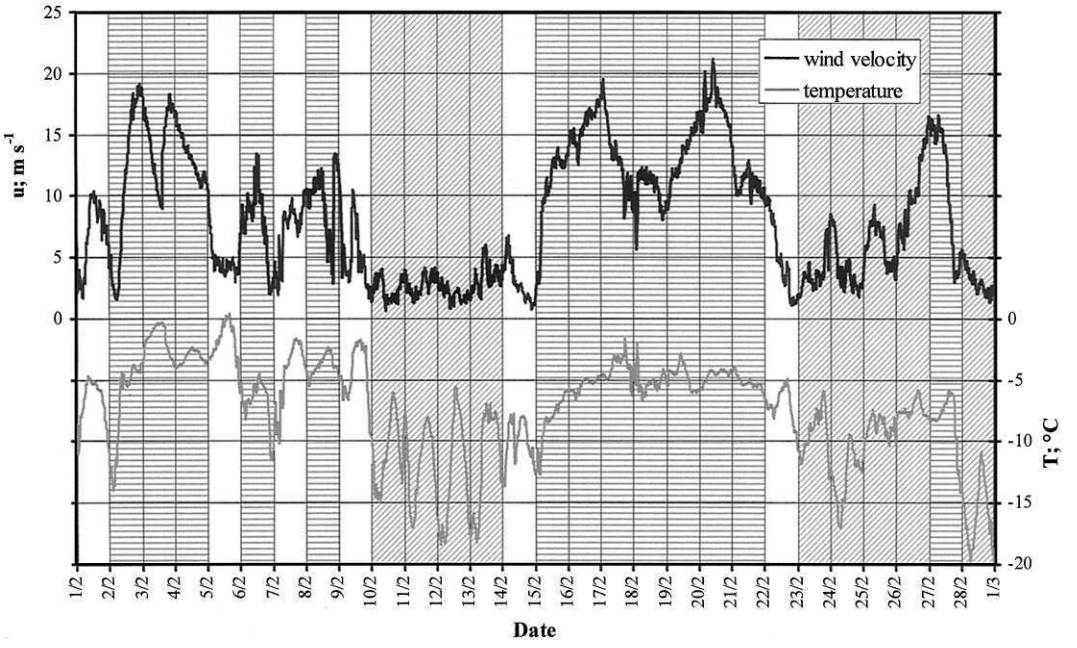

Fig. 2. Time series of air temperature and wind velocity measured at Neumayer station during February 1999. Periods with strong snow drift are indicated by vertically hatched areas; periods with low wind speeds and temperatures by diagonally hatched areas.

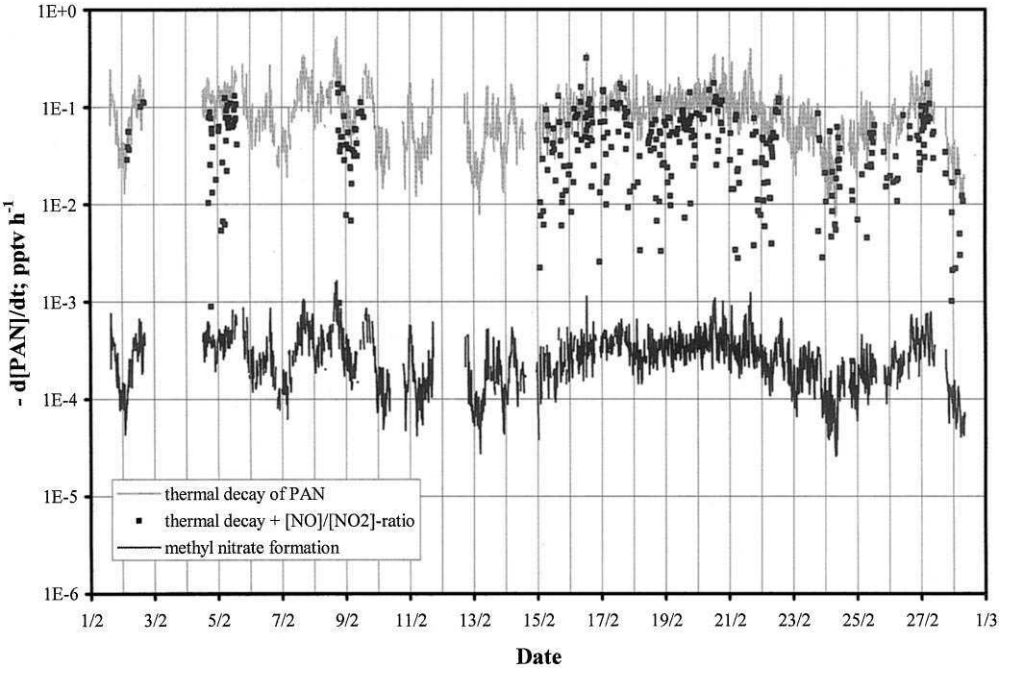

Fig. 3. Calculated PAN decay rates during PEAN'99. The grey line corresponds to the thermal decay calculated using Eq. (1); the squares include thermal decay and $[NO]/[NO_2]$ ratio following Eq. (2); the black line corresponds to simulated methyl formation rates using reaction rate constant given by Senum et al. (1986).

5×10^{-2} pptv h^{-1} during the day with a sun shine duration of 12 h, a total decay of 0.6 pptv d^{-1} may be estimated. This decay is equivalent to the concurrent NO_x production because one additional NO_2 molecule is formed during the decay of a PAN molecule.

Despite of the long lifetime, the observed PAN mixing ratios exhibit a high variability. Jobson et al. (1999) reported variability–lifetime relationships for different regions in the troposphere and the stratosphere. They found a general relationship of the form

$$s_{\ln X} = A\tau^b \tag{3}$$

with $s_{\ln X}$ the standard deviation of the ln of the mixing ratios, τ the lifetime in d, and A and b adjustable parameters. For the PEAN'99 campaign we calculated a standard deviation of the PAN mixing ratio of $s_{\ln[PAN]} = 0.44$ and a mean PAN lifetime of $\tau = 30.3$ d taking into account the thermal decomposition and the NO to NO_2 ratio. Jobson et al. (1999) reported a maximum range of 1.6–4.3 for parameter A for organic compounds observed in remote marine and arctic regions. With these upper and lower limits of A and the measured quantities $s_{\ln[PAN]}$ and τ_{PAN}, we can calculate a range of -0.38 to -0.67 for the exponent b for our study using Eq. (3).

Jobson et al. (1999) demonstrated that the exponent b is correlated to the distance from source regions. The lower limit of $b = -1$ can be expected for a region isolated from any sources like Antarctica, because for this condition the variability results solely from the amount of photochemical degradation in different air masses. In contrast, the estimated range for b in this study is considerably higher. Given that the measured variability $s_{\ln[PAN]}$ is correct, the deviation of the estimated range for b to the expected value of -1 can be explained by a shorter PAN lifetime. The actual PAN lifetime is probably less than the calculated lifetime of 30.3 d due to further reactions of the acetyl peroxy radicals, reactions of PAN with OH and/or PAN photolysis; however, at the earth surface the last two reactions can be neglected (Roberts, 1990). Instead, PAN deposition to the snow surface may be responsible for a significant decrease of the PAN lifetime in the PBL of Antarctica. With the observed PAN variability and the expected parameter $b = -1$, we obtain lifetimes in the range of 4–10 d using values of 1.6 and 4.3 for parameter A in Eq. (3). A PAN flux of $2–5 \times 10^{10}$ molecules m^{-2} s^{-1} is already sufficient to deplete a 100 m thick PBL with a homogeneous PAN mixing ratio of 13 pptv within 4–10 d.

The role of PAN acting as a precursor of NO_x has been investigated for the remote troposphere over the tropical South Atlantic and South Pacific (Heikes et al., 1996; Jacob et al., 1996; Schultz et al., 1999). Although PAN mixing ratios were less than 5 pptv in the marine boundary layers, PAN decomposition accounted for NO_x production rates of a few pptv h^{-1} which was mainly due to the much higher temperatures in tropical latitudes. Further modelling studies have shown that these NO_x production rates were sufficient to establish NO_x mixing ratios of less than 10 pptv. Observations made in the middle to lower summertime troposphere over Alaska have indicated that under certain conditions the thermal decomposition of PAN alone could account for the concurrent measured NO_x abundance in the lower 6-km tropospheric column (Singh et al., 1992b), whereas in other cases the middle tropospheric (4–6 km) abundance of NO_x may have been controlled by the degradation of other organic nitrates due to photolysis or reaction with OH (Jacob et al., 1992).

Assuming the same mechanisms for the oxidation of NO_x in the lower troposphere at higher northern and southern latitudes, the NO_x decay rates can be estimated. Jacob et al. (1992) demonstrated that the main chemical sink is the reaction of NO_2 with OH forming nitric acid HNO_3. For this reaction they found averaged rates of 2 pptv h^{-1} in the lower 1 km of the troposphere over the North American continent. This rate was calculated for a mean NO_x concentration of 25 pptv (Sandholm et al., 1992) which was a factor of 5.7 higher than the NO_x mixing ratios of this study. Therefore, it can be expected that the NO_x decay rates were also lower by the same factor giving a value of approximately 0.35 pptv h^{-1}. This rate is still higher than the maximum NO_x formation rate due to thermal PAN decay (see. Fig. 3), thus indicating that PAN decomposition was probably not sufficient to maintain observed NO_x mixing ratios (Fig. 4). However, global modelling studies (e.g. Wang et al., 1998) show that surface OH concentrations in higher southern latitudes in January can be lower by a factor of 2–4 compared to northern mid-latitudes where PAN decay rates are comparable to NO_x destruction rates (Jacob et al., 1992). Taking into account these uncertainties in the OH mixing ratios during the campaign, the calculation of the NO_x destruction of 0.7 pptv h^{-1} is only a rough estimate. A modelling study using the measured mixing ratios as input parameters is necessary for a more precise comparison.

The appearance of methyl nitrate in the atmosphere has been at least partly attributed to a uni-molecular cyclic decomposition of PAN (Stephens, 1969; Senum et al, 1986; Roberts, 1990) due to the reaction

$$CH_3C(O)OONO_2 \rightarrow CH_3ONO_2 + CO_2. \tag{R5}$$

Although this pathway has been proven to be much less important than it once was thought to be, and may not occur at all (Orlando et al., 1992; Roumelis and Glavas, 1992), we used the rate coefficient reported by Senum et al. (1986) to derive an upper limit for the methyl nitrate formation. The calculated PAN decay rates equivalent to the methyl nitrate formation rates are shown in Fig. 3. Even these upper limits were always less than 10^{-3} pptv h^{-1}. During a former summer campaign at Neumayer, methyl nitrate mixing ratios in the range

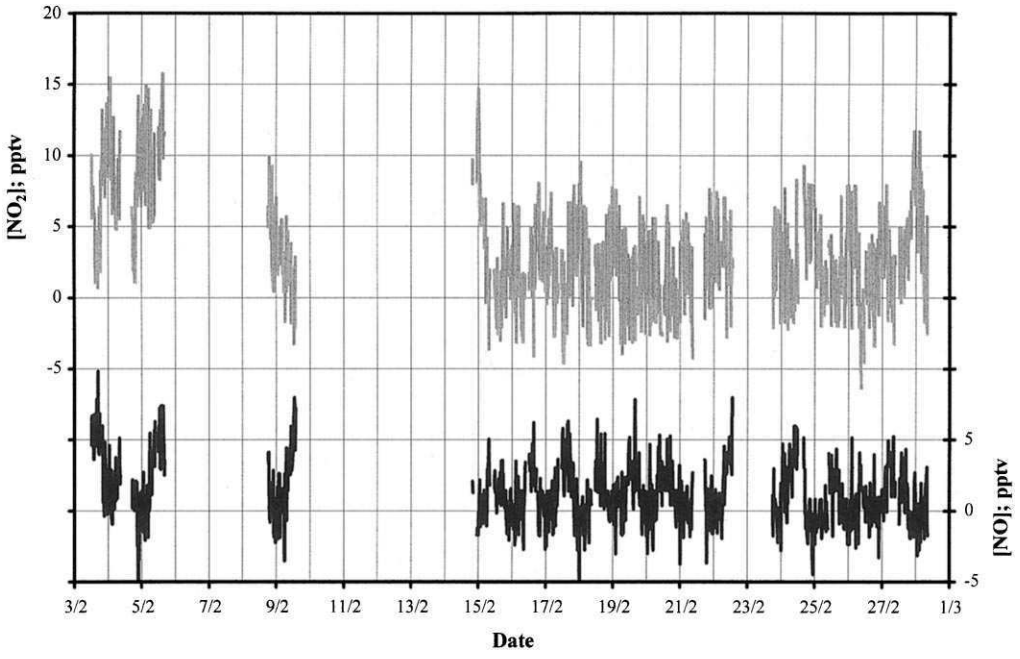

Fig. 4. Time series of NO and NO_2 measured at Neumayer station during PEAN'99.

of 27–46 pptv with a mean concentration of 37 ± 7 pptv have been observed (Jones et al., 1999). These results have been confirmed by alkyl nitrate measurements during this study (Jones et al., 2000b). It can be concluded that the homogeneous formation of methyl nitrate in the gas phase due to reaction (R5) was negligible and other sources like long-range transport or oceanic emissions must be invoked to explain the local budget of methyl nitrate.

3.3. NO_y budget

Another focus of the campaign was to compare PAN concentrations with concentrations of other reactive nitrogen compounds. Therefore, we present additional measurements of HNO_3 and p-NO_3^-. The observed inorganic nitrate concentrations are shown in Fig. 5. The values correspond to mean concentrations for the sampling periods of individual filters represented by horizontal bars. Mixing ratios of HNO_3 and p-NO_3^- were in the range of 1.8–8 pptv and 1.3–11.7 pptv, respectively. Averaged mixing ratios of 4 pptv for both compounds were calculated (see Table 1).

The sum of reactive nitrogen compounds (NO_y) is thought to consist primarily of the sum of NO, NO_2, HONO, HNO_3, HO_2NO_2, NO_3, $2N_2O_5$, PAN and p-NO_3^- (e.g. Sandholm et al., 1994). Other organic nitrates may contribute as well. The distribution of the individual nitrogen-containing species has been subject to several intensive field studies (Bradshaw et al., 1998). The results have shown that in large parts of the troposphere NO_y is dominated by NO_x, PAN and inorganic nitrate, however, their contributions vary systematically. The NO_x contribution is normally highest in regions with strong anthropogenic sources, PAN dominates in rural areas in temperate latitudes with active photochemistry including oxidation of organic compounds or at low temperatures at high northern latitudes and higher altitudes of the northern hemisphere, while the contribution of inorganic nitrate is highest in other remote parts of the troposphere. These variations can be mainly explained by the sources and sinks of the individual species, because the tropospheric lifetimes of PAN and inorganic nitrate are considerably longer compared to other nitrogen containing species like NO_x, NO_3, N_2O_5 or HONO.

Similarly, the mean concentrations of PAN and NO_x observed in this study differ by a factor of 3. This ratio, however, remains highly uncertain taking into account the errors for both values in the low pptv range. Nevertheless, PAN concentrations were higher than NO_x concentrations most of the time of the campaign (Fig. 6). The mean ratio is in reasonable agreement with the PAN to NO_x ratio of 10 pptv to 6 pptv estimated for the campaign in 1997 at Neumayer (Jones et al., 1999). Nevertheless, this ratio is low compared to most of the values reported for Arctic regions. At higher northern latitudes PAN contributed up to 90% of measured NO_y (e.g. Barrie et al., 1989; Solberg et al., 1997) inferring high PAN to NO_x

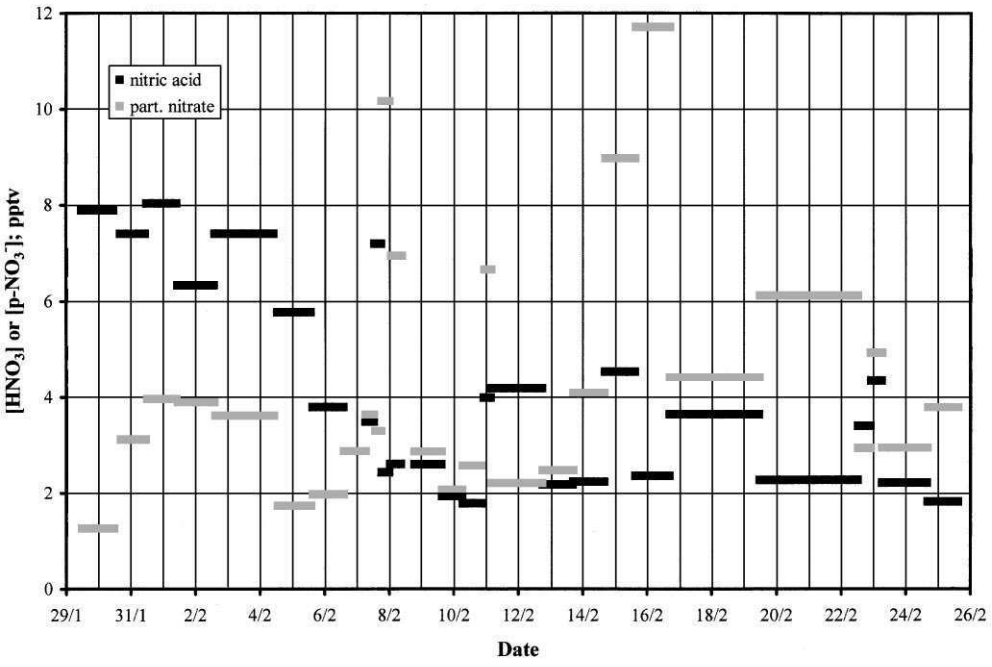

Fig. 5. Time series of HNO_3 and p-NO_3^- measured at Neumayer station during PEAN'99.

Table 1
Summary of mixing ratios (pptv) of individual odd-nitrogen species measured at Neumayer station, during PEAN'99

NO_y (i)	*N*	Minimum	Maximum	Mean	S.D.	Median
PAN	1544	< 5	47.9	13.1[a]	7.3	11.5
NO	977	< 1	9.8	1.2	2.2	1
NO_2	977	< 1	15.7	3.2	3.7	2.8
NO_x[b]	977	< 2	20.2	4.4	3.2	3.8
HNO_3	1867	1.8	8.0	4.0	2.0	3.6
p-NO_3^-	1867	1.3	11.7	4.2	2.4	3.8

[a]Mean value calculated using 2.5 pptv if [PAN] < 5 pptv.
[b]$NO_x = NO + NO_2$.

ratios. However, these high ratios were normally found during early springtime. Due to the negligible photochemical oxidation during the Arctic polar night, organic precursors of PAN are enriched in the Arctic troposphere leading to a significant PAN production of 1–2 pptv h^{-1} in large Arctic areas with increased radiation after polar sunrise (Solberg et al., 1997; Jacobi et al., 1999). According to these processes, PAN mixing ratios in the Arctic exhibit a strong seasonality with highest values during spring and decreasing concentrations during summer (Bottenheim et al., 1994) corresponding to high PAN to NO_x ratios in spring and lower ratios in summer. Thus, mean PAN and NO_x concentrations observed in the lowest 3000 m of the troposphere over the North American high latitudes in July/August 1988 were equal (Bradshaw et al., 1998), probably also as a result of continental NO_x emissions. Compared to these results, the PAN to NO_x ratio in this study was only slightly higher and, therefore, lower than expected taking into account the long distance to continental NO_x source regions. The lower ratio may be at least partly attributed to a photochemical production of NO_x within the firn layer. Additional investigations during PEAN'99 indicated a possible NO_x source strength of 5 pptv d^{-1} in the PBL (Jones et al., 2000a) which is significantly higher than homogeneous NO_x production of 0.6 pptv d^{-1} due to the decay of PAN. Furthermore, the results of this study show that HNO_3 and NO_x concentrations were

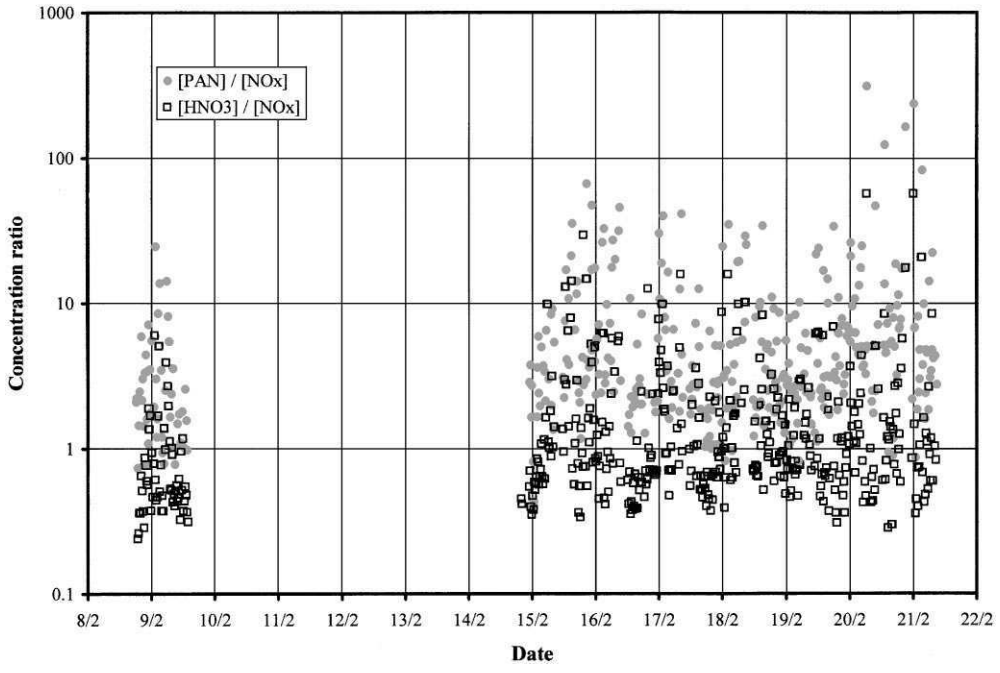

Fig. 6. Temporal variation of PAN to NO_x and HNO_3 to NO_x ratios at Neumayer station during PEAN'99.

comparable during the campaign. Although this ratio is also highly uncertain due to the uncertainties of the measurements, it is still obvious that observed HNO_3 to NO_x ratios were considerably lower than expected from results of modelling studies for remote tropospheric air masses (Chatfield, 1994). Simulated $[HNO_3]/[NO_x]$ ratios are in the range of 15–100 compared to measured ratios rarely exceeding a value of 10 (Fig. 6). A lower ratio compared to simulated values can be due to several processes not included in the model like an additional source of NO_x, an additional sink of inorganic nitrate or a conversion of HNO_3 to NO_x. Chatfield (1994) and Fan et al. (1994) argued that a conversion of HNO_3 in acid aerosols in the presence of formaldehyde could occur in the upper troposphere. However, the low $[HNO_3]/[NO_x]$ ratios are also consistent with a significant emission of NO_x from the firn layer.

3.4. PAN fluxes

Reactive nitrogen compounds can possibly play an important role in air–snow exchange influencing nitrate concentrations in the ice. The knowledge of these processes is crucial for a correct interpretation of nitrate signals in ice cores. Details of the mechanism of the deposition and evaporation of nitrogen containing compounds are still unknown. Singh et al. (1992a) as well as Dibb et al. (1998) speculated that the transfer of PAN can be of great importance for the deposition of nitrate to glaciers in Greenland. PAN deposition could be of similar importance for the Antarctic ice sheet taking into account that PAN contributes significantly to NO_y in higher southern latitudes.

Therefore, we performed consecutive measurements of PAN mixing ratios at two different heights (2.5 and 0.1 m above the snow surface). Due to the analysis time of 10 min for each sample, measurements with a time resolution of 20 min were obtained at both heights linearly interpolated to calculate mixing ratios and differences in the mixing ratios between both heights every 10 min (Fig. 7). The differences exhibited a strong variability within the range of $\pm$ 30 pptv. The average of the difference for the whole campaign was [PAN](2.5 m) − [PAN](0.1 m) = (0.2 $\pm$ 6.6) pptv. It must be noted that due to the precision of the PAN analyser only concentration differences higher than 6 pptv can be resolved.

We further calculated PAN fluxes using the friction velocity u^* which was obtained iteratively from Monin–Obukhov surface layer similarity theory with the following integrated equations:

$$L = \frac{u^{*2}T}{\kappa g T^*}, \tag{4}$$

$$\frac{\kappa u_{10\mathrm{m}}}{u^*} = \ln\left(\frac{z_{10\mathrm{m}}}{z_0}\right) + \alpha_{\mathrm{M}} \cdot \frac{z_{10\mathrm{m}}}{L} \tag{5}$$

$$\frac{\kappa(T_{10\mathrm{m}} - T_{2\mathrm{m}})}{T^*} = \mathrm{Pr}\ln\left(\frac{z_{10\mathrm{m}}}{z_{2\mathrm{m}}}\right) + \alpha_{\mathrm{T}}\, z_{10\mathrm{m}} - \frac{z_{2\mathrm{m}}}{L} \tag{6}$$

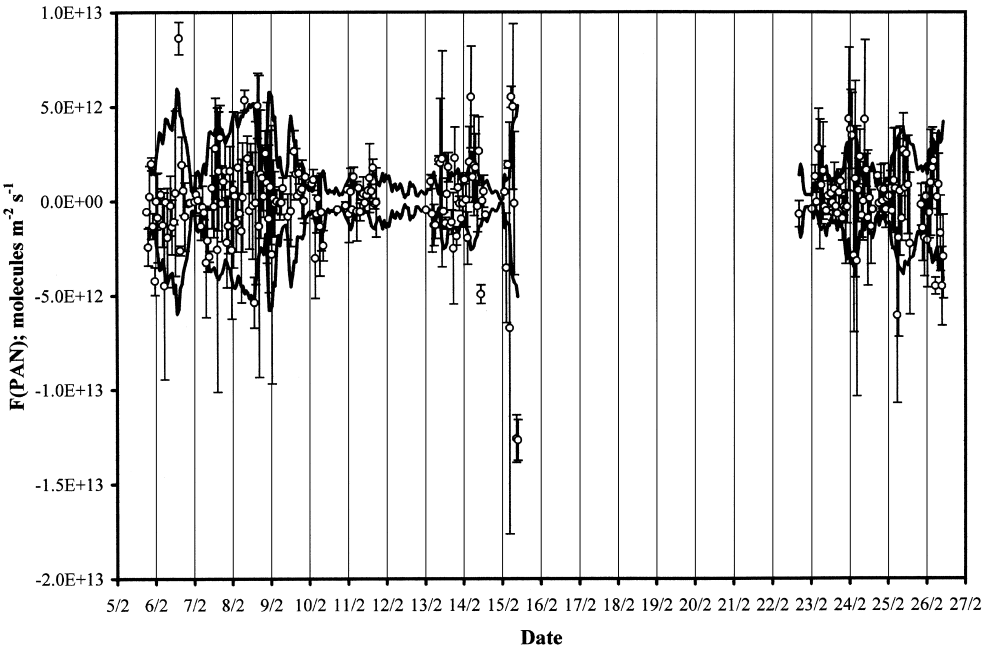

Fig. 7. Calculated 1-h-means of PAN fluxes during PEAN'99. Error bars indicate calculated standard deviations. Positive values correspond to fluxes from the atmosphere to the snow. The lines show the range of fluxes calculated with PAN concentration differences of $\pm$ 6 pptv.

with L being the Monin–Obukhov length; T the mean temperature; κ the von Karmans constant ($= 0.40$); T^* the scaling temperature; u the wind speed; z/L the stability parameter; z_0 the aerodynamic roughness length; and Pr the turbulent Prandtl number ($= 0.83$). Prandtl number, roughness length and the empirical constants α_M and α_T have been obtained from measurements at Halley station for typical conditions in Antarctica (King and Anderson, 1994). The values of $Pr = 0.83$, $z_0 = 5.6 \cdot 10^{-5}$ m, $\alpha_M = 5.7$ and $\alpha_T = 4.6$ were also applied for the calculations in this study. Moreover, the Monin–Obukhov length provides a measure of the stability of the surface layer. While the calculation of u^* is only applicable at unstable ($L < 0$) and neutral conditions ($L \gg 0$), values of u^* were rejected if $0 \leqslant L \leqslant 4$ m. PAN fluxes F(PAN) were calculated using the following equation:

$$F(\mathrm{PAN}) = \kappa u^* z \frac{[\mathrm{PAN}]_{2.5\mathrm{m}} - [\mathrm{PAN}]_{0.1\mathrm{m}}}{\Delta z} \qquad (7)$$

with z being the logarithmic mean of the measuring heights ($= 0.5$ m) and $\Delta z = 2.5$–0.1 m $= 2.4$ m.

Fig. 7 shows the time series of the averaged 1-h-means of the PAN fluxes. In this case, positive values correspond to fluxes from the atmosphere to the snow and vice versa. Like the concentration differences, a great deal of variability is present in the calculated PAN fluxes and regular variations were not observed. Moreover, almost all of the values are within the range given by the uncertainty of the PAN concentration measurements. Fig. 7 also shows the upper and lower limit of the PAN flux calculated with concentration differences of $[\mathrm{PAN}]_{2.5\mathrm{m}} - [\mathrm{PAN}]_{0.1\mathrm{m}} = \pm 6$ pptv. Therefore, no predominant direction of the PAN flux can be given. The results can only be used to estimate limits of the PAN exchange between the troposphere and the underlying snow pack. Except for three outliers on 15 February, all values including the standard deviations are within the range of $\pm 1 \times 10^{13}$ molecules m^{-2} s^{-1}. The averaged PAN flux was -4×10^{10} molecules m^{-2} s^{-1} and was more than two orders of magnitude lower than the limits of the observed range. Overall, it appears that if there was any PAN transfer, it was considerably less than the limits of $\pm 1 \times 10^{13}$ molecules m^{-2} s^{-1}.

Compared to NO_y fluxes observed at Summit, Greenland (Dibb et al., 1998) the calculated upper limit for PAN fluxes for this study is one order of magnitude lower. Arctic PAN mixing ratios, however, are considerably higher than in Antarctica resulting in higher fluxes between atmosphere and ice under same conditions. On the other hand, the limit is still two orders of magnitude higher than the production rate of NO and NO_2 of 9×10^{10} molecules m^{-2} s^{-1} observed in Antarctic snow (Jones et al., 2000). Additionally, a PAN flux of 5×10^{10} molecules m^{-2} s^{-1} would lead to a PAN lifetime of less

than 10 d due to deposition assuming a 100 m thick PBL with a homogenous PAN concentration of 13 pptv. This lifetime is much shorter than the value calculated for homogeneous PAN decomposition and is in much better agreement with the variability–lifetime relationship of PAN.

4. Conclusions

Although the observed mean PAN concentrations in Antarctica of 13 pptv are in good agreement with the results of global modelling studies, PAN is less important in tropospheric nitrogen chemistry at higher southern latitudes compared to other remote tropospheric regions probably due to its long chemical lifetime even in the Antarctic PBL. Moreover, even though PAN concentrations were sometimes higher than model predictions and were high compared to concentrations of NO_x and inorganic nitrate, homogeneous PAN decomposition is probably not an important source of photochemically active nitrogen compounds. Consequently, further modelling studies are necessary to investigate the role of PAN in tropospheric photochemistry at higher southern latitudes.

Despite the fact that this investigation of PAN fluxes between the atmosphere and snow using the gradient method was limited by the analyser's precision, resulting in a lower limit of verifiable fluxes of $\pm 1 \times 10^{13}$ molecules m^{-2} s^{-1}, even significantly lower PAN fluxes can be of importance for the exchange of nitrogen-containing compounds between the atmosphere and the surface snow in Antarctica. The variability of the PAN concentrations which is considerably higher than expected for a long living trace gas in a remote tropospheric region could be explained by the rapid deposition of PAN onto the ice shield. Further measurements with higher resolution and precision are necessary to investigate if PAN fluxes between the atmosphere and snow can be important either for the exchange of nitrogen-containing compounds between the atmosphere and ice or for the PAN destruction and formation in the PBL of Antarctica.

While it can be assumed that long-range transport enhances PAN concentrations considerably above the mean concentration, PAN deposition onto the snow surface may be crucial for the determination of PAN lifetimes in the PBL. Further investigations are necessary to quantify both processes because of their potential to influence the PAN budget in high southern latitudes, thus altering the role of a major contributor of NO_y in a vast area.

Acknowledgements

The authors thank the scientists and technicians of the Neumayer overwintering crews of the years 1998/1999 and 1999/2000 for their assistance. Moreover, we thank the two anonymous reviewers for their helpful comments on the manuscript. The trajectories have been provided by the German Weather Service (DWD). This research was partially supported by grants from the Deutscher Akademischer Austauschdienst (DAAD) and the British Research Council (BRC). This paper is contribution No. 1690 of the Alfred Wegener Institute for Polar and Marine Research.

References

Barrie, L.A., den Hartog, G., Bottenheim, J.W., Landsberger, S., 1989. Anthropogenic aerosols and gases in the lower troposphere at Alert Canada in April 1986. Journal of Atmospheric Chemistry 9, 101–127.

Beine, H.J., Jaffe, D.A., Blake, D.R., Atlas, E., Harris, J., 1996. Measurements of PAN, alkyl nitrates, ozone, and hydrocarbons during spring in interior Alaska. Journal of Geophysical Research 101, 12613–12619.

Bottenheim, J.W., Gallant, A.J., 1989. PAN over the Arctic, observations during AGASP-2 in April 1986. Journal of Atmospheric Chemistry 9, 301–316.

Bottenheim, J.W., Gallant, A.J., Brice, K.A., 1986. Measurements of NO_y species and O_3 at 82°N latitude. Geophysical Research Letters 13, 113–116.

Bottenheim, J.W., Barrie, L.A., Atlas, E., 1993. The partitioning of nitrogen oxides in the lower Arctic troposphere during spring 1988. Journal of Atmospheric Chemistry 17, 15–27.

Bottenheim, J.W., Sirois, A., Brice, K.A., Gallant, A.J., 1994. Five years of continuous observations of PAN and ozone at a rural location in eastern Canada. Journal of Geophysical Research 99, 5333–5352.

Bradshaw, J., Sandholm, S., Talbot, R., 1998. An update on reactive odd-nitrogen measurements made during recent NASA Global Tropospheric Experiment programs. Journal of Geophysical Research 103, 19129–19148.

Bridier, I., Caralp, F., Loirat, H., Lesclaux, R., Veyret, B., Becker, K.H., Reimer, A., Zabel, F., 1991. Kinetic and theoretical studies of the reactions $CH_3C(O)O_2 + NO_2 + M \leftrightarrow CH_3C(O)O_2NO_2 + M$ between 248 and 393 K and between 30 and 760 Torr. Journal of Physical Chemistry 95, 3594–3600.

Carroll, M.A., Thompson, A.M., 1995. NO_x in the non-urban troposphere. In: Barker, J.R. (Ed.), Progress and Problems in Atmospheric Chemistry. World Scientific, Singapore, pp. 198–255.

Chatfield, R.B., 1994. Anomalous HNO_3/NO_x ratio of remote tropospheric air: conversion of nitric acid to formic acid and NO_x? Geophysical Research Letters 21, 2705–2707.

DeMore, W.B., Sander, S.P., Golden, D.M., Hampson, R.F., Kurylo, M.J., Howard, C.J., Ravishankara, A.R., Kolb, C.E., Molina, M.J., 1997. Chemical kinetics and photochemical data for use in stratospheric modeling. Evaluation 12, Jet Propulsion Laboratory, Pasadena.

Dibb, J.E., Talbot, R.W., Munger, J.W., Jacob, D.J., Fao, S.-M., 1998. Air–snow exchange of HNO_3 and NO_y at summit. Greenland. Journal of Geophysical Research 103, 3475–3486.

Fan, S.-M., Jacob, D.J., Mauzerall, D.L., Bradshaw, J.D., Sandholm, S.T., Blake, D.R., Singh, H.B., Talbot, R.W., Gregory, G.L., Sachse, G.W., 1994. Origin of tropospheric NO_x over subarctic eastern Canada in summer. Journal of Geophysical Research 99, 16867–16877.

Heikes, B., Lee, M., Jacob, D., Talbot, R., Bradshaw, J., Singh, H., Blake, D., Anderson, B., Fuelberg, H., Thompson, A.M., 1996. Ozone, hydroperoxides, oxides of nitrogen and hydrocarbon budgets in the marine boundary layer over the South Atlantic. Journal of Geophysical Research 101, 24221–24234.

Jacob, D.J., Wofsy, S.C., Bakwin, P.S., Fan, S.-M., Harriss, R.C., Talbot, R.W., Bradshaw, J.D., Sandholm, S.T., Singh, H.B., Browell, E.V., Gregory, G.L., Sachse, G.W., Shipham, M.C., Blake, D.R., Fitzjarrald, D.R., 1992. Summertime photochemistry of the troposphere at high northern latitudes. Journal of Geophysical Research 97, 16421–16431.

Jacob, D.J., Heikes, B.G., Fan, S.-M., Logan, J.A., Mauzerall, D.L., Bradshaw, J.D., Singh, H.B., Gregory, G.L., Talbot, R.W., Blake, D.R., Sachse, G.W., 1996. Origin of ozone and NO_x in the tropical troposphere: a photochemical analysis of aircraft observations over the South Atlantic basin. Journal of Geophysical Research 101, 24235–24250.

Jacobi, H.-W., Schrems, O., 1999. Peroxyacetyl nitrate (PAN) distribution over the South Atlantic Ocean. Physical Chemistry Chemical Physics 1, 5517–5521.

Jacobi, H.-W., Weller, R., Bluszcz, T., Schrems, O., 1999. Latitudinal distribution of peroxyacetyl nitrate (PAN) over the Atlantic Ocean. Journal of Geophysical Research 104, 26901–26912.

Jaffe, D.A., Berntsen, T.K., Isaksen, I.S.A., 1997. A global three-dimensional chemical transport model: 2. Nitrogen oxides and nonmethane hydrocarbon results. Journal of Geophysical Research 102, 21281–21296.

Jobson, J.T., McKeen, S.A., Parrish, D.D., Fehsenfeld, F.C., Blake, D.R., Goldstein, A.H., Schauffler, S.M., Elkins, J.W., 1999. Trace gas mixing ratio variability versus lifetime in the troposphere and stratosphere: observations. Journal of Geophysical Research 104, 16113–16901.

Jones, A.E., Weller, R., Minikin, A., Wolff, E.W., Sturges, W.T., McIntyre, H.P., Leonard, S.R., Schrems, O., Baugitte, S., 1999. Oxidized nitrogen chemistry and speciation in the Antarctic troposphere. Journal of Geophysical Research 104, 21355–21366.

Jones, A.E., Weller, R., Wolff, E.W., Jacobi, H.-W., 2000a. Speciation and rate of photochemical NO and NO_2 production in Antarctic snow. Geophysical Research Letters 27, 345–348.

Jones, A.E., McIntyre, H., Sturges, W., Weller, R., Wolff, E.W., Jacobi, H.-W., Mulvaney, R., 2000b. Methyl nitrate at Neumayer, Antarctica – Signal of diurnal variability? in preparation.

King, J.C., Anderson, P.S., 1994. Heat and vapour fluxes and scalar roughness lengths over an Antarctic ice shelf. Boundary Layer Meteorology 69, 101–121.

Kleindienst, T.E., 1994. Recent developments in the chemistry and biology of peroxyacetyl nitrate. Research of Chemical Intermediates 20, 335–384.

Moxim, W.J., Levy II, H., Kasibhatla, P.S., 1996. Simulated global tropospheric PAN: its transport and impact on NO_x. Journal of Geophysical Research 101, 12621–12638.

Müller, K.P., Rudolph, J., 1992. Measurements of peroxyacetylnitrate in the marine boundary layer over the Atlantic. Journal of Atmospheric Chemistry 15, 361–367.

Munger, J.W., Jacob, D.J., Fan, S.-M., Colman, A.S., Dibb, J.E., 1999. Concentrations and snow-atmosphere fluxes of reactive nitrogen at Summit. Greenland. Journal of Geophysical Research 104, 13721–13734.

Muthuramu, K., Shepson, P.B., Bottenheim, J.W., Jobson, B.T., Niki, H., Anlauf, K.G., 1994. Relationships between organic nitrates and surface ozone destruction during Polar Sunrise Experiment 1992. Journal of Geophysical Research 99, 25369–25378.

Orlando, J.J., Tyndall, G.S., Calvert, J.G., 1992. Thermal decomposition pathways for peroxyacetyl nitrate (PAN): Implications for atmospheric methyl nitrate levels. Atmospheric Environment 26A, 3111–3118.

Roberts, J.M., 1990. The atmospheric chemistry of organic nitrates. Atmospheric Environment 24A, 243–287.

Roumelis, N., Glavas, S., 1992. Thermal decomposition of peroxyacetyl nitrate in the presence of O_2, NO_2 and NO. Monatshefte der Chemie 123, 63–72.

Rudolph, J., Vierkorn-Rudolph, B., Meixner, F.X., 1987. Large-scale distribution of peroxyacetylnitrate results from the STRATOZ III flights. Journal of Geophysical Research 92, 6653–6661.

Sandholm, S.T., Bradshaw, J.D., Chen, G., Singh, H.B., Talbot, R.W., Gregory, G.L., Blake, D.R., Sachse, G.W., Browell, E.V., Barrick, J.D.W., Shipham, M.A., Bachmeier, A.S., Owen, D., 1992. Summertime tropospheric observations related to N_xO_y distributions and partitioning over Alaska: Arctic Boundary Layer Expedition 3A. Journal of Geophysical Research 97, 16481–16509.

Sandholm, S., Olsen, J., Bradshaw, J., Talbot, R., Singh, H., Gregory, G., Blake, D., Anderson, B., Sachse, G., Barrick, J., Collins, J., Klemm, K., Lefer, B., Klemm, O., Gorzelska, K., Herlth, D., O'Hara, D., 1994. Summertime partitioning and budget of NO_y compounds in the troposphere over Alaska and Canada: ABLE 3B. Journal of Geophysical Research 99, 1837–1861.

Schrimpf, W., Müller, K.P., Johnen, F.J., Lienaerts, K., Rudolph, J., 1995. An optimized method for airborne peroxyacetyl nitrate (PAN) measurements. Journal of Atmospheric Chemistry 22, 303–317.

Schultz, M.G., Jacob, D.J., Wang, Y., Logan, J.A., Atlas, E.T., Blake, D.R., Blake, N.J., Bradshaw, J.D., Browell, E.V., Fenn, M.A., Flocke, F., Gregory, G.L., Heikes, B.G., Sachse, G.W., Sandholm, S.T., Shetter, R.E., Singh, H.B., Talbot, R.W., 1999. On the origin of tropospheric ozone and NO_x over the tropical South Pacific. Journal of Geophysical Research 104, 5829–5843.

Senum, G.I., Fajer, R., Gaffney, J.S., 1986. Fourier transform infrared spectroscopic study of the thermal stability of peroxyacetyl nitrate. Journal of Physical Chemistry 90, 152–156.

Seinfeld, J.H. and Pandis, S.N., 1998. Atmospheric Chemistry and Physics, 1st Edition. Wiley, New York.

Singh, H.B., Salas, L.J., Viezee, W., 1986. Global distribution of peroxyacetyl nitrate. Nature 321, 588–591.

Singh, H.B., O'Hara, D., Herlth, D., Bradshaw, J.D., Sandholm, S.T., Gregory, G.L., Sachse, G.W., Blake, D.R., Crutzen, P.J., Kanakidou, M.A., 1992a. Atmospheric measurements of peroxyacetyl nitrate and other organic nitrates at high latitudes:

possible sources and sinks. Journal of Geophysical Research 97, 16511–16522.

Singh, H.B., Herlth, D., O'Hara, D., Zahnle, K., Bradshaw, J.D., Sandholm, S.T., Talbot, R., Crutzen, P.J., Kanakidou, M., 1992b. Relationship of peroxyacetyl nitrate to active and total odd nitrogen at northern high latitudes: influence of reservoir species on NO_x and O_3. Journal of Geophysical Research 97, 16523–16530.

Singh, H.B., Herlth, D., O'Hara, D., Zahnle, K., Bradshaw, J.D., Sandholm, S.T., Talbot, R., Gregory, G.L., Sachse, G.W., Blake, D.R., Wofsy, S.C., 1994. Summertime distribution of PAN and other reactive nitrogen species in the northern high-latitude atmosphere of eastern Cananda. Journal of Geophysical Research 99, 1821–1835.

Singh, H.B., Herlth, D., Kolyer, R., Chatfield, R., Viezee, W., Salas, L.J., Chen, Y., Bradshaw, J.D., Sandholm, S.T., Talbot, R., Gregory, G.L., Anderson, B., Sachse, G.W., Browell, E., Bachmeier, A.S., Blake, D.R., Heikes, B., Jacob, D., Fuelberg, H.E., 1996. Impact of biomass burning emissions on the composition of the South Atlantic troposphere: reactive nitrogen and ozone. Journal of Geophysical Research 101, 24203–24219.

Singh, H.B., Viezee, W., Chen, Y., Thakur, A.N., Kondo, Y., Talbot, R.W., Gregory, G.L., Sachse, G.W., Blake, D.R., Bradshaw, J.D., Wang, Y., Jacob, D.J., 1998. Latitudinal distribution of reactive nitrogen in the free troposphere over the Pacific Ocean in late winter/early spring. Journal of Geophysical Research 103, 28237–28246.

Singh, H.B., Viezee, W., Chen, Y., Bradshaw, J., Sandholm, S., Blake, D., Blake, N., Heikes, B., Snow, J., Talbot, R., Browell, E., Gregory, G., Sachse, G., Vay, S., 2000. Biomass burning influences on the composition of the remote South Pacific troposphere: analysis based on observations from PEM-Tropics-A. Atmospheric Environment 34, 635–644.

Solberg, S., Krognes, T., Stordal, F., Hov, O., Beine, H.J., Jaffe, D.A., Clemitshaw, K.C., Penkett, S.A., 1997. Reactive nitrogen compounds at Spitsbergen in the Norwegian Arctic. Journal of Atmospheric Chemistry 28, 209–255.

Stephens, E.R., 1969. The formation, reactions, and properties of peroxyacyl nitrates (PANs) in photochemical air pollution. Advances in Environmental Science and Technology 1, 119–146.

Talbot, R.W., Dibb, J.E., Scheuer, E.M., Kondo, Y., Koike, M., Singh, H.B., Salas, L.B., Fukui, Y., Ballenthin, J.O., Meads, R.F., Miller, T.M., Hunton, D.E., Viggiano, A.A., Blake, D.R., Blake, N.J., Atlas, E., Flocke, F., Jacob, D.J., Jaegle, L., 1999. Reactive nitrogen budget during the NASA SONEX mission. Geophysical Research Letters 26, 3057–3060.

Wagenbach, D., Görlach, U., Moser, K., Münnich, K.O., 1988. Coastal Antarctic aerosol: the seasonal pattern of its chemical composition and radionuclide content. Tellus 40B, 426–436.

Wang, Y., Logan, J.A., Jacob, D.J., 1998. Global simulation of tropospheric O_3–NO_x–hydrocarbon chemistry, 2. Model evaluation and global ozone budget. Journal of Geophysical Research 103, 10727–10755.

Warneck, P., Zerbach, T., 1992. Synthesis of peroxyacetyl nitrate in air by acetone photolysis. Environmental Science and Technology 26, 74–79.

Publication 3.1.4

Fischer, R., R. Weller, H.-W. Jacobi, and K. Ballschmiter,

Levels and pattern of volatile organic nitrates and halocarbons in the air at Neumayer Station (70°S), Antarctic,

Chemosphere **48**, 981-992, 2002.

PERGAMON

Chemosphere 48 (2002) 981–992

CHEMOSPHERE

www.elsevier.com/locate/chemosphere

Levels and pattern of volatile organic nitrates and halocarbons in the air at Neumayer Station (70°S), Antarctic

Ralf Fischer [a,1], Rolf Weller [b], Hans-Werner Jacobi [b,2], Karlheinz Ballschmiter [a,*]

[a] *Department of Analytical and Environmental Chemistry, University of Ulm, Albert-Einstein-Allee 11, D-89081 Ulm, Germany*
[b] *Alfred-Wegener-Institute for Polar and Marine Research, Am Handelshafen 12 D-27570 Bremerhaven, Germany*

Received 13 February 2001; received in revised form 14 February 2002; accepted 28 February 2002

Abstract

Levels and patterns of C1–C4/C9 organic nitrates were measured for the first time in Antarctica. The sampling was done by adsorptive enrichment on Tenax TA followed by thermodesorption cold-trap high resolution capillary gas chromatography with electron capture detection. 2–70 l air on-column have been analyzed this way. C1–C9 alkyl mononitrates, C2–C4 alkyl dinitrates, C2–C4 hydroxy alkyl nitrates, and halocarbons could be identified in air samples collected near the German Neumayer Research Station, Antarctica, in February 1999. Volatile biogenic and anthropogenic halocarbons were used to assess the origin of the air parcels analyzed. The average concentration measured for $\sum$C2–C6 alkyl nitrates was in the range of 9.2 ± 1.8 ppt(v), while the sum of the mixing ratios of six C2–C4 hydroxy alkyl nitrates was in the range of 1.1 ± 0.2 ppt(v). Moreover, C2–C4 alkyl dinitrates were found at levels near the detection limit of 0.1–0.5 ppt(v). The concentrations of organic nitrates found in Antarctic air represent ultimate baseline levels due to chemical and physical loss processes during long-range transport in the air. The South Atlantic and the Antarctic Ocean as a general secondary source for organic nitrates in terms of an air/sea exchange equilibrium has to be evaluated yet, but it seems logical. Our results confirm the common assumption that there are no biogenic marine sources of C2–C9 organonitrates. We have found a level of >80 ppt(v) for methyl nitrate. This level if it can be confirmed in a systematic survey requires a strong biogenic source of methyl nitrate in the Antarctic Ocean.

Keywords: Alkyl mononitrates; Methyl nitrate; Hydroxy alkyl nitrates; Alkyl dinitrates; Air; Antarctica; Thermal desorption; Capillary gas chromatography; Baseline levels; Long-range transport

1. Introduction

The troposphere has to be considered in general as an oxidative medium with the tendency for species to be converted to a more oxidized state. The results of the light induced photochemistry and oxidation chemistry of hydrocarbons in air depend on the levels of the reaction of starting radicals such as OH, or NO_3, and on the levels of trace gases like odd-nitrogen NO_y, (particularly NO_x ($NO + NO_2$) as main part), ozone, and organosulfur compounds (Atlas et al., 1992a,b; Carroll et al., 1992; Barrie et al., 1994; Kondo et al., 1997; Platt

* Corresponding author. Tel.: +49-731-502-2750; fax: +49-731-502-2763.
E-mail address: karlheinz.ballschmiter@chemie.uni-ulm.de (K. Ballschmiter).
[1] Present address: Dr. Th. Böhme KG, Isardamm 79-83, D-82538 Geretsried.
[2] Present address: Department of Hydrology and Water Research, 1133 E. North Campus Dr., University of Arizona, Tucson, AZ 85721-0011, USA.

0045-6535/02/$ - see front matter
PII: S0045-6535(02)00110-8

and Le Bras, 1997). As a result of combustion emissions, levels of NO_x greatly enhanced over those in the background troposphere can be found in urban and densely inhabited continental areas. NO_x is the key in the organonitrogen chemistry of the urban troposphere. When NO and NO_2 are present in sunlight, ozone formation occurs as a result of photolysis of NO_2 at wavelength $\lambda < 424$ nm.

$$NO_2 + h\nu \rightarrow NO + O(^3P) \quad (1)$$

$$O(^3P) + O_2 + M \rightarrow O_3 + M^{\ddagger} \quad (2)$$

On the other hand, ozone reacts with NO to regenerate NO_2.

$$O_3 + NO \rightarrow NO_2 + O_2 \quad (3)$$

Therefore the steady-state ozone concentration is approximated by Eq. (4)

$$[O_3] = \frac{J_1[NO_2]}{k_3[NO]} \quad (4)$$

Expression (4) is named the *photostationary state relation*. The ozone concentration is in a first approximation proportional to the NO_2/NO ratio, which means high NO_2 levels lead to high ozone concentrations. Conversion of NO to NO_2 by HO_2 or peroxyalkyl radicals (7a) will lead to increases in ozone and deviation from Eq. (4).

Members of the NO_y pool are also involved in these processes by increasing or reducing NO_x levels in the air. Alkyl nitrates as parts of the NO_y pool are therefore of potential interest.

Alkyl nitrates besides being compounds of the atmospheric chemistry are used as propellants, and explosives (Köhler and Meyer, 1995). Together with the alkyl nitrites they are a group of potent pharmaceuticals, e.g. isosorbid dinitrate is a powerful vasodilator (Ahlner et al., 1991). None of the technical and pharmaceutical uses leads however to a general environmental contamination. Local contaminations by explosives may occur.

The source of alkyl nitrates in the troposphere is the conversion of hydrocarbons (Fraser et al., 1997). OH/O_2 (5a) or NO_3/O_2 (5b) attack on an aliphatic carbon–hydrogen or an olefinic C=C bond forms peroxyalkyl radicals RO_2 (6). They are also formed by a thermolysis/O_2 reaction (5c) of long chain alkoxy radicals and by the photolysis (5d) of carbonyl compounds followed by the addition of O_2. The reaction of peroxyalkyl radicals with NO leads to nitrogen dioxide and alkoxy radicals—finally stabilizing as carbonyl compounds (7a) and (7b)—or in a side reaction to alkyl nitrates (reactions (7c)) (Atkinson et al., 1982; Finlayson-Pitts and Pitts, 1986; Atkinson, 1990; Seinfeld and Pandis, 1998).

- Formation of alkyl radicals (initial step):

$$RH + OH^{\cdot} \rightarrow R^{\cdot} + H_2O \quad (5a)$$

$$RH + NO_3^{\cdot} \rightarrow R^{\cdot} + HNO_3 \quad (5b)$$

$$R'RHC\text{–}O^{\cdot} + \Delta \rightarrow R^{\cdot} + R'HC{=}O \quad (5c)$$

$$R'(C{=}O)R + h\nu \rightarrow R^{\cdot} + {\cdot}R'C{=}O \quad (5d)$$

- Formation of peroxyalkyl radicals:

$$R^{\cdot} + O_2(+M) \rightarrow RO_2^{\cdot}(+M^{\ddagger}) \quad (6)$$

- Formation of stable products:

$$RO_2^{\cdot} + NO \rightarrow RO^{\cdot} + NO_2 \quad (7a)$$

$$RO^{\cdot} + O_2 \rightarrow R_1R_2CO + HO_2 \quad (7b)$$

$$RO_2^{\cdot} + NO(+M) \rightarrow (RO_2NO)(+M^{\ddagger}) \rightarrow RONO_2 \quad (7c)$$

This reaction scheme may repeat itself with alkyl nitrates leading finally to carbonyl alkyl nitrates or to non-vicinal alkyl dinitrates.

The reaction of alkenes with either ·OH during daytime or with $NO_3^{\cdot}$ during nighttime in the presence of NO_x leads to the formation of multifunctional organic nitrates like hydroxy alkyl nitrates or alkyl dinitrates (O'Brien et al., 1995; O'Brien et al., 1997; Kastler and Ballschmiter, 1998; Kastler and Ballschmiter, 1999). Moreover, organic nitrates formed by the reaction of isoprene have recently been reported (Werner et al., 1999). A detailed summary of the reaction schemes leading to alkyl nitrates is given by Roberts (Roberts, 1990).

The yield of alkyl nitrates in the branching of the reaction of a peroxyalkyl radical with NO (7c) increases from <0.014 for ethane to 0.33 for octane. Thus a wide range of homologues and isomeric alkyl nitrates is expected in the atmosphere. The decreasing concentrations of long-chain alkanes are partly offset by the increased yields of alkyl nitrate formation (Atkinson et al., 1982; Schneider et al., 1998a).

While for alkyl mononitrates $\leqslant$C5 the dominant loss process is photolysis (8) (Clemitshaw et al., 1997), alkyl nitrates with more than five C-atoms and multifunctional alkyl nitrates are mainly degraded by OH radicals (9) (Talukdar et al., 1997).

- Atmospheric chemistry of alkyl nitrates

$$RONO_2 + h\nu \rightarrow RO^{\cdot} + NO_2^{\cdot} \quad (8)$$

$$RONO_2 + OH^{\cdot} \rightarrow \text{multifunctional nitrates, polar products} \quad (9)$$

In continental air alkyl nitrates contribute 2% to the NO_y budget, increasing up to 15% for marine air (Atlas et al., 1992a,b). They are a sink of the NO_y pool par-

ticularly during polar winters. Thus, in arctic air masses the alkyl nitrates can enrich up to 20% of the total NO_y budget (Bottenheim et al., 1993). Photodegradation of alkyl nitrates results in the formation of NO_x. They can act as an important NO_x source in the polar regions with highest release rates of NO_x during polar sunrise.

Since the first measurements of alkyl nitrates in the marine atmosphere 1988 by Atlas (Atlas, 1988), this class of compounds found increasing interest. Several studies took place in the USA, Canada and Germany. Moreover field campaigns took place in the Pacific air (equatorial and Hawaiian region) and the Atlantic air on board RV "Meteor" (Schneider and Ballschmiter, 1999) and RV "Polarstern" (Fischer et al., 2000). In spite of increasing activities in this field of atmospheric chemistry the number of studies in polar regions is limited.

Concentrations in the low ppt(v) range were found for the North Pacific air by Atlas (Atlas et al., 1992a,b; Atlas et al., 1993). Roberts measured concentrations of 14 ± 8.3 ppt(v) for $\sum$C1–C4 alkyl nitrates at Chebogue Point, Nova Scotia (Roberts et al., 1998). de Kock found mean concentrations of 17.5 ± 8.4 ppt(v) for C3–C5 alkyl nitrates at the South African southeast coast (de Kock and Anderson, 1994). More recently Schneider reported levels of 3–8 ppt(v) for $\sum$C3–C5 alkyl nitrates for the South Atlantic air (Schneider, 1998a,b; Schneider and Ballschmiter, 1999). Fischer reported a mean concentration of 1.7 ppt(v) for $\sum$C4 + C5 alkyl nitrates for the North Atlantic air and 1.3 ppt(v) for $\sum$C4 + C5 for the South Atlantic air (Fischer, 1999; Fischer et al., 2000). Fischer gives a global overview on the levels of short chain alkyl nitrates at different continental and marine sampling sites (Fischer and Ballschmiter, 2001).

O'Brien reported 1995 for the first time the occurrence of four alkyl hydroxy nitrates and one alkyl dinitrate (O'Brien et al., 1995; O'Brien et al., 1997). Recently additional hydroxy alkyl nitrates and 30 alkyl dinitrates were identified in urban air (Kastler and Ballschmiter, 1998; Kastler and Ballschmiter, 1999; Fischer et al., 2000).

We believe to be the first to present in this work levels and patterns of higher organic nitrates in the lower troposphere of the Antarctic. Furthermore we compare the occurrence of alkyl nitrates with the levels of halocarbons as atmospheric markers. A comparison with values obtained in South Atlantic air places the Antarctic data in a greater spatial context.

2. Short hand nomenclature of organic nitrates

Schneider and Ballschmiter recently introduced a shorthand nomenclature of alkyl mononitrates that correlates the structure of a specific alkyl nitrate to the hydrocarbon precursor (Schneider and Ballschmiter, 1996). In our extended shorthand nomenclature the expression organic nitrates represents the whole family of mono- and multifunctional alkyl nitrates (Table 1) keeping the basic settings given by Schneider and Ballschmiter (Fischer et al., 2000).

The longest *unbranched* alkyl chain is taken as the skeleton of the molecule; e.g. C7 means in this case that the longest unbranched carbon chain has seven C-atoms. Furthermore we define for *unbranched* alkyl nitrates that the nitrooxy group possesses the highest priority and is numbered first.

For *branched* alkyl nitrates the alkyl side chains possess now the highest priority above all other groups in the molecule, and therefore the positions of alkyl side chains are numbered first. M is used for methyl, and E is used for ethyl side chains, respectively.

This convention is particularly important and helpful if isomeric hydrocarbon skeletons have to be distinguished. For a better understanding we explain the abbreviations introducing some examples for alkyl mononitrates, alkyl dinitrates, hydroxy alkyl nitrates, keto alkyl nitrates, and alicyclic alkyl nitrates.

Alkyl mononitrates: 2,4M5C7 indicates a heptyl chain with two methyl groups at the 2 and 4 position and the nitrooxy group at the 5 position, specifically a 2,4-dimethyl-5-nitrooxyheptane.

Alkyl dinitrates: 2,3M1,4C5 would be a alkyl dinitrate with a carbon skeleton of five atoms, with two methyl groups at the 2 and 3 position, and two nitrooxy groups at position 1 and 4, specifically a 2,3-dimethyl-1,4-dinitrooxy pentane.

Hydroxy alkyl nitrates: OH is used for the hydroxy group. 3OH1C4 would be 3-hydroxy-1-nitrooxy butane.

Keto alkyl nitrate: The letter O labels the carbonyl group, e.g. 2O1C5 is a 2-keto-1-nitrooxy pentane.

Alicyclic alkyl nitrates: The letters *c* and *t* are used for *cis* and *trans* positions, respectively. Cy indicates an alicyclic skeleton. *c*1,2CyC6 indicates a *cis*-1,2-dinitrooxy cyclohexane.

Aryl alkyl nitrates: Aryl alkyl nitrates are named considering the phenyl- or naphthyl group as a substituent of the alkyl chain (Woidich et al., 1999).

3. Position of the Neumayer Research Station in the Antarctic

The Neumayer Station (70°39′S, 8°15′W) was established in 1992 on the Ekström Shelf Ice as a research observatory for geophysical, meteorological and air chemistry measurements. Fig. 1 shows the geographical position of the research station. The snow-covered station is located on shelf ice that is 200 m thick and almost flat. The shelf ice margin where supply ships (e.g. RV "Polarstern") dock is 10 km away. The isolated location

Table 1
IUPAC and short style nomenclature of the alkyl mononitrates and short-chain alkyl hydroxy- and dinitrates identified in the Antarctic air samples

No.	IUPAC	Abbreviation	No.	IUPAC	Abbreviation
C_n			C_n		
	Alkyl mononitrates			Alkyl dinitrates	
1	Nitrooxy-methane	C1	2	1,2-Dinitrooxy-ethane	1,2C2
2	Nitrooxy-ethane	C2	3	1,2-Dinitrooxy-propane	1,2C3
3	1-Nitrooxy-propane	1C3		1,3-Dinitrooxy-propane	1,3C3
	2-Nitrooxy-propane	2C3	4	1,3-Dinitrooxy-butane	1,3C4
4	1-Nitrooxy-butane	1C4		2,3-Dinitrooxy-butane	2,3C4
	2-Nitrooxy-butane	2C4		2-Methyl-1,2-dinitrooxy-propane	2M1,2C3
	2-Methyl-1-nitrooxy-butane	2M1C3	5	2,3-Dinitrooxy-pentane	2,3C5
5	1-Nitrooxy-pentane	1C5	6	2-Methyl-3,4-dinitrooxy-pentane	2M3,4C5
	2-Nitrooxy-pentane	2C5		Hydroxy alkyl nitrates	
	3-Nitrooxy-pentane	3C5	3	1-Hydroxy-2-nitrooxy-propane	1OH2C3
	2-Methyl-3-nitrooxy-butane	2M3C4		2-Hydroxy-1-nitrooxy-propane	2OH1C3
6	1-Nitrooxy-hexane	1C6	4	3-Hydroxy-2-nitrooxy-butane	3OH2C4
	2-Nitrooxy-hexane	2C6		4-Hydroxy-2-nitrooxy-butane	4OH2C4
	3-Nitrooxy-hexane	3C6	5	2-Hydroxy-1-nitrooxy-pentane	2OH1C5
7	1-Nitrooxy-heptane	1C7		1-Hydroxy-2-nitrooxy-pentane	1OH2C5
	2-Nitrooxy-heptane	2C7	6	2-Hydroxy-3-nitrooxy-hexane	2OH3C6
	3-Nitrooxy-heptane	3C7		4-Hydroxy-3-nitrooxy-hexane	4OH3C6
	4-Nitrooxy-heptane	4C7		2-Methyl-4-hydroxy-5-nitrooxy-pentane	2M4OH5C5
8	1-Nitrooxy-octane	1C8		2-Methyl-5-hydroxy-4-nitrooxy-pentane	2M5OH4C5

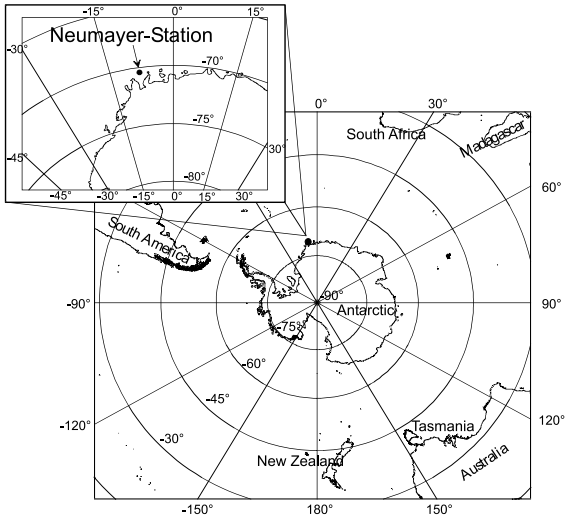

Fig. 1. Geographical position of Neumayer Station; on the Ekström Shelf ice in the Atka Bay, Northeast Weddell Sea (70°39″S, 8°15″W).

of the station makes it a valuable reference site for measurements under conditions of extreme air purity. In addition, the proximity to the ice margin permits the detection of substances released from the ocean to the atmosphere. Table 2 summarizes the meteorological parameters related to the Neumayer Station during the sampling period.

4. Experimental

4.1. Air sampling procedure

The air sampling was done by pulling air through glass tubes (160 mm length, 3 mm, i.d.) filled with 80–100 mg of Tenax TA, 60–80 mesh (Chrompack, Middelburg, Netherlands) at a flow rate of 80–100 ml/min with a sampling pump (SKC model 222-3, Eighty Four, Pennsylvania, United States). Two sampling tubes connected in series have been used to control the sampling efficiency. Volumes of 2–68 l air were sampled. The sampling tubes were flame-sealed in larger glass tubes for transport and were kept refrigerated until analysis.

To detect the whole range of alkyl nitrates parallel sampling of low volumes of 2 l for C2 up to C5 alkyl nitrates and high volumes of 50–70 l as well for alkyl nitrates $C > 5$ is recommended. In polar regions the breakthrough loss due to sampling temperatures is negligible.

4.2. Analytical procedure: GC separation, detection and quantitation

The high resolution gas chromatography with electron capture detection (HRGC/ECD) chromatographic separation was performed on a Chrompack Model 9001 gas chromatograph equipped with a thermal desorption cold trap (TCT) device (Chrompack, Middelburg,

Table 2
Meteorological parameters related to the Antarctic air samples

Sample	Date	Sample volume (l)	Air temperature (°C)	Wind direction	Wind velocity ($m\,s^{-1}$)	Humidity (%)
NM 1	13.02.1999	2.0	−7.5	130°SE	4	75
NM 2	22.02.1999	30.2	−5.5	75°ENE	5	73
NM 3	22.02.1999	68.0	−10.0	160°ESE	3	87
NM 4	26.02.1999	10.8	−6.3	90°E	12	96

Netherlands). We used a DB-1701 capillary (58 m × 0.312 mm i.d. × 1.0 μm film thickness, J&W Scientific, Folsom, United States). A detailed description of the analytical conditions is given in (Fischer et al., 2000). Quantitation was done by external calibration with solutions containing known amounts of alkyl nitrates and halocarbons. The limit of detection based on a 30 l air sample was about 0.3 ng/m^3 or 0.05 ppt(v) for alkyl nitrates and 0.2 ng/m^3 or 0.02 ppt(v) for the three halocarbons trichloroethane, tetrachloroethene and bromoform. The overall error for the alkyl nitrates and halocarbons was estimated to be less than ±20% (Fischer, 1999).

5. Results

The measured concentrations of organic nitrates and halocarbons of this work are summarized in Table 3. The results presented in this work are unique for organic nitrates. Table 4 lists all literature data and compares them with the results of this work. Highest in abundance are the short chain alkyl mononitrates C2, 1C3, 2C3 and 2C4. This observation is consistent with the literature data for Arctic regions (Table 4). The alkyl nitrate levels for the Arctic regions are one order of magnitude higher than the values found in the Antarctic, indicating that the sampling sites in the North are closer to the highly industrialized regions of the North American continent. In terms of the vicinity to non-point sources the Arctic and Antarctic regions have to be considered differently; the effects of a limited photodegradation in the respective polar nights will be similar.

Fig. 2a and b depict TCT–HRGC–ECD chromatograms of air samples collected at Neumayer Station, Antarctica. To our knowledge these are the first chromatograms showing alkyl nitrates in the air of a South Polar region.

The biogenic marker dibromomethane and tribromomethane (bromoform) show relative to alkyl nitrates higher mixing ratios indicating marine emissions sources (the sampling location is only 10 km away from the coastal line). Anthropogenic markers like carbontetrachloride and 1,1,1-trichloroethane with long k_{OH}

Table 3
Mixing ratios for the alkyl mononitrates, hydroxy alkyl nitrates, alkyl dinitrates, and bromo- and chloro-halocarbons in the Antarctic air in ppt(v) ($n = 2$–4)

Mononitrates	Mean (ppt(v))	Hydroxy nitrates	Mean (ppt(v))	Halocarbons	Mean (ppt(v))
C1($n = 1$)	84	2OH1C4	<LOD	Tetrachloromethane	95
C2	4.6	2OH1C3	0.03	1,1,1-Trichloroethane	75
1C3	1.1	RR-3OH2C4[a]	0.3	Trichlorethene	<LOD
2C3	0.7	1OH2C3/RS-3OH2C4[a]	0.8	Tetrachlorethene	0.3
1C4	0.03			Hexachloroethane	0.06
2C4/2M1C3	0.5	1OH2C4	0.02	Dibromomethane	0.8
1C5	0.7	3OH1C4	0.01	Bromodichloromethane	0.05
2C5	<LOD	∑OH	1.1	Dibromochloromethane	0.02
3C5	0.03			Bromoform	0.3
				1,2-Dibromoethane	0.1
		Dinitrates			
1C6	0.5	1,2C3/1,2C2	0.5		
2C6	1.0	2M1,2C3	0.1		
3C6	0.08				
2C7	0.18	∑ C4 + C5	1.3		
4C7	0.02	∑ C3–C6	4.6		

Limit of detection (LOD) = 0.01 ppt(v).
[a] RR/SS-3OH2C4; RS/SR-3OH2C4 co-elution with 1OH2C3.

Table 4
Comparison of mixing ratios of alkyl nitrates in the Antarctic air with Arctic and Alaska reference data in ppt(v)

	Antarctic (this work)	Alert, Canada		Arctic, Canada[a]
		Polar night[b]	Polar day[b]	
1C3	1.11	3.33	3.14	3.96
2C3	0.49	12.44	13.08	12.5
1C4	0.03	1.7	1.18	2.05
2C4/2M1C3	0.48	18.41	13.73	13.98
2M3C4	<LOD	4.84	2.32	2.65
1C5	0.71	1.01	0.53	1.03
2C5	<LOD	5.44	2.47	4.18
3C5	0.03	4.31	2.31	3.02
2C6	0.08	2.46	0.98	1.50
3C6	0.95	4.27	1.65	2.55
2C7	0.18	1.45	0.56	–
3C7	(0.01)	1.86	0.68	–
$\sum$C2–C6	9.2	–	–	34[c]
$\sum$C3–C7	–	–	–	144[d]

Limit of detection (LOD) = 0.01 ppt(v).
[a] Canadian Arctic (69°N–83°N) "Polar Sunrise Experiment" April 1992 (Leaitch et al., 1994).
[b] Alert, Northwest Territories of Canada, "Polar Sunrise Experiment" January–April 1992, Polar night January–March; day period March–April (Muthuramu et al., 1994).
[c] Poker Flat Research Rang, Alaska (64°N/147°W) winter/spring 1993 (Beine et al., 1996).
[d] Canadian Arctic March–April 1988 (Bottenheim et al., 1993).

lifetimes (τ = month to years) were also found, but markers with short k_{OH} lifetime like trichloroethene ($\tau = 7$ days) are below the limit of detection (<0.01 ppt(v)).

The patterns of the Antarctic air samples are quite similar to the patterns found in the South Atlantic Trade Wind region. Fig. 2c depicts for comparison a chromatogram of this marine region, taken during the ALBATROSS campaign on board of RV "Polarstern" (ANT XIV/1) at 10.4°S/25.5°W (Fischer et al., 2000). The Antarctic and the Southern Trades apparently represent baseline levels of clean marine air in terms of organic nitrates.

5.1. Levels of anthropogenic halocarbons in Antarctic air

The mixing ratios for the long-lived halocarbons (Table 3) are in good agreement with earlier measurements. We found 95 ppt(v) for tetrachloromethane ($\tau = 42a$) while Derwent measured 101 ppt(v) in Ireland (Derwent et al., 1998). This indicates a more or less even global distribution in the troposphere. For 1,1,1-trichlorethane we observed 75 ppt(v) ($\tau = 4.8a$); estimations by Derwent for 1999 results in ratios of 70–80 ppt(v) (Derwent et al., 1998). The situation seems to be similar as observed for tetrachloromethane. The mean value for hexachloroethane is in the range of 0.06 ppt(v) and somewhat lower than 0.24 ppt(v) observed by Atlas in 1993 for the Pacific (Atlas et al., 1993). For medium lived C_2^- halocarbons like tetrachlorethene we observed a mean value of 0.3 ppt(v). During the Albatross–Campaign we found similar mixing ratios in the South Atlantic Ocean and levels by a factor 3 higher for the North Atlantic (Fischer et al., 2000). The good correlation of the measured halocarbon ratios with literature data backs the accuracy of our analytical procedure.

6. Discussion

To interpret the data of the South Polar region in a wider spatial context we enclose the data of the Albatross–Campaign, which also covered the South Atlantic (Fischer et al., 2000).

6.1. Levels of butyl nitrates in marine and Antarctic air

Fig. 3 is a plot of the mixing ratios of the 2C4, the secondary, and the 1C4, the primary butyl nitrate along the Atlantic Ocean (Albatross–Campaign) and at Neumayer Station, Antarctic. The main emission sources are in the industrialized areas of the Northern hemisphere. The accumulation in the Northern hemisphere is enhanced in fall and wintertime by a reduced photodegradation. The concentration for 2-butyl nitrate (2C4) in the coastal region is 3.5–5 ppt(v). An average value of 1 ± 0.2 ppt(v) is observed for 1-butyl nitrate (1C4) in the air of the North Atlantic. A 2C4/1C4 ratio close to 4 indicates a recent continental input or marine local input by islands.

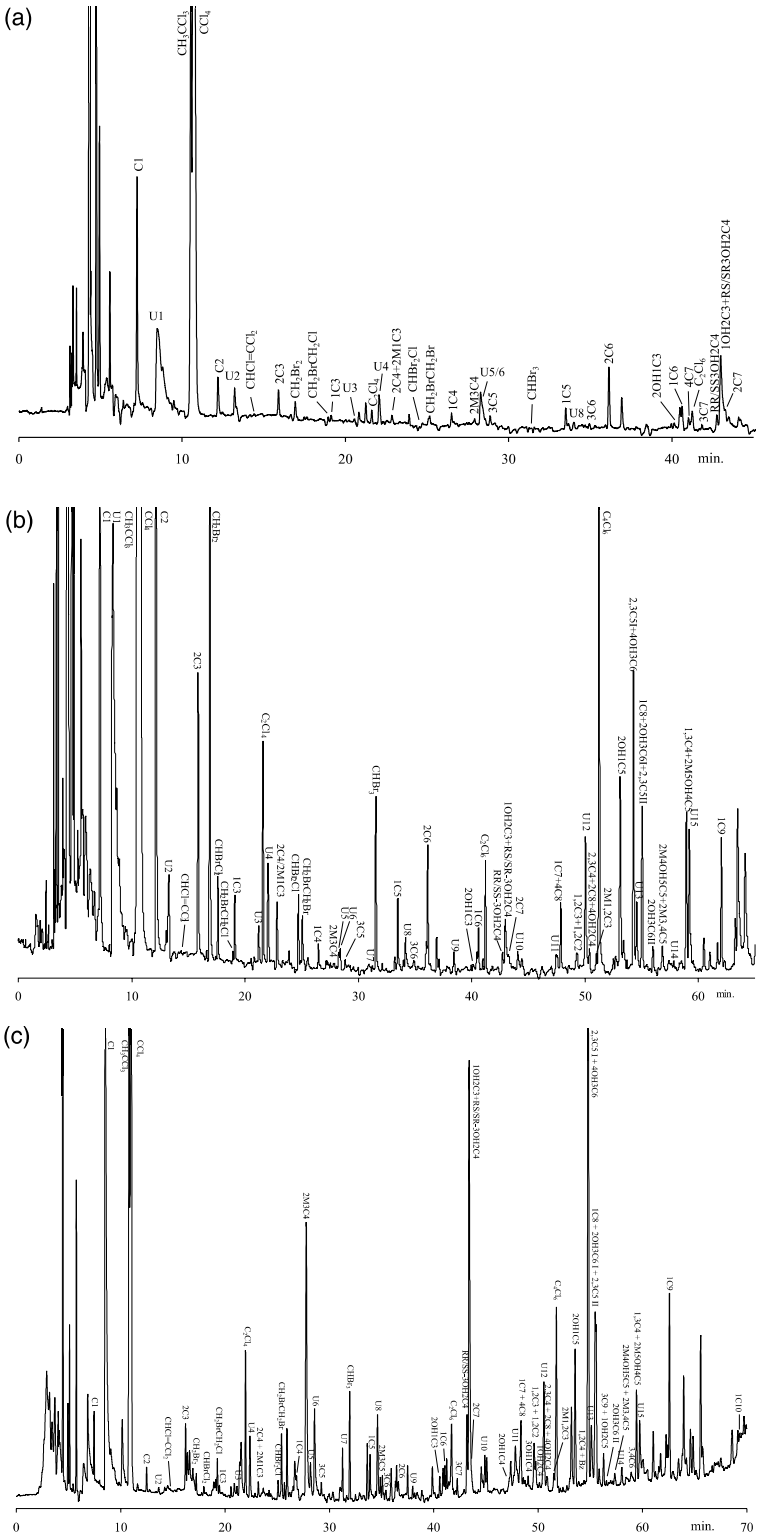

Fig. 2. (a) TCT–HRGC(DB-1701)/ECD chromatogram of an Antarctic air sample, taken at Neumayer Station, sampling and on-column volume (a) 2.0 l (sample NM 1), (b) 68 l (sample NM 3). (c) TCT–HRGC(DB-1701)/ECD chromatogram of a South Atlantic air sample of the trade wind region 10.4°S/25.5°W, sampling and on-column volume 105 l.

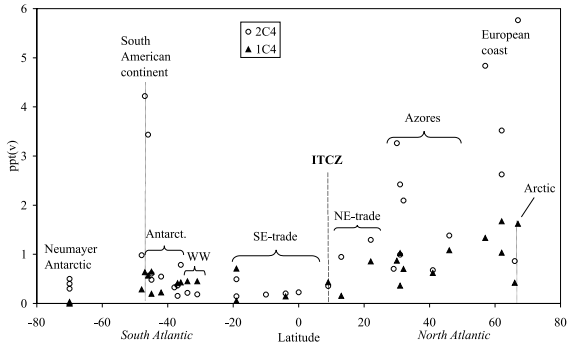

Fig. 3. Distribution of butyl nitrates from 67°N to 70°S over the Atlantic Ocean mainly across 30°W longitude (Albatross–Campaign on board RV Polarstern ANT XIV/1, 1996) and at the Neumayer Station, 1999.

In the South Atlantic trade wind region the values for 2C4 decrease to 0.2 ± 0.05 ppt(v) leading to a 2C4/1C4 ratio to about 1 and even below 1. The levels of 2C4 rise again to 0.4 ± 0.08 ppt(v) in the west wind belt of the South Atlantic and remain at 0.4 ± 0.1 ppt(v) for air collected at the Neumayer Station. The levels of 1C4 decrease from 1.0 ± 0.2 ppt(v) in the Northern hemisphere passing the intertropical convergence zone (ITCZ) to the south to levels of 0.4 ± 0.08 ppt(v). A further decrease to levels down to the limit of detection of 0.05 ppt(v) is observed for the air at the Neumayer Station. The 2C4/1C4 ratio covers a span between 0.2 and 7.0 reflecting in one part the dominance of 1C4 in "old" air masses and also a very low level of possible local input in the Antarctic. In the latter case only the dominant 2C4 would be detected.

6.2. Characterization of the age of air masses

An air mass is called "young" if pollution deriving from densely inhabited regions with a corresponding level of traffic and industrial emissions is observed. Several attempts have been made to characterize air mass ages. Atherton used a pure deductive kinetic model (Atherton, 1989). Other models consider differences in photochemical degradation velocities using pairs of molecules or groups of molecules like carbon monoxide and alkyl nitrates (Roberts et al., 1996), PAN and alkyl nitrates (Buhr et al., 1990), hydrocarbons and alkyl nitrates (Roberts et al., 1998), NO_y and NO_x (Trainer et al., 1991), two isomeric alkyl nitrates (Flocke et al., 1998; Schneider and Ballschmiter, 1999) or consider the presence of benzyl nitrate (Schneider et al., 1998a; Schneider and Ballschmiter, 1999). Here we present two different approaches to characterize the "age" of air masses. It is the 2-butyl-, 2-pentyl nitrate/tetrachloroethene quotient (traffic/industry indicator) and the ratio of isomeric pentyl nitrates (traffic indicator).

6.3. The 2-butyl-, 2-pentyl nitrate/tetrachlorethene ratio as an air mass marker

Here, we present a method based on the differences in the degradation rates of short chain alkyl nitrates and semi-stable halocarbons (e.g. tetrachloroethene). Short chain alkyl nitrates are formed in all regions with traffic that are releasing significant NO and short chain hydrocarbon emissions. Butyl- and pentyl nitrates are degraded by photolysis and OH on their long-range transport finally reaching remote areas like the Antarctic. The anthropogenic halocarbons emerge basically from industrialized continental regions and then undergo photochemistry on their long-range transport. They are degraded mainly by OH radicals and only to a minor extent by photolysis (Class and Ballschmiter, 1986).

The k_{OH} lifetime of tetrachloroethene is in the range of 4 month. Tetrachloroethene shows a three-step decrease in the global mixing ratios in the lower troposphere (Wiedmann et al., 1994). A first decrease is observed when going from continental air to marine air of the Northern hemisphere. This is a mixture of a decrease by degradation and by mixing of the source air with less polluted air of the Northern Hadley cell of the general circulation. The second decrease is observed in the Northern tropics and a third one when passing the ITCZ reaching the air of South East Trades of the Southern hemisphere. This clearly indicates the separation of the air masses of both hemispheres in the lower troposphere by the ITCZ. This has been observed for other anthropogenic volatile chlorocarbons before (Class and Ballschmiter, 1986).

The butyl nitrates do not give this clear difference in atmospheric levels but decrease more or less continuously in going to remote regions. The increased levels around the Azores indicate the importance of quasi-local inputs in the marine atmosphere due to traffic on these islands. Fig. 5a depicts the ratios of the mixing ratios of the secondary alkyl nitrates 2-butyl- and 2-pentyl nitrate relative to tetrachloroethene (C_2Cl_4) in the air of the Atlantic Ocean and in the air of Neumayer Station. Three clusters are formed. Marine air influenced by air masses coming from the South American continent is characterized by a surplus of 2-butyl and 2-pentyl nitrates relative to tetrachloroethene. Unpolluted marine air has low mixing ratios for 2-pentyl nitrate itself and the ratio $2C5/C_2Cl_4$ is <1 indicating a strong degradation for 2-pentyl nitrate. The third cluster represents the global baseline level. It is characterized by the fact that both the ratios for $2C4/C_2Cl_4$ and $2C5/C_2Cl_4$

are well below 1. This third cluster represents the photochemically aged pollution depleted air masses.

6.4. The ratio of isomeric pentyl nitrates as an air mass marker

A further method to decide about the origin or age of an air parcel is to compare the levels of the isomeric pentyl nitrates. In the case of pentyl nitrates significantly increased mixing ratios for primary and secondary pentyl nitrates are found with a surplus of secondary pentyl nitrates (3C5 > 2C5 > 1C5). Very low concentrations of secondary pentyl nitrates, and in contrast noticeably higher concentrations of 1-pentyl nitrates characterize aged air masses (e.g. collected in remote marine or Antarctic regions). The former sequence of the levels in air 3C5 > 2C5 > 1C5 turns now to 1C5 ≫ 3C5 > 2C5. The mixing ratio for 2C5 in the air of the Antarctic Neumayer Station is below the limit of detection (Table 3). The missing of 2C5 and barely detectable traces of 3C5 while 1C5 can be measured confirm that highly degraded air masses were collected.

6.5. Methyl nitrate in Antarctic air

The level found for methyl nitrate found in the Antarctic is unexpectedly high and requires a specific discussion. The branching ratio for the atmospheric reaction Eqs. (7a)–(7c) is normally set close to zero for C1. Degradation of peroxyacetylnitrate (PAN) by the loss of CO_2 or the esterfication of methanol with nitric acid on aerosols (Senum et al., 1986; Orlando et al., 1992; Fan et al., 1994) can result in higher yields of metyl nitrate in polluted continental air.

The reaction of methyl nitrate with OH is the major loss process. The reaction rate constant was first measured by Gaffney et al. (Gaffney et al., 1986). It has recently be redetermined (Kakesu et al., 1997).

Methyl nitrate is very volatile and substantial breakthrough losses will occur if not specific precautions (low sample volume, high amount of adsorbent, low temperature) are set to sample this very volatile alkyl nitrate by adsorption techniques. A correct quantitation of methyl nitrate is therefore difficult and requires optimized sampling conditions. We have found a level of >80 ppt(v) for methyl nitrate in the low volume sample. Co-elution with other compounds in the gas chromatogram of our sample can be excluded by identification of the C1 peak by HRGC/MSD. Recently Jones measured methyl nitrate from 27 to 46 ppt(v) and ethyl nitrate from 5 to 13 ppt(v) sampled at Neumayer Station 1997 (Jones et al., 1999).

Walega et al. found for methyl nitrate 4 ppt(v) at Mauna Loa, Hawaii (Walega et al., 1992) and Flocke et al. measured 8 ppt(v) in the air over the North Atlantic (Flocke et al., 1998). Atlas supposed a marine emission source for methyl nitrate (Atlas et al., 1997). In the marine boundary layer (MBL) maximum concentrations were found as high as 50 ppt(v) near Christmas Island (1–3°N) and concentrations of 20–35 ppt(v) near Western Samoa (13°S) during ACE 1 (Blake et al., 1999). The authors conclude that methyl nitrate has a significant equatorial marine source. The most logic biogenic source would be the methylation of nitrate ions. We may observe a similar reaction for the nitrate ion leading to methyl nitrate as it is found for the methylation of chloride (Urhahn and Ballschmiter, 1998). Methionine methyl sulfonium chloride (MMSL) e.g. gave an intense release of monohalomethanes when mixed in a buffer with potassium halides.

6.6. Levels of hydroxy alkyl nitrates in marine and Antarctic air

Fig. 4 is a plot of the mixing ratios of hydroxy alkyl nitrates along the Atlantic Ocean (Albatross–Campaign) and at Neumayer Station, Antarctic. All of the observed compounds are vicinal hydroxy alkyl nitrates. Hence, their formation pathway via OH radical addition to olefins is most likely. We observe a NH/SH gradient of about factor 3 with 4.3 ± 0.8 ppt(v) for the sum of 4 hydroxy alkyl nitrates in the air of the Northern hemisphere and 1.6 ± 0.3 ppt(v) in the South Atlantic air. The mixing ratio for hydroxy alkyl nitrates in the air of the Neumayer Station is with 1.2 ± 0.2 ppt(v) somewhat lower than in the South Atlantic air. In accordance with previous discussions the formation of secondary alkyl radicals is preferred to the formation of primary ones (Kastler, 1999). Therefore, if 1-alkenes are degraded by OH radicals, the yield of 1-hydroxy-2-nitrooxy-alkanes must be higher than the yield for 2-hydroxy-1-nitrooxy alkanes. This is consistent with our observations.

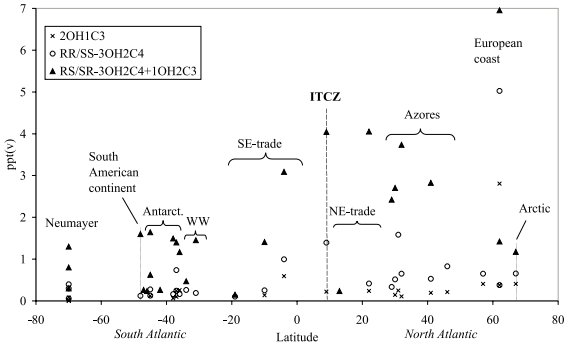

Fig. 4. Distribution of hydroxy propyl- and butyl nitrates from 67°N to 70°S over the Atlantic Ocean and at Neumayer Station.

6.7. Principal compound analysis (PCA) of organic nitrates in marine and Antarctic air

The principal compound analysis is a statistical model to compare the pattern of air samples between different regions. The theoretical feedback of the method is given in (Smith, 1991). The *n*-dimensional expression is reduced to a two dimensional expression. The distance between two points is a measure of the similarity of air samples. Fig. 5b depicts the PCA of all marine and Antarctic air samples. 15 locations and the ratios of 14 alkyl mononitrates are the basis for the PCA given here.

A grouping of air masses is also obtained by plotting two ratios of selected air constituents. This approach has been used to characterize air masses by their complex pattern of polychlorinated biphenyls (PCBs) (Schreitmüller et al., 1994). We have plotted here the ratios of the mixing ratio of 2-butyl nitrate/tetrachloroethene versus 2-pentyl nitrate/tetrachlorethene. The results are given in Fig. 5a. Three clusters of air masses can be differentiated. Cluster I contains all sampling locations representing global baseline levels. Cluster II summarizes marine air samples with slightly polluted air, indicating the influence of islands. The last cluster contains polluted air coming in from the South American continent. The PCA as an independent method confirms the characterization of marine and polar air samples as discussed above.

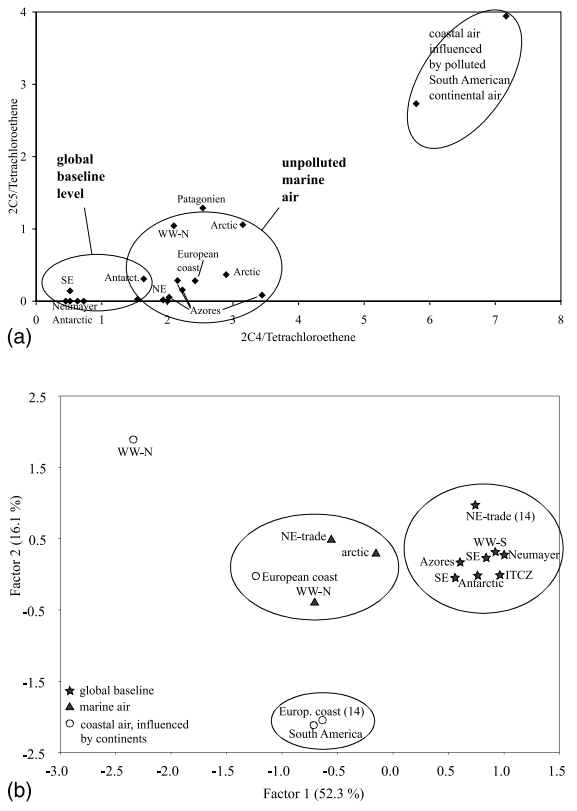

Fig. 5. Grouping of air masses by (a) mixing ratio of 2-butyl nitrate/tetrachloroethene versus 2-pentyl nitrate/tetrachlorethene, (b) PCA of organic nitrates in marine air.

7. Conclusion

In this paper we presented for the first time a data set of higher organic nitrates in the air of the German South Polar Neumayer Station. We are in a unique position to discuss and compare the levels and patterns of alkyl nitrates and halocarbons in the air of the Atlantic Ocean and in the air of the South Polar region. The organonitrate concentrations in the marine and Antarctic samples reached only 1–10% of the continental samples. The mixing ratio in the South East Trade Wind region and in the air of Neumayer Station are similar and represents the global baseline level for the organonitrates. This is a strong indication for the long-range transport of these molecules. No new alkyl nitrate formation is expected due to the lack of NO_x sources in the marine and the Antarctic atmosphere. Methyl nitrate seems to be the exception from this rule. A biogenic source for this compound appears to be likely as it has been discussed before.

Halocarbons can be used as marker molecules to distinguish between inhabited and biogenic sources. The ratio of tetrachloroethene to secondary alkyl nitrates can be used as a tool to decide about the origin and age of an air parcel analyzed. The ratio of the isomeric pentyl nitrates can also be used to characterize air masses.

References

Ahlner, J., Andersson, R.G.G., Torfgard, K., Axelsson, K.L., 1991. Organic nitrate esters: Clinical use and mechanisms of actions. Pharmacol. Rev. 43, 351–353.

Atherton, C.S., 1989. Organic nitrates in remote marine environments: evidence for long- range transport. Geophys. Res. Lett. 16, 1289–1292.

Atkinson, R., 1990. Gas-phase tropospheric chemistry of organic compounds: a review. Atmos. Environ. 24A, 1–41.

Atkinson, R., Aschmann, S.M., Carter, W.P.L., Winer, A.M., Pitts, J.N., 1982. Alkyl nitrates formation from the NO_x-air photooxidations of C2–C8 *n*-alkanes. J. Phys. Chem. 86, 4563–4569.

Atlas, E., 1988. Evidence for >C3 alkyl nitrates in rural and remote atmospheres. Nature 331, 426–428.

Atlas, E., Flocke, F., Schauffler, S., Stroud, V., Blake, D., Rowland, F.S., Singh, H., 1997. Evidence for marine sources of atmospheric alkyl nitrates: measurements over the tropical Pacific Ocean during PEM tropics. Posterbeitrag, American Geophysical Union (AGU) 78 (46) Fall Meeting, Supplement.

Atlas, E., Pollock, W., Greenberg, J., Heidt, L., 1993. Alkyl nitrates, nonmethane hydrocarbons and halocarbon gases over equatorial Pacific Ocean during Saga 3. J. Geophys. Res. 98, 16 933–16 947.

Atlas, E., Ridley, B.A., Hübler, G., Walega, J.G., Carroll, M.A., Montzka, D.D., Huebert, B.J., Norton, R.B., Grahek, F.E., Schauffler, S., 1992a. Partitioning and budget of NO_y species during the Mauna Loa Observatory Photochemistry Experiment. J. Geophys. Res. 97, 10 449–10 462.

Atlas, E., Schauffler, S.M., Merrill, J.T., Hahn, J., Ridley, B.A., Walega, J.G., Greenberg, J., Heidt, L., Zimmerman, P.B., 1992b. Alkyl nitrate and selected halocarbon measurements at Mauna Loa Observatory, Hawaii. J. Geophys. Res. 97, 10 331–10 348.

Barrie, L.A., Li, S.M., Toom, D.L., Landsberger, S., Sturges, W.T., 1994. Lower tropospheric measurements of halogens, nitrates, and sulphur oxides during Polar Sunrise Experiment 1992. J. Geophys. Res. 99, 25 453–25 467.

Beine, H.J., Jaffe, D.A., Blake, D.R., Atlas, E., Harris, J., 1996. Measurement of PAN, alkyl nitrates, ozone, and hydrocarbons during spring in interior Alaska. J. Geophys. Res. 101, 12 613–12 619.

Blake, N.J., Blake, D.R., Wingenter, O.W., Sive, B.C., Kang, C.H., Thornton, D.C., Bandy, A.R., Atlas, E., Flocke, F., Harris, J.M., Rowland, F.S., (1999). Aircraft measurements of the latitudinal, vertical, and seasonal variations of NMHCS, methyl nitrate, methyl halides, and DMS during the first aerosol characterization experiment. (ACE 1) J. Geophys. Res. 104, 21 803-21 817.

Bottenheim, J.W., Barrie, L.A., Atlas, E., 1993. The partitioning of nitrogen oxides in the lower Arctic troposphere during spring 1988. J. Atmos. Chem. 17, 15–27.

Buhr, M.P., Parrish, D.D., Norton, R.B., Fehsenfeld, F.C., Sievers, R.E., 1990. Contribution of organic nitrates to the total reactive nitrogen budget at a rural Eastern US site. J. Geophys. Res. 95, 9809–9816.

Carroll, M.A., Ridley, B.A., Montzka, D.D., Hübler, G., Walega, J.G., Norton, R.B., Huebert, B.J., Grahek, F.E., 1992. Measurements of nitric oxide and nitrogen dioxide during the Mauna Loa Observatory Photochemistry Experiment. J. Geophys. Res. 97, 10 361–10 374.

Class, T., Ballschmiter, K., 1986. Chemistry of organic traces in air VI: distribution of chlorinated C1–C4 hydrocarbons in air over the northern and Southern Atlantic Ocean. Chemosphere 15, 413–427.

Clemitshaw, K.C., Williams, J., Rattigan, O.V., Shallcross, D.E., Law, K.S., Cox, R.A., 1997. Gas-phase ultraviolet absorption cross-sections and atmospheric lifetimes of several C2–C5 alkyl nitrates. J. Photochem. Photobiol A: Chem. 102, 117–126.

de Kock, A.C., Anderson, C.R., 1994. The measurement of C3–C5 alkyl nitrates at a coastal sampling site in the Southern hemisphere. Chemosphere 29, 299–310.

Derwent, R.G., Simmonds, P.G., O'Doherty, S., Ryall, D.B., 1998. The impact of the Montreal protocol on halocarbon concentrations in Northern hemisphere baseline and European air masses at Mace Head, Ireland over a ten year period from 1987–1996. Atmos. Environ. 32, 3689–3702.

Fan, S.M., Jacob, D.J., Mauzerall, J.D., Bradshaw, D., Sandholm, S.T., Blake, D., Singh, H.B., Talbot, R., Gregory, G.L., Sachse, G.W., 1994. Origin of tropospheric NO_x over subarctic Eastern Canada in summer. J. Geophys. Res. 99, 16 867–16 877.

Finlayson-Pitts, B.J., Pitts Jr., J.N., 1986. Atmospheric Chemistry: Fundamentals and Experimentals Techniques. John Wiley & Sons, New York.

Fischer, R.G., 1999. Vorkommen und Umweltverhalten der C_1–C_{10} organischen Nitrate in kontinentaler und mariner Luft. Dissertation Dr. rer. nat., Universität Ulm.

Fischer, R.G., Ballschmiter, K., 2001. Global occurrence and pattern of short chain alkyl nitrates. In: Proceedings Symposium Atmospheric Reactive Compounds. Bayreuth 1999, in press.

Fischer, R.G., Kastler, J., Ballschmiter, K., 2000. Levels and pattern of alkyl nitrates, multifunctional alkyl nitrates, and halocarbons in the air over the Atlantic Ocean. J. Geophys. Res. 105, 14 473–14 494.

Flocke, F., Volz-Thomas, A., Buers, H.J., Pätz, H.W., Garthe, H.J., Kley, D., 1998. Long-term measurements of alkyl nitrates in Southern Germany 1. General behavior and seasonal and diurnal variation. J. Geophys. Res. 103, 5729–5745.

Fraser, M.P., Cass, G.R., Simoneit, B.R.T., Rasmussen, R.A., 1997. Air quality model evaluation data for organics 4. C_2–C_{36} non-aromatic hydrocarbons. Environ. Sci. Technol. 31, 2356–2367.

Gaffney, J.S., Fajer, R., Senum, G.I., Lee, J.H., 1986. Measurement of the reactiviy of OH with methyl nitrate: implication for prediction of alkyl nitrate–OH reaction rates. Int. J. Chem. Kinetics 18, 399–407.

Jones, A.E., Weller, R., Minikin, A., Wolff, S., Sturges, W.T., McIntyre, M.E., Leonard, S.R., Schrems, O., Bauguitte, S., 1999. Oxidized nitrogen chemistry and speciation in the Antarctic troposphere. J. Geophys. Res. 104, 21 355–21 366.

Kakesu, M., Bandow, H., Takenaka, N., Maeda, Y., et al., 1997. Kinetic measurements of methyl and ethyl nitrate reactions with OH radicals. Int. J. Chem. Kinetics 29, 933–941.

Kastler, J., 1999. Analytik, Massenspektrometrie und Vorkommen multifunktioneller Alkylnitrate in belasteter und unbelasteter Atmosphäre. Dissertation Dr. rer. nat., Universität Ulm.

Kastler, J., Ballschmiter, K., 1998. Bifunctional alkyl nitrates—trace constituents of the atmosphere. Fresenius J. Anal. Chem. 360, 812–816.

Kastler, J., Ballschmiter, K., 1999. Identification of alkyl dinitrates in ambient air of Central Europe. Fresenius J. Anal. Chem. 363, 1–4.

Köhler, J., Meyer, R., 1995. Explosivstoffe. VCH, Weinheim.

Kondo, Y., Koike, M., Kawakami, S., Singh, H.B., Nakajiama, H., Gregory, G.L., Blake, D.R., Sachse, G.W., Merrill, J.T., Newell, R.E., 1997. Profiles and partitioning of reactive nitrogen over Pacific Ocean in winter and early spring. J. Geophys. Res. 102, 28 405–28 424.

Leaitch, W.R., Barrie, L.A., Bottenheim, J.W., Li, S.M., Shepson, P.B., Muthuramu, K., Yokouchi, Y., 1994. Airborne observations related to ozone depletion at Polar Sunrise. J. Geophys. Res. 99, 25 499–25 517.

Muthuramu, K., Shepson, P.B., Bottenheim, J.W., Jobson, B.T., Niki, H., Anlauf, K.G., 1994. Relationsships between organic nitrates and surface ozone destruction during Polar

Sunrise Experiment 1992. J. Geophys. Res. 99, 25 369–25 378.

O'Brien, J.M., Shepson, P.B., Muthuramu, K., Hao, C., Hastie, D.R., 1995. Measurement of alkyl and multifunctional organic nitrates at a rural site in Ontario. J. Geophys. Res. 100, 22 795–22 804.

O'Brien, J.M., Shepson, P.B., Wu, Q., Biesenthal, T.A., Bottenheim, J.W., Wiebe, H.A., Anlauf, K.G., Brickell, P., 1997. Production and distribution of organic nitrates, and their relationship to carbonyl compounds in an urban environment. Atmos. Environ. 31, 2059–2069.

Orlando, J.J., Tyndall, G.S., Calvert, J.G., 1992. Thermal decomposition pathways for peroxyacetyl nitrate (PAN)—implications for atmospheric methyl nitrate levels. Atmos. Environ. Part A—General Topic 17, 3111–3118.

Platt, U., Le Bras, G., 1997. Influence of DMS on the O_x–NO_y partitioning and the NO_x distribution in the marine background atmosphere. Geophys. Res. Lett. 24, 1935–1938.

Roberts, J.M., 1990. The atmospheric chemistry of organic nitrates. Atmos. Environ. 24A, 243–287.

Roberts, J.M., Bertman, S.B., Parrish, D.D., Fredrick, C., Fehsenfeld, F.C., Jobson, B.T., Niki, H., 1998. Measurement of alkyl nitrates at Chebogue Point, Nova Scotia during the 1993 North Atlantic Regional Experiment (NARE) intensive. J. Geophys. Res. 130, 13 569–13 580.

Roberts, J.M., Parrish, D.D., Norton, R.B., Bertman, S.B., Holoway, J.S., Trainer, M., Fehsenfeld, F.C., Carroll, M.A., Albercook, G.M., Wang, T., Forbes, G., 1996. Episodic removal of NO_y species from the marine boundary layer over the North Atlantic. J. Geophys. Res. 101, 28 947–28 960.

Schneider, M., Ballschmiter, K., 1996. Separation of diastereomeric and enantiomeric alkyl–nitrates—systematic approach to chiral discrimination on cyclodextrin LIPODEX-D. Chem. Eur. J. 2, 539–544.

Schneider, M., Ballschmiter, K., 1999. C3–C14 alkyl nitrates in remote South Atlantic air. Chemosphere 38, 233–244.

Schneider, M., Deissler, A., Ballschmiter, K., 1998a. Levels and patterns of C1–C15 alkyl nitrates, perchloroethene, and bromoform in Californian air. ACS, Division of Environmental Chemistry Reprints of Extended Abstracts 38, 18–20.

Schneider, M., Luxenhofer, O., Deissler, A., Ballschmiter, K., 1998b. C_1–C_{15} alkyl nitrates, benzyl nitrate, and bifunctional nitrates: measurements in Californian and South Atlantic Air and global comparison using C_2Cl_4 and $CHBr_3$ as marker molecules. Environ. Sci. Technol. 32, 3055–3062.

Schreitmüller, J., Vigneron, M., Bacher, R., Ballschmiter, K., 1994. Pattern analysis of polychlorinated biphenyls (PCB) in Marine Air of the Atlantic Ocean. Int. J. Environ. Anal. Chem. 57, 33–52.

Seinfeld, J.H., Pandis, S.N., 1998. Atmospheric Chemistry and Physics—From Air Pollution to Climate Change. John Wiley & Sons, New York.

Senum, G.I., Fajer, R., Gaffney, J.S., 1986. Fourier transform infrared spectroscopic study of the thermal stability of peroxyacetyl nitrate. J. Phys. Chem. 90, 152–156.

Smith, G.L., 1991. Principal component analysis. an introduction. Anal. Proc. 28, 150–151.

Talukdar, R.K., Burkholder, J.B., Hunter, M., Gilles, M.K., Roberts, J.M., Ravishankara, A.R., 1997. Atmospheric fate of several alkyl nitrates: part 2 UV absorption cross-sections and photodissoziation quantum yields. J. Chem. Soc. Farad. Trans. 93, 2797–2805.

Trainer, M., Buhr, M.P., Curran, C.M., Fehsenfeld, F.C., Hsie, E.Y., Liu, S.C., Norton, R.B., Parrish, D.D., Williams, E.J., 1991. Observations and modeling of the reactive nitrogen photochemistry at a rural site. J. Geophys. Res. 96, 3045–3063.

Urhahn, T., Ballschmiter, K., 1998. Chemistry of the biosynthesis of halogenated methanes: C1-organohalogens as pre-industrial chemical stressors in the environment? Chemosphere 37, 1017–1032.

Walega, J.G., Ridley, B.A., Madronich, S., Grahek, F.E., Shetter, J.D., Sauvain, T.D., Hahn, J., Merill, J.T., Bodhaine, B.A., Robinson, E., 1992. Observations of peroxyacetyl nitrate, peroxypropionyl nitrate, methyl nitrate and ozone during Mauna Loa Observatory Photochemistry Experiment. J. Geophys. Res. 97, 10 311–10 330.

Werner, G., Kastler, J., Looser, R., Ballschmiter, K., 1999. Organic nitrates of isoprene as atmospheric compounds. Angew. Chem. Int. Ed. 38, 1634–1637.

Wiedmann, T.O., Güthner, B., Class, T., Ballschmiter, K., 1994. Global distribution of tetrachloroethene in the troposphere: measurements and modeling. Environ. Sci. Technol. 28, 2321–2329.

Woidich, S., Froescheis, O., Luxenhofer, O., Ballschmiter, K., 1999. EI and NCI-mass spectrometry of arylalkyl nitrates and their occurrence in urban air. Fresenius J. Anal. Chem. 364, 91–99.

Publication 3.1.5

Weller, R., A.E. Jones, A. Wille, H.-W. Jacobi, H. McIntyre, W.T. Sturges, M. Huke, and D. Wagenbach,

Seasonality of reactive nitrogen oxides (NO_y) at Neumayer Station, Antarctica,

J.Geophys.Res. **107** (D23), 4673, doi:10.1029/2002JD002495, 2002.

Seasonality of reactive nitrogen oxides (NO_y) at Neumayer Station, Antarctica

R. Weller,[1] A. E. Jones,[2] A. Wille,[3] H.-W. Jacobi,[1] H. P. McIntyre,[4] W. T. Sturges,[4] M. Huke,[5] and D. Wagenbach[5]

Received 30 April 2002; revised 9 July 2002; accepted 15 August 2002; published 3 December 2002.

[1] NO, NO_y (total reactive nitrogen oxides), gaseous HNO_3, and particulate nitrate ($p\text{-}NO_3^-$) were measured at Neumayer Station from February 1999 to January 2000. In addition, during February 1999, the NO_y component species peroxyacetyl nitrate (PAN) and methyl, ethyl, i-propyl, and n-propyl nitrates were determined. We found a mean NO_y mixing ratio of 46 ± 29 pptv, with significantly higher values between February and end of May (58 ± 35 pptv). Between February and November, the (HNO_3 + $p\text{-}NO_3^-$)/NO_y ratio was extremely low (around 0.22) and in contrast to NO_y the seasonality of $p\text{-}NO_3^-$ and HNO_3 showed a distinct maximum in November and December, leading to a (HNO_3 + $p\text{-}NO_3^-$)/NO_y ratio of 0.66. Trajectory analyses and radioisotope measurements (^{7}Be, ^{10}Be, ^{210}Pb, and ^{222}Rn) indicated that the upper troposphere or stratosphere was the main source region of the observed NO_y with a negligible contribution of ground-level sources at northward continents. Frequent maxima of NO_y mixing ratios up to 100 pptv are generally associated with air mass transport from the free troposphere of continental Antarctica, while air masses with the lowest NO_y mixing ratios were typically advected from the marine boundary layer. *INDEX TERMS:* 0330 Atmospheric Composition and Structure: Geochemical cycles; 0322 Atmospheric Composition and Structure: Constituent sources and sinks; 0365 Atmospheric Composition and Structure: Troposphere—composition and chemistry; 0368 Atmospheric Composition and Structure: Troposphere—constituent transport and chemistry; *KEYWORDS:* reactive nitrogen oxides, nitric acid, NO, alkyl nitrates

Citation: Weller, R., A. E. Jones, A. Wille, H.-W. Jacobi, H. P. McIntyre, W. T. Sturges, M. Huke, and D. Wagenbach, Seasonality of reactive nitrogen oxides (NO_y) at Neumayer Station, Antarctica, *J. Geophys. Res.*, *107*(D23), 4673, doi:10.1029/2002JD002495, 2002.

1. Introduction

[2] Reactive nitrogen oxides generally refer to the sum of oxidized nitrogen species in the atmosphere (NO_y = NO + NO_2 + HNO_3 + HNO_2 + HONO + PAN + organic nitrates + NO_3 + 2 N_2O_5 + $XONO_2$... where PAN is peroxyacetyl nitrate, and X is a halogen atom). Atmospheric chemistry of NO_y components is closely linked with interconversion between its members, while the percentage that each individual component contributes to the total NO_y budget clearly varies at different locations and with time in the atmosphere [e.g., *Thakur et al.*, 1999]. Due to the role of NO and NO_2 in determining the oxidation capacity of the troposphere, knowledge of the natural background concentration of oxidized nitrogen compounds is pivotal in judging the impact of human activity on the oxidizing capacity of the Earth's atmosphere [e.g., *Logan*, 1983; *Kleinman*, 1994]. Apart from the remote South Pacific and South Atlantic, Antarctica seems to be the only remaining area where the almost natural tropospheric NO_y budget may be studied. Interestingly, recent field campaigns at Neumayer Station have revealed photochemical NO_x production from the upper firn layer [*Jones et al.*, 2000], a process which may have a dramatic impact on the summertime NO_x budget and boundary layer photochemistry in central Antarctica [*Davis et al.*, 2001]. Another motivation to investigate the chemistry and budget of NO_y especially at high latitudes arises in view of serious deficits in the interpretation of nitrate signals in ice cores. Ice cores carry an invaluable potential in providing proxies to elucidate climate and chemical composition of the past atmosphere, and hence to assess the evolution of our present one. While nitrate is one of the most abundant ionic impurities of polar ices, translation into past atmospheric changes remained enigmatic [*Wolff*, 1995; *Wagenbach*, 1996] since even the major source of background NO_y (and hence nitrate in the ice) is not well known. Both lightning and downward transport of N_2O derived NO_y from the stratosphere were suggested as the origin of nitrate in Antarctica [*Legrand and Delmas*, 1986; *Wagenbach et al.*, 1998], whereas no anthropogenic effect could be revealed [*Legrand and Mayewski*,

[1]Alfred-Wegener-Institut für Polar- und Meeresforschung, Bremerhaven, Germany.
[2]British Antarctic Survey, Natural Environment Research Council, High Cross, Cambridge, UK.
[3]Metrohm AG, Herisau, Switzerland.
[4]School of Environmental Sciences, University of East Anglia, Norwich, UK.
[5]Institut für Umweltphysik, Universität Heidelberg, Heidelberg, Germany.

0148-0227/02/2002JD002495$09.00

1997]. In contrast to Antarctica, Arctic ice core nitrate records [*Legrand and Mayewski*, 1997; *Fischer et al.*, 1998] and atmospheric measurements [*Honrath and Jaffe*, 1992; *Wofsy et al.*, 1992] clearly revealed a dramatic impact of anthropogenic emissions on the Arctic NO_y budget.

[3] In this paper we present reactive nitrogen oxide measurements conducted during the PEAN'99 summer campaign (Photochemical Experiment at Neumayer, February 1999) and the succeeding overwintering period at the German Antarctic research station Neumayer. During February 1999, mixing ratios of NO_y and the individual components NO, NO_2, HNO_3, particulate nitrate (p-NO_3^-), PAN, and methyl, ethyl, i-propyl, and n-propyl nitrates (CH_3ONO_2, $C_2H_5ONO_2$, $C_3H_7ONO_2$, and $(CH_3)_2CHONO_2$, respectively) were determined, while during the overwintering period from March 1999 to January 2000 the measuring program was restricted to NO, NO_y, HNO_3, and p-NO_3^-. For the first time, year-round NO_y and NO measurements in Antarctica could be realized allowing the observed NO_y and nitrate seasonality to be discussed in terms of source assignment and associated implications for the interpretation of Antarctic nitrate ice core records under present-day climatic conditions. These evaluations are backed up by year-round observations of atmospheric radioisotope concentrations (^{7}Be, ^{10}Be, and ^{210}Pb). In addition, supporting information on air mass characterization arriving at Neumayer came from daily back trajectory studies.

2. Measurement Techniques

2.1. Measurement Site and Meteorological Conditions

[4] All measurements were made either at, or close to, the Air Chemistry Observatory, Neumayer Station (70°39′S, 8°15′W), where meteorological data are collected continuously [*König-Langlo et al.*, 1998]. During the summer months, the bay and the nearby ice edge are mainly free of sea ice and there is always open water present. Other than a few nunataks about 100 km south of the station there are no ice-free land surfaces near Neumayer, and the probability of contact with air masses from ice-free continents is small. The prevailing winds are from the east, but with strong switches to westerly winds from time to time. The air mass transport pattern to Neumayer Station was investigated by *Kottmeier and Fay* [1998] and a more detailed picture on the climatology at Neumayer Station is given by *König-Langlo et al.* [1998].

[5] Local pollution by vehicles and the base itself is a potential problem for many measurements concerning the background status of the Antarctic troposphere. Consequently, a central aspect of the technical concept of the air chemistry observatory lies in the possibility of contamination-free sampling of aerosols and trace gases. This is realized by several means: the Air Chemistry Observatory is situated in a clean air facility approximately 1.5 km south of Neumayer. Due to the fact that northerly wind directions are very rare, contamination from the base can be excluded for most of the time. The power supply (20 kW) is provided by cable from the main station, thus no fuel driven generator is operated in the observatory vicinity. Contamination-free sampling is controlled by the permanently recorded wind velocity, wind direction and by the condensation nuclei (CN) concentration. Contamination was indicated if one of the following criteria was given: wind direction within a 330°–30° sector, wind velocity <2.2 m s^{-1} and/or CN concentrations (measured by a TSI CNC3022A particle counter) >1200 cm^{-3} during summer, >800 cm^{-3} during spring/autumn and >400 cm^{-3} during winter. The CN threshold values were chosen on the basis of our nearly 20-year long CN record from Neumayer, demonstrating that CN concentrations above the corresponding levels can usually be traced back to local pollution.

[6] For the present study, daily 5-day back trajectories were calculated by the German Weather Service (Deutscher Wetterdienst, DWD) based on the global model of the DWD. In all cases the air masses reached Neumayer at 1200 UTC. Throughout this work the time is given in UTC, corresponding to a shift of +32 min relative to the solar time and trace compound concentrations are given in pptv, ppbv, or at scm^{-3} (parts per 10^{12} or 10^9 by volume or atoms per standard m^3).

2.2. NO, NO_2, and NO_y

[7] We measured NO, NO_2, and NO_y using two chemiluminescence detectors coupled with a photolytical NO_2 and an Au/CO catalyzed NO_y convertor, respectively. NO_y was determined by reduction to NO (gold catalyst at 300°C with 0.3% CO) and a chemiluminescence detector (Eco Physics CLD 780 TR). The values for NO_y are derived from 200-s integrations, binned to give 30-min averages. The instruments were run under controlled conditions, including checks and tests for instrument performance carried out on a daily basis throughout the year as well as prior to leaving for Antarctica. While a detailed discussion of accuracy determination and measurement technique is given by *Jones et al.* [1999, 2001] and *Weller and Schrems* [1996], only some details, concerning the reliability of the NO_y time series, will be reported here. The conversion efficiency of the NO_y convertor was checked weekly with NO_2 using NIST traceable NO standard mixtures (1.03 ± 0.05 ppmv NO in N_2, Messer Griesheim, Germany) for dynamic dilution to the range between 3 and 10 ppbv NO. Former tests revealed that the instrument showed a linear response down to at least 25 pptv NO [*Weller and Schrems*, 1996]. NO_2 was generated by gas phase titration of NO calibration mixtures with ozone. The conversion efficiency factor was found to be essentially constant at 0.95 ± 0.03, showing no systematic change over 1 year of continuous operation of the convertor. Similarly, laboratory experiments were carried out to determine the conversion efficiency of HNO_3 both before leaving for Antarctica and on return. The HNO_3 conversion efficiency was found to vary between 0.72 and 0.93. We forwent cleaning of the gold catalyst since it seemed to enhance the conversion efficiency only for a few hours. In addition, the response of the NO detector was determined before, during, and after the overwintering with different certified NO calibration mixtures, showing that the sensitivity of the NO detector remained essentially stable. At the end of the measuring period in January 2000, NO_y mixing ratios were comparable with those measured in January/February 1997 [*Weller et al.*, 1999] and February 1999, which underlines the stable performance of the equipment.

[8] Considerable care must be taken when evaluating NO_y data, as the operationally defined number NO_y^* resulting from the measurement may not represent the real, above

Table 1. Mixing Ratios and Error Limits (±Accuracy) of Individual NO_y Component Species Measured During PEAN'99 Campaign

Date	CH_3ONO_2 [pptv]	$C_2H_5ONO_2$ [pptv]	$(CH_3)_2CHONO_2$ [pptv]	$C_3H_7ONO_2$ [pptv]	PAN [pptv]	HNO_3 [pptv]	$NO + NO_2$ [pptv]	Sum [pptv]	NO_y^* [pptv]
8 February	8.0 ± 0.6	1.8 ± 0.13	1.2 ± 0.1	0.7 ± 0.06	8.7 ± 3.0	2.6 ± 0.6	7.6 ± 4.0	30.6 ± 5.1	35.1 ± 12
17 February	8.5 ± 0.65	1.9 ± 0.13	0.9 ± 0.1	–	9.0 ± 3.0	3.6 ± 0.8	4.6 ± 3.5	28.6 ± 4.8	45.1 ± 16
18 February	9.4 ± 0.7	2.2 ± 0.15	0.7 ± 0.07	0.9 ± 0.07	9.1 ± 3.0	3.6 ± 0.8	2.1 ± 2.0	28.1 ± 4.0	42.2 ± 15
19 February	10.8 ± 0.8	2.9 ± 0.2	1.3 ± 0.12	1.0 ± 0.08	11.3 ± 3.0	2.3 ± 0.5	3.4 ± 3.0	33.1 ± 4.4	24.7 ± 8.6
20 February	10.7 ± 0.8	2.9 ± 0.2	1.1 ± 0.12	1.1 ± 0.09	12.5 ± 3.0	2.3 ± 0.5	1.6 ± 1.6	32.2 ± 3.6	16.0 ± 5.6

NO, NO_2, and NO_y^* represent mean values over the respective HNO_3 sampling interval, while the alkyl nitrate data correspond to sampling periods of typically 30 min.

defined NO_y in the ambient atmosphere, for our data NO_y^* includes the sum of inorganic oxidized nitrogen and PAN plus the converted fraction of the light alkyl nitrates. As discussed by *Jones et al.* [1999], we do not consider that it will include p-NO_3^-. Recognizing the difficulties with HNO_3 sampling because of uptake to surfaces, some proportion of HNO_3 is likely to be missing from the measured NO^*_y. We determined the inlet efficiency factor to be 0.7 ± 0.2. This causes no substantial problems, however, as HNO_3 mixing ratios were in the lower pptv range, except of the period from November to January, when the NO_y^* values were corrected for inlet efficiency (0.7) and conversion efficiency (0.8). Much more problematic is the conversion efficiency of methyl nitrate, which seems to be a dominant NO_y^* component species at Neumayer at least during summer [*Jones et al.*, 1999]. To our knowledge, conversion efficiencies for methyl nitrate are not available and we did not succeed in developing a suitable calibration source for the NO_y convertor. During the PEAN'99 campaign, coinciding alkyl nitrates, HNO_3, PAN, NO_x, and NO_y^* measurements were available for an overall period of 72 hours. Assuming a uniform conversion efficiency of 1.0 for all components, a comparison of the budget from the sum of the individual compounds and the measured NO_y^* showed that NO_y^* agrees on average within the error limits (Table 1). This is consistent with results obtained with the same convertor type at Jungfraujoch, Switzerland by *Zellweger et al.* [2000]. Here NO_y^* was 22% higher than the individually measured NO_y components. *Zellweger et al.* [2000] attribute this discrepancy to the presence of alkyl nitrates, which were not measured.

[9] In order to ensure that the influence of local NO_y sources or instrumental artifacts did not affect the data presented here, the raw NO_y^* and NO data records were subject to a detailed and conservative screening procedure. Exclusively the diesel generator of the nearby Neumayer Station and frequent motor vehicle usage during polar summer must be considered as possible contamination source. Contamination was indicated by the criteria described in section 2.1. In addition, the NO_y^* convertor showed disturbingly high background noise after calibration procedures or instrument failures caused by occasional power outages. All NO_y^* data recorded within such periods were discarded and not considered for further evaluation. In all, we obtained reliable NO_y^* data from about 73.1% of the total available time between 1 February 1999 and 17 January 2000. The most extensive data losses of about 77% occurred in February when instrumental problems in the setup phase and detailed performance tests were conducted.

[10] The precision of the NO_y^* measurement on a 2 σ basis was determined to be around ±20% in the concentration range between 10 and 100 pptv. The accuracy is highly dependent on the composition of ambient NO_y, given the possible differences in conversion efficiency of the various components. Assuming that the conversion efficiencies of all component species not experimentally determined here was 0.75 ± 0.25, the overall accuracy of the NO_y^* measurement was ±35% from February to November. From early November to late January, the portion of HNO_3 was between 21% and 41% of the total NO_y^* amount. Therefore the variable transmission and conversion efficiencies of HNO_3 were most decisive leading to an accuracy of ±31% during this period.

2.3. HNO_3 and p-NO_3^-

[11] During the PEAN'99 summer campaign nitric acid and p-NO_3^- were sampled for 24-hour time periods using a 3-stage PFA filter holder system, including a Teflon and two nylon (Nylasorb) filters (all 1 μm pore size). During the overwintering a Teflon/nylon/cellulose filter combination (Whatman 541 cellulose filter impregnated with K_2CO_3 to sample acidic gases and SO_2) was used and the temporal resolution was 7 days. The filter systems were housed within the Neumayer Air Chemistry Observatory. Ambient air was drawn through a ventilated stainless steel inlet stack (total height 8–9 m above the snow surface). While the Teflon filter collected p-NO_3^-, gaseous HNO_3 passing the Teflon filter or reemitted from it was collected by the nylon backup filters. For the 24-hour (7 days) sampling period, derived errors were 21% (15%) and 9% (7%) for HNO_3 and p-NO_3^-, respectively, with a combined error for total inorganic nitrate (HNO_3 + p-NO_3^-) of 11% (9%). The detection limit, derived from 2 σ of the blank values, was found to be 1 pptv (about 0.5 pptv) for both p-NO_3^- and gaseous nitrate. Further details are described by *Jones et al.* [1999].

2.4. Additional Measurements During PEAN'99: PAN and Alkyl Nitrates

[12] Preconditioned 800 and 3200 mL stainless steel flasks were filled to roughly 3.2 bar at regular intervals during the campaign, using a metal bellows pump after thorough flushing of the whole system with ambient air. Whenever possible, flasks were filled at ground level roughly 50 m upwind of the Air Chemistry Observatory. The whole air samples were analyzed using a gas chromatograph equipped with an electron capture detector (ECD, Ni-63 foil). The respective accuracies were ±7.5% for CH_3ONO_2, ±7% for $C_2H_5ONO_2$, ±9.2% for $C_3H_7ONO_2$, and ±8% for $(CH_3)_2CHONO_2$. In total we analyzed 96 flasks for alkyl nitrates, sampled between 7 and 23 February. The mean mixing ratios (±s.d.) were 9.5 ± 1.4 pptv CH_3ONO_2, 2.3 ± 0.5 pptv $C_2H_5ONO_2$, 1.1 ± 0.8

$C_3H_7ONO_2$, and 1.2 ± 0.5 pptv $(CH_3)_2CHONO_2$. In the course of this study we found that the calibration used to calculate $RONO_2$ mixing ratios in our previous paper on NO_y^* speciation at Neumayer in 1997 [*Jones et al.*, 1999] may have been in error. The calibration of methyl and ethyl nitrates presents particular challenges, requiring synthesis of the pure compounds, and coanalysis of dynamically diluted effusion from diffusion tubes by both chemiluminescence and ECD. Of particular note was the discovery that humidity levels have a profound effect on the sensitivity and reproducibility of the ECD determination of $RONO_2$. A new calibration was performed with a humidification system in place and the 1997 results were reassessed in the light of this [*McIntyre*, 2001]. $RONO_2$ mixing ratios are now thought to have been overestimated by about a factor of 3, explaining why NO_y^* estimated from summation of individual species did, on occasions, exceeded the direct chemiluminescence measurement of NO_y^*. Applying the revised calibration to the 1997 data resulted in an estimated average NO_y^* from summation of species of 25 ± 5 pptv, lower than the original estimate of 39 ± 6 pptv, and within the error of the mean chemiluminescence measurement of 30 ± 20 pptv. Only methyl and ethyl nitrates were considered in the 1997 study, but the work here shows that C_3 nitrates contribute at most only one or two pptv of NO_y^*, and there was no evidence of significant levels of higher alkyl nitrates in the ECD traces either then or in the current study. The revised measurements of methyl and ethyl nitrate from 1997 (10 ± 2 and 3 ± 1 pptv, respectively) are now in good agreement with the averages from this study (see above).

[13] The method for the PAN measurements is based on electron capture gas chromatography with cryogenic preconcentration technique [*Schrimpf et al.*, 1995]. Details of the commercial analyzer (Meteorologie Consult GmbH, Glashütten, Germany) were recently described [*Jacobi et al.*, 1999]. A PAN detection limit of 5 pptv was obtained referring to two times the standard deviation of the noise. Multipoint calibrations were performed at the beginning and at the end of the campaign and showed good agreement, resulting in an estimated overall accuracy of ±15% or ±3 pptv, whatever is higher [*Jacobi et al.*, 2000].

2.5. ^{7}Be, ^{10}Be, ^{210}Pb, and Solar Irradiance Measurements

[14] These measurements are part of the long-term measuring program carried out since 1983 at Neumayer (http://www.awi-bremerhaven.de/GPH/SPUSO.html). Aerosol borne ^{7}Be, ^{10}Be, and ^{210}Pb were collected on cellulose filters (2× Whatman 541 in series, diameter 240 mm) by continuous high volume aerosol sampling (120 m^3 hr^{-1}, sampling interval 2 weeks) through the stainless steel stack of the Air Chemistry Observatory. After return to the Heidelberg laboratory the ^{7}Be and ^{210}Pb activities were determined by high resolution γ-spectroscopy as described by *Wagenbach et al.* [1988], ^{10}Be was measured by accelerator mass spectroscopy. 1σ counting errors were generally between 5% and 15% for ^{7}Be (depending on the decay time before analyses) and typically 10% for ^{210}Pb. UV solar radiation was measured routinely by an UV radiometer (Eppley, USA, 300–370 nm) and an UV-B spectroradiometer covering the spectral range from 280 to 320 nm with a spectral resolution better than 1.35 nm at an absolute wavelength precision of 0.01 nm and a detection threshold of 10^{-7} W m^{-2} nm^{-1} [*Seckmeyer et al.*, 1998].

3. Results and Discussion

3.1. NO_y^* Data Presentation

[15] In Figure 1 the entire NO_y^* time series is presented. Note that due to high HNO_3 mixing ratios, NO_y^* data between 1 November 1999 (day of the year, DOY = 305) and 17 January 2000 (DOY = 382) was corrected for the inlet and conversion efficiency of HNO_3. In Figure 2, HNO_3, the sum of p-NO_3^- and HNO_3 (total nitrate) and the mean NO_y^* mixing ratio averaged over each aerosol sampling interval are shown. A similar seasonal cycle of HNO_3 and total nitrate mixing ratios was measured through the years 1997, 1998, and 2000. From the NO_y^* time series the following overall picture emerges: NO_y^* mixing ratios showed a broad maximum during late summer and fall, while a minimum could be observed during polar night. The frequency distribution of the NO_y^* mixing ratios matches a normal distribution skewed to higher values (Table 2). A comparison of the p-NO_3^-/HNO_3 with NO_y^* data revealed that except for the months November, December, and January the HNO_3/NO_y^* and the $(HNO_3 + p\text{-}NO_3^-)/NO_y^*$ ratios were rather low. Only from November to January, HNO_3 seemed to be a major NO_y^* component species (Table 3).

[16] As mentioned in the experimental section, measuring reactive nitrogen oxides by catalytic reduction/chemical luminescence technique (CR/CL) may be susceptible to several artifacts. Although a discrepancy between the NO_y^* determined by CR/CL and the sum of individual NO_y component species was not confirmed by our limited data set, we will assess if the presented features of the NO_y^* time series might be caused by systematic composition change of NO_y, though the sum of NO_y compounds was apparently constant. If we assume an uniform and high conversion efficiency of the reactive and thermally unstable component species PAN, NO_3, HNO_4, N_2O_5, $ClONO_2$, and $BrONO_2$, which may constitute a significant part of the NO_y budget during polar night, the most critical NO_y component is CH_3ONO_2 due to its probably low conversion efficiency. But even assuming a conversion efficiency as low as 0.5, methyl nitrate variations with amplitudes higher than 20 pptv would have been needed to explain the NO_y^* maxima observed from March to June. This is rather unrealistic, especially considering the relatively constant methyl nitrate mixing ratios around 9 pptv observed in February. Up to now the source of methyl nitrate is unclear, although recent studies point to a marine origin [*Talbot et al.*, 2000]. However, during the PEAN'99 campaign trajectories did not indicate that advection of marine air was linked with enhanced methyl nitrate mixing ratios. It is likely that marine emissions are widespread throughout the Southern Hemisphere. Combined with its relatively long tropospheric residence time, especially in higher latitudes, a reasonably uniform background concentration of methyl nitrate could be anticipated throughout the year. *Flocke et al.* [1998] discussed gas phase production of CH_3ONO_2 that could be relevant for the upper troposphere and lower stratosphere. Regarding the very low CH_3ONO_2/NO_y ratio of <0.1 found in upper tropospheric air [*Talbot et al.*, 2000],

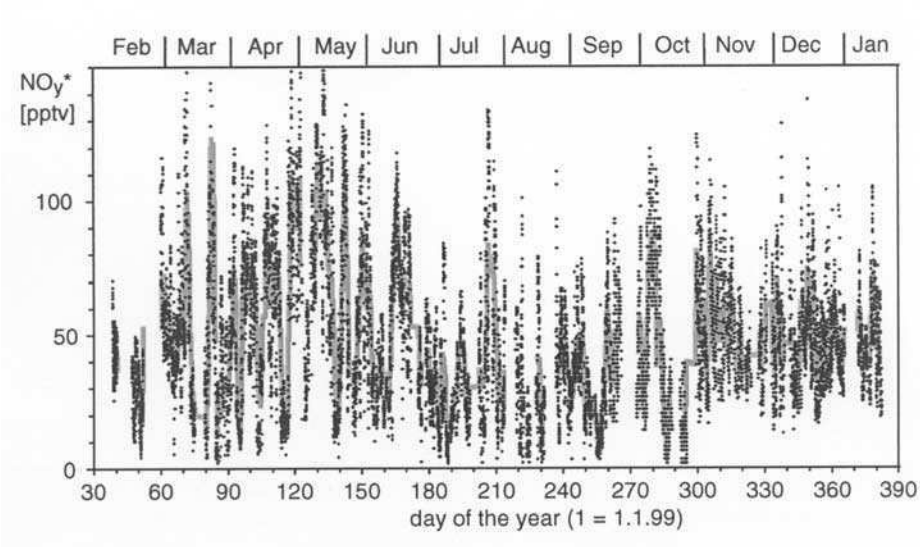

Figure 1. Measured NO_y^* time series. Dots represent 30-min averages, and the gray line corresponds to 24-hour running means.

an impact of varying methyl nitrate mixing ratios on the observed NO_y^* seasonality may be negligible.

3.2. Photochemical Aspects

[17] Reemission of deposited NO_y [*Weller et al.*, 1999] and solar radiation induced NO_x emissions from the firn layer [*Honrath et al.*, 1999; *Jones et al.*, 2000, 2001] may partly be responsible for diurnal NO_y^* variations associated with NO_y^* maxima in the late afternoon frequently observed from November 1999 to January 2000 (Figure 3). Similar to our results obtained in January and February 1997 [*Weller et al.*, 1999], the occurrence of such diurnal NO_y^* cycles during

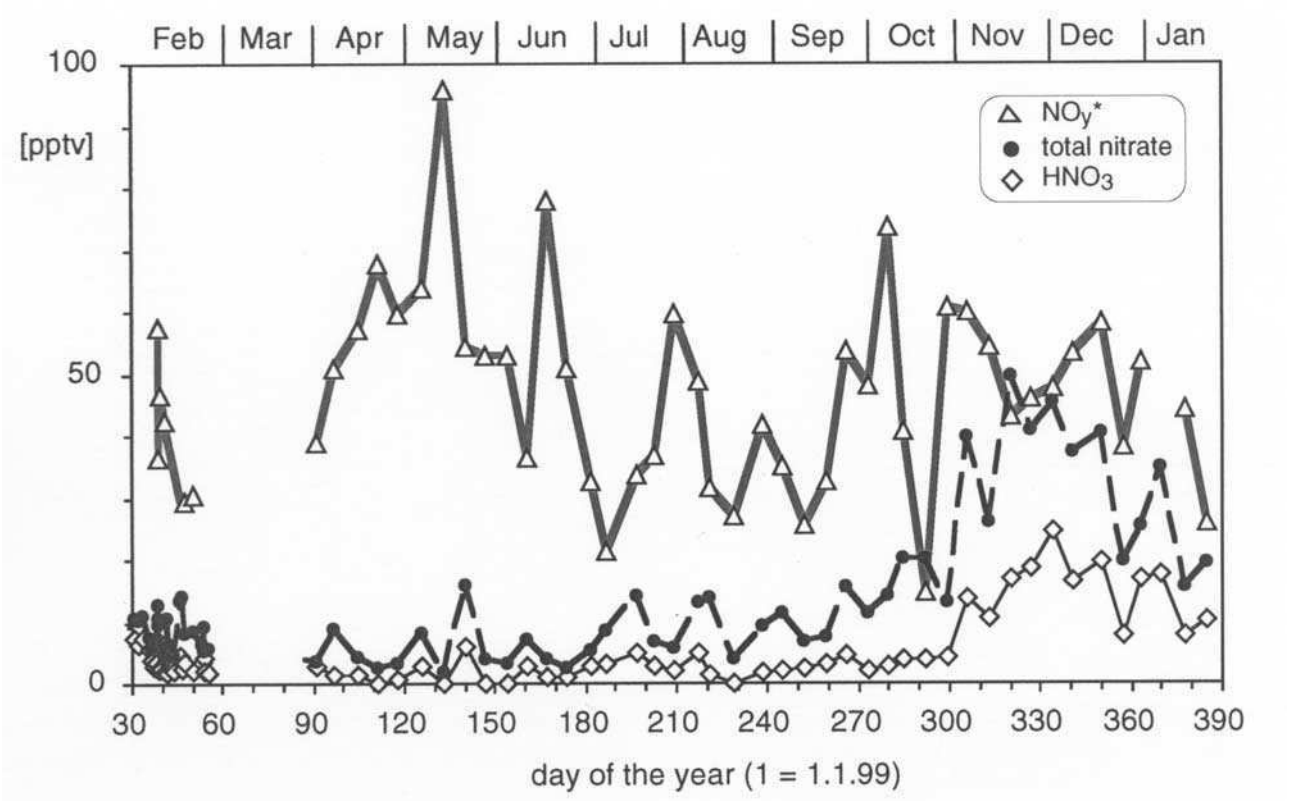

Figure 2. Seasonality of NO_y^* (triangles) in comparison with HNO_3 (diamonds) and total nitrate (closed circles). The NO_y^* mixing ratios equal averages for corresponding aerosol sampling periods (1 week).

Table 2. Statistics of the NO_y^* Measurement at Neumayer

Period	NO_y^* mean ± s.d. [pptv]	Skewness
1 February to 31 May (DOY 32–151)	58 ± 35	0.99
1 June to 17 January (DOY 152–382)	44 ± 23	0.63
All data (DOY 32–382)	49 ± 29	1.05

polar summer was linked with the variability of the surface inversion strength and the actinic radiation. Apart from these special cases, NO_y^* signals and surface inversion strength (defined as the temperature difference between 10 and 2 m altitude, $\Delta T_{10m-2\ m}$) or radiation were generally not correlated, indicating that this process appeared to be secondary regarding the NO_y^* balance at Neumayer. However, recent investigations indicate that in continental Antarctica photochemically recycled nitrate from the upper firn layer, i.e., emissions of NO_x (=NO + NO_2) produced by postdepositional photolysis of nitrate, leads to a dramatic accumulation of NO within the flat surface inversion layer [*Davis et al.*, 2001]. There, and in coastal sites with pronounced katabatic winds, during austral summer a significant if not dominant part of the NO_y^* balance might be controlled by this process. Although Neumayer is clearly not among such sites, the seasonal maximum of the NO signals appears at the end of the ozone hole period in early December. In Figure 4, NO mixing ratios are presented in comparison with short wave UV radiation (measured at 300 nm, spectral width 1.35 nm), which may have caused an increased nitrate photolysis within the upper firn layer during this period. Note, that the observed NO maximum during early December was primarily not caused by enhanced NO_2 photolysis rates. NO_2 photolysis frequencies are roughly comparable to the UV irradiance between 300 and 370 nm as measured by the Eppley radiometer [*Junkermann et al.*, 1989] exhibiting a nearly constant level from early December to the end of January (Figure 4). However, a statistically significant correlation between shortwave UV-radiation and near surface NO mixing ratios was not found, most probably blurred by the variable stability of the boundary layer. In addition, our NO levels were an order of magnitude lower than the values found by *Davis et al.* [2001] at South Pole with NO_y^* mixing ratios showing no significant increase. On the other hand, it is well known that especially in central Antarctica a large part of deposited nitrate is exposed to postdepositional losses [e.g., *Röthlisberger et al.*, 2002]. One may speculate whether the maximum in HNO_3 and p-NO_3^- mixing ratios can partly be attributed to enhanced HNO_3 and NO_x emissions from central Antarctic snowfields, but an assessment of this problem would deserve dedicated model calculations.

3.3. Major NO_y^* Source Assignment

[18] From March to May a peculiar alternation between high and low NO_y^* mixing ratios was observed. This period, which also embraces the seasonal NO_y^* maximum, coincides with the beginning of the polar winter and the development of the polar vortex [*Schoeberl and Hartmann*, 1991]. Regarding 5-day back trajectories it emerged that in most cases a change occurred from advection of marine boundary layer air masses resulting in low NO_y^* mixing ratios to down mixing of air parcels from continental Antarctica causing events of increasing or maximum NO_y^* signals (Figure 5). Note that only trajectories of the following two categories are presented: (1) air masses from the marine boundary layer below the 800 hPa level and (2) air masses from the free troposphere over continental Antarctica, originating above the 700 hPa level. The first category showed mean NO_y^* mixing ratios of 44 ± 18 pptv, while the latter bore significantly higher NO_y^* levels of 63 ± 26 pptv. The remaining trajectories were less characteristic, i.e., a clear classification in marine boundary layer or continental free troposphere air masses was not possible. Although no trajectory could eventually be traced back to the stratosphere and in some cases a clear connection between air mass origin and NO_y^* extrema was not evident, it is obvious that during this period low NO_y^* mixing ratios were preferentially found in marine boundary layer air while higher NO_y^* levels could be assigned to advection from the free troposphere above the inland ice. Regarding the whole NO_y^* record, this differentiation was not so pronounced and barely significant: advection from marine areas within 800–1000 hPa showed NO_y^* mixing ratios of 40 ± 15 pptv, while NO_y^* mixing ratios in air masses from the free troposphere of continental Antarctica (above 700 hPa) were only slightly higher (49 ± 24 pptv, Figure 6).

[19] ^{7}Be, whose equilibrium mixing ratios steadily increase with altitude showing a maximum in the lower stratosphere, is only a poor tracer for stratospheric intrusions. Actually, the observed NO_y^* record clearly showed no correlation with ^{7}Be activity levels at Neumayer. As outlined by *Wagenbach et al.* [1988], ^{7}Be activities have to be normalized by ^{210}Pb activities in order to cancel the down-mixing efficiency from the free troposphere to the surface layer. By this means, ^{7}Be/^{210}Pb ratios are a suitable tracer for down-mixing of stratospheric or upper tropospheric air masses. Figure 7 presents the mean NO_y^* mixing ratios during corresponding radioisotope sampling intervals (2 weeks) and the calculated ^{7}Be/^{210}Pb activity ratio. Although the ^{7}Be/^{210}Pb maximum preceded the NO_y^* maximum, the overall seasonality looks quite similar and a significant positive covariance exists (90% significance level, N = 25, r = 0.35). In contrast, ^{210}Pb activity was anticorrelated (99.5% significance level, N = 25, r = 0.56). Again atmospheric ^{222}Rn whose major sources are the ice-free continents is measured routinely at Neumayer and exhibits there regular enhanced levels on the diurnal timescale (so-called radon storms) showed virtually no

Table 3. HNO_3/NO_y^* and $(HNO_3 + p\text{-}NO_3^-)/NO_y^*$ Ratios Measured at Neumayer

Period	HNO_3/NO_y^* (±s.d.)	$(HNO_3 + p\text{-}NO_3^-)/NO_y^*$ (±s.d.)
1 February to 31 October (DOY 32–304)	0.06 ± 0.05	0.22 ± 0.2
1 November to 31 January (DOY 305–382)	0.31 ± 0.1	0.69 ± 0.23
All data (DOY 32–382)	0.12 ± 0.1	0.33 ± 0.3

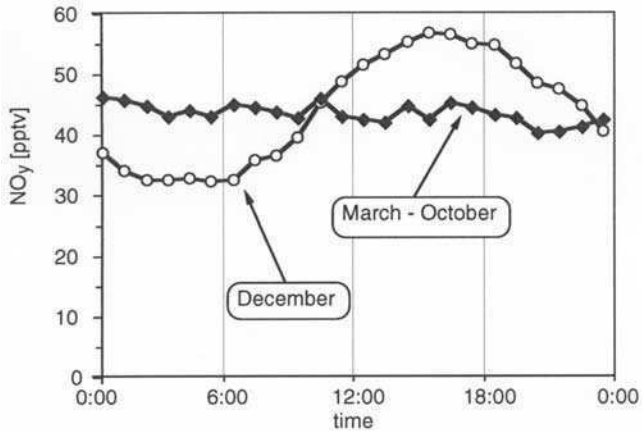

Figure 3. Mean diurnal cycles of NO_y^* (filled diamonds from March to October; circles for December). Each time interval represents the corresponding average over the mentioned observation period. The daily maximum of the solar UV radiation is at 1232 UTC (local noon).

correlation with NO_y^* mixing ratios. In addition, black carbon (BC), which can be regarded as a tracer for biomass burning, clearly showed a different seasonality compared with NO_y^* in Antarctica. BC concentrations measured since 1995 at Neumayer with an aethalometer (Magee Scientific AE10iE) are maximal between July and October, while at Halley [*Wolff and Cachier*, 1998] and South Pole [*Bodhaine*, 1995] the seasonal BC maxima appear in October. All these findings argue against a NO_y ground-level source at northward continents favoring instead a stratospheric or upper tropospheric NO_y origin.

[20] In the following we try to assess the NO_y associated with stratospheric air by using ^{10}Be and ^{7}Be data from Neumayer. Unfortunately, the ^{10}Be data for 1999 are only seasonally resolved (i.e., 3-month means), but for the years 1983–1986 ^{10}Be records with 2 weeks and 1990/1991 with monthly resolution were available. Therefore we used a normalized ^{10}Be mean annual cycle based on the high resolution data set and scaled to the mean of the 1999 data. Another critical point is the assumption of equal tropospheric lifetimes of the Be-bearing aerosol (about 30 days according to *Shaw* [1982]) and NO_y (*Logan et al.* [1981] estimated a free tropospheric HNO_3 residence time of 5–55 days for 4–10 km altitude). Our calculations are based on a simple two-box approach under steady state assumptions as previously described by *Raisbeck et al.* [1981], which allows elucidation of the contribution of stratospheric air arriving at ground level from ^{10}Be and ^{7}Be measurements. The stratospheric and

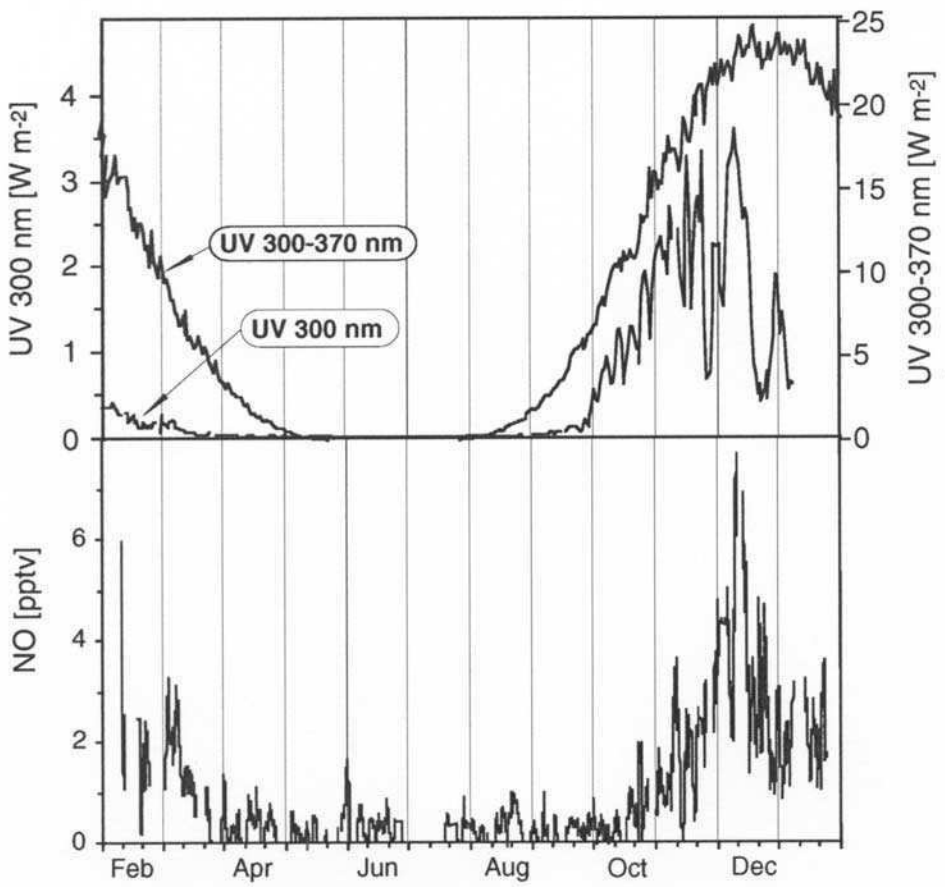

Figure 4. Seasonality of the measured NO mixing ratios (24-hour running means), solar radiation at 300 nm (daily averages, measured by the spectroradiometer), and solar UV radiation from 300 to 370 nm (daily averages, measured by the UV radiometer).

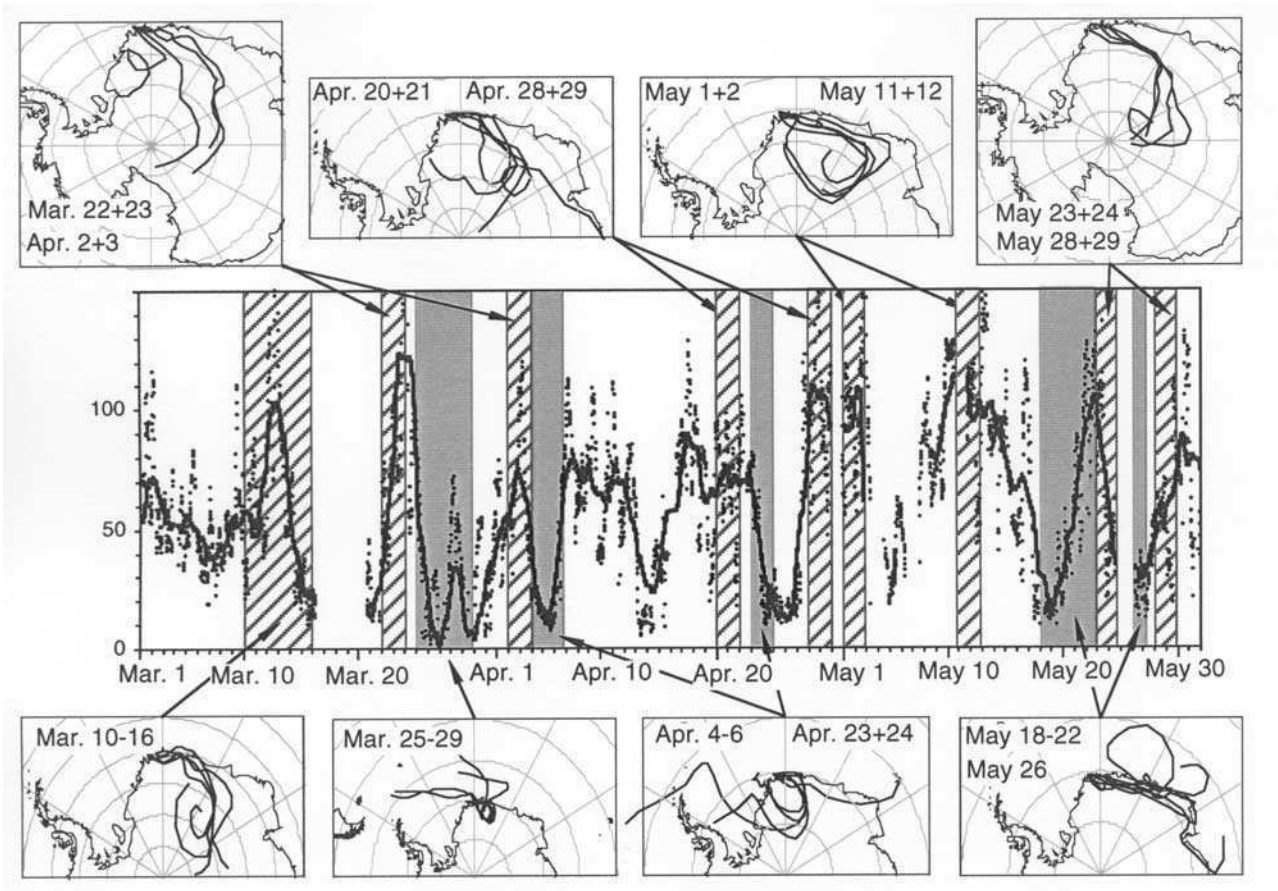

Figure 5. Details of the measured NO_y^* time series from March to May 1999. Dots represent 30-min averages, the gray line corresponds to 24-hour running means. Also shown are 5-day back trajectories arriving at Neumayer at 1200 UTC during marked periods (gray: marine air masses; hatched: air masses from the continental free troposphere.) For details, see text.

tropospheric box inventories are described by the following equation:

$$\frac{[^{10}Be]}{[^{7}Be]} = \frac{P_{10} + J_{10}}{P_7 + J_7}\left(1 + \frac{\tau}{\tau_7}\right)$$

P_i and J_i are the production rates and fluxes of the corresponding beryllium isotope ^{i}Be into the box, τ_7 is the radioactive lifetime of ^{7}Be (77 days) and τ the residence time of aerosol in the atmospheric box. The production ratio $P_{10}/P_7 = 0.52$ [*Masarik and Beer*, 1999] is expected to be constant throughout the atmosphere. The stratospheric lifetime used to estimate the stratospheric ^{10}Be/^{7}Be ratio is assumed to be 1 year [*Raisbeck et al.*, 1981] which is on the lower end of the range derived from ^{90}Sr profiles by *Johnston* [1989]. The model is employed to derive the stratospheric ^{10}Be fraction $[^{10}Be]_{sf}$ seen at Neumayer which in turn is used to estimate the associated stratospherically derived NO_y fraction $[NO_y]_{sf}$ where $[NO_y]_s/[^{10}Be]_s$ denotes the respective ratio in the stratosphere:

$$[NO_y]_{sf} = [^{10}Be]_{sf}\left(\frac{[NO_y]_s}{[Be]_s}\right)$$

A stratospheric ^{10}Be concentration of 4×10^6 at scm^{-1} was assumed from respective production rate [*Masarik and Beer*, 1999] and aerosol lifetime. The corresponding NO_y mixing ratio in the lower stratosphere varied between 3 and 6 ppbv according to *Gao et al.* [1997]. Accordingly a range for $([NO_y]_s/[^{10}Be]_s)$ between 0.75×10^{-15} and 1.5×10^{-15} m^3 atm^{-1} has been employed. The result of this estimate indicates that the seasonality of surface NO_y at Neumayer could be caused by stratospheric air mass intrusions, although the NO_y^* maximum appeared about 2–3 months later (Figure 8). In addition our admittedly crude estimate demonstrates that most of the NO_y^* measured at Neumayer originated most probably from the stratosphere, leaving little room for a supplementary tropospheric NO_y contribution. Nevertheless a plausible explanation for the observed NO_y^* maximum early May 1999 can not be given on the basis of our results. Note that we used a mean seasonal cycle of the ^{10}Be/^{7}Be ratio, because data from 1999 were only available in 3-month means. Accordingly a close coincidence between the seasonality of NO_y^* and ^{10}Be/^{7}Be can not be anticipated. The seasonalities of alkyl nitrate and PAN sources coming into question are not clear. However, for these NO_y component species, accounting for about 70% of the total NO_y^* during austral summer at Neumayer, a stratospheric source should be negligible.

[21] Recent field measurements, satellite observations and model simulations suggest lightning activity to play an

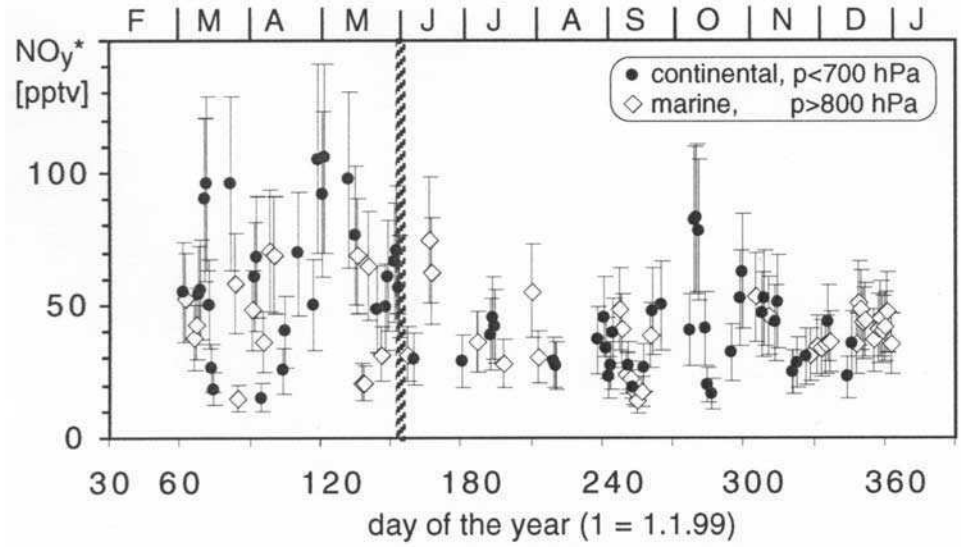

Figure 6. Daily mean NO_y^* mixing ratios classified according to the origin of advected air masses. The line separates the period of high NO_y^* variability. For details, see text.

important role in determining the NO_y budget of the upper troposphere [*Zhang et al.*, 2000; *Tie et al.*, 2001; *Bond et al.*, 2002] and may also be a significant source for Antarctic NO_y. However, the seasonal maximum of lightning activity in southern Africa occurs from December to February [*Zhang et al.*, 2000; *Bond et al.*, 2002], hence preceding the observed NO_y^* maximum at Neumayer by 3–5 months.

3.4. Comparison With Seasonality of Total Nitrate and Arctic NO_y

[22] Our results constitute the first year-round NO_y^* record from Antarctica. From the high Arctic, up to now, the sole seasonal cycle of NO_y^* was recorded by *Honrath and Jaffe* [1992] at Barrow (a coastal station in Alaska, 71°19′N, 156°37′W) using a similar technique. They observed maximum NO_y^* mixing ratios of about 500–700 pptv in late winter/early spring while during polar summer median values were as low as 70 pptv. These results are consistent with more recent measurements conducted at Summit, Greenland, during the summers of 1994 and 1995 [*Dibb et al.*, 1998; *Munger et al.*, 1999]. Compared to the Arctic maximum, NO_y^* mixing ratios measured at Neumayer were lower by nearly an order of magnitude with a different seasonal cycle. In the Arctic, maximum total nitrate (HNO_3 + p-NO_3^-) mixing ratios between 25 and 90 pptv can be found in late January/February [*Barrie and Hoff*, 1985], while the annual maximum at coastal Antarctic sites is again different and appears in late austral spring (November). In the Arctic, the HNO_3/NO_y^* ratio is very low, around 0.01 during summer [*Dibb et al.*, 1998; *Munger et*

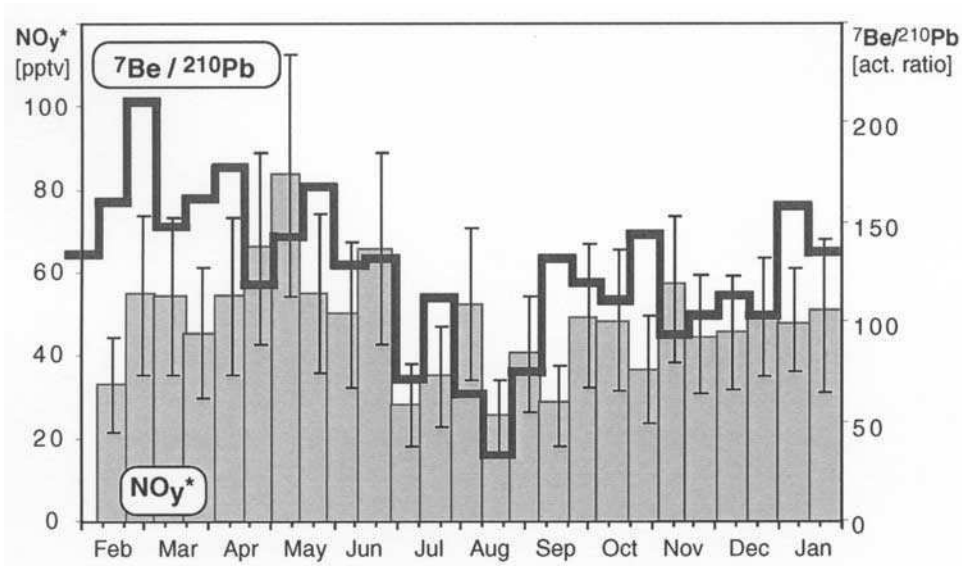

Figure 7. Seasonality of NO_y^* (gray bars) in comparison with $^7Be/^{210}Pb$ activity ratios (thick line). The NO_y^* mixing ratios equal averages for the corresponding radionuclide sampling periods (2 weeks).

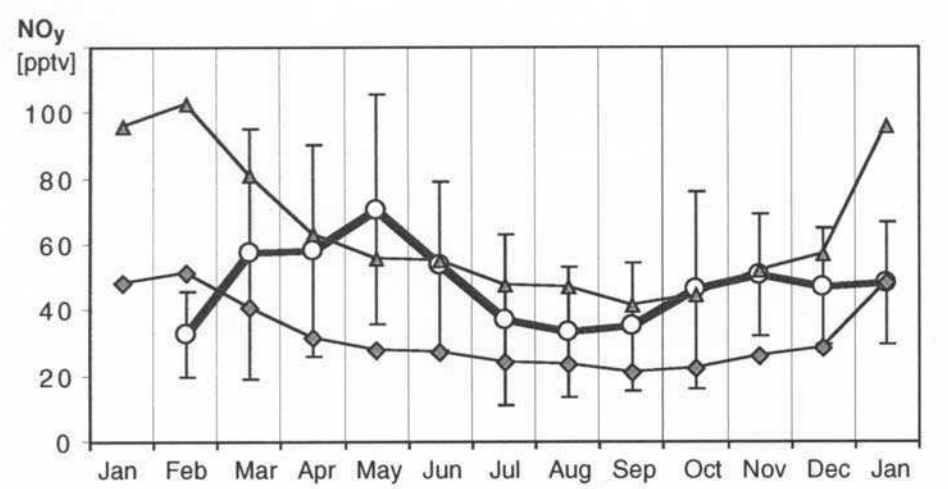

Figure 8. Measured NO_y^* (circles) in comparison with the stratospheric component of NO_y calculated from the ^7Be and ^{10}Be data, assuming a stratospheric NO_y mixing ratio of 3 ppbv (shaded diamonds) and 6 ppbv (shaded triangles). All data have been averaged to calendar months. In addition for NO_y^*, the standard deviation of the individual means is shown.

al., 1999] while at Neumayer a value of 0.31 is typical for the same season. PAN seems to be the dominating reactive nitrogen component in the Arctic, at least during winter and spring [*Solberg et al.*, 1997]. Unfortunately, for Antarctica a NO_y-budget assessment is only possible for February, indicating that organic nitrates, i.e., PAN and methyl nitrate, are the main compounds. A strong impact of industrial emissions, which accumulate in the Arctic troposphere during winter/spring, is evident [*Ottar*, 1989; *Honrath and Jaffe*, 1992; *Wofsy et al.*, 1992]. Other important sources for Arctic NO_y are natural fires and intrusions of stratospheric air masses [*Wofsy et al.*, 1992]. In Antarctica, on the other hand, stratospheric input and (sub-) tropical lightning activities were put forward as dominant sources, at best for HNO_3 and p-NO_3^- [*Legrand and Delmas*, 1986; *Wolff*, 1995; *Wagenbach et al.*, 1998]. As discussed in detail by *Wagenbach et al.* [1998], the seasonal total nitrate maximum most probably reflects stratospheric nitrate input associated with the sedimentation and evaporation of polar stratospheric clouds (PSCs). The observed seasonal maximum of NO_y^* appeared in April/May, too early for PSC sedimentation but roughly consistent with the annual maximum of stratospheric air mass intrusions. Although the seasonality of the total nitrate and NO_y^* signal at Neumayer is clearly different and thus no obvious correlation between atmospheric nitrate (HNO_3 + p-NO_3^-) and NO_y^* mixing ratios is evident, the stratosphere seems to be the main source region.

4. Conclusions

[23] Trajectory analyses and radioisotope variability (^7Be, ^{10}Be and ^{210}Pb) consistently indicated an upper tropospheric or stratospheric NO_y^* source region, although the seasonal maximum observed in early May could not be explained by any potential NO_y source. Our results did not support the northward continents or marine boundary layer to be a significant source for NO_y^* measured at Neumayer. Thus our findings support the idea that nitrate signals archived in Antarctic ice cores under present-day climatic conditions are dominated by a stratospheric source [*Wagenbach et al.*, 1998]. Our results do not indicate a locally enhanced (coastal or ice-edge) marine source of CH_3ONO_2. Most probably methyl nitrate mixing ratios observed at Neumayer represent a background level induced by uniform marine emissions throughout the Southern Hemisphere. Coinciding year-round measurements of individual NO_y component species, in particular NO + NO_2, PAN, $RONO_2$, and HNO_3 are necessary to overcome ambiguities concerning the source region and budget of Antarctic reactive nitrogen oxides. Present atmospheric models symptomatically overpredict upper tropospheric HNO_3/NO_y ratios indicating a serious shortfall in understanding chemistry and budget of reactive nitrogen oxides in the (global) upper troposphere. Nevertheless, dedicated modeling efforts specifically designed for trace component conversion and transport to Antarctica and for the remobilization of oxidized nitrogen species from the upper firn layer would be indispensable to elucidate possible source regions of NO_y compounds finally controlling ice core nitrate variability.

[24] **Acknowledgments.** The authors would like to thank G. König-Langlo for providing the meteorological data used in this contribution. We also acknowledge the valuable comments of three anonymous referees, which helped to improve the paper. Special thanks go to the technicians and scientists of the Neumayer overwintering crews of the years 1998 and 1999.

References

Barrie, L. A., and R. M. Hoff, Five years of air chemistry observations in the Canadian Arctic, *Atmos. Environ.*, *19*, 1995–2010, 1985.

Bodhaine, B. A., Aerosol absorption measurements at Barrow, Mauna Loa, and the South Pole, *J. Geophys. Res.*, *100*, 8967–8975, 1995.

Bond, D. W., S. Steiger, R. Zhang, X. Tie, and R. Orville, The importance of NO_x production by lightning in the tropics, *Atmos. Environ.*, *36*, 1509–1519, 2002.

Davis, D., et al., Unexpected high levels of NO observed at the South Pole, *Geophys. Res. Lett.*, *28*, 3625–3628, 2001.

Dibb, J. E., R. W. Talbot, J. W. Munger, D. J. Jacob, and S.-M. Fan, Air-snow exchange of HNO_3 and NO_y at Summit, Greenland, *J. Geophys. Res.*, *103*, 3475–3486, 1998.

Fischer, H., D. Wagenbach, and S. Kipfstuhl, Sulfate and nitrate firn concentrations on the Greenland ice sheet, 2, Temporal anthropogenic deposition changes, *J. Geophys. Res.*, *103*, 21,935–21,942, 1998.

Flocke, F., E. Atlas, S. Madronich, S. M. Schauffler, K. Aikin, J. J. Margitan, and T. P. Bui, Observations of methyl nitrate in the lower stratosphere during STRAT: Implications for its gas phase production mechanisms, *Geophys. Res. Lett.*, *25*, 1891–1894, 1998.

Gao, R. S., et al., Partitioning of the reactive nitrogen reservoir in the lower stratosphere of the Southern Hemisphere: Observations and modeling, *J. Geophys. Res.*, *102*, 3935–3949, 1997.

Honrath, R. E., and D. A. Jaffe, The seasonal cycle of nitrogen oxides in the arctic troposphere at Barrow, Alaska, *J. Geophys. Res.*, *97*, 20,615–20,630, 1992.

Honrath, R. E., M. C. Peterson, S. Guo, J. E. Dibb, P. B. Shelson, and B. Cambell, Evidence of NO_x production within or upon ice particles in the Greenland snowpack, *Geophys. Res. Lett.*, *26*, 695–698, 1999.

Jacobi, H.-W., R. Weller, T. Bluszcz, and O. Schrems, Latitudinal distribution of peroxyacetyl nitrate (PAN) over the Atlantic Ocean, *J. Geophys. Res.*, *104*, 26,901–26,912, 1999.

Jacobi, H.-W., R. Weller, A. E. Jones, P. S. Anderson, and O. Schrems, Peroxyacetyl nitrate (PAN) concentrations in the Antarctic troposphere measured during the photochemical experiment at Neumayer (PEAN'99), *Atmos. Environ.*, *34*, 5235–5247, 2000.

Jones, A. E., R. Weller, A. Minikin, E. W. Wolff, W. T. Sturges, H. P. McIntyre, S. R. Leonard, O. Schrems, and S. Bauguitte, Oxidized nitrogen chemistry and speciation in the Antarctic troposphere, *J. Geophys. Res.*, *104*, 21,355–21,366, 1999.

Jones, A. E., R. Weller, E. W. Wolff, and H.-W. Jacobi, Speciation and rate of photochemical NO and NO_2 production in Antarctic snow, *Geophys. Res. Lett.*, *27*, 345–348, 2000.

Jones, A. E., R. Weller, P. S. Anderson, H.-W. Jacobi, E. W. Wolff, O. Schrems, and H. Miller, Measurements of NO_x emissions from the Antarctic snowpack, *Geophys. Res. Lett.*, *28*, 1499–1502, 2001.

Johnston, H., Evaluation of excess carbon 14 and strontium 90 data for suitability to test two-dimensional stratospheric models, *J. Geophys. Res.*, *94*, 18,485–18,493, 1989.

Junkermann, W., U. Platt, and A. Volz-Thomas, A photoelectric detector for the measurement of photolysis frequencies of ozone and other atmospheric molecules, *J. Atmos. Chem.*, *8*, 203–227, 1989.

Kleinman, L. I., Low and high NO_x tropospheric photochemistry, *J. Geophys. Res.*, *99*, 16,831–16,838, 1994.

König-Langlo, G., J. C. King, and P. Pettré, Climatology of the three coastal Antarctic stations Dumont d'Urville, Neumayer, and Halley, *J. Geophys. Res.*, *103*, 10,935–10,946, 1998.

Kottmeier, C., and B. Fay, Trajectories in the Antarctic lower troposphere, *J. Geophys. Res.*, *103*, 10,947–10,959, 1998.

Legrand, M. R., and R. J. Delmas, Relative contributions of tropospheric and stratospheric sources to nitrate in Antarctic snow, *Tellus*, *38B*, 236–249, 1986.

Legrand, M., and P. Mayewski, Glaciochemistry of polar ice cores: A review, *Rev. Geophys.*, *35*, 219–243, 1997.

Logan, J. A., M. J. Prather, S. C. Wofsy, and M. B. McElroy, Tropospheric chemistry: A global perspective, *J. Geophys. Res.*, *86*, 7210–7254, 1981.

Logan, J. A., Nitrogen oxides in the troposphere: Global and regional budgets, *J. Geophys. Res.*, *88*, 10,785–10,807, 1983.

McIntyre, H. P., The measurement and implications of short chain alkyl mono-nitrates in contemporary tropospheric and aged polar firn air, Ph.D. thesis, Univ. of East Anglia, Norwich, UK, 2001.

Masarik, J., and J. Beer, Simulation of particle fluxes and cosmogenic nuclide production in the Earth's atmosphere, *J. Geophys. Res.*, *104*, 12,099–12,111, 1999.

Munger, J. W., D. J. Jacob, S.-M. Fan, A. S. Colman, and J. E. Dibb, Concentration and snow-atmosphere fluxes of reactive nitrogen at Summit, Greenland, *J. Geophys. Res.*, *104*, 13,721–13,734, 1999.

Ottar, B., Arctic air pollution: A Norwegian perspective, *Atmos. Environ.*, *23*, 2349–2356, 1989.

Raisbeck, G. M., F. Yiou, M. Fruneau, J. M. Loiseaux, M. Lieuven, and J. C. Ravel, Cosmogenic $^{10}Be/^{7}Be$ as a probe of atmospheric transport processes, *Geophys. Res. Lett.*, *8*, 1015–1018, 1981.

Röthlisberger, R., et al., Nitrate in Greenland and Antarctic ice cores: A detailed description of post-depositional processes, *Ann. Glaciol.*, in press, 2002.

Schoeberl, M. R., and D. L. Hartmann, The dynamics of the stratospheric polar vortex and its relation to springtime ozone depletions, *Science*, *251*, 46–52, 1991.

Schrimpf, W., K. P. Müller, F. J. Johnen, K. Lienaerts, and J. Rudolph, An optimized method for airborne peroxyacetyl nitrate (PAN) measurements, *J. Atmos. Chem.*, *22*, 303–317, 1995.

Seckmeyer, G., B. Mayer, and G. Bernhard, The 1997 status of solar UV spectroradiometry in Germany: Results from the national intercomparison of UV spectroradiometers Garmisch Partenkirchen, Germany, in *Fraunhofer Institut Atmosphärische Umweltforschung Schriftenreihe*, vol. 55, edited by W. Seiler, pp. 1–166, Shaker Verlag, Aachen, 1998.

Shaw, G. E., On the resident time of Antarctic ice sheet sulfate aerosol, *J. Geophys. Res.*, *87*, 4309–4313, 1982.

Solberg, S., T. Krognes, F. Stordal, Ø. Hov, H. J. Beine, D. A. Jaffe, K. C. Clemitshaw, and S. A. Penkett, Reactive nitrogen compounds at Spitsbergen in the Norwegian Arctic, *J. Atmos. Chem.*, *28*, 209–225, 1997.

Talbot, R. W., et al., Tropospheric reactive odd nitrogen over the South Pacific in austral springtime, *J. Geophys. Res.*, *105*, 6681–6694, 2000.

Thakur, A. N., H. B. Singh, P. Mariani, Y. Chen, Y. Wang, D. J. Jacob, G. Brasseur, J.-F. Müller, and M. Lawrence, Distribution of reactive nitrogen species in the remote free troposphere: Data and model comparisons, *Atmos. Environ.*, *33*, 1403–1422, 1999.

Tie, X., R. Zhang, G. Brasseur, L. Emmons, and W. Lei, Effects of lightning on reactive nitrogen and nitrogen reservoir species in the troposphere, *J. Geophys. Res.*, *106*, 3167–3178, 2001.

Wagenbach, D., U. Görlach, K. Moser, and K. O. Münnich, Coastal Antarctic aerosol: The seasonal pattern of its chemical composition and radionuclide content, *Tellus*, *40B*, 426–436, 1988.

Wagenbach, D., Coastal Antarctica: Atmospheric chemical composition and atmospheric transport, in *Chemical Exchange Between the Atmosphere and Polar Snow, NATO ASI Ser.*, vol. 43, edited by E. W. Wolff and R. C. Bales, pp. 173–199, Springer-Verlag, New York, 1996.

Wagenbach, D., M. Legrand, H. Fischer, F. Pichlmayer, and E. W. Wolff, Atmospheric near-surface nitrate at coastal Antarctic sites, *J. Geophys. Res.*, *103*, 11,007–11,020, 1998.

Weller, R., and O. Schrems, Photooxidants in the marine Arctic troposphere in summer, *J. Geophys. Res.*, *101*, 9139–9147, 1996.

Weller, R., A. Minikin, G. König-Langlo, O. Schrems, A. E. Jones, E. W. Wolff, and P. S. Anderson, Investigating possible causes of the observed diurnal variability in Antarctic NO_y, *Geophys. Res. Lett.*, *26*, 2853–2856, 1999.

Wofsy, S. C., et al., Atmospheric chemistry in the Arctic and Subarctic: Influence of natural fires, industrial emissions, and stratospheric inputs, *J. Geophys. Res.*, *97*, 16,731–16,746, 1992.

Wolff, E. W., Nitrate in polar ice, in *Ice Core Studies of Global Biogeochemical Cycles, NATO ASI Ser.*, vol. 30, edited by R. J. Delmas, pp. 195–224, Springer-Verlag, New York, 1995.

Wolff, E. W., and H. Cachier, Concentrations and seasonal cycle of black carbon in aerosol at a coastal Antarctic station, *J. Geophys. Res.*, *103*, 11,033–11,041, 1998.

Zellweger, C., M. Ammann, B. Buchmann, P. Hofer, M. Lugauer, R. Rüttimann, N. Streit, E. Weingartner, and U. Baltensperger, Summertime NO_y speciation at the Jungfraujoch, 3580 m above sea level, Switzerland, *J. Geophys. Res.*, *105*, 6655–6667, 2000.

Zhang, R., N. T. Sanger, R. E. Orville, X. Tie, W. Randel, and E. R. Williams, Enhanced NO_x by lightning in the upper troposphere and lower stratosphere inferred from the UARS global NO_2 measurements, *Geophys. Res. Lett.*, *27*, 685–688, 2000.

M. Huke and D. Wagenbach, Institut für Umweltphysik, Universität Heidelberg, D-69120 Heidelberg, Germany.

H.-W. Jacobi and R. Weller, Alfred-Wegener-Institut für Polar- und Meeresforschung, D-27570 Bremerhaven, Germany. (rweller@awi-bremerhaven.de)

A. E. Jones, British Antarctic Survey, Natural Environment Research Council, High Cross, Madingley Road, Cambridge CB3 0ET, UK.

H. P. McIntyre and W. T. Sturges, School of Environmental Sciences, University of East Anglia, Norwich NR4 7TJ, UK.

A. Wille, Metrohm AG, CH-9101 Herisau, Switzerland.

3.2 Field measurements of the exchange of reactive compounds between the atmosphere and the snow

Publication 3.2.1

Jones, A.E., R. Weller, E.W. Wolff, and H.-W. Jacobi,

Speciation and rate of photochemical NO and NO_2 production in Antarctic snow,

Geophys.Res.Lett. **27**, 345-348, 2000.

GEOPHYSICAL RESEARCH LETTERS, VOL. 27, NO. 3, PAGES 345-348, FEBRUARY 1, 2000

Speciation and Rate of Photochemical NO and NO_2 Production in Antarctic Snow

A.E. Jones[1], R.Weller[2], E.W. Wolff[1], H-W. Jacobi[2]

Abstract. Measurements were made of NO and NO_2, in controlled experiments to investigate their production from snow. Throughout a diurnal cycle, measurements were made of ambient air and air from inside a snowblock. Enhanced concentrations of NO and NO_2 (up to 15 pptv and 32 pptv respectively) were measured inside the snowblock. The production rate inside the block varied with intensity of incident radiation, and reached a maximum of $1.1x10^6$ molecs/cm^3/s for NO and $2.1x10^6$ molecs/cm^3/s for NO_2. A second experiment, in which the snowblock was alternately exposed to sunlight and then shaded, confirmed that the diurnal production was driven by photochemistry rather than some other diurnally varying factor. Concentrations of nitrate in the snowblock did not change as a result of 50 hours of experiments, confirming that if nitrate is the source reservoir, it can not be rapidly depleted. Snowpack production may contribute significantly to NO_x concentrations in the Antarctic lower troposphere.

Introduction.

The existence of a diurnal variation in NO_y (= NO + NO_2 + HNO_3 + PAN + alkyl nitrates etc.) was observed in a measurement campaign at the German Antarctic research station, Neumayer (70°S, 8°W), in summer 1997 [*Weller et al.*, 1999]. A diurnal cycle in a tracer such as NO_y implies regular changes in either sources or sinks (or both) of one or more component family members. The NO_y data clearly showed an influence from local meteorology and some exchange of HNO_3 at the snow surface was also observed, but this could not account for the magnitude of the diurnal NO_y changes. Given that the Antarctic troposphere is remote from major pollution sources, any process which might influence concentrations of active chemicals, such as NO_x, clearly has important implications for regional tropospheric chemistry. It is potentially also an added complication in the quest to translate the ice core nitrate signal into one for past concentrations of NO_x [*Wolff*, 1995].

A recent paper reporting work from Summit, Greenland, suggested that photochemical reactions occurring within or upon surface snow produced NO_x from a N-reservoir compound within the snow [*Honrath et al.*, 1999]. There was some evidence in the reported measurements of a photochemical influence on NO_x production and the authors suggested that photolysis of nitrate, present in surface snow, may be a source of NO_2.

To investigate these findings further, we carried out controlled experiments during the PEAN 1999 (Photochemical Experiment at Neumayer) summer campaign, aimed at i) confirming the photochemical nature of the observed NO_x production, ii) determining whether NO or NO_2 was the dominant product, and iii) quantifying the source of both NO and NO_2. The experiments were based around comparing concentrations of both NO and NO_2 in ambient air, and in air that was sucked through a porous block of snow, supported so that all sides were exposed to the air and light. Any differences in concentration were thus a product of the snowblock activity. The experiments were carried out on days with a high incidence of solar radiation, and in a sheltered location to minimise any influence of varying wind speeds.

Experimental

Measurements were carried out at Neumayer's atmospheric observatory located 1.5 km upwind of the station [*Jones et al*, 1999]. An EcoPhysics PLC760, for photolytic conversion of NO_2 to NO, and an EcoPhysics CLD780TR, for chemiluminescent detection of NO, were used to measure NO and NO_2 [*Weller and Schrems*, 1996; *Jones et al.*, 1999]. The CLD780TR used either an integration time of 60 secs (later averaged into 5 minute means) or 200 secs (averaged into 20 minute means). The calculated accuracy of the NO and NO_2 measurements was ±2 pptv and ±4 pptv respectively, with an average detection limit for 20 minute averaging (2σ of background signal [*Weller and Schrems*, 1996]) of 2.0 pptv NO and 3.5 pptv NO_2.

A snowblock, roughly 20 cm x 20 cm x 20 cm, was cut from surface snow using cleaned equipment to avoid contamination. The block dimensions were then measured accurately. In the middle of the uppermost face, a hole (diameter=3 cm, depth=9 cm) was cut into the block. The block was then supported on two horizontal poles 1 m above the snow surface. All sides were thus exposed to the air and sunlight. A teflon filter holder with diameter slightly greater than 3cm was inserted into the hole to a depth of 2.5 cm so that the hole was sealed from outside ambient air. Two 10 m long PFA inlet lines (4 mm id) were connected to the CLD780TR *via* a 3-way teflon valve. One line was attached to the teflon filter holder in the snowblock such that any air entering this line would have passed through the snowblock from the air outside. The other line sampled ambient air 1 m above the ground adjacent to the snowblock. The flow rate to the CLD780TR was 1500 cm^3/min such that the residence time of air in the inlet lines was 5 seconds. The volume of the snowblock was 10.14 dm^3. Assuming 50% of the volume was air (ie. a snow density of 0.45g.cm^{-3}), and an equal flow of air

[1]British Antarctic Survey, Natural Environment Research Council, Cambridge, UK

[2]Alfred-Wegener-Institute for Polar and Marine Research, Bremerhaven, Germany.

Paper number 1999GL010885.
0094-8276/00/1999GL010885$05.00

through the block from all directions, the residence time of air in the snowblock was 3.4 minutes. Two specific experiments were carried out. Furthermore, snow samples taken from the snowblock, and from the pit from which it was dug, were analysed for nitrate (NO_3^-).

1. Diurnal measurement.

Measurements of NO and NO_2 were made continually throughout a day/night cycle, from 14:00 on February 22nd to 16:00 on February 23rd. The inlet line switched between sampling ambient air and the snowblock air roughly every 1 to 2 hours, allowing representative NO and NO_2 averages to be calculated. The results are shown in Figure 1. Figure 1a) shows the variation in NO, with a clear diurnal variation in ambient air, with zero NO during the night, and a maximum of roughly 9 pptv around noon. The concentrations of NO in air that has passed through the snowblock follow a similar cycle, but the concentrations during the daylight hours are substantially larger than those in ambient air, with an average of 22 pptv around noon on the first day. During nighttime, concentrations of NO in both ambient air and snowblock air drop to zero. Figure 1b) shows the variation in NO_2. The diurnal variation in ambient air has a minimum around midday and a maximum (roughly 16 pptv) around midnight. However, air that has passed through the snowblock shows a totally different diurnal cycle, with maximum NO_2 mixing ratios around noon and minimum during the night. During the day, mixing ratios of NO_2 in snowblock air are consistently higher than in ambient air, reaching around 35 pptv on both days. During the night, the mixing ratios effectively track those of ambient air.

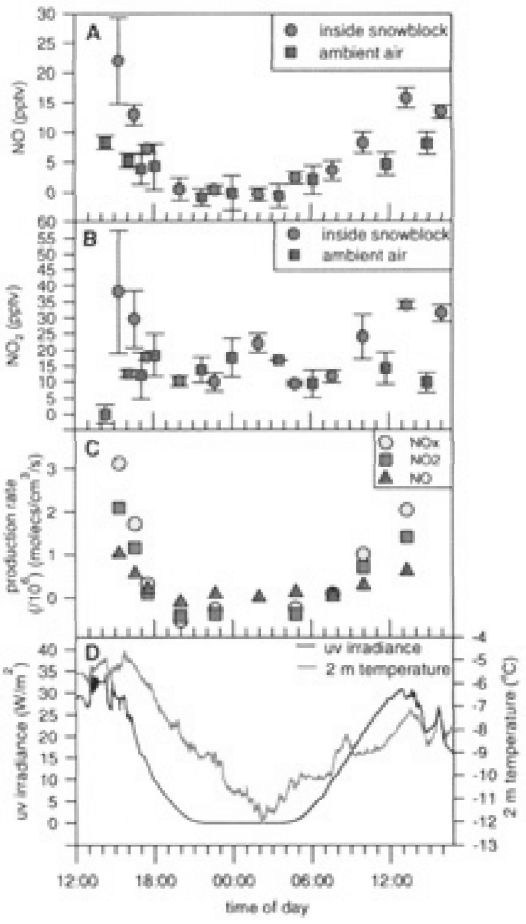

Figure 1. Measurements of a) NO and b) NO_2, both in ambient air and from air within the snowblock. The "snowblock air" has recently been ambient, the change in NO and NO_2 concentration is caused by processes within the snowblock. Measurements are for a complete diurnal cycle, and each data point shown is the average of between 30 minutes and 2 ½ hours of sampling. Error bars are the standard deviation of the individual measurements. c) Production rate of NO, NO_2, and therefore NO_x from the snowblock, over a diurnal cycle. d) Variation in ultraviolet irradiance (290 to 385 nm), and ambient air temperature at 2m height, during the period of the experiment.

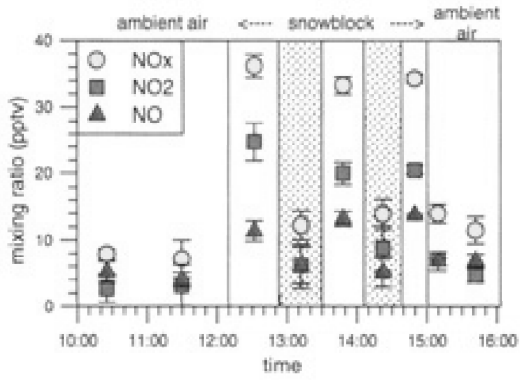

Figure 2. Measurements of NO, NO_2, and NO_x in the "shading experiment". The first and final sections (1 and 7) are measurements made in ambient air. Middle sections are measurements made within the snowblock, alternatively fully exposed to sunlight and fully shaded to eliminate any photochemical activity. Periods of shading are indicated by stipling.

It is now possible to calculate production rates of NO and NO_2 over the day. This was done by interpolating the data from Figures 1a) and b) onto a common time axis and deriving the magnitude of NO, NO_2 and thereby NO_x produced. The production rate per unit volume of the block (ie. snow + air) is calculated from:

$$\textit{production (molecs/cm}^3\textit{/s)} = \frac{\Delta NO,\ \Delta NO_2 \text{ or } \Delta NO_x \text{ (pptv)} * LN * FR}{\textit{volume of block (cm}^3\textit{)}}$$

where $\Delta NO = (NO_{snowblock} - NO_{ambient\ air})$, $\Delta NO_2 = (NO_{2\ snowblock} - NO_{2\ ambient\ air})$, $\Delta NO_x = (NO_{x\ snowblock} - NO_{x\ ambient\ air})$, LN = Loschmidt's number = 2.69×10^{19} molecules/cm^3, FR = flow rate (cm^3/s). The result is shown in Figure 1c). The production rates of NO and NO_2 reached a maximum of 1.1×10^6 molecs/cm^3/s and 2.1×10^6 molecs/cm^3/s respectively, and fell to essentially zero between 19:00 and 07:00 on these days. In terms of mixing ratio, an increase of 47 pptv of NO_x was measured early afternoon on Feb 22nd. Figure 1d) shows the variation in ultra violet irradiance (290 to 385 nm) measured

with an Eppley TUVR radiometer, and ambient air temperature at 2 m height, during the experiment.

2. Shading experiment.

Measuring over a diurnal cycle is clearly a good start when looking for photochemical effects, but other parameters, such as temperature, also vary on a diurnal timescale (as shown by Figure 1d). Care is therefore needed when interpreting diurnal variations. With this in mind, an experiment was carried out on Feb 24th to directly control the amount of sunlight reaching the snowblock over short time intervals. Initially, measurements of NO and NO_2 were made in ambient air, to provide a reference. The inlet line was then connected to the snowblock as previously described, and a measurement integration time of 60 seconds selected. Measurements of NO and NO_2 were then made from air that had passed through the snowblock which was exposed to full sun. This was done for 40 minutes, such that a representative number of measurements were made and meaningful averages could be calculated. The snowblock was then "shaded" by carefully wrapping aluminium foil around all sides of the block to shade it from the sun, while ensuring that the foil was loose enough not to restrict the air flow. The air from the snowblock was then measured for a further 40 minutes. The shading was then removed so that the sequence of measuring the snowblock "unshaded" and "shaded" could be repeated. After several cycles, measurements of NO and NO_2 were repeated in the ambient air for reference.

The results from this experiment are shown in Figure 2. The dramatic increase in both NO and NO_2 mixing ratios during the "sunlit" phases as opposed to the "shaded" phases is immediately obvious. Mixing ratios of NO and NO_2 during the "shaded" phases are essentially the same as in the ambient air measured at the start and end of the experiment, at ~6 pptv and ~5 pptv respectively. However, during the "sunlit" phases, mixing ratios of NO rose to an average of 13 pptv, and those of NO_2 rose to 22 pptv. Furthermore, the changes in concentration between the "sunlit" and the "shaded" modes were extremely rapid in both directions, and evident in the first measurement made after the change in light intensity. This experiment demonstrates conclusively that the source of NO_x is dominated by photochemistry in the snow.

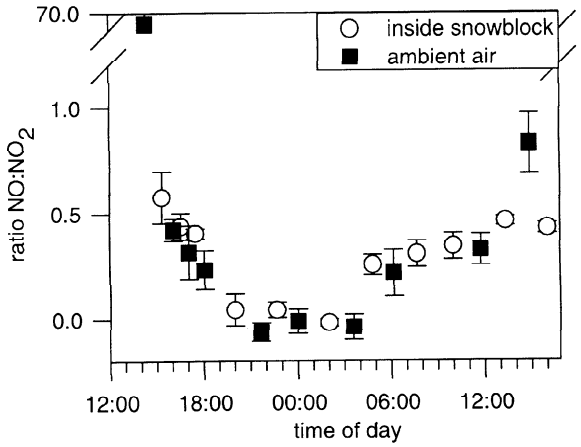

Figure 3. Ratio of $NO:NO_2$ in both ambient air and in the snowblock, from February 22nd to 23rd. The ratio is derived from the data of Figure 1. Error bars are based around standard error of the mean; for the first point they are out of range of the plot, at ±65.9, ie. ratio range from 3.4 to 135.5.

3. Snow analysis.

Duplicate snow samples were taken both from the snowpit at the time of cutting the snowblock, and from the snowblock itself at the end of the experiment. The samples were analysed while at Neumayer using an ion chromatograph to measure concentrations of NO_3^-. The upper 4 cm of the snowblock comprised of freshly deposited wind-blown snow with relatively low concentrations of nitrate (~30 ng/g). Concentrations increased with depth to a smooth profile of roughly 50 ng/g throughout the rest of the block. The profile from the aged snowblock was essentially the same as that of the snow pit from which it was dug: no significant change in nitrate concentration in the snowblock occurred between the time the snowblock was dug, and the time that the experiments ended (~50 hours).

Discussion

We have provided clear evidence that photochemical activity in surface snow in Antarctica can significantly increase concentrations of both NO and NO_2 in firn air. An important question is what is the mechanism supplying the additional NO_x, and what is the reservoir species. These are likely to be the same as those responsible for the observed NO_x production at Summit [*Honrath et al.*, 1999]. Having measured both NO and NO_2, we looked at the ratio $NO:NO_2$ for clues. The ratio of $NO:NO_2$ in both ambient air and the snowblock has a clear diurnal variation, with minimum during the night rising to a noon maximum (Figure 3). The difference occurs in the early afternoon, when the ratio in ambient air rises sharply to a high maximum (due to the decline in NO_2 - see Figure 1b), while the ratio within the snowblock declines due to the relatively much greater concentrations of NO_2. Unless radically different chemistry occurs inside the snowblock to that outside (ie. for the drivers of the $NO:NO_2$ partitioning: $j(NO_2)$, O_3 and RO_2), this strongly suggests a source of NO_2 within the firn. If nitrate is the reservoir for this production, its erosion appears to be slow. Taking even the lowest snow nitrate concentration in the block (30 ng/g) and the highest production rate shown in Figure 1c), the nitrate reservoir in the snowblock would be sufficient for 2 years of NO_x production, so it is not surprising that we see no loss in snow nitrate over a few days.

Although the production is within the firn, and the calculated production rates do not immediately translate into an atmospheric source strength, some exchange between firn and atmosphere will undoubtably occur and influence local photochemistry. *Dibb et al.* [1998] reported air/snow fluxes of NO_y at Summit that were not accounted for by HNO_3 exchange. The production rate per unit area receiving sunlight can be estimated assuming a surface area of 1450 cm^2 (=3 sides of the block, since not all sides were receiving full sunlight). The average production rate of NO_x for the day in Figure 1) would be 9×10^6 molecs/cm^2/s, which if fully vented would be enough to replenish a 50 m thick inversion layer by ~5 pptv of NO_x per day. Assuming a concentration of OH of

4×10^5 molecs/cm^3 [*Crutzen*, 1994] and with the main sink of NO_x being reaction with OH, the lifetime of NO_x is of the order of 24hours. The calculated NO_x source from the snowpack could therefore make a significant contribution.

The implications of this study are numerous and significant. Firstly, a key goal of studying ice core nitrate is to reconstruct past levels of NO_x [*Wolff*, 1995]. This study suggests a significant influence of local variables (particularly uv irradiance and concentration of nitrate in snow) on tropospheric NO_x concentrations over Antarctica. Reconstructing past tropospheric NO_x in polar regions from the local ice core nitrate signal could therefore be possible. However, the ultimate goal is the global picture, and for this, the complete derivation (sources and deposition mechanisms as well as re-cycling) of snowpack (and hence ice core) nitrate must be known. Secondly, at low accumulation sites concentrations of nitrate in ice cores drop off rapidly with depth [*Wagnon et al.*, 1999] and although remobilisation and re-emission are suggested as causes, the mechanism is not fully understood. Photolytic decay is a potential contributor to this observed loss. Finally, the influence on polar tropospheric chemistry must be considered. The annual cycle of surface ozone measured at South Pole [*Schnell et al.*, 1991] shows a secondary maximum in late spring coincident with the current annual maximum in uv-B radiation [*Booth et al.*, 1994]. Based on the competition between the reactions HO_2 + NO and $HO_2 + O_3$, the balance between production and destruction of ozone at South Pole in springtime (30 ppbv O_3, -30°C) is of the order 5 pptv NO, ie. the pivotal concentration of NO is of the order reported for coastal Antarctica [*Jefferson et al.*, 1998; *Jones et al.*, in press]. The growing intensity of uv radiation arising from growth of the Antarctic ozone hole [*Farman et al*, 1985, *Jones and Shanklin*, 1995] might have provided an increased source for NO_x, switching this clean air regime to ozone production during late spring. Photochemical activity in polar snow has recently been proposed as a source of HCHO [*Sumner and Shepson*, 1999], although another study attributed elevated HCHO to temperature-dependent degassing of HCHO deposited with snowfall [*Hutterli et al.*, 1999]. If there is a photochemical source, and considering the increase in uv radiation, the snowpack could increasingly have become an important source for peroxy radicals, and hence OH, to the troposphere. It is evident from these observations that the chemistry of the polar regions, although "clean", is nonetheless extremely complex. The role of the snow surface in influencing a range of chemical reactions could be extremely significant.

Acknowledgements. The authors would like to thank G. König-Langlo and B. Loose for providing the meteorological data used in this study.

References

Booth, C.R., T.B. Lucas, J.H. Morrow, C.S. Weiler, P.A. Penhale, The US NSF/Antarctic Program's Network for Monitoring Ultraviolet Radiation, in *Ultraviolet Radiation in Antarctica: Measurements and Biological research*, (C.S. Weiler and P.A. Penhale, eds.), AGU Antarctic Research Series, vol. 62, AGU, Washington, D.C., 17-37, 1994.

Crutzen, P., Global tropospheric chemistry, in *Low-temperature chemistry of the atmosphere*, NATO ASI Series I, vol. 21 (editor G.K. Moortgat et al.), *465-498,* Springer-Verlag, New York, N.Y., 1994.

Dibb, J.E., R.W. Talbot, J.W. Munger, D.J. Jacob, S.-M. Fan, Air-snow exchange of HNO_3 and NO_y at Summit, Greenland, *J. Geophys. Res., 103*, 3475-3486, 1998.

Farman, J.C., B.G. Gardiner, and J.D. Shanklin, Large losses of total ozone in Antarctica reveal seasonal ClOx/NOx interaction, *Nature, 315,* 207-210, 1985.

Honrath, R.E., M.C. Peterson, S. Guo, J.E. Dibb, P.B. Shelson, B. Cambell, Evidence of NO_x production within or upon ice particles in the Greenland snowpack, *Geophys. Res. Lett., 26*, 695-698, 1999.

Hutterli, M.A., R. Röthlisberger, R.C. Bales, Atmosphere-to-snow-to-firn transfer studies of HCHO at Summit, Greenland, *Geophys. Res. Lett., 26*, 1691-1694, 1999.

Jefferson, A., D.J. Tanner, F.L. Eisele, D.D. Davis, G. Chen, J. Crawford, J.W. Huey, A.L. Torres, H. Berresheim, OH photochemistry and methane sulfonic acid formation in the coastal Antarctic boundary layer, *J. Geophys. Res., 103,* 1647-1656, 1998.

Jones, A.E., R. Weller, A. Minikin, E.W. Wolff, W.T. Sturges, H.P. McIntyre, S.R. Leonard, O. Schrems, S. Bauguitte, Oxidised Nitrogen Chemistry and Speciation in the Antarctic Troposphere, *J. Geophys. Res.*, 1999.

Jones, A.E. and J.D. Shanklin, Continued decline of total ozone over Halley, Antarctica, since 1985, *Nature, 376,* 409-411, 1995.

Schnell, R.C., S.C. Liu, S. J. Oltmans, R.S. Stone, D.J. Hofmann, E.G. Hutton, T. Deshler, W.T. Sturges, J.W. Harder, S.D. Sewell, M. Trainer, J.M Harris, Decrease of summer tropospheric ozone concentrations in Antarctica, *Nature, 351*, 726-729, 1991.

Sumner, A.M. and P.B. Shepson, Snowpack production of formaldehyde and its effect on the Arctic troposphere, *Nature, 398*, 230-233, 1999.

Wagnon, P., R.J. Delmas, and M.Legrand, Loss of volatile acidic species from upper firn layers at Vostok, Antarctica, *J. Geophys. Res., 104*, 3423-3431, 1999.

Weller, R. and O. Schrems, Photooxidants in the marine arctic troposphere in summer, *J. Geophys. Res., 101*, 9139-9147, 1996.

Weller, R., A.E. Jones, E.W. Wolff, A.Minikin, P.S. Anderson, G. König-Langlo, O. Schrems, Investigating possible causes of the observed diurnal variability in Antarctic NO_y, *Geophys. Res. Lett.*, 1999.

Wolff, E., Nitrate in polar ice, in *Ice core studies of global biogeochemical cycles,* NATO ASI Series I, vol. 30 (editor R.J. Delmas), *195-224,* Springer-Verlag, New York, N.Y., 1995.

A.E. Jones, E.W. Wolff, British Antarctic Survey, Natural Environment Research Council, High Cross, Madingley Road, Cambridge, CB3 0ET, UK. (a.jones@bas.ac.uk)

R. Weller, H.W. Jacobi, AlfredWegerner Institut für Polar- und Meeresforschung, 27570 Bremerhaven, Germany (rweller@awi-bremerhaven.de)

(Received June 29, 1999; revised October 19, 1999; accepted November 11, 1999)

Publication 3.2.2

Jones, A.E., R. Weller, P.S. Anderson, H.-W. Jacobi, E.W. Wolff, H. Miller, and O. Schrems,

Measurements of NO_x emissions from the Antarctic snowpack,

Geophys.Res.Lett. **28**, 1499-1502, 2001.

GEOPHYSICAL RESEARCH LETTERS, VOL. 28, NO. 8, PAGES 1499-1502, APRIL 15, 2001

Measurements of NO_X emissions from the Antarctic snowpack

A.E. Jones[1], R. Weller[2], P.S. Anderson[1], H.-W. Jacobi[2], E.W. Wolff[1], O. Schrems[2], H. Miller[2]

Abstract. It has been shown that NO_x is produced photochemically within the snowpack of polar regions. If emitted to the atmosphere, this process could be a major source of NO_x in remote snowcovered regions. We report here on measurements made at the German Antarctic station, Neumayer, during austral summer 1999, aimed at detecting and quantifying emissions of NO_x from the surface snow. Gradients of NO_x were measured, and fluxes calculated using local meteorology measurements. On the 2 days of flux measurements, the derived fluxes showed continual release from the snow surface, varying between ~0 and $3x10^8$ molecs/cm^2/s. When not subject to turbulence, the variation was coincident with the uv diurnal cycle, suggesting rapid release once photochemically produced. Scaling the diurnal average of Feb. 7th ($1.3x10^8$ molecs/cm^2/s) suggests an annual emission over Antarctica of the order 0.0076TgN.

Introduction

The chemistry of oxidised nitrogen species at high latitudes is proving to be surprisingly complex. Original polar studies were aimed at understanding the nitrate record in ice cores, which hold the potential to reconstruct concentrations of NO_x during past historic times [*Wolff*, 1995]. For this purpose it is necessary to understand both the background chemistry determining NO_x concentrations in the polar troposphere, and also any exchange processes between the snow and the air. Neither of these is currently fully understood.

Two recent studies have focussed on NO_x in the interstitial air within the snowpack of Greenland [*Honrath et al.*, 1999] and Antarctica [*Jones et al.*, 2000]. Several conclusions have been drawn from these studies: i) that in these locations, NO_x concentrations within the snowpack interstitial air are higher than those of the overlying atmosphere; ii) that this arises because of *in situ* production, possibly from the breakdown of nitrate impurities in the snow; iii) that this production is driven by photochemistry; and iv) that it appears that NO_2 rather than NO is the dominant product. Given that this has been observed in both polar regions, and that nitrate is a common impurity in snow and ice, it is likely that this process will occur in any snow-covered areas of the world. In snow-covered areas remote from anthropogenic emissions, such as Antarctica, this process could be the dominant source of NO_x to the regional atmosphere.

No study has yet attempted to directly identify nor quantify emissions of NO_x from snow, although there are observations which are in accord with such a process. *Weller et al.* [1999] report a diurnal variation of NO_y in the Antarctic troposphere which, although modulated by local meteorology, seemed to have a surface source. *Ridley et al.* [2000] reported diurnal cycle in both NO_x and NO_y at Alert, which they attribute to release of NO_x from the snow surface. In Greenland, *Dibb et al.* [1998] noted that gradients of HNO_3 could not explain fluxes of NO_y, either in magnitude or direction. *Munger et al.* [1999] suggested reversible adsorption of compounds such as PAN to ice surfaces as an explanation but emissions of NO_x could account for some of the NO_y fluxes.

We report here measurements made during the PEAN 1999 (Photochemical Experiment at Neumayer) summer campaign designed to detect and quantify NO_x emissions from the Antarctic snowpack, and to asses factors controlling the emissions

Experimental

1. Overview

The measurements were carried out from 5-7th February 1999 at the German Antarctic station, Neumayer (70°39'S, 8°15'W) [*Jones et al.*, 1999; *Weller et al.*, 1999]. The experiment required measurements of NO_x at two different heights. Because of instrument configuration, such a measurement is not straightforward and it was necessary to use two instrument systems. The first was an EcoPhysics PLC760, for photolytic conversion of NO_2 to NO, coupled to an EcoPhysics CLD780TR for chemiluminescent detection of NO. Automatic measurements with a PLC760/CLD780TR combination can either switch between NO_2 and NO measurement modes at a single location, or between measuring in one mode at two different heights. The system was therefore used to measure in the NO_2 mode at two different heights. This avoided a possible offset that might be present if each height level is sampled with a different detector. The measurement derived is not a direct value of NO_2, but represents the mixing ratio of NO plus the fraction of NO_2 that is photolytically converted to NO, and is referred to as NO.c. This conversion fraction was derived regularly throughout the 7 week measurement campaign from calibration tests and was $(0.65\pm0.06) \times NO_2$. The formula for derivation of NO_2 is therefore:

$$NO_2 = 1/0.65 \times (NO.c - NO) \quad (1)$$

In order to derive NO_2, and thereby NO_x, a measurement of NO is also required, so a second CLD780TR was employed to derive NO. This instrument was dedicated to a different experiment, however, and could therefore only measure at a single height. The influence of this on the derived gradients of NO_x is fully discussed below.

A mast was erected in a clean sector away from the observatory. Two 10 m PFA inlet lines (4mm i.d.) were attached at a height of 0.02 m and 2.5 m above the snow surface respectively. They were connected to the PLC760/CLD780TR system by a teflon switching valve, allowing the instrument to switch automatically between the inlet lines. Using a flow rate of 1500 cm^3 minute^{-1}, the residence time for samples in the inlet line was 5 seconds. A third inlet line at 1.5 m height connected to the CLD780TR for measurement of NO only.

2. Artefacts, accuracy and precision

Both detectors were calibrated according to the method described by *Weller and Schrems* [1996] the only exception being

[1] British Antarctic Survey, Natural Environment Research Council, Cambridge, UK

[2] Alfred-Wegener-Institute for Polar and Marine Research, Bremerhaven, Germany.

Paper number 2000GL011956.
0094-8276/01/2000GL011956$05.00

that 1.03 (±5%) ppmv NO in N_2 (Messer Griesheim) was used for dynamic dilution to between 3 ppbv and 10 ppbv NO. NO_2 was generated by gas phase titration of the NO calibration mixtures. The potential artefact arising through production of NO_2 within the system from the reaction $NO+O_3$ [*Ridley et al.*, 1988] was assessed to be constant (due to constant ambient O_3 mixing ratios) and at worst 4% in the photolysis cell and less than 2.3% in the inlet lines. Both CLD780TRs were integrated for 200 secs and the data averaged to 20 minute means. The calculated accuracy, including all artefacts, was ±2 pptv NO and ±4 pptv NO_2 with an average detection limit for 20 minute means (2σ of background signal) of 2.0 pptv NO and 3.5 pptv NO_2 (see *Weller and Schrems* [1996] for details). Earlier laboratory tests showed that the instrument is capable of detecting spikes of less than 2 pptv NO/NO_2 mixtures on a 20 minute time base. Given that we are considering the difference between two measurements made with the same instrument, a key parameter is the precision of the instrument (see *Weller and Schrems* [1996] for details of derivation). The 2σ uncertainty of the 20 minute averages was 1.5 pptv NO_x, so that gradients greater than 2.1 pptv are significant on a 2σ level.

3. Error analysis for gradient measurements

To address the potential for instrumental bias, NO was measured in parallel with both detectors for 6 days prior to the flux measurements. The mean difference of the measured NO was 0.26 pptv (s.d. 2.2 pptv) ie. data from the two systems agree within the quoted error margin. The NO.c measurements were made with the same instrument and under the same conditions so the errors arise from the precision of the instrument (±15%) and the accuracy of the conversion fraction (±10%).

To derive gradients of NO_x it was necessary to assume that NO measured at 1.5 m height is representative of NO at both 0.02 m and 2.5 m, ie. that there was no gradient in NO. This assumption is unlikely to be correct and introduces a quantifiable bias into the derived gradients. We assess the limits on the size of the bias here.

$$\Delta NO_x = \frac{1}{0.65}\Delta NO.c - (\frac{1}{0.65} - 1)\Delta NO \quad (2)$$

The difference between the NO_x mixing ratios at 0.02 m height and 2.5 m height, given the conversion fraction of 0.65, and following the relationship in Eq'n 1 is:

$$\Delta NO_x^* = \frac{1}{0.65}\Delta NO.c \quad (3)$$

where Δ denotes the mixing ratio at 0.02 m height minus that at 2.5 m. Because we assume that NO is constant, we actually calculate: and our error is equal to 0.54ΔNO. If the true ΔNO is positive, assuming a zero gradient will lead to a positive bias in ΔNO_x, and vice versa.

A gradient in NO might arise from three causes:

i) if NO were deposited to the snow surface this would cause ΔNO to be negative (higher mixing ratio at 2.5 m). However, we currently have no reason to expect that such deposition occurs indeed we expect the opposite (see iii below).

ii) If NO_2 is emitted from snow and by 2.5 m height it has still not reached photochemical equilibrium with NO (through photolysis of NO_2 and the reaction of NO with O_3 or RO_2), then the ratio NO/NO_2 can be expected to increase with increasing height from the surface, making ΔNO negative. However, the timescale for vertical mixing at the site during the period of the measurements can be calculated as a few seconds (following *Garratt*, 1994) while the timescale for photolysis of NO_2 at noon in early February is around 1 minute. The NO/NO_2 ratio should therefore not be altered substantially from this cause.

iii) If NO is also emitted from the snow surface (perhaps some NO_2 is already photolysed before the air leaves the surface), and given the time required to reach photostationary state, then NO should decrease with height, ie. ΔNO would be positive. This seems to be the most likely scenario. From our previous work using a block of snow [*Jones et al.*, 2000], we found that during daylight when NO_x was being photochemically produced, the NO in the snow interstitial air was roughly 50% of the NO_2. Under these conditions, $\Delta NO \approx 0.5\Delta NO_2$. With our error of 0.54ΔNO it follows that:

$$\Delta NO_x^* = 1.2\Delta NO_x \quad (4)$$

In other words, under reasonable conditions we estimate that our assumption of constant NO causes our derived NO_x gradients to be up to 20% higher than the real ones.

Deriving fluxes

Various methods can be used to derive fluxes of chemical species depending on hardware available and the location of the flux measurements (eg. tree canopy, open water etc.) as is fully discussed by *Dabbert et al.* [1993]. For our work, fluxes of NO_x were derived from gradients in vertical NO_x concentrations and an eddy diffusivity as described by *Dabbert et al.* [1993].With this approach, the flux of a species and its vertical gradient are linked by a coefficient of proportionality, *K*. For fluxes of NO_x, the relationship can be written:

$$F(NO_x) = K_{NO_x}\frac{d(NO_x)}{dz} \quad (5)$$

K_{NOx} has not previously been measured, but following Monin-Obukhov surface layer similarity theory [*Stull*, 1988], it has a similar form to K_H, the transfer coefficient for heat. Following *King and Anderson* [1994], K_H can be derived from:

$$K_H = U_*.\kappa.z\left(\Pr + \alpha_T\frac{z}{L}\right) \quad (6)$$

where κ = von Kármán's constant (= 0.40); z = logarithmic mean of the measurement heights ($\ln^{-1}((\ln(2.5m) + \ln(0.02m))/2)$) (=0.22 m), U_* is the friction velocity. For neutral to moderate stability, as encountered in Antarctica during the summertime, $\alpha_T.z/L$ is negligible [*King and Anderson*, 1994]. The equivalent turbulent Prandtl number *Pr* for NO_x is unknown, but as similar numbers for heat and moisture are ≈1 [*King and Anderson*, 1994] it is reasonable to take *Pr* for $NO_x = 1$. Therefore, K_{NOx}, the transfer coefficient for NO_x, is derived:

$$K_{NO_x} = U_*.\kappa.z \quad (7)$$

U_* can be derived iteratively given a wind speed, temperature gradient and an assumed surface roughness [*King and Anderson*, 1994], parameters which are all available for Neumayer [e.g. *König*, 1985]. The mean error on U_* when $U_* > 0.2$ is 10%. Fluxes of NO_x, $F(NO_x)$, were then calculated from:

$$F(NO_x) = U_*.\kappa.z\frac{[NO_x]_{2.5m} - [NO_x]_{0.02m}}{\Delta z} \times LN \quad (8)$$

where *LN* = Loschmidt's number = number of molecules per cm^3 air (= 2.69×10^{19}) and Δz = 2.5 m - 0.02 m = 2.48 m. Positive fluxes represent release of NO_x from the snowpack to the atmosphere.

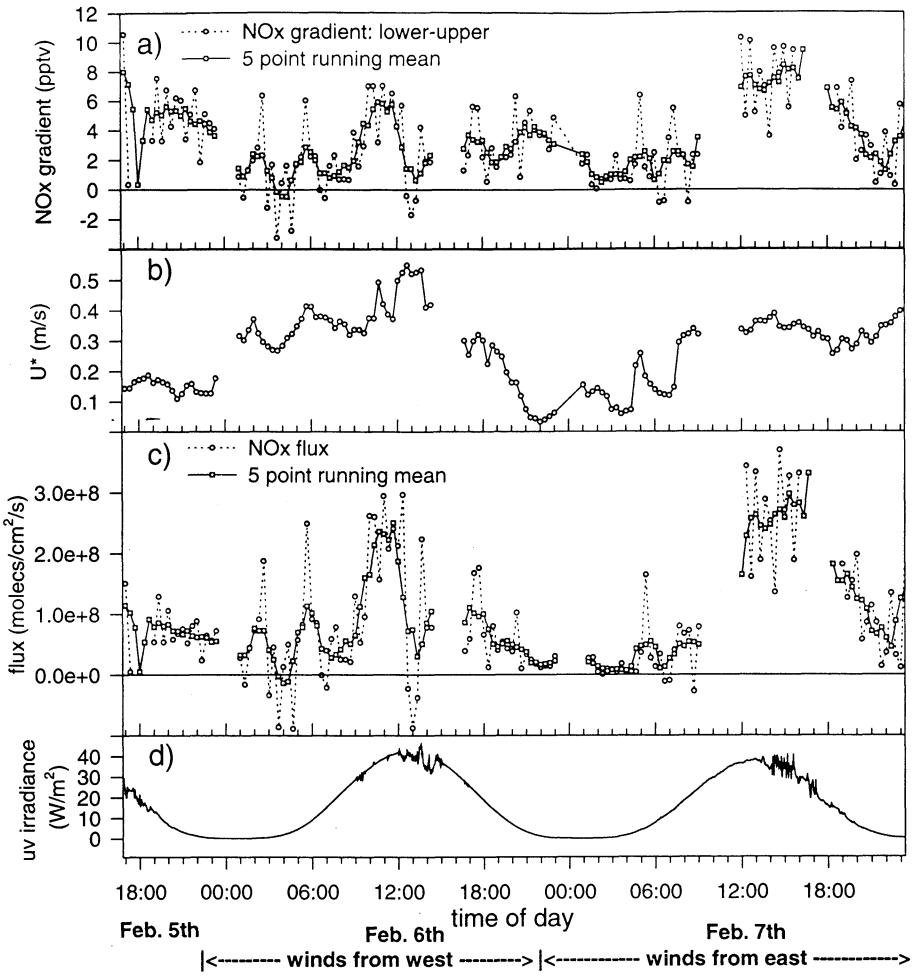

Figure 1. a) Gradients of NO_x derived from measurements at 2 cm - 2.5 m. Based upon considerations of instrument precision, gradients greater than 1.5 pptv are significant at the 2σ level; b) Variation in the friction velocity, U_*, which governs turbulent transfer, on the days of gradient measurements; c) Fluxes of NO_x derived from the measured gradients and U_*. Note that those measured during westerly winds are subject to turbulence. During easterly winds, the measurements are not influenced by turbulence; d) Diurnal variation in ultra violet irradiance (290 to 385 nm) on the days of measurements.

Combined errors from uncertainties in gradients and in U_* can thus be quoted as +10%/-30%.

Results

Figure 1a shows the gradient in NO_x (0.02 m - 2.5 m) measured on all days of the experiment. Gradients are generally positive and greater than the 2σ uncertainty. The magnitude varies between 0 and 9 pptv, based on a 5 point running mean. However, from 21:00 on Feb. 5th until 21:30 on Feb. 6th, winds were from the west and the inlets prone to turbulence from a nearby container. These data should thus be treated with appropriate caution. On Feb. 7th, with consistent easterly winds all day and no issues of turbulence, a noticeable diurnal cycle is evident. Figure 1b shows the variation of U_*, the friction velocity, during the same measurement period. U_* was smaller during the night (of the order 0 to 0.1 m/s) and with a tendency for larger U_* (up to 0.5 m/s) during the day. As a result, the transfer coefficient for NO_x, K_{NOx} (Eq'n 7), also varies in a similar way during the period of measurements. The NO_x flux, $F(NO_x)$, derived from the gradients and U_* is shown in Figure 1c. The calculated fluxes show significant variability, with essentially zero flux during the night, but reaching noon maxima of up to ~3 (+0.3/-0.9) x 10^8 molecs/cm²/s. NO_x is thus clearly being emitted from the snow to the overlying atmosphere throughout the majority of the day. Figure 1d shows the measured uv irradiance (290 to 385 nm) over these days, which also shows regular maxima at noon and nighttime minima.

Discussion and conclusions

When measurements were not disrupted by turbulence, the fluxes of NO_x varied in a regular manner with minima during the night and maxima around noon. Although U_*, driven by wind speed and temperature, clearly has an influence on NO_x fluxes, from ~02:00 to 22:00 on Feb. 7th, U_* is relatively constant but the flux of NO_x shows a marked diurnal variation. Given that we know NO_x is produced photochemically within the snowpack [*Jones et al.*, 2000], this strongly suggests that changes in uv irradiance is driving the flux. Furthermore, the NO_x flux decreases at the same time as the uv irradiance declines suggesting that photochemically-produced NO_x does not accumulate within the snowpack. We note that the measurements of *Honrath et al.* [1999] showed elevated concentrations of NO_x at 10 cm depth within the snowpack during daylight which also declined when the intensity of uv irradiance

dropped. With a diffusivity of around 10^{-5} m^2s^{-1} [Schwander et al., 1988], the venting timescale for this depth is 16 minutes, suggesting venting of photochemically produced NO_x on this timescale.

The impact of the NO_x flux on the overlying atmosphere will vary throughout the year according to production rate and seasonally-varying chemistry. For Neumayer on Feb. 7th, the mean daytime (i.e. from 06:00 to 21:00) NO_x flux, $F(NO_x)$, was $1.7x10^8$ molec/cm^2/s. Assuming the dominant NO_x loss occurs from reaction of NO_2 with OH (even at twilight the calculated photolysis rate of NO_3 is an order of magnitude greater than reaction with DMS, so that the latter does not provide an alternative sink for NO_x during this part of the day) and that photochemical equilibrium between NO and NO_2 is reached within a minute, the increase in the NO_x mixing ratio within a uniformly mixed layer of height z can be estimated from:

$$\frac{d[NO_x]}{dt} \approx \frac{F(NO_x)}{z} - k[OH][NO_2] \qquad (9)$$

With $k=2.4x10^{-11}(T/300)^{-1.3}$ cm^3 s^{-1} [*DeMore et al.*, 1994], a daily averaged $[OH]\approx 2x10^5$ molec cm^{-3} [*Jefferson et al.*, 1998] and a mixed layer height of 300m, the calculated NO_x increase between 06:00 and 21:00 is 9.6 pptv, close to the observed NO_x increase of ~10 pptv. Clearly this calculation is sensitive to the mixed layer height, and further the profile shape of NO_x emitted from the snow surface will be strongly influenced by the stability of the overlying boundary layer so will not always be uniformly mixed.

On a regional scale, if the source of NO_x is photolysis of nitrate impurities in the firn [*Honrath et al.*, 1999], and given the high concentrations of nitrate in polar snow [*Wolff*, 1995] we can assume that this production is occuring throughout the Antarctic continent. An average annual NO_x flux can be derived by scaling the Feb. 7th flux ($1.3x10^8$ molecs/cm^2/s) according to the relative uv irradiance (15.4 W/m^2 on Feb. 7th cf. 8.97 W/m^2 for the year). With an ice-covered surface of Antarctica of 13,340,000 km^2 [*Bartholomew*, 1985], an annual emission rate of 0.0076 TgN can be derived. Any tropospheric NO_x deposited as HNO_3 can potentially be recycled, but additionally, any nitrate deposited more directly to the snowpack can provide a source of new NO_x to the Antarctic troposphere. The source of NO_x from the snowpack is potentially very significant to Antarctica which is remote from most anthropogenic and biogenic sources. With regards the quest to derive atmospheric NO_x mixing ratios from concentrations of nitrate in ice cores, the findings presented here add a further twist and highlight an additional important factor that must be considered. Further measurements are clearly needed to derive a representative flux throughout the year and for different snow types.

Acknowledgements. G. König-Langlo is thanked for providing meteorological data used in this study, and H.K. Roscoe for help with instrumentation. Constructive comments and suggestions from two anonymous referees are gratefully acknowledged. This research was partly supported by grants from the Deutscher Akademischer Austauschdients (DAAD) and the British Council.

References

Bartholomew, J. and Son Ltd., *The Times Atlas of the World*, Times Books Ltd. London, 1985.

Dabberdt, W.F., D.H. Lenschow, T.W. Horst, P.R. Zimmermann, S.P. Oncley, A.C. Delany, Atmosphere-surface exchange measurements, *Science 260,* 1472-1481, 1993.

DeMore, W.B., S.P. Sander, D.M. Golden, R.F. Hampson, M.J. Kurylo, C.J. Howard, A.R. Ravishankara, C.E. Kolb, and M.J. Molina, Chemical kinetics and photochemical data for use in stratospheric modeling, Evaluation number 11, JPL Publ., 94-26, 1, 1994.

Dibb, J. E., R.W. Talbot, J.W. Munger, D.J. Jacob, and S.-M. Fan, Air-snow exchange of HNO3 and NOy at Summit, Greenland, *J. Geophys. Res., 103,* 3475-3486, 1998.

Garratt, J.R., *The Atmospheric Boundary Layer*, pp 247, Cambridge University Press, Cambridge, 1994.

Honrath, R.E., M.C. Peterson, S. Guo, J.E. Dibb, P.B. Shepson, and B. Cambell, Evidence of NO_x production within or upon ice particles in the Greenland snowpack, *Geophys. Res. Lett., 26,* 695-698, 1999.

Jefferson, A., D.J. Tanner, F.L. Eisele, D.D. Davis, G. Chen, J. Crawford, J.W. Huey, A.L. Torres, H. Berresheim, OH photochemistry and methane sulfonic acid formation in the coastal Antarctic boundary layer, *J. Geophys. Res., 103,* 1647-1656, 1998.

Jones, A.E., R. Weller, A. Minikin, E.W. Wolff, W.T. Sturges, H.P. McIntyre, S.R. Leonard, O. Schrems, and S. Bauguitte, Oxidised nitrogen chemistry and speciation in the Antarctic troposphere, *J. Geophys. Res. 104,* 21355-21366, 1999.

Jones, A.E., R. Weller, E.W. Wolff, and H.-W. Jacobi, Speciation and rate of photochemical NO and NO2 production in Antarctic Snow, *Geophys. Res. Lett., 27,* 345-348, 2000.

King, J.C. and P.S. Anderson, Heat and vapour fluxes and scalar roughness lengths over an Antarctic ice shelf. *Boundary Layer Meteorology 69,* 101-121, 1994.

König, G., Roughness length of an Antarctic ice shelf, *Polarforschung*, 55, no. 1, pp 27-32, 1985.

Munger, J.W., D.J. Jacob, S.-M. Fan, A.S. Colman, J.E. Dibb, Concentrations and snow-atmosphere fluxes of reactive nitrogen at Summit, Greenland, *J. Geophys. Res., 104,* 13,721-13,734, 1999

Ridley, B.A., M.A. Carroll, G.L. Gregory and G.W. Sachse, NO and NO2 in the troposphere: Technique and measurements in regions of a folded tropopause, *J. Geophys. Res., 93,* 15813-15830, 1988.

Ridley, B., J. Walega, D. Montzka, F. Grahek, E. Atlas, F. Flocke, V. Stroud, J. Deary, A. Gallant, H. Boudries, J. Bottenheim, K. Anlauf, D. Worthy, A.L. Sumner, B. Splawn, and P. Shepson, Is the Arctic surface layer a source and sink of NOx in winter/spring?, *J. Atmos. Chem, 36,* 1-22, 2000.

Schwander, J., B. Stauffer, and A. Sigg, Air mixing in firn and the age of the air at pore close-off, *Ann. Glaciol. 10,* 141-145, 1988.

Stull, R.B., *An Introduction to Boundary Layer Meteorology*, Kluwer, Dordrecht, 1988.

Weller, R. and O. Schrems, Photooxidants in the marine arctic troposphere in summer, *J. Geophys. Res., 101,* 9139-9147, 1996.

Weller, R., A.E. Jones, E.W. Wolff, A. Minikin, P.S. Anderson, G. König-Langlo, and O. Schrems, Investigating possible causes of the observed diurnal variability in Antarctic NOy, *Geophys. Res. Lett. 26,* 2853-2856, 1999.

Wolff, E., Nitrate in polar ice, in *Ice core studies of global biogeochemical cycles*, NATO ASI Series I, vol. 30 (editor R.J. Delmas), *195-224,* Springer-Verlag, New York, N.Y., 1995.

A.E. Jones, E.W. Wolff, P.S. Anderson, British Antarctic Survey, Natural Environment Research Council, High Cross, Madingley Road, Cambridge, CB3 0ET, UK. (e-mail: a.jones@bas.ac.uk)

R. Weller, H.-W. Jacobi, O. Schrems, H. Miller, Alfred-Wegener Institut für Polar- und Meeresforschung, 27570 Bremerhaven, Germany. (e-mail: r.weller@awi-bremerhaven.de)

(Received June 27, 2000; revised January 22, 2001;
accepted January 27, 2001)

Publication 3.2.3

Hutterli, M.A., J.R. McConnell, R.W. Stewart, H.-W. Jacobi, and R.C. Bales,

Impact of temperature-driven cycling of hydrogen peroxide (H_2O_2) between air and snow on the planetary boundary layer,

J.Geophys.Res. **106**, 15395-15404, 2001.

JOURNAL OF GEOPHYSICAL RESEARCH, VOL. 106, NO. D14, PAGES 15,395–15,404, JULY 27, 2001

Impact of temperature-driven cycling of hydrogen peroxide (H_2O_2) between air and snow on the planetary boundary layer

Manuel A. Hutterli,[1] Joseph R. McConnell,[2] Richard W. Stewart,[3] Hans-Werner Jacobi,[1] and Roger C. Bales[1]

Abstract. Hydrogen peroxide (H_2O_2) contributes to the atmosphere's oxidizing capacity, which determines the lifetime of atmospheric trace species. Measured bidirectional summertime H_2O_2 fluxes from the snowpack at Summit, Greenland, in June 1996 reveal a daytime H_2O_2 release from the surface snow reservoir and a partial redeposition at night. The observations also provide the first direct evidence of a strong net summertime H_2O_2 release from the snowpack, enhancing average boundary layer H_2O_2 concentrations approximately sevenfold and the OH and HO_2 concentrations by 70% and 50%, respectively, relative to that estimated from photochemical modeling in the absence of the snowpack source. The total H_2O_2 release over a 12-day period was of the order of 5×10^{13} molecules m^{-2} s^{-1} and compares well with observed concentration changes in the top snow layer. Photochemical and air-snow interaction modeling indicate that the net snowpack release is driven by temperature-induced uptake and release of H_2O_2 as deposited snow, which is supersaturated with respect to ice-air partitioning, approaches equilibrium. The results show that the physical cycling of H_2O_2 and possibly other volatile species is a key to understanding snowpacks as complex physical-photochemical reactors and has far reaching implications for the interpretation of ice core records as well as for the photochemistry in polar regions and in the vicinity of snowpacks in general.

1. Introduction

Hydrogen peroxide (H_2O_2) is a significant reservoir for the gas phase oxidants OH and HO_2 and is itself a powerful oxidant in the liquid phase. It thus plays a major role in determining the oxidizing capacity of the atmosphere [*Thompson*, 1992]. In the last decade, ice core records of H_2O_2 were established in part to provide a validation tool for global photochemical models investigating changing atmospheric composition and chemistry [*Sigg and Neftel*, 1991; *Thompson*, 1992; *Anklin and Bales*, 1997]. However, the reliability of these records was questioned when it was found that measured atmospheric H_2O_2 concentrations at Summit (72.6° N, 38.5° W, 3200 m elevation) were higher than predicted by gas phase photochemistry alone and that H_2O_2 concentrations in fresh snow were higher than those in equilibrium with the atmosphere, suggesting considerable exchange of H_2O_2 between the snow and atmosphere [*Conklin et al.*, 1993; *Neftel et al.*, 1995; *Fuhrer et al.*, 1996; *McConnell et al.*, 1997]. However, past studies have failed to directly measure H_2O_2 release from the snowpack [*Bales et al.*, 1995a, 1995b; *Fuhrer et al.*, 1996]. Further, there is strong evidence that formaldehyde (HCHO) desorbs from surface snow in response to diurnal and seasonal temperature changes, leading to H_2O_2 production [*Fuhrer et al.*, 1996; *Hutterli et al.*, 1999; *Couch et al.*, 2000]; this would also occur if HCHO was produced by heterogeneous photochemical reactions in the snow [*Fuhrer et al.*, 1996; *Sumner and Shepson*, 1999]. To further complicate the matter, it has recently been speculated that heterogeneous photochemical production of nitrogen oxides (NO_x) in snow might induce H_2O_2 production [*Jones et al.*, 2000; *Honrath et al.*, 2000].

The present study had three goals. The first was to directly determine H_2O_2 fluxes from the snowpack at Summit with continuous gradient measurements and to compare them with independent estimates based on H_2O_2 concentration changes in the near surface snow. The second goal was to test whether the measurements are consistent with temperature-dependent air-ice par-

[1]Department of Hydrology and Water Resources, University of Arizona, Tucson, Arizona.
[2]Desert Research Institute, Reno, Nevada.
[3]NASA Goddard Space Flight Center, Greenbelt, Maryland.

Paper number 2001JD900102.
0148-0227/01/2001JD900102$09.00

titioning alone, using an existing transfer model [*McConnell et al.*, 1998]. The third goal was to investigate the impact of measured H_2O_2 and HCHO fluxes on atmospheric H_2O_2 and HCHO mixing ratios using a photochemical model and to compare the results with the measurements.

2. Methods

The work was carried out at an electrically heated laboratory module situated 400 m SE of the main structures at the Greenland Ice Sheet Project (GISP2) Camp at Summit, Greenland (72.6° N, 38.5° W, 3200 m elevation) from June 4 to 20, 1996. H_2O_2 was continuously monitored in the air, with the instrument intake line mounted on a lift located 4 m upwind of the laboratory. The lift automatically switched the intake line between heights of 0.06 m and 3.5 m above the snow surface every 12 min. The 7 m long 1/4" perfluoroalkoxy (PFA) intake line was insulated and heated to prevent condensation and was tested several times during the field season for H_2O_2 losses and contamination by comparing various intake lines of different lengths. No artifacts were detected. Note that the use of a single intake line instead of one at each height reduces possible artificial concentration gradients due to line losses. On June 20, H_2O_2 was also measured in the firn air in the top few centimeters of the snowpack, by simply sticking the intake line into a small hole in the surface snow that was made with a polytetrafluoroethylene (PTFE) tool.

Gas phase measurements were done according to *Sigg et al.* [1992] by drawing air (~ 1 L min^{-1} (STP)) and pumping H_2O_2 free water (0.4 mL min^{-1}) together into a coil scrubber, resulting in 100% H_2O_2 collection efficiency. Subsequently, the H_2O_2 content in the water was continuously analyzed by fluorescence spectrometry after derivatization with 4-ethylphenol in the presence of peroxidase [*Sigg et al.*, 1992]. However, instead of raising the pH by adding a NaOH solution with a separate channel, the sample-reagent mixture was pumped through a short membrane tubing (Accurel) that was suspended over a 25% NH_3 solution. Calibrations were performed twice a day by running liquid standards through the coil scrubber while it was flushed with H_2O_2-free air, which was generated by pumping ambient air through a MnO_2 column. Those standards were compared with liquid standards measured directly to check for H_2O_2 losses in the coil scrubber. No losses were detected. The detector was kept at 25°C ±1°C. The baseline was determined every hour by measuring H_2O_2-free air through the intake line. Analytical precision, defined as 3 times the signal noise, was 40 pptv and the accuracy better than 20%.

Sets of five surface snow samples were collected daily at various times (Figure 1e). Each set represented a 2-cm-deep "minipit" with a vertical resolution of 0.5 cm and the top 0.5 cm layer sampled twice. During high winds, drifting snow samples were collected. However, it was not possible to distinguish between pure drifting snow and the fresh snow that apparently fell during those time periods, so that the samples are potentially a mixture of both. Some pure fresh snow samples were also collected in glass bottles using a high density polyethylene funnel (Figure 1e). Shallow firn cores extending down to 4 m were also collected. H_2O_2 and HCHO concentrations in the various snow samples were simultaneously determined according to *Röthlisberger et al.* [2000] in the field within less than a day after sampling. A more detailed description of the sampling procedures, a representative H_2O_2 concentration profile in the firn, and the HCHO results are given by *Hutterli et al.* [1999]. Firn temperatures were measured with a standard digital thermometer (Technotherm 300, ± 0.3°C).

Meteorological data were obtained from the GISP2 Automatic Weather Station at Summit (http://uwamrc.ssec.wisc.edu/aws/awsproj.html). Air temperatures were measured at 0.5 and 3.0 m, and wind speed and wind direction were measured at 3 m above the snow surface. Ozone was measured as documented previously [*Bales et al.*, 1995b]. Fog observations were made intermittently and thus reflect only a lower limit for the number of actual fog events.

3. Models

Photochemical modeling was conducted using the NASA Goddard Space Flight Center model [*Stewart and Thompson*, 1996] adapted for Summit conditions (72.3°N, 3 km elevation, and mixed layer height of 100 m [*Neftel et al.*, 1995; *Bales et al.*, 1995b]). A simulation of the measured H_2O_2 and HCHO [*Hutterli et al.*, 1999] fluxes was also included in the model. The model fluxes had the same maximum magnitude and diurnal variation as the observations but were assumed to have a sinusoidal form. In a box model, these fluxes (molecules m^{-2}s^{-1}) must be converted to sources (molecules m^{-3}s^{-1}) and to this end we usually used a mixed layer height of 100 m to determine the appropriate H_2O_2 and HCHO source functions. Such sources scale directly with the assumed mixed layer height and some results for an assumed 200 m value are indicated in the text and figures.

The lateral extent of the model domain is implicit in an assumed mixing time, a parameter used to specify the coupling to the ambient atmosphere [*Stewart et al.*, 1983]. The mixing time is an e-folding time that, in absence of chemistry, would tend to equilibrate the computed species in the box with the fixed values in the ambient atmosphere. In the present model the assumed mixing time is 1 year, so the box is nearly isolated. Water vapor is calculated assuming a relative humidity of 80%. Column-integrated ozone amounts and ozone (O_3), carbon monoxide (CO), and methane (CH_4) observations were used at 3-hour intervals to constrain the model chemistry. The values are based on either satellite measurements or measurements at remote sites in the Northern Hemisphere from the National Oceanic and Atmospheric Administration (NOAA) [*GLOBALVIEW-CH4*, 1999] (data are available on www.cmdl.

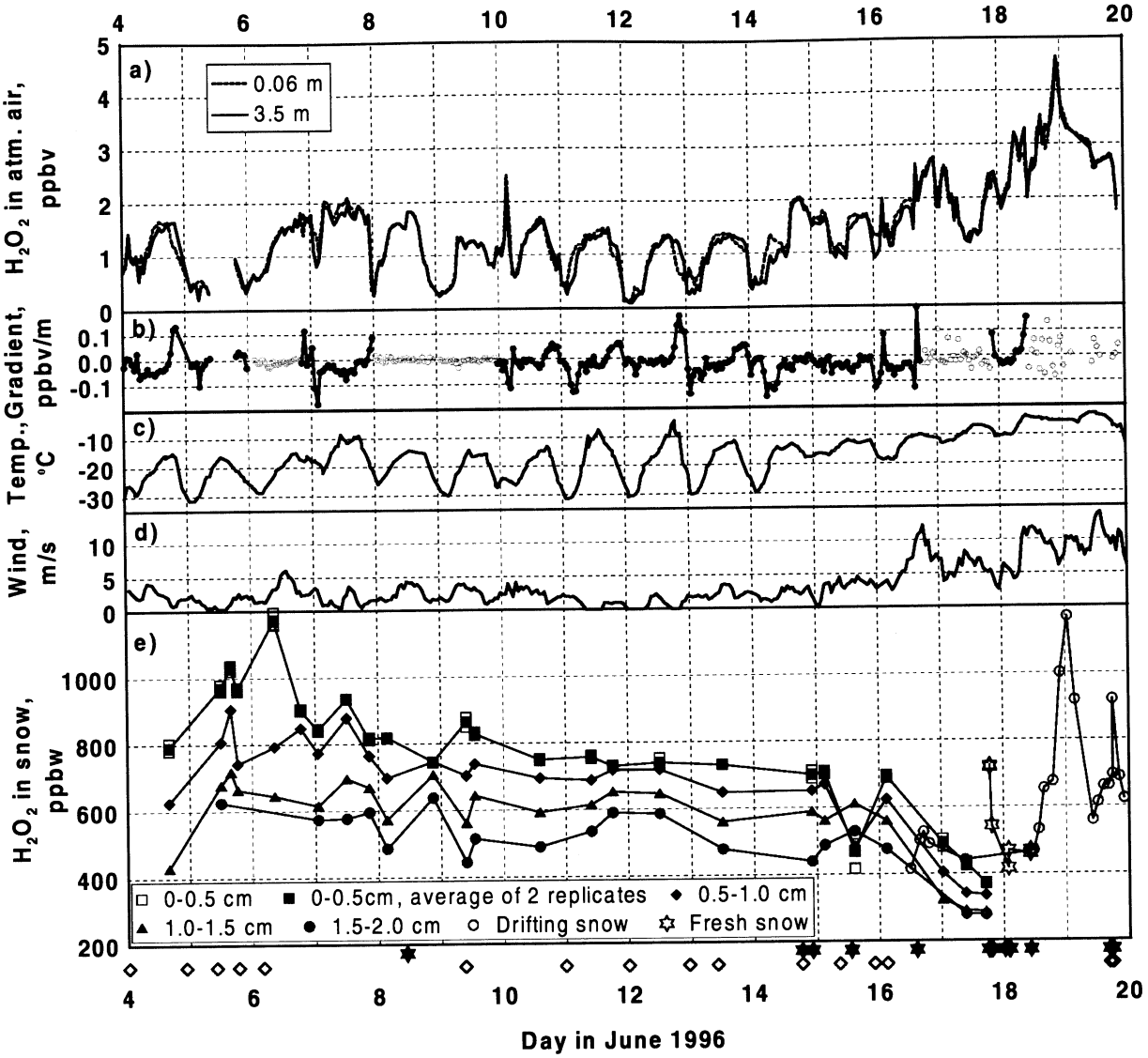

Figure 1. Results of H_2O_2 and meteorological measurements at Summit. Diamonds below the time axis indicate reported fog, and stars indicate snow precipitation. (a) Atmospheric H_2O_2 mixing ratios. (b) Corresponding H_2O_2 gradients between 3.5 and 0.06 m. Open circles are measurements at fixed height of 3.5 m, which do not represent gradients, but rather the variability of the H_2O_2 mixing ratios in the air on timescales of the gradient measurements (~20 min). (c) Air temperature (3 m). (d) Wind speed (3 m). (e) H_2O_2 concentrations in the top snow layers in parts per billion by weight (ppbw). Drifting snow is a mixture of fresh and wind-blown snow.

noaa.gov/info/ftpdata.html). Ozone was further verified using the few available measurements at Summit.

The chemical mechanism used in the present mode is similar to that of *Stewart and Thompson* [1996]. Oxidation of ethene has been added as have reactions involving Cl and Br. As explained in the reference, changing the reaction scheme in the model is handled by a preprocessor and does not require any code modification. The added reactions are all from *DeMore et al.* [1997]. To construct the continuity equations, the model uses 113 reactions and photolyses rates among 48 variable species along with specified physical production and loss terms for some species. Photolysis rates are interpolated from table values generated from the model of *Madronich* [1987]. These tables are written as functions of column-integrated ozone amounts and zenith angle. The kinetic data used are mostly taken from *DeMore et al.* [1997] and *Atkinson et al.* [1992]. The reactions are those following the photolyses of O_3 to produce $O(^1D)$ and the subsequent reaction of some of the latter with water vapor to form OH. In addition to methane, oxidation of ethane (C_2H_6) and ethene (C_2H_4) are included in the model. Ethane values are maintained by an assumed constant flux chosen to give nighttime values in the 2-3 ppbv range consistent with the values measured by *Jobson et al.* [1994] during the Polar Sunrise Experiment. Ethene values measured elsewhere may be about a factor of 2 lower [*Poisson*

et al., 2000] and a flux adjusted to give ~1 ppbv nighttime values was used. Both species are substantially oxidized during the Arctic day. The overall odd nitrogen background is maintained by a specified constant NO source and is about 4 pptv (NO_x). Since ozone is constrained by observed values in this model, the effect of varying assumed NO_x source is small relative to that in a model with ozone responsive to NO_x changes. Methyl chloride (CH_3Cl) and methyl bromide (CH_3Br) are also included in the chemistry to provide a basic source of halogens. CH_3Cl is held fixed at 600 pptv [*Graedel and Keene*, 1995] and CH_3Br at 10 pptv [*Yokouchi et al.*, 2000]. First-order loss of several species to the ice/snow surface is computed using deposition velocities taken from the summary of *Seinfeld and Pandis* [1998].

The numerical methods used in the model have been described by *Stewart* [1993, 1995] and *Stewart and Thompson* [1996]. The model was run in a time-dependent mode constrained by observations. Temperature, column-integrated ozone amount, and concentrations of methane, carbon monoxide, and ozone were used to update the model at 3-hour intervals. Reaction rates and physical source and loss values are updated every 10 min during a simulation to ensure that photolysis rates are computed at reasonable intervals. The model has previously been employed in Monte Carlo studies of modeling uncertainties [*Stewart and Thompson*, 1996] and in studies related to snow-to-firn transfer of H_2O_2 at the South Pole [*McConnell et al.*, 1998].

The transfer model described by *McConnell et al.* [1998] was used to model the exchange of H_2O_2 between the air and the snowpack. The simulation of the uptake and release of H_2O_2 by snow as environmental conditions change is simulated by the one-dimensional advection-dispersion equation and grain-scale spherical diffusion. Both air-snow partitioning of H_2O_2 and diffusion rates in ice are strongly temperature dependent, with coefficients derived from independent laboratory experiments [*Conklin et al.*, 1993]. In addition to temperature, rates of uptake and release are closely related to grain size and firn ventilation.

In the simulations reported here, we used a 100-layer model with layer thicknesses of 0.5 cm. Measured atmospheric concentrations at 3.5 m provided the upper boundary condition. Firn temperatures were modeled using measured air temperatures and diffusion into the snowpack [*Schwander et al.*, 1997]. Comparison with measurements shows that modeled values in the top few centimeters of the snowpack can be off by up to a few degrees on certain days [*Hutterli*, 1999]. This can be explained with uncertainties inherent in air and snow temperature measurements and with the fact that potential radiation effects [*Colbeck*, 1989] are not taken into account in the model. However, measured temperatures in deeper layers are reproduced within less than 0.5°C, indicating that average temperatures also of the top snow layers are accurately described on daily and longer term timescales [*Hutterli*, 1999]. The uncertainties in the temperature model thus do not significantly affect the average flux estimates. However, on shorter timescales they may have contributed to differences between the modeled and measured H_2O_2 firn air concentrations (Table 1).

Table 1. Comparison of the June 20 H_2O_2 Firn Air Measurements With Model Results[a]

Time, LST	Air Temperature, °C	C_a, ppbv	C_{fa}, ppbv	C_{fa}^{mod}, ppbv
1000	-12	0.60	2.1	1.7
1600	-11	0.76	1.8	1.9
2400	-20	0.62	1.0	0.9

[a] C_a, atmospheric H_2O_2 mixing ratio; C_{fa}, firn air H_2O_2 mixing ratio; C_{fa}^{mod}, modeled firn air H_2O_2 mixing ratio, 0-2.5 cm average.

Molecular diffusion within the firn air was parameterized according to *Hutterli et al.* [1999], with typical H_2O_2 diffusivities of the order of $2.2\times10^{-5}\,m^2\,s^{-1}$. The initial concentration of H_2O_2 in the snowpack was based on surface snow measurements for the top 2 cm and a snowpit profile of concentration from 2 cm to 50 cm depth, sampled in the same area as the surface snow measurements on June 4 [*Hutterli et al.*, 1999]. H_2O_2 was assumed to initially be distributed uniformly within the snow grains. This simplification might have an impact on the modeled fluxes in the first few days. However, it is not expected to influence the total H_2O_2 release because the initial H_2O_2 distribution within the snow grains adapts fast due to the high diffusion rates at the measured temperatures.

4. Results and Discussion

4.1. Atmospheric Measurements

Atmospheric H_2O_2 showed a distinct diurnal cycle closely linked to temperature with hourly H_2O_2 mixing ratios averaging 1.4 ppbv (range 0.09-4.6 ppbv) for both heights (Figure 1a), consistent with prior summertime measurements [*Bales et al.*, 1995b; *Sigg et al.*, 1992]. From June 4 to 16, wind speed was generally below 5 m s^{-1} (Figure 1d), and fog built up during nearly every night, resulting in rime deposition.

During this period, H_2O_2 gradients in the air above the snow showed a distinct diurnal cycle with positive values (uptake) from evening to midnight and negative values (release) during the rest of the day (Figures 2a and 2b). H_2O_2 gradients were generally between ±0.1 ppbv m^{-1} (Figures 1b and 2b), with an average of -0.020 ppbv m^{-1} which is below the detection limits of earlier studies [*Bales et al.*, 1995b]. From June 17 to 21 there was less nighttime cooling, higher daily mean temperatures (Figure 1c) and wind speeds were up to 15 m s^{-1}, resulting in drifting snow and a higher variability and no distinct diurnal cycle in the H_2O_2 gradients (Figures 1a and 1b). The lifetime of H_2O_2 of less than

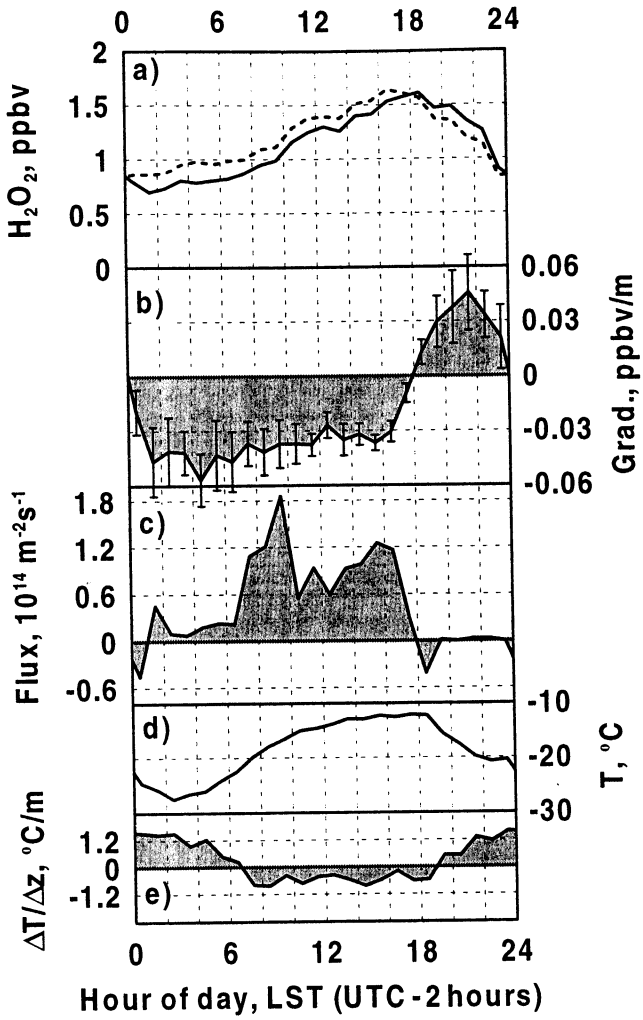

Figure 2. Average diurnal cycles in Local Standard Time (LST) for the period from June 4 to June 16, 1996 (hour of day averages are based on 10-min data). (a) Atmospheric H_2O_2 mixing ratios. (b) Corresponding H_2O_2 gradients between 3.5 and 0.06 m with standard deviation of the mean. (c) Calculated H_2O_2 fluxes from the snowpack. (d) Air temperature. (e) Air temperature gradient.

2 days at Summit in summer and the remoteness of the site limit the potential impact of long-range transport of H_2O_2 on atmospheric concentrations at Summit. However, the meteorological conditions during the period after June 16 indicated more vigorous long range transport (i.e., lower transport times of air masses from potential direct H_2O_2 sources to Summit). A contribution from H_2O_2 enriched air masses to the high concentrations during this period can thus not be excluded.

H_2O_2 fluxes were determined from the gradient measurements and diffusion coefficients calculated based on the Monin-Obukhov similarity theory according to

$$F = -K_{zz}\frac{\partial C}{\partial z} = -\frac{\kappa u_* z}{\phi(z/L)}\frac{\partial C}{\partial z}, \quad (1)$$

where C is the atmospheric concentration, z is the height, F is the particle flux, K_{zz} is the turbulent diffusion coefficient, κ (set to 0.40) is the von Karman constant, u_* is the friction velocity, and $\phi(z/L)$ is an empirically determined function defining the flux-profile relationship, which is assumed to depend only on the stability parameter z/L, with L the Monin-Obukhov length [*Seinfeld and Pandis,* 1998]. Variable u_* was obtained iteratively following *King et al.* [1996], using the same parameters and integrated ϕ functions that were determined empirically over the Antarctic ice shelf at Halley station for stable and neutral conditions [*King and Anderson,* 1994]. For unstable conditions the ϕ functions proposed by *Högström* [1988] were used. Finally, the fluxes F were obtained by integrating (1) from measurement heights z_1 to z_2 and inserting the observed atmospheric concentrations $C(z_1)$ and $C(z_2)$.

Implicit in the above flux calculations is the assumption of a constant flux at all heights at any given time. For unstable to moderately stable conditions this is justified by the long characteristic times of chemical reactions involving H_2O_2 (lifetime of ~43 hours at Summit in summer) compared to transport time between the measurement heights (seconds to minutes). This also holds for HCHO (lifetime 3.7 hours at Summit in summer) released by the snowpack, which represents a potentially significant radical source increasing H_2O_2 production [*Hutterli et al.,* 1999]. Stable conditions, with K_{zz} values less than 0.1% of those for unstable conditions, do not contribute significantly to the average H_2O_2 flux and can thus be neglected.

Average H_2O_2 fluxes for each hour of the day for the 12-day period between June 4 and 16 are shown in Figure 2c. Nighttime fluxes are lower due to more stable stratification compared to daytime, when temperature gradients show stratification becoming unstable (Figure 2e). Two outliers, when high wind in combination with a very strong negative temperature gradient led to unreasonably high mixing, were removed from the 164 hourly values. Values for K_{zz} ranged from less than 10^{-5} to 0.9 m^{2}s^{-1}, with an average of 0.13 m^{2}s^{-1} for the 12-day period (K_{zz} values lower than the typical molecular diffusivity of 2.4×10^{-5} m^{2}s^{-1} for H_2O_2 under Summit conditions were replaced by this value for consistency; however, this had no effect on the flux calculations). The average flux (± standard deviation of the mean) during this period was $(4.9\pm0.9)\times10^{13}$ m^{-2} s^{-1} ($(6.3\pm1.3)\times10^{13}$ m^{-2}s^{-1} including the outliers). Error propagation calculations based on the meteorological data indicate an uncertainty of the average flux of less than a factor of 2.

4.2. Photochemical Model Runs

Without including H_2O_2 and HCHO fluxes from the snowpack, the gas phase photochemical model results predict average summertime mixing ratios of approximately 0.21 and 0.024 ppbv for H_2O_2 and HCHO, respectively for Summit (Figure 3). This is about one seventh and one tenth of the observed 1.4 and 0.23 ppbv [*Hutterli et al.,* 1999], respectively. This inability of gas phase photochemistry to replicate the observed summer high-latitude H_2O_2 and HCHO mixing ratios has

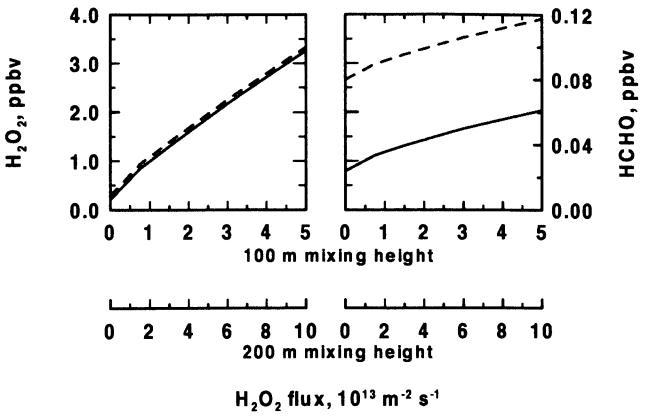

Figure 3. Modeled atmospheric H_2O_2 and HCHO mixing ratios as a function of H_2O_2 fluxes for two mixing heights. Solid lines indicate results calculated without a HCHO flux, and dotted lines indicate results calculated with a HCHO flux of $1\times10^{13}\,m^{-2}s^{-1}$.

been encountered in other model studies [e.g., *Fuhrer et al.,* 1996]. H_2O_2 fluxes in the observed range of 1.5×10^{13} to $5\times10^{13}\,m^{-2}s^{-1}$ increase the H_2O_2 mixing ratios to 1.3-3.3 ppbv (0.8-1.8 ppbv) and HCHO mixing ratios to 0.039-0.061 ppbv (0.033-0.055 ppbv), respectively, assuming a typical mixing height of 100 m (200 m) for Summit [*Bales et al.,* 1995b]. Inclusion of the reported HCHO flux of $1\times10^{13}\,m^{-2}s^{-1}$ [*Hutterli et al.,* 1999] into the model adds an additional 0.06 ppbv of HCHO and increases H_2O_2 by about 0.1 ppbv (100 m mixing height), consistent with estimates from earlier model simulations [*Hutterli et al.,* 1999]. While modeled H_2O_2 levels fall within the observed range, modeled HCHO concentrations are lower than observed. The combined effect of the H_2O_2 and HCHO fluxes increases the OH and HO_2 concentrations by $\sim$70% and $\sim$50%, respectively (100 m mixing height).

While the measured diurnal variation in atmospheric H_2O_2 is about a factor of 4 ($\sim$0.4 to $\sim$1.6 ppbv), the gas phase photochemistry alone results in a diurnal change of only 20%, indicating that heterogeneous processes are also taking place. Including a strong heterogeneous deposition due to fog formation and taking into account the generally lower mixing height at nighttime would increase this amplitude as well as alter the flux - mixing ratio relationship shown in Figure 3 (see section 4.5).

Although the details of halogen activation mechanisms are not completely understood, the role of halogen atoms in Arctic photochemistry is well established [*Rudolph et al.,* 1999; *Boudries and Bottenheim,* 2000]. This role is episodic and is associated with ozone depletion events [*Solberg et al.,* 1996]. There is neither direct or indirect evidence for halogen atom involvement during the time of the Summit observations, nor evidence ruling out such involvement. We have therefore performed a few model runs to estimate the effect that reactions involving chlorine might have on H_2O_2 and HCHO mixing ratios. The oxidation of CH_3Cl and CH_3Br by OH, included in all model runs, does not produce enough active halogen to influence the mixing ratios of other species. We have therefore included a chlorine source to maintain a Cl atom concentration of the order of $10^{10}\,m^{-3}$ [*Rudolph et al.,* 1999]. This increased the H_2O_2 and HCHO mixing ratios by 0.9 and 0.18 ppbv, respectively, due to Cl atom reaction with methane and other hydrocarbons. Without considering the effect of the observed H_2O_2 and HCHO fluxes, a Cl atom concentration similar to that inferred by *Jobson et al.* [1994] increases computed peroxide and formaldehyde concentrations to within about 20% and 13%, respectively, of their observed values. This suggests that halogen photochemistry may, when considered in conjunction with observed H_2O_2 and HCHO fluxes, help resolve discrepancies in the magnitude of observed and computed concentrations. A potential source of Cl atoms may be the proposed HCl volatilization from snow [*Wagnon et al.,* 1999]. However, the reaction of HCl with OH producing Cl atoms appears to be too slow to provide a major Cl source. Due to lack of evidence for halogen involvement at the time of the Summit observations, we have not attempted a best fit of observed H_2O_2 and HCHO fluxes and halogen sources to modeled concentrations.

4.3. Firn Air

Firn air measurements 5 cm below the snow surface on June 20 revealed H_2O_2 mixing ratios up to 3.5 times atmospheric concentrations, consistent with H_2O_2 release by the snow grains (Table 1). Note that due to the porous nature of the firn, the firn air measured is a mixture of atmospheric and firn air, and mixing ratios represent lower limits for actual values. Modeled firn air concentrations for corresponding times and depths agree with the measurements with differences less than 20% (Table 1). The latter are explainable by uncertainties in the surface snow concentrations after June 18 (no minipit data) and the uncertainties in the modeled snow temperatures in the top layers. Previous firn air measurements deeper down (below 25 cm) revealed values near or below the atmospheric level [*Bales et al.,* 1995a], which is consistent with lower temperatures and lower H_2O_2 concentrations in those firn layers.

4.4. Snow

H_2O_2 concentrations in the surface snow layers generally decreased with depth and replicate samples from the top layer had relatively low variability (Figure 1e). The drifting snow samples (open circles in Figure 1e), which could also contain fresh snow (see methods), showed concentrations up to 1200 parts per billion by weight (ppbw). Up to and including June 16 snow falls were light and not expected to contribute significantly to the surface snow samples. Fresh snow collected the night of June 17 had concentrations between 415 ppbw and 720 ppbw (stars in Figure 1e). Pit measurements revealed the typical seasonal H_2O_2 signal with high values ($\sim$350 ppbw) in summer layers and low values ($\sim$50 ppbw) in winter layers [*Hutterli et al.,* 1999]. All

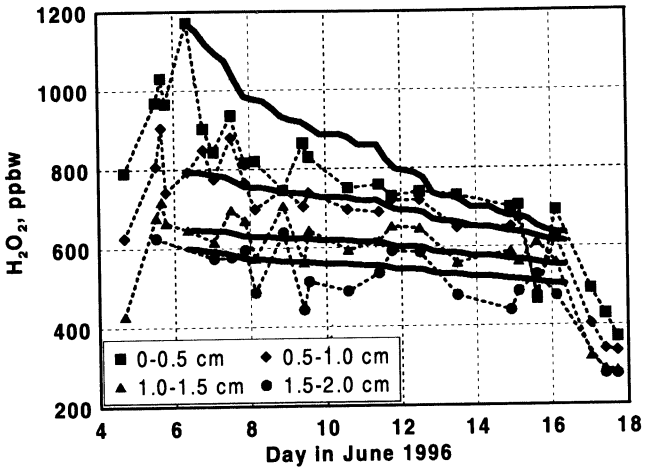

Figure 4. Measured and corresponding modeled (solid lines) H_2O_2 concentrations in the surface snow using a grain radius of 120 μm (100 μm for the top layer).

previous summer peak values in the pit profile were below 400 ppbw.

The strong H_2O_2 decrease in the top 2-cm snow layer (Figure 1e) from June 6 to June 16 corresponds to a mean H_2O_2 flux of $3.3\times10^{13}\,m^{-2}\,s^{-1}$ (snow density $350\,kg\,m^{-3}$, decrease of $23\,ppbw\,d^{-1}$). Simulating the uptake and release of H_2O_2 from the snow with the transfer model as environmental conditions change shows that deeper layers also significantly contributed to the net flux. Both air-snow partitioning and rates of uptake and release are related to grain size. While the latter was not measured, using effective grain radii within published values led to a good agreement between the modeled and measured evolution of the near-surface snow profiles (Figure 4). As near-surface snow grain radii are significantly smaller than at depth [*Waddington et al.*, 1996], the top 0.5 cm snow layer was set to a constant 100 μm, while only the values for the deeper layers were varied. Table 2 summarizes the model results. The minipit data (and the corresponding flux estimate) were best reproduced with effective snow grain radii of about 120 μm (Figure 4) for those layers. In this case, with a modeled flux from the top 2 cm snow layer of $3.2\times10^{13}\,m^{-2}\,s^{-1}$ ($3.3\times10^{13}\,m^{-2}\,s^{-1}$ from the minipit measurements), the modeled total net flux from the snowpack was $4.6\times10^{13}\,m^{-2}\,s^{-1}$. This is in excellent agreement with the independently determined average flux based on the gradient measurements ($4.9\times10^{13}\,m^{-2}\,s^{-1}$), thus confirming physical uptake/release as the dominant process. Note that if the net H_2O_2 flux revealed by the gradient measurements was due to heterogeneous photochemical H_2O_2 production in the snowpack, the snow would tend to take up the produced H_2O_2 [*Conklin et al.*, 1993], leading to an increase rather than the observed decrease of H_2O_2 concentrations in the snow. Because the combination of grain size and H_2O_2 diffusivity in ice determines the release of H_2O_2, instead of adjusting the grain size, the temperature dependance of the diffusivity could be varied within its uncertainty range as well (changing the diffusivities within a factor of 2-3). While this alters the value of the optimal effective grain size, it does not significantly affect the resulting fluxes. By adjusting the grain size, the model is tuned to account implicitly also for other temperature-dependent processes, such as evaporation and condensation of water vapor on ice crystal surfaces, which are expected to affect the H_2O_2 uptake and release through cocondensation and coevaporation [*Sigg et al.*, 1992].

The very strong depletion of the surface snow layers between June 16 and June 18 ($177\,ppbw\,d^{-1}$, corresponding to $2.5\times10^{14}\,m^{-2}\,s^{-1}$) are coincident with high temperatures, very high wind speeds, and elevated atmospheric H_2O_2 mixing ratios, consistent with the temperature-dependent uptake/release hypothesis. Increased sublimation rates expected during such conditions would accelerate the H_2O_2 depletion in the snow. Part of the depletion could also be due to a removal of the top snow layer by the wind and/or its mixing with lower concentration drifting snow. However, this alone would not explain the elevated atmospheric mixing ratios. The concurrence of high H_2O_2 concentrations in fresh and drifting snow samples with high atmospheric values further stress the close link between the two.

Deposition of fresh snow could explain the higher surface snow layer concentration after June 18. The early June increase in surface snow H_2O_2 concentration occurred during an exceptional fog event lasting from June 4, 22:30 Local Standard Time (LST; UTC - 2 hours) through June 6, 04:00 LST that deposited ~1 cm of surface hoar. The concentration was in the range of previous fog and hoar measurements (680 up to 2550 ppbw), agreed with that based on cocondensation theory [*Sigg et al.*, 1992] and was supersaturated with respect to air-snow equilibrium [*Conklin et al.*, 1993; *McConnell et al.*, 1997].

Thus fresh snow and extensive fog deposition can result in higher concentrations in surface snow and can temporarily mask the long-term H_2O_2 release. The previously reported net H_2O_2 increase in surface snow over a 17-day-long period without fresh snow deposition [*Bales et al.*, 1995b] does not exclude a release. Over the 17-day period, the surface snow concentration revealed H_2O_2 enrichments in the course of a day

Table 2. Modeled Mean H_2O_2 Fluxes From the Snowpack Between June 6 and 16

Grain Radius,[a] μm	F_{2cm},[b] $10^{13}\,m^{-2}\,s^{-1}$	F_{total},[c] $10^{13}\,m^{-2}\,s^{-1}$
100	3.52	5.68
120	3.24	4.61
150	2.98	3.70
180	2.80	3.19
250	2.56	2.59

[a]Grain radius fixed at 100 μm in the top 0.5 cm.
[b]H_2O_2 flux from the top 2 cm snow layer.
[c]Total H_2O_2 flux from the snowpack.

consistent with the reported fog deposition, followed by gradual decreases over several days as expected from the uptake/release hypothesis.

4.5. Fog

While the transfer model reveals a temporary H_2O_2 uptake by the cold surface snow on many nights, it is plausible that fog deposition dominates nighttime H_2O_2 depletion from air [*Sigg et al.*, 1992; *Bergin et al.*, 1996]. Heterogeneous deposition due to fog formation, which occurred on virtually every night during the first 12 days of the measurements, and the lower mixing heights at night can explain the discrepancy. This is supported by sporadic observations in the field linking the fast H_2O_2 depletion in the air to the formation of radiative fog. In fact, modeled fog formation and deposition suggested a complete depletion of atmospheric H_2O_2 in the air [*Bergin et al.*, 1996] which is in contradiction to our measurements. However, these measurements may represent H_2O_2 in the air and in fog droplets, as no attempt was made to prevent the latter from entering the system. This indicates that during fog events much of the H_2O_2 may be present in the fog droplets.

Nighttime ground fog strongly influences atmospheric H_2O_2 mixing ratios and also impacts the surface snow concentrations. However, apart from the exceptional fog event from June 4 to June 6 discussed in the previous section, the impact of fog deposition on surface snow appeared to be small. Specifically, during the June 6 to 16 period, fog observations, minipit measurements and visual surface snow inspection do not indicate a significant impact of fog deposition on the surface snow H_2O_2 concentrations. One exception might have been the fog event on June 9. After this event, fresh surface frost and an increase in surface snow concentrations exceeding the general spatial variability was seen. However, accounting for the potential additional H_2O_2 release following fog deposition increased the H_2O_2 flux estimate based on the minipit measurements by less than 10% and was therefore neglected.

Fog droplets that are in or close to Henry's equilibrium with the air become highly oversaturated when they freeze. Though rime and surface hoar start releasing H_2O_2 right after formation, the H_2O_2 escaping into the atmosphere is immediately scavenged again by depositing fog droplets and redeposited until the fog droplet flux to the surface stabilizes or decreases, which occurs before air temperatures rise [*Bergin et al.*, 1996]. This change in water flux would thus explain why the snowpack started to release H_2O_2 around midnight, hours before the temperature began to rise (Figure 2). *Sigg et al.*'s [1992] suggestion that the reevaporation of freshly formed hoar was responsible for the rise of the H_2O_2 mixing ratios only holds after the temperature starts to rise. *Bergin et al.* [1996] attributed the morning increase of H_2O_2 in the air to downmixing of higher concentration air from above the fog. However, the atmosphere generally remained stable until around 07:00 LST (Figure 2e) and downmixing is incompatible with the direction of the measured gradients.

5. Conclusions

While heterogeneous photochemical H_2O_2 production in snow can not be excluded, our results show that physical processes are necessary and sufficient to explain the H_2O_2 measurements in snow and air. They show that polar snow and most likely clean, dry snow in general acts as a reservoir for atmospheric H_2O_2. High concentrations of H_2O_2 are incorporated into snow when it forms (cocondensation, riming). Once on the ground, the H_2O_2 both degasses from the snow as it approaches equilibrium and cycles between the atmosphere and surface snow in response to the diurnal temperature cycle and the deposition/evaporation of water. This (re)cycling increases the average H_2O_2 concentration by a factor of 7 above what it would be without a snowpack source, thus contributing ~85% of the H_2O_2 in the planetary boundary layer during the warm part of the day at Summit in summer 1996. The cycling also causes a significant depletion from the air at night. Much of the nighttime atmospheric H_2O_2 may be present in fog droplets, where it represents a strong oxidant that may significantly enhance sulfate deposition [*Bergin et al.*, 1996]. Slow H_2O_2 degassing from snow accounted for the decrease in surface snow concentrations, although modeling studies indicate that the snow is generally buried before reaching equilibrium with the atmosphere at Summit.

This release does not only significantly increase the oxidizing capacity in the planetary boundary layer but also in the firn air in the top snow layers, possibly affecting heterogeneous (photo-)chemistry at the snow crystal surfaces. The temperature dependence of the H_2O_2 release suggests a strong seasonal variation of the fluxes with generally higher values during the warmer months modulated by the timing and concentration of snow accumulation. It further implies that volatile contaminants physically removed from the atmosphere and immobilized in the snow during winter could be partially reemitted in spring while snow temperatures rise. In order to understand the photochemistry in the polar boundary layer and to quantitatively interpret chemical ice core records of volatile species, highly nonlinear physical processes as well as heterogeneous photochemistry in the snowpack must be considered and their impact on regional to global scale assessed.

Acknowledgments. Field measurements were made under the European project EV5V-0412 Transfer of Aerosols and Gases to Greenland Snow and Ice. C.R. Stearns, University of Wisconsin-Madison, funded by NSF, provided the AWS-data (http://uwamrc.ssec.wisc.edu/aws/awsproj.html) and J.E. Dibb provided fresh snow observations. Carbon monoxide and ozone measurements were made available by the National Oceanic and Atmospheric Administration (NOAA), Climate Monitoring and Diagnostics Laboratory (CMDL), Carbon Cycle Group. The Swiss and U.S. National Science Foundations provided financial support. H.W.J. thanks the Deutsche Forschungsgemeinschaft (DFG) for a stipend. We thank C.M. Brown-Mitic and R. Röthlisberger for valuable discussions.

References

Anklin, M., and R. C. Bales, Recent increase in H_2O_2 concentration at Summit, Greenland, *J. Geophys. Res., 102*, 19,099–19,104, 1997.

Atkinson, R., D. L. Baulch, R. F. Hampson Jr., J. A. Kerr, and J. Troe, Evaluated kinetic and photochemical data for atmospheric chemistry, *J. Phys. Chem. Ref. Data, 21*, suppl. IV, 1125–1568, 1992.

Bales, R. C., M. V. Losleben, J. R. McConnell, K. Fuhrer, and A. Neftel, H_2O_2 in snow, air and open pore space in firn at Summit, Greenland, *Geophys. Res. Lett., 22*, 1261–1264, 1995a.

Bales, R. C., J. R. McConnell, M. V. Losleben, M. H. Conklin, K. Fuhrer, A. Neftel, J. E. Dibb, J. D. W. Kahl, and C. R. Stearns, The diel variations of H_2O_2 in Greenland: A discussion of the cause and effect relationship, *J. Geophys. Res., 100*, 18,661–18,668, 1995b.

Bergin, M. H., S. N. Pandis, C. I. Davidson, J.-L. Jaffrezo, J. E. Dibb, A. G. Russell, and H. D. Kuhns, Modeling of the processing and removal of trace gas and aerosol species by Arctic radiation fogs and comparison with measurements, *J. Geophys. Res., 101*, 14,465–14,478, 1996.

Boudries, H., and J. W. Bottenheim, Cl and Br atom concentrations during a surface boundary layer ozone depletion event in the Canadian High Arctic, *Geophys. Res. Lett., 27*, 517–520, 2000.

Colbeck, S. C., Snow-crystal growth with varying surface temperatures and radiation penetration, *J. Glaciol., 35*, 23–29, 1989.

Conklin, M. H., A. Sigg, A. Neftel, and R. C. Bales, Atmosphere-snow transfer function for H_2O_2: Microphysical considerations, *J. Geophys. Res., 98*, 18,367–18,376, 1993.

Couch, T. L., A. L. Sumner, T. M. Dassau, P. B. Shepson, and R. E. Honrath, An investigation of the interaction of carbonyl compounds with the snowpack, *Geophys. Res. Lett., 27*, 2241–2244, 2000.

DeMore, W. B., S. P. Sander, D. M. Golden, R. F. Hampson, M. J. Kurylo, C. J. Howard, A. R. Ravishankara, C. E. Kolb, and M. J. Molina, Chemical kinetics and photochemical data for use in stratospheric modeling, *JPL Publ., 97-12*, 1997.

Fuhrer, K., M. Hutterli, and J. R. McConnell, Overview of recent field experiments for the study of the air-snow transfer of H_2O_2 and HCHO, in *Chemical Exchange Between the Atmosphere and Polar Snow, NATO ASI Ser. I, Vol. 43*, pp. 307-318, Springer-Verlag, New York, 1996.

GLOBALVIEW-CH4, *Cooperative Atmospheric Data Integration Project - Methane* [CD-ROM], NOAA Clim. Monit. and Diagnostics Lab., Boulder, Colo., 1999.

Graedel, T. E., and W. C. Keene, Tropospheric budget of reactive chlorine, *Global Biogeochem. Cycles, 9*, 47–77, 1995.

Högström, U., Non-dimensional wind and temperature profiles in the atmospheric surface layer: A re-evaluation, *Boundary Layer Meteorol., 42*, 55–78, 1988.

Honrath, R. E., S. Guo, M. C. Peterson, M. P. Dziobak, J. E. Dibb, and M. A. Arsenault, Photochemical production of gas phase NO_x from ice crystal NO_3^-, *J. Geophys. Res., 105*, 24,183–24,190, 2000.

Hutterli, M. A., Luft-Firn Transferstudien von HCHO und H_2O_2 zur Interpretation von Eisbohrkerndaten, Ph.D. thesis, Phys. Inst., Univ. of Bern, Bern, Switzerland, 1999.

Hutterli, M. A., R. Röthlisberger, and R. C. Bales, Atmosphere-to-snow-to-firn transfer studies of HCHO at Summit, Greenland, *Geophys. Res. Lett., 26*, 1691–1694, 1999.

Jobson, B. T., H. Niki, Y. Yokouchi, J. Bottenheim, F. Hopper, and R. Leaitch, Measurements of C_2-C_6 hydrocarbons during the Polar Sunrise 1992 Experiment: Evidence for Cl and Br atom chemistry, *J. Geophys. Res., 99*, 25,355–25,368, 1994.

Jones, A. E., R. Weller, E. W. Wolff, and H.-W. Jacobi, Speciation and rate of photochemical NO and NO_2 production in Antarctic snow, *Geophys. Res. Lett., 27*, 345–348, 2000.

King, J. C., and P. S. Anderson, Heat and water vapor fluxes and scalar roughness lengths over an Antarctic ice shelf, *Boundary Layer Meteorol., 69*, 101–121, 1994.

King, J. C., P. S. Anderson, M. C. Smith, and S. D. Mobbs, The surface energy and mass balance at Halley, Antarctica during winter, *J. Geophys. Res., 101*, 19,119–19,128, 1996.

Madronich, S., Photodissociation in the atmosphere, 1. Actinic flux and the effect of ground radiation and clouds, *J. Geophys. Res., 92*, 9740–9752, 1987.

McConnell, J. R., J. R. Winterle, R. C. Bales, A. M. Thompson, and R. W. Stewart, Physically based inversion of surface snow concentrations of H_2O_2 to atmospheric concentrations at South Pole, *Geophys. Res. Lett., 24*, 441–444, 1997.

McConnell, J. R., R. C. Bales, R. W. Stewart, A. M. Thompson, and M. R. Albert, Physically based modeling of atmosphere-to-snow-to-firn transfer of H_2O_2 at South Pole, *J. Geophys. Res., 103*, 10,561–10,570, 1998.

Neftel, A., R. C. Bales, and D. J. Jacob, H_2O_2 and HCHO in polar snow and their relation to atmospheric chemistry, in *Ice Core Studies of Global Biogeochemical Cycles, NATO ASI Ser I, vol. 30*, edited by R. J. Delmas, pp. 249–264, Springer-Verlag, New York, 1995.

Poisson, N., M. Kanakidou, and P. J. Crutzen, Impact of non-methane hydrocarbons on tropospheric chemistry and the oxidizing power of the global troposphere: 3-dimensional modelling results, *J. Atmos. Chem., 36*, 157–230, 2000.

Röthlisberger, R., M. Bigler, M. A. Hutterli, S. Sommer, B. Stauffer, H. G. Junghans, and D. Wagenbach, Technique for continuous high-resolution analyses of trace substances in firn and ice cores, *Environ. Sci. Technol., 34*, 338–342, 2000.

Rudolph, J., R. F. Ban, A. Thompson, K. Anlauf, and J. Bottenheim, Halogen atom concentrations in the Arctic troposphere derived from hydrocarbon measurements: Impact on the budget of formaldehyde, *Geophys. Res. Lett., 26*, 2941–2944, 1999.

Schwander, J., T. Sowers, J.-M. Barnola, T. Blunier, A. Fuchs, and B. Malaiz, Age scale of the air in the Summit ice: Implications for glacial-interglacial temperature change, *J. Geophys. Res., 102*, 19,483–19,493, 1997.

Seinfeld, J. H., and S. N. Pandis, *Atmospheric Chemistry and Physics*, John Wiley, New York, 1998.

Sigg, A., and A. Neftel, Evidence for a 50% increase in H_2O_2 over the past 200 years from a Greenland ice core, *Nature, 351*, 557–559, 1991.

Sigg, A., T. Staffelbach, and A. Neftel, Gas phase measurements of hydrogen peroxide in Greenland and their meaning for the interpretation of H_2O_2 records in ice cores, *J. Atmos. Chem., 14*, 223–232, 1992.

Solberg, S., N. Schmidbauer, A. Semb, F. Stordal, and O. Hov, Boundary-layer ozone depletion as seen in the Norwegian Arctic in spring, *J. Atmos. Chem., 23*, 301–332, 1996.

Stewart, R. W., Multiple steady states in atmospheric chemistry, *J. Geophys. Res., 98*, 20,601–20,611, 1993.

Stewart, R. W., Dynamics of the low to high NO_x transition in a simplified tropospheric photochemical model, *J. Geophys. Res., 100*, 8929–8943, 1995.

Stewart, R. W., and A. M. Thompson, Kinetic data impre-

cisions in photochemical rate calculations: Means, medians, and temperature dependence, *J. Geophys. Res., 101*, 20,953–20,964, 1996.

Stewart, R. W., S. Hameed, and G. Matloff, A model study of the effects of intermittent loss on odd nitrogen concentrations in the lower troposphere, *J. Geophys. Res., 88*, 10,697–10,707, 1983.

Sumner, A.-L., and P. B. Shepson, Snowpack production of formaldehyde and its effect on the Arctic troposphere, *Nature, 398*, 230–233, 1999.

Thompson, A. M., The oxidizing capacity of the Earth's atmosphere: Probable past and future changes, *Science, 256*, 1157–1168, 1992.

Waddington, E. D., J. Cunningham, and S. L. Harder, The effects of snow ventilation on chemical concentrations, in *Chemical Exchange Between the Atmosphere and Polar Snow, NATO ASI Ser. I, vol. 43*, pp. 403–451, Springer-Verlag, New York, 1996.

Wagnon, P., R. J. Delmas, and M. Legrand, Loss of volatile acid species from upper firn layers at Vostok, Antarctica, *J. Geophys. Res., 104*, 3423–3431, 1999.

Yokouchi, Y., L. A. Barrie, D. Toom-Sauntry, Y. Nojiri, Y. Fujinuma, Y. Inuzuka, H. J. Li, H. Akimoto, and S. Aoki, Latitudinal distribution of atmospheric methyl bromide: Measurements and modeling, *Geophys. Res. Lett., 27*, 697–700, 2000.

R. C. Bales, M. A. Hutterli, and H.-W. Jacobi, Department of Hydrology and Water Resources, University of Arizona, Tucson, AZ 85721. (roger@hwr.arizona.edu; manuel@hwr.arizona.edu; hwj@hwr.arizona.edu)

J. R. McConnell, Desert Research Institute, Water Resources Center, 2215 Raggio Parkway, Reno, NV 89512. (jmcconn@dri.edu)

R. W. Stewart, NASA GSFC, Code 916, Greenbelt, MD 20771. (stewart@oasis.gsfc.nasa.gov)

(Received September 25, 2000; revised January 31, 2001; accepted February 3, 2001.)

Publication 3.2.4

Yang, J., R.E. Honrath, M.C. Peterson, J.E. Dibb, A.L. Sumner, P.B. Shepson, M. Frey, H.-W. Jacobi, A. Swanson, and N. Blake,

Impacts of snowpack photochemistry on levels of OH and peroxy radicals at Summit, Greenland,

Atmos.Environ. **36**, 2523-2534, 2002.

PERGAMON

Atmospheric Environment 36 (2002) 2523–2534

ATMOSPHERIC ENVIRONMENT

www.elsevier.com/locate/atmosenv

Impacts of snowpack emissions on deduced levels of OH and peroxy radicals at Summit, Greenland

J. Yang[a], R.E. Honrath[a,*], M.C. Peterson[a], J.E. Dibb[b], A.L. Sumner[c], P.B. Shepson[c], M. Frey[d], H.-W. Jacobi[d], A. Swanson[e], N. Blake[e]

[a] *Department of Civil and Environmental Engineering, Michigan Technological University, 1400 Townsend Dr. Houghton, MI 49931-1295, USA*

[b] *Climate Change Research Center, University of New Hampshire, Durham, USA*

[c] *Departments of Chemistry, and Earth and Atmospheric Science, Purdue University, Indiana, USA*

[d] *Department of Hydrology and Water Resources, University of Arizona, USA*

[e] *Department of Chemistry, University of California, Irvine, USA*

Received 4 June 2001; received in revised form 1 October 2001; accepted 11 January 2002

Abstract

Levels of OH and peroxy radicals in the atmospheric boundary layer at Summit, Greenland, a location surrounded by snow from which HO_x radical precursors are known to be emitted, were deduced using steady-state analyses applied to $(OH + HO_2 + CH_3O_2)$, $(OH + HO_2)$, and OH–HO_2 cycling. The results indicate that HO_x levels at Summit are significantly increased over those that would result from O_3 photolysis alone, as a result of elevated concentrations of HONO, HCHO, H_2O_2, and other compounds. Estimated midday levels of $(HO_2 + CH_3O_2)$ reached 30–40 pptv during two summer seasons. Calculated OH concentrations averaged between 05:00 and 20:00 (or 21:00) exceeded 4×10^6 molecules cm^{-3}, comparable to (or higher than) levels expected in the tropical marine boundary layer. These findings imply rapid photochemical cycling within the boundary layer at Summit, as well as in the upper pore spaces of the surface snowpack. The photolysis rate constants and OH levels calculated here imply that gas-phase photochemistry plays a significant role in the budgets of NO_x, HCHO, H_2O_2, HONO, and O_3, compounds that are also directly affected by processes within the snowpack.

Keywords: HO_x; Oxidants; Steady-state model; Arctic boundary layer; Ice photochemistry

1. Introduction

A series of studies over the past several years have demonstrated that processes within surface snowpacks result in the release (and in some cases, the uptake) of a variety of photochemically active compounds. It appears that these effects are largely driven by three processes: photodissociation of nitrate ion present within the surface layer of ice crystals in the snowpack (Honrath et al., 2000), temperature-dependent adsorption or cocondensation onto, and desorption from, ice surfaces (e.g. Bales et al., 1995), and autocatalytic release of halogen compounds, resulting from reactions on ice surfaces (Tang and McConnell, 1996). (The latter process has been clearly documented only near the marine boundary layer and is not considered in detail here.)

It is likely that these processes significantly alter levels of HO_x $(OH + HO_2)$ in the atmospheric boundary layer above snowpacks. Photodissociation of nitrate ion near the surface of ice crystals is believed to be the source of NO_x release observed from sunlight-irradiated snow (e.g. Honrath et al., 1999), and, if so, results in the production of OH radicals at the site of photodissociation. The fate of this OH is not known, but in the

*Corresponding author.
E-mail address: reh@mtu.edu (R.E. Honrath).

1352-2310/02/$ - see front matter
PII: S1352-2310(02)00128-0

presence of ubiquitous organic matter, it may result in the production and release of photolabile oxidized compounds, such as formaldehyde (Sumner and Shepson, 1999). In addition, there is direct evidence of impacts of snowpack emissions on ambient atmospheric concentrations of a variety of compounds that play direct roles in the budgets of HO_x compounds. These compounds include HONO (Zhou et al., 2001; Dibb et al., 2002) and H_2O_2 (Jacobi et al., 2002) (OH sources), HCHO (Sumner and Shepson, 1999; Jacobi et al., 2002) (an HO_2 source), and NO_x (Ridley et al., 2000; Davis et al., 2001; Honrath et al., 2002) (which largely determines the partitioning of HO_x). Recent measurements at the South Pole, which indicate that OH concentrations are higher than expected (Mauldin et al., 2001), are consistent with the expectation that the net result of these impacts is likely to increase atmospheric OH concentrations.

As part of a series of studies designed to determine the impact of snowpack photochemistry upon atmospheric and snow composition, measurements of nitrogen oxides and other species were made during two summer field seasons at Summit, Greenland (38.4°E, 72.55°N, 3200 m altitude), a site surrounded by snow for > 350 km in all directions. In this work, we analyze these measurements to deduce atmospheric levels of peroxy radicals (PO_2, which in this analysis includes HO_2 and CH_3O_2) and OH at Summit during the summers of 1999 and 2000. Our goal is to quantify the magnitude of PO_2 and OH levels at Summit and to investigate the dominant gas-phase processes in their budgets. In particular, measurements of each of the important OH precursor compounds were made, allowing us to quantify their relative importance to the OH budget. We do not directly relate PO_2 and OH levels to snowpack emissions of their precursors in this paper. However, companion papers in this issue present measurements of the vertical fluxes of some of the precursor compounds above the Summit snowpack (Honrath et al., 2002; Jacobi et al., 2002).

2. Methods

PO_2 and OH concentrations were estimated using steady-state analyses. This technique makes use of the fact that the daytime rates of formation and destruction of short-lived radicals are rapid, relative to the rates of change of radical concentrations, as is the rate of cycling among members of rapidly cycling radical families. Steady state was applied in three ways. First, the partitioning of HO_x between OH and HO_2 was calculated by setting the reactions interconverting these two compounds at steady-state. Second, the total concentration of (HO_x plus CH_3O_2) (referred to as CHO_x) was determined by setting the sources and sinks of this compound group equal to one another. Finally, the steady-state of OH was assessed. In this analysis, we have not calculated the partitioning of peroxy radicals between HO_2 and CH_3O_2, but rather set the ratio $\alpha = [HO_2]/[PO_2]$. The true value of α at boundary layer sites (and at Summit in particular) is not well known. We have conducted simulations with α varying from 0.5 to 0.9, spanning the range deduced in some previous steady-state modeling analyses (e.g. Cantrell et al., 1997; Zanis et al., 1999). The choice of α affects the self-consistency of the results, as indicated by the balance of OH and HO_x formation and destruction rates; this is discussed in Section 3.3.

Table 1 presents the reactions used in each steady-state analysis. The ratio $[OH]/[HO_2]$ was calculated by setting the total rate of reactions converting OH to HO_2 (reactions (1)–(5)) equal to total rate of reactions converting HO_2 to OH (reactions (6) and (7)). The concentration of PO_2 was then determined by setting the total rate of formation of CHO_x (due to reactions (9)–(14)) equal to the total rate of CHO_x destruction (via reactions (15)–(21)).

This method necessarily results in equality between the rates of formation and destruction of CHO_x. It does not, however, need to result in equal rates of formation and destruction of other radical families. The rates of formation and destruction of HO_x and OH were therefore also calculated. The rate of HO_x formation is calculated from the same set of reactions used for CHO_x, with the exception that reactions (14) and (16) produce and destroy, respectively, only one HO_x (rather than two CHO_x), and reaction (17) does not remove HO_x. Similarly, the rate of OH formation was determined from reactions (6), (7), and (9)–(12), and the rate of OH destruction was determined from reactions (1)–(5) and (18)–(21), plus two additional reactions:

$$OH + CH_4 \rightarrow CH_3O_2 + H_2O, \quad (22)$$

$$OH + CH_3OOH \rightarrow CH_3O_2 + H_2O. \quad (23)$$

2.1. Measurement techniques

NO and NO_2 were determined as described by Honrath et al. (2002), using measurements at heights of 80–95 cm in 1999 and of 47 and 200 cm in 2000. NO and NO_2 measurements were obtained every ~7 min; the calculations presented below were conducted at the times of these measurements.

O_3 was determined each minute at the same heights as NO_x, using commercial ultraviolet absorbance instruments, with different instruments used during 1999 and 2000. The instrument used during 2000 was compared to a NIST-traceable instrument at the NOAA CMDL laboratory, and agreed within 4% (S. Oltmans, NOAA CMDL, personal communication, 2001). Based on an

Table 1
Reactions used in the steady-state analyses

$OH \rightleftharpoons HO_2$ Cycling

$OH \rightarrow HO_2$ reactions:

$$OH + CO \xrightarrow{O_2} HO_2 + CO_2 \quad (1)$$

$$OH + O_3 \rightarrow HO_2 + O_2 \quad (2)$$

$$OH + HCHO \xrightarrow{O_2} HO_2 + H_2O + CO \quad (3)$$

$$OH + H_2O_2 \rightarrow HO_2 + H_2O \quad (4)$$

$$OH + H_2 \xrightarrow{O_2} HO_2 + H_2O \quad (5)$$

$HO_2 \rightarrow OH$ reactions:

$$HO_2 + NO \rightarrow OH + NO_2 \quad (6)$$

$$HO_2 + O_3 \rightarrow OH + 2O_2 \quad (7)$$

CHO_x ($HO_2 + OH + CH_3O_2$) Steady-state

Sources:

$$O_3 + h\nu \rightarrow O_2 + O(^1D) \quad (+0) \quad (8)$$

$$O(^1D) + H_2O \rightarrow 2OH \quad (+2) \quad (9)$$

$$HONO + h\nu \rightarrow OH + NO \quad (+1) \quad (10)$$

$$H_2O_2 + h\nu \rightarrow 2OH \quad (+2) \quad (11)$$

$$CH_3OOH + h\nu \xrightarrow{O_2} OH + HO_2 + HCHO \quad (+2) \quad (12)$$

$$HCHO + h\nu \xrightarrow{O_2} 2HO_2 + CO \quad (+2) \quad (13)$$

$$CH_3CHO + h\nu \rightarrow CH_3O_2 + HO_2 + CO \quad (+2) \quad (14)$$

Sinks:

$$HO_2 + HO_2 \rightarrow H_2O_2 + O_2 \quad (-2) \quad (15)$$

$$HO_2 + CH_3O_2 \rightarrow CH_3OOH + O_2 \quad (-2) \quad (16)$$

$$CH_3O_2 + CH_3O_2 \rightarrow \text{products} \quad (-2) \quad (17)$$

$$OH + HO_2 \rightarrow H_2O + O_2 \quad (-2) \quad (18)$$

$$OH + NO_2 \xrightarrow{M} HNO_3 \quad (-1) \quad (19)$$

$$OH + NO \xrightarrow{M} HONO \quad (-1) \quad (20)$$

$$OH + CH_3CHO \rightarrow CH_3CO + H_2O \quad (-1) \quad (21)$$

intercomparison with this instrument, the instrument used during 1999 was determined to be biased low by 20%, and the 1999 measurements were therefore adjusted by the factor 1.25.

Nitrous acid was sampled at a height of ~1 m (1999) and 80 cm (with occasional measurements at heights of 200 and 400 cm) (2000) using mist chambers, and was analyzed as nitrite using ion chromatography, using methods described previously for HNO_3 (Dibb et al., 1998) and discussed by Dibb et al. (2002). These samples reflect average concentrations over 24- to 38-min measurement periods. A small number (5 observations; 2% of the total number) of unusually high HONO mixing ratios which exceeded the mean of the remaining data by more than four standard deviations were removed from the 1999 dataset; none were removed from the 2000 dataset. HONO measurements from mist chamber samples that overlapped the NO_x measurement times were used in calculations; NO_x measurements with no overlapping mist chamber sample were excluded from calculations.

Formaldehyde was determined during 1999 at a height of 1 m using a modified version of the fluorometric method described by Fan and Dasgupta (1994). During 2000, the methods described by Jacobi et al. (2002) were used, and measurements were at heights of 143 and 152 cm. HCHO measurements were interpolated to the NO_x measurement times; periods when the interpolation would have exceeded 1 h were excluded from calculations.

Hydrogen peroxide was determined using the methods described by Jacobi et al. (2002). Measurement heights during 1999 were 60–100 cm; during 2000, H_2O_2 was determined at the same heights at HCHO. H_2O_2 was interpolated in the same manner as HCHO.

CH_4, non-methane hydrocarbons, and (in 2000) CO were determined in ambient-air canister samples taken ~1–6 times each day and analyzed using gas chromatography with flame ionization detection (GC/FID) (Blake and Rowland, 1986; Hurst, 1990; Swanson et al., 2002). CO and CH_4 levels were relatively constant; average values were used for each season (with the exception that 1999 CO was estimated from previous high latitude observations; Novelli, 1998). Non-methane hydrocarbons were determined to be insignificant as OH sinks (destroying less than 5% of the amount reacting with CO and CH_4), and are not analyzed further here.

Water vapor concentrations were calculated from hourly average measurements of relative humidity obtained from the Summit meteorological station (K. Steffen, Univ. Colorado, personal communication, 2001). CH_3CHO was estimated from HCHO measurements, using an estimated [CH_3CHO]:[HCHO] ratio of 0.5, based on measurements at Alert (P. Shepson, pers. commun., 2000; see also Grannas et al., 2002). CH_3OOH was set equal to the measured H_2O_2, based on previous measurements in Antarctica (Riedel et al., 2000). H_2 was set at a mixing ratio of 500 ppbv (Warneck, 2000).

2.2. Photodissociation rate constants

Photolysis rate constants were calculated using a radiative transfer model constrained by the measured downwelling component of J_{NO_2}. The Phodis radiative transfer model, Version 0.40 (Kylling et al., 1995) was

used in six-stream, pseudo-spherical mode, assuming clear-sky conditions, using a standard subarctic summer atmosphere, and without addition of aerosol. Surface albedo was set to 0.95, based on previous analyses of the albedo of clean snow in the ultraviolet (Warren, 1982; Junkermann, 1994; Dickerson et al., 1982). The overhead ozone column was obtained from TOMS measurements, and varied daily. Absorption cross sections and quantum yields recommended by DeMore et al. (1997) were used, with the exception of acetaldehyde, for which we used the recommendations of Atkinson (1994), and O_3, for which the updated quantum yield was used (Sander et al., 2000).

Calculated J-values for all compounds were corrected for the effects of clouds using a comparison of measured and modeled J_{NO_2}. (This method implicitly assumes that the effect of clouds is independent of wavelength, which it is not (e.g. Kylling et al., 1997). However, the potential error introduced by this assumption is judged to be small relative to other sources of uncertainty in the steady-state analyses.) The downwelling component of the NO_2 photodissociation rate constant was determined with a 2-π Metcon filterradiometer. Radiometer sensitivity was referenced to the manufacturer's transfer standard and temperature correction was applied to account for temperature dependence of the NO_2 absorption cross section and quantum yield (Volz-Thomas et al., 1996). During clear-sky periods, the measured and modeled J_{NO_2} values differed by a nearly constant ratio, with average measured/modeled equal to 0.820, similar to the findings of Simpson et al. (2002) using the same filterradiometer during the ALERT 2000 study. All measured values were adjusted by the factor of 0.820 to agree with the model results. The effect of clouds was then taken into account by multiplying all model-calculated photodissociation rate constants by the ratio of J_{NO_2} (adjusted measurements)/J_{NO_2} (model), at each measurement time.

3. Results and discussion

A summary of the main parameters used in the PO_2 and OH calculations is provided in Table 2. The required simultaneous measurements were available most frequently during the late morning to late evening period. During late night and early morning, insufficient data were obtained for adequate precision of average estimated concentrations. Missing measurements entirely precluded calculations for times before 05:00 (1999 and 2000) or after 20:00 (1999) or 21:00 (2000). The two seasons differed significantly in the levels of many compounds, especially HCHO, H_2O_2, and HONO; the cause of these differences is unknown. Conditions during 2000 were also calmer and sunnier (see also Honrath et al., 2002).

In the remainder of this section, we first present and discuss the estimated CHO_x ($PO_2 + OH$) and OH levels, calculated using $\alpha = [HO_2]/[PO_2] = 0.7$. This is followed by a brief discussion of the degree to which the calculated sources and sinks of OH and HO_x balance. Finally, as the calculated concentrations are quite high, the impacts of in situ photochemistry on the budgets of NO_x, HCHO, H_2O_2, and O_3, species that are also affected by snowpack emission or deposition, are assessed.

3.1. Estimated peroxy radicals

The diurnal cycle of calculated peroxy radical mixing ratios is shown in Fig. 1. These mixing ratios, reaching average midday peaks of $\sim$42 and 32 pptv in 1999 and 2000, respectively, are somewhat higher than or similar to those observed at other remote regions (e.g. Hauglustaine et al., 1996; Davis et al., 1996; Penkett et al., 1997). However, this similarity is deceptive, because the sources of HO_x at Summit are significantly different from those at these other sites, which are characterized by higher water vapor concentrations and a larger radical source from ozone photolysis.

A comparison to calculated and measured peroxy radicals at Mauna Loa is instructive, because of the amount of information available from the MLOPEX studies and the fact that Mauna Loa is a surface-based site that is similar in some ways to Summit. The two sites are roughly equivalent in terms of pressure altitude (atmospheric pressure at both locations is 690 ± 10 hPa), but Summit differs greatly from Mauna Loa in three respects: the presence of snow, which has a much higher albedo than the volcanic rock at Mauna Loa, its latitude, which results in larger solar zenith angles, and colder temperatures (median -10°C), which alter reaction rate constants and, more importantly, result in lower water vapor concentrations ($<50\%$ of those at Mauna Loa during summer). The presence of snow at Summit results in much higher sunlight intensity at longer wavelengths, and as a result midday values of J_{NO_2} calculated at Summit exceed those calculated at Mauna Loa during spring and summer (Lantz et al., 1996) by a factor of 2.4. However, at shorter wavelengths, increased O_3 absorption in the longer slant light path at Summit counteracts this effect, with the result that noontime J_{O^1D} values at Summit are approximately equal to those calculated at Mauna Loa during spring (Shetter et al., 1996). The combination of similar O_3 photolysis rate constants and lower water vapor results in a reduced HO_x source from O_3 photolysis at Summit.

Midday peroxy radical mixing ratios measured at Mauna Loa during the summertime MLOPEX 2d intensive averaged 25 pptv, while a steady-state model similar to the one used in this study predicted a value of $\sim$38 pptv (Cantrell et al., 1996). These values thus

Table 2
Summary of input parameters

	1999		2000	
Parameter	Mean	Range	Mean	Range
NO (pptv) (10:00–14:00)	24.7	8.3–40.8	16.0	4.4–36.6
NO_2 (pptv) (10:00–14:00)	32.7	7.9–55.4	15.2	0–58.5
NO_x (pptv) (full period)	49.4	2.2–90.0	39.7	0–106.
O_3 (ppbv)	40.5	28.4–48.7	51.9	39.9–62.8
HONO (pptv)	7.24	1.1–18.7	12.7	3.1–26.6
HCHO (ppbv)	0.74	0.03–1.9	0.12	0.058–0.20
H_2O_2 (ppbv)	1.78	0.85–2.77	0.72	0.22–1.52
CO (ppbv)	90	—	110	92–127
CH_4 (ppbv)	1800	1800–1820	1816	1792–1835
H_2O (% v/v)	0.40	0.17–0.60	0.29	0.13–0.50
J_{NO_2} (model) (s^{-1})	0.015	$8.07 \times 10^{-3} - 0.0211$	0.0162	8.00×10^{-3}-0.0223
(10:00–14:00)	0.0149	0.0155–0.0211	0.0196	0.0162–0.0223
J_{O^1D} (model) (s^{-1})	2.15×10^{-5}	$3.26 \times 10^{-6} - 4.30 \times 10^{-5}$	2.21×10^{-5}	$2.50 \times 10^{-6} - 4.27 \times 10^{-5}$
(10:00–14:00)	3.23×10^{-5}	$2.44 \times 10^{-5} - 4.30 \times 10^{-5}$	3.38×10^{-5}	$2.32 \times 10^{-5} - 4.27 \times 10^{-5}$
J_{HONO} (model) (s^{-1})	3.23×10^{-3}	$1.74 \times 10^{-3} - 4.69 \times 10^{-3}$	3.59×10^{-3}	$1.70 \times 10^{-3} - 4.98 \times 10^{-3}$
(10:00–14:00)	4.21×10^{-3}	$3.44 \times 10^{-3} - 4.69 \times 10^{-3}$	4.36×10^{-3}	$3.59 \times 10^{-3} - 4.98 \times 10^{-3}$

Ranges reflect the range of measurements used in steady-state calculations, which include the subset of all measurements that included simultaneous observations of all required species. Photolysis rate constants therefore apply to the period 05:00–20:00 for 1999, and 05:00–21:00 for 2000.

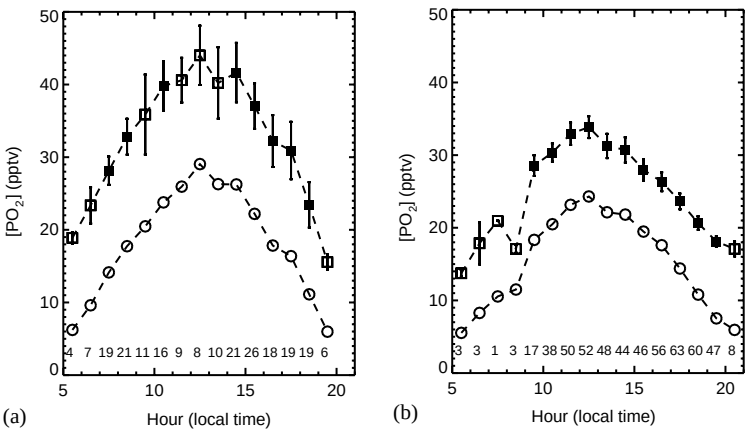

Fig. 1. The diurnal cycle of peroxy radical mixing ratio calculated using CHO_x balance with $[HO_2]/[PO_2] = 0.7$ for (a) summer, 1999, and (b) summer, 2000. Symbols indicate the mean in each 1 h time bin; error bars extend ± 2 standard errors of the mean. The number of measurements contributing to each 1 h mean is indicated above the x-axis; means calculated from fewer than 15 measurements are indicated by open symbols. The open circles connected by dashed lines show the $[PO_2]$ that would result if ozone photolysis were the only significant source of HO_x radicals.

approximately span the average midday peroxy radical levels calculated for Summit. However, the observed peroxy radical levels at Mauna Loa were consistent with production dominated by ozone photolysis (reactions (8) and (9)), and destruction dominated by peroxy radical recombination (Cantrell et al., 1996). Model simulations of Mauna Loa HO_x levels also indicate that O_3 photolysis is the dominant HO_x source (Hauglustaine et al., 1999), and this is generally also the case at remote marine boundary layer sites (Penkett et al., 1997). Were this the case at Summit, the combination of O_3 mixing ratios and J_{O^1D} values similar to those at Mauna Loa, and significantly lower water vapor concentrations, would result in peroxy radical mixing ratios significantly lower than those observed at Mauna Loa, and significantly lower than those calculated for Summit.

This is illustrated by the dashed lines in Fig. 1, which indicate the peroxy radical mixing ratios that would balance radical production from ozone photolysis with radical destruction by reactions (15)–(17).

3.2. Estimated OH radical

The diurnal cycle of OH concentrations calculated by the steady-state method is shown in Fig. 2. The diurnal cycles during 1999 and 2000 differ in shape, largely as a result of the differing levels of HCHO, H_2O_2, and HONO noted above (see also the discussion of HO_x sources, below). OH concentrations peak at 5–8 $\times$ 10^6 molecules cm^{-3}. These peak levels are similar to noontime OH concentrations during spring and summer at the somewhat similar Mauna Loa site (which, again, would be unexpected if ozone photolysis were the dominant radical source). [OH] at Mauna Loa was estimated using a steady-state model similar to that used here (Cantrell et al., 1996) and directly measured (Eisele et al., 1996): noontime simulated and measured concentrations at Mauna Loa reached 4–6 $\times$ 10^6 molecules cm^{-3} on most days. The diurnal variation of [OH] at Summit is flatter than that at Mauna Loa, however, reflecting the increased importance at Summit of photolysis of compounds more sensitive than O_3 to longer-wavelength actinic flux. The resulting daily average Summit OH concentration (averaged over the total period of calculations—05:00–20:00 in 1999, 05:00–21:00 in 2000—and equal to 4.8×10^6 and 4.5×10^6 molecules cm^{-3} during 1999 and 2000, respectively) is significantly higher than the mean levels calculated by global models, which reach $\sim 1 \times 10^6$ at the latitude and altitude of Summit during July (Wang et al., 1998). Indeed, it is larger than those in the tropics, the region believed to be responsible for a majority of the globally integrated OH atmospheric oxidation, due to the high OH concentrations there ($\lesssim 3.5 \times 10^6$; Crutzen and Zimmerman, 1991). (Elevated OH levels at Summit may be confined to a much smaller boundary layer, however.)

3.3. Sources and sinks of OH and HO_x

Table 3 summarizes the total sources and sinks, integrated over 15 (1999) or 16 (2000) h, for CHO_x, OH, and HO_x. Since a balance of CHO_x was the basis of these calculations, CHO_x balances exactly. The reactions that make up the OH budget are displayed in Fig. 3; the OH budget is imbalanced, with sources exceeding sinks by 20% (1999) or 46% (2000) at $\alpha = [HO_2]/[PO_2] = 0.7$. This imbalance improves as the assumed value of α increases, but an imbalance persists even at a value of 0.9. This suggests that an OH sink or sinks, resulting in the formation of HO_2 and not included in the reactions listed in Table 1, may have been present.

The budget of HO_x is nearly balanced, changing from an excess of sources at $\alpha = 0.5$ to an excess of sinks at $\alpha = 0.7$. The sources and sinks of HO_x are shown in Fig. 4. It is here that the impact of snowpack emissions on HO_x becomes most apparent. Ozone photolysis, the major source of HO_x in most remote boundary-layer sites, is exceeded in importance on a daily-average basis by formaldehyde photolysis in 1999, and is equaled in importance by HONO photolysis in 2000. In both years, O_3 photolysis contributes $<35\%$ of the total daily-average source of HO_x (calculated using the full calculation period at $\alpha = 0.7$).

3.4. Relevance to the budgets of NO_x, HONO, H_2O_2, and HCHO

Since the lifetime of OH is extremely short, the vertical scale over which elevated OH concentrations are present depends on the lifetimes of the precursor

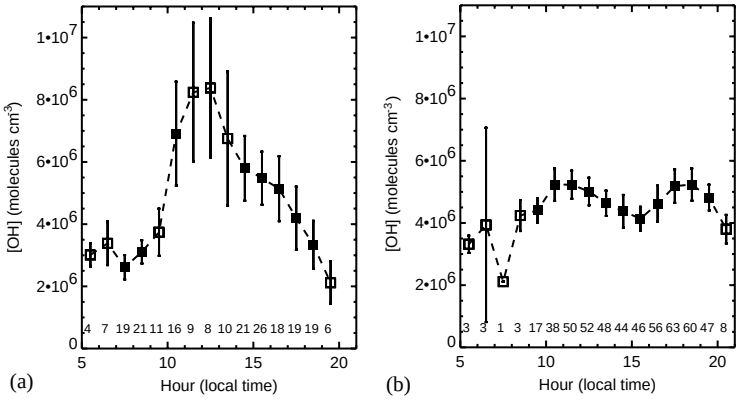

Fig. 2. The diurnal cycle of [OH] during (a) summer, 1999, and (b) summer, 2000, presented as described for Fig. 1.

Table 3
Summary of radical source and sink balances

	2000			1999		
	$\alpha = 0.5$	$\alpha = 0.7$	$\alpha = 0.9$	$\alpha = 0.5$	$\alpha = 0.7$	$\alpha = 0.9$
CHO_x						
Sources	0.111	0.111	0.111	0.195	0.195	0.195
Sinks	0.111	0.111	0.111	0.195	0.195	0.195
OH						
Sources	0.166	0.183	0.200	0.209	0.229	0.249
Sinks	0.0994	0.125	0.151	0.152	0.190	0.228
Source/Sink	1.67	1.46	1.33	1.37	1.20	1.09
Noon [OH]	4.0×10^6	5.0×10^6	6.0×10^6	6.8×10^6	8.4×10^6	9.9×10^6
HO_x						
Sources	0.111	0.111	0.111	0.193	0.193	0.193
Sinks	0.0974	0.114	0.134	0.180	0.210	0.244
Source/Sink	1.14	0.97	0.83	1.07	0.92	0.79
Noon [PO_2]	38	34	32	50	44	41
Noon [HO_2]	19	24	29	25	31	37

Reaction rates reflect averages over the period of data (05:00–20:00 for 1999, and 05:00–21:00 for 2000), in units of pptv/s; [PO_2] and [HO_2] are displayed in units of pptv; [OH] is displayed in units of molecules cm^{-3}. $\alpha = [HO_2]/([HO_2] + [CH_3O_2])$.

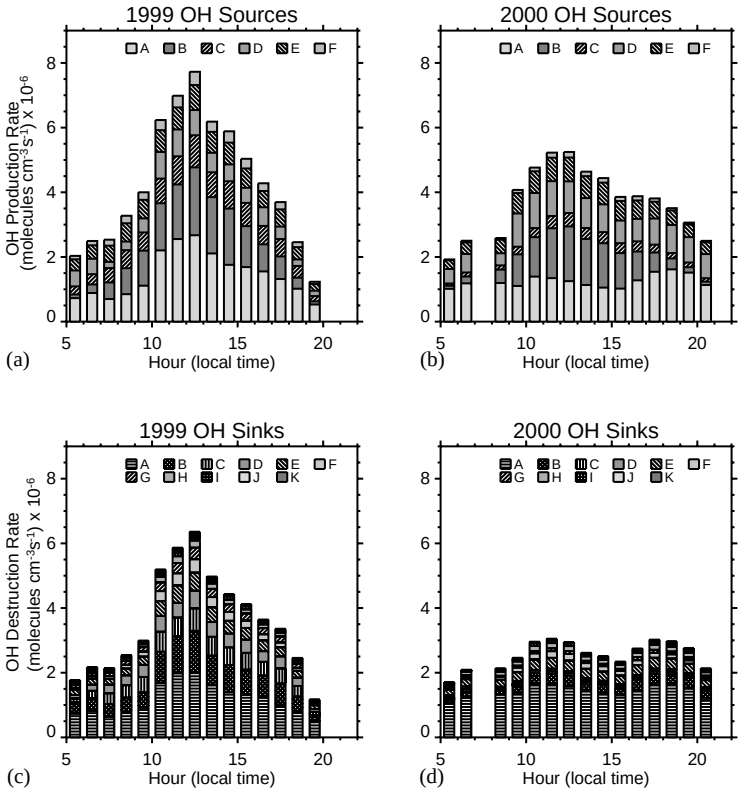

Fig. 3. The diurnal cycle of the magnitude of the most important OH sources (a and b) and sinks (c and d). Results for 1999 are shown in parts a (sources) and d (sinks); results for 2000 are shown in parts b (sources) and d (sinks). OH sources include $HO_2 + NO$ (region A), $O_3 + h\nu$ (B), $H_2O_2 + h\nu$ (C), $HONO + h\nu$ (D), $O_2 + HO_2$ (E), and $CH_3OOH + h\nu$ (F). OH sinks include OH reaction with CO (region A), CH_3OOH (B), HCHO (C), CH_3CHO (D), CH_4 (E), HO_2 (F), H_2O_2 (G), O_3 (H), H_2 (I), NO_2 (J), and NO (K).

compounds and the intensity of vertical mixing at Summit. The impact of photochemistry on the atmospheric lifetimes of NO_x, H_2O_2, and HCHO also impacts the degree to which nitrate, H_2O_2, and HCHO ultimately incorporated into glacial ice reflect local photochemical cycling, relative to the degree they reflect the composition of the larger atmosphere. To explore these issues, we briefly discuss the photochemical sources and sinks of these compounds.

Table 4 displays the main in situ sources and sinks of NO_x, HONO, H_2O_2, HCHO, and O_3. With the exception of HONO, rates of destruction are slow enough that these compounds are expected to mix throughout the boundary layer. The sinks of NO_2 and HONO may be compared to the NO_x, HONO, and HNO_3 fluxes determined using gradient measurements during summer 2000 (Honrath et al., 2002). To do this, a vertical dimension over which the calculated gas-phase rates apply is required. Helmig et al. (2002) measured midday boundary layer heights of 70–250 m during the 2000 study; the minimum height of 70 m is used here as a rough estimate of the daily averaged height over which the reaction rates summarized in Table 4 apply, since a surface-based inversion generally developed in the late evening.

The degree to which conditions at the sampling inlets were characteristic of those throughout the 70 m mixed layer is, however, dependent on the intensity of turbulent mixing. This may have been resulted in non-homogeneous conditions in two ways. First, snowpack interstitial air concentrations of NO_2 greatly exceed those of NO (Dibb et al., 2002). Emitted NO_2 and NO may approach steady state as they diffuse through the snowpack, but whether this is the case is not known. The estimated characteristic times for turbulent mixing from the snow surface to the NO_x inlets at 47 and 200 cm were 22 and 68 s, respectively (median values calculated during periods when measurements were made at those heights), estimated as $\tau_t = z/(\kappa u_*)$ (Lenschow and Delany, 1987), where $\kappa = 0.4$ is the von Karman constant, and the friction velocity u_* was determined from eddy covariance measurements (Honrath et al., 2002). Since these values are less than the period required for approach to NO_2–NO steady state, it is

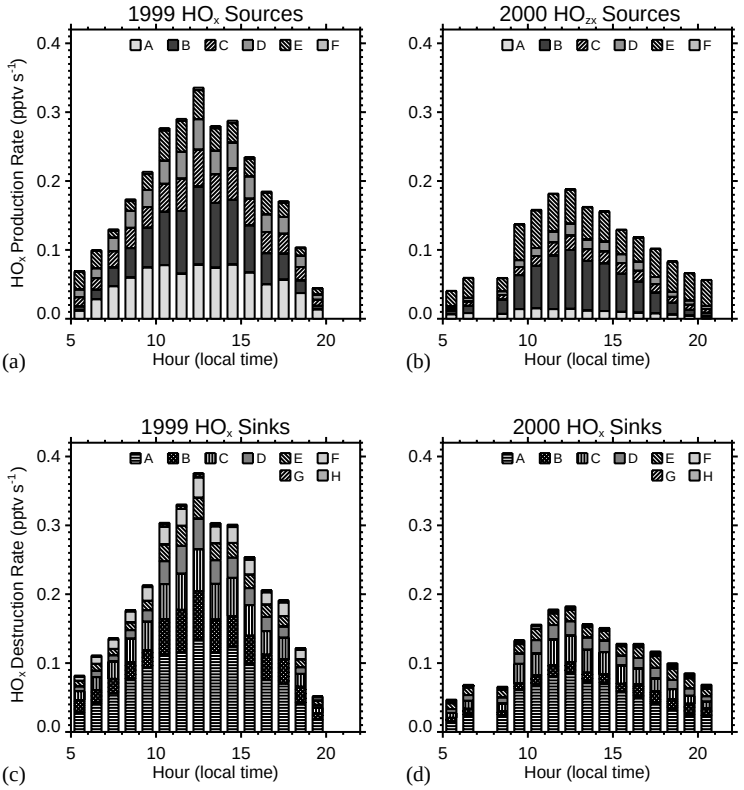

Fig. 4. The diurnal cycle of the magnitude of the most important HO_x sources (a and b) and sinks (c and d). Results for 1999 are shown in parts a (sources) and c (sinks); results for 2000 are shown in parts b (sources) and d (sinks). Sources include HCHO + *hv* (region A), O_3 + *hv* (B), H_2O_2 + *hv* (C), CH_3OOH + *hv* (D), HONO + *hv* (E), and CH_3CHO + *hv* (F). HO_x sinks include $HO_2 + HO_2$ (region A), $OH + CH_3OOH$ (B), $HO_2 + CH_3O_2$ (C), $OH + HO_2$ (D), $OH + CH_4$ (E), $OH + CH_3CHO$ (F), $OH + NO_2$ (G), and OH + NO (H).

Table 4
Impacts on the budgets of non-HO_x species

		Average rate (pptv/h)			
		1999		2000	
Compound	Reaction	0500–2000	1000–1400	0500–2100	1000–1400
NO_x	Sink: $NO_2 + OH$	8.6	14.6	4.4	4.4
HONO	Sink: $HONO + h\nu$	92.9	147.1	142.9	184.8
	Source: $NO + OH$	3.2	6.1	3.1	2.6
H_2O_2	Sink: $H_2O_2 + h\nu$	56.1	82.2	21.2	32.0
	Source: $HO_2 + HO_2$	144.0	215.2	86.3	138.6
	Source: $OH + OH$	0.02	0.03	0.01	0.01
HCHO	Sink: $HCHO + OH$	83.0	120.1	13.8	15.1
	Sink: $HCHO + h\nu$	98.8	133.4	17.3	25.2
	Source: $CH_4 + OH$[a]	<60.4	<97.3	<49.0	<58.2
O_3	Source: $NO + HO_2$	279.1	461.8	217.4	232.5
	Source: $NO + CH_3O_2$	115.2	190.6	90.0	96.1
	Sink: $O_3 + h\nu(+H_2O)$	95.0	169.2	70.8	133.6
	Sink: $O_3 + HO_2$	103.7	134.3	96.0	127.6
	Sink: $O_3 + OH$	22.9	37.6	23.7	27.8

[a] The rate of the reaction of CH_4 with OH provides an upper limit on the rate of formaldehyde formation, since most of the CH_3O_2 radicals ultimately formed are expected to react with HO_2 in this low-NO_x environment. (The minimum fraction forming HCHO, calculated assuming that all PO_2 is HO_2, is approximately 13%.)
Results are shown for steady-state calculations with $\alpha = 0.7$.

possible that NO_2/NO ratios at the sampling inlets were higher than those applicable aloft. If so, then the volume–average rate of the $NO_2 + OH$ reaction shown in Table 4 would be overestimated. Second, the lifetime of HONO ($1/J_{HONO} \geqslant 200$ s) is less than the period required for mixing throughout a 70 m height. This implies that the HONO sink shown in Table 4 is overestimated and further implies that the boundary-layer-average HO_x source from HONO photolysis is less than that at the sampling height. (In contrast, the lifetimes of HCHO and H_2O_2 are much longer, and those compounds are expected to mix throughout the mixed layer.)

The 05:00–20:00 average NO_2 destruction rate during 2000, shown in Table 4, would be balanced by a surface NO_x emission of 1.7×10^{12} molecules m^{-2} s^{-1} (all surface fluxes will be specified in these units). It would also be expected to be balanced by HNO_3 deposition of an equivalent amount. The 24 h average gradient-based NO_x flux estimate was 2.5×10^{12}, in relatively good agreement with this gas-phase destruction rate. However, a corresponding HNO_3 deposition was not observed (the average HNO_3 deposition flux was only 7.2×10^{11}). As noted above, it is possible that the measured NO_2 concentrations were higher than those at steady-state; if so, then the average rate of HNO_3 production would be less. This comparison implies export of NO_x from the Summit boundary layer. There is a much larger degree of disagreement between the average rate of HONO photolysis (equivalent to a surface emission of 5.3×10^{13}) and the gradient-based HONO emission (4.6×10^{11}). While it is likely that HONO concentrations are not constant throughout the boundary layer, as noted above, this discrepancy cannot be resolved by presuming that HONO's lifetime precludes it from mixing throughout the full height of the midday boundary layer; the measured HONO emission flux would be exceeded by photolysis in a layer shallower than the height at which HONO was measured.

Vertical fluxes of HCHO and H_2O_2 were also measured during the 2000 season, using gradient techniques (Jacobi et al., 2002). These species are both emitted from and deposited to the snowpack. The rate of gas-phase destruction of HCHO, through a 70 m boundary layer, is equivalent to a surface emission of 1.1×10^{13}, a value larger than the maximum emission flux and much larger than the net daily HCHO emission. However, gas-phase production from CH_4 oxidation probably partially counteracts this. H_2O_2 production exceeds H_2O_2 destruction, with the net effect of gas-phase chemistry equivalent to a surface deposition of 2.1×10^{13}. This is similar in magnitude to the maximum rate of H_2O_2 deposition, but is much greater than the net deposition averaged over the study period (Jacobi et al., 2002). Deposition of H_2O_2 in fog may account for this discrepancy. These results indicate that gas-phase chemistry rapidly cycles HCHO and H_2O_2 that is emitted from, and deposited to, the snowpack.

The impact of the O_3 production and destruction reactions summarized in Table 4 is a net ozone production of 2.6 ppbv (1999) and 1.8 ppbv (2000) during the 15- (1999) or 16-h (2000) calculation period. (If $[NO_2]/[NO]$ at the NO_x inlet was greater than the steady-state value, then the actual rate of O_3 production would exceed this value.) Significant net O_3 production is not apparent in the diurnal cycle of O_3 measured at Summit, which is weak but implies net destruction (Helmig et al., 2002). Since photochemical O_3 destruction has been observed in the interstitial air of the snowpack at Summit (Peterson and Honrath, 2001), it is possible that deposition on the snow surface exceeds the in situ production.

4. Summary and conclusions

Measurements of a suite of radical-source and -sink compounds during two summer seasons were used to constrain a steady-state model of radical sources and sinks at Summit, Greenland. In contrast to other remote surface measurement sites, ozone photolysis was not the dominant source of radicals. Photolysis of HCHO, HONO, and H_2O_2 (all measured at elevated mixing ratios attributed to snowpack emissions) and CH_3OOH (estimated), together increased the HO_x production rate by a factor of $\gtrsim 3$. The result is that midday peroxy radical levels (32–42 pptv) are comparable to those at lower latitude and altitude sites with higher water vapor concentrations, and average OH concentrations ($> 4 \times 10^6$ molecules cm^{-3} during the period of calculation: 05:00–20:00 or 21:00) exceed daily average levels in the tropical marine boundary layer.

The calculated photolysis rate constants and OH concentrations reveal some gaps in our understanding of photochemistry in the Summit boundary layer. The calculated HONO destruction rate greatly exceeds the HONO emission flux. Gas-phase reactions of H_2O_2 and HCHO also imply that photochemistry in the atmospheric boundary layer plays an important role in the budgets of these species. The integrated rate of $NO_2 +$ OH reaction is $\sim 70\%$ of the measured NO_x flux, and may be overestimated. This suggests that some of the emitted NO_x is exported to the overlying atmosphere. A moderate rate of net O_3 production (2–3 ppbv/day) is calculated. This in situ production must compete against photochemical destruction in the snowpack (Peterson and Honrath, 2001) and an unusually high rate of O_3 deposition to the snow surface (Helmig et al., 2002). Finally, although the HO_x budget was approximately balanced, that of OH was not, suggesting the presence of an unidentified OH sink which produced HO_2.

These results imply that the atmospheric boundary layer in snow-covered regions is quite active photochemically, and imply rapid chemical cycling of ($NO_x +$ HONO), HCHO, and H_2O_2 within the boundary layer. Since concentrations of the radical precursors are significantly elevated in the interstitial air of the near-surface sunlit snowpack (Sumner and Shepson, 1999; Dibb et al., 2002), it is likely that photochemistry is even more active there. Future direct measurements of OH, HO_2, and the radical precursor compounds analyzed here, made at heights ranging from within or near the snowpack surface to several tens of meters above, are needed to test the prediction of significantly elevated HO_x levels and to better constrain the vertical extent over which elevated HO_x is present.

Acknowledgements

The assistance of M. Dziobak, S. Guo and Y. Lu in the NO_x measurements, helpful conversations with Bill Simpson (Univ. Alaska Fairbanks) regarding the J_{NO_2} measurements, and logistical support provided by PICO and the NY ANG are appreciated. We are grateful to the Danish Polar Board and the Greenlandic Home Rule government for granting us permission to work at Summit. This work was supported by the National Science Foundation under Grant No. 9979497.

References

Atkinson, R., 1994. Gas-phase tropospheric chemistry of organic compounds. Journal of Physical Chemical Reference Data Monograph 2, 1–216.

Bales, R.C., Losleben, M.V., McConnell, J.R., Fuhrer, K., Neftel, A., 1995. H_2O_2 in snow, air, and open pore space in firn at Summit, Greenland. Geophysical Research Letters 22, 1261–1264.

Blake, D.R., Rowland, F.S., 1986. World-wide increase in tropospheric methane, 1978–1983. Journal of Atmospheric Chemistry 4, 43–62.

Cantrell, C.A., Shetter, R.E., Calvert, J.G., Eisele, F.L., Williams, E., Baumann, K., Brune, W.H., Stevens, P.S., Mather, J.H., 1997. Peroxy radicals from photostationary state deviations and steady state calculations during the tropospheric OH photochemistry experiment at Idaho Hill, Colorado, 1997. Journal of Geophysical Research 102, 369–378.

Cantrell, C.A., Shetter, R.E., Gilpin, T.M., Calvert, J.G., 1996. Peroxy radicals measured during Mauna Loa observatory photochemistry experiment 2: the data and first analysis. Journal of Geophysical Research 101, 14643–14652.

Crutzen, P.J., Zimmerman, P.H., 1991. The changing photochemistry of the troposphere. Tellus 43AB, 136–151.

Davis, D., Nowack, J.B., Chen, G., Buhr, M., Arimoto, R., Hogan, A., Eisele, F., Mauldin, L., Tanner, D., Shetter, R., Lefer, B., McMurry, P., 2001. Unexpected high levels of NO measured at South Pole. Geophysical Research Letters 28, 3625–3628.

Davis, D.D., et al., 1996. Assessment of ozone photochemistry in the western North Pacific as inferred from PEM-West, observations during the fall of 1991. Journal of Geophysical Research 101, 2111–2134.

DeMore, W.B., Sander, S.P., Golden, D.M., Hampson, R.F., Kurylo, M.J., Howard, C.J., Ravishankara, A.R., Kolb, C.E., Molina, M.J., 1997. Chemical kinetics and photochemical data for use in stratospheric modeling, evaluation number 12. Technical Report JPL Publication 97-4, NASA Jet Propulsion Laboratory.

Dibb, J.E., Arsenault, M., Peterson, M.C., Honrath, R.E., 2002. Fast nitrogen oxide photochemistry in Summit, Greenland snow. Atmospheric Environment 36, 2501–2511.

Dibb, J.E., Talbot, R.W., Munger, J.W., Jacob, D.J., Fan, S.-M., 1998. Air–snow exchange of HNO_3 and NO_y at Summit Greenland. Journal of Geophysical Research 103, 3475–3486.

Dickerson, R.R., Stedman, D.H., Delany, A.C., 1982. Direct measurement of ozone and nitrogen dioxide photolysis rates in the troposphere. Journal of Geophysical Research 87, 4933–4946.

Eisele, F.L., Tanner, D.J., Cantrell, C.A., Calvert, J.G., 1996. Measurements and steady state calculations of OH concentrations at Mauna Loa observatory. Journal of Geophysical Research 101, 14665–14679.

Grannas, A.M., Shepson, P.B., Guimbaud, C., Sumner, A.L., Albert, M., Simpson, W., Dominé, F., Boudries, H., Bottenheim, J., Beine, H.J., Honrath, R., Zhou, X., 2002. A study of photochemical and physical processes affecting carbonyl compounds in the arctic atmospheric boundary layer. Atmospheric Environment 36, 2733–2742.

Hauglustaine, D.A., Madronich, S., Ridley, B.A., Flocke, S.J., Cantrell, C.A., Eisle, F.L., Shetter, R.E., Tanner, D.J., Ginoux, P., Atlas, E.L., 1999. Photochemistry and budget of ozone during the Mauna Loa observatory photochemistry experiment (MLOPEX 2). Journal of Geophysical Research 104, 30275–30307.

Hauglustaine, D.A., Madronich, S., Ridley, B.A., Walega, J.G., Cantrell, C.A., Shetter, R.E., Hübler, G., 1996. Observed and model-calculated photostationary state at Mauna Loa Observatory during MLOPEX 2. Journal of Geophysical Research 101, 14681–14696.

Helmig, D., Boulter, J., David, D., Birks, J., Cullen, N., Steffen, K., Johnson, B.J., Oltmans, J.W., 2002. Ozone and meteorological boundary-layer conditions at Summit, Greenland, during June 3–12, 2000. Atmospheric Environment 36, 2595–2608.

Honrath, R.E., Guo, S., Peterson, M.C., Dziobak, M.P., Dibb, J.E., Arsenault, M., 2000. Photochemical production of gas-phase NO_x from sunlight irradiation of ice-crystal NO_3^-. Journal of Geophysical Research 105, 24183–24190.

Honrath, R.E., Lu, Y., Peterson, M.C., Dibb, J.E., Arsenault, M.., et al., 2002. Vertical fluxes of NO_x, HONO, and HNO_3 above the snowpack at Summit, Greenland. Atmospheric Environment 36, 2629–2640.

Honrath, R.E., Peterson, M.C., Guo, S., Dibb, J.E., Shepson, P.B., Campbell, B., 1999. Evidence of NO_x production within or upon ice particles in the Greenland snowpack. Geophysical Research Letters 26, 695–698.

Hurst, D.F., 1990. Seasonal variations in the latitudinal distribution of tropospheric carbon monoxide, 1986–1988. Ph.D. Thesis, University of California, Irvine.

Jacobi, H.-W., Frey, M.M., Hutterli, M.A., Bales, R.C., Schrems, O., Cullen, N.J., Steffen, K., Koehler, C., 2002. Measurements of hydrogen peroxide and formaldehyde exchange between the atmosphere and surface snow. Atmospheric Environment 36, 2619–2628.

Junkermann, W., 1994. Measurements of the J_{O^1D} actinic flux within and above stratiform clouds and above snow surfaces. Geophysical Research Letters 21, 793–796.

Kylling, A., Albold, A., Seckmeyer, G., 1997. Transmittance of a cloud is wavelength-dependent in the UV-range: Physical interpretation. Geophysical Research Letters 24, 397–400.

Kylling, A., Stamnes, K., Tsay, S.-C., 1995. A reliable and efficient two-stream algorithm for spherical radiative transfer: Documentation of accuracy in realistic layered media. Journal of Atmospheric Chemistry 21, 115–150.

Lantz, K.O., Shetter, R.E., Cantrell, C.A., Flocke, S.J., Calvert, J.G., Madronich, S., 1996. Theoretical, actinometric, and radiometric determinations of the photolysis rate coefficient of NO_2 during the Mauna Loa Observatory photochemistry experiment 2. Journal of Geophysical Research 101, 14613–14629.

Lenschow, D.H., Delany, A.C., 1987. An analytic formulation for NO and NO_2 flux profiles in the atmospheric surface layer. Journal of Atmospheric Chemistry 5, 301–309.

Mauldin, R.L., Eisele, F.L., Tanner, D.J., Kosciuch, E., Shetter, R., Lefer, B., Hall, S.R., Nowak, J.B., Buhr, M., Chen, G., Wang, P., Davis, D., 2001. Measurements of OH, H_2SO_4, and MSA at the South Pole during ISCAT. Geophysical Research Letters 28, 3629–3632.

Novelli, P.C., 1998. Distributions and recent changes of carbon monoxide in the lower troposphere. Journal of Geophysical Research 103, 19015–19033.

Penkett, S.A., Monks, P.S., Carpenter, L.J., Clemitshaw, K.C., Ayers, G.P., Gillett, R.W., Galbally, I.E., Mayer, C.P., 1997. Relationships between ozone photolysis rates and peroxy radical concentrations in clean marine air over the Southern Ocean. Journal of Geophysical Research 102, 12805–12817.

Peterson, M.C., Honrath, R.E., 2001. Observations of rapid photochemical destruction of ozone in snowpack interstitial air. Geophysical Research Letters 28, 511–514.

Riedel, K., Weller, R., Schrems, O., König-Langlo, G., 2000. Variability of tropospheric hydroperoxides at a coastal surface site in Antarctica. Atmospheric Environment 34, 5225–5234.

Ridley, B., Walega, J., Montzka, D., Grahek, F., Atlas, E., Flocke, F., Stroud, V., Deary, J., Gallant, A., Boudries, H., Bottenheim, J., Anlauf, K., Worthy, D., Sumner, A.L., Shepson, P., 2000. Is the Arctic surface layer a source and sink of NO_x in winter/spring?. Journal of Atmospheric Chemistry 36, 1–22.

Sander, S.P., Friedl, R.R., DeMoore, W.B., Golden, D.M., Kurylo, M.J., Hampson, R.F., Huie, R.E., Moortgat, G.K., Ravishankara, A.R., Kolb, C.E., Molina, M.J., 2000. Chemical kinetics and photochemical data for use in stratospheric modeling: Supplement to evaluation

12: Update of key reactions. Technical Report JPL Publication 00-3, NASA Jet Propulsion Laboratory.

Shetter, R.E., Cantrell, C.A., Lantz, K.O., et al., S.J.F., 1996. Actinometric and radiometric measurement and modeling of the photolysis rate coefficient of ozone to $O(^1d)$ during Mauna Loa Observatory Photochemistry Experiment 2. Journal of Geophysical Research 101, 14631–14641.

Simpson, W.R., King, M.D., Beine, H.J., Honrath, R.E., Peterson, M.C., 2002. Atmospheric photolysis rate coefficients during the Polar Sunrise Experiment ALERT 2000. Atmospheric photolysis rates suring the Polar Sunrise Experiment ALERT2000 field campaign. Atmospheric Environment 36, 2471–2480.

Sumner, A., Shepson, P., 1999. Snowpack production of formaldehyde and its impact on the Arctic troposphere. Nature 398, 230–233.

Swanson, A.L., Blake, N.J., Blake, D.R., Rowland, F.S., Dibb, J.E., 2002. Photochemically induced production of CH_3Br, CH_3I, C_2H_5I, ethene, and propene within surface snow. Atmospheric Environment 36, 2671–2682.

Tang, T., McConnell, J.C., 1996. Autocatalytical release of bromine from Arctic snow pack during polar sunrise. Geophysical Research Letters 23, 2633–2636.

Volz-Thomas, A., Lerner, A., Pätz, H.-W., Schultz, M., McKenna, D.S., Schmitt, R., Madronich, S., Röth, E.P., 1996. Airborne measurements of the photolysis frequency of NO_2. Journal of Geophysical Research 101, 18613–18627.

Wang, Y., Logan, J.A., Jacob, D.J., 1998. Global simulation of tropospheric O_3–NO_x-hydrocarbon chemistry: 2. Model evaluation and global ozone budget. Journal of Geophysical Research 103, 10727–10756.

Warneck, P., 2000. Chemistry of the Natural Atmosphere. Academic Press, New York.

Warren, S.G., 1982. Optical properties of snow. Reviews of Geophysics and Space Physics 20, 67–89.

Zanis, P., Monks, P.S., Schuepbach, E., Penkett, S.A., 1999. On the relationship of $HO_2 + RO_2$ with $j(O^1D)$ during the Free Tropospheric Experiment (FREETEX '96) at the Jungfraujoch Observatory (3590 m above sea level) in the Swiss Alps. Journal of Geophysical Research 104, 26913–26925.

Zhou, X., Beine, H.J., Honrath, R.E., Fuentes, J.D., Simpson, W., Shepson, P.B., Bottenheim, J.W., 2001. Snowpack photochemical production of HONO: a major source of OH in the Arctic boundary layer in springtime. Geophysical Research Letters 28, 4087–4090.

Publication 3.2.5

Jacobi, H.-W., M.M. Frey, M.A. Hutterli, R.C. Bales, O. Schrems, N.J. Cullen, K. Steffen, and C. Koehler,

Measurements of hydrogen peroxide and formaldehyde exchange between the atmosphere and surface snow at Summit, Greenland,

Atmos.Environ. **36**, 2619-2628, 2002.

PERGAMON

Atmospheric Environment 36 (2002) 2619–2628

ATMOSPHERIC ENVIRONMENT

www.elsevier.com/locate/atmosenv

Measurements of hydrogen peroxide and formaldehyde exchange between the atmosphere and surface snow at Summit, Greenland

Hans-Werner Jacobi[a,*], Markus M. Frey[a], Manuel A. Hutterli[a], Roger C. Bales[a], Otto Schrems[b], Nicolas J. Cullen[c], Konrad Steffen[c], Cathi Koehler[d]

[a] *Department of Hydrology and Water Resources, University of Arizona, P.O. Box 210011, 1133 E. North Campus Dr., Tucson, AZ 85721-0011, USA*

[b] *Alfred Wegener Institute for Polar and Marine Research, Am Handelshafen 12, 27570 Bremerhaven, Germany*

[c] *CIRES, CB 216, University of Colorado, Boulder, CO 80309, USA*

[d] *Manchester High School, Earth and Space Science, Manchester, CT 06040, USA*

Received 6 June 2001; received in revised form 7 September 2001; accepted 17 September 2001

Abstract

Tower-based measurements of hydrogen peroxide (H_2O_2) and formaldehyde (HCHO) exchange were performed above the snowpack of the Greenland ice sheet. H_2O_2 and HCHO fluxes were measured continuously between 16 June and 7 July 2000, at the Summit Environmental Observatory. The fluxes were determined using coil scrubber-aqueous phase fluorometry systems together with micrometeorological techniques. Both compounds exhibit strong diel cycles in the observed concentrations as well as in the fluxes with emission from the snow during the day and the evening and deposition during the night. The averaged diel variations of the observed fluxes were in the range of $+1.3\times10^{13}$ molecules $m^{-2}s^{-1}$ (deposition) and -1.6×10^{13} molecules $m^{-2}s^{-1}$ (emission) for H_2O_2 and $+1.1\times10^{12}$ and -4.2×10^{12} molecules $m^{-2}s^{-1}$ for HCHO, while the net exchange per day for both compounds were much smaller. During the study period of 22 days on average $(0.8^{+4.6}_{-4.3})\times10^{17}$ molecules m^{-2} of H_2O_2 were deposited and $(7.0^{+12.6}_{-12.2})\times10^{16}$ molecules m^{-2} of HCHO were emitted from the snow per day. A comparison with the inventory in the gas phase demonstrates that the exchange influences the diel variations in the boundary layer above snow covered areas. Flux measurements during and after the precipitation of new snow shows that $<16\%$ of the H_2O_2 and more than 25% of the HCHO originally present in the new snow were available for fast release to the atmospheric boundary layer within hours after precipitation. This release can effectively disturb the normally observed diel variations of the exchange between the surface snow and the atmosphere, thus perturbing also the diel variations of corresponding gas-phase concentrations.

Keywords: Hydrogen peroxide; Formaldehyde; Greenland; Air–snow exchange; Tropospheric composition; Polar atmospheric chemistry

1. Introduction

Formaldehyde (HCHO) and hydrogen peroxide (H_2O_2) are key compounds regarding the chemical composition of the Earth's atmosphere. Both are important secondary products formed during the oxidation of organic compounds (e.g. Jenkin and

*Corresponding author. Present address: Alfred Wegener Institute for Polar and Marine Research, Am Handelshafen 12, 27570 Bremerhaven, Germany.

E-mail address: hwjacobi@awi-bremerhaven.de (H.-W. Jacobi).

1352-2310/02/$ - see front matter
PII: S1352-2310(02)00106-1

Clemitshaw, 2000). At the same time, they influence the oxidation capacity of the troposphere because they are important precursors of radicals like OH and HO_2 (Crawford et al., 1999). Therefore, both compounds have been used to investigate photochemical processes in the troposphere (e.g. Weller et al., 2000; Lee et al., 2000; Chance et al., 2000) and to validate the performance of numerical photochemistry models (e.g. Jaeglé et al., 2000; Solberg et al., 2001).

Recently, HCHO and H_2O_2 in polar regions have attracted a lot of interest due to two different reasons. It has been discussed that HCHO and H_2O_2 can play critical roles in the atmospheric boundary layer (ABL) at high latitudes during the occurrence of ozone (O_3) depletion events that are commonly observed during polar sunrise in Arctic areas (McConnell et al., 1992). While the effective O_3 destruction is caused by reactions with chlorine (Cl) and bromine (Br) atoms (Barrie et al., 1988, 1994; Mickle et al., 1989; Bottenheim et al., 1990; Jobson et al., 1994; Solberg et al., 1996; Ariya et al., 1998; Ramacher et al., 1999), Cl and Br atoms also react quickly with HCHO and are transformed into non-reactive compounds like HCl and HBr that are subsequently removed from the gas phase (Barrie et al., 1988; Shepson et al., 1996). In contrast, Michalowski et al. (2000) pointed out that the reaction of HCHO with BrO might lead to the formation of HOBr initiating subsequent heterogeneous reactions increasing halogen atom concentrations. H_2O_2 could also contribute to the formation of gas-phase molecular bromine (Br_2) as a consequence of the reaction of H_2O_2 with bromide (Br^-) in the aqueous phase (McConnell et al., 1992). Besides the involvement of both compounds in important photochemical processes, H_2O_2 and HCHO are conserved in surface snow and ice cores providing valuable information about the oxidation capacity of the past troposphere (Staffelbach et al., 1991; Thompson et al., 1993; Neftel et al., 1995; Fuhrer et al., 1996; Hutterli et al., 1999, 2001). Knowledge of the exchange between the atmosphere and the underlying snowpack is important for the development of transfer functions that link concentrations in the snowpack and in the gas phase.

Gas-phase H_2O_2 and HCHO concentrations have been investigated at several different sites in the Arctic. Combined field and modeling studies have indicated, that current gas-phase chemistry models are unable to account for H_2O_2 (Neftel et al., 1995; McConnell et al., 1997a; Hutterli et al., 2001) and HCHO concentrations (McConnell et al., 1992; De Serves, 1994; Sander et al., 1997; Rudolph et al., 1999; Hutterli et al., 1999) commonly observed at high latitudes. Model results also indicate that emissions from the snowpack can sustain measured gas-phase concentrations of H_2O_2 and HCHO (Shepson et al., 1996; Michalowski et al., 2000; Hutterli et al., 1999, 2001). Nevertheless, only few attempts have been made to measure fluxes above the snowpack. Vertical HCHO profiles at Alert, Canada, presented by Sumner and Shepson (1999), displayed higher concentrations close to the snow surface compared to ambient concentrations. Moreover, Hutterli et al. (1999) calculated HCHO fluxes from the snowpack at Summit, Greenland, using either measured ambient and interstitial air concentrations or surface snow measurements that are sufficiently high to compete with known HCHO formation pathways in the gas phase. Hutterli et al. (2001) also reported diel variations of H_2O_2 fluxes above the snowpack indicating a temperature-driven recycling between air and snow.

In this paper we report observations of H_2O_2 and HCHO gradients above a snowpack combined for the first time with direct measurements of diffusion coefficients using eddy correlation technique. The impact of the derived fluxes on observed diel variations in the ABL is discussed. A precipitation event is analyzed to demonstrate how regular diel variations of concentrations and fluxes are effectively disturbed by emissions from new snow.

2. Experimental

Ambient gas-phase concentrations of H_2O_2 and HCHO were continuously measured at the Greenland Environmental Observatory Summit (GEO Summit) on top of the Greenland ice sheet (72.6°N, 38.5°W, 3200 m elevation) from 5 June to 9 July 2000. Ambient air was drawn through heated and insulated inlet lines (0.635 cm ID PFA tubes) to the analyzers installed in a trench located 400 m south of the main camp and ~3 m below the snow surface. From 16 June to 7 July gradient measurements of both compounds above the snowpack were performed. For this purpose the inlet line was mounted on a lift that automatically switched every 8 min between two heights (1 and 152 or 1 and 143 cm). Because the concentrations could be affected by contamination from emissions of the main camp the data was filtered using ambient NO_x and NO_y concentrations (Honrath et al., this issue). Concentrations were discarded when either $[NO] \geqslant 100$ pptv or $[NO_x] \geqslant 200$ pptv or $[NO_y] \geqslant 1000$ pptv. When NO_x and NO_y concentrations were not available, data were also abandoned if the wind came from northerly directions ($330° \leqslant WD \leqslant 30°$).

Gas-phase H_2O_2 and HCHO were absorbed from the sample air stream into an aqueous solution using coil scrubbers followed by derivatization and fluorometric detection. Both instruments have previously been described in detail (Hutterli et al., 2001; Riedel et al., 1999). H_2O_2 was stripped from an ambient airflow (~1.2 l min^{-1} (STP)) by H_2O_2 free water running at ~0.2 ml min^{-1}) into a coil scrubber. After raising the pH, the aqueous phase H_2O_2 concentration was

analyzed by UV fluorescence spectroscopy after derivatization with 4-ethylphenol in the presence of peroxidase. Calibrations were performed daily by running liquid standards through the scrubber while flushing with H_2O_2-free air generated by pumping ambient air through a column filled with manganese dioxide–copper oxide mixture (Hopcalite®, Callery Chemical Company, USA). The same zero air was used to monitor the baseline every hour. The limit of detection (LOD) of the instrument was 70 pptv corresponding to 3 times the standard deviation of the noise level measured with zero air and the accuracy was estimated to be better than 25%. It is well known that the applied method is also sensitive to higher organic peroxides (Lee et al., 2000). Therefore, we used a second channel equipped with a manganese dioxide catalyst to selectively destroy H_2O_2 (Lee et al., 2000). The signal of the second channel always remained below the detection limit in agreement with previous data from Summit (Sigg et al., 1992) and gives us confidence that organic peroxides did not interfere substantially with our H_2O_2 measurements. Gas-phase HCHO concentrations were obtained using a commercial analyzer (AL4001, Aero-Laser GmbH, Germany). HCHO was collected by drawing air ($\sim$0.6–0.8 l min^{-1} (STP)) and pumping acid solution (0.05 M H_2SO_4) at a rate of $\sim$0.2 ml min^{-1} together into a coil scrubber. The analysis in the aqueous phase is based on the Hantzsch reaction of HCHO with pentane-2,4-dione and NH_3 followed by fluorometric detection. While the reaction chamber and the fluorescence cell were kept at 60°C, the scrubber was held at a constant temperature of 16°C to increase the stripping efficiency to more than 96% (Riedel et al., 1999). The zero air for the H_2O_2 instrument was also used to hourly determine the baseline for the HCHO measurements. A LOD of 30 pptv and an accuracy of $<$25% were achieved.

The primary flux measurement systems utilized to determine the turbulent structure of the near-surface boundary layer were two eddy covariance (EC) systems including two three-dimensional sonic anemometers with fine wire thermocouples and two ultraviolet hygrometers (CSAT3, FW05, KH20; all Campbell Scientific, USA) mounted on profile arms 1 and 2 m above the snow surface, respectively. These instruments were reoriented so that they pointed into the prevailing wind direction during the measurement period. The measurements were performed at 50 Hz using a data logger (CR5000, Campbell Scientific, USA) connected directly to a computer housed near the measurement tower. Supporting measurements were wind speed, temperature and relative humidity measured at 0.5, 1, and 2 m above the snow surface on a separate tower. A three-dimensional coordinate rotation on the time series u, v, and w were performed after Kaimal and Finnigan (1994), which aligned the time series with the mean wind vector, forcing v and w means to zero. Turbulence statistics were generated for 10 min periods in post processing to coincide with those calculated from the supporting measurements. The two EC systems were utilized to investigate the accuracy of the turbulence measurements resulting in deviations of $<$15% in all cases (Cullen and Steffen, 2001).

Further micrometeorological data (temperature, wind speed, wind direction, pressure, relative humidity) is available on the web pages of GEO Summit (http://www.hwr.arizona.edu/geosummit/data.html).

3. Results

Fig. 1 shows observed HCHO and H_2O_2 time series. Due to different experiments the inlets were mounted at different heights. The time series presented here are assembled from all measurements at heights between 1 and 2 m above the snow surface. For the measuring period from 5 June until 8 July 2000, average concentrations were 0.65 and 120 pptv for H_2O_2 and HCHO, respectively. An increasing trend for HCHO was observed with average concentrations of $<$100 pptv in the first week and almost 180 pptv in the last week. Most of the days both compounds exhibit diel cycles with low concentrations during the night and higher concentrations during the day as shown in Fig. 2. However, maximum concentrations are reached either in the evening (H_2O_2) or in the morning (HCHO).

Fluxes of HCHO and H_2O_2 were determined using an integrated flux-gradient approach based on Monin–Obukhov similarity theory. Direct measurements of the heat and momentum fluxes using the eddy correlation technique enabled determination of the Obukhov length L, a key independent variable in the steady state, horizontally homogenous ABL. Specification of the flux–profile relationships required to calculate fluxes of HCHO and H_2O_2 reduces to knowledge of the stability function ϕ_m as a function of z/L (e.g. Businger et al., 1971; Dyer, 1974) with the height above the snow surface z. Once functions of ϕ_m were established changes to the turbulent exchange coefficient for momentum (K_m) with stability were determined, enabling fluxes of HCHO and H_2O_2 to be expressed in terms of concentration gradients in the vertical direction z using Eq. (1):

$$F = K_m(z)\frac{\partial C}{\partial z} = \frac{\kappa u_* z}{\phi_m(z/L)}\frac{\partial C}{\partial z} = \text{const.} \quad (1)$$

with von Karman constant κ (=0.4), friction velocity u_*, and concentration C. Since the application of the flux–profile relationship also includes the premise of constant fluxes with height, Eq. (1) can be solved in the integrated form (2).

$$F = \frac{\kappa u_* \int_{C(z_1)}^{C(z_2)} \partial C}{\int_{z_1}^{z_2} (\phi_m(z/L)/z)\,\partial z} = \frac{\kappa u_* (C(z_2) - C(z_1))}{\int_{z_1}^{z_2} (\phi_m(z/L)/z)\,\partial z}. \quad (2)$$

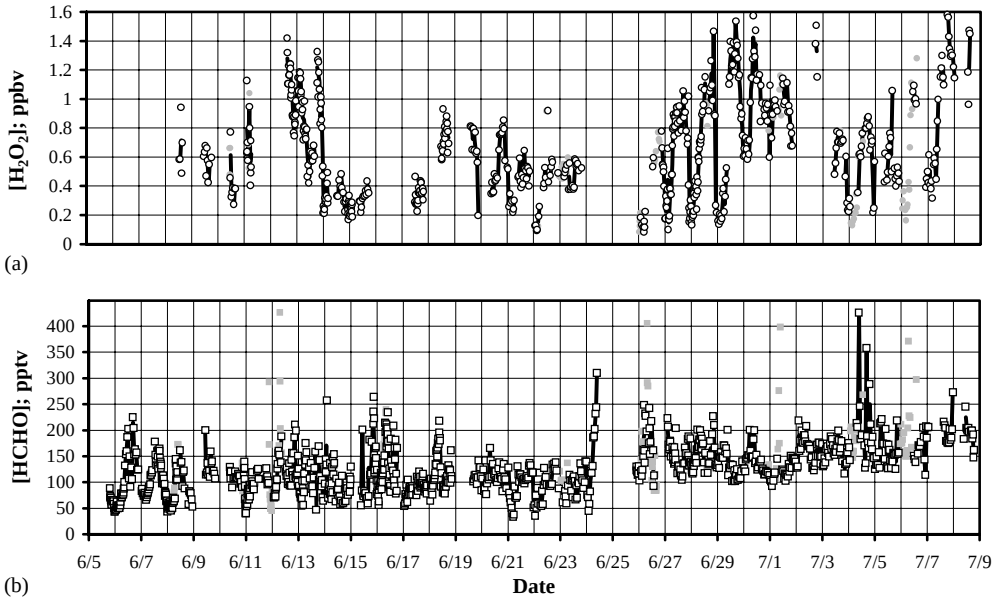

Fig. 1. Time series of H_2O_2 (a) and HCHO (b) concentrations measured at Summit, Greenland, in June–July 2000. Symbols mark 10 min averages; lines show 1 h averages. Grey symbols indicate discarded data (see text) also including HCHO concentrations between 400 and 1400 pptv (not shown).

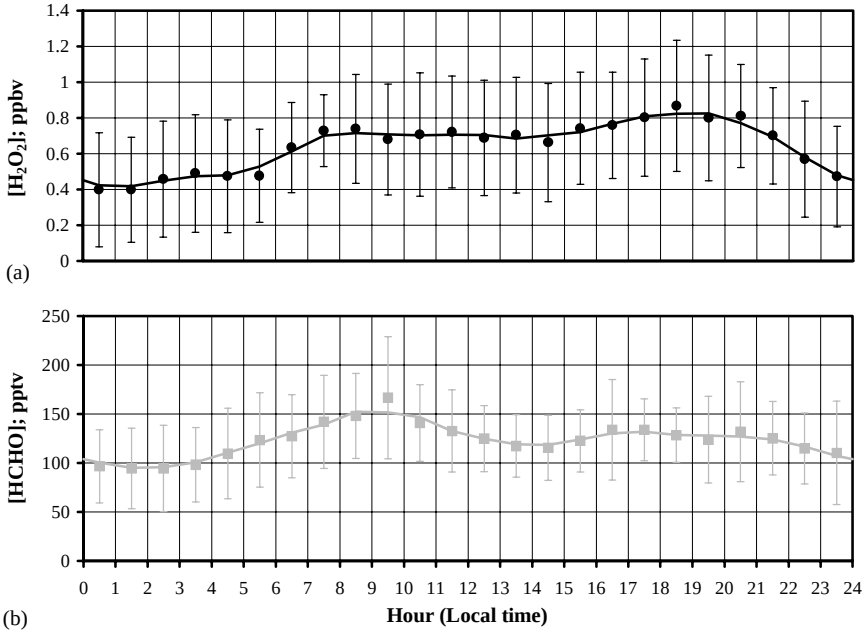

Fig. 2. Diel variations of H_2O_2 (a) and HCHO (b) concentrations measured at Summit, Greenland, in June–July 2000. Symbols mark 1 h bins; lines show 3 h running averages. Error bars indicate calculated standard deviations.

Gradient measurements, friction velocities, and Obukhov lengths are available for a 22-day period (16 June–7 July). For unstable conditions the stability function $\phi(z/L) = (1 - 16z/L)^{-0.25}$ was used, while for stable cases the function $\phi(z/L) = 1 + 4.6z/L$ was applied, which reduces under neutral conditions ($L \gg 1$) to $\phi(z/L) = 1$. Because the concentrations were alternately measured at two heights with an integration time

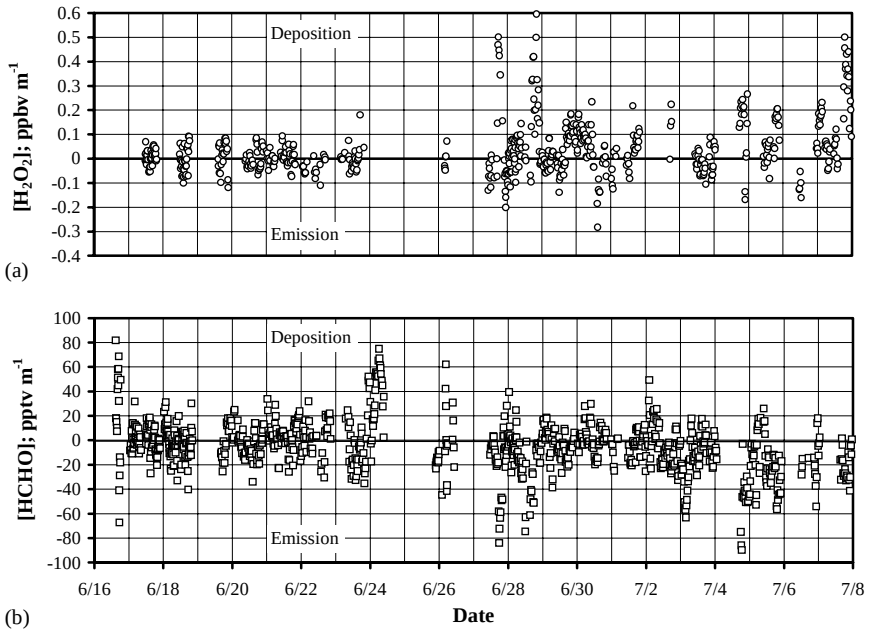

Fig. 3. Time series of H_2O_2 (a) and HCHO (b) concentration gradients measured at Summit, Greenland, in June–July 2000.

of 8 min at each height, consecutive measurements in one height were used to linearly interpolate the value at one height for the point of time of the measurement at the other height. The concentration gradients shown in Fig. 3 were calculated as (upper level concentration measurement)−(lower level concentration measurement). As a result, a positive gradient represents trace gas deposition and a negative gradient indicates trace gas emission. Each gradient was used to calculate the flux with the appropriate micrometeorological coefficients. The fluxes for the whole period were averaged within 1 h bins to obtain average diel variations for both compounds (Fig. 4). Average H_2O_2 fluxes vary between $+1.3$ and -1.6×10^{13} molecules $m^{-2}s^{-1}$. On the other hand, average HCHO fluxes show a smaller amplitude between $+1.1$ and -4.2×10^{12} molecules $m^{-2}s^{-1}$. Fig. 4 also indicates the range of the middle 50% of the flux data that were used to calculate errors of the amounts exchanged between air and snow per day (Table 1). These errors and ranges illustrate that the observed fluxes exhibit a large variability, which is mainly caused by an inherent natural variability of the fluxes due to variable meteorological conditions. Compared to the natural variability, uncertainties in the flux calculations and analytical errors are small. Nevertheless, the 50% range also demonstrates that a majority of the individual diel cycles measured on different days follow distinct patterns, reflected by the averaged diel variations of both compounds, with common features like emissions during the day and deposition during the night. The average turning point from deposition to emission occurs around 10:00 in the morning for H_2O_2 and HCHO. While HCHO emissions continue until midnight, H_2O_2 fluxes change their directions already at 17:00 in the evening. Highest average H_2O_2 deposition rates were observed between 17:00 and 21:00 in the evening. The average net fluxes during the course of 1 day correspond to a daily deposition of 8×10^{16} molecules m^{-2} of H_2O_2 and a daily emission of 7×10^{16} molecules m^{-2} of HCHO.

During the measuring period we had the opportunity to measure fluxes during one night with a new snow event. Fluxes calculated for the period between 29 June and 1 July are shown in Fig. 5. While fluxes measured on 29 June and the first half of 30 June reflect typical diel variations for both compounds close to average diel variations depicted in Fig. 4, the results for the night from 30 June to 1 July demonstrate the impact of <1 cm new snow that precipitated in the course of this night. H_2O_2 and HCHO fluxes clearly show strong emissions during the night at a time when normally slight emission or deposition occur. Highest emission rates for H_2O_2 were observed between 21:00 on 30 June and 2:00 on 1 July, whereas highest emission rates for HCHO were measured $\sim$2–3 h later. Total amounts released were 6.7×10^{17} molecules m^{-2} of H_2O_2 between 21:00 and 2:00 and 8.1×10^{16} molecules m^{-2} of HCHO between 24:00 and 4:00.

4. Discussion

The most prominent feature in the H_2O_2 gas-phase concentrations is its distinct diel variation that has been

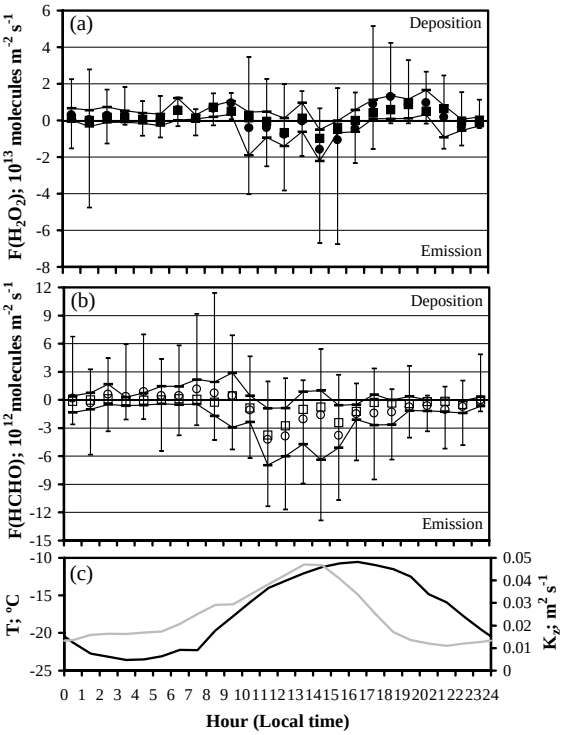

Fig. 4. Diel variations measured at Summit, Greenland, between 16 June and 7 July 2000. H_2O_2 (a) and HCHO (b) fluxes. The average and median of the data in each 1 h bin are indicated by a circle and a box, respectively; the vertical lines connected by solid lines indicate the middle 50% of the data; and the error bars the middle 95% of the data, (c) 1 h averages of surface snow temperature and eddy diffusion coefficient.

Table 1
Gas-phase inventories, averaged exchange rates, and net photochemical production or destruction rates measured during the field season 2000 at Summit, Greenland

	H_2O_2	HCHO
Maximum gas phase inventory[a], molecules m^{-2}	1.4×10^{18}	2.5×10^{17}
Minimum gas phase inventory[b], molecules m^{-2}	0.4×10^{18}	0.9×10^{17}
Difference in gas phase inventory; molecules m^{-2}	1.0×10^{18}	1.6×10^{17}
Daily deposition[c]; molecules m^{-2}	$(2.7^{+2.9}_{-2.3}) \times 10^{17}$	$(1.8^{+4.5}_{-1.8}) \times 10^{16}$
Daily emission[c]; molecules m^{-2}	$(1.9^{+2.1}_{-1.7}) \times 10^{17}$	$(8.8^{+10.8}_{-7.7}) \times 10^{16}$
Daily net exchange[c]; molecules m^{-2}	$(0.8^{+4.6}_{-4.3}) \times 10^{17}$	$(7.0^{+12.6}_{-12.2}) \times 10^{16}$
	Deposition	Emission
Daily net photochemical production/destruction[d]; molecules m^{-2}	1.5×10^{18}	6.5×10^{17}
	Production	
Destruction		
Total emission after new snow event; molecules m^{-2}	6.7×10^{17}	8.1×10^{16}

[a] Estimated using an ABL height of 90 m (Helmig et al., 2002), $[H_2O_2] = 0.82$ ppbv, and [HCHO] = 150 pptv.

[b] Estimated using an ABL height of 50 m (see text), $[H_2O_2] = 0.42$ ppbv, and [HCHO] = 95 pptv.

[c] Errors are calculated using the maxima and minima of the middle 50% of the data of the fluxes indicated in Fig. 4.

[d] Estimated using an ABL height of 90 m and average rates given by Yang et al. (2002) for 5:00–21:00.

observed in all previous studies at Summit (Sigg et al., 1992; Bales et al., 1995a, b; Fuhrer et al., 1996; McConnell et al., 1997b; Hutterli et al., 2001). For example, during this field season highest concentrations were found between 17:00 and 21:00 with an average of 0.82 ppbv, whereas lowest values averaging to 0.42 ppb were measured between 0:00 and 3:00. In comparison to previous studies, the H_2O_2 concentrations are lower and the diel cycle is less pronounced. In addition, we observed a diel cycle in the HCHO concentrations in the gas phase with highest concentrations between 7:00 and 10:00 and lowest concentrations between midnight and 3:00. The averages for these 3 h periods are 150 and 95 pptv. This diel variation is less marked compared to H_2O_2 and has not been observed in former studies at Summit (Fuhrer et al., 1996; Hutterli et al., 1999). The average HCHO concentrations in 2000 were also lower compared to observations at Summit in 1996 (Hutterli et al., 1999). The differences between this study and former results are possibly due to the meteorological conditions. During long periods, the wind speed was very low ($<4\,m\,s^{-1}$). Moreover, fresh snowfalls, which can substantially disturb diel variations of H_2O_2 and HCHO (see below), occurred only twice during the measuring period.

The observed fluxes show that H_2O_2 and HCHO are exchanged between the surface snow and the gas phase. Since fluxes in both directions occur, the surface snowpack can be considered as a temporary reservoir for H_2O_2 and HCHO during the night. While this mechanism was suggested for H_2O_2 by Sigg et al. (1992), we demonstrate here that it can also be applied to HCHO. Obviously, such a mechanism has the potential to contribute to observed diel variations. Likewise, a comparison of the observed concentrations with the direction of the fluxes demonstrates partial agreement. The emissions of both compounds during the day and deposition during the night can explain elevated concentrations at daytime. These results are in agreement with previous measurements of H_2O_2 fluxes above

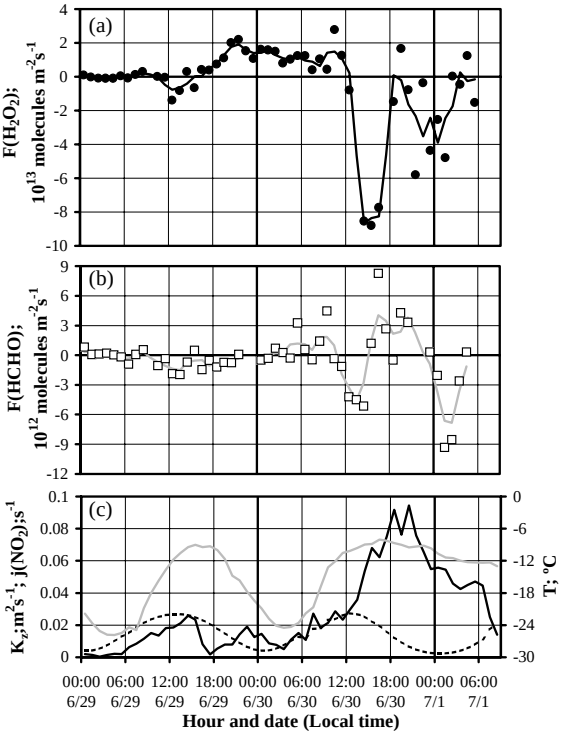

Fig. 5. H_2O_2 and HCHO fluxes, surface snow temperature, eddy diffusion coefficient, and photolysis rate of NO_2 measured at Summit, Greenland, between 29 June and 1 July 2000, (a) H_2O_2 flux. Filled circles mark 1 h averages; line represents 3 h running averages, (b) HCHO flux. Open squares mark 1 h averages; line represents 3 h running averages, (c) 1 h averages of surface snow temperature (gray line), eddy diffusion coefficient (black line), and $j(NO_2)$ (dashed line).

the snow surface (Hutterli et al., 2001) indicating that emissions with highest values between 8:00 and 16:00 contributed to observed diel variations in H_2O_2 gas-phase concentrations.

To evaluate the impact of the exchange on the diel variations in the gas phase, we compare the change in the total amount present in the ABL (= inventory) with the measured daily emission and deposition. Table 1 shows estimated maximum and minimum inventories in the gas phase using maximum and minimum concentrations of 0.82 and 0.42 ppbv for H_2O_2 and 150 and 95 pptv for HCHO. We also used averaged ABL heights of 90 m during daytime (Helmig et al., this issue) and 50 m during nighttime corresponding to the median of mixing heights calculated from friction velocities and Obukhov lengths for stable conditions between 0:00 and 3:00 (Seibert et al., 2000). Then, the difference in the maximum and minimum inventories can be compared with daily deposited and emitted amounts, which are summarized in Table 1. In general, the results suggest that bi-directional fluxes in the boundary layer are an important mechanism influencing diel cycles of H_2O_2 and HCHO in the ABL over the snowpack at Summit. However, the diel variations cannot be explained solely by the exchange with the snow pack. Moreover, increase and decrease of the concentrations do not coincide with changes in the direction of the fluxes. For example, HCHO concentrations start rising at 4:00 and falling at 21:00, although deposition and emission still continue until 9:00 and 1:00, respectively. A similar time shift is apparent in the case of H_2O_2.

Photochemical reactions governing the production and destruction of H_2O_2 and HCHO involve OH and HO_2 reactions and direct photolysis. Since OH and HO_2 concentrations closely follow diel variations in UV radiation, photochemical processing of H_2O_2 and HCHO becomes more vigorous with increasing radiation intensity. In fact, increase and decrease of the H_2O_2 and HCHO diel variations at the transitions between day and night seem to be dominated by photochemical reactions since both correlate well with $j(NO_2)$ (Fig. 5) which corresponds to the intensity of UV radiation. Yang et al. (this issue) report average production and destruction rates for several species obtained from photolysis rates and calculated OH and HO_2 concentrations. Their results show that the photochemical sources and sinks of H_2O_2 and HCHO are not in equilibrium resulting in a net production of H_2O_2 and a net destruction of HCHO (Table 1). Although the exchange with the surface snow partly counteracts the photochemical imbalances, it accounts only for $<10\%$ of photochemically produced H_2O_2 and destroyed HCHO. Note, that the photochemical production of HCHO is uncertain since it depends on the branching ratio for the reaction of methyl peroxyradicals with either NO or HO_2. The net destruction given in Table 1 is calculated using a ratio of 0.13 (Yang et al., this issue) and would turn into a net photochemical production at a ratio of higher than 0.66. The non-equilibrium of photochemical transformation plus exchange at the snow surface for H_2O_2 and HCHO indicates that additional processes must be considered to fully explain the diel variations and are discussed in the following.

One important removal mechanism for H_2O_2 is the formation of fog (Bergin et al., 1996; Hutterli et al., 2001) that regularly occurred at night during the field season. Bergin et al. (1996) demonstrated that H_2O_2 could be fully depleted in the presence of fog if equilibrium according to Henry's law between concentrations in the fog droplets and in the gas phase is assumed. A calculated H_2O_2 flux of 5.5×10^{18} molecules m^{-2} was obtained in a case study of a fog event at Summit lasting for 10 h during one night (Bergin et al., 1996). This value is more than 10 times the daily dry deposition obtained in this study (Table 1) demonstrating that fog deposition can be very effective and is sufficient to remove the photochemically

produced excess H_2O_2. The transfer of HCHO into droplets and subsequent deposition to the surface snow could also cause an additional deposition of HCHO. Due to the lower Henry's law coefficient the removal is probably less effective in agreement with the less pronounced diel cycle.

Another possible mechanism having the potential to influence gas-phase concentration in the ABL is the entrainment of air from above into the ABL due to increasing mixing layer heights during the course of the day. This can either lead to an increase or decrease of H_2O_2 and HCHO depending on concentrations in the free troposphere relative to concentrations in the ABL. This process might be reflected by the fast increase of HCHO and H_2O_2 during the morning when the shallow and stable nocturnal ABL is obliterated assuming that the deposition during the night decreases the concentrations in the ABL compared to the layer above. Overall, further studies to distinguish between H_2O_2 and HCHO in the gas phase and in fog are needed to fully understand the cycling between the ABL and the surface snow. In addition, detailed investigations of the structure of the ABL are necessary to elaborate the impact of emission, deposition, and vertical transport on H_2O_2 and HCHO concentrations in the ABL.

The new snow event and its effect observed during the night from 30 June to 1 July demonstrates that the system ABL plus underlying snowpack cannot be regarded as a closed system with negligible exchange at the upper and lower boundary. New snow influences the surface snow concentrations as well as the magnitude and direction of the flux between snow and ABL as observed during this specific night (Fig. 4). The total amount of H_2O_2 released during the night was more than 3 times the amount normally released during 1 day (Table 1). This difference was less dramatic in the case of HCHO, and the amount emitted during the night with the new snow event almost equalled the amount normally released during the course of 1 day. Accordingly, the effect on the concentrations in the ABL is more pronounced in the case of H_2O_2 (Fig. 1). In most of the nights before and after the event, H_2O_2 concentrations dropped to values around 0.2–0.4 ppbv during the night while in this specific night considerably higher concentrations between 0.6 and 1.1 ppbv were observed. HCHO concentrations showed almost no deviation from the normal diel variation. However, another effect of the synoptic weather situation concealed the possible impact of extraordinary emissions. Unstable conditions reflected in the high values of the eddy diffusion coefficients (Fig. 5) prevented the development of a shallow nocturnal ABL, thus diluting the emitted amounts in a much deeper layer compared to other nights. While no measurements of the H_2O_2 and HCHO concentrations in the new snow of this event are available, previous measurements have revealed that in general new snow initially contains higher concentrations of both compounds compared to surface snow (Bales et al., 1995b) and that the concentrations drop rapidly within a few hours (Hutterli et al., 1999, 2001).

The emitted amount and the timing of the emission are analyzed to estimate the lability of both compounds in the new snow. This estimate can only constitute an upper limit since the higher snow temperature during the specific night (Fig. 5) could also cause enhanced emissions of deeper snow layers. Surface snow samples were taken on 1 July at 8:00 after the new snow event. We found H_2O_2 and HCHO concentrations of 12.1 and 0.65 μM in the top 1 cm of the snow and densities of 0.05 and 0.06 $g\,cm^{-3}$, respectively, corresponding to H_2O_2 and HCHO amounts of 3.6×10^{18} molecules m^{-2} and 2.3×10^{17} molecules m^{-2} after the emission during the past night. Adding the emitted amounts during the night (Table 1) leads to an estimate of the total amount in the new snow before precipitation resulting in 4.3×10^{18} molecules m^{-2} of H_2O_2 and 3.1×10^{17} molecules m^{-2} of HCHO. The comparison shows more than 25% of the HCHO amount, but $<16\%$ of the H_2O_2 amount was available for emission during the first night after precipitation indicating that a higher percentage of HCHO is present at the surface compared to H_2O_2.

Couch et al. (2000) demonstrated that the immediate release after snowfall can be attributed to the surface-bound component. Accordingly, a laboratory investigation of the uptake of H_2O_2 demonstrated that it is accumulated on the ice surface as well as incorporated into the bulk ice with an estimated upper limit of 20% present at the surface at –12.5°C (Conklin et al., 1993). This limit is slightly higher than the released amount obtained in our study, which also represents only an upper limit for the amount present at the surface layer since during the first hours after precipitation recrystallization occurs that also leads to the evaporation of part of the bulk ice crystals.

5. Conclusions

Long-term measurements revealed that HCHO concentrations in the ABL over the snowpack at Summit, Greenland follow a diel cycle similar to H_2O_2 diel variations with higher concentrations during the day and lower concentrations during the night. These diel variations are at least partly caused by bi-directional fluxes of both species between the atmosphere and the underlying snowpack indicating that the snow acts as a temporary reservoir during the course of a day. During this study the emitted and deposited amounts of H_2O_2 and HCHO nearly canceled each other during 24 h resulting in small net deposition of H_2O_2 and net emission of HCHO. Photochemistry as well as emission and deposition of H_2O_2 and HCHO must be taken into

account to reproduce diel variations in the ABL. Due to the importance of both compounds in tropospheric photochemistry the bi-directional exchange should be included in modeling studies undertaken to investigate photochemical processes above snow covered areas like O_3 depletion or halogen activation occurring in the polar ABL. Since no measurements of the ABL height and no measurements above the ABL were performed the role of changing mixing heights and entrainment from higher layers cannot be addressed. These measurements are necessary in future studies to establish a comprehensive budget of H_2O_2 and HCHO in the ABL in polar regions and to reproduce observed diel cycles.

New snow disturbs regular uptake and release processes leading to the emission of considerable quantities of H_2O_2 and HCHO into the ABL within hours after the beginning of the precipitation event. A rough analysis of the new snow event shows that more than 25% of the HCHO and almost 16% of the H_2O_2 incorporated in the new snow are available for rapid release after precipitation. Although a larger HCHO fraction was released, the emission maximum was delayed by several hours compared to H_2O_2.

Acknowledgements

Financial support by the National Science Foundation (NSF), grants OPP-9813442 and OPP-9813311, is gratefully acknowledged. HWJ thanks the Deutsche Forschungsgemeinschaft (DFG) for a research stipend. Moreover, NSF funded the participation of CK through the program Teachers Experiencing Antarctica and the Arctic (TEA). Assistance and equipment during the field experiments were provided by the Summit summer crew, VECO Polar Resources, the Air National Guard, and the University of Bern, Switzerland.

References

Ariya, P.A., Jobson, B.T., Sander, R., Niki, H., Harris, G.W., Hopper, J.F., Anlauf, K.G., 1998. Measurements of C_2–C_7 hydrocarbons during the polar sunrise experiment 1994: further evidence for halogen chemistry in the troposphere. Journal of Geophysical Research 103, 13169–13180.

Bales, R.C., McConnell, J.R., Losleben, M.V., Conklin, M.H., Fuhrer, K., Neftel, A., Dibb, J.E., Kahl, J.D.W., Stearns, C.R., 1995a. Diel variations of H_2O_2 in Greenland: a discussion of the cause and effect relationship. Journal of Geophysical Research 100, 18661–18668.

Bales, R.C., Losleben, M.V., McConnell, J.R., Fuhrer, K., Neftel, A., 1995b. H_2O_2 in snow, air and open pore space in firn at Summit, Greenland. Geophysical Research Letters 22, 1261–1264.

Barrie, L.A., Bottenheim, J.W., Schnell, R.C., Crutzen, P.J., Rasmussen, R.A., 1988. Ozone destruction and photochemical reactions at polar sunrise in the lower Arctic atmosphere. Nature 334, 138–141.

Barrie, L.A., Staebler, R., Toom, D., Georgi, B., den Hartog, G., Landsberger, S., Wu, D., 1994. Arctic aerosol size-segregated chemical observations in relation to ozone depletion during Polar Sunrise Experiment 1992. Journal of Geophysical Research 99, 25439–25451.

Bergin, M.H., Pandis, S.N., Davidson, C.I., Jaffrezo, J.-L., Dibb, J.E., Russell, A.G., Kuhns, H.D., 1996. Modeling of the processing and removal of trace gas and aerosol species by Arctic radiation fogs and comparison with measurements. Journal of Geophysical Research 101, 14465–14478.

Bottenheim, J.W., Barrie, L.A., Atlas, E., Heidt, L.E., Niki, H., Rasmussen, R.A., Shepson, P.B., 1990. Depletion of lower tropospheric ozone during Arctic spring: the Polar Sunrise Experiment 1988. Journal of Geophysical Research 95, 18555–18568.

Businger, J.A., Wyngaard, J.C., Izumi, Y., Bradley, E.F., 1971. Flux–profile relationships in the atmospheric surface layer. Journal of Atmospheric Sciences 78, 181–189.

Chance, K., Palmer, P.I., Spurr, R.J.D., Martin, R.V., Kurosu, T.P., Jacob, D.J., 2000. Satellite observations of formaldehyde over North America from GOME. Geophysical Research Letters 27, 3461–3464.

Conklin, M.H., Sigg, A., Neftel, A., Bales, R.C., 1993. Atmosphere–snow transfer for H_2O_2: microphysical considerations. Journal of Geophysical Research 98, 18367–18376.

Couch, T.L., Sumner, A.L., Dassau, T.M., Shepson, P.B., Honrath, R.E., 2000. An investigation of the interaction of carbonyl compounds with the snowpack. Geophysical Research Letters 27, 2241–2244.

Crawford, J., Davis, D., Olsen, J., Chen, G., Liu, S., Gregory, G., Barrick, J., Sachse, G., Sandholm, S., Heikes, B., Singh, H., Blake, D., 1999. Assessment of upper tropospheric HO_x sources over the tropical pacific based on NAS GTE/PEM data: net effect on HO_x and other photochemical parameters. Journal of Geophysical Research 104, 16255–16273.

Cullen, N., Steffen, K., 2001. Unstable near-surface boundary conditions in summer on top of the Greenland ice sheet. Geophysical Research Letters 28, 4491–4493.

De Serves, C., 1994. Gas phase formaldehyde and peroxide measurements in the Arctic atmosphere. Journal of Geophysical Research 99, 25391–25398.

Dyer, A.J., 1974. A review of flux–profile relationships. Boundary-Layer Meteorology 7, 363–372.

Fuhrer, K., Hutterli, M., McConnell, J.R., 1996. Overview of recent field experiments for the study of the air–snow transfer of H_2O_2 and HCHO. In: Wolff, E., Bales, R.C. (Eds.), Chemical Exchange between the Atmosphere and Polar Snow. NATO ASI Series I, Vol. 43. Springer, Berlin, pp. 307–318.

Helmig, D., Boulter, J., David, D., Birks, J., Cullen, N., Steffen, K., 2002. Ozone and meteorological boundary-layer conditions at Summit, Greenland. Atmospheric Environment 36, 2595–2608.

Honrath, R.E., Lu, Y., Peterson, M.C., Dibb, J.E., Arsenault, M.A., Cullen, N.J., Steffen, K., 2002. Vertical fluxes of NO_x, HONO and HNO_3 above the snowpack at summit, greenland. Atmospheric Environment 36, 2629–2640.

Hutterli, M.A., Röthlisberger, R., Bales, R.C., 1999. Atmosphere-to-snow-to-firn transfer studies of HCHO at Summit, Greenland. Geophysical Research Letters 26, 1691–1694.

Hutterli, M.A., McConnell, J.R., Stewart, R.W., Jacobi, H.-W., Bales, R.C., 2001. Impact of temperature-driven cycling of hydrogen peroxide (H_2O_2) between air and snow on the planetary boundary layer. Journal of Geophysical Research 106, 15395–15404.

Jaeglé, L., Jacob, D.J., Brune, W.H., Faloona, I., Tan, D., Heikes, B.G., Kondo, Y., Sachse, G.W., Anderson, B., Gregory, G.L., Singh, H.B., Pueschel, R., Ferry, G., Blake, D.R., Shetter, R.E., 2000. Photochemistry of HO_x in the upper troposphere at northern midlatitudes. Journal of Geophysical Research 105, 3877–3892.

Jenkin, M.E., Clemitshaw, K.C., 2000. Ozone and other secondary photochemical pollutants: chemical processes governing their formation in the planetary boundary layer. Atmospheric Environment 34, 2499–2527.

Jobson, B.T., Niki, H., Yokouchi, Y., Bottenheim, J., Hopper, F., Leaitch, R., 1994. Measurements of C_2–C_6 hydrocarbons during the Polar Sunrise 1992 Experiment: evidence for Cl atom and Br atom chemistry. Journal of Geophysical Research 99, 25355–25368.

Kaimal, J.C., Finnigan, J.J., 1994. Atmospheric Boundary Layer Flows: their Structure and Measurement. Oxford University Press, Cambridge.

Lee, M., Heikes, B.G., O'Sullivan, D.W., 2000. Hydrogen peroxide and organic hydroperoxide in the troposphere: a review. Atmospheric Environment 34, 3475–3494.

McConnell, J.C., Henderson, G.S., Barrie, L., Bottenheim, J., Niki, H., Langford, C.H., Templeton, E.M.J., 1992. Photochemical bromine production implicated in arctic boundary-layer ozone depletion. Nature 355, 150–152.

McConnell, J.R., Winterle, J.R., Bales, R.C., Thompson, A.M., Stewart, R.W., 1997a. Physically based inversion of surface snow concentrations of H_2O_2 to atmospheric concentrations at South Pole. Geophysical Research Letters 24, 441–444.

McConnell, J.R., Bales, R.C., Winterle, J.R., Kuhns, H., Stearns, C.R., 1997b. A lumped parameter model for the atmosphere-to-snow transfer function for hydrogen peroxide. Journal of Geophysical Research 102, 26809–26818.

Michalowski, B.A., Francisco, J.S., Li, S.-M., Barrie, L.A., Bottenheim, J.W., Shepson, P.B., 2000. A computer model study of multiphase chemistry in the Arctic boundary layer during polar sunrise. Journal of Geophysical Research 105, 15131–15145.

Mickle, R.E., Bottenheim, J.W., Leaitch, W.R., Evans, W., 1989. Boundary layer ozone depletion during AGASP-II. Atmospheric Environment 23, 2443–2449.

Neftel, A., Bales, R.C., Jacob, D.J., 1995. H_2O_2 and HCHO in polar snow and their relation to atmospheric chemistry. In: Delmas, R. (Ed.), Ice Core Studies of Global Biogeochemical Cycles, NATO ASI Series I, Vol. 30. Springer, Berlin, pp. 249–264.

Ramacher, B., Rudolph, J., Koppmann, R., 1999. Hydrocarbon measurements during tropospheric ozone depletion events: evidence for halogen atom chemistry. Journal of Geophysical Research 104, 3633–3653.

Riedel, K., Weller, R., Schrems, O., 1999. Variability of formaldehyde in the Antarctic troposphere. Physical Chemistry Chemical Physics 1, 5523–5527.

Rudolph, J., Fu, B.R., Thompson, A., Anlauf, K., Bottenheim, J., 1999. Halogen atom concentrations in the arctic troposphere derived from hydrocarbon measurements: impact on the budget of formaldehyde. Geophysical Research Letters 26, 2941–2944.

Sander, R., Vogt, R., Harris, G.W., Crutzen, P.J., 1997. Modeling the chemistry of ozone, halogen compounds, and hydrocarbons in the Arctic troposphere during spring. Tellus 49B, 522–532.

Seibert, P., Beyrich, F., Gryning, S.-E., Joffre, S., Rasmussen, A., Tercier, P., 2000. Review and intercomparison of operational methods for the determination of the mixing height. Atmospheric Environment 34, 1001–1027.

Shepson, P.B., Shirju, A.-P., Hopper, J.F., Barrie, L.A., Young, V., Niki, H., Dryfhout, H.J., 1996. Sources and sinks of carbonyl compounds in the Arctic Ocean boundary layer: Polar Ice Flow Experiment. Journal of Geophysical Research 101, 21081–21089.

Sigg, A., Staffelbach, T., Neftel, A., 1992. Gas phase measurements of hydrogen peroxide in Greenland and their meaning for the interpretation of H_2O_2 records in ice cores. Journal of Atmospheric Chemistry 14, 223–232.

Solberg, S., Schmidbauer, N., Semb, A., Strodal, F., Hov, Ø., 1996. Boundary layer ozone depletion as seen in the Norwegian Arctic in spring. Journal of Atmospheric Chemistry 23, 301–332.

Solberg, S., Dye, C., Walker, S.-E., Simpson, D., 2001. Long-term measurements and model calculations of formaldehyde at rural European monitoring sites. Atmospheric Environment 35, 195–207.

Staffelbach, T., Neftel, A., Stauffer, B., Jacob, D., 1991. A record of atmospheric methane sink from formaldehyde in polar ice cores. Nature 349, 603–605.

Sumner, A.L., Shepson, P.B., 1999. Snowpack production of formaldehyde and its effect on the Arctic troposphere. Nature 398, 230–233.

Thompson, A.M., Chappellaz, J.A., Fung, I.Y., Kucsera, T.L., 1993. The atmospheric CH_4 increase since the last glacial maximum, 2, interactions with oxidants. Tellus B 45, 242–357.

Weller, R., Schrems, O., Boddenberg, A., Gäb, S., Gautrois, M., 2000. Meridional distribution of hydroperoxides and formaldehyde in the marine boundary layer of the Atlantic (48°N–35°S) measured during the Albatross campaign. Journal of Geophysical Research 105, 14401–14412.

Yang, J., Honrath, R.E., Peterson, M.C., Dibb, J.E., Sumner, A.L., Shepson, P.B., Frey, M., Jacobi, H.-W., Swanson, A., Blake, N., 2002. Impacts of snowpack photochemistry on levels of OH and peroxy radicals at Summit, Greenland. Atmospheric Environment 36, 2523–2534.

Publication 3.2.6

Dassau, T.M., A.L. Sumner, S.L. Koeniger, P.B. Shepson, J. Yang, R.E. Honrath, N.J. Cullen, K. Steffen, H.-W. Jacobi, M. Frey, and R.C. Bales,

Investigation of the role of the snowpack on atmospheric formaldehyde chemistry at Summit, Greenland,

J.Geophys.Res. **107** (D19), 4394, doi:10.1029/2002JD002182, 2002.

Investigation of the role of the snowpack on atmospheric formaldehyde chemistry at Summit, Greenland

Terra M. Dassau, Ann Louise Sumner, and Stormy L. Koeniger
Department of Chemistry, Purdue University, West Lafayette, Indiana, USA

Paul B. Shepson
Department of Chemistry, Purdue University, West Lafayette, Indiana, USA
Department of Earth and Atmospheric Sciences, Purdue University, West Lafayette, Indiana, USA

Jie Yang and Richard E. Honrath
Department of Civil and Environmental Engineering, Michigan Technological University, Houghton, Michigan, USA

Nicolas J. Cullen and Konrad Steffen
Cooperative Institute for Research in Environmental Sciences, University of Colorado, Boulder, Colorado, USA

Hans-Werner Jacobi, Markus Frey, and Roger C. Bales
Department of Hydrology and Water Resources, University of Arizona, Tucson, Arizona, USA

Received 7 February 2002; revised 1 May 2002; accepted 10 June 2002; published 10 October 2002.

[1] Ambient gas-phase and snow-phase measurements of formaldehyde (HCHO) were conducted at Summit, Greenland, during several summers, in order to understand the role of air-snow exchange on remote tropospheric HCHO and factors that determine snowpack HCHO. To investigate the impact of the known snowpack emission of HCHO, a gas-phase model was developed that includes known chemistry relevant to Summit and that is constrained by data from the 1999 and 2000 field campaigns. This gas-phase-only model does not account for the high ambient levels of HCHO observed at Summit for several previous measurement campaigns, predicting approximately 150 ppt from predominantly CH_4 chemistry, which is ~25–50% of the observed concentrations for several years. Simulations were conducted that included a snowpack flux of HCHO based on HCHO flux measurements from 2000 and 1996. Using the fluxes obtained for 2000, the snowpack does not appear to be a substantial source of gas-phase HCHO in summer. The 1996 flux estimates predict much higher HCHO concentrations, but with a strong diel cycle that does not match the observations. Thus, we conclude that, although the flux of HCHO from the surface likely has a significant impact on atmospheric HCHO above the snowpack, the time–dependent fluxes need to be better understood and quantified. It is also necessary to identify the HCHO precursors so we can better understand the nature and importance of snowpack photochemistry. *INDEX TERMS:* 0322 Atmospheric Composition and Structure: Constituent sources and sinks; 0365 Atmospheric Composition and Structure: Troposphere—composition and chemistry; 1863 Hydrology: Snow and ice (1827); 3367 Meteorolgy and Atmospheric Dynamics: Theoretical modeling

Citation: Dassau, T. M., et al., Investigation of the role of the snowpack on atmospheric formaldehyde chemistry at Summit, Greenland, *J. Geophys. Res.*, *107*(D19), 4394, doi:10.1029/2002JD002182, 2002.

1. Introduction

[2] There has recently been considerable interest in air–snow exchange, as chemical species trapped in ice cores contain information regarding long-term changes in atmospheric composition [*Yang et al.*, 1997; *Haan and Raynaud*, 1998; *Stauffer*, 2000]. One of the important concerns about atmospheric change relates to the possibility that emissions of trace gases such as NO_x and VOCs may influence the oxidizing power of the atmosphere [*Thompson*, 1995] and thus, indirectly, impact changes in radiatively active gases, such as CH_4. Ice core formaldehyde (HCHO) can be used as a tool for estimating the historical oxidizing capacity of the atmosphere [*Staffelbach et al.*, 1991], i.e., as a proxy for OH radicals, the principal atmospheric oxidant. However, our understanding of factors that control polar atmospheric HCHO and thus air-snow-ice transfer is weak.

[3] Carbonyl compounds are oxidation products of hydrocarbons, and HCHO is a dominant carbonyl com-

0148-0227/02/2002JD002182$09.00

pound produced in this process [*Atkinson et al.*, 1999]. Methane oxidation is the largest source of HCHO in the remote troposphere [*Jaegle et al.*, 2001], as shown in reactions (1)–(5).

$$CH_4 + OH \rightarrow CH_3 + H_2O \quad (1)$$

$$CH_3 + O_2 \rightarrow CH_3OO \quad (2)$$

$$CH_3OO + HO_2 \rightarrow CH_3OOH + O_2 \quad (3)$$

$$CH_3OO + NO \rightarrow CH_3O + NO_2 \quad (4)$$

$$CH_3O + O_2 \rightarrow HCHO + HO_2 \quad (5)$$

[4] There is a considerable interest regarding carbonyl compounds in polar regions because the carbonyl compound data in glacial ice core records may be used to infer changes in the composition of the atmosphere [*Staffelbach et al.*, 1991] and they can be important sources and sinks of radicals [*Shepson et al.*, 1996; *Sumner and Shepson*, 1999]. HCHO photolysis, in this environment, is a very important source of HO_x (HO_2 and OH) radicals, as shown in reactions (6a)–(10) and given the rapid HO_2/OH interconversion shown in reactions (9)–(11).

$$HCHO + h\upsilon \rightarrow H_2 + CO \quad (6a)$$

$$\rightarrow H + CHO \quad (6b)$$

$$H + O_2 \rightarrow HO_2 \quad (7)$$

$$CHO + O_2 \rightarrow HO_2 + CO \quad (8)$$

$$HO_2 + NO \rightarrow OH + NO_2 \quad (9)$$

$$O_3 + HO_2 \rightarrow 2\,O_2 + OH \quad (10)$$

$$OH + CO(+O_2) \rightarrow CO_2 + HO_2 \quad (11)$$

[5] Recent measurements [*Fuhrer et al.*, 1996; *Hutterli et al.*, 1999; *Jacobi et al.*, 2002] show HCHO concentrations in the Summit, Greenland atmospheric boundary layer to be higher than can be predicted by photochemical models, implying that there must be a neglected HCHO source. *Hutterli et al.* [1999] discussed that fresh fallen snow and buried winter snowfall contain HCHO concentrations that are in excess of values that represent equilibrium with the atmosphere, and as a result, the snowpack emits HCHO. In the upper two meters of the snowpack, the HCHO concentration exhibits a maximum just below the surface and then decreases with depth, but with seasonal oscillations, showing winter maxima. HCHO concentrations in the firn air are always higher than in ambient air during the summer [*Fuhrer et al.*, 1996; *Hutterli et al.*, 1999]. It has also been shown that HCHO in surface snow can be photochemically produced, and that this contributes to the large atmospheric HCHO concentrations at the time of polar sunrise, near the Arctic Ocean [*Sumner and Shepson*, 1999; *Sumner et al.*, 2002]. It has been determined that snowpack nitrate ions can photolyze in the snowpack to produce oxidizing radicals, according to reactions (12) and (13) [*Honrath et al.*, 1999, 2000; *Dibb et al.*, 2002].

$$NO^-_{3(aq)} + h\upsilon \rightarrow NO_{2(aq)} + O^-_{(aq)} \quad (12)$$

$$O^-_{(aq)} + H_2O \rightarrow OH_{(aq)} + OH^-_{(aq)} \quad (13)$$

These reactions show that NO_x and HO_x radicals are produced in the snowpack condensed phase [*Honrath et al.*, 2000], and since HCHO is produced from OH radical oxidation of a wide variety of organic precursors [*Zhou and Mopper*, 1997], it is likely that HCHO can be photochemically produced in the snowpack. Actinic radiation is known to penetrate 10–20 cm into the snowpack and thus HCHO will also be photochemically destroyed [*King and Simpson*, 2001; *Peterson et al.*, 2002]. Photochemical processing of HCHO in the snowpack thus complicates the interpretation of ice core HCHO, as it takes several months for deposited species to be buried beneath the photic surface layer [*Peterson et al.*, 2002].

[6] In this paper, we employ field experiments and associated modeling to address the extent of our understanding of atmospheric HCHO above the snowpack at Summit, Greenland, including the nature of air-snow exchange processes and gas-phase photochemistry that may account for the ambient concentrations. Our overall goal is to ascertain the role of the snowpack on atmospheric HCHO chemistry.

2. Experimental Methods

[7] All new measurements presented in this paper were conducted on the Greenland ice sheet at the Summit, Greenland Environmental Observatory (38.4°W, 72.55°N, 3200 m elevation) during the summers of 1999 and 2000. Measurements of gas-phase HCHO were conducted from 27 June to 16 July 1999 and snow samples were collected from 5 June to 3 July 2000 and analyzed at the Purdue laboratory.

2.1. Gas-Phase HCHO Measurements

[8] In 1999, we conducted measurements of gas-phase HCHO, as well as measurements of HCHO in the firn air. Gas-phase HCHO was measured using a flow injection analysis instrument with fluorescence detection [*Fan and Dasgupta*, 1994; *Sumner et al.*, 2002], which was located in a wood enclosure built beneath the snowpack. Briefly, gas-phase HCHO was extracted into water through a 60 cm Nafion membrane diffusion scrubber and was reacted with 1,3-cyclohexanedione and ammonium acetate to produce a fluorescent product (emission at 465 nm). Gas-phase standards were generated from two permeation sources that yielded gas-phase concentrations in the 100–600 ppt and 1.8–8.0 ppb range after dilution, and were sampled every 2 hours during the field study. Monomeric HCHO was produced by passing a length of FEP Teflon tubing through solid paraformaldehyde in a heated (40°C) aluminum cylinder. A similar commercial gas-phase standard (Kin-Tek) used α-polyoxymethylene at 60°C to produce HCHO(g). The permeation rate of each device was determined using 2,4-dinitrophenylhydrazine (DNPH) derivatization and HPLC analysis [*Sirju and Shepson*, 1995].

Table 1. Summary of HCHO Measurement Methods for 1993 to 2000

Year	Chemical reaction	Scrubber used	Inlet height, m
1993	1,3-cyclohexanedione	Nafion membrane diffusion scrubber[a]	1
1994	1,3-cyclohexanedione	Nafion membrane diffusion scrubber[a]	1
1996	2,4-pentanedione	Wet effluent diffusion denuder[b]	1
1999	1,3-cyclohexanedione	Nafion membrane diffusion scrubber	1
2000	2,4-pentanedione	Coil scrubber[c]	1.52 or 1.43

[a] *Staffelbach et al.* [1997]. Due to the interference from H_2O_2, HCHO concentrations may be up to 20–30% high.
[b] *Hutterli et al.* [1999].
[c] *Jacobi et al.* [2002].

[9] The inlet line (PFA-Teflon) for gas-phase measurements was positioned 15 meters southeast of the sampling tower, where ambient air was sampled at a height 1 m above the snowpack. A second inlet line was also used during special experiments to allow for alternate sampling from two different locations. A Teflon filter pack (1 μm) was used to remove snow crystals and particulate matter from the ambient air. Data were excluded when snow crystals were found in the ambient sampling line. There is a known interference from H_2O_2 with this method [*Li et al.*, 2001] due to its reaction with cyclohexanedione to form a competing fluorescent product. The sensitivity to HCHO relative to H_2O_2 was determined to be 1:0.035 [*Sumner*, 2001], making the interference only important at low HCHO/H_2O_2 ratios. Because of the high HCHO levels measured at Summit in 1999, and an average H_2O_2 concentration of 1.6 ppb, the hydrogen peroxide interference was determined to be unimportant (ranging from 1 to 11% of the total signal with an average of 4%), compared to the measurement uncertainty. Our instrument has been successfully intercompared with a tunable diode laser (TDL), using the same calibration system, and has been shown to agree very well with a correlation coefficient of 0.95 [*MacDonald et al.*, 1998; *Sumner*, 2001] when the response of our instrument was plotted against the TDL-determined concentration (slope = 0.94 ± 0.03; intercept = 50 ± 40 ppt). For this experiment, however, contributions to the total signal were observed from the inlets, likely from degassing of HCHO from condensation on the inlet walls. This resulted in a high detection limit (3s) of 350 ppt, where the uncertainty in the measurements is approximately +30/−50%. The instrumental precision, based on replicate injections of a gas-phase standard, was ∼10%.

[10] In this paper, we compare computer model output not only to our 1999 measurements, but also to Summit data from 1993, 1994, 1996, and 2000 [*Fuhrer et al.*, 1996; *Hutterli et al.*, 1999; *Jacobi et al.*, 2002]. HCHO measurements for previous years were determined in a similar manner to 1999, as they all involved the reaction of a cyclic dione, in the presence of ammonium ions, to produce a fluorescent product. Table 1 shows a summary of the HCHO measurement methods.

[11] Snowpack interstitial air was sampled using a stainless steel probe, constructed by the Purdue University Jonathan Amy Facility for Chemical Instrumentation. The probe consisted of a 5.1 cm diameter stainless steel cylinder (supported by a perforated aluminum base), through which a length of 6.4 mm Teflon sample line was inserted, terminating at a Teflon filter pack (1 μm) mounted at the bottom of the tube. The probe was positioned by first making a hole in the snowpack with a second stainless steel tube, of the same dimensions. The probe was then inserted into the bored hole, minimizing the disturbance to the surrounding snowpack. A Type K (Chromel/Alomel) thermocouple was mounted at the tip of the probe and temperatures were monitored with a hand-held Omega digital readout.

2.2. Snow Sampling and Analysis

[12] In 2000, snow samples were collected at Summit and transported to Purdue University for determination of aldehydes, strong acid anions, carboxylic acids, and total organic carbon. Snow samples to be analyzed for total organic carbon (TOC) and aldehydes and ketones were collected in 30 mL and 250 mL glass jars, respectively, with Teflon-lined lids, while snow samples to be analyzed for strong acid anions and carboxylic acids were collected in 100 mL brown, opaque Nalgene high density polyethylene (HDPE) bottles. Sample bottles were precleaned by washing with soap, rinsing, and soaking in Millipore water overnight (repeated twice), followed by three additional rinses. Bottles were tested for leaching of anions, carboxylic acids, and HCHO and were found not to contaminate samples when allowed to remain below 0°C. Millipore water sent to Summit was used to fill identical bottles, which were then frozen and sent back to Purdue where they were analyzed to blank-correct all snow samples. Snow samples were collected from an HDPE tray designed to collect fresh snowfall, and from the surface of the snowpack. All samples remained frozen for the duration of the field study, during transport, and storage at the Purdue laboratory (less than 6 months before analysis).

[13] Snow sample aldehydes and ketones were determined using DNPH derivatization, and separation by high performance liquid chromatography (HPLC) with UV detection at 360 nm (Supelcosil LC-8 column, 25 cm × 4.6 mm ID, Waters 990). The snow samples were melted in a room temperature water bath. Once melted, a 5 mL aliquot of the sample was removed, 0.1 mL acidified DNPH (∼7 mM) was added, the contents were briefly shaken by hand, and reaction was allowed to proceed for 1 hour [*Keiber and Mopper*, 1990] before HPLC injection via a 500 μL sample loop. Gradient elution was conducted by mixing reservoir A (100% acetonitrile) and B (10% acetonitrile in water, pH 2.6), with a constant total flow rate of 1.5 mL min^{-1}. The program profile was as follows (%A/%B): 36/64 for 2 min, increasing to 50/50 over 4 min, constant at 50/50 for 8 min, then to 80/20 over 10 min, and then 100/0 for 20 min.

[14] Liquid-phase carbonyl compound standards were prepared by serial dilution of a HCHO solution standardized using the sodium sulfite method, as described by *Walker* [1964], and using pure aldehydes and ketones. However,

Table 2. Gas-Phase Reactions Used in the HCHO Photochemistry Model, With Rate Constants (second order in cm^3 $molecule^{-1}$ sec^{-1}, first order in sec^{-1} calculated for 255 K, P = 0.67 atm)

Reaction	k(T) or J
OH Reactions	
$OH + CH_4 \rightarrow CH_3OO$	2.39×10^{-15}[a]
$CH_3CH_3 + OH \rightarrow CH_3CH_2OO$	1.41×10^{-13}[a]
$HCHO + OH \rightarrow CO + HO_2$	9.30×10^{-12}[a]
$CH_3CHO + OH \rightarrow CH_3C(O)OO$	1.89×10^{-11}[a]
$CO + OH \rightarrow HO_2$	1.90×10^{-13}[a]
$OH + NO_2 \rightarrow HNO_3$	1.60×10^{-11}[b]
$OH + NO \rightarrow HONO$	3.60×10^{-11}[b]
$OH + HO_2 \rightarrow H_2O$	1.28×10^{-10}[b]
$OH + O_3 \rightarrow HO_2$	4.01×10^{-14}[b]
$HNO_3 + OH \rightarrow NO_3$	2.53×10^{-13}[b]
$OH + H_2 \rightarrow HO_2$	2.16×10^{-15}[b]
$CH_3OOH + OH \rightarrow HCHO + OH$	2.11×10^{-12}[a]
$CH_3OOH + OH = CH_3OO$	4.00×10^{-12}[a]
$H_2O_2 + OH \rightarrow HO_2$	1.55×10^{-12}[b]
$CH_3C(O)CH_3 + OH \rightarrow CH_3C(O)CH_2OO$	1.43×10^{-13}[a]
$C_2H_4 + OH \rightarrow 1.90\ HCHO$	9.00×10^{-12}[b]
$C_3H_6 + OH \rightarrow HCHO + CH_3CHO$	3.00×10^{-11}[b]
$CH_3C(O)OONO_2 + OH \rightarrow HCHO + NO_3$	3.00×10^{-14}[a]
$RO_2 + NO$ Reactions	
$CH_3OO + NO \rightarrow NO_2 + HCHO + HO_2$	8.56×10^{-12}[a]
$CH_3CH_2OO + NO \rightarrow NO_2 + CH_3CHO + HO_2$	1.11×10^{-11}[a]
$NO + HO_2 \rightarrow NO_2 + OH$	9.33×10^{-12}[b]
$CH_3C(O)OO + NO \rightarrow NO_2 + CH_3OO$	2.17×10^{-11}[b]
$CH_3C(O)CH_2OO + NO \rightarrow HCHO + CH_3C(O)OO + NO_2$	8.00×10^{-12}[c]
$RO_2 + RO_2$ Reactions	
$CH_3OO + CH_3OO \rightarrow CH_3OH + HCHO$	2.67×10^{-13}[a]
$CH_3OO + CH_3OO \rightarrow 2\ HCHO + 2\ HO_2$	1.07×10^{-13}[a]
$CH_3OO + HO_2 \rightarrow CH_3OOH$	8.09×10^{-12}[a]
$CH_3CH_2OO + HO_2 \rightarrow CH_3CH_2OOH$	1.30×10^{-12}[a]
$CH_3CH_2OO + CH_3OO \rightarrow CH_3CH_2OH + HCHO$	6.00×10^{-14}[d]
$CH_3CH_2OO + CH_3OO \rightarrow CH_3OH + CH_3CHO$	8.00×10^{-14}[d]
$CH_3CH_2OO + CH_3OO \rightarrow CH_3CHO + 2\ HO_2 + HCHO$	6.00×10^{-14}[d]
$CH_3OO + CH_3C(O)OO \rightarrow HCHO + HO_2 + CH_3OO$	6.39×10^{-12}[a]
$CH_3OO + CH_3C(O)OO \rightarrow CH_3C(O)OH + HCHO$	6.39×10^{-12}[a]
$CH_3CH_2OO + CH_3C(O)OO \rightarrow CH_3CHO + HO_2 + CH_3OO$	5.00×10^{-12}[a]
$CH_3CH_2OO + CH_3C(O)OO \rightarrow CH_3CHO + CH_3C(O)OH$	5.00×10^{-12}[a]
$CH_3C(O)OO + HO_2 \rightarrow CH_3C(O)OOH$	2.27×10^{-11}[b]
$2\ CH_3C(O)OO \rightarrow 2\ CH_3OO$	2.06×10^{-11}[a]
$CH_3C(O)CH_2OO + HO_2 \rightarrow CH_3C(O)CH_2OOH$	9.00×10^{-12}[e]
$RO_2 + NO_2$ Reactions	
$CH_3OO + NO_2 \rightarrow CH_3OONO_2$	7.50×10^{-12}[a]
$CH_3CH_2OO + NO_2 \rightarrow CH_3CH_2OONO_2$	8.80×10^{-12}[a]
$CH_3C(O)OO + NO_2 \rightarrow CH_3C(O)OONO_2$	1.39×10^{-11}[a]
$HO_2 + NO_2 \rightarrow HO_2NO_2$	5.90×10^{-12}[b]
RO_2NO_2 Reactions	
$CH_3OONO_2 \rightarrow CH_3OO + NO_2$	1.14×10^{-2}[a]
$CH_3CH_2OONO_2 \rightarrow CH_3CH_2OO + NO_2$	1.46×10^{-2}[a]
$CH_3C(O)OONO_2 \rightarrow CH_3C(O)OO + NO_2$	1.51×10^{-7}[a]
$HO_2NO_2 \rightarrow HO_2 + NO_2$	5.40×10^{-4}[e]
Misc. Reactions	
$O_3 + NO \rightarrow NO_2$	8.36×10^{-15}[e]
$O(^1D) \rightarrow O_3$	$5.69 \times 10^{+8}$[b]
$O(^1D) \rightarrow 2\ OH$	$7.47 \times 10^{+6}$[b]
$HO_2 + O_3 \rightarrow OH$	1.55×10^{-15}[b]
$2\ HO_2 \rightarrow H_2O_2$	2.42×10^{-12}[b]
$NO_2 + O_3 \rightarrow NO_3$	8.06×10^{-18}[b]
$NO_2 + NO_3 \rightarrow N_2O_5$	1.50×10^{-12}[b]
$N_2O_5 \rightarrow NO_2 + NO_3$	1.31×10^{-4}[e]
$NO + NO_3 \rightarrow 2\ NO_2$	2.92×10^{-11}[b]
Photolysis Reactions	
$NO_2 \rightarrow NO + O_3$	Variable[f]
$O_3 \rightarrow O(^1D)$	Variable[f]
$HONO \rightarrow OH + NO$	Variable[f]
$HCHO \rightarrow 2\ HO_2 + CO$	Variable[f]
$HCHO \rightarrow H_2 + CO$	Variable[g]
$NO_3 \rightarrow NO_2 + O_3$	Variable[h]
$NO_3 \rightarrow NO$	Variable[h]
$CH_3CHO \rightarrow CH_3OO + HO_2 + CO$	Variable[f]
$CH_3C(O)CH_3 \rightarrow CH_3OO + CH_3C(O)OO$	Variable[f]
$CH_3OOH \rightarrow OH + HO_2 + HCHO$	Variable[f]
$H_2O_2 \rightarrow 2\ OH$	Variable[f]
Emissions	
HONO	Variable[i]
HCHO	Variable[j]
H_2O_2	Variable[j]
Depositions	
HNO_3	8.00×10^{-5}[h]
N_2O_5	8.00×10^{-5}[h]
HCHO	Variable[j]
H_2O_2	Variable[j]

[a] *Atkinson et al.* [1999].
[b] *DeMore et al.* [1997].
[c] *Sehested et al.* [1998].
[d] *Villeneuve and Lesclaux* [1996].
[e] *Atkinson et al.* [1997].
[f] Curve fitting and interpolation of *Yang et al.* [2002] values.
[g] Scaling of JHCHO1 from *Simpson et al.* [2002] equations and JHCHO2.
[h] Scaled from or based upon the *Michalowski et al.* [2000] NO_3 and NO_2.
[i] Simulation of ambient concentrations.
[j] *Jacobi et al.* [2002].

HCHO was the only compound detected in snow above the method detection limit (5×10^{-8} M). The coefficient of variance for the method, as determined by analyzing repeated samples was 7%; whereas, for the triplicate sample analysis (which includes sample concentration variability), it was 44%.

[15] Strong acid anions (F^-, Cl^-, NO_3^-, and SO_4^{2-}), and carboxylic acid anions (lactate, acetate, propionate, formate, methylsulfonate, and oxalate) were determined in melted snow samples using ion chromatography (Dionex DX-500 IC, 200 μL sample loop). Samples were separated using a Dionex AS11 separation column and an AG11 guard column using a gradient program increasing from 0.2 mM NaOH to 38.25 mM NaOH over 20 min at a flow rate of 2 mL min^{-1}. Anions were detected via conductivity using a Dionex ASRS-Ultra II micromembrane suppressor in autorecycle mode. Calibrations were achieved by serial dilution of freshly prepared acid and anion standards.

[16] Snow-phase total organic carbon (TOC) was measured using an automated Shimadzu TOC-5000A analyzer with an ASI-5000A autosampler. TOC was calculated as the difference between measured total carbon and inorganic carbon, detected as CO_2 via nondispersive infrared absorption. The instrument determines total carbon by combustion of all organic material to CO_2 with the use of platinum on alumina catalyst at 680°C. Inorganic carbon was measured by acidifying all carbonates to CO_2 using 25% phosphoric acid. Solutions of potassium hydrogen phthalate and sodium carbonate/bicarbonate were used for total carbon and inorganic carbon standards, respectively. All analyzed samples were well above the instrument limit of detection of 50 μg L^{-1} for total carbon and 30 μg L^{-1} for inorganic carbon. The coefficient of the variance for the TOC measurements was 13% based on replicate analysis of the same sample and 50% based on triplicate sampling, which includes snowpack concentration variability and sampling artifacts.

Table 3. Initial Gas-Phase Concentrations for Model Species

Species	Initial concentration	Constant/variable
CH_4	1.8 ppm	Constant
CH_3CH_3	713 ppt	Constant
H_2	580 ppb	Constant
CO	114 ppb	Constant
O_3	40 ppb	Constant
$CH_3C(O)CH_3$	1.2 ppb	Constant
H_2O_2	452 ppt	Variable
HCHO	100 ppt	Variable
CH_3CHO	8 ppt	Variable
NO	7 ppt	Variable
NO_2	40 ppt	Variable
NO_3	10 ppt	Variable
HONO	2 ppt	Variable
C_2H_4	9 ppt	Constant
C_3H_6	6 ppt	Constant

2.3. Gas-Phase Photochemistry Model

[17] The zero-dimensional box model of atmospheric photochemistry was developed using the Chemical Reactions Modeling System (CREAMS) which improved on previous models [e.g., *Neftel et al.*, 1995] by constraining the model given time varying, measured gas-phase concentrations for many species on the basis of observations during the 1999 and 2000 field campaigns. Specifically, we included a flux of HONO from the snowpack as shown to occur by *Honrath et al.* [2002], in which the magnitude of the time varied flux (with a cosine dependence following radiation) was altered until the model simulated NO, NO_2, and HONO agreed with observations [*Dibb et al.*, 2002; Honrath et al., unpublished data]. The model incorporates methane, ethane, ethene, propene, and acetone chemistry and includes time varying photolysis rate constants for NO_2, O_3, NO_3, HONO, HCHO, H_2O_2, CH_3OOH, $CH_3C(O)CH_3$, and CH_3CHO, which were calculated based on radiation measurements [*Yang et al.*, 2002]. Adding the chemistry of other organic molecules measured at Summit (Swanson et al., unpublished data), such as methanol, at the highest measured concentration, does not contribute significantly to HCHO production. The 65 reactions included in this model are shown in Table 2, with the appropriate rate constants, calculated from Arrhenius expressions (where available) for T = 255K and P = 0.67 atm. Initial concentrations for simulated species are listed in Table 3. In general, species that were not produced in the model and have long lifetimes were input at constant concentrations; those that were reaction products and/or short-lived were allowed to vary.

3. Results and Discussion

3.1. Ambient HCHO Measurements

[18] Ambient air HCHO concentrations from 3 to 18 July 1999 are presented in Figure 1. H_2O_2 data are also presented as H_2O_2 is a product of HCHO photolysis from the HO_2 self-reaction and is thus related to HCHO. The range of observed HCHO concentrations was 300–1500 ppt, which is, on average, higher than previous measurements. Previous investigators reported HCHO concentrations in the range of 50–200 ppt [*Jacobi et al.*, 2002], 200–300 ppt [*Hutterli et al.*, 1999], and 200–600 ppt [*Fuhrer et al.*, 1996]. Although the estimated uncertainty in the 1999 measurements is relatively high, we believe the data reflect a real interannual difference in HCHO concentrations. As shown in Figure 1, H_2O_2 and HCHO concentrations appear to be correlated. Although both species exhibit a pronounced diel cycle early in this measurement period, the diel cycle is not consistently present. *Fuhrer et al.* [1996] and *Hutterli et al.* [1999] did not observe a diel cycle, but the most recent gas-phase measurements [*Jacobi et al.*, 2002] do indicate the presence of a diel cycle. On 3, 5, and 8 July, a pattern is evident that shows HCHO reaching a maximum concentration in the late morning/early afternoon. In Figure 2, these data are plotted along with radiation and

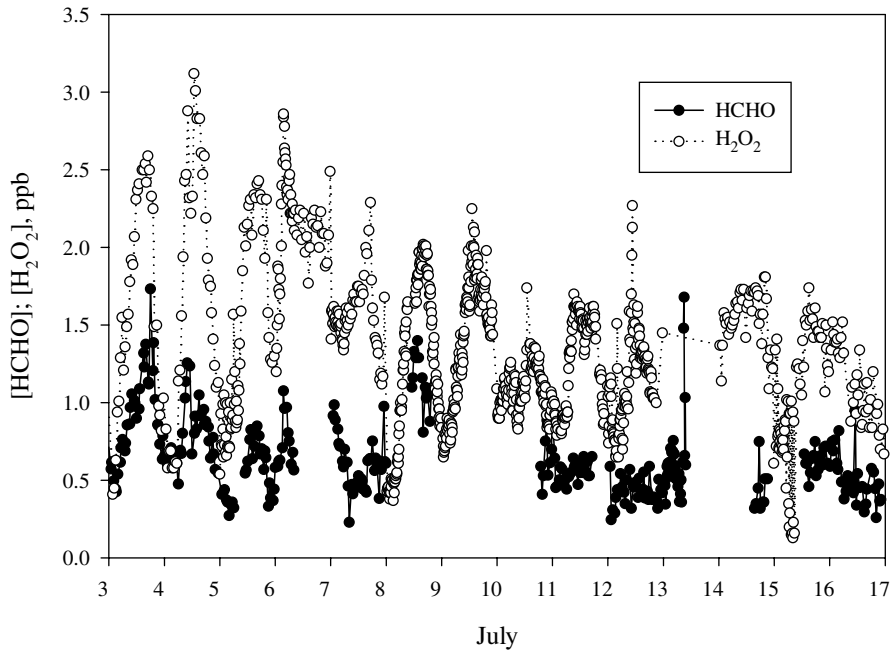

Figure 1. Ambient HCHO and H_2O_2 mixing ratios (in ppb) from 3 to 17 July 1999.

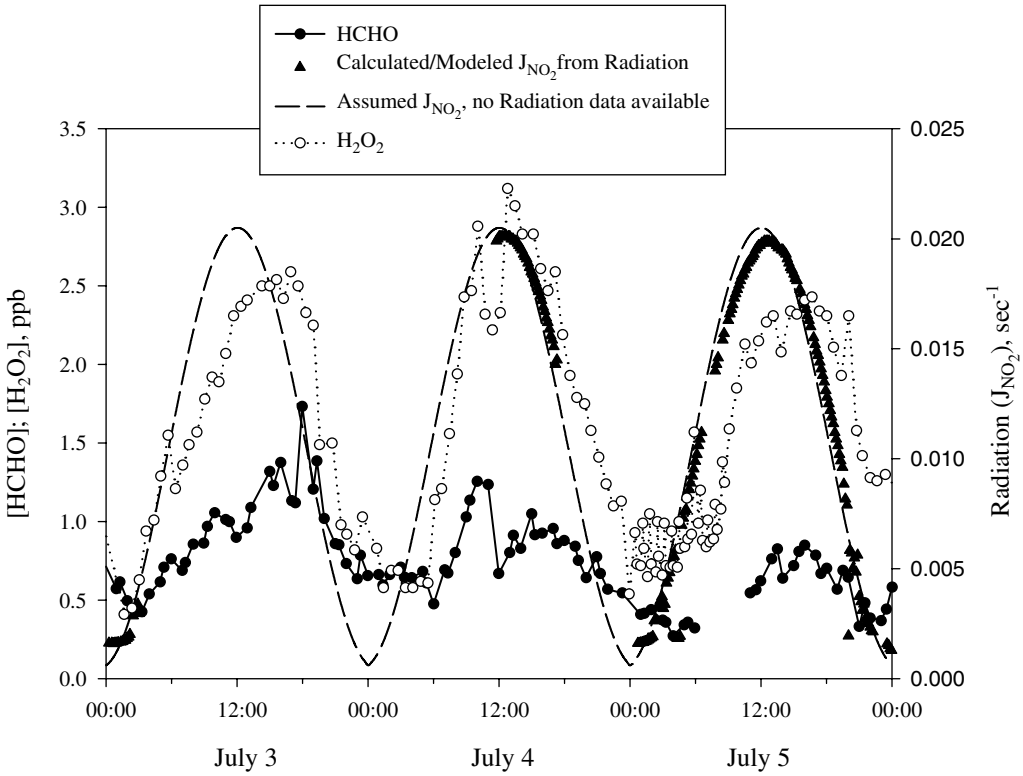

Figure 2. Ambient HCHO and H_2O_2 mixing ratios (in ppb) from 3 to 6 July 1999. Modeled relative radiation (scaled to measured radiation) is also plotted as J_{NO2}. Where measured radiation is not available, a best-fit estimate of the data is presented (dashed line).

H_2O_2 to show that their variability has a similar pattern to radiation (and temperature). NO_2 photolysis rate constants (J_{NO2}), calculated from radiation measurements [*Yang et al.*, 2002], are shown to represent radiation. On average, for these days, both HCHO and H_2O_2 maximize after solar noon.

[19] Using all available data for this time period, the 1999 HCHO concentrations were plotted against temperature and radiation measurements to determine the extent of their correlation. It was found that ambient HCHO correlated with both variables with correlation coefficients (r^2) of 0.50. It is important to note that, while the HCHO observations are high relative to those from other years, the same is true for H_2O_2. Previous investigations found ambient H_2O_2 at levels typically between 0.2 and 1.2 ppb, considerably lower than those shown in Figure 2 [*Fuhrer et al.*, 1996; *Jacobi et al.*, 2002]. The large concentration of H_2O_2 (in 1999) and correlation with HCHO is consistent with the fact that HCHO photolysis will be an important source of HO_2 radicals, as shown by reaction (14).

$$HO_2 + HO_2 \rightarrow H_2O_2 + O_2 \qquad (14)$$

3.2. Snowpack HCHO Processing and Snow Composition

[20] An important issue for interpretation of both gas-phase HCHO, as well as ice core concentrations is that of postdepositional photochemical processing. *Haan et al.* [2001] propose that photolysis of HCHO is a source of the photochemical production of CO from sunlit snow. The recent data by *Couch et al.* [2000] and *Burkhart et al.* [2002] imply that the HCHO–methylene glycol equilibrium in snow lies to the unhydrated side. If this is the case, it will be photolyzed on a timescale that is short (<1 day) relative to its burial time (~several months). As discussed by *Fuhrer et al.* [1996], *Sumner and Shepson* [1999], and *Sumner et al.* [2002], HCHO could be photochemically produced in the snowpack as well. Indeed, if HCHO can be photochemically destroyed in the surface snowpack condensed phase on timescales comparable to the gas-phase lifetime (i.e., a few hours), some photochemical production is necessary to sustain the observed condensed-phase concentrations.

[21] To examine the potential for photochemical production of HCHO in the snowpack, firn air measurements in 1999 were obtained with alternating ambient measurements to examine the relationship between snowpack gas-phase HCHO concentrations and the ambient concentrations above. The snowpack temperature was also measured from the tip of the snow probe sampling the firn air. To isolate the radiation variable, we used a 1 m × 2 m rectangular piece of Styrofoam to shade the snow surface. In this experiment, the Styrofoam was suspended approximately 15 cm above the snowpack surface, to shade the snowpack. This allowed for the control of radiation penetrating into the snowpack, without significantly affecting snowpack temperature or ventilation. In this experiment, as shown in Figure 3, ambient HCHO concentrations were constant, simplifying the analysis of the radiation impact. During this experiment, the HCHO concentrations in the firn air were greater (~5 times) than those in the ambient air aloft, implying a flux to the atmosphere throughout the day, in accord with previous

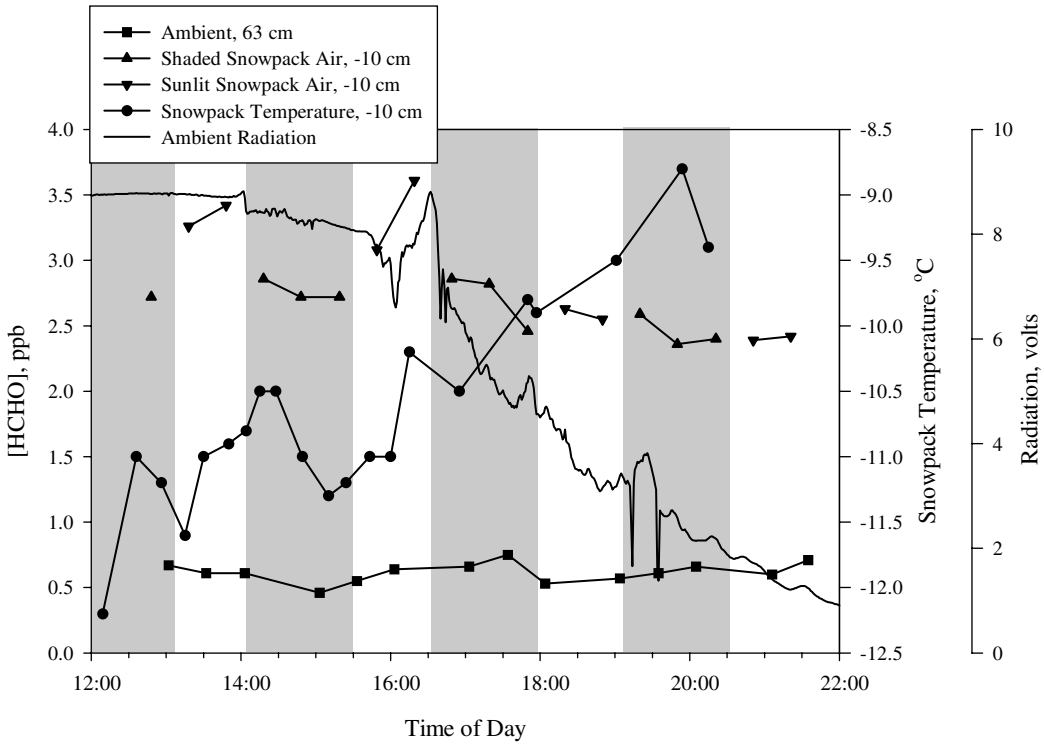

Figure 3. Firn air shading experiment, 15 July 1999. This plot shows the effect of shading and unshading the snow surface on snowpack air at −10 cm. Ambient HCHO (in ppb) is shown by the squares, and snowpack air HCHO (in ppb) is shown by the triangles (inverted triangles depict unshaded snowpack air and upright triangles depict shaded snowpack air). Radiation signal decreases throughout the measurement period and is shown by the solid line, whereas snowpack temperature (in °C) increases and is shown by the circles.

observations [*Fuhrer et al.*, 1996; *Hutterli et al.*, 1999; *Sumner and Shepson*, 1999; *Jacobi et al.*, 2002]. In the early afternoon, when radiation was high, covering and uncovering the snowpack produced a significant result: HCHO levels were higher when the snowpack was exposed to ambient radiation and decreased when this radiation was removed. Thus radiation induced a larger snowpack efflux of HCHO to the atmosphere. Comparable results were also obtained in 2000 for similar firn air experiments. At lower radiation levels (i.e., after 1800), this effect was not apparent. An interesting note is that the snowpack temperature increased throughout this experiment, while the covered snowpack air concentrations were slowly decreasing. Thus during these experiments, if thermal desorption were the cause of the short-timescale changes in the interstitial air HCHO concentrations, that desorption would have to occur from other depths (presumably lower) and diffuse to the inlet depth. The result shown in Figure 3 is more likely caused by snowpack photochemical production, a conclusion that is consistent with the results of *Sumner et al.* [2002] for Alert, Nunavut.

[22] HCHO and other carbonyl compounds can be produced from condensed-phase OH oxidation of organic matter, where the OH radicals may be produced from reactions (12) and (13). To better understand the chemistry, it is necessary to understand the composition of the organic material in the snow. With this in mind, we conducted measurements of the total organic carbon content of snow and determined the concentrations of snow-phase carboxylic acids and HCHO. On 6 June 2000, a sample was obtained immediately after a snow event. This is of interest, as the carbon in this snow will result mainly from what is incorporated in snowfall, rather than from dry deposition. For this particular snow sample, we found a total organic carbon content of 1.85 mg C L^{-1} and an inorganic carbon content of 1.08 mg C L^{-1}. Of that organic carbon, HCHO accounted for 1.93%, while the carboxylic acids and MSA accounted for 1.76% (1.18% acetate, 0.32% propionate, 0.21% formate, 0.03% MSA, 0.02% lactate). Thus, we can account for only ~4% of the total organic carbon content. This is the first attempt to account for the snowpack organic carbon budget at Summit. *Twickler et al.* [1986] measured organic carbon levels in the Greenland snowpack between 0 and 150 cm (~40 km southwest of Dye 3, 44.87°W, 65.01°N). Their average TOC concentration was 0.11 mg L^{-1}, with a range of 0.03–0.32 mg L^{-1}, lower than our measurements. It is clear that in order to understand the condensed-phase organic chemistry that leads to production of a wide variety of photochemical oxidation products, additional work is needed to characterize the nature and source of the organic matter in the snowpack. As in the gas phase, the snowpack could contain larger organic materials that can oxidize to produce HCHO. Large alkanes, aldehydes, alcohols, aromatics, and fulvic acids have been observed in Antarctic snow [*Desderi et al.*, 1998; *Cincinelli et al.*, 2001; *Calace et al.*, 2001] and other high alpine sites

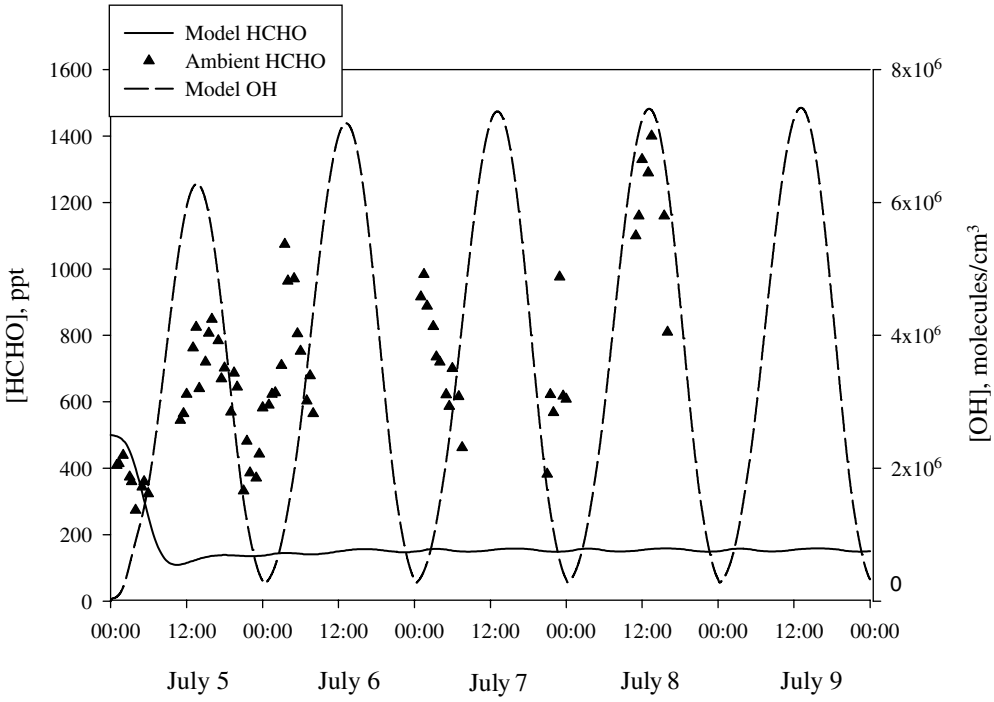

Figure 4. Five-day model simulation of HCHO at Summit, Greenland, 5 to 10 July 1999. Model output (solid line) is compared to 1999 HCHO mixing ratios (triangles, in ppt). Simulated OH is plotted as the dashed line (in molecules cm^{-3}).

[*Grollert and Puxbaum*, 2000], so it is reasonable to assume that significant HCHO precursors are also present in the snowpack at Summit.

3.3. Model Simulations

3.3.1. Base Photochemical Model

[23] To evaluate our understanding of Summit HCHO chemistry, we conducted a 5-day simulation corresponding to conditions during 5 to 9 July 1999 (chosen because of full data coverage), as shown in Figure 4. As discussed by *Dibb et al.* [2002], HONO levels are surprisingly high in the snowpack air (~80 ppt) as compared to ambient concentrations (~5–20 ppt, generally) and have a significant impact on ambient HO_x levels [*Yang et al.*, 2002] when released into the atmosphere. The simulated OH levels, shown in Figure 4, demonstrate a solar noon peak of $\sim 7 \times 10^6$ molecules cm^{-3}. These OH concentrations are higher than previously expected, but agree with calculations of *Yang et al.* [2002], who predict an OH maximum of 5×10^6 to 8×10^6 molecules cm^{-3}. As shown, the model yields a nearly constant HCHO concentration after ~1 day. The gas-phase-only model results in HCHO concentrations of 148–156 ppt. The observed 1999 gas-phase concentrations were as much as 5 times greater than those predicted by the model, assuming only gas-phase photochemical production. To thoroughly examine the model measurement comparison, we also present in Figure 5 all previously reported HCHO measurement data for Summit, shown as diel average concentrations. For each field campaign, the diurnally averaged atmospheric HCHO concentration data for the full measurement period are plotted. Modeled HCHO is lower than measured for all but the 2000 campaign (even without a snowpack flux of HCHO; for 2000, observed average [HCHO] = 125 ± 34, (N = 41) during the 1200–1300 time period), and are significantly lower than most of the 1993, 1994, and 1999 HCHO data. Specifically, the model simulation indicates a noon [HCHO] = 155 ppt and the observed diurnal average concentrations and variability (1s) are 404 ± 52 ppt (N = 13), 321 ± 89 ppt (N = 37), and 751 ± 290 ppt (N = 8), respectively for 1993, 1994, and 1999 between 1200 and 1300. The 1996 observed diurnal average is significantly higher than the model at some points, but not throughout the day (noon average = 215 ± 47 ppt, N = 5). These results imply that emission from the snowpack may significantly impact gas-phase concentrations. If gas-phase HCHO concentrations are determined in part by emission of various species from the snowpack, there could be significant interannual variability, at a minimum, because of variations in the HCHO flux, and the HONO flux. The HONO flux (which largely determines surface layer OH) will be dependent on the deposition rates for HNO_3 and particle/snow NO_3^- [*Honrath et al.*, 2000]. The base model, which does not include a contribution to HCHO from the snowpack, does not exhibit any diel cycle. The lack of a diel cycle is consistent with the 1996 data [*Hutterli et al.*, 1999] and the 10 to 17 July 1999 data. The 2000 data [*Jacobi et al.*, 2002] shows a diurnal variation in HCHO, which maximizes in the morning. This is not evident in the gas-phase base model and implies that if there is a diurnal cycle in gas-phase HCHO, it is not caused by known gas-phase photochemistry.

[24] Previous models predicted a summer, noontime HCHO concentration of ~90 ppt, and attributed the discrepancy between model prediction and ambient concentration to an underestimate of the HCHO sources [*Neftel et*

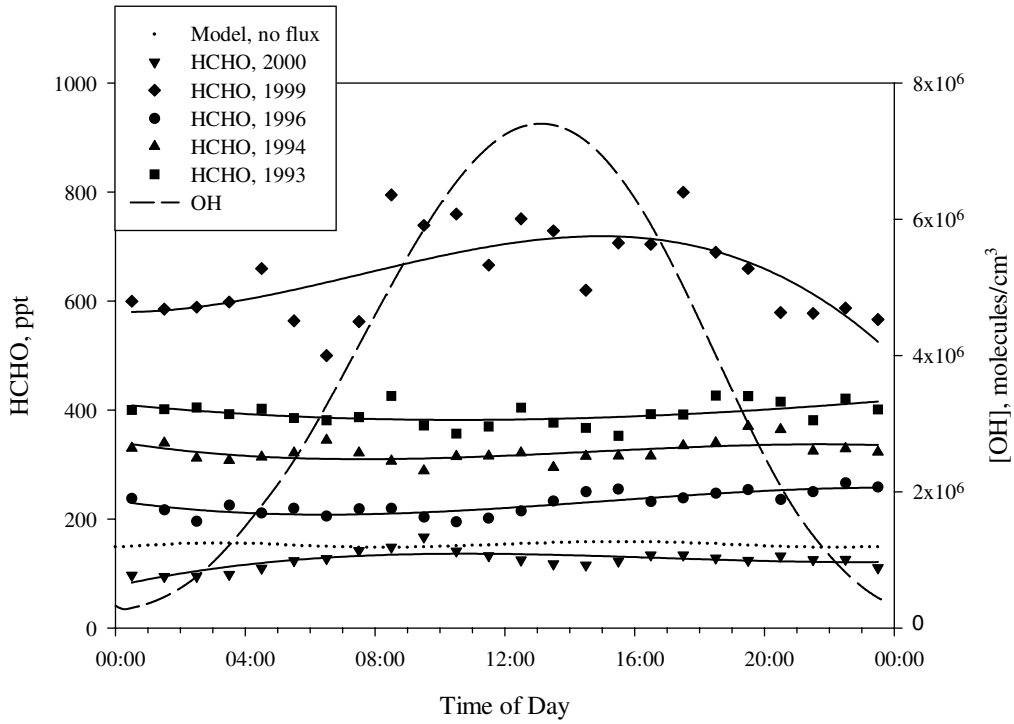

Figure 5. Comparison of modeled HCHO to 5 years of ambient data. Modeled HCHO is shown in this plot for 7 July 1999 (small dots). These values are compared to diel averages for all 5 years of HCHO data. The curves that correspond to each data set are cubic polynomial fits. In addition, OH (in molecules cm^{-3}) is shown for comparison.

al., 1995]. Our updated model predicts higher levels of gas-phase HCHO, at 156 ppt for the same season and time. The difference is largely due to the greater OH concentrations in this model, resulting from inclusion of HONO emission from the snowpack, and also to more efficient conversion of CH_3OO to CH_3O via NO (reaction (4)), resulting from NO_x emissions from the snowpack. To examine the relative importance of various HCHO sources, we calculated the rates of each reaction that produced HCHO in our model, from noon to 1300 on 7 July 1999, including the role of input via the surface flux. The results are shown in Table 4. Clearly CH_3OO, from the reaction of CH_4 + OH (reaction (1)), is the most important HCHO source in the model. Although CH_3OOH (methylhydroperoxide) oxidation is important, this species is also produced largely from CH_4 oxidation.

3.3.2. Snowpack Flux Estimates

[25] It is now well known that HCHO can efflux from the snowpack, particularly from fresh fallen snow [*Hutterli et al.*, 1999; *Houdier et al.*, 2002], and the data in Figure 3 suggest that snowpack photochemistry may enhance this flux. These two facts imply that the snowpack could be an important source of ambient HCHO, and may account for the difference in measurement and model predictions. Thus, we wish to use the measured HCHO fluxes from the snowpack to examine the effect of this additional HCHO source on gas-phase HCHO.

[26] *Hutterli et al.* [1999] reported HCHO fluxes ranging from 1.4×10^{12} to 8.8×10^{12} molecules m^{-2} sec^{-1}, as determined during the summer of 1996, based on five snow-phase HCHO gradient measurements conducted on different dates and times. However, the calculated fluxes were lower limits, and their best estimate average snowpack HCHO flux, determined via modeling, for June at Summit, Greenland was reported as 1.0×10^{13} molecules m^{-2} sec^{-1}. *Jacobi et al.* [2002] found the HCHO flux to be diurnally varying, and both emission and deposition of HCHO and H_2O_2 were shown to occur from and to the snowpack. This is consistent with the results of *Grannas et al.* [2002]. In

Table 4. Relative Production Rates for HCHO from the Gas-Phase Model Between Solar Noon and 1300 (top)

Sources of HCHO from model output	
Reactants	% of total HCHO production
CH_3OO + NO	78.7
CH_3OOH + OH	5.52
C_2H_4 + OH	5.34
CH_3OOH + hv	4.13
C_3H_6 + OH	3.29
$CH_3C(O)CH_3$ + OH	2.33
CH_3OO + CH_3OO	0.39
CH_3OO + $CH_3C(O)OO$	0.26
PAN + OH	0.06
CH_3OO + CH_3CH_2OO	0.00
Sources of CH_3OO from model output	
Reactants	% of total CH_3OO production
CH_4 + OH	77.0
CH_3OOH + OH	10.3
$CH_3C(O)OO$ + NO	7.07
$CH_3C(O)CH_3$ + hv	5.28
CH_3CHO + hv	0.36
2 $CH_3C(O)OO$	0.06
CH_3CH_2OO + $CH_3C(O)OO$	0.00

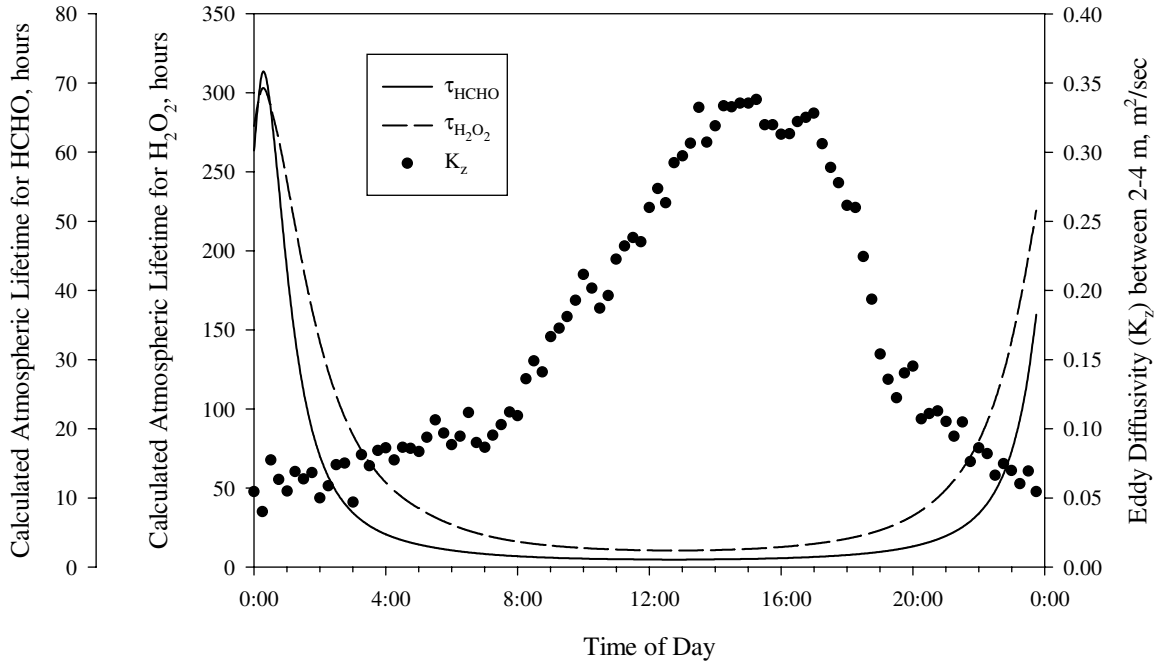

Figure 6. Diurnal variation of atmospheric lifetime and eddy diffusivity. Calculated atmospheric lifetime is plotted for HCHO (solid line, in hours) and H_2O_2 (dashed line, in hours). The points represent the eddy diffusivity calculated between 2 and 4 m (in m^2 sec^{-1}).

addition, *Perrier et al.* [2002] propose that photochemical production of HCHO can occur within the snowpack causing an immediate release of HCHO to the atmosphere. This would result in a diel cycle consistent with the *Jacobi et al.* [2002] findings. To translate these flux values to volumetric fluxes, for use in our 0-D model, we assumed an appropriate atmospheric mixing height. At Summit, in July, potential temperature generally increases with altitude, a condition that inhibits convective mixing [*Helmig et al.*, 2002]; however, shortly after the short-wave radiation reaches its maximum value, unstable conditions can occur, as discussed by *Cullen and Steffen* [2002] for the Summit 2000 experiment. But, because the mixing time through the boundary layer can considerably exceed the lifetimes of photochemically active species, under all stability conditions, the concept of a ''mixed layer'' is inaccurate (e.g., for HCHO). In our model, we invoke the concept of ''effective mixing height,'' defined as the vertical scale a particular species can diffuse over one lifetime. This calculation is time and species dependent, as it relies on the lifetime of the particular species and the eddy diffusivity. To simulate the impact of emission of these species using our model, we calculated a volumetric flux, $F_v = F_z/Z_i$, where Z is the effective mixing height for species i, i.e., $Z_i = (K_z \tau_i)^{1/2}$. For this calculation, we assume that an emitted species mixes vertically over a spatial scale equivalent to the distance it can diffuse in one lifetime [*Guimbaud et al.*, 2002]. Here τ_i is the calculated time varying atmospheric lifetime of species i, and Kz is the time-varying eddy diffusivity (the minimum lifetime is 1.1 hours for HCHO and 10.5 hours for H_2O_2 at 1245 local time). For this calculation, diurnally varying eddy diffusivity values (K_z) were determined for heights between two and four meters, as described by *Honrath et al.* [2002]. The K_z values are shown in Figure 6, along with time varying lifetimes for HCHO and H_2O_2. A complication with this method is that the eddy diffusivity measurements may be underestimated, as we are using values obtained for two to four meters as representative of those over the full effective mixing height. Thus the calculated effective mixing heights may be low (or in other words, our volumetric input rates may be too large), since eddy diffusivities increase with altitude. Thus effective mixing heights used are lower limits, and the volumetric input rates are upper limit values. We calculated volumetric fluxes for HCHO and H_2O_2 from the time varying flux measurements of *Jacobi et al.* [2002], and using the calculated Z_i's, which are shown in Figure 7. The H_2O_2 flux was then included in our model as time varying, zero-dimensional emission and deposition rates, and the model output was determined with and without the HCHO flux. The resulting fluxes are plotted for both species in Figure 7, where positive numbers represent emission from the snowpack and negative numbers represent deposition. Also shown is the flux used by *Hutterli et al.* [1999] in their modeling, scaled to an average of 1.0×10^{13} molecules m^{-2} sec^{-1} (with the same shape and deposition values as the *Jacobi et al.* [2002] flux) generated by multiplying the emission terms of the *Jacobi et al.* [2002] flux data by 11.6. This flux was then converted to a volumetric input rate based on our time varied effective mixing height. These two flux determinations, from which we calculated the volumetric fluxes required by our model, are the only two published determinations. Because of apparent interannual variability of fluxes (as seen from the large difference in magnitude between 1996 and 2000 flux measurements), we will examine each of the 2 years separately and compare the

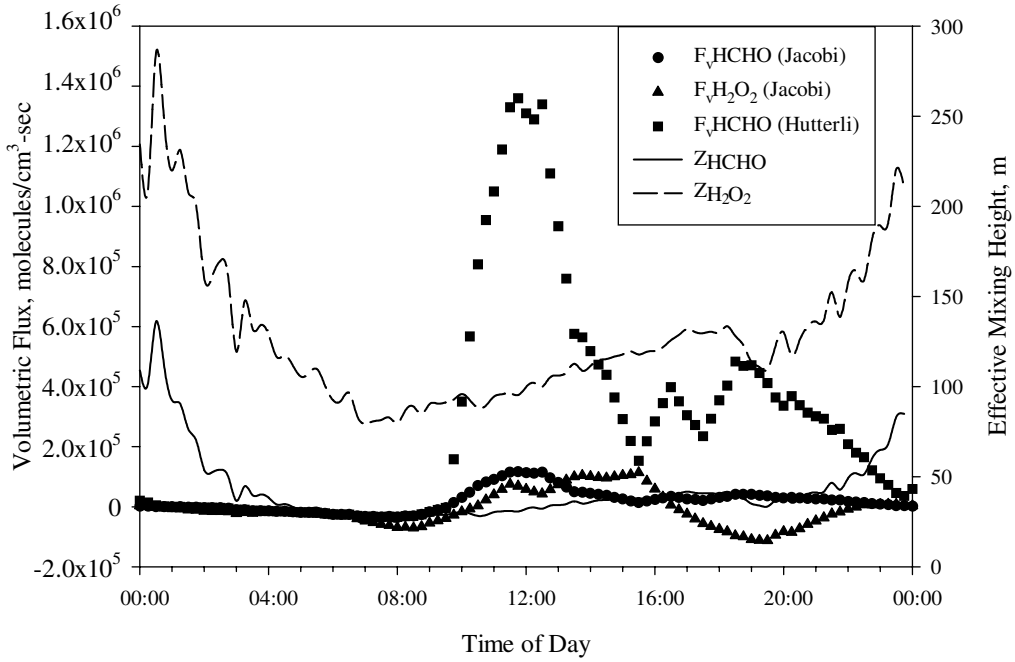

Figure 7. Diurnal variation of volumetric flux and mixing height. The two lines represent effective mixing height for HCHO (solid line) and H_2O_2 (dashed line). The symbols represent determinations of volumetric flux based upon the mixing heights plotted in this figure. The circles are the HCHO flux measured in 2000, the triangles are the H_2O_2 flux measured in 2000 [*Jacobi et al.*, 2002], and the squares are the HCHO flux used to model the 1996 field season [*Hutterli et al.*, 1999]. For the fluxes, positive numbers represent emission from the snowpack and negative numbers represent deposition.

model predictions to both the diurnal average for that year and to a representative day for each field campaign.

3.3.3. Case 1: Summer 2000

[27] Figure 8 (top) shows the model simulations and data for the 2000 field campaign, using the 2000 measured snowpack fluxes [*Jacobi et al.*, 2002]. 18 June 2000 was chosen as a representative day as it possesses a diel cycle consistent with the calculated average, has concentrations in the range of the majority of the data, and has good data coverage. Even without the addition of a flux, the model overestimates HCHO, as compared to the ambient data. When the 2000 flux is added, the simulated HCHO exhibits more of a diel cycle, maximizing right after noon and minimizing in the morning. This is inconsistent with the diel cycle observed in the ambient data, which shows a maximum in the morning, where the model predicts the lowest HCHO concentration, due to nighttime snowpack uptake. The addition of the flux also does not substantially increase HCHO concentration, but does contribute to the early afternoon peak. Between noon and 1300, the snowpack flux contribution to atmospheric HCHO production is 13%, with methane oxidation remaining the dominant HCHO precursor.

3.3.4. Case 2: Summer 1996

[28] As a first estimate of the HCHO flux for the 1996 campaign, we used the *Hutterli et al.* [1999] model flux value, 1.0×10^{13} molecules m^{-2} sec^{-1}, as an average flux for the month of June, scaled to the same diurnal profile found in 2000 and converted to a volumetric flux as before. Although *Hutterli et al.* [1999] did not detect or discuss a diurnally varying HCHO flux, since the *Jacobi et al.* [2002] flux is similar in shape to the diel cycle of temperature, it is reasonable to assume that the flux profile is similar year-to-year. The model results and ambient data are shown in Figure 8 (bottom). 14 June 1996 was chosen as a representative day because it had good data coverage, no diel cycle (consistent with the results of *Hutterli et al.* [1999]) and had concentrations in the range of the majority of the data (although slightly smaller than the diurnal average concentrations). For 14 June 1996, the gas-phase base model does a good job of accounting for the ambient HCHO concentrations. However, adding the diurnally varying *Hutterli et al.* [1999] best estimate flux predicts much higher daytime concentrations of HCHO, specifically a noon maximum of ~400 ppt. Between noon and 1300, the model predicts a snowpack flux contribution to atmospheric HCHO production of 64%. At all other times of the day, gas-phase photochemical production is a more important source than is the snowpack. The model also predicts a large diel cycle for HCHO, maximizing right after noon. The magnitude of the maximum HCHO concentrations and the presence of a diurnal variation in HCHO are both inconsistent with the 1996 data. Interestingly, the model output is more consistent in shape with the data shown in Figure 2 for 1999 (i.e., HCHO maximizes right after noon).

[29] As a diurnally varying snowpack flux for HCHO was not specifically observed in 1996, we also applied the *Hutterli et al.* [1999] flux as a constant input for comparison. Thus in Figure 8, we also show the simulated HCHO using the *Hutterli et al.* [1999] average value as a constant flux (but varying volumetric input rate, due to the time

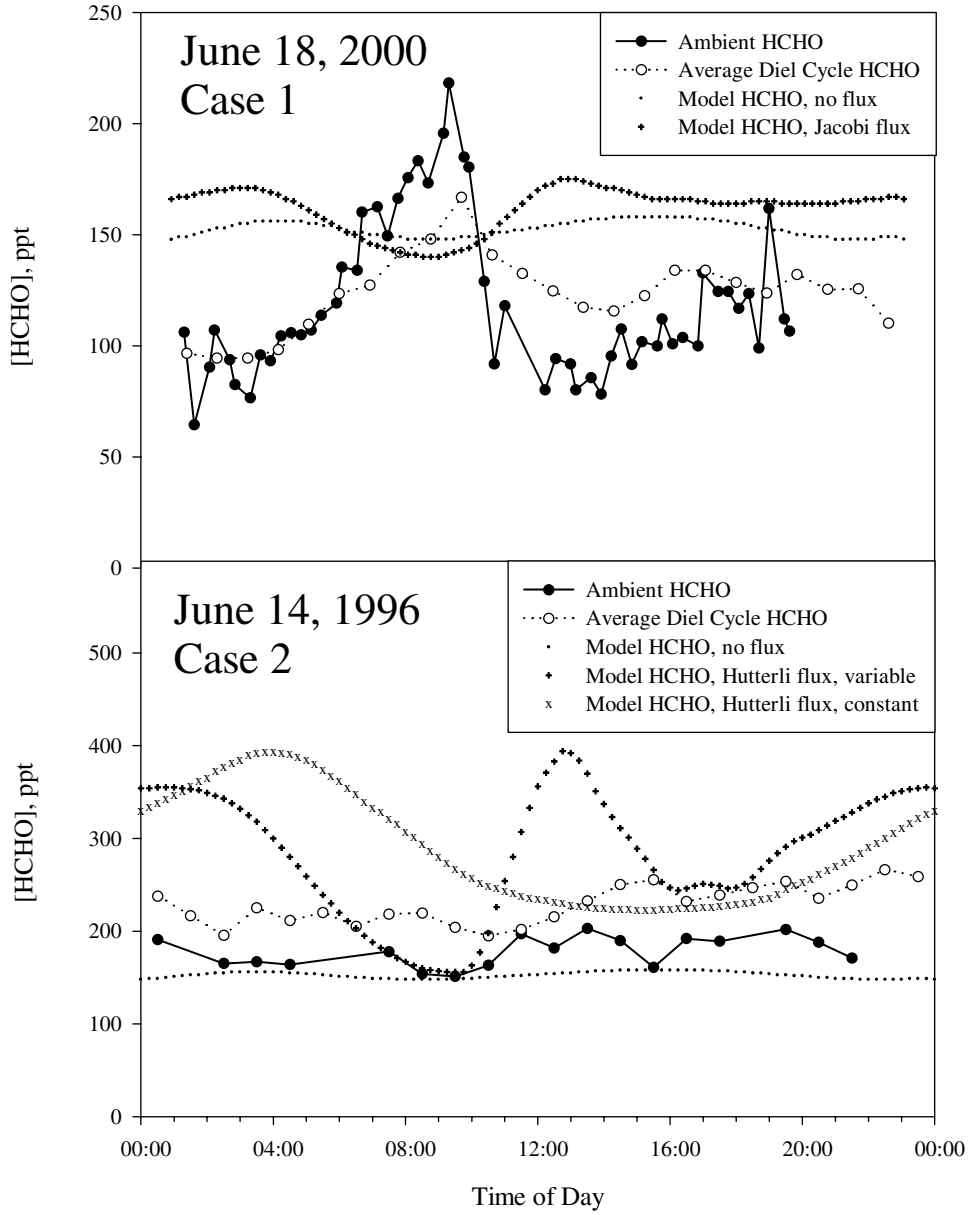

Figure 8. Comparison of measured and simulated HCHO for 2000 and 1996. Modeled HCHO is shown without a snowpack flux (small dots), with the *Jacobi et al.* [2002] flux (Case 1-2000, crosses), with the *Hutterli et al.* [1999] average flux scaled to the shape of the *Jacobi et al.* [2002] flux (Case 2-1996, crosses), and the *Hutterli et al.* [1999] average flux as a constant input (Case 2-1996, x symbols). Ambient data from representative days of each field campaign (solid circles) and the average diel cycle for each field campaign (open circles) are also shown.

varying effective mixing height). In both cases, the 24-hour integrated HCHO flux is the same. With this treatment, the model predicted a HCHO maximum of 400 ppt in the early morning, roughly twice that observed, and a broad minimum in the early afternoon. For both flux treatments, the early morning maximum predicted is inconsistent with the observations. For this simulation, the snowpack efflux contribution to atmospheric HCHO production between noon and 1300 is much lower, at 12%.

3.3.5. Discussion

[30] It is clear with these two cases that although the combination of gas-phase photochemistry and snowpack flux can account for the average observed concentrations, our model does not capture the diel cycle in HCHO observed in some, but not all, of the data sets. Although we used the June average best estimate flux from the work of *Hutterli et al.* [1999], the actual calculated fluxes ranged from 1.4×10^{12} to 8.8×10^{12} molecules m^{-2} sec^{-1}, which were estimated from measurements of the concentrations gradient in the firn air. The *Jacobi et al.* [2002] diel average flux was 6.9×10^{11} molecules m^{-2} sec^{-1}, an order of magnitude smaller. If these two studies are correct, there must be a large interannual variability in HCHO flux. The flux of HCHO from the snowpack is dependent on both

temperature and snowpack HCHO concentration, as well as snow grain physical and chemical morphology. Comparing ambient temperature to HCHO concentration for all years shows no correlation between the two variables (within each measurement period). In addition, the average temperatures for all 5 years are similar, with a standard deviation of the average of 1.9°C. In fact, in 1996, temperature increased throughout the study (by ~15°C), and the gas-phase HCHO concentration did not correlate with this change. Surface snowpack HCHO concentrations for the 5 years compared here are also similar [*Fuhrer et al.*, 1996; *Hutterli et al.*, 1999; *Jacobi et al.*, 2002]. However, as discussed by *Hutterli et al.* [1999], assessment of the impact of desorption-driven flux requires knowledge of the vertical distribution of HCHO throughout the top ~1 meter of the snowpack. It is clear that much more flux measurement data is needed to enable quantitative and predictive understanding of the relationships between snowpack temperature, composition, radiation, and HCHO fluxes.

[31] The discrepancy between the observations and both model simulations imply that we do not yet fully understand gas-phase HCHO chemistry at Summit. Although it is possible that the snowpack HCHO flux is highly variable, it is also possible that we are missing a gas-phase photochemical source term. In support of this argument, *Singh et al.* [2001] reported large concentrations of oxygenated organic compounds in the remote troposphere. They found, among other compounds, high levels of methanol (~900 ppt) and methylhydroperoxide (~1 ppb; our model only predicts ~120 ppt), both of which are HCHO precursors. HCHO precursors, such as methylhydroperoxide, are in turn likely produced from oxidation of larger unidentified organic precursors, which could also produce HCHO directly. There is a wide range of potential sources; as an example, *Warneke et al.* [1999] reported that abiotic decay of biomass produces products such as HCHO, CH_3CHO, $CH_3C(O)CH_3$, and CH_3OH. If atmospheric particulate matter contains biosphere-derived components, heterogeneous oxidation (e.g., via O_3) of that organic particulate matter could be a possible HCHO source. A variety of large organic molecules can be oxidized to produce HCHO. It has been hypothesized that oxygenated VOCs can be produced by ozonolysis of unsaturated fatty acids incorporated in inverted micelle aerosols [*Ellison et al.*, 1999]. This could allow for the transport of carbonyl compound precursors to remote environments and the free troposphere, such as Summit. Our snowpack analytical data make it clear that we do not understand the sources of organic carbon to the Summit surface. Thus, there is a great need for analytical work with respect to the organic composition in both the gas and the snowpack phases.

4. Conclusions

[32] The model simulations of ambient HCHO using 1996 and 2000 HCHO flux measurement data show conflicting results that do not simulate (and often underpredict) ambient concentrations. The firn air experiment described here indicates that HCHO can be photochemically produced in the snowpack. However, the importance of this to the flux, and the snowpack and ambient HCHO concentrations is as yet unclear. The result for HCHO can now be taken in the context of recent reports of HCHO, CH_3CHO, and acetone production in the snowpack at Alert [*Guimbaud et al.*, 2002; *Grannas et al.*, 2002; *Boudries et al.*, 2002; *Sumner et al.*, 2002], as well as production of alkyl halides and alkenes at Summit [*Swanson et al.*, 2002], and CO production in Alpine snow [*Haan et al.*, 2001]. Indeed, it is very interesting that *Haan et al.* [2001] show that CO photoproduction is well correlated with snowpack TOC levels, and conclude that HCHO is likely a CO precursor. The *Swanson et al.* [2002] report makes it clear that the sunlit snowpack exhibits active and interesting organic photochemistry. In order to understand the production of HCHO in the snowpack, additional research into the nature of its precursors in the snowpack must be conducted. It is also clearly necessary to better quantify and understand environmental variables that influence the HCHO flux from the snowpack.

[33] **Acknowledgments.** We thank the Summit 1999 and 2000 summer crew, the Polar Ice Coring Office, the VECO Polar Resources, the 109th Air National Guard personnel, and the National Science Foundation (grant 9907376OPP) for support of this work. We also gratefully acknowledge Matt Arsenault for his help in obtaining the snow samples analyzed here and Aaron Swanson for helpful discussions.

References

Atkinson, R., D. L. Baulch, R. A. Cox, R. F. Hampson, J. A. Kerr, M. J. Rossi, and J. Troe, Evaluated kinetic and photochemical data for atmospheric chemistry: Supplement VI, *J. Phys. Chem. Ref. Data*, *26*, 1329–1499, 1997.

Atkinson, R., D. L. Baulch, R. A. Cox, R. F. Hampson, J. A. Kerr, M. J. Rossi, and J. Troe, Evaluated kinetic and photochemical data for atmospheric chemistry, organic species: Supplement VII, *J. Phys. Chem. Ref. Data*, *28*, 191–393, 1999.

Boudries, H., J. W. Bottenheim, C. Guimbaud, A. Grannas, P. B. Shepson, S. Houdier, S. Perrier, and F. Domine, Distribution and trends of oxygenated hydrocarbons in the high Arctic derived from measurements in the atmospheric boundary layer and interstital snow air during the ALERT 2000 field campaign, Alert 2000, *Atmos. Environ.*, *36*, 2573–2583, 2002.

Burkhart, J. F., M. Hutterli, and R. C. Bales, Partitioning of formaldehyde between air and ice at −35°C to −5°C, *Atmos. Environ.*, in press, 2002.

Calace, N., B. M. Petronio, R. Cini, A. M. Stortini, B. Pampaloni, and R. Udisti, Humic marine matter and insoluble materials in Antarctic snow, *Int. J. Environ. Anal. Chem.*, *79*, 331–348, 2001.

Couch, T. L., A. L. Sumner, T. M. Dassau, P. B. Shepson, and R. E. Honrath, An investigation of the interaction of carbonyl compounds with the snowpack, *Geophys. Res. Lett.*, *27*, 2241–2244, 2000.

Cincinelli, A., P. G. Desderi, L. Lepri, L. Checchini, M. Del Bubba, and R. Udisti, Marine contribution to the chemical composition of coastal and inland Antarctic snow, *Int. J. Environ. Anal. Chem.*, *74*, 283–299, 2001.

Cullen, N., and K. Steffen, Unstable near-surface boundary conditions in summer on top of the Greenland ice sheet, *Geophys. Res. Lett.*, *28*, 4491–4492, 2002.

DeMore, W. B., S. P. Sander, D. M. Golden, R. F. Hampson, M. J. Kurylo, C. J. Howard, A. R. Ravishankara, C. E. Kolb, and M. J. Molina, Chemical kinetics and photochemical data for use in stratospheric modeling: Evaluation number 12, *JPL Publ. 97-4*, 1–266, 1997.

Desderi, P. G., L. Lepri, R. Udisti, L. Checchini, M. Del Bubba, R. Cini, and A. Stortini, Analysis of organic compounds in Antarctic snow and their origin, *Int. J. Environ. Anal. Chem.*, *71*, 331–351, 1998.

Dibb, J. E., M. Arsenault, M. C. Peterson, and R. E. Honrath, Fast nitrogen oxide photochemistry in Summit, Greenland snow, *Atmos. Environ.*, *36*, 2501–2511, 2002.

Ellison, G. B., A. F. Tuck, and V. Vaida, Atmospheric processing of organic aerosols, *J. Geophys. Res.*, *104*, 11,633–11,641, 1999.

Fan, Q., and P. K. Dasgupta, Continuous automated determination of atmospheric formaldehyde at the parts per trillion level, *Anal. Chem.*, *66*, 551–556, 1994.

Fuhrer, K., M. Hutterli, and J. R. McConnell, Overview of recent field experiments for the study of the air-snow transfer of H_2O_2 and HCHO, in *Chemical Exchange Between the Atmosphere and Polar Snow*, NATO ASI, pp. 307–318, Springer-Verlag, New York, 1996.

Grannas, A. M., et al., Carbonyl compounds and surface photochemistry in the arctic marine boundary layer, *Atmos. Environ.*, *36*, 2733–2742, 2002.

Grollert, C., and H. Puxbaum, Lipid organic aerosol and snow composition at a high alpine site in the fall and the spring season and scavenging ratios for single compounds, *Water Air Soil Pollut.*, *117*, 157–173, 2000.

Guimbaud, C., et al., Snowpack processing of acetaldehyde and acetone in the Arctic atmospheric boundary layer, *Atmos. Environ.*, *36*, 2743–2752, 2002.

Haan, D., and D. Raynaud, Ice core record of CO variations during the last two millennia: Atmospheric implications and chemical interactions within the Greenland ice, *Tellus*, *50B*, 253–262, 1998.

Haan, D., Y. Zuo, V. Gros, and A. M. Brenninkmeijer, Photochemical production of carbon monoxide in snow, *J. Atmos. Chem.*, *40*, 217–230, 2001.

Helmig, D., J. Boulter, D. David, J. Birks, N. Cullen, K. Steffen, B. Johnson, and S. Oltmans, Ozone and meteorological boundary-layer conditions at Summit, Greenland during 3–21 June 2000, *Atmos. Environ.*, *36*, 2595–2608, 2002.

Honrath, R. E., M. C. Peterson, S. Guo, J. E. Dibb, P. B. Shepson, and B. Campbell, Evidence of NO_x production and release within the snowpack at Summit, Greenland, *Geophys. Res. Lett.*, *26*, 695–698, 1999.

Honrath, R. E., S. Guo, M. C. Peterson, M. P. Dziobak, J. E. Dibb, and M. A. Arsenault, Photochemical production of gas phase NO_x from ice crystal NO_3^-, *J. Geophys. Res.*, *105*, 24,183–24,190, 2000.

Honrath, R. E., Y. Lu, M. C. Peterson, J. E. Dibb, M. A. Arsenault, N. J. Cullen, and K. Steffen, Vertical fluxes of NO_x, HONO, and HNO_3 above the snowpack at Summit, Greenland, *Atmos. Environ.*, *36*, 2629–2640, 2002.

Houdier, S., S. Perrier, F. Domine, A. Cabanes, L. Legagneux, A. M. Grannas, C. Guimbaud, P. B. Shepson, H. Boudries, and J. W. Bottenheim, Acetaldehyde and acetone in the Arctic snowpack during the ALERT2000 field campaign: Snowpack composition, incorporation processes and atmospheric impact, *Atmos. Environ.*, *36*, 2609–2618, 2002.

Hutterli, M. A., R. Rothlisberger, and R. C. Bales, Atmosphere-to-snow-to-firn transfer studies of HCHO at Summit, Greenland, *Geophys. Res. Lett.*, *26*, 1691–1694, 1999.

Jacobi, H. W., M. M. Frey, M. A. Hutterli, R. C. Bales, O. Schrems, N. J. Cullen, K. Steffen, and C. Koehler, Measurements of hydrogen peroxide and formaldehyde exchange between the atmosphere and surface snow at Summit, Greenland, *Atmos. Environ.*, *36*, 2619–2628, 2002.

Jaegle, L., D. J. Jacob, W. H. Brune, and P. O. Wennberg, Chemistry of HO_x radicals in the upper troposphere, *Atmos. Environ.*, *35*, 469–489, 2001.

Keiber, R. J., and K. Mopper, Determination of picomolar concentrations of carbonyl compounds in natural waters, including seawater, by liquid chromatography, *Environ. Sci. Technol.*, *24*, 1477–1481, 1990.

King, M. D., and W. R. Simpson, Extinction of UV radiation in Arctic snow at Alert, Canada (82 degrees N), *J. Geophys. Res.*, *106*, 12,499–12,507, 2001.

Li, J., P. K. Dasgupta, Z. Genfa, and M. A. Hutterli, Measurement of atmospheric formaldehyde with a diffusion scrubber and light-emitting diode: Liquid-core waveguide based fluorometry, *Field Anal. Chem. Technol.*, *5*, 2–12, 2001.

MacDonald, A. M., et al., Results of a formaldehyde intercomparison study in Ontario, paper presented at Am. Geophys. Union Fall Meet., San Francisco, Calif., 6–12 December 1998.

Michalowski, B., J. S. Francisco, Y. Li, S. M. Li, and P. B. Shepson, A study of multiphase chemistry in the Arctic boundary layer during polar sunrise, *J. Geophys. Res.*, *105*, 15,131–15,145, 2000.

Neftel, A., R. C. Bales, and D. J. Jacob, H_2O_2 and HCHO in polar snow and their relation to atmospheric chemistry, in *Ice Core Studies of Global Biogeochemical Cycles*, NATO ASI, pp. 249–264, Springer-Verlag, New York, 1995.

Perrier, S., S. Houdier, F. Domine, A. Cabanes, L. Legagneux, A. L. Sumner, and P. B. Shepson, Formaldehyde in Arctic snow. Incorporation into ice particles and evolution in the snowpack, *Atmos. Environ.*, *36*, 2695–2705, 2002.

Peterson, M., D. Barber, and S. Green, Monte Carlo modeling and measurement of actinic flux levels in Summit, Greenland snowpack, *Atmos. Environ.*, *36*, 2541–2551, 2002.

Sehested, J., L. K. Christensen, O. J. Nielsen, M. Bilde, T. J. Wallington, W. F. Schneider, J. J. Orlando, and G. S. Tyndall, Atmospheric chemistry of acetone: Kinetic study of the $CH_3C(O)CH_2O_2$ + NO/NO_2 reactions and decomposition of $CH_3C(O)CH_2O_2NO_2$, *Int. J. Chem. Kinet.*, *30*, 475–489, 1998.

Shepson, P. B., A. P. Sirju, J. F. Hopper, L. A. Barrie, V. Young, H. Niki, and H. Dryfhout, Sources and sinks of carbonyl compounds in the Arctic Ocean boundary layer: Polar Ice Floe Experiment, *J. Geophys. Res.*, *101*, 21,081–21,089, 1996.

Simpson, W. R., M. D. King, H. J. Beine, R. E. Honrath, and X. Zhou, Radiation-transfer modeling of snowpack photochemical processes during ALERT 2000, *Atmos. Environ.*, in press, 2002.

Singh, H., Y. Chen, A. Staudt, D. Jacob, D. Blake, B. Heikes, and J. Snow, Evidence from the Pacific troposphere for large global sources of oxygenated organic compounds, *Nature*, *410*, 1078–1081, 2001.

Sirju, A. P., and P. B. Shepson, A laboratory and field investigation of the DNPH cartridge technique for the measurement of atmospheric carbonyl compounds, *Environ. Sci. Technol.*, *29*, 384–392, 1995.

Staffelbach, T., A. Neftel, B. Stauffer, and D. Jacob, A record of the atmospheric methane sink from formaldehyde in polar ice cores, *Nature*, *349*, 603–605, 1991.

Staffelbach, T., et al., Photochemical oxidant formation over southern Switzerland: Results from summer 1994, *J. Geophys. Res.*, *102*, 23,345–23,362, 1997.

Stauffer, B., Long term climate records from polar ice, *Space Sci. Rev.*, *94*, 321–336, 2000.

Sumner, A. L., The role of formaldehyde in tropospheric ozone chemistry, Ph.D. Thesis, Purdue Univ., West Lafayette, IN, 2001.

Sumner, A. L., and P. B. Shepson, Snowpack production of formaldehyde and its effect on the Arctic troposphere, *Nature*, *398*, 230–233, 1999.

Sumner, A. L., et al., Atmospheric chemistry of formaldehyde in the Arctic troposphere at Polar Sunrise, and the influence of the snowpack, *Atmos. Environ.*, *36*, 2553–2562, 2002.

Swanson, A. L., N. J. Blake, J. E. Dibb, M. R. Albert, D. R. Blake, and F. S. Rowland, Photochemically induced production of CH_3Br, CH_3I, C_2H_5I, ethene, and propene within surface snow, *Atmos. Environ.*, *36*, 2671–2682, 2002.

Thompson, A. M., The oxidizing capacity of the Earth's atmosphere: Probably past and future changes, *Science*, *256*, 1157–1165, 1995.

Twickler, M. S., M. J. Spencer, W. B. Lyons, and P. A. Mayewski, Measurement of organic carbon in polar snow samples, *Nature*, *320*, 156–158, 1986.

Villenave, E., and R. Lesclaux, Kinetics of the cross reactions of CH_3O_2 and $C_2H_5O_2$ radicals with selected peroxy radicals, *J. Phys. Chem.*, *100*, 14,372–14,388, 1996.

Walker, J. F., *Formaldehyde*, 3rd edition, Van Nostrand Reinhold, New York, 1964.

Warneke, C., T. Karl, H. Judmaier, A. Hansel, A. Jordan, and W. Lindinger, Acetone, methanol, and other partially oxidized volatile organic emissions from dead plant matter by abiological processes: Significance for atmospheric HO_x chemistry, *Glob. Biogeochem. Cycles*, *13*, 9–17, 1999.

Yang, C., P. A. Mayewski, M. S. Twickler, and S. Whitlow, Major features of glaciochemistry over the last 110,000 years in the Greenland Ice Sheet Project 2 ice core, *J. Geophys. Res.*, *102*, 23,289–23,299, 1997.

Yang, J., R. E. Honrath, M. C. Peterson, J. E. Dibb, A. L. Sumner, P. B. Shepson, M. Frey, H. W. Jacobi, A. Swanson, and N. Blake, Impacts of snowpack emissions on deduced levels of OH and peroxy radicals at Summit, Greenland, *Atmos. Environ.*, *36*, 2523–2534, 2002.

Zhou, X., and K. Mopper, Photochemical production of low-molecular-weight carbonyl compounds in seawater and surface microlayer and their air–sea exchange, *Mar. Chem.*, *56*, 201–213, 1997.

T. M. Dassau, S. L. Koeniger, P. B. Shepson, and A. L. Sumner, Department of Chemistry, Purdue University, West Lafayette, IN, USA. (terra@highstream.net)

R. E. Honrath and J. Yang, Department of Civil and Environmental Engineering, Michigan Technological University, Houghton, MI, USA.

N. J. Cullen and K. Steffen, Cooperative Institute for Research in Environmental Sciences, University of Colorado, Boulder, CO, USA.

R. C. Bales, M. Frey, and H.-W. Jacobi, Department of Hydrology and Water Resources, University of Arizona, Tucson, AZ, USA.

Publication 3.2.7

Jacobi, H.-W., R.C. Bales, R.E. Honrath, M.C. Peterson, J.E. Dibb, A.L. Swanson, and M.R. Albert,

Reactive trace gases measured in the interstitial air of surface snow at Summit, Greenland,

Atmos.Environ. **38**, 1687-1697, 2004.

AE International – Polar Regions

Atmospheric Environment 38 (2004) 1687–1697

ATMOSPHERIC ENVIRONMENT

www.elsevier.com/locate/atmosenv

Reactive trace gases measured in the interstitial air of surface snow at Summit, Greenland

Hans-Werner Jacobi[a,b,*], Roger C. Bales[a,1], Richard E. Honrath[c], Matthew C. Peterson[c], Jack E. Dibb[d], Aaron L. Swanson[e,2], Mary R. Albert[f]

[a] *Department of Hydrology and Water Resources, University of Arizona, 1133 E. North Campus Drive, Tucson, AZ 85721, USA*
[b] *Alfred Wegener Institute for Polar and Marine Research, Am Handelshafen 12, 27570 Bremerhaven, Germany*
[c] *Department of Civil and Environmental Engineering, Michigan Technological University, 1400 Townsend Drive, Houghton, MI 49931, USA*
[d] *Climate Change Research Center, Institute for the Study of Earth, Oceans and Space, University of New Hampshire, 39 College Road, Durham, NH 03824, USA*
[e] *Department of Chemistry, University of California at Irvine, 516 Rowland Hall, Irvine, CA 92697, USA*
[f] *US Army Cold Regions Research and Engineering Laboratory, 72 Lyme Road, Hanover, NH 03755, USA*

Received 3 March 2003; received in revised form 22 December 2003; accepted 7 January 2004

Abstract

Concentration measurements of nitric oxide (NO), nitrogen dioxide (NO_2), nitrous acid (HONO), nitric acid (HNO_3), formaldehyde (HCHO), hydrogen peroxide (H_2O_2), formic acid (HCOOH) and acetic acid (CH_3COOH) were performed in air filtered through the pore spaces of the surface snowpack (firn air) at Summit, Greenland, in summer 2000. In general, firn air concentrations of NO, NO_2, HONO, HCHO, HCOOH, and CH_3COOH were enhanced compared to concentrations in the atmospheric boundary layer above the snow. Only HNO_3 and H_2O_2 normally exhibited lower concentrations in the firn air. In most cases differences were highest during the day and lowest during nighttime hours. Shading experiments showed a good agreement with a photochemical NO_x source in the surface snow. Patterns of H_2O_2, CH_3COOH, and HNO_3 observed within the surface snow-firn air system imply that the number of molecules in the snow greatly exceeded that in the firn air. Deduced partitioning indicates that the largest fractions of the acids were present at the ice grain–air interface. In all cases, the number of molecules located at the interface was significantly higher than the amount in the firn air. Therefore, snow surface area and surface coverage are important parameters, which must be considered for the interpretation of firn air concentrations.

Keywords: Trace gases; Air-snow exchange; Firn air; Polar atmospheric chemistry; Greenland

1. Introduction

Recent experiments have demonstrated that surface snow in polar regions can act as a photochemical reactor influencing concentrations of a wide variety of important tropospheric trace gases like ozone and nitrogen containing compounds in the atmospheric boundary layer (ABL) over snow-covered regions (e.g. Honrath et al., 2000a, 2002; Jones et al., 2000, 2001; Peterson and Honrath, 2001). Moreover, the exchange of trace gases present in the snow (e.g. H_2O_2) with the ABL is of great

*Corresponding author. Alfred Wegener Institute for Polar and Marine Research, Am Handelshafen 12, 27568 Bremerhaven, Germany. Tel.: +49-471-4831-1493; fax: +49-471-4831-1425.

E-mail address: hwjacobi@awi-bremerhaven.de (H.-W. Jacobi).

[1] Present address: University of California, P.O. Box 2039, Merced, CA 95344, USA.

[2] Present address: Cooperative Institute for Research in Environmental Sciences, Colorado University, 1850 Table Mesa Drive, Boulder, CO 80309, USA.

1352-2310/$ - see front matter © 2004 Elsevier Ltd. All rights reserved.
doi:10.1016/j.atmosenv.2004.01.004

importance for the interpretation of firn and ice core profiles of these gases (McConnell et al., 1997; Hutterli et al., 1999, 2001). Since firn air constitutes the link between the ABL and the snow, gases exchanging between the snow and the atmosphere pass through the firn air. Firn air comprises only a small portion of the ABL-snow system, making it sensitive to even small changes in temperature (through firn-air partitioning) or atmospheric concentrations.

In order to gain further insight into the role of the firn air, simultaneous measurements of key species in the firn air were performed during the summer 2000 on the Greenland ice sheet. In this paper, we report the first simultaneous observations of nitric oxide (NO), nitrogendioxide (NO_2), nitrous acid (HONO), nitric acid (HNO_3), formaldehyde (HCHO), hydrogen peroxide (H_2O_2), formic acid (HCOOH), and acetic acid (CH_3COOH) in the firn air at multiple depths with varying temperatures and radiation levels and investigate the extent to which concentrations are controlled by the partitioning between surface snow and firn air.

2. Experimental

Firn air was intensively sampled from 19 to 23 June, 2000 at the Summit Environmental Observatory on top of the Greenland ice sheet (72.6° N, 38.5° W, 3200 m elevation) using three different inlet lines. For the NO and NO_2 measurements a PFA-Teflon tube terminated with a PFA-Teflon filter pack was positioned at the bottom of a narrow hole, which was refilled with excavated snow. Firn air samples for the measurements of H_2O_2 and HCHO were drawn through a heated and insulated inlet line (0.635 cm ID PFA tubes) mounted in a PVC tube (6.03 cm OD, 5.08 cm ID) with a length of 43 cm. Another piece of the same PVC tube was used to drill holes into the surface snow. After placing the PVC tube with the inlet line into the hole, it was carefully sealed with surface snow (Fig. 1). A similar set-up with a 2-m length of heated 0.95 cm OD PFA tubing with a Teflon pre-filter was used for firn air sampling of HONO, HNO_3, HCOOH, and CH_3COOH (Dibb and Arsenault, 2002). The distance between the inlets was <2 m. Applied flow rates were on the order of 20 l min^{-1} for the acids and <2 l min^{-1} for the other compounds. Measurements were made at depths of 10 and 30 cm below the snow surface. In each case, a second similar inlet line was used to sample either ambient air or, in the case of NO_x for certain periods, firn air at a different depth. Measurements were made with instruments described in detail previously, using a chemiluminescence technique for NO and NO_2 (Honrath et al., 2002), fluorometric detection for HCHO and H_2O_2 (Jacobi et al., 2002), and mist chamber sampling followed by ion chromatographic detection for HONO, HNO_3, HCOOH, and CH_3COOH (Dibb and Arsenault, 2002; Dibb et al., 2002). NO_2 photodissociation rate constants were determined with a 2-π Metcon filterradiometer (Yang et al., 2002).

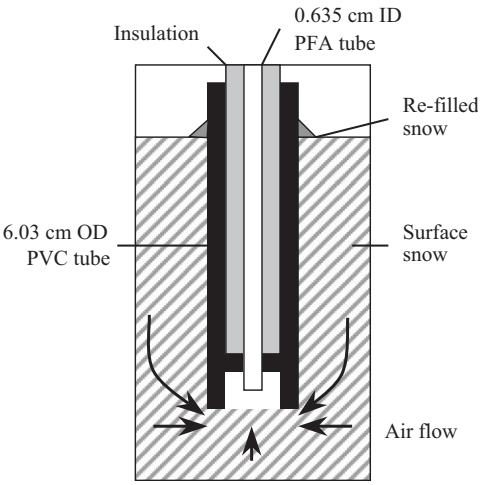

Fig. 1. Schematic drawing of the inlet line used for sampling H_2O_2 and HCHO in the firn air.

Even with a perfect seal at the sampler–snow interface, significant amounts of atmospheric air is drawn down through the surface snow into the sample inlets (Albert et al., 2002). Air reaching the inlets has been filtered through firn at a range of depths and layers, and does not represent simply air that has been in contact with distinct snow layers (Bales et al., 1995a). In addition, the sampler-induced flow rates are at least an order of magnitude larger than flows induced by natural ventilation, and are many orders of magnitude higher than movement from diffusion (Albert et al., 2002); thus we cannot use models based on diffusion for quantitative interpretation of these data. Moreover, the inlets for different samplers have vastly different flow rates and were at different locations in the snow, inducing three-dimensional interstitial flow patterns that further complicate interpretation. In spite of these complications, the data are the first of their kind and do help to give insight into physical and photochemical interactions in the near-surface snow.

To investigate the influence of photochemical processes, the sampling area was shaded for periods of 30 min–2 h using pieces ($\sim$4 m^2) of aluminum-covered insulation boards (20 June, 10:56–13:02 and 15:15–17:35; 22 June, 10:11–11:11, 12:22–13:25, 14:42–15:39 and 16:54–17:52), plexiglass (21 June, 8:59–11:04), or polyethylene (PE) film (22 June, 19:06–20:10) mounted $\sim$15 cm above the snow surface. After finishing the firn air measurements, a snow pit was dug within the sampling area on 24 June. Snow samples of this pit were analyzed for concentrations of H_2O_2 and NO_3^-,

density, and surface area. The surface area was determined from quantitative microscopy on two-dimensional thick sections of snow (Albert and Shultz, 2002). While the grain sizes determined by this method agree with visual observations, the surface area is sometimes affected by three-dimensional effects. Preliminary comparison of the side-by-side determination of the surface area of windpack and hoar in a thin snowpack at Alert, Canada by gas adsorption techniques (Dominé et al., 2002) and by imaging show differences as large as 25% (M. Albert, unpublished data).

3. Results

The firn air sampling was done near a tower that had been in place for many years, and the physical characteristics of the snow at the site had different characteristics than snow in undisturbed areas (Albert and Shultz, 2002), primarily due to foot traffic from previous years and drift patterns near the tower. Fig. 2 shows the stratigraphy and permeability profile of the snow at the sampling site. The snow was primarily fine-grained wind packed snow interspersed with layers of hoar. No dendritic forms were observed. The packed, low permeability snow below depths of 40 cm was trafficked snow that was deposited in the previous year, and the undisturbed snow from the current year lay above that. The specific surface area steadily decreased from 210 $cm^2 g^{-1}$ near –13 cm depth to 130 $cm^2 g^{-1}$ near –28 cm depth. The densities in the subsamples used for surface area determinations were essentially constant in the range 0.22–0.23 $g cm^{-3}$. Although these densities were lower than those shown in Fig. 2, we used the surface area (210 $cm^2 g^{-1}$) and density (0.22 $g cm^{-3}$) measured on the same sample from –13 depth in further analysis of the firn air measurements at –10 cm depth. H_2O_2 concentrations in the same snow pit decreased from 17.0 μM at the surface (0 to –3 cm depth) to 4.9 μM in the depth range of –24 to –28 cm. Between –7 and –13 cm depth, the concentration was 11.5 μM. Similarly, NO_3^- decreased from 5.0 μM at the surface to 0.6 μM in the depth range of –24 to –27 cm. Between –9 and –12 cm depth, a NO_3^- concentration of 2.3 μM was found.

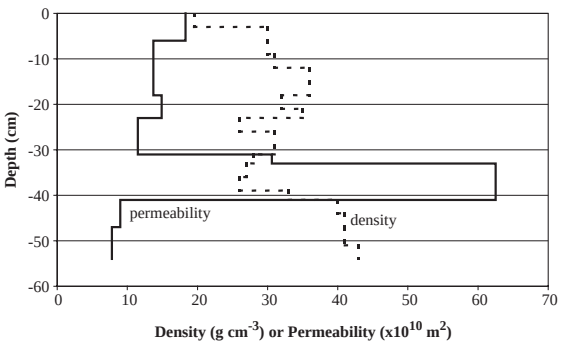

Fig. 2. Density and permeability measured in a snow pit within the firn air sampling area.

Figs. 3–6 show time series of concentration measurements above and below the snow surface for the period 19–22 June. This period includes six shading experiments with the aluminum-covered insulation boards and single shading experiments using either plexiglass or PE film. The last shading experiment with the PE film, which is partly transparent to UV and visible radiation (the transmission increases from 30% at 350 nm to 50% at 600 nm), was conducted to investigate whether the shading would cause an effect due to a change in the ventilation between firn air and ABL. Since changes in firn air concentrations were not observed during this experiment, changes in air flow patterns due to the shading of the sampling area was neglected.

The most pronounced diel cycles in the firn air were observed for NO and NO_2. NO concentrations in the firn air at –10 and –30 cm were similar, and were much higher than ambient concentrations during daytime (Fig. 3a). There were immediate, strong drops in NO at both levels during each shading period. During the longer shading experiments on June 20, the firn air concentrations dropped to ambient levels. NO levels immediately increased upon removing the shading, increasing to levels observed before the shading. NO_2 at –10 cm slowly decreased during the shading experiment whereas NO_2 at –30 cm first jumped to higher values followed by a steady decrease (Fig. 3b). Again, the opposite behavior was found after unshading. Even at night firn air NO_2 was elevated compared to ambient levels.

The diel cycle in the H_2O_2 concentration that was observed in the ABL was attenuated in the firn air at –10 cm (Fig. 4a). Ambient and firn air concentrations were comparable late at night. However, after sunrise ambient concentrations increased more than did those in the firn air, while firn air concentrations at –10 and –30 cm were comparable. Shading experiments did not affect H_2O_2 concentrations in the firn air.

Firn air concentrations of HCHO also exhibited a diel cycle at a depth of –10 cm (Fig. 4b). Late at night firn air and ambient concentrations were comparable. However, after sunrise firn air concentrations increased more than ambient concentrations and peaked around 19:00. At this time ambient and firn air concentrations at –10 cm differed by about 150 pptv. Although firn air concentrations at –30 cm on 22 June were further enhanced compared to firn air concentrations at –10 cm on the previous days, a diel cycle was less obvious. Firn air concentrations at –10 cm dropped by 50 to 60 pptv during the two shading periods on 20 June, while the experiments produced negligible effects on HCHO concentrations at –30 cm on 22 June.

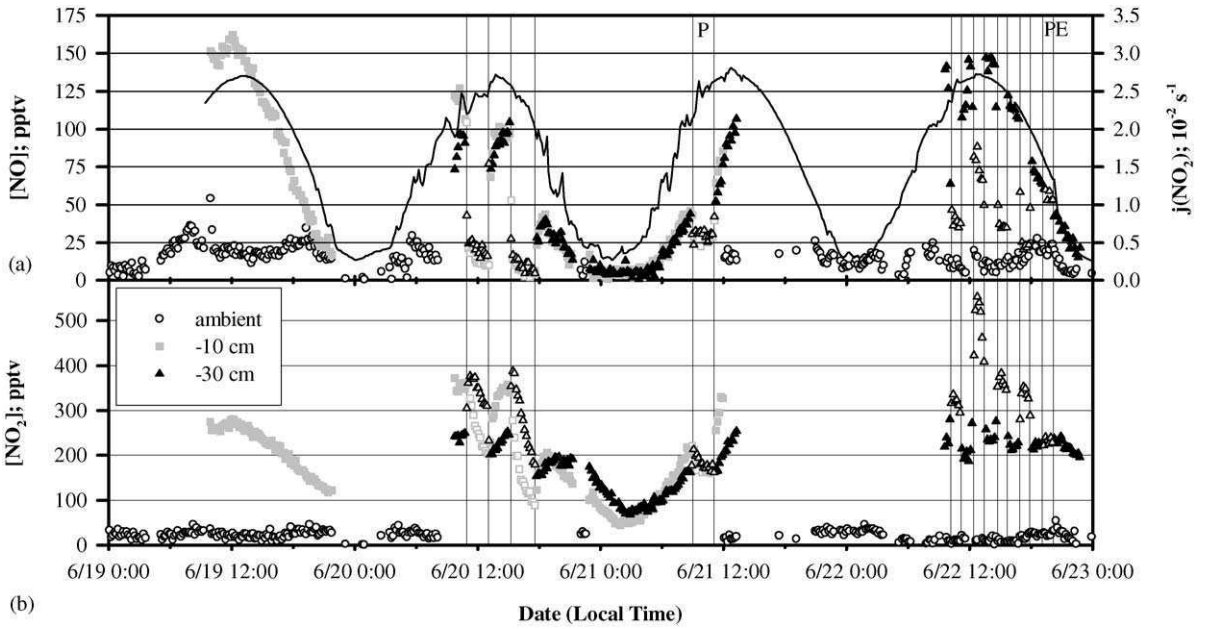

Fig. 3. Time series of 10-min averages of (a) NO and (b) NO_2 concentrations above and below the snow surface measured from 19 to 22 June. Also shown is the photolysis rate of NO_2 $j(NO_2)$ above the snow surface (a). Firn air concentrations during shading experiments are marked by open symbols with beginning and end of each experiment indicated by vertical lines (P: plexiglass, PE: PE film, others: aluminum; see text).

Quite high interstitial air concentrations were found for HCOOH and CH_3COOH (Dibb and Arsenault, 2002). In contrast to ambient concentrations, which exhibited slightly higher concentrations during the day than at night, firn air concentrations were always in the range of 1500–4600 pptv for HCOOH and 2500–5500 pptv for CH_3COOH with no distinct diel cycle (Fig. 5). Also, concentrations were not affected during the shading experiments. HONO showed a behavior comparable to the organic acids; however, concentrations were much smaller (Fig. 6a). Shading experiments produced ambiguous results with the first shading experiment on 20 June resulting in a slight increase in HONO at –10 cm and with a strong decrease during the second shading experiment. HNO_3 exhibited the lowest firn air concentrations of all measured compounds (Fig. 6b). At –10 and –30 cm concentrations were comparable and remained below 20 pptv. The largest differences between firn air and ambient concentrations occurred at daytime, owing to the diel cycle of HNO_3 in the ABL.

4. Discussion

4.1. Relationship to fluxes measured above the snow surface

Firn air is connected both to the surface snow and the ABL above the snow. Therefore, we can expect that the exchange measured above the snow surface correlates to the gradient between ambient and firn air concentrations. During the summer 2000 field season fluxes above the snow surface of NO_x, HONO, HNO_3, H_2O_2 and HCHO were measured (Honrath et al., 2002; Jacobi et al., 2002). Honrath et al. (2002) reported upward fluxes of NO_x and HONO and downward fluxes of HNO_3. The average diel cycle of each compound shows its maximum flux around noon, with negligible exchange during the night. These cycles agree well with the observed elevated firn air concentrations of NO_x and HONO and the reduced firn air concentrations of HNO_3. NO_2 and HONO firn air concentrations also remained higher than ambient levels at night and, thus, could cause emissions all day. However, at night very stable conditions normally develop in the ABL at Summit (Cullen and Steffen, 2001) limiting the turbulence to very low values. Therefore, even in the presence of large concentration gradients the exchange can remain negligible, in agreement with the measured fluxes.

The diel cycles of the exchange of H_2O_2 and HCHO followed similar patterns: emissions of both compounds during the day and a slight uptake at night (Jacobi et al., 2002). Daytime gradients of HCHO and nighttime gradients of H_2O_2 matched the previously reported direction of the fluxes above the snow surface, whereas those at other times did not. The reason for this disagreement could be that the fluxes of H_2O_2 and

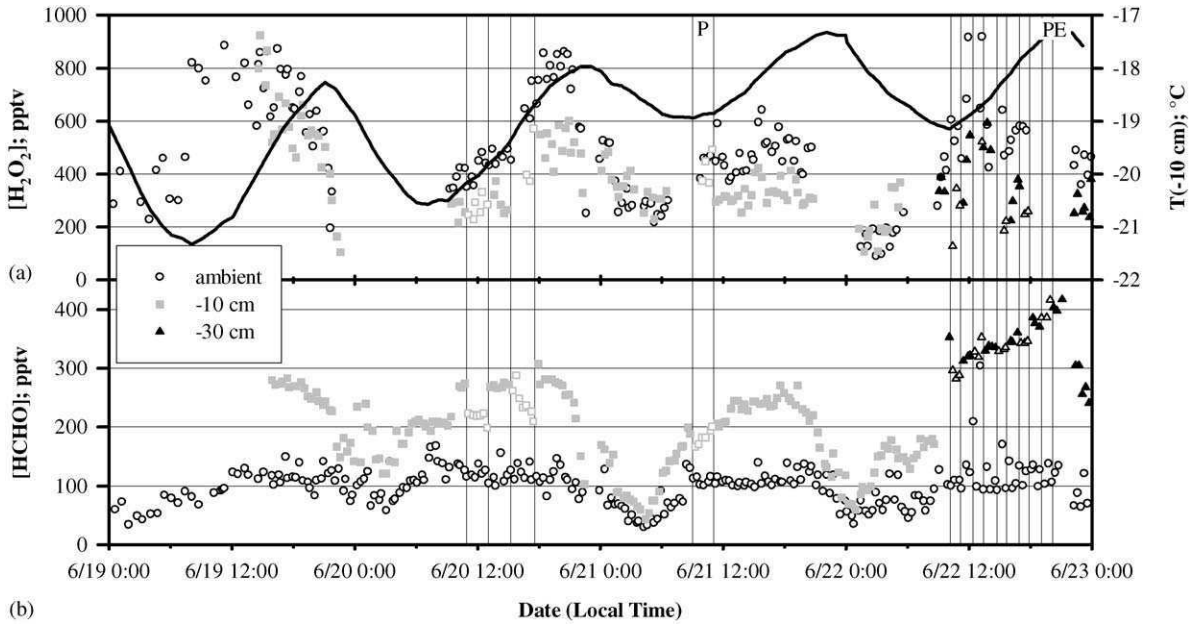

Fig. 4. Time series of 10-min averages of (a) H_2O_2 and (b) HCHO concentrations above and below the snow surface measured from 19 to 22 June. Also shown is the firn air temperature T at –10 cm (a). Firn air concentrations during shading experiments are marked by open symbols with beginning and end of each experiment indicated by vertical lines (P: Plexiglass, PE: PE film, others: aluminum; see text).

HCHO are dominated by the exchange with only the top few centimeters or millimeters of the snow surface (Hutterli et al., 2001). The amounts of H_2O_2 and HCHO stored in the top layer of the snow are sufficient to sustain the measured fluxes to the ABL as well as to deeper layers of the snow (Jacobi et al., 2002). However, differences between firn air and ambient concentrations may also be an artifact of the flow rates and patterns as described above, and points to the need for firn air sampling using much lower flow rates.

Thus, although gradients between ambient and firn air at –10 cm are considerably easier to quantify than gradients in the ABL, due to the much higher concentration differences, these gradients appear to be good indicators of fluxes between the surface snow and the ABL only for NO_x, HONO, and HNO_3.

4.2. Photochemistry in the firn air

It has been demonstrated that the transfer of different trace gases between snow and air depends on temperature dependent physical and/or photochemical processes (Bales et al., 1995b; Sumner and Shepson, 1999; Hutterli et al., 1999, 2001; Couch et al., 2000; Honrath et al., 2000a; Jones et al., 2000). We can expect that the same processes also influence firn air concentrations. To investigate the effects of the physical and photochemical processes, we made a quantitative comparison using maxima of the firn air concentrations and maxima of temperature and radiation in the surface snow. Radiation levels peak between 12:00 and 13:00. In contrast, snow temperatures peaked between 19:00 and 21:00 at –10 cm and between 21:00 and 23:00 at –30 cm.Thus, photochemically produced species should exhibit highest firn air concentrations at noon while maxima of species dominated by ice-air partitioning should occur concomitant with the temperature maxima at night. However, since the sampled firn air is not restricted to a distinct layer, the correlation with the temperature is probably rather weak. In contrast, the agreement with the radiation intensity should be much better because the maximum of the photochemical production occurs in all layers at the same time.

Accordingly, an unambiguous classification is only possible in the cases of NO and NO_2. Highest firn air concentrations of NO and NO_2 normally occurred around noon (Fig. 3) indicating the photochemical production of NO_x ($=NO+NO_2$) in the surface snowpack (Honrath et al., 2000a; Jones et al., 2000, 2001), which has been attributed to the photolysis of the NO_3^- dissolved in the snow (Honrath et al., 2000b). Linear regressions of [NO], [NO_2], and [NO_x] with the photolysis rate $j(NO_2)$ measured at –10 cm on 19 June gave correlation coefficients (R^2) of 0.89, 0.91, and 0.90, respectively. A similar simple interpretation of the results of the shading experiments is hampered by the

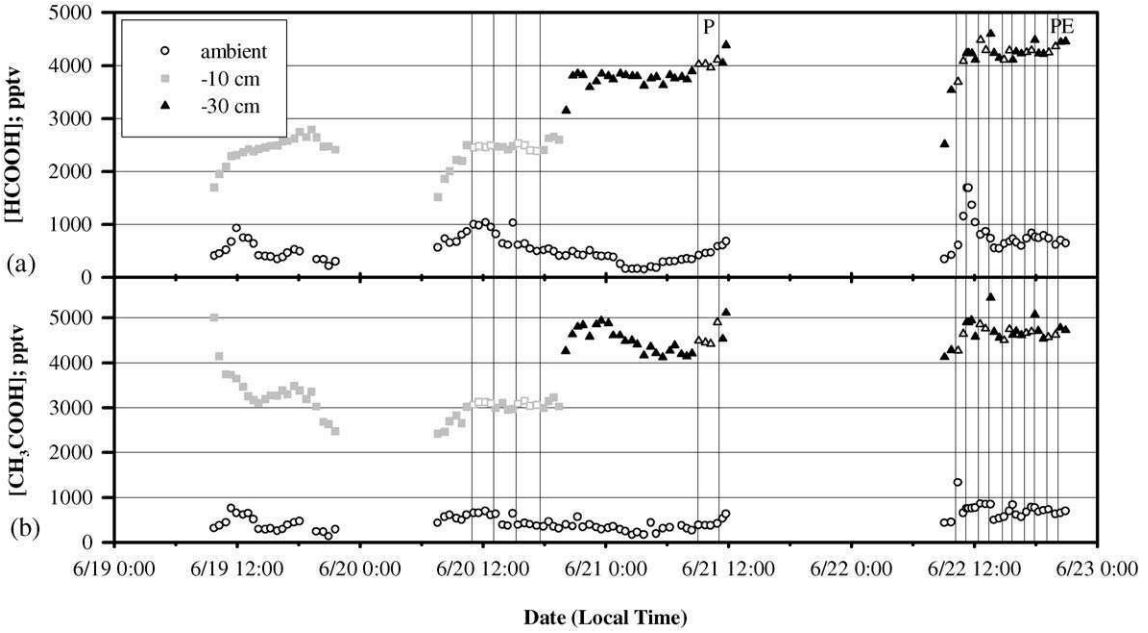

Fig. 5. Time series of (a) HCOOH and (b) CH_3COOH concentrations above and below the snow surface measured from 19 to 22 June. Sampling periods lasted between 19 and 38 min. Firn air concentrations during shading experiments are marked by open symbols with beginning and end of each experiment indicated by vertical lines (P: Plexiglass, PE: PE film, others: aluminum; see text).

fact that NO and NO_2 are connected by a very fast photochemical cycle involving the reactions of NO with O_3 and HO_2 and the photolysis of NO_2. However, the NO–NO_2 cycling has no effect on NO_x, which can be analyzed regarding the effect of the shading experiments. NO_x in the firn air decreased during all shading experiments and increased after unshading except after experiments late in the afternoon. These effects were more pronounced at –10 compared to –30 cm and are also in good agreement with a photochemical NO_x source in the snowpack. The shading immediately stops photochemical reactions in the snowpack as well as the photolysis of NO_2, while the reaction of NO with O_3 is much less affected due to the more steady O_3 concentrations. Therefore, the quick drop in firn air NO and the constant or increasing NO_2 concentrations immediately after shading may be attributed to the shift in the photochemical NO_x-O_3-cycle and the continuing steady decrease of both compounds due to the missing photochemical production in the snowpack.

H_2O_2 and HCHO also exhibited lower firn air concentrations at night versus daytime, indicating a possible photochemical contribution to elevated firn air values. However, maximum concentrations during the afternoon occurred later than the radiation maxima, but prior to temperature maxima. A better correlation might be obscured by the firn air sampling technique, which samples a mixture of ambient air and firn air from shallower depths, where the temperature maxima occur earlier than at –10 and –30 cm.We assume that a combination of chemical and physical processes determined measured HCHO firn air concentrations. Since H_2O_2 concentrations in the firn air were lower than ambient values, a significant direct photochemical H_2O_2 source seems unlikely.

For HCOOH, CH_3COOH, HONO, and HNO_3 the results are more ambiguous because no full diel cycles were measured. The available data show rather constant concentrations for all compounds at –10 and –30 cm.This result is surprising in the case of HONO, which can also be a product of the NO_3^- photolysis similar to NO_x (Mack and Bolton, 1999) and which normally exhibits higher firn air concentrations with increased radiation levels (Dibb et al., 2002; Zhou et al., 2001). Several effects can cause the differences in the behavior of HONO and NO_x. First, the very high flow rates for the sampling of the acidic compounds might have obscured any photochemical effect by diluting the firn air with a much larger volume of air mostly including ambient air. Second, even if HONO and NO_x are produced by the same photochemical mechanism in the snow, the release of HONO into the firn air could be affected by its properties in the surface region of the ice crystals, which is commonly called quasi-liquid layer (QLL) because it is less ordered and exhibits different properties than the solid ice. Such a QLL could act as a reservoir for HONO, but not for NO and NO_2. Thus, the HONO release could be dominated by

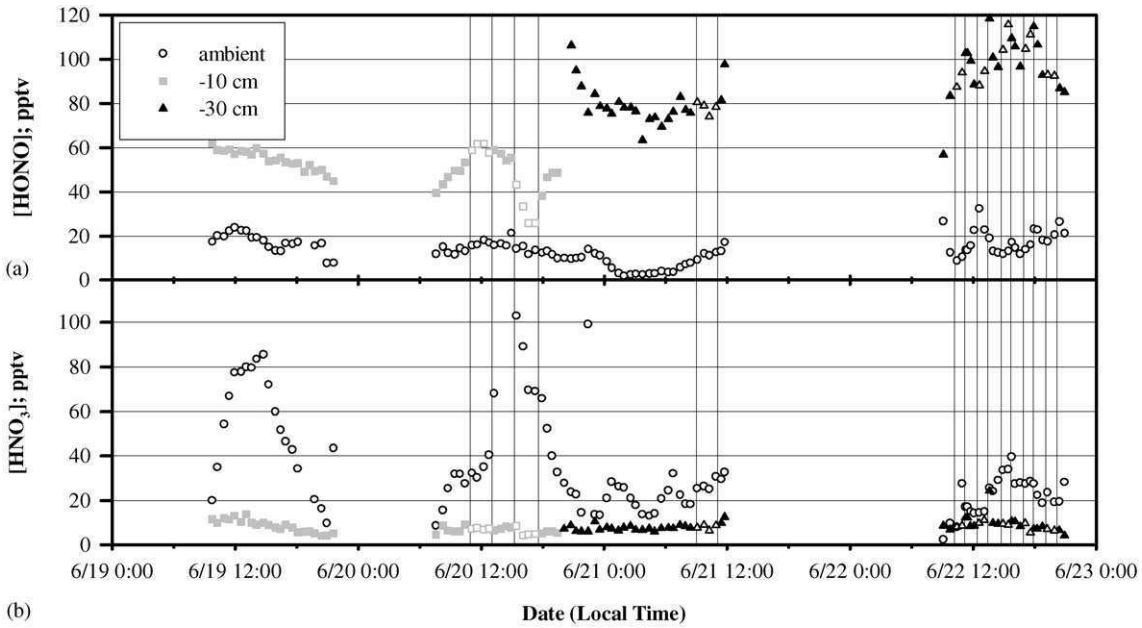

Fig. 6. Time series of (a) HONO and (b) HNO_3 concentrations above and below the snow surface measured from 19 to 22 June. Sampling periods lasted between 19 and 38 min. Firn air concentrations during shading experiments are marked by open symbols with beginning and end of each experiment indicated by vertical lines (P: Plexiglass, PE: PE film, others: aluminum; see text).

physical equilibria, which follow diel cycles different to the radiation cycles. Third, constant HONO concentrations could result if the most dominant sources and sinks follow similar diel cycles. For example, if the NO_3^- photolysis is the most important production process and the HONO photolysis the most important sink, both reactions would exhibit similar diel cycles that vary according to the radiation intensity. Nevertheless, the measurable nighttime HONO concentrations may also indicate a heterogeneous HONO production from NO_2 in the surface snow like observed in previous laboratory experiments (e.g. Finlayson-Pitts et al., 2003).

4.3. Air–snow partitioning

In order to further examine the influence of the temperature-dependent equilibrium between snow and firn air, we analyzed the air–snow partitioning considering the bulk ice, the ice grain–air interface, and the adjacent firn air. We assume that the equilibrium between the firn air and the interface is quickly established. Therefore, we used measured firn air concentrations to calculate surface coverages for the compounds, which have been measured directly in laboratory experiments or can be deduced from partitioning data. With the specific surface areas, the amounts located at the interface are calculated and subtracted from the amounts measured in the snow samples if necessary.

The distribution in Table 1 presents the results for H_2O_2, CH_3COOH, and HNO_3 following this procedure. The numbers reveal some important features for the air–snow partitioning of reactive trace gases. For example, the largest fractions are restricted to the condensed phase, with less than 0.1% present in the firn air in all three cases. The snow–air equilibrium constants are in the range of 2.9×10^4, 230, and 4.6×10^5 M atm^{-1} for H_2O_2, CH_3COOH, and HNO_3. The constant for H_2O_2 falls well in the range estimated from previous field studies (e.g. McConnell et al., 1997). Practically, all the H_2O_2 and HNO_3 are located in the bulk ice, while a significant fraction of CH_3COOH is present at the interface.

The different distribution of H_2O_2 and CH_3COOH in the condensed phase is somewhat surprising. However, it agrees well with several results of previous studies. First, bulk acetate concentrations in polar snow are very low compared to concentrations in rain in remote regions (Chebbi and Carlier, 1996) possibly due to low concentrations in the bulk ice (Table 1). On the other hand, the H_2O_2 uptake during the formation of fresh snow seems to be dominated by co-condensation leading to uniformly distributed H_2O_2 concentrations in the bulk ice of fresh snow (Sigg et al., 1992). Second, since large amounts of CH_3COOH are available at the interface, its degassing from aging snow can be expected to occur much faster than the degassing of H_2O_2, which is to a large extent limited by the slow diffusion within

Table 1
Properties of the ice-firn air system and partitioning of H_2O_2, CH_3COOH, and HNO_3 at a depth of –10 cm[a]

		Bulk ice	Interface	Firn air
	Volume or surface area per volume unit	0.24 $cm^3\,cm^{-3}$[b]	46 $cm^2\,cm^{-3}$[c]	0.76 $cm^{-3}\,cm^{-3}$[d]
H_2O_2	Concentration or surface coverage	11.5 μM[e]	$\sim 10^{10}\,cm^{-2}$[f]	560 pptv[g]
	Number of molecules per volume unit	$1.7 \times 10^{15}\,cm^{-3}$	$4.6 \times 10^{11}\,cm^{-3}$	$8.2 \times 10^{9}\,cm^{-3}$
	Fraction	1	3×10^{-4}	5×10^{-6}
CH_3COOH	Concentration or surface coverage	0.38 μM[h]	$3.8 \times 10^{11}\,cm^{-2}$[i]	3000 pptv[j]
	Number of molecules per volume unit	$5.5 \times 10^{13}\,cm^{-3}$	$1.7 \times 10^{13}\,cm^{-3}$	$4.4 \times 10^{10}\,cm^{-3}$
	Fraction	0.76	0.24	6×10^{-4}
HNO_3	Concentration or surface coverage	2.3 μM[e]		7 pptv[k]
	Number of molecules per volume unit	$3.3 \times 10^{14}\,cm^{-3}$	$2.5 \times 10^{9}\,cm^{-3}$[l]	$1.0 \times 10^{8}\,cm^{-3}$
	Fraction	1	8×10^{-6}	3×10^{-7}

[a] Calculations for June 19, 15:00–22:00 ($T = -19°C$; $\rho_{air} = 1.93 \times 10^{19}\,cm^{-3}$).
[b] Calculated with the measured snow density of 0.22 $g\,cm^{-3}$ and the ice density of 0.92 $g\,cm^{-3}$ at $T = -19°C$.
[c] Product of surface area (210 $cm^2\,g^{-1}$) and volume density (0.22 $g\,cm^{-3}$).
[d] (1–0.24) $cm^3\,cm^{-3}$.
[e] Measured bulk snow concentration.
[f] Clegg and Abbatt (2001).
[g] see Fig. 4a.
[h] Calculated with an average CH_3COOH bulk snow concentration of 0.5 μM (Dibb et al., 1994; De Angelis and Legrand, 1995; Legrand and Mayewski, 1997) taking into account the amount located at the interface.
[i] Sokolov and Abbatt (2002).
[j] see Fig. 5b.
[k] see Fig. 6b.
[l] Calculated with a partitioning coefficient of $n_{interface}/n_{firn\ air} = 25$ obtained from the adsorption enthalpy and entropy of HNO_3 (Bartels-Rausch et al., 2002).

the ice matrix. Accordingly, field studies have shown that the loss of H_2O_2 from surface snow occurs over weeks to months (e.g. Bales et al., 1995b), while CH_3COOH in surface snow can significantly decrease within hours to days (Dibb et al., 1994; De Angelis and Legrand, 1995).

Molecular dynamics simulations demonstrate that HCOOH and CH_3COOH are trapped at the ice surface (Compoint et al., 2002). These calculations show that the incorporation of HCOOH in the bulk is more likely compared to CH_3COOH. Nevertheless, we assume that a somewhat lower, however still significant fraction of HCOOH is located at the interface of the crystals, since HCOOH concentrations in the firn and firn air behave similar to CH_3COOH.

To further investigate photochemical reactions occurring in the snow, it would be important to know if the reactive compounds are in the solid ice, dissolved in the QLL, or adsorbed on the ice crystal-air interface. For example, Honrath et al. (2000b) discussed that the photochemistry of NO_3^- is different in all three environments. Unfortunately, the laboratory studies of Clegg and Abbatt (2001) and Sokolov and Abbatt (2002) regarding the surface coverages of H_2O_2 and CH_3COOH were performed at lower temperatures below 245 K and possibly without the presence of a QLL. Thus, these experimental results do not allow distinguishing between adsorbed amounts and amounts present in the QLL. In addition, Bartels-Rausch et al. (2002) stressed that their results are only valid for the amount of undissociated HNO_3 adsorbed at the surface of the ice crystal. Thus, the "bulk ice" quantity shown for NO_3^- in Table 1 includes NO_3^- in the QLL as well as in the bulk ice (but does not include adsorbed NO_3^- at the ice grain-air interface). Distribution coefficients for the partitioning of HNO_3 between ice and liquid water indicate that most of this NO_3^- is likely to be in the QLL. Gross (2003) obtained an average distribution coefficient (ice/liquid water) for NO_3^- of 2.3×10^{-4}, in a series of experiments using $NaNO_3$ and KNO_3, while Thibert and Dominé (1998) reported a much smaller distribution coefficient for HNO_3 (5×10^{-6} at $-19°C$). Even if the QLL volume were only $\sim 10^{-4}$ of the total (equivalent to a layer on the ice surface with a thickness of 2.5×10^{-6} cm), these distribution coefficients imply that 80–100% of the NO_3^- is present in the QLL.

Although HNO_3 is almost exclusively present in the condensed phase within the firn–firn air system, the

calculations suggest that by far the largest fraction is present in the QLL and, thus, available for release to the atmosphere. Indeed, substantial postdepositional losses from surface snow have been reported (e.g. Fischer et al., 1998; Wagnon et al., 1999). Moreover, the main source of the NO_x produced by irradiated surface snow is most probably the photolysis of nitrate present in the QLL rather than the photolysis of nitrate in the bulk ice.

Since considerably higher amounts of the trace gases are located at the interface compared to amounts in the firn air, firn air concentrations are expected to be very sensitive to physical parameters like temperature or surface area. For example, a simultaneous decrease of H_2O_2 and temperature at –10 cm during the night from 20 to 21 June was observed (Fig. 4a). Between 22:00 and 7:00, the snow temperature dropped from about –18°C to –19°C, while H_2O_2 declined from around 500–300 pptv. Laboratory studies gave an enthalpy of $\Delta H^\circ = -55\,\mathrm{kJ\,mol^{-1}}$ for the temperature dependence of the ice-atmosphere equilibrium of H_2O_2 below –11°C (Conklin et al., 1993). Therefore, the temperature drop would lead to a concentration decrease of $<10\%$ as long as all other parameters remain constant. This is much less than the observed decline of 40%, which would require a temperature drop of 5 K. Measurements of the H_2O_2 uptake on ice resulted in a more or less constant surface coverage in the temperature range between 218 and 238 K (Clegg and Abbatt, 2001). Nevertheless, a slight temperature dependence of the surface coverage well below the uncertainty of the laboratory experiments (Clegg and Abbatt, 2001) could explain a decrease of H_2O_2 in the firn air on the order of 200 pptv due to the exceeding amounts present at the surface compared to the firn air. In addition, Dibb and Arsenault (2002) noted that firn air profiles of CH_3COOH at Summit exhibited large fluctuations of 800–2200 pptv between profiles measured with time lags of 4–5 h. With the surface coverage given in Table 1, a change in the surface area of only 0.2% could explain fluctuations in firn air concentrations on the order of 2200 pptv.

Cabanes et al. (2002) studied trends of surface areas of Arctic snow. They found that the surface area of fresh snow decreased significantly with rates between 19 and $730\,\mathrm{cm^2\,g^{-1}\,day^{-1}}$. However, the surface area of older underlying snow remained rather stable (Dominé et al., 2002). The temperature gradients during this study were too low to induce metamorphism leading to an increase in the surface area. Therefore, decreasing surface areas can explain observed increases, but not the also observed quick drops in firn air concentrations of CH_3COOH. More likely are differences in firn air concentrations that may be related to snow characteristics and/or spatial variability at the sampling site.

Nevertheless, surface area and surface coverage are possibly as important as the temperature in determining equilibria between snow and firn air and thus firn air concentrations. Cabanes et al. (2002) calculated that the surface area and the temperature-dependent adsorption could affect HNO_3 concentrations not only in the firn air, but even in the boundary layer. As discussed above, complications due to the varying flow rates and flow patterns make detailed model interpretation of the data untenable for the current study. However, small changes in the physical characteristics of snow, especially the surface area, may yield significant differences in firn air concentrations.

Exchange with the ABL also affects firn air concentrations. For example, the average H_2O_2 flux measured above the snow surface (Jacobi et al., 2002) during 20 June, 22:00–21 June, 7:00 resulted in a slight emission, on the order of 1.5×10^8 molecules $\mathrm{m^{-2}\,s^{-1}}$, contributing to the drop in the measured firn air concentration at –10 cm.This small flux could remove the entire H_2O_2 amount in the firn air of the top 30 cm of the snow within <1 h, were it not replenished from the condensed phase.

5. Conclusions

The comparison of trace gas concentration profiles above and below the snow surface during day and night and during shading experiments revealed that firn air concentrations are determined by photochemical reactions, temperature-dependent equilibria between the surface snow and adjacent firn air, and the exchange between the firn air and the air above the snow. Removal of NO_x during shading experiments confirms previous results demonstrating that considerable amounts are produced in the surface snow and released to the firn air due to photochemical processes. However, during the shading experiments two different regimes were identified indicating that the release from the snowpack is considerably slower than the rates in the photochemical NO_x-O_3 cycle. Nevertheless, features like elevated NO_2 firn air concentrations at night remain unexplained warranting a more detailed study of the mechanism of NO_x production in surface snow and the photochemical NO_x reactions in the firn air. Mixing ratios of H_2O_2, CH_3COOH, and HNO_3 in the firn air mainly depend on gas and snow phase equilibria. The analysis of the firn air data indicate that a large fraction of CH_3COOH is present at the ice grain–air interface making adsorption to the snow and the surface area of the snow very important parameters for firn air concentrations. Despite the lack of laboratory data for HCOOH, we conclude that it is also mainly located in the QLL or at the grain–air interface based on the similarities in the behavior of HCOOH and CH_3COOH in the firn and firn air.

However, further laboratory studies of the ice-gas phase equilibria and surface coverage of ice at

temperatures close to the freezing point are needed. For example, the results could be used to analyze whether observed diel cycles of alkyl nitrates in the firn air (Swanson et al., 2002) are caused by phase partitioning or photochemical production. Since most of the NO_3^- is probably located in the QLL, it seems likely that the NO_x production is also governed by reactions in this layer. Therefore, laboratory experiments in a broad range of temperatures could demonstrate the importance of the QLL for the NO_3^- photolysis in ice and snow. For the correct description of the conditions within the firn and the firn air, further information about the nature and properties of the QLL of the snow grains is needed. For example, Dubowski et al. (2002) conclude that some properties of the QLL differ from those of supercooled water. The results underline the obvious need to characterize the amount and properties of this layer using for example NMR techniques (Cho et al., 2002) and to include this knowledge in models describing the transfer of trace gases between firn and firn air.

Acknowledgements

Financial support by the National Science Foundation (NSF), grants OPP-9813311, OPP-9813442, OPP-9910303, and OPP-9907330, is gratefully acknowledged. HWJ thanks the Deutsche Forschungsgemeinschaft (DFG) for a research stipend. The Summit summer crew, VECO Polar Resources, and the Air National Guard provided assistance and equipment during the field experiments.

References

Albert, M.R., Shultz, E.F., 2002. Snow and firn properties and air–snow transport processes at Summit, Greenland. Atmospheric Environment 36, 2789–2797.

Albert, M.R., Grannas, A.M., Bottenheim, J., Shepson, P.B., Perron, F.E., 2002. Processes and properties of snow-air transfer in the high Arctic with application to interstitial ozone at Alert, Canada. Atmospheric Environment 36, 2779–2787.

Bales, R.C., Losleben, M.V., McConnell, J.R., Fuhrer, K., Neftel, A., 1995a. H_2O_2 in snow, air and open pore space in firn at Summit, Greenland. Geophysical Research Letters 22, 1261–1264.

Bales, R.C., McConnell, J.R., Losleben, M.V., Conklin, M.H., Fuhrer, K., Neftel, A., Dibb, J.E., Kahl, J.D.W., Stearns, C.R., 1995b. Diel variations of H_2O_2 in Greenland: a discussion of the cause and effect relationship. Journal of Geophysical Research 100, 18661–18668.

Bartels-Rausch, T., Eichler, B., Zimmermann, P., Gäggeler, H.W., Ammann, M., 2002. The adsorption enthalpy of nitrogen oxides on crystalline ice. Atmospheric Chemistry and Physics 2, 235–247.

Cabanes, A., Legagneux, L., Dominé, F., 2002. Evolution of the specific surface area and of crystal morphology of Arctic fresh snow during the ALERT 2000 campaign. Atmospheric Environment 36, 2767–2777.

Chebbi, A., Carlier, P., 1996. Carboxylic acids in the troposphere, occurrence, sources, and sinks: a review. Atmospheric Environment 30, 4233–4249.

Cho, H., Shepson, P.B., Barrie, L.A., Cowin, J.P., Zaveri, R., 2002. NMR investigation of the quasi-brine layer in ice/brine mixtures. Journal of Physical Chemistry B 106, 11226–11232.

Clegg, S.M., Abbatt, J.P.D., 2001. Uptake of gas-phase SO_2 and H_2O_2 by ice surfaces: dependence on partial pressure, temperature, and surface acidity. Journal of Physical Chemistry A 105, 6630–6636.

Compoint, M., Toubin, C., Picaud, S., Hoang, P.N.M., Girardet, C., 2002. Geometry and dynamics of formic and acetic acids adsorbed on ice. Chemical Physics Letters 365, 1–7.

Conklin, M.H., Sigg, A., Neftel, A., Bales, R.C., 1993. Atmosphere-snow transfer for H_2O_2: microphysical considerations. Journal of Geophysical Research 98, 18367–18376.

Couch, T.L., Sumner, A.L., Dassau, T.M., Shepson, P.B., Honrath, R.E., 2000. An investigation of the interaction of carbonyl compounds with the snowpack. Geophysical Research Letters 27, 2241–2244.

Cullen, N.J., Steffen, K., 2001. Unstable near-surface boundary conditions in summer on top of the Greenland ice sheet. Geophysical Research Letters 28, 4491–4493.

De Angelis, M., Legrand, M., 1995. Preliminary investigations of post depositional effects on HCl, HNO_3, and organic acids in polar firn layers. In: Delmas, R. (Ed.), Ice Core Studies of Global Biogeochemical Cycles, NATO ASI Series I, Vol. 30. Springer, Berlin, pp. 361–381.

Dibb, J.E., Arsenault, M., 2002. Should not snowpacks be a source of monocarboxylic acids? Atmospheric Environment 36, 2513–2522.

Dibb, J.E., Talbot, R.W., Bergin, M.H., 1994. Soluble acidic species in air and snow at Summit, Greenland. Geophysical Research Letters 21, 1627–1630.

Dibb, J.E., Arsenault, M., Peterson, M.C., Honrath, R.E., 2002. Fast nitrogen oxide photochemistry in Summit, Greenland snow. Atmospheric Environment 36, 2501–2511.

Dominé, F., Cabanes, A., Legagneux, L., 2002. Structure, microphysics, and surface area of the Arctic snowpack near Alert during the ALERT 2000 campaign. Atmospheric Environment 36, 2753–2765.

Dubowski, Y., Colussi, A.J., Boxe, C., Hoffmann, M.R., 2002. Monotonic increase of nitrite yields in the photolysis of nitrate in ice and water between 238 and 294 K. Journal of Physical Chemistry A 106, 6967–6971.

Finlayson-Pitts, B.J., Wingen, L.M., Sumner, A.L., Syomin, D., Ramazan, K.A., 2003. The heterogeneous hydrolysis of NO_2 in laboratory systems and in outdoor and indoor atmospheres: an integrated mechanism. Physical Chemistry Chemical Physics 5, 223–242.

Fischer, H., Wagenbach, D., Kipfstuhl, J., 1998. Sulfate and nitrate firn concentrations on the Greenland ice sheet, 1. Large-scale geographical deposition changes. Journal of Geophysical Research 103, 21927–21934.

Gross, G.W., 2003. Nitrates in ice: uptake; dielectric response by the layered capacitor method. Canadian Journal of Physics 81, 439–450.

Honrath, R.E., Peterson, M.C., Dziobak, M.P., Dibb, J.E., Arsenault, M.A., Green, S.A., 2000a. Release of NO_x from sunlight-irradiated midlatitude snow. Geophysical Research Letters 27, 2237–2240.

Honrath, R.E., Guo, S., Peterson, M.C., Dziobak, M.P., Dibb, J.E., Arsenault, M.A., 2000b. Photochemical production of gas phase NO_x from ice crystal NO_3^-. Journal of Geophysical Research 105, 24183–24190.

Honrath, R.E., Lu, Y., Peterson, M.C., Dibb, J.E., Arsenault, M.A., Cullen, N.J., Steffen, K., 2002. Vertical fluxes of photochemically important compounds above the snowpack at Summit, Greenland. Atmospheric Environment 36, 2629–2640.

Hutterli, M.A., Röthlisberger, R., Bales, R.C., 1999. Atmosphere-to-snow-to-firn transfer studies of HCHO at Summit, Greenland. Geophysical Research Letters 26, 1691–1694.

Hutterli, M.A., McConnell, J.R., Stewart, R.W., Jacobi, H.-W., Bales, R.C., 2001. Impact of temperature-driven cycling of hydrogen peroxide (H_2O_2) between air and snow on the planetary boundary layer. Journal of Geophysical Research 106, 15395–15404.

Jacobi, H.-W., Frey, M.M., Hutterli, M.A., Bales, R.C., Schrems, O., Cullen, N.J., Steffen, K., Koehler, C., 2002. Long-term measurements of hydrogen peroxide and formaldehyde exchange between the atmosphere and surface snow at Summit, Greenland. Atmospheric Environment 36, 2619–2628.

Jones, A.E., Weller, R., Wolff, E.W., Jacobi, H.-W., 2000. Speciation and rate of photochemical NO and NO_2 production in Antarctic snow. Geophysical Research Letters 27, 345–348.

Jones, A.E., Weller, R., Anderson, P.S., Jacobi, H.-W., Wolff, E.W., Schrems, O., Miller, H., 2001. Measurements of NO_x emissions from the antarctic snowpack. Geophysical Research Letters 28, 1499–1502.

Legrand, M., Mayewski, P., 1997. Glaciochemistry of polar ice cores: a review. Reviews of Geophysics 35, 219–243.

Mack, J., Bolton, J.R., 1999. Photochemistry of nitrite and nitrate in aqueous solution: a review. Journal of Photochemistry and Photobiology A 128, 1–13.

McConnell, J.R., Bales, R.C., Winterle, J.R., Kuhns, H., Stearns, C.R., 1997. A lumped parameter model for the atmosphere-to-snow transfer function for hydrogen peroxide. Journal of Geophysical Research 102, 26809–26818.

Peterson, M.C., Honrath, R.E., 2001. Observations of rapid photochemical destruction of ozone in snowpack interstitial air. Geophysical Research Letters 28, 511–514.

Sigg, A., Staffelbach, T., Neftel, A., 1992. Gas phase measurements of hydrogen peroxide in Greenland and their meaning for the interpretation of H_2O_2 records in ice cores. Journal of Atmospheric Chemistry 14, 223–232.

Sokolov, O., Abbatt, J.P.D., 2002. Adsorption to ice of n-alcohols (ethanol to 1-hexanol) acetic acid, and hexanal. Journal of Physical Chemistry A 106, 775–782.

Sumner, A.L., Shepson, P.B., 1999. Snowpack production of formaldehyde and its effect on the Arctic troposphere. Nature 398, 230–233.

Swanson, A.L., Blake, N.J., Dibb, J.E., Albert, M.R., Blake, D.R., Rowland, F.S., 2002. Photochemically induced production of CH_3Br, CH_3I, C_2H_5I, ethene, and propene within surface snow at Summit, Greenland. Atmospheric Environment 36, 2671–2682.

Thibert, E., Dominé, F., 1998. Thermodynamics and kinetics of the solid solution of HNO_3 in ice. Journal of Physical Chemistry B 102, 4432–4439.

Wagnon, P., Delmas, R.J., Legrand, M., 1999. Loss of volatile acid species from upper firn layers at Vostok, Antarctica. Journal of Geophysical Research 104, 3423–3431.

Yang, J., Honrath, R.E., Peterson, M.C., Dibb, J.E., Sumner, A.L., Shepson, P.B., Frey, M., Jacobi, H.-W., Swanson, A., Blake, N., 2002. Impacts of snowpack photochemistry on deduced levels of OH and peroxy radicals at Summit, Greenland. Atmospheric Environment 36, 2523–2534.

Zhou, X., Beine, H.J., Honrath, R.E., Fuentes, J.D., Simpson, W., Shepson, P.B., Bottenheim, J.W., 2001. Snowpack photochemical production of HONO: a major source of OH in the Arctic boundary layer in springtime. Geophysical Research Letters 28, 4087–4090.

3.3 Laboratory experiments with artificial snow samples

Publication 3.3.1

Jacobi, H.-W., B. Kwakye-Awuah, and O. Schrems,

Photochemical decomposition of hydrogen peroxide (H_2O_2) and formaldehyde (HCHO) in artificial snow,

Ann.Glaciol. **39**, 29-33, 2004.

Photochemical decomposition of hydrogen peroxide (H_2O_2) and formaldehyde (HCHO) in artificial snow

Hans-Werner JACOBI, Bright KWAKYE-AWUAH, Otto SCHREMS

Alfred Wegener Institute for Polar and Marine Research, Am Handelshafen 12, D-27570 Bremerhaven, Germany
E-mail: hwjacobi@awi-bremerhaven.de

ABSTRACT. Laboratory-made snow doped with either hydrogen peroxide (H_2O_2) or formaldehyde (HCHO) was exposed to radiation in the ultraviolet and visible range, resulting in a decomposition of both compounds. These experiments demonstrate that, besides the photolysis of nitrate, further photochemical reactions of atmospheric relevant compounds can take place in snow. Under similar conditions the decomposition of H_2O_2 is more efficient than that of HCHO. Since the decompositions in the experiments follow first-order reaction kinetics, we suggest that the same products as in photolysis reactions in the liquid phase are produced. If similar reactions also take place in natural snow covers, these reactions would have several important consequences. The reactions could represent pathways for the generation of highly reactive radicals in the condensed phase, enhancing the photochemical activity of surface snow and modifying the oxidation capacity of the atmospheric boundary layer. The photolysis could also constitute an additional sink for H_2O_2 and HCHO in surface snow, which should be taken into account for the reconstruction of atmospheric concentrations of both compounds from concentration profiles in surface snow and ice cores.

INTRODUCTION

Photochemical reactions in snow have recently attracted strong interest (e.g. Dominé and Shepson, 2002, and references therein). Several field studies at different locations in polar and mid-latitude regions have demonstrated that reactive nitrogen oxides are produced in the surface layers of irradiated snow covers and are subsequently emitted to the atmosphere (Honrath and others, 1999, 2000a, 2002; Jones and others, 2000, 2001; Ridley and others, 2000; Davis and others, 2001; Beine and others, 2002). Moreover, other reactive compounds like hydrogen peroxide (H_2O_2) and formaldehyde (HCHO), which are present in the snow and the atmosphere, can effectively be transferred in both directions between both compartments (Hutterli and others, 2001, 2002; Jacobi and others, 2002). Such processes modify the chemical composition and the oxidation capacity of the boundary layer over snow-covered regions (Ridley and others, 2000; Chen and others, 2001; Yang and others, 2002).

In addition, H_2O_2, HCHO and nitrate concentrations in ancient atmospheres would constitute important constraints for investigations of the chronological development of the atmospheric composition. Thus, a better understanding of the transfer processes of reactive species is needed to calculate atmospheric concentrations from profiles in surface snow, firn and ice cores. Transfer models for H_2O_2 and HCHO including physical processes in the atmosphere and the surface layers of the snow have so far been developed (McConnell and others, 1998; Hutterli and others, 1999, 2002). However, these models potentially suffer from the lack of consideration of photochemical processes taking place in irradiated snow.

Recent laboratory experiments have shown that the photolysis of nitrate incorporated in snow is responsible for producing nitrogen oxides (Honrath and others, 2000b; Dubowski and others, 2001, 2002; Cotter and others, 2003). Other species absorbing solar radiation in the troposphere are compounds like ozone, nitrate radical, organic peroxides and aldehydes (e.g. Finlayson-Pitts and Pitts, 2000). However, among these species only hydrogen peroxide (H_2O_2) and formaldehyde (HCHO) are incorporated in natural snow in considerable amounts. Indeed, Haan and others (2001) suggested that the HCHO photolysis could be responsible for observed CO production in sunlit snow. Therefore, we investigated whether H_2O_2 and HCHO can undergo photochemical reactions in snow. Consequently, we performed experiments with laboratory-made snow samples containing only H_2O_2 or HCHO to prevent further photochemical reactions, which possibly would lead to the concurrent production of both compounds.

EXPERIMENTAL

Solutions for the generation of artificial snow were prepared by adding 30% H_2O_2 (Merck, Darmstadt, Germany) or 37% HCHO (Merck) solutions to Milli-Q water. The diluted solutions were transferred into a stainless-steel tank. The tank was pressurized to $2–3 \times 10^5$ Pa and the liquid was forced through a brass nozzle producing a fine spray, which was collected in a wide-mouth Dewar flask filled with liquid nitrogen. The ice produced in this way was transferred into a walk-in cold room at –20°C, where it was collected on aluminum foil. After evaporation of the remaining liquid nitrogen, small amounts of the ice were ground with an electric mill and passed through a stainless-steel sieve with a mesh size of 0.5 mm. Following sieving, the snow was stored overnight in 1 L Schott bottles covered with aluminum foil and sealed with zero-air traps, which were filled with Hopcalite (Aero-Laser, Garmisch-Partenkirchen, Germany) to allow further degassing of nitrogen and to prevent the condensation of H_2O_2 or HCHO on the snow.

The experimental set-up for the photolysis experiments is shown in Figure 1. A 1000 W mercury-arc lamp (Oriel Instruments, Stratford, CT) installed in the cold room was

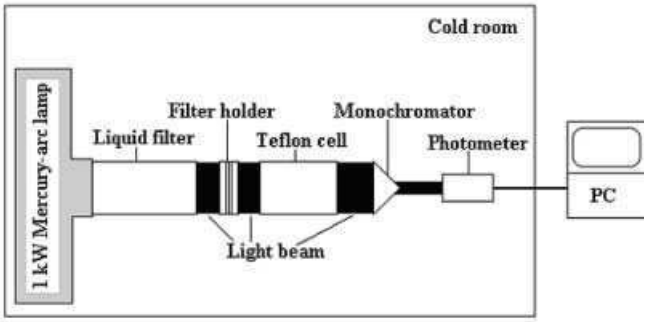

Fig. 1. Experimental system used for the photolysis experiments.

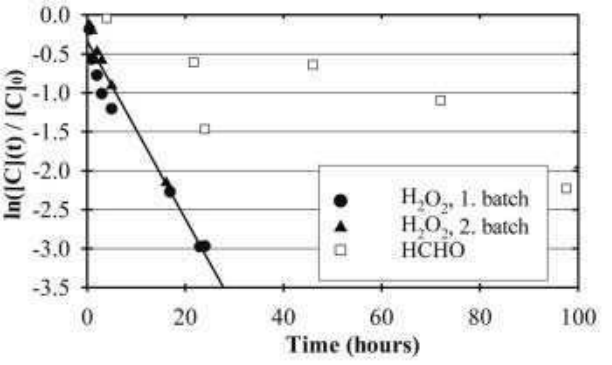

Fig. 2. Logarithm of relative H_2O_2 and HCHO concentrations in artificial snow as a function of irradiation time. $[H_2O_2]_0 = 9.5$–$9.8\,\mu$M, $[HCHO]_0 = 12$–$69\,\mu$M. The experiments were made with the 1 cm cell.

used as a light source. The emission intensity was regulated by the output of the lamp's power supply, which was set to 440 W. A water filter consisting of a cuvette filled with Milli-Q water and equipped with quartz windows was directly coupled to the output of the lamp housing condenser. The water absorbed the infrared radiation, which was sufficient to keep the water in the liquid state and to prevent the snow sample from melting. The transmittance of the water filter was >80% between 250 and 700 nm. The snow samples were filled into cylindrical Teflon cells equipped with quartz windows. Since the Teflon cell has the same inner diameter (4.6 cm) as the liquid cell, the snow sample was completely illuminated by the light beam. Two different cells with path lengths of 1 and 10.5 cm, respectively, were used.

The intensity of the irradiance transmitted through the cell was measured with a photodetector (SED 400, International Light, Newburyport, MA) connected to a recently calibrated radiometer (IL1700, International Light). The photodetector captured data over the range ~280–385 nm with a maximum sensitivity at 350 nm. The spectral resolution of the irradiance was obtained using a monochromator (Oriel Instruments, Stratford, CT) with a bandwidth of 2 nm.

The wavelength range of the emitted light was varied with two long-pass filters. The 50% cut-on points of these filters were either 295 nm (WG 295, Schott Glas, Mainz, Germany) or 360 nm (WG 360, Schott Glas). The output of the lamp shows two bands with maximum intensities around 310 and 370 nm. The long-pass filter WG 295 reduces only the intensity of the band at the lower wavelength and has a negligible influence on the intensity of the second band. The second long-pass filter, WG 360, entirely blocks the radiation of the first band and reduces the intensity of the second band at 370 nm by approximately 50%. However, the radiation in the visibility range remains almost unchanged.

H_2O_2 and HCHO concentrations in the snow were determined before and after each experiment. When the cell was filled for a new experiment, a sample of the same batch of snow was kept in an airtight bottle. After the experiment the snow from the 1 cm cell was transferred into a single bottle. The snow from the 10.5 cm cell was sampled in several layers and stored in different bottles. The snow samples were melted and immediately analyzed for H_2O_2 by titration with potassium permanganate solution or for HCHO by iodometric titration. Initial concentrations in the freshly prepared snow were approximately 9.4 mM for H_2O_2 and 12–69 mM for HCHO. Detection limits of the titrations were 0.25 mM for H_2O_2 and 0.5 mM for HCHO.

RESULTS

All experiments with the 1 cm cell show that H_2O_2 and HCHO in the artificial snow samples are decomposed during the irradiation with light in the ultraviolet (UV) and visible range. Figure 2 shows the logarithm of the ratio of the final and initial concentrations as a function of the irradiance time. It demonstrates that increasing the durations of the irradiation results in more effective decomposition of both compounds.

Assuming a first-order decay due to a photolysis reaction as described in Equation (1), the decrease of the concentrations can be expressed by Equation (2).

$$C + h\nu \rightarrow \text{prod.} \tag{1}$$

$$\ln\left(\frac{[C](t)}{[C]_0}\right) = -kt \tag{2}$$

with $C = H_2O_2$ or HCHO, $[C](t)$ the concentration after the experiment, $[C]_0$ the initial concentration, k the first-order reaction rate constant, and t the duration of the experiment.

In the case of H_2O_2, experiments were performed with two different batches of artificial snow. Separate regressions of the results of the two batches resulted in slopes of $-(0.11 \pm 0.01)\,h^{-1}$ and $-(0.13 \pm 0.01)\,h^{-1}$, respectively. These results are in excellent agreement and indicate that the results are reproducible and independent of the batches.

Regression lines for the decay of both compounds are shown in Figure 2, resulting in calculated slopes of $-(0.11 \pm 0.01)\,h^{-1}$ for H_2O_2 including all experiments and $-(0.017 \pm 0.007)\,h^{-1}$ for HCHO. These values show that under comparable conditions the decay of H_2O_2 occurs more than a factor of 5 faster than the decay of HCHO. Moreover, the regression coefficients of $R^2 = 0.97$ and 0.62 for H_2O_2 and HCHO indicate that the decomposition of both compounds can well be described by a first-order reaction.

Results of the experiments with the 10.5 cm cell are shown in Figure 3. As expected, the decomposition of both compounds is more effective in the surface layers that were directly exposed to the irradiation. Deeper layers show very small or even no decomposition of both compounds due to the effective attenuation of the irradiation intensities in the snow (e.g. Peterson and others, 2002). In order to investigate

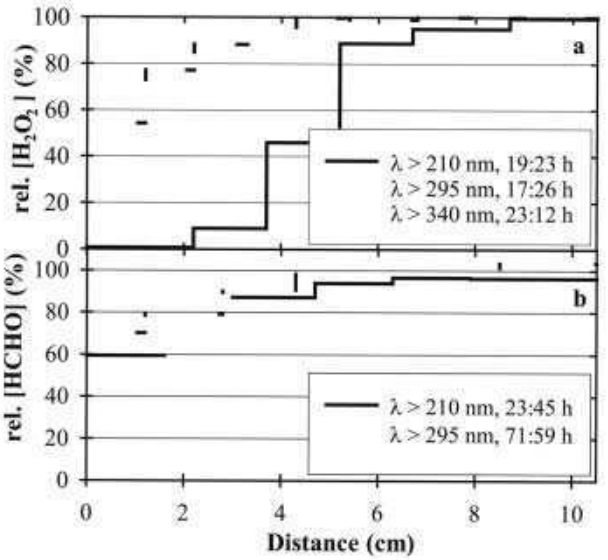

Fig. 3. Percentage of remaining (a) H_2O_2 and (b) HCHO in artificial snow samples after irradiation experiments. Samples were illuminated from the left; applied wavelengths and durations are indicated.

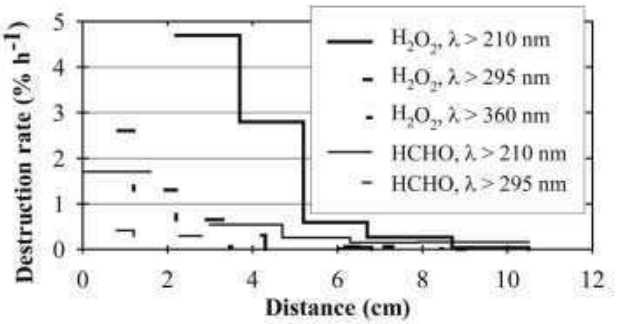

Fig. 4. Decomposition rates of H_2O_2 and HCHO during photolysis experiments with artificial snow.

the decay as a function of the wavelength, additional experiments with long-pass filters were performed. To compare the results of the different experiments with different duration, decomposition rates in per cent per hour were calculated (Fig. 4). Adding the long-pass filters obviously leads to smaller decomposition rates for both compounds, demonstrating that the decay of both compounds is more sensitive to irradiation in the UV than in the visible range. As in the experiments with the 1 cm cell, the decomposition of H_2O_2 is more effective than the decomposition of HCHO under comparable conditions.

DISCUSSION

H_2O_2 in the gas and liquid phase as well as HCHO in the gas phase significantly absorb solar radiation (e.g. Finlayson-Pitts and Pitts, 2000). Therefore, photolytic reactions are well-known sinks for both compounds in the atmosphere. For the first time, our results demonstrate that H_2O_2 and HCHO incorporated in artificial snow can also be destroyed if the snow is illuminated by radiation in the UV and visible range. These reactions can constitute additional pathways for the destruction of reactive compounds in natural snow covers due to photochemical reactions. Currently, only the photolysis of nitrate in snow has been investigated (Honrath and others, 2000b; Dubowski and others, 2001, 2002; Cotter and others, 2003) as a key reaction for the photochemical activity of surface snow layers. However, the results of this study imply that the photochemical activity of illuminated snow is possibly more diverse than previously thought.

The decays follow first-order kinetics as expected for the direct photolysis of both compounds. Such photolysis reactions also occur in the liquid phase according to reactions (3) and (4):

$$H_2O_2 + h\nu \rightarrow 2OH \quad (3)$$

$$H_2C(OH)_2 + h\nu \rightarrow H + HC(OH)_2. \quad (4)$$

In liquid solutions, HCHO is only present in the hydrated form $H_2C(OH)_2$ (Bell, 1966). Since the artificial snow is produced from liquid solutions, which are very rapidly frozen, we assume that in the artificial snow HCHO also exists in the hydrated form. Absorption of the hydrated HCHO in the aqueous phase in the UV range is much smaller than the absorption of H_2O_2 in aqueous solution. Therefore, in contrast to the H_2O_2 photolysis, this reaction is not included in tropospheric liquid-phase chemical models (e.g. Herrmann and others, 2000). Accordingly, the decay of HCHO in artificial snow also occurs more slowly than the decay of H_2O_2. If the HCHO photolysis proceeds via the fission of one of the C-H bonds as shown in reaction (4), H atoms are produced, which can react further with oxygen to form HO_2. Assuming that reactions (3) and (4) also occur in natural snow covers, they would constitute new pathways for the production of the highly reactive radicals OH and HO_2. These radicals could initiate further reactions in the snow or could be released into the interstitial air of the snowpack, where they could enhance the oxidation capacity of the interstitial air.

However, several difficulties exist in seeking to apply the experimental results with artificial snow samples to snow covers under natural conditions. These deficiencies are discussed in more detail.

The properties of the artificial snow samples are not directly comparable to natural snow, mainly due to the different production processes. In the atmosphere, ice crystals are formed by freezing of supercooled droplets or nucleation on ice-forming nuclei (Petrenko and Whitworth, 1999). The incorporation of H_2O_2 and HCHO into ice crystals is probably governed by co-condensation (Sigg and others, 1992). Although this mechanism should lead to rather uniform concentrations throughout the ice crystal, it has been shown that, in fresh precipitating snow and aged snow in the snowpack, large fractions of both compounds are located on the surface or within the surface layer of the crystals (Hutterli and others, 2002; Jacobi and others, 2002). In contrast, the shock freezing of the artificial snow leads most probably to ice crystals with evenly distributed H_2O_2 and HCHO. Due to the low diffusion coefficients of both compounds in ice of $<10^{-10}$ cm^{-2} s^{-1} (McConnell and others, 1998; Perrier and others, 2003), the molecules would require >100 days to diffuse from the middle to the surface of the artificial snow crystal. Therefore we assume that, in our experiments, H_2O_2 and HCHO were always rather uniformly distributed in the ice lattice. Nevertheless, H_2O_2

and HCHO molecules, which are present in a quasi-liquid surface layer, are most likely more effectively photolyzed than molecules incorporated in the ice lattice. Thus, we assume that under natural conditions, with larger fractions of both impurities present at the grain surfaces, the decay of both compounds could be even more effective than in our experiments.

The H_2O_2 and HCHO concentrations in the artificial snow samples were considerably higher than concentrations found in natural snow samples. Concentrations determined in snow samples from Antarctica and Greenland range from 1 to 35 μM for H_2O_2 (e.g. McConnell and others, 1998; Hutterli and others, 2001) and 0.1 to 2 μM for HCHO (e.g. Riedel and others, 1999; Hutterli and others, 2002). In addition, the irradiation intensities in the experiments were also considerably higher than the intensities of the solar radiation reaching the Earth's surface. To estimate this difference, we measured the radiation intensity in our experiments and compared it to measured intensities at the German research station Neumayer (70°39′ S) in Antarctica, where radiation in the wavelength range 300–370 nm is continuously measured with a total UV radiometer (TUVR; Eppley, Newport, RI). The measured radiation data can be retrieved via the Internet (http://www.awi-bremerhaven.de/MET/Neumayer/radiation.html). Highest daily averages of the radiation intensities occur in December and reach values of 23–27 W m^{-2}. In contrast, in our experiments the radiation intensity in the same wavelength range corresponded to a value of approximately 1200 W m^{-2} at the surface of the artificial snow samples. Thus, we assume that the concentration levels of the produced OH and HO_2 radicals in the snow were significantly higher in our experiment than in natural surface snow. These high levels may initiate further reactions, leading to an additional destruction of the impurities. Further experiments with lower H_2O_2 and HCHO concentrations and lower radiation intensities are needed.

Post-depositional loss processes may have important implications for the interpretation of H_2O_2 and HCHO profiles in surface snow and ice cores. Understanding and accounting for such reactions are essential for reconstructing past atmospheric composition. However, current transfer models of H_2O_2 and HCHO do not include photochemical reactions in the surface snow layer (McConnell and others, 1998; Hutterli and others, 1999, 2002). Interestingly, such transfer models based only on physical processes have successfully been applied to model measured H_2O_2 and HCHO properties at different locations (e.g. H_2O_2 and HCHO profiles retrieved from shallow ice cores; relationships between atmospheric and surface snow concentrations; fluxes between the snow surface and the atmosphere).

The discrepancy between measured and modeled field measurements, on the one hand, and our laboratory experiments, on the other, has several possible explanations. The photolysis of H_2O_2 and HCHO in natural snow may not be significant. If we compare again the radiation intensities in our experiment with the intensity measured at Neumayer (see above), we applied intensities which were roughly a factor of 50 higher than the maxima of daily means of the measured solar radiation intensities. For the comparison, we use the results of the experiments with the 295 nm long-pass filter, since the filter strongly reduces the radiation below 295 nm, comparable to the spectrum of the solar radiation reaching the Earth's surface. In these experiments, we obtained decomposition rates of 2.6 and 0.4% h^{-1} for H_2O_2 and HCHO in the surface layer of the snow (Fig. 4). Divided by a factor of 50, these decomposition rates correspond to 1.2% d^{-1} or 8.4% week^{-1} for H_2O_2, and 0.19% d^{-1} or 1.3% week^{-1} for HCHO. These rates are not negligible and would lead to observable losses in natural snow covers, at least in the case of H_2O_2. However, such losses can be obscured either by the deposition of H_2O_2 and HCHO from the atmosphere or by the photochemical production in the surface snow. Field measurements have shown that the transfer of both compounds between the atmosphere and the underlying surface snow occurs (Hutterli and others, 2001, 2002; Jacobi and others, 2002). Although bi-directional fluxes have been observed, deposition occurred normally during the night (Jacobi and others, 2002), and in summer the net fluxes were directed from the snow to the atmosphere (Hutterli and others, 2001, 2002; Jacobi and others, 2002). Therefore, such fluxes are not able to balance a photochemical decay, which potentially occurred in the surface snow layers. The possibility that the photochemical decay of H_2O_2 and HCHO is matched by a concurrent photochemical production is intriguing. Such mechanisms were proposed by Sumner and Shepson (1999) and were further elaborated by Dominé and Shepson (2002). Organic material is quite abundant even in the snow in polar regions (Dassau and others, 2002) and could act as a precursor for the photochemical formation of H_2O_2 and HCHO, which are typical products during the oxidation of organic compounds in the atmospheric gas and liquid phase (Finlayson-Pitts and Pitts, 2000). If similar photochemical mechanisms also take place in the surface snow, the production of H_2O_2 and HCHO is possible.

CONCLUSIONS

An effective decomposition of H_2O_2 and HCHO in laboratory-made snow was observed under the influence of highly intense UV and visible radiation. Further experiments with lower radiation intensities comparable to the solar radiation are needed before the results can be applied to processes occurring in natural snow covers. Additionally, lower trace compound concentrations should be applied and product studies should be performed.

However, if such reactions take place in natural snow, our experiments demonstrate that the decomposition rates are not negligible. The photochemical activity of the surface snow would depend not only on the photolysis of nitrate, but also on the photolysis of H_2O_2 and HCHO, which are always present in natural snow due to their solubility. Further laboratory and modeling studies are needed to better characterize photochemical processes in the snow and their effects on the composition of the atmospheric boundary layer above natural snow covers as well as on the concentration profiles of H_2O_2 and HCHO conserved in snow, firn and ice cores.

ACKNOWLEDGEMENT

Financial support by the Deutsche Forschungsgemeinschaft (DFG), grant JA 932/5-1, is gratefully acknowledged.

REFERENCES

Beine, H. J., R. E. Honrath, F. Dominé, W. R. Simpson and J. D. Fuentes. 2002. NO_x during background and ozone depletion periods at Alert: fluxes above the snow surface. *J. Geophys. Res.,* **107**(D21), 4584. (10.1029/2002JD002082.)

Bell, R. P. 1966. The reversible hydration of carbonyl compounds. *Adv. Phys. Organic Geochem.,* **4**, 1–29.

Chen, G. *and 12 others*. 2001. An investigation of South Pole HO_x chemistry: comparison of model results with ISCAT observations. *Geophys. Res. Lett.,* **28**(19), 3633–3636.

Cotter, E. S. N., A. E. Jones, E. W. Wolff and S.-B. Baugitte. 2003. What controls photochemical NO and NO_2 production from Antarctic snow? Laboratory investigation assessing the wavelength and temperature dependence. *J. Geophys. Res.,* **108**(D4), 4147. (10.1029/2002JD002602.)

Dassau, T. M. *and 10 others*. 2002. Investigation of the role of the snowpack on atmospheric formaldehyde chemistry at Summit, Greenland. *J. Geophys. Res.,* **107**(D19), 4394. (10.1029/2002JD002182.)

Davis, D. *and 11 others*. 2001. Unexpected high levels of NO observed at South Pole. *Geophys. Res. Lett.,* **28**(19), 3625–3628.

Dominé, F. and P. B. Shepson. 2002. Air–snow interactions and atmospheric chemistry. *Science,* **297**(5586), 1506–1510.

Dubowski, V., A. J. Colussi and M. R. Hoffmann. 2001. Nitrogen dioxide release in the 302 nm band photolysis and spray-frozen aqueous nitrate solutions: atmospheric implications. *J. Phys. Chem., Ser. A,* **105**(20), 4928–4932.

Dubowski, V., A. J. Colussi, C. Boxe and M. R. Hoffmann. 2002. Monotonic increase of nitrite yields in the photolysis of nitrate in ice and water between 238 and 294 K. *J. Phys. Chem., Ser. A,* **106**(30), 6967–6971.

Finlayson-Pitts, B. J. and J. N. Pitts. 2000. *Chemistry of the upper and lower atmosphere.* San Diego, CA, Academic Press.

Haan, D., Y. Zuo, V. Gros and C. A. M. Brenninkmeijer. 2001. Photochemical production of carbon monoxide in snow. *J. Atmos. Chem.,* **40**(3), 217–230.

Herrmann, H., B. Ervens, H.-W. Jacobi, R. Wolke, P. Nowacki and R. Zellner. 2000. CAPRAM2.3: a chemical aqueous phase radical mechanism for tropospheric chemistry. *J. Atmos. Chem.,* **36**(3), 231–284.

Honrath, R. E., M. C. Peterson, S. Guo, J. E. Dibb, P. B. Shepson and B. Campbell. 1999. Evidence of NO_x production within or upon ice particles in the Greenland snowpack. *Geophys. Res. Lett.,* **26**(6), 695–698.

Honrath, R. E., S. Guo, M. C. Peterson, M. P. Dziobak, J. E. Dibb and M. A. Arsenault. 2000a. Photochemical production of gas phase NO_x from ice crystal NO_3^-. *J. Geophys. Res.,* **105**(D19), 24,183–24,190.

Honrath, R. E., M. C. Peterson, M. P. Dziobak, J. E. Dibb, M. A. Arsenault and S. A. Green. 2000b. Release of NO_x from sunlight-irradiated midlatitude snow. *Geophys. Res. Lett.,* **27**(15), 2237–2240.

Honrath, R. E. *and 6 others*. 2002. Vertical fluxes of NO_x, HONO, and HNO_3 above the snowpack at Summit, Greenland. *Atmos. Environ.,* **36**(15–16), 2629–2640.

Hutterli, M. A., R. Röthlisberger and R. C. Bales. 1999. Atmosphere-to-snow-to-firn transfer studies of HCHO at Summit, Greenland. *Geophys. Res. Lett.,* **26**(12), 1691–1694.

Hutterli, M. A., J. R. McConnell, R. W. Stewart, H.-W. Jacobi and R. C. Bales. 2001. Impact of temperature-driven cycling of hydrogen peroxide (H_2O_2) between air and snow on the planetary boundary layer. *J. Geophys. Res.,* **106**(D14), 15,395–15,404.

Hutterli, M. A., R. C. Bales, J. R. McConnell and R. W. Stewart. 2002. HCHO in Antarctic snow: preservation in ice cores and air–snow exchange. *Geophys. Res. Lett.,* **29**(8). (10.1029/2001GL014256.)

Jacobi, H.-W. *and 7 others*. 2002. Measurements of hydrogen peroxide and formaldehyde exchange between the atmosphere and surface snow at Summit, Greenland. *Atmos. Environ.,* **36**(15–16), 2619–2628.

Jones, A. E., R. Weller, E. W. Wolff and H.-W. Jacobi. 2000. Speciation and rate of photochemical NO and NO_2 production in Antarctic snow. *Geophys. Res. Lett.,* **27**(3), 345–348.

Jones, A. E. *and 6 others*. 2001. Measurements of NO_x emissions from the Antarctic snowpack. *Geophys. Res. Lett.,* **28**(8), 1499–1502.

McConnell, J. R., R. C. Bales, R. W. Stewart, A. M. Thompson, M. R. Albert and R. Ramos. 1998. Physically based modeling of atmosphere-to-snow-to-firn transfer of H_2O_2 at South Pole. *J. Geophys. Res.,* **103**(D9), 10,561–10,570.

Perrier, S., P. Sassin and F. Dominé. 2003. Diffusion and solubility of HCHO in ice: preliminary results. *Can. J. Phys.,* **81**(1–2), 319–324.

Peterson, M., D. Barber and S. Green. 2002. Monte Carlo modeling and measurements of actinic flux levels in Summit, Greenland snowpack. *Atmos. Environ.,* **36**(15–16), 2545–2551.

Petrenko, V. F. and R. W. Whitworth. 1999. *Physics of ice.* Oxford, etc., Oxford University Press.

Ridley, B. *and 15 others*. 2000. Is the Arctic surface layer a source and sink of NO_x in winter/spring? *J. Atmos. Chem.,* **36**(1), 1–22.

Riedel, K., R. Weller and O. Schrems. 1999. Variability of formaldehyde in the Antarctic troposphere. *Phys. Chem. Chem. Phys.,* **1**(24), 5523–5527.

Sigg, A., T. Staffelbach and A. Neftel. 1992. Gas phase measurements of hydrogen peroxide in Greenland and their meaning for the interpretation of H_2O_2 records in ice cores. *J. Atmos. Chem.,* **14**(1–4), 223–232.

Sumner, A. L. and P. B. Shepson. 1999. Snowpack production of formaldehyde and its effect on the Arctic troposphere. *Nature,* **398**(6724), 230–233.

Yang, J. *and 9 others*. 2002. Impacts of snowpack emissions on deduced levels of OH and peroxy radicals at Summit, Greenland. *Atmos. Environ.,* **36**(15–16), 2523–2534.

Publication 3.3.2

Blunier, T., G. Floch, H.-W. Jacobi, and E. Quansah,
Isotopic view on nitrate loss in Antarctic surface snow,
Geophys.Res.Lett. **32**, L13501, doi: 10.1029/2005GL023011, 2005.

Isotopic view on nitrate loss in Antarctic surface snow

Thomas Blunier,[1] Grégoire L. Floch,[1] Hans-Werner Jacobi,[2] and Emmanuel Quansah[2]

Received 17 March 2005; revised 24 May 2005; accepted 6 June 2005; published 8 July 2005.

[1] Massive post-depositional processes alter the nitrate concentration in polar firn where the annual snow accumulation is low. This hinders a direct atmospheric interpretation of the ice core nitrate record. Fractionation of nitrate isotopes during post-depositional nitrate loss may allow estimating the amount of nitrate loss in the past. We measured $\delta^{15}N$ of nitrate in two Antarctic surface cores from the Dome C area. In concert with the known concentration decrease with depth we observe an increase in the isotopic signature. Assuming a Rayleigh type process we find an isotope effect of $\varepsilon = -54‰$. We measured the fractionation factor for photolysis in the laboratory and obtained $\varepsilon = -11.7 \pm 1.4‰$. As the observed fractionation factor in the firn is much lower this rules out that photolysis in the surface snow is the main process leading to the dramatic nitrate loss in the top centimeters of the firn. **Citation:** Blunier, T., G. L. Floch, H.-W. Jacobi, and E. Quansah (2005), Isotopic view on nitrate loss in Antarctic surface snow, *Geophys. Res. Lett.*, *32*, L13501, doi:10.1029/2005GL023011.

1. Introduction

[2] Nitrate (NO_3^-) deposition is the final fate of various N species in polar regions [*Wolff*, 1995]. Therefore, NO_3^- from polar ice cores can potentially be used to investigate the atmospheric cycle of reactive nitrogen compounds. Nitrogen compounds have an important impact on atmospheric chemistry and the oxidation capacity of the atmosphere. Unfortunately, it turned out that NO_3^- undergoes massive depositional and post-depositional processes in the firn. This hinders a direct atmospheric interpretation of the ice core NO_3^- records [*Röthlisberger et al.*, 2002].

[3] In Antarctica's low accumulation areas most of the NO_3^- deposited at the surface is lost when the snow reaches a few decimeters depth [*Mayewski and Legrand*, 1990; *Röthlisberger et al.*, 2000]. On the other hand, high accumulation sites (e.g., Summit, Greenland) presently preserve more than 90% of the initial NO_3^- [*Burkhart et al.*, 2004]. Here the annual cycle in the concentration is preserved and also the isotopic composition of NO_3^- appears largely unaffected by post-depositional processes [*Hastings et al.*, 2004].

[4] *Mulvaney et al.* [1998] describe the depositional processes affecting NO_3^- in surface snow as a short-term equilibrium between the atmosphere and the snowpack where uptake and loss operate over the daily cycle with a net loss over weeks and months. The seasonal NO_3^- signal is preserved in this process although smoothed by diffusion. At very low accumulation sites the net loss of NO_3^- continues over several years and results in a complete loss of the annual signal for very low accumulations sites like Vostok, or Dome C.

[5] Key parameters determining NO_3^- loss are established but are not clearly quantified [*Dibb and Whitlow*, 1996; *Mayewski and Legrand*, 1990; *Röthlisberger et al.*, 2000]. They include temperature-accumulation, near surface air concentration, elevation, and presence of other species in snow (see *Burkhart et al.* [2004] for a compilation). Major candidates for the loss process in Antarctica as well as in Greenland are photolysis and re-evaporation. The latter may be related to wind driven effects [*Mulvaney et al.*, 1998].

[6] In low accumulation sites snow remains relatively long in close proximity to the surface and thus in range of radiation of intense UV. Therefore, it seems possible that photolysis is the main process leading to the NO_3^- loss [*Röthlisberger et al.*, 2002]. Nonetheless, a model study suggests that only 40% of the NO_3^- content can be depleted by photolysis for conditions found at Dome C [*Wolff et al.*, 2002].

[7] The isotopic composition of NO_3^- deposited on the snow depends on the NO_3^- sources and the chemical reactions taking place during the transport to the deposition site [*Freyer et al.*, 1996]. The isotope composition in freshly fallen snow is expected to equal the one in the atmosphere above the snow [*Hastings et al.*, 2004]. *Wagenbach et al.* [1998] present Antarctic atmospheric $\delta^{15}N$ values varying from 0 to −50‰. In a pioneer study *Freyer et al.* [1996] measured $\delta^{15}N$ of NO_3^- in ice cores from Greenland, Antarctica and the Alps. They found increasing $\delta^{15}N$ values with the inverse accumulation rate for Holocene samples. This increase goes along with a NO_3^- concentration decrease for most sites, which is interpreted as originating from a loss process in the freshly fallen snow. Thus, the changes in the nitrogen (and oxygen) isotope composition of NO_3^- may allow for the reconstruction of the atmospheric NO_3^- concentration once the fractionation processes in the firn are understood.

[8] Here we investigate the first 15 cm of a firn core taken at the EPICA-DC site in the austral summer of 2003 by means of isotope analysis. Dome C (75°06′S, 123°21′E, altitude 3233 m a.s.l.) has an annual mean temperature of −54.5°C and a snow accumulation rate of 25.0 kg m^{-2} $year^{-1}$ (corresponding to about 7.4 cm of snow per year at the surface). At this low accumulation site the NO_3^- concentration decreases by orders of magnitude over the first 10 cm of firn. Release in the form of HNO_3 and photolysis of NO_3^- have been proposed as the cause for this loss [*Röthlisberger et al.*, 2002]. Further we determined the fractionation factor for $\delta^{15}N$ of NO_3^- associated with photolysis of NO_3^- in snow. Based on laboratory and

[1]Climate and Environmental Physics, Physics Institute, University of Bern, Bern, Switzerland.
[2]Alfred Wegener Institute for Polar and Marine Research, Bremerhaven, Germany.

0094-8276/05/2005GL023011$05.00

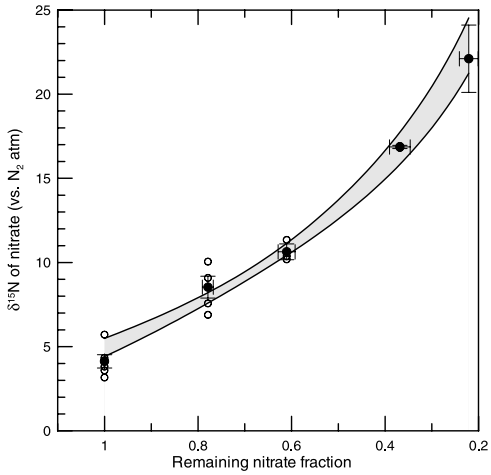

Figure 1. $\delta^{15}N$ of NO_3^- measured in artificial snow versus the remaining NO_3^- fraction after exposure to radiation. Circles are replicate isotope measurements using the same snow sample. Dots are mean values with error bars. The gray area represents the one sigma spread of the Monte Carlo simulations for the Rayleigh type process. The calculated fractionation factor is $\varepsilon = -11.7 \pm 1.4‰$, where $\varepsilon = (\alpha - 1)$.

firn measurements we are able to show that photolysis is not the sole process responsible for the NO_3^- loss in the firn.

2. Measurements

[9] We measure NO_3^- isotopes using a microbiological method developed by Sigman et al. [*Sigman et al.*, 2001]. The method is based on the isotopic analysis of nitrous oxide (N_2O) generated from NO_3^- by denitrifying bacteria. We use *Pseudomonas Chlororaphis*, which lacks N_2O reductase activity, and follow the protocol for bacteria cultivation by *Sigman et al.* [2001]. 2 ml aliquots of bacteria slush are added to 20 ml sample vials. Remnant N_2O in the vials is removed by purging ultrapure helium carrier gas at 20 ml/min for 2–4 hours, before melt water from the samples (or artificial snow) is added to the cultures. After an overnight incubation, the bacteria quantitatively converted NO_3^- to N_2O. A poison (NaOH) is injected to lysis the bacteria and stop the reaction. Using a helium carrier gas, N_2O is stripped from each sample vial and analyzed by a GC/MS system (Thermo Finnigan MAT 253). With standards we obtain a reproducibility of ±15 ppb for the concentration and ±0.2‰ for $\delta^{15}N$. All measurements are made versus a N_2O standard gas. Each batch of samples includes samples with NO_3^- standards (IAEA-N3), which have an assigned $\delta^{15}N$ of 4.7‰ versus atmospheric N_2.

[10] Our system is designed to work with a sample amount of 10 nmole of NO_3^-. To obtain 10 nmole of NO_3^- the volume of the sample (i.e., the amount of snow) added to the bacteria slush varies depending upon the concentration of each sample. As the concentration in the snow decreases rapidly over the first few centimeters, the sample volumes vary between 1 and 8 ml from the surface to 15 cm depth. We observe that for low concentration samples the transfer of NO_3^- to N_2O is slightly reduced. Along with the reduced transfer comes a strong $\delta^{15}N$ fractionation of several per mil. We overcame this problem by adding more bacteria to the low NO_3^- concentration samples. The bacteria concentration was kept constant at values corresponding to the sample protocol of *Sigman et al.* [2001] regardless of the sample size.

3. Laboratory Experiment

[11] Fractionation factors for the various possible reactions in firn are unknown. We determined the fractionation factor for photolysis of NO_3^- in a laboratory experiment. At AWI artificial snow was produced from a solution of $NaNO_3$ in ultrapure water (MilliQ) with an initial concentration of about 780 ppb. The solution was sprayed into a Styrofoam cup filled with liquid nitrogen. The generated ice chunks were ground and passed through a sieve. After storage over night, the artificial snow samples were exposed to intense UV and visible radiation in the range of 200 nm to ~900 nm [see *Jacobi et al.*, 2005]. The experiments were performed at −20°C with exposition times ranging from 0.5 to 3 h.

[12] Previous experiments performed under identical conditions regarding initial NO_3^- concentration, radiation intensity, and temperature demonstrated an exponential decay of NO_3^- within the first 5 h of the experiments with a photolysis rate of 0.5 h^{-1} [*Quansah*, 2004]. This photolysis rate was used to calculate remaining NO_3^- fractions in the snow samples used for the isotope analyses. In the previous experiments, nitrite concentrations showed a steep increase followed by a fast decrease leading to a maximum in the nitrite concentrations after experiments lasting between 0.5 and 1 h. Using the previously observed nitrite concentrations, we estimate that the nitrite-to-nitrate ratios are equal to or smaller than 0.08 in all samples used for the isotope analysis. Since the experiments were performed in closed cells, it is not clear if the detected nitrite is a decay product or if it is formed from decay products, which were not removed during the experiments. We also do not completely rule out that some NO_3^- is reformed from gaseous decay products like NO_2. The exposed snow was transported to Bern for isotope analysis (Figure 1).

[13] We calculate the fractionation factor of the photolysis reaction for this Rayleigh type experiment.

$$\frac{R_f}{R_0} = f^{(\alpha-1)} \tag{1}$$

R_0 and R_f are the isotope ratios $^{15}N/^{14}N$ of the initial NO_3^- and the remaining NO_3^- fraction f. The same equation can be written with concentrations and δ-values versus an arbitrary standard with the isotope ratio value R_{St}.

$$\frac{R_f}{R_{St}} \cdot \frac{R_{St}}{R_0} = \frac{\delta_f + 1}{\delta_0 + 1} = f^{(\alpha-1)} \tag{2}$$

$$\ln(\delta_f + 1) = (\alpha - 1) \cdot \ln f + \ln(\delta_0 + 1) \tag{3}$$

[14] A simple linear regression of the data allows the calculation of the fractionation factor (Equation 3). However, this method does not account for the individual

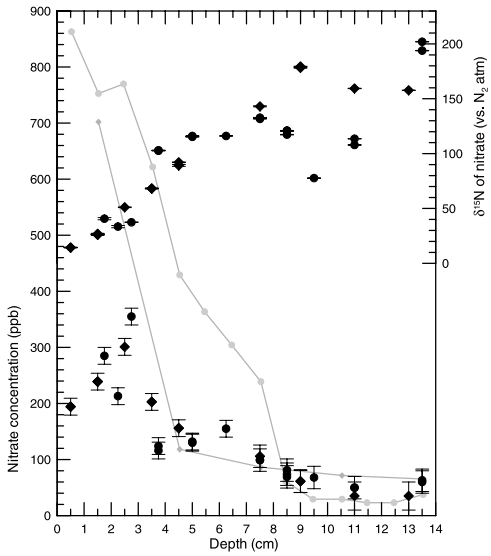

Figure 2. $\delta^{15}N$ and concentrations of NO_3^- from the Dome C area versus depth. Grey dots and diamonds are concentration measurements from a snow pit taken in 1999 [*Röthlisberger et al.*, 2000]. Dots and diamonds are individual samples from adjacent cores taken in 2003. Error bars show one sigma analytical errors. Concentrations were estimated from the mass spectrometer measurements.

uncertainties for $\delta^{15}N$ values and concentrations, which are quite substantial. Therefore, we do a Monte Carlo simulation taking into account these uncertainties (Figure 1). The exposition times are used to calculate the NO_3^- concentrations, which are accurate to the 2% range. We obtain a fractionation factor of $\varepsilon = -11.7 \pm 1.4‰$, where $\varepsilon = (\alpha - 1)$. Our bacteria do feed on NO_3^- and nitrite forming finally N_2O. Therefore the calculated fractionation factor includes a fraction of maximal 8% nitrite in our samples (see above). Depending on how this nitrite is formed we may under- or overestimate the photolytic fractionation factor for NO_3^-.

4. Antarctic Samples

[15] Two adjacent firn cores were sampled at Dome C during the austral summer of 2003. The cores were stored in polyethylene tubes and kept below −20°C until analyzed. We measured the first 15 cm of both cores, which covers about two years of precipitation. Both concentration profiles are typical for Dome C and low accumulations sites, with a drastic drop of 350 ppb to 50 ppb in the first ten centimeters of the firn (Figure 2). In deeper strata the concentration remains stable at low levels [*Röthlisberger et al.*, 2000].

[16] Samples were taken from the inner and the outer part of the core. We observe systematically higher NO_3^- concentrations and lower isotopic values in the outer section of the cores. On average the concentration difference between outer and inner sample is 41 ± 11 ppb with an average $\delta^{15}N$ difference of −26 ± 6‰. Apparently the polyethylene tube is a source of light NO_3^-. In a core sampled and stored in a similar way than the Dome C samples discussed here, we investigated how deep the contamination entered the core. We found that the contamination has entered the outermost 2 cm of the core. As these measurements have been made six months later than the isotope measurements, we are confident that our Dome C results from the inner core section are free from a contamination from the sampling tubes.

[17] In Figure 3, $\delta^{15}N$ values of the inner section are plotted against NO_3^- concentrations. The resolution depends on the NO_3^- concentration of the ice core. In the top 2 cm we measured samples every 0.5 cm. Further down the core the resolution decreases due to the lower concentration in order to match the sample size minimum of about 10 nmoles of NO_3^-.

5. Results and Discussion

[18] At high accumulation sites annual variations in concentration and isotope values are visible in the first meter of firn [*Hastings et al.*, 2004]. No annual variations are obvious in the concentration [*Röthlisberger et al.*, 2000] or nitrogen isotope records (Figure 2) at Dome C. The two cores and similar concentration studies show, that both concentration and isotope signals are highly variable in adjacent cores. Nevertheless, a clear trend of lower concentrations with increasing isotope values is visible. Apparently the removal process for NO_3^- prefers the lighter isotope. Assuming that NO_3^- is removed irreversibly from the firn we can use the Rayleigh equation to calculate the fractionation coefficient α of the sum of the processes involved. For the natural samples we do not know the original surface concentration and, therefore, the fraction *f*. However, the fractionation coefficient can also be calculated without that knowledge. We substitute $f = C_f/C_0$ where C_0 and C_f are the original surface concentration and the concentration of the remaining fraction *f*, respectively and obtain:

$$\ln(\delta_f + 1) = (\alpha - 1)\ln C_f + \underbrace{[\ln(\delta_0 + 1) - (\alpha - 1)\ln C_0]}_{b} \quad (4)$$

[19] We find $\varepsilon = -53.9‰$, where $\varepsilon = (\alpha - 1)$ (Figure 3). Due to the high local variability the uncertainty of this isotope effect is relatively large (9.7‰). As the fractionation

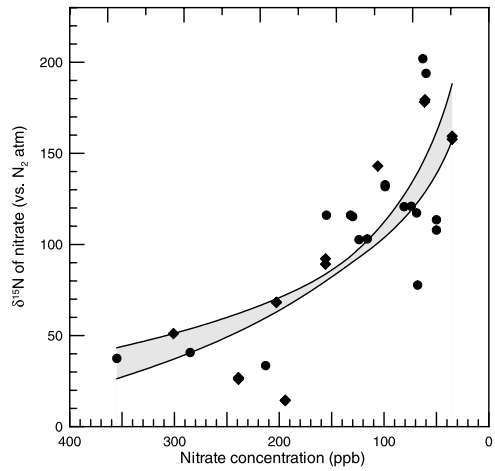

Figure 3. $\delta^{15}N$ of NO_3^- versus concentration for samples taken in the austral summer of 2003 (Figure 2). The gray area represents the one sigma spread of the Monte Carlo simulations for a Rayleigh type process.

coefficient for photolysis is only $\varepsilon = -11.7 \pm 1.4‰$ we conclude, that photolysis is probably not the dominant loss process in the near surface snow.

[20] There is, however, the possibility that photolysed NO_3^- is recycled, accumulating photolytic fractionations to the observed isotope effect. Such a process would involve the photolysis of NO_3^- in the snow generating nitrogen oxides (NO_x), its release to the firn air [*Jones et al.*, 2000], the reoxidation of NO_x to NO_3^- in the gas phase, which then is again deposited to the snow. Such a recycling in the atmosphere could explain the strong fractionation observed in the natural snow only, if it involves at least one step with a strong $\delta^{15}N$ enrichment. Such an enrichment has been observed, however, not under conditions that lead to a significant NO_3^- production. Under conditions that lead to a significant production of NO_3^- the redeposited NO_3^- is isotopically light [*Heaton et al.*, 2004]. This is in line with a recent finding from *Hastings et al.* [2004] and makes it unlikely that recycling of photolysed NO_3^- explains the observed isotope fractionation in the firn.

[21] At Neumayer Station (70°39′S, 08°15′W) the isotope values of NO_3^- vary between about 0‰ in the austral summer and −50‰ in the austral winter. The annual mean value for the time period 1986 to 1992 is $-21.6 \pm 9.9‰$ [*Wagenbach et al.*, 1998]. First measurements on filter samples from the Dome C site show a similar signal. The top samples ("surface") show relatively low concentrations compared to the values found by *Röthlisberger et al.* [2000] with elevated isotope values of up to +40‰. It is likely that we did not catch the surface snow or that the first sample suffered from loss processes during the transport. The Rayleigh approach allows also the calculation of a surface concentration based on a surface isotope value from the intercept b of the regression (Equation 4).

$$C_0 = \left(\frac{\delta_0 + 1}{e^b}\right)^{1/(\alpha-1)} \quad (5)$$

[22] Assuming that the initial $\delta^{15}N$ signature of NO_3^- in fresh snow corresponds to the annual mean value found for Neumayer Station, we calculate a surface NO_3^- concentration of about 900 ppb consistent with published data for the Dome C area [*Röthlisberger et al.*, 2000].

[23] We are aware that assuming a Rayleigh type fractionation is an oversimplification of the processes in the firn. Nevertheless, this simple approach demonstrates that photolysis alone is not responsible for the loss process in the near surface snow. *Wolff et al.* [2002] estimate that only 40% of the NO_3^- is removed by photolysis reactions. With our data this would result in a fractionation factor of the other non photolytic process(es) of about −80‰. The most promising candidate is re-evaporation of NO_3^-. The next step will be to simulate re-evaporation in the lab and to determine its fractionation factor.

[24] Once fractionation factors for individual loss processes in the firn are known they will help to disentangle their relative contribution to the total NO_3^- loss. If we understand the fractionation of NO_3^- isotopes during post-depositional processes isotope measurements from ice cores may ultimately allow estimating the amount of post-depositional NO_3^- loss in the past. Combined with the existing high resolution NO_3^- concentration records it may be possible to reconstruct the true past atmospheric NO_3^- concentration in polar areas.

[25] **Acknowledgments.** This work was supported by the University of Bern, the Swiss National Science Foundation, and the German Research Foundation (DFG). We thank Danny Sigman (Princeton University) for his open door policy concerning the denitrifier method and Ernst Schweingruber (University of Bern) for his support with the bacteria cultures. We also thank Manuel Hutterli, Regine Röthlisberger (University of Bern), Dietmar Wagenbach (University of Heidelberg), and Eric Wolff (British Antarctic Survey) for discussion and comments. We thank the EPICA crews for their work in the field. We also thank Meredith G. Hastings and an anonymous reviewer for critical but constructive comments.

References

Burkhart, J. F., M. Hutterli, R. C. Bales, and J. R. McConnell (2004), Seasonal accumulation timing and preservation of nitrate in firn at Summit, Greenland, *J. Geophys. Res.*, *109*, D19302, doi:10.1029/2004JD004658.

Dibb, J. E., and S. I. Whitlow (1996), Recent climate anomalies and their impact on snow chemistry at South Pole, 1987–1994, *Geophys. Res. Lett.*, *23*, 1115–1118.

Freyer, H. D., K. Kobel, R. J. Delmas, D. Kley, and M. R. Legrand (1996), First results of N-15/N-14 ratios in nitrate from alpine and polar ice cores, *Tellus, Ser. B*, *48*, 93–105.

Hastings, M. G., E. J. Steig, and D. M. Sigman (2004), Seasonal variations in N and O isotopes of nitrate in snow at Summit, Greenland: Implications for the study of nitrate in snow and ice cores, *J. Geophys. Res.*, *109*, D20306, doi:10.1029/2004JD004991.

Heaton, T. H. E., P. Wynn, and A. M. Tye (2004), Low $^{15}N/^{14}N$ ratios for nitrate in snow in the high Arctic (79°N), *Atmos. Environ.*, *38*, 5611–5621.

Jacobi, H.-W., B. Kwakye-Awuah, and O. Schrems (2005), Photochemical decomposition of hydrogen peroxide (H_2O_2) and formaldehyde (HCHO) in artificial snow, *Ann. Glaciol.*, in press.

Jones, A. E., R. Weller, E. W. Wolff, and H. W. Jacobi (2000), Speciation and rate of photochemical NO and NO_2 production in Antarctic snow, *Geophys. Res. Lett.*, *27*, 345–348.

Mayewski, P. A., and M. R. Legrand (1990), Recent increase in nitrate concentration of Antarctic snow, *Nature*, *346*, 258–260.

Mulvaney, R., D. Wagenbach, and E. W. Wolff (1998), Postdepositional change in snowpack nitrate from observation of year-round near-surface snow in coastal Antarctica, *J. Geophys. Res.*, *103*, 11,021–11,031.

Quansah, E. (2004), Photochemical decomposition of nitrate (NO_3^-) in artificial snow, M.S. thesis, Univ. of Bremen, Bremen, Germany.

Röthlisberger, R., M. A. Hutterli, S. Sommer, E. W. Wolff, and R. Mulvaney (2000), Factors controlling nitrate in ice cores: Evidence from the Dome C deep ice core, *J. Geophys. Res.*, *105*, 20,565–20,572.

Röthlisberger, R., et al. (2002), Nitrate in Greenland and Antarctic ice cores: A detailed description of post-depositional processes, *Ann. Glaciol.*, *35*, 209–216.

Sigman, D., K. L. Casciotti, M. Andreani, C. Barford, M. Galanter, and J. K. Böhlke (2001), A bacterial method for the nitrogen isotopic analysis of nitrate in seawater and freshwater, *Anal. Chem.*, *73*, 4145–4153.

Wagenbach, D., M. Legrand, H. Fischer, F. Pichlmayer, and E. W. Wolff (1998), Atmospheric near-surface nitrate at coastal Antarctic sites, *J. Geophys. Res.*, *103*, 11,007–11,020.

Wolff, E. W. (1995), Nitrate in Polar Ice, in *Ice Core Studies of Global Biogeochem. Cycles*, edited by R. J. Delmas, pp. 195–224, Springer, New York.

Wolff, E. W., A. E. Jones, T. J. Martin, and T. C. Grenfell (2002), Modelling photochemical NO_x production and nitrate loss in the upper snowpack of Antarctica, *Geophys. Res. Lett.*, *29*(20), 1944, doi:10.1029/2002GL015823.

T. Blunier and G. L. Floch, Climate and Environmental Physics, Physics Institute, University of Bern, Sidlerstrasse 5, CH-3012 Bern, Switzerland. (blunier@climate.unibe.ch)

H.-W. Jacobi and E. Quansah, Alfred Wegener Institute for Polar and Marine Research, Am Handelshafen 12, D-27570 Bremerhaven, Germany.

Publication 3.3.3

Jacobi, H.-W., T. Annor, and E. Quansah,

Investigation of the photochemical decomposition of nitrate, hydrogen peroxide, and formaldehyde in artificial snow,

J.Photochem.Photobiol. A **179**, 330-338, 2006.

Available online at www.sciencedirect.com
SCIENCE DIRECT
Journal of Photochemistry and Photobiology A: Chemistry 179 (2006) 330–338
Journal of Photochemistry and Photobiology A:Chemistry
www.elsevier.com/locate/jphotochem

Investigation of the photochemical decomposition of nitrate, hydrogen peroxide, and formaldehyde in artificial snow

Hans-Werner Jacobi *, Thompson Annor, Emmanuel Quansah

Alfred Wegener Institute for Polar and Marine Research, Am Handelshafen 12, 27570 Bremerhaven, Germany

Received 19 July 2005; received in revised form 22 August 2005; accepted 1 September 2005
Available online 7 October 2005

Abstract

Species like nitrate (NO_3^-), hydrogen peroxide (H_2O_2), and formaldehyde (HCHO) are ubiquitous trace compounds in snow. Photochemical reactions of these compounds in the snow can have important implications for the composition of the atmospheric boundary layer in snow-covered regions and for the interpretation of concentration profiles in snow and ice regarding the composition of the past atmosphere. Therefore, we performed laboratory experiments to investigate such reactions in artificially produced snow samples. Artificial snow samples allow to execute experiments under defined and reproducible conditions and to investigate single reactions. All reactions were carried out under comparable experimental conditions and indicated that the photolysis of H_2O_2 and NO_3^- occurred equally fast, while the photolysis of HCHO was considerably slower. Moreover, the photolysis of HCHO was only observed if initial concentrations were much higher than found in natural snow samples. These results indicate that the H_2O_2 and NO_3^- reactions are possibly equally important in natural snow covers regarding the formation of OH radicals, while the photolysis of HCHO is probably negligible. Nitrite (NO_2^-) was observed as one of the products of the NO_3^- photolysis; however, it was itself photolyzed at a higher rate than NO_3^-. After a certain photolysis period ($\geq$8 h) the NO_3^- and NO_2^- concentrations in the snow remained constant at a level of 10% of the initial nitrogen content. This is probably due to a recycling of the anions from nitrogen oxides in the gas phase of the reaction cells indicating that the chemical reactions occur in or near the surface layer of the snow crystals.

Keywords: Photochemical reactions; Snow; Nitrate; Hydrogen peroxide; Formaldehyde

1. Introduction

The chemical transformation of many compounds in the atmosphere is initiated and driven by photochemical reactions. Such reactions occurring in the atmospheric gas and liquid phases have extensively been studied (e.g. [1]). Recently, photochemical reactions in the tropospheric ice phase also attracted a lot of interest. Among these are photochemical reactions taking place in the upper layers of the natural snow covers in polar and alpine regions [2]. Because of their ubiquity in the troposphere and their high water solubility, species like nitric acid (HNO_3), hydrogen peroxide (H_2O_2), and formaldehyde (HCHO) are common trace compounds in natural snow samples even in remote polar regions [3]. It can be expected that photochemical reactions in snow take place, since these and further organic compounds present in the snow [4,5] can absorb solar radiation, which can penetrate into deeper layers (several tens of centimeters) of the snow [6,7]. Indeed, several field and laboratory studies have indicated that a variety of photochemical processes can occur in natural surface snow under the influence of solar radiation [5,8–25]. For example, the photolysis of nitrate (NO_3^-) has been identified as one of the key reactions. Therefore, it has been the goal of several laboratory experiments to investigate the reaction mechanism and the reaction products at temperatures typical for natural snow covers [16–20]. More recently, the photolysis reactions of H_2O_2 and HCHO have been the subject of laboratory studies [21,25]. Nevertheless, reliable information about the photochemical reaction mechanism in surface snow is still missing. For example, several authors have proposed that in addition to or initiated by the NO_3^- photolysis organic compounds present in the snow are transformed into highly reactive organic compounds like formaldehyde (HCHO) or acetone [2,5,15].

The photochemical processes in snow have two important implications. First, they affect the composition of the atmospheric boundary layer in snow-covered areas due to the release

* Corresponding author. Tel.: +49 471 4831 1493; fax: +49 471 4831 1425.
E-mail address: hwjacobi@awi-bremerhaven.de (H.-W. Jacobi).

1010-6030/$ – see front matter © 2005 Elsevier B.V. All rights reserved.
doi:10.1016/j.jphotochem.2005.09.001

of photochemically produced compounds like nitrogen oxides (NO_x). For example, under stable atmospheric conditions, NO_x mixing ratios can reach values in the order of several hundreds of parts per trillion by volume (ppt V) even in remote polar regions [13,14]. Such high levels of NO_x influence the atmospheric oxidation capacity due to their role in the formation of hydroxl radicals and ozone. Second, the photochemical processing can alter the concentrations of the trace compounds in the snow after deposition. This can have a large impact on the interpretation of the concentration profiles in the snow and in firn and ice cores. Such profiles can be utilized to reconstruct concentrations of the compounds in the paleo-atmosphere if so-called transfer functions are known, which relate snow concentrations to atmospheric concentrations [3]. Transfer functions for NO_3^-, H_2O_2, and HCHO would be of great importance since these compounds can potentially be used to determine the role of reactive nitrogen species and the oxidation of methane in the atmosphere in the past (e.g. [26]).

Here, we present laboratory experiments concerning the photochemical transformation of NO_3^-, H_2O_2, and HCHO in snow, since in most of the previous laboratory studies ice samples rather than snow samples were used. Our experiments were performed using artificially produced snow samples in order to control initial conditions and prevent side reactions. All experiments were performed under equal experimental conditions to obtain results, which are comparable at least for the applied experimental conditions. The applicability and the importance of the observed reactions for the photochemistry occurring in natural snow are discussed.

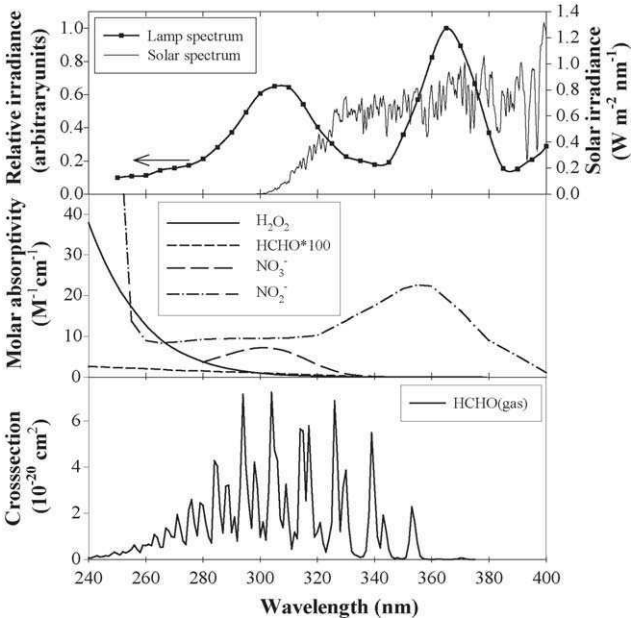

Fig. 1. Comparison of the lamp emission with the solar irradiance measured in Antarctica and with absorption spectra of the investigated compounds. (Top) emission spectrum of the mercury lamp measured behind the water filter with a grating monochromator (77250, Oriel) and a radiometer (IL1700, International Light) connected to a calibrated light sensor (SED400, International Light) and a solar spectrum measured at the German station Neumayer (70°39′S, 08°15′W) between 12:36 and 12:47 UTC on December 12, 2003 [50]. (Middle) absorption spectra in aqueous solution of H_2O_2 at 1 °C [21], HCHO measured at 20 °C (more than 99% present in the gem-diol form [38], the absorption coefficients are multiplied by 100), NO_3^- at 5 °C [20], and NO_2^- at room temperature [51]. (Bottom) absorption spectrum of HCHO in the gas phase at 25 °C [52].

2. Experimental methods

Solutions for the generation of artificial snow were prepared from Milli-Q water (conductivity larger than 18 MΩ) by adding either 30% H_2O_2 (Merck, Darmstadt, Germany), 37% HCHO (Merck, Darmstadt, Germany), or sodium nitrate (Merck, Darmstadt, Germany). All chemicals were used without further purification. Two liters of solutions with initial concentrations of $\sim 9 \times 10^{-6}$ M NO_3^-, $\sim 1 \times 10^{-2}$ M and $\sim 2 \times 10^{-5}$ M H_2O_2, or $\sim 6 \times 10^{-3}$ M and $\sim 3 \times 10^{-6}$ M HCHO were prepared. The preparation of the solutions with the low initial concentrations involved an additional dilution step. The final solutions were transferred into a stainless steel tank, which was pressurized with ambient air to 2–3 $\times 10^5$ Pa. Applying this pressure, the liquid was forced through a 1 mm hollow cone brass nozzle producing a fine spray, which was collected in a Styrofoam container filled with liquid nitrogen. The produced chunks of ice were transferred into a walk-in cold room at $T = -20 \pm 3$ °C, where the equipment for the further handling of the ice and snow was stored before using. First, the ice chunks were collected on a piece of aluminum foil. Small portions of the ice were ground with an electric mill and passed through a stainless steel test sieve (Retsch, Haan, Germany) with a mesh size of 0.5 mm. Afterwards, the snow was stored in 1 L Schott bottles covered with aluminum foil and sealed with traps filled with Hopcalite (Aero-Laser, Garmisch-Partenkirchen, Germany) to allow further degassing of nitrogen and to prevent the condensation of impurities on the snow. Newly prepared snow was stored at least overnight before using for the experiments to ensure that the nitrogen was completely removed.

Details of the experimental set-up for the photolysis experiments are described by Jacobi et al. [25]. The samples were irradiated using a 1000 W Mercury-arc lamp (Oriel Instruments, Stratford, CT) installed in the walk-in cold room. The emission intensity was regulated by the output of the lamp's power supply, which was set to 460 W. A water filter was used to absorb the infrared radiation. The transmittance of the water filter was higher than 80% between 250 and 700 nm. The emission spectrum measured behind the water filter is shown in Fig. 1. The snow samples (7–9 g) were loosely filled into 1-cm-long Teflon cells with a volume of 32 cm^3. During the experiments the cells were entirely illuminated by the light beam. Water filter and cells were equipped with quartz windows (Suprasil, Heraeus, Hanau, Germany).

The concentrations of the trace compounds in the snow were determined before and after each experiment. When filling the cell for a new experiment, a sample of the same batch of snow was kept in an airtight bottle. After the experiment the snow was completely removed from the cell and filled into an airtight bottle. The bottles were stored in the dark at −20 °C and the samples were melted before analysis.

Concentrations of H_2O_2 and HCHO in the melted samples were determined by multiple titrations with potassium

permanganate solution (H_2O_2) or by iodometric titration (HCHO). The detection limits and the errors of the titration methods were 1×10^{-4} M for H_2O_2 and 4×10^{-4} M for HCHO representing in each case the addition of a single droplet of the titrant. Lower concentrations were determined with commercial analyzers using fluorometric methods (AL2001CL and AL4001, Aero-Laser, Garmisch-Partenkirchen, Germany). Both instruments have previously been described in detail [27,28]. The instruments are normally used for gas phase measurements. However, they can be switched into the liquid mode to introduce liquid samples directly into the instruments. The analyzers were calibrated at least twice daily using diluted standard solutions and Milli-Q water. Initial concentrations of the standard solutions were also obtained by the titration methods. The limits of detection calculated from three times the standard deviation of the signal for Milli-Q water were 6×10^{-8} M for H_2O_2 and 5×10^{-8} M for HCHO, while the overall error in the μM range was in the order of 3%.

An ion chromatography system, normally operated to analyze natural snow samples from both polar regions [29], was used to perform the anion (NO_3^- and NO_2^-) analysis in the artificial snow samples. The system was calibrated with a range of standard solutions and Milli-Q water before and after the analysis of the samples. The overall error for both anions was on the order of 5%.

3. Results

Experiments with four different batches of artificial snow were performed in the case of H_2O_2. In all experiments a decrease of the H_2O_2 concentrations with increasing duration of the irradiation was observed. The decomposition can be described by a first-order rate law in agreement with previous experiments [25]:

$$\frac{d[c]}{dt} = -k_{1st}[c] \quad (1)$$

$$\ln\left(\frac{[c]}{[c]_0}\right) = -k_{1st}t \quad (2)$$

The first-order rate constant k_{1st} corresponds to the experimental photolysis rate j_{exp}. Fig. 2 shows a plot of the logarithm of the relative concentrations of $[H_2O_2]$ and $[H_2O_2]_0$ after and before the experiments as a function of time t. The plot demonstrates that the experiments with durations up to 6 h can be described by Eq. (2) in agreement with known photodegradation of H_2O_2 due to the following reaction:

$$H_2O_2 + h\nu \rightarrow 2\,OH \quad (R1)$$

We performed linear regressions separately for the high and low initial concentrations resulting in matching values for j_{R1} of 0.48 ± 0.03 and $0.48 \pm 0.09\,h^{-1}$, respectively. Here and in all further cases, the reported errors of the experimental photolysis rates are the statistical errors of the fitting procedure.

Different results were obtained in the case of the HCHO photolysis (Fig. 3). As reported previously [25], the decomposition of the impurity was observed with initial concentrations in the mM range due to the following reaction:

$$HCHO + h\nu \rightarrow \text{products} \quad (R2)$$

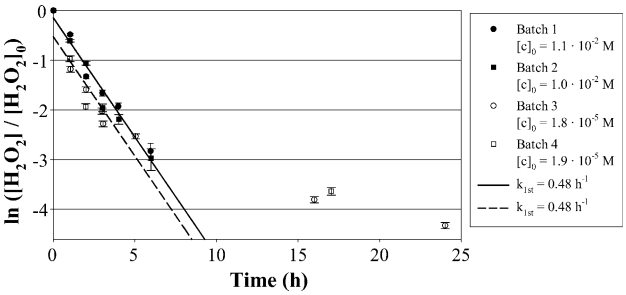

Fig. 2. Plot of the logarithm of the relative H_2O_2 concentrations before and after each photolysis experiment vs. the duration of the experiments. Different symbols represent the four different batches of artificial snow. Error bars are determined by error propagation using the analytical errors. The full line was calculated by linear regression for the high initial concentrations, the dashed line for the low initial concentrations.

The experimental photolysis rate obtained from the slope of a linear regression of the data points for the high initial concentration resulted in a value of $j_{R2} = 0.103 \pm 0.008\,h^{-1}$. Lower initial concentrations led to puzzling results with decreasing concentrations in one of the experiments and increasing concentrations in the other two experiments. Neither experiment with low initial concentrations showed a first-order decrease as observed in the experiments with the high initial concentration.

The photolysis of NO_3^- in ice or snow leads to the formation of several products like NO_x, HONO, and NO_2^- (e.g. [10,12,18]). Using an ion chromatography system, we were able to detect both NO_3^- and NO_2^- concentrations in the snow samples. The results are shown in Fig. 4. Initial NO_3^- concentrations were in the order of 13×10^{-6} M. Even before the photolysis experiments the prepared snow always contained small amounts of NO_2^- in the order of $5–10 \times 10^{-8}$ M. In all experiments a first-order loss of NO_3^- was observed in the experiments lasting up to 5 h (Fig. 4a). A linear regression fit was performed for these data points resulting in an observed photolysis rate of $j_{R3} = 0.49 \pm 0.02\,h^{-1}$. Extending the duration of the photolysis further led to relatively constant NO_3^- concentrations with an average of approximately 9% of the initial NO_3^- concentrations.

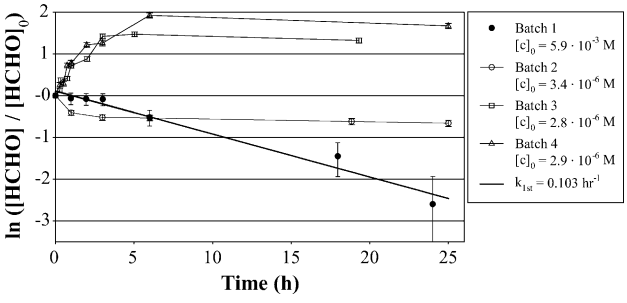

Fig. 3. Plot of the logarithm of the relative HCHO concentrations before and after each photolysis experiment vs. the duration of the experiments. Different symbols represent the four different batches of artificial snow. Error bars are determined by error propagation using the analytical errors. The full line was calculated by linear regression for the high initial concentrations. The lines between the open symbols are only visual guides.

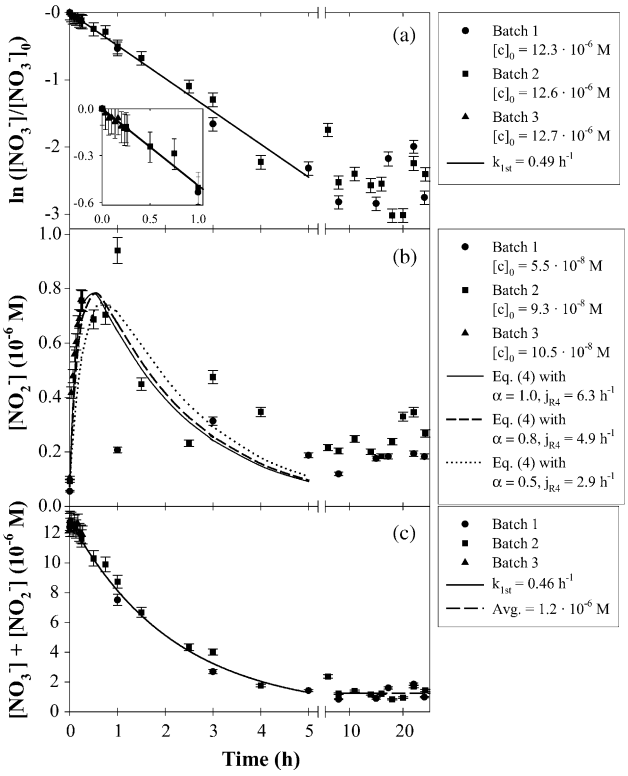

Fig. 4. (a) Plot of the logarithm of the relative NO_3^- concentrations before and after each photolysis experiment vs. the duration of the experiments. Different symbols represent the three different batches of artificial snow. Error bars are determined by error propagation using the analytical errors. The full line was calculated by linear regression for experiments with durations of up to 5 h. The inset shows an enlargement of the results of the experiments up to 1 h duration. (b) Plot of the NO_2^- concentrations after each photolysis experiment vs. the duration of the experiments. Error bars are determined from the analytical errors. The lines represent calculated profiles using Eq. (5) with a range of NO_2^- yields α and calculated NO_2^- photolysis rates j_{R4} (see text). (c) Plot of the sum of NO_3^- and NO_2^- concentrations as a function of the duration of the experiments. Error bars are determined from the analytical errors. The full line was calculated by linear regression for the experiments with durations of up to 5 h. The dashed line represents the average of all concentrations of the experiments beyond 8 h irradiation.

While NO_3^- concentrations decreased, NO_2^- concentrations showed a steep increase followed by a fast decrease leading to a maximum in the nitrite concentrations after experiments lasting between 0.5 and 1 h. Such a concentration–time profile can be described with a simple mechanism including the simultaneous production and destruction of NO_2^-. Several laboratory studies concerning the photolysis of NO_3^- in ice [17,18,20] have demonstrated that the reaction proceeds via two different channels comparable to the mechanism in the aqueous phase [30]:

$$NO_3^- + h\nu(+H^+) \rightarrow NO_2 + OH \quad \text{(R3a)}$$

$$NO_3^- + h\nu \rightarrow NO_2^- + O \quad \text{(R3b)}$$

$$NO_2^- + h\nu \rightarrow \text{products} \quad \text{(R4)}$$

Therefore, we assume that the observed overall photolysis of NO_3^- represents the sum of the two channels (R3a) and (R3b). Assuming that the reactions (R3) and (R4) are the most important driving forces for the conversion of NO_3^- to NO_2^- in our experiments, we recognize that NO_2^- is produced via reaction (R3b) and is simultaneously destroyed by the direct photolysis (R4). Taking into account the NO_2^- yield α for the reaction (R3), we can deduce the reaction rate law (3) for NO_2^- using the simple mechanism including reactions (R3a), (R3b), and (R4):

$$\frac{d[NO_2^-]}{dt} = \alpha j_{R3}[NO_3^-] - j_{R4}[NO_2^-] = \alpha j_{R3}[NO_3^-]_0 \exp(-j_{R3}t) - j_{R4}[NO_2^-] \quad (3)$$

The analytical solution for Eq. (3) results in the following equation for the concentration–time profiles of NO_2^- (see Appendix A):

$$[NO_2^-] = [NO_2^-]_0 \exp(-j_{R4}t) + \frac{\alpha j_{R3}[NO_3^-]_0}{j_{R4} - j_{R3}}[\exp(-j_{R3}t) - \exp(-j_{R4}t)] \quad (4)$$

Eq. (4) can be applied to the analysis of the measured NO_2^- concentrations if the NO_2^- yield α is known. The NO_2^- yield α can be calculated using the quantum yields of OH ϕ_{OH} and NO_2^- $\phi_{NO_2^-}$ for the NO_3^- photolysis:

$$\alpha = \frac{\phi_{NO_2^-}}{\phi_{OH} + \phi_{NO_2^-}} \quad (5)$$

Dubowski et al. [17,18] and Chu and Anastasio [20] investigated the OH and NO_2^- quantum yields of the reactions (R3a) and (R3b) in ice as function of temperature and in the case of ϕ_{OH} also as a function of wavelength. At $T = -20\,^\circ C$ the obtained quantum yield ϕ_{OH} varied between 6×10^{-4} [17] and 2.8×10^{-4} [20], while a quantum yield $\phi_{NO_2^-}$ of 1.5×10^{-3} [18] was reported. Applying these numbers we obtain values between 0.71 and 0.84 for α.

We analyzed the NO_2^- concentrations of the batches 1–3 for experiments lasting up to 5 h, since the temporal development of the NO_3^- concentrations in these experiments can be described by a first-order loss (Fig. 4a). The data were fitted using a Marquardt–Levenberg non-linear least squares fitting procedure in SigmaPlot (SPSS, Chicago, IL), which was performed for different NO_2^- yields α in the range from 1 to 0.5 accounting for the uncertainty in the reported quantum yields. The resulting concentration–time profiles are shown in Fig. 4b. The shape of the profiles is more or less independent of the chosen NO_2^- yield α in the selected range and in good agreement with the measured data. Nevertheless, the calculated NO_2^- photolysis rate j_{R4} decreases by more than 50% from 6.3 to 2.9 h^{-1} if the NO_2^- yield α decreases from 1.0 to 0.5. Fig. 5 shows the linear dependence of the calculated NO_2^- photolysis rate j_{R4} as a function of the NO_2^- yield α. Taking also into account the high variability of the measured NO_2^- concentrations for the different snow batches (Fig. 4b), the NO_2^- photolysis rate remains rather uncertain. Moreover, the additional reaction of NO_2^- with the OH radical produced in reaction (R3b) could also contribute to the destruction of NO_2^-. The effect of such reaction increases with a decreasing NO_2^- yield α. Nevertheless, the experimental

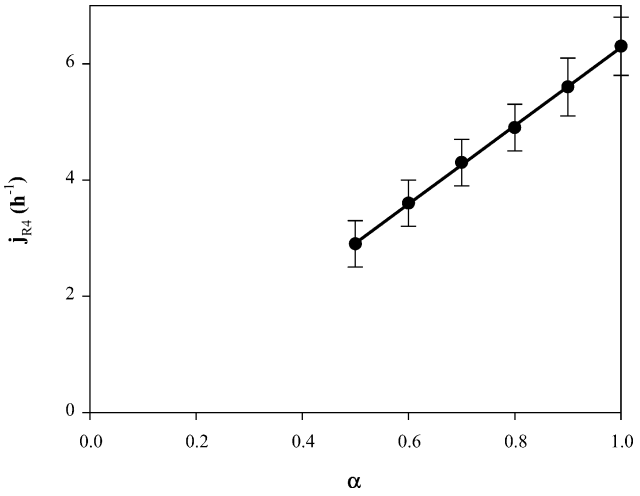

Fig. 5. Calculated experimental rates j_{R4} for the photolysis of NO_2^- as a function of the NO_2^- yield α of the NO_3^- photolysis. The photolysis rates were obtained by non-linear least squares fitting procedures using Eq. (4) with varying NO_2^- yields (see text). The error bars represent calculated statistical errors. The line shows the result of a linear regression using all data points ($R^2 = 0.9995$).

photolysis rate of NO_2^- is certainly higher than the photolysis rate of NO_3^-.

We also analyzed the concentrations of total nitrogen in the snow as the sum of the concentrations of NO_3^- and NO_2^-. Since NO_3^- dominates the total nitrogen budget, we also obtained an exponential decay with increasing durations of the experiments (Fig. 4c). The first-order loss rate of $j = 0.46 \pm 0.01\ h^{-1}$ is calculated by linear regression for the experiments with durations up to 5 h and is somewhat smaller than the overall photolysis rate of NO_3^-. Total nitrogen in the snow remained relatively constant beyond 8 h irradiation. The average of the remaining nitrogen amounts to $(1.2 \pm 0.2) \times 10^{-6}$ M, which constitutes approximately 10% of the initial nitrogen concentrations.

4. Discussion

Our results permit the comparison of the photolysis reactions of different trace compounds in snow, since the experiments were performed under similar conditions allowing the evaluation of relative photolysis rates of the different compounds. The smallest photolysis rate of $0.103 \pm 0.008\ h^{-1}$ was observed in the case of HCHO, while the H_2O_2 and NO_3^- photolysis rates of 0.48 ± 0.09 and $0.49 \pm 0.02\ h^{-1}$ are comparable. Moreover, a decomposition of HCHO was only observable with high initial concentrations. Similar results for HCHO and H_2O_2 with initial concentrations in the mM range were reported previously [25]. This order of the photolysis rates agrees well with the absorption spectra of the three compounds in the aqueous phase as shown in Fig. 1. While H_2O_2 and NO_3^- show significant absorption bands overlapping with the emission spectrum of the lamp, the HCHO absorption is significantly lower.

The disagreeing results obtained in the experiments with low initial HCHO concentrations are possibly due to the fact that a simultaneous photochemical production of HCHO in snow occurs. Similar results were reported by Grannas et al. [5], who found increasing HCHO concentrations in snow samples from the Arctic and the Antarctic after irradiating with UV radiation. They concluded that the HCHO production is caused by the presence of organic material in the snow, which undergoes oxidation either through photolysis or the attack by OH radicals. Similar processes are possible in our experiments, too. Although using Milli-Q water, the prepared solutions and therefore the snow samples will not be absolutely carbon-free. The maximum HCHO increase observed in the experiments with the batches 3 and 4 corresponds to 10×10^{-6} or 17×10^{-6} M (Fig. 3). However, such large contaminations of the Milli-Q water with organic matter seem very unlikely. We rather suspect that the snow became contaminated during the production process of the artificial snow. This could also explain the disagreeing results including the observation of an HCHO decrease in the case of batch 2 showing that possibly no contamination occurred in this case (Fig. 3). Interestingly, such contaminations seem to have a negligible effect on the H_2O_2 decomposition. In the atmospheric gas and aqueous phase H_2O_2 is formed by the recombination of two HO_2 radicals [31]. Although HO_2 is also produced during the oxidation of organic compounds, the formation rate of H_2O_2 in snow seems to be much smaller compared to HCHO. This is in agreement with previous field studies as summarized by Dominé and Shepson [2], who concluded that photochemical reactions in surface snow can lead to the production of carbonyl compounds. In contrast, the photochemical production of H_2O_2 in surface snow has not been observed yet (e.g. [32]). Moreover, from laboratory experiments Anastasio and Jordan [33] deduced H_2O_2 formation rates in the snowpack of Alert, Canada, caused by the deposition and photolysis of particulate chromophores. Compared to the bulk H_2O_2 concentration in the snow, they found that the photoformation is probably only a minor source.

Under the applied experimental conditions, the H_2O_2 and NO_3^- photolysis reactions occur equally fast in the snow. This result would have important implications for the photochemistry occurring in natural snow covers, because the photolysis of NO_3^- in ice and snow has recently attracted a lot of interest. Field [8–14] and laboratory experiments [16–19] have demonstrated that the NO_3^- photolysis in surface snow is responsible for the formation of reactive nitrogen oxides like NO, NO_2, and HONO in the surface snow, which are subsequently emitted to the atmosphere [12,14,34–36] influencing the chemistry of the boundary layer above the snow cover. Moreover, the NO_3^- photolysis is widely regarded as a source of OH radicals in surface snow, which initiates several oxidation reactions. Unfortunately, our experimental conditions are not directly comparable to conditions in the natural surface snow regarding the irradiation intensity and spectrum and the generation of the snow. For example, Jacobi et al. [25] reported that in the range from 300 to 370 nm the integral irradiation intensity of the lamp is more than 40 times higher than the maximum solar irradiance measured at a coastal station in Antarctica. Moreover, the lamp emits irradiation in the UV range down to 230 nm, which is only partly absorbed by the water filter, while the actinic flux reaching the Earth's surface becomes negligible below wavelengths of 290 nm (Fig. 1). Therefore, the relative rate of the

H_2O_2 photolysis to the NO_3^- photolysis is probably higher in our experiments compared to natural conditions because the absorption coefficients of H_2O_2 in the aqueous phase in the range of 230–280 nm are higher than the comparable absorption coefficients of NO_3^- (Fig. 1). Nevertheless, the experiments demonstrate that the photochemistry in natural snow covers is not only driven by the NO_3^- photolysis, but also by the photolysis of other light-absorbing species. Since H_2O_2 is omni-present in natural snow samples (e.g. [3]), its photolysis needs to be taken into account if an accurate description of the photochemistry is required. Chu and Anastasio [21] even concluded that in all investigated polar environments the OH production in the surface snow could be dominated by the H_2O_2 photolysis. The produced OH radicals can have a further impact on the conversion of higher organic compounds like chlorophenols in the snow as discussed by Klánová et al. [37].

Only in the case of the NO_3^- photolysis a direct observation of the formation of one of the products was possible. Our measurements show that the generated NO_2^- is itself photo labile and undergoes a photochemical reaction, which is faster than the NO_3^- photolysis as expected from a comparison of the absorption spectra of both compounds (Fig. 1). According to processes in the aqueous phase [30], the most likely products of the NO_2^- photolysis are NO and O^-. O^- is quickly protonated forming the OH radical. Therefore, each photolyzed NO_3^- molecule results in the formation of one OH molecule either directly in reaction (R3a) or via the NO_2^- photolysis. Further, N-containing products are the nitrogen oxides NO and NO_2. These are highly volatile and thus are probably released to the gas phase. The NO_x production and release to the gas phase as a result of the radiation of NO_3^- dissolved in ice or snow has been observed in several laboratory studies [16,17,19]. Therefore, we conclude that the missing fraction of the initial total nitrogen in the snow in our experiments constitutes the released NO_x. Since our experiments are performed in closed cells, the generated nitrogen oxides cannot escape. The volume of the gas phase in the experimental cells amounts to about 24 cm^3. The missing fraction of total nitrogen in the experiments lasting longer than 8 h is about 11×10^{-6} M (Fig. 4c). With a mass of snow of approximately 8 g, the released amount of nitrogen would result in the formation of more than 70 ppmV NO_x in the gas phase of the cells. Under these conditions side reactions are likely leading to the reformation of NO_3^- in the snow. Therefore, we assume that the constant total nitrogen in the snow in the experiments lasting longer than 8 h is due to the recycling of NO_3^- from NO_x previously released to the gas phase of the cells.

Like in the gas and aqueous phase, the photolysis of H_2O_2 in ice samples leads to the formation of OH radicals, which was demonstrated by using a radical scavenger like benzoic acid [21]. Thus, we assume that OH radicals are also produced upon the photolysis of H_2O_2 in the artificial snow like in our experiments. In the case of HCHO the products are not well known. In the aqueous phase more than 99% of the HCHO is hydrated forming the gem-diol ($CH_2(OH)_2$), which is much more soluble in water [38]. However, the absorption of radiation in the UV and visible range by the gem-diol form is negligible (Fig. 1). Moreover, Couch et al. [39] concluded from snow chamber experiments that the HCHO present in the surface layer of natural snow grains is most likely not hydrated. We are currently not able to distinguish if the hydrated or non-hydrated form of HCHO is present in the artificial snow. Nevertheless, the HCHO decay observed with the high initial concentration point to the fact that under these conditions a significant HCHO fraction must be present in the non-hydrated from. Due to the properties of the carbonyl group only the non-hydrated HCHO can absorb the applied radiation as demonstrated by the absorption spectrum of HCHO in the gas phase (Fig. 1). If HCHO is the photochemically active form in our experiments, we must consider that two different reaction channels are possible like in the gas phase [1]:

$$HCHO + h\nu \rightarrow H + CHO \quad \text{(R2a)}$$

$$HCHO + h\nu \rightarrow H_2 + CO \quad \text{(R2b)}$$

In the gas phase the products formed in reaction channel (R2a) quickly undergo subsequent reactions with O_2 generating compounds like HO_2 and CO [1]. However, further studies concerning the possible stable products like CO will be needed to elucidate the reaction mechanism of the HCHO photolysis in snow. Due to the volatility of CO it is also likely that it is released to the gas phase, where it would be possible to quantify the CO production with a high time resolution.

Large fractions of all three investigated compounds are removed from the snow during the long-term experiments. For example, less than 2% of the initial H_2O_2 was found in the snow after an irradiation period of 24 h (Fig. 2). Remaining fractions of HCHO and total nitrogen in the snow amounted to values around 10% (Figs. 3 and 4c). As discussed above, the most likely fate of the reaction products in the case of the NO_3^- photolysis is the release to the gas phase. However, even for the longest experiments the diffusion of NO_3^- in the solid ice is negligible. A diffusion coefficient of 6.6×10^{-11} cm^2 s^{-1} was reported for HNO_3 in ice at −20 °C [40]. Using $\langle x^2 \rangle = 2Dt$ and $t \leq 25$ h = 90,000 s, the maximum traveled distance x of HNO_3 amounts to 34 μm, which is small compared to the maximum radius of the snow crystals of 250 μm. This indicates that before the start of the experiments a large fraction of the NO_3^- must be present close to the surface enabling a quick transfer of the products from the snow to the gas phase. This is somewhat surprising since due to the applied snow production method involving the shock-freezing of the solution in liquid nitrogen a rather uniform distribution of the NO_3^- throughout the snow grains would be plausible. The diffusion of NO_3^- to the surface of the snow grains during the storage time of the artificial snow is also not feasible because with the above mentioned diffusion coefficient a period of more than 50 days would be necessary to move a distance of 250 μm within the solid ice. In contrast, the maximum storage time of the samples was less than 3 weeks. Regarding the NO_3^- distribution in the snow grains, the artificial snow seems to resemble natural snow quite closely. For example, Jacobi et al. [41] concluded from measurements of HNO_3 in the interstitial air of the surface snow and nitrate measurements in the snow in Greenland, that 80–100% of the nitrate is present in the surface layer of the snow grains. Since we did not follow the product formation during the experiments with H_2O_2 and HCHO, we are

not able to determine the distribution of these trace compounds within the snow grains.

5. Conclusions

Our results show that the photochemistry occurring in the sunlit snow is very diverse. Besides the photolysis of NO_3^-, the photolysis of H_2O_2 seems to be fast enough to contribute to the formation of OH radicals in the snow. Like in the tropospheric gas and aqueous phase the OH radical is probably the most important driving force for the oxidation of organic compounds in sunlit snow. The oxidation likely leads to the formation of volatile compounds such as aldehydes, ketones, and carboxylic acids. Most of these compounds have been detected in surface snow even in the remote polar areas [15,42,43]. Moreover, the emissions of several volatile compounds from the sunlit snow have been observed in the Arctic [44–46] influencing the chemistry in the boundary layer in snow-covered areas [2]. OH radicals can also contribute to the formation and release of molecular chlorine (Cl_2) and bromine (Br_2) if the snow contains chloride and bromide [2]. Cl_2 and Br_2 are easily photolyzed by radiation in the visible range forming halogen atoms [1], which can contribute to the removal of ozone, the oxidation of organic compounds, and the formation and deposition of reactive gaseous mercury [47]. Therefore, photochemical reactions in the snow have the potential to alter the surface snow composition as well as the composition of the boundary layer above snow-covered areas.

One of the major effects of a changing snow composition is the interpretation of concentration profiles in firn and ice cores. The interpretation of NO_3^- profiles is currently hampered by the fact that a transfer function relating snow and atmospheric concentrations has not been established. A fast drop in NO_3^- concentrations in the surface snow with depth has been recorded at several polar locations [48]. However, the drop is probably caused by a site-specific combination of the photolysis and the re-evaporation of deposited NO_3^-. Unfortunately, the different contributions have not been quantified yet, although several investigations have indicated that the photolysis is a minor, albeit not negligible factor (e.g. [48,49]). Since the H_2O_2 photolysis in snow occurs at a comparable rate, we suggest that at least for low accumulation sites, where the surface snow is exposed to the solar radiation for long periods, the photodecomposition of H_2O_2 needs to be taken into account.

In the case of NO_3^-, we concluded that a large fraction of the trace compound was located close to the surface of the snow grains. This indicates that although the artificial snow production process is vastly different from the process of ice crystal formation in the atmosphere, the distribution of this specific compound is comparable in natural and artificial snow grains. Nevertheless, further laboratory experiments are needed including the simultaneous investigation of the decomposition of the initial trace compound and the formation of stable products either in the snow or in the adjacent gas phase. With such experiments more information about the reaction mechanism, the product distribution, and the distribution of the trace compounds within the snow grains can be obtained.

Acknowledgements

Financial support by the Deutsche Forschungsgemeinschaft (DFG), grant JA 932/5-1, is gratefully acknowledged. We thank the two anonymous reviewers for valuable comments.

Appendix A

The reaction rate law for NO_2^- (Eq. (A1)) can be transformed into a differential equation (Eq. (A2)) with a general analytical solution (Eq. (A3)) with the differentiation constant $\mathrm{diff}_{\mathrm{const}}$ and the further constants c_1–c_3.

$$\frac{d[NO_2^-]}{dt} = \alpha j_{R3}[NO_3^-]_0 \exp(-j_{R3}t) - j_{R4}[NO_2^-] \quad \text{(A1)}$$

$$y' + c_1 y = c_2 \exp(-c_3 t) \quad \text{(A2)}$$

$$y = \mathrm{diff}_{\mathrm{const}} \exp(-c_1 t) + \frac{c_2}{c_1 - c_3}\exp(-c_3 t) \quad \text{(A3)}$$

The transformed rate law corresponds to the equation (Eq. (A4)):

$$\frac{d[NO_2^-]}{dt} + j_{R4}[NO_2^-] = \alpha j_{R3}[NO_3^-]_0 \exp(-j_{R3}t) \quad \text{(A4)}$$

with the constants $c_1 = j_{R4}$, $c_2 = \alpha j_{R3}[NO_3^-]_0$, and $c_3 = j_{R3}$. Introducing these constants into (Eq. (A3)) yields the following solution for the reaction rate law:

$$[NO_2^-] = \mathrm{diff}_{\mathrm{const}} \exp(-j_{R4}t) + \frac{\alpha j_{R3}[NO_3^-]_0}{j_{R4} - j_{R3}} \exp(-j_{R3}t) \quad \text{(A5)}$$

The NO_2^- concentration at $t = 0$ is set to the initial NO_2^- concentration $[NO_2^-]_0$ and can be used to calculate the differentiation constant $\mathrm{diff}_{\mathrm{const}}$:

$$\mathrm{diff}_{\mathrm{const}} = [NO_2^-]_0 - \frac{\alpha j_{R3}[NO_3^-]_0}{j_{R4} - j_{R3}} \quad \text{(A6)}$$

Applying this constant, we derive the final expression for the reaction rate law of NO_2^-:

$$[NO_2^-] = [NO_2^-]_0 \exp(-j_{R4}t) + \frac{\alpha j_{R3}[NO_3^-]_0}{j_{R4} - j_{R3}}[\exp(-j_{R3}t) - \exp(-j_{R4}t)] \quad \text{(A7)}$$

References

[1] B.J. Finlayson-Pitts, J.N. Pitts, Chemistry of the Upper and Lower Atmosphere: Theory, Experiments, and Applications, Academic Press, San Diego, 2000.
[2] F. Dominé, P.B. Shepson, Air-snow interactions and atmospheric chemistry, Science 279 (2002) 1506–1510.
[3] M. Legrand, P. Mayewski, Glaciochemistry of polar ice cores: a review, Rev. Geophys. 35 (1997) 219–243.
[4] C. Anastasio, A.L. Jordan, Photoformation of hydroxyl radical and hydrogen peroxide in aerosol particles from Alert, Nunavut: implications for aerosol and snowpack chemistry in the Arctic, Atmos. Environ. 38 (2004) 1153–1166.

[5] A.M. Grannas, P.B. Shepson, T.R. Filley, Photochemistry and nature of organic matter in Arctic and Antarctic snow, Global Biogeochem. Cycles 18 (GB1006) (2004), doi:10.1029/2003GB002133.
[6] M.D. King, W.R. Simpson, The extinction of UV radiation in Arctic snow at Alert, Canada (82°N), J. Geophys. Res. 106 (2001) 12499–12507.
[7] M. Peterson, D. Barber, S. Green, Monte Carlo modeling and measurements of actinic flux levels in Summit, Greenland snowpack, Atmos. Environ. 36 (2002) 2545–2551.
[8] R.E. Honrath, M.C. Peterson, S. Guo, J.E. Dibb, P.B. Shepson, B. Campbell, Evidence of NO_x production within or upon ice particles in the Greenland snowpack, Geophys. Res. Lett. 26 (1999) 695–698.
[9] R.E. Honrath, M.C. Peterson, M.P. Dziobak, J.E. Dibb, M.A. Arsenault, S.A. Green, Release of NO_x from sunlight-irradiated midlatitude snow, Geophys. Res. Lett. 27 (2000) 2237–2240.
[10] A.E. Jones, R. Weller, E.W. Wolff, H.-W. Jacobi, Speciation and rate of photochemical NO and NO_2 production in Antarctic snow, Geophys. Res. Lett. 27 (2000) 345–348.
[11] B. Ridley, J. Walega, D. Montzka, F. Grahek, E. Atlas, F. Flocke, V. Stroud, J. Deary, A. Gallant, H. Boudries, J. Bottenheim, K. Anlauf, D. Worthy, A.L. Sumner, B. Splawn, P. Shepson, Is the Arctic surface layer a source and sink of NO_x in winter/spring? J. Atmos. Chem. 36 (2000) 1–22.
[12] X. Zhou, H.J. Beine, R.E. Honrath, J.D. Fuentes, W. Simpson, P.B. Shepson, J.W. Bottenheim, Snowpack photochemical production of HONO: a major source of OH in the arctic boundary layer in springtime, Geophys. Res. Lett. 28 (2001) 4087–4090.
[13] D. Davis, J.B. Nowak, G. Chen, M. Buhr, R. Arimoto, A. Hogan, F. Eisele, L. Mauldin, D. Tanner, R. Shetter, B. Lefer, P. McMurry, Unexpected high levels of NO observed at South Pole, Geophys. Res. Lett. 28 (2001) 3625–3628.
[14] R.E. Honrath, Y. Lu, M.C. Peterson, J.E. Dibb, M.A. Arsenault, N.J. Cullen, K. Steffen, Vertical fluxes of NO_x, HONO, and HNO_3 above the snowpack at Summit, Greenland, Atmos. Environ. 36 (2002) 2629–2640.
[15] A.L. Sumner, P.B. Shepson, Snowpack production of formaldehyde and its effect on the Arctic troposphere, Nature 398 (1999) 230–233.
[16] R.E. Honrath, S. Guo, M.C. Peterson, M.P. Dziobak, J.E. Dibb, M.A. Arsenault, Photochemical production of gas phase NO_x from ice crystal NO_3^-, J. Geophys. Res. 105 (2000) 24183–24190.
[17] Y. Dubowski, A.J. Colussi, M.R. Hoffmann, Nitrogen dioxide release in the 302 nm band photolysis of spray-frozen aqueous nitrate solutions. Atmospheric implications, J. Phys. Chem. A 105 (2001) 4928–4932.
[18] Y. Dubowski, A.J. Colussi, C. Boxe, M.R. Hoffmann, Monotonic increase of nitrite yields in the photolysis of nitrate in ice and water between 238 and 294 K, J. Phys. Chem. A 106 (2002) 6967–6971.
[19] E.S.N. Cotter, A.E. Jones, E.W. Wolff, S.J.-B. Baugitte, What controls photochemical NO and NO_2 production from Antarctic snow? Laboratory investigation assessing the wavelength and temperature dependence, J. Geophys. Res. 108 (D4) (2003) 4147, doi:10.1029/2002JD002602.
[20] L. Chu, C. Anastasio, Quantum yields of hydroxyl radical and nitrogen dioxide from the photolysis of nitrate on ice, J. Phys. Chem. A 107 (2003) 9594–9602.
[21] L. Chu, C. Anastasio, Formation of hydroxyl radical from the photolysis of frozen hydrogen peroxide, J. Phys. Chem. A 109 (28) (2005) 6264–6271.
[22] D. Haan, Y. Zuo, V. Gros, C.A.M. Brenninkmeijer, Photochemical production of carbon monoxide in snow, J. Atmos. Chem. 40 (2001) 217–230.
[23] P. Klán, I. Holoubek, Ice (photo)chemistry. Ice as a medium for long-term (photo)chemical transformations—environmental implications, Chemosphere 46 (2002) 1201–1210.
[24] P. Klán, J. Klánová, I. Holoubek, P. Čupr, Photochemical activity of organic compounds in ice induced by sunlight irradiation: the Svalbard project, Geophys. Res. Lett. 30 (6) (2003) 1313, doi:10.1029/2002GL016385.
[25] H.-W. Jacobi, B. Kwakye-Awuah, O. Schrems, Photochemical decomposition of hydrogen peroxide (H_2O_2) and formaldehyde (HCHO) in artificial snow, Ann. Glaciol. 39 (2004) 29–33.
[26] T. Staffelbach, A. Neftel, B. Stauffer, D. Jacob, A record of atmospheric methane sink from formaldehyde in polar ice cores, Nature 349 (1991) 603–605.
[27] K. Riedel, R. Weller, O. Schrems, Variability of formaldehyde in the Antarctic troposphere, Phys. Chem. Chem. Phys. 1 (1999) 5523–5527.
[28] K. Riedel, R. Weller, O. Schrems, G. König-Langlo, Variability of tropospheric hydroperoxides at a coastal surface site in Antarctica, Atmos. Environ. 34 (2000) 5225–5234.
[29] F. Göktas, H. Fischer, H. Oerter, R. Weller, S. Sommer, H. Miller, A glacio-chemical characterization of the new EPICA deep-drilling site on Amundsenisen, Dronning Maud Land, Antarctica, Ann. Glaciol. 35 (2002) 347–354.
[30] J. Mack, J.R. Bolton, Photochemistry of nitrite and nitrate in aqueous solution: a review, J. Photochem. Photobiol. A 128 (1999) 1–13.
[31] A.V. Jackson, C.N. Hewitt, Atmosphere hydrogen peroxide and organic hydroperoxides: a review, Crit. Rev. Environ. Sci. Technol. 29 (1999) 175–228.
[32] H.-W. Jacobi, M.M. Frey, M.A. Hutterli, R.C. Bales, O. Schrems, N.J. Cullen, K. Steffen, C. Koehler, Measurements of hydrogen peroxide and formaldehyde exchange between the atmosphere and surface snow at Summit, Greenland, Atmos. Environ. 36 (2002) 2619–2628.
[33] C. Anastasio, A.L. Jordan, Photoformation of hydroxyl radical and hydrogen peroxide in aerosol particles from Alert, Nunavut: implications for aerosol and snowpack chemistry in the Arctic, Atmos. Environ. 38 (2004) 1153–1166.
[34] A.E. Jones, R. Weller, P.S. Anderson, H.-W. Jacobi, E.W. Wolff, O. Schrems, H. Miller, Measurements of NO_x emissions from the Antarctic snowpack, Geophys. Res. Lett. 28 (2001) 1499–1502.
[35] J.E. Dibb, M. Arsenault, M.C. Peterson, R.E. Honrath, Fast nitrogen oxide photochemistry in Summit, Greenland snow, Atmos. Environ. 36 (2002) 2501–2511.
[36] H.J. Beine, R.E. Honrath, F. Dominé, W.R. Simpson, J.D. Fuentes, NO_x during background and ozone depletion periods at Alert: fluxes above the snow surface, J. Geophys. Res. 107 (D21) (2002) 4584, doi:10.1029/2002JD002082.
[37] J. Klánová, P. Klán, D. Heger, I. Holoubek, Compariosn of the effects of UV, H_2O_2/UV and γ-irradiation processes on frozen and liquid water solutions of monochlorphenols, Photochem. Photobiol. Sci. 2 (2003) 1023–1031.
[38] R.P. Bell, The reversible hydration of carbonyl compounds, Adv. Phys. Org. Chem 4 (1966) 1–29.
[39] T.L. Couch, A.L. Sumner, T.M. Dassau, P.B. Shepson, R.E. Honrath, An investigation of the interaction of carbonyl compounds with the snowpack, Geophys. Res. Lett. 27 (2000) 2241–2244.
[40] E. Thibert, F. Dominé, Thermodynamics and kinetics of the solid solution of HNO_3 in ice, J. Phys. Chem. B 102 (1998) 4432–4439.
[41] H.-W. Jacobi, R.C. Bales, R.E. Honrath, M.C. Peterson, J.E. Dibb, A.L. Swanson, M.R. Albert, Reactive trace gases measured in the interstitial air of surface snow at Summit, Greenland, Atmos. Environ. 38 (12) (2004) 1687–1697.
[42] J.E. Dibb, M. Arsenault, Should not snowpacks be a source of monocarboxylic acids? Atmos. Environ. 36 (2002) 2513–2522.
[43] S. Houdier, S. Perrier, F. Dominé, A. Cabanes, L. Legagneux, A.M. Grannas, C. Guimbaud, P.B. Shepson, H. Boudries, J.W. Bottenheim, Acetaldehyde and acetone in the Arctic snowpack during the ALERT2000 campaign. Snowpack composition, incorporation processes and atmospheric impact, Atmos. Environ. 36 (2002) 2609–2618.
[44] H. Boudries, J.W. Bottenheim, C. Guimbaud, A.M. Grannas, P.B. Shepson, S. Houdier, S. Perrier, F. Dominé, Distribution and trends of oxygenated hydrocarbons in the high arctic derived from measurements in the atmospheric boundary layer and interstitial snow air during the ALERT2000 field campaign, Atmos. Environ. 36 (2002) 2573–2583.
[45] A.M. Grannas, P.B. Shepson, C. Guimbaud, A.L. Sumner, M. Albert, W. Simpson, F. Domine, H. Boudries, J. Bottenheim, H.J. Beine, R. Honrath, X. Zhou, A study of photochemical and physical processes affecting carbonyl compounds in the Arctic atmospheric boundary layer, Atmos. Environ. 36 (2002) 2733–2742.

[46] C. Guimbaud, A.M. Grannas, P.B. Shepson, J.D. Fuentes, H. Boudries, J.W. Bottenheim, F. Dominé, S. Houdier, S. Perrier, T.B. Bisenthal, B.G. Splawn, Snowpack processing of acetaldehyde and acetone in the arctic atmospheric boundary layer, Atmos. Environ. 36 (2002) 2743–2752.

[47] W.H. Schroeder, K.G. Anlauf, L.A. Barrie, J.Y. Lu, A. Steffen, D.R. Schneeberger, T. Berg, Arctic springtime depletion of mercury, Nature 394 (1998) 331–332.

[48] R. Röthlisberger, M.A. Hutterli, E.W. Wolff, R. Mulvaney, H. Fischer, M. Bigler, K. Goto-Azuma, M.E. Hansson, U. Ruth, M.-L. Siggaard-Andersen, J.P. Steffensen, Nitrate in Greenland and Antarctic ice cores: a detailed description of post-depositional processes, Ann. Glaciol. 35 (2002) 209–216.

[49] T. Blunier, G.L. Floch, H.-W. Jacobi, E. Quansah, Isotopic view on nitrate loss in Antarctic surface snow, Geophys. Res. Lett. 32 (2005) L13501, doi:10.1029/2005GL023011.

[50] S. Wuttke, Radiation conditions in an Antarctic environment, accessible at http://www.muk.uni-hannover.de/institut/bibliothek/pdf-diss/Dissertation_Wuttke.pdf, Ph.D. Thesis, University Hannover, Germany, 2005.

[51] S.J. Strickler, M. Kasha, Solvent effects on the electronic absorption spectrum of nitrite ion, J. Am. Chem. Soc. 85 (1963) 2899–2901.

[52] R. Meller, G.K. Moortgat, Temperature dependence of the absorption cross sections of formaldehyde between 223 and 323 K in the wavelength range 225–375 nm, J. Geophys. Res. 105 (2000) 7089–7101.

Publication 3.3.4

Jacobi, H.-W., and B. Hilker,
A mechanism for the photochemical transformation of nitrate in snow,
J.Photochem.Photobiol. A **185**, 371-382, 2007.

Available online at www.sciencedirect.com
ScienceDirect
Journal of Photochemistry and Photobiology A: Chemistry 185 (2007) 371–382
Journal of Photochemistry and Photobiology A:Chemistry
www.elsevier.com/locate/jphotochem

A mechanism for the photochemical transformation of nitrate in snow

Hans-Werner Jacobi *, Birgit Hilker

Alfred Wegener Institute for Polar and Marine Research, Am Handelshafen 12, 27570 Bremerhaven, Germany

Received 1 June 2006; received in revised form 29 June 2006; accepted 30 June 2006
Available online 8 July 2006

Abstract

Photochemical reactions of trace compounds in snow have important implications for the composition of the atmospheric boundary layer in snow-covered regions and for the interpretation of concentration profiles in snow and ice regarding the composition of the past atmosphere. One of the prominent reactions is the photolysis of nitrate, which leads to the formation of OH radicals in the snow and to the release of reactive nitrogen compounds, like nitrogen oxides (NO and NO_2) and nitrous acid (HONO) to the atmosphere. We performed photolysis experiments using artificial snow, containing variable initial concentrations of nitrate and nitrite, to investigate the reaction mechanism responsible for the formation of the reactive nitrogen compounds. Increasing the initial nitrite concentrations resulted in the formation of significant amounts of nitrate in the snow. A possible precursor of nitrate is NO_2, which can be transformed into nitrate either by the attack of a hydroxy radical or the hydrolysis of the dimer (N_2O_4). A mechanism for the transformation of the nitrogen-containing compounds in snow was developed, assuming that all reactions took place in a quasi-liquid layer (QLL) at the surface of the ice crystals. The unknown photolysis rates of nitrate and nitrite and the rates of NO and NO_2 transfer from the snow to the gas phase, respectively, were adjusted to give an optimum fit of the calculated time series of nitrate, nitrite, and gas phase NO_x with respect to the experimental data. Best agreement was obtained with a ~25 times faster photolysis rate of nitrite compared to nitrate. The formation of NO_2 is probably the dominant channel for the nitrate photolysis. We used the reaction mechanism further to investigate the release of NO_x and HONO under natural conditions. We found that NO_x emissions are by far dominated by the release of NO_2. The release of HONO to the gas phase depends on the pH of the snow and the HONO transfer rate to the gas phase. However, due to the small amounts of nitrite produced under natural conditions, the formation of HONO in the QLL is probably negligible. We suggest that observed emissions of HONO from the surface snow are dominated by the heterogeneous formation of HONO in the firn air. The reaction of NO_2 on the surfaces of the ice crystals is the most likely HONO source to the gas phase.

Keywords: Photochemical reactions; Snow; Nitrate; Nitrite; Nitrogen oxides

1. Introduction

Photochemical reactions leading to the chemical transformation of trace compounds in the atmosphere do not only occur in the atmospheric gas and liquid phases, but also in the tropospheric ice phase. Such reactions can take place in the upper layers of the natural snow-covers in polar and alpine regions [1]. The photolysis of nitrate (NO_3^-) was first identified as an important photochemical reaction in this environment [2]. This reaction is considered as one of the key reactions in surface-snow and has been the subject of a series of field [2–17] and laboratory studies [18–27]. Nitrate photolysis has an impact on the composition of and processes in the surface-snow. It also affects the atmosphere after the release of volatile and reactive nitrogen compounds to the gas phase [28,29].

Nitrate is one of the dominating anions found in snow samples in both polar regions [30]. However, the photochemical processing can alter the concentrations in the snow after deposition. Significant losses of nitrate from the surface snow at polar sites with very low snow accumulation rates were attributed to the NO_3^- photolysis [24,31]. This effect influences the interpretation of NO_3^- profiles in firn and ice cores, which can convolute information obtained about levels of reactive nitrogen compounds in the atmosphere in the past [32]. In addition, NO_3^- photolysis can affect further trace compounds in the snow. Laboratory experiments have shown that it leads to the formation of highly reactive hydroxyl (OH) radicals in the snow

* Corresponding author. Tel.: +49 471 4831 1493; fax: +49 471 4831 1425.
E-mail address: hwjacobi@awi-bremerhaven.de (H.-W. Jacobi).

1010-6030/$ – see front matter © 2006 Elsevier B.V. All rights reserved.
doi:10.1016/j.jphotochem.2006.06.039

[22] in agreement with well-known aqueous phase processes [33]. The generated OH has the potential to attack organic compounds, eventually leading to the formation of oxidized hydrocarbons like formaldehyde, acetaldehyde, and acetone [1,34,35].

Evidence of the formation of more volatile compounds, which are quickly released to the gas phase, is supported by several field and laboratory studies. Emissions of nitrogen oxides ($NO_x = NO + NO_2$) from the surface snow under the influence of solar radiation have been reported from several Arctic [2,4,11,12], Antarctic [5–7,15], as well as a mid-latitude sites [3]. Nitrous acid (HONO) has also been found to be released from the surface snow at non-marine polar sites [8,11,16], although HONO fluxes from alkaline snow seem to be negligible or even directed to the snow [17,36]. These emissions are driven by the strongly enhanced concentrations of the reactive nitrogen compounds in the interstitial air of the surface snow compared to ambient concentrations [9,14,16]. They have a strong effect on photochemical processes occurring in the atmospheric boundary layer above snow-covered regions. NO_x mixing ratios affected by emissions from the snowpack can reach values on the order of several hundreds of pptV (parts per trillion by volume) under stable atmospheric conditions, even in remote polar regions [7,11,15]. In addition, HONO concentrations up to 70 pptv have been reported for polar regions [8,9,16,17,37]. However, the applied collecting techniques using mist chambers or aqueous scrubbers are prone to interferences for example by pernitric acid (HO_2NO_2), raising concerns about the actual HONO concentrations in polar regions [16,28,38]. Recently, Liao [38] reported simultaneous HONO measurements at South Pole station using laser-induced fluorescence (LIF) and mist chamber-ion chromatography (MC-IC) techniques. They found that the results from the MC-IC measurements were about seven times higher than the LIF measurements. Nevertheless, the reported NO_x and HONO levels have a profound effect on the photochemistry of the polar boundary layer since both compounds are involved in the formation and destruction of OH and hydroperoxyl radicals (HO_2) and ozone [28,29], thus influencing the oxidation capacity of the boundary layer.

Although the strong impact of the NO_3^- photolysis is evident, a full mechanistic understanding of the transformation of nitrogen-containing compounds in the snow is still not available. Previous laboratory studies have focused on different aspects, like the photolytic decomposition of NO_3^- [24,27], the formation of products like OH [20,22] and nitrite (NO_2^-) [19,20,27] and the release of NO_x to the gas phase [18,19,21,23,25,26].

Here, we present a series of laboratory experiments performed with artificial snow samples. Results of photolysis experiments with different initial concentrations of NO_3^- and NO_2^- are used to develop a reaction mechanism for the photochemical transformation of NO_3^- and NO_2^-. The mechanism is further adapted to conditions during previous field experiments performed at Summit, Greenland. The modeled results regarding the emissions of NO_x and HONO are compared to the field measurements, indicating that the main photochemical processes occurring in the natural snow-cover can successfully be reproduced using the proposed mechanism.

2. Experimental methods

Details of the preparation of artificial snow samples have been described previously [27,39]. In short, liquid solutions were prepared from Milli-Q water (resistance larger than 18 MΩ) by adding sodium nitrate or sodium nitrite (both Merck, Darmstadt, Germany) and transferred into a stainless steel tank. From the pressurized tank the solution was sprayed into liquid nitrogen. In a cold room below −25 °C, the resulting ice was ground with an electric mill, passed through a test sieve with a mesh size of 0.5 mm, and stored at least overnight in 1 L glass bottles covered with aluminum foil.

The experimental set-up was similar to previously performed photolysis experiments [27,39]. A mercury-arc lamp (Oriel Instrument, Stratford, CT) with a maximum power input of about 1000 W was used as the light source. For the experiments the power input was reduced to 500 W. A 10 cm long liquid-filter filled with Milli-Q water was directly coupled to the output of the lamp housing condenser to absorb the infrared radiation. The transmittance of the water filter was about 80% between the wavelengths of 250 and 700 nm [27]. An additional 10 cm long cylindrical extension made of white synthetic material was fixed to the end of the liquid-filter. The snow samples were filled into cylindrical 1 cm long Teflon cells, equipped with quartz windows. The reaction cells were easily attached to the end of the extension, which was equipped with a flange with an inner-diameter equal to the outer-diameter of the cells. The snow sample was completely illuminated by the light beam since the liquid-filter, the cylindrical extension, and the reaction cells had the same inner-diameter of 4.6 cm (Fig. 1).

The experiment was installed inside an opening of a freezer so that two-thirds of the extension and the entire reaction cell were located inside the freezer, which was regulated to a temperature of −31 to −30 °C. Before each experiment, the filled cell was stored several hours in the freezer to assure that the temperature of the snow was in equilibrium with the freezer's temperature. To start and end the single experiments, the cell was either placed inside or removed from the flange of the extension reaching through a second, normally closed opening of the freezer.

The NO_3^- and NO_2^- concentrations in the snow were determined before and after each experiment. When filling the cell for a new experiment, a sample of the same batch of snow was kept in an airtight bottle. After the experiment, the snow was

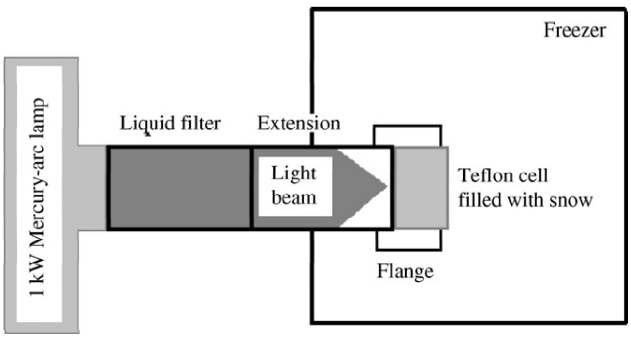

Fig. 1. Experimental system of the photolysis experiments.

Table 1
Measured initial concentrations of NO_3^- and NO_2^- in the snow samples, calculated liquid QLL fraction, and corresponding calculated initial concentrations in the QLL

Batch	Temperature (°C)	C_{bulk}[a] (μM)		φ_{H_2O}[b] ($\times 10^{-5}$)	C_T^{0}[c] (mM)	
		$[NO_3^-]_0$	$[NO_2^-]_0$		$[NO_3^-]_0$	$[NO_2^-]_0$
1	−31	10.84	0.161	3.42	317	4.71
2	−31	9.97	0.185	3.29	303	5.62
3	−30	1.66	3.28	2.33	71.2	141
4	−31	0.757	11.72	3.64	20.8	322
[d]	−20	12.55	0.084	4.65	270	1.80
[e]	−20	4.4	0	1.94	230	0

[a] Concentrations measured in the melted snow samples.
[b] Liquid fraction calculated using Eq. (4).
[c] QLL concentrations calculated using Eq. (3).
[d] Concentrations and QLL fraction calculated for the experiments presented by Jacobi et al. [27].
[e] Concentrations and QLL fraction calculated for average NO_3^- concentration measured in surface snow during the summer of 2000 at Summit [11].

completely removed from the cell and filled into a second air-tight bottle. The bottles were stored in the dark at −20 °C and the melted samples were analyzed using an ion chromatography system [27]. The system was always calibrated with a range of standard solutions and Milli-Q water before and after the analysis of the samples. The analytical error was $\pm 3 \times 10^{-8}$ M for NO_3^- and $\pm 4 \times 10^{-8}$ M for NO_2^- or ±10%, whichever is larger.

3. Results

Photolysis experiments with four different batches of artificial snow were performed with varying initial concentrations of NO_3^- and NO_2^- (Table 1). Batches 1 and 2 contained the highest initial NO_3^- concentrations ($\sim 10^{-5}$ M) in the presence of almost negligible NO_2^- amounts. Irradiation caused a logarithmic decomposition of NO_3^- during the experiments (Fig. 2a). In the same experiments NO_2^- was first produced reaching a concentration maximum in the experiments lasting around 30 min. Thereafter, NO_2^- decreased after longer irradiation periods. However, the behavior of both compounds changed with elevated initial NO_2^- concentrations. The results of the batches 3 and 4 demonstrate that with higher initial NO_2^- concentrations the drop in the NO_3^- concentrations was delayed or even absent (Fig. 2b and c). Increasing the NO_2^- concentration to 1.2×10^{-5} M even caused a significant production of NO_3^- (Fig. 2c). On the other hand, the NO_2^- concentrations showed a steady decrease in the batches 3 and 4 with increasing irradiation times.

4. Discussion

4.1. Development of a reaction mechanism for the transformation of NO_3^- and NO_2^- in snow

The experimental results cannot be reconciled with the following previously proposed reaction sequence [27]:

$$NO_3^- \xrightarrow{h\nu} NO_2^- \xrightarrow{h\nu} NO_x$$

Such a reaction sequence is in conflict with the observation of the formation of NO_3^- in the experiments with significant initial NO_2^- concentrations. Additional reactions are needed to describe the experimental data. According to the known reaction

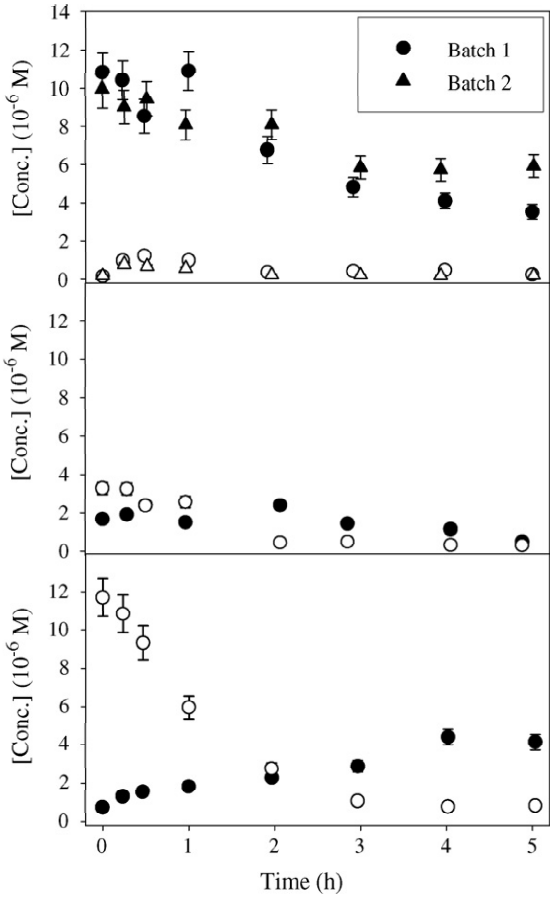

Fig. 2. Plots of the NO_3^- (filled symbols) and NO_2^- concentrations (open symbols) measured in the melted snow after each photolysis experiment vs. the duration of the experiments: (a) batches 1 and 2, (b) batch 3, and (c) batch 4 (initial concentrations see Table 1). Error bars represent analytical errors. If no error bar is visible, the errors are smaller than the size of the symbols.

mechanism in the aqueous phase [33] NO_2^- can be oxidized to NO_3^- via the formation of nitrogen dioxide (NO_2). Using NO_2^- as a precursor, NO_2 formation can occur through two different pathways: attack by OH (R1) and photolysis of NO_2^- (R2) with the subsequent oxidation of NO by dissolved oxygen (R3):

$$NO_2^- + OH \rightarrow NO_2 + OH^- \quad (R1)$$

$$NO_2^-(+H^+) \xrightarrow{h\nu} NO + OH \quad (R2)$$

$$2NO + O_2 \rightarrow 2NO_2 \quad (R3)$$

In the reaction (R2) an oxide radical ion (O^-) is first generated, which immediately adds a proton to yield OH radicals [40]. NO_2 can subsequently be oxidized to NO_3^- either by the formation of the dimer N_2O_4 followed by hydrolysis (R4) [25] or by the attack of an OH radical (R5):

$$2NO_2 + H_2O \rightarrow NO_3^- + NO_2^- + 2H^+ \quad (R4)$$

$$NO_2 + OH \rightarrow NO_3^- + H^+ \quad (R5)$$

Two reaction channels are possible during the photolysis of NO_3^-: either the formation of NO_2 (R6) or NO_2^- (R7):

$$NO_3^-(+H^+) \xrightarrow{h\nu} NO_2 + OH \quad (R6)$$

$$NO_3^- \xrightarrow{h\nu} NO_2^- + O \quad (R7)$$

An additional product of reaction (R7) is the oxygen atom (O). It can react with dissolved oxygen to produce ozone (R8) and with NO_3^- producing additional NO_2^- (R9):

$$O + O_2 \rightarrow O_3 \quad (R8)$$

$$NO_3^- + O \rightarrow NO_2^- + O_2 \quad (R9)$$

Additional reactions leading to the formation of NO_2^- is the reaction of OH with NO (R10) and the reaction of NO with NO_2 with the subsequent hydrolysis of N_2O_3 (R11):

$$NO + OH \rightarrow NO_2^- + H^+ \quad (R10)$$

$$NO + NO_2 + H_2O \rightarrow 2NO_2^- + 2H^+ \quad (R11)$$

Due to the experimental conditions, we also need to take into account the photolysis of NO_2 to NO in the snow (R12):

$$NO_2 \xrightarrow{h\nu} NO + O \quad (R12)$$

Finally, due to the low solubility the nitrogen oxides are transferred to the gas phase (R13) and (R14):

$$NO \rightarrow NO_{gas} \quad (R13)$$

$$NO_2 \rightarrow NO_{2\,gas} \quad (R14)$$

The full reaction mechanism used for the analysis of the experimental data is shown in Table 2. We used aqueous phase kinetic data for the rate constants of the bimolecular reactions. If temperature-dependent rate constants were available, they were extrapolated to sub-freezing temperatures (Table 2).

The rate constants of the NO_2^- and NO_3^- photolysis reactions (R2), (R6), and (R7) and the rates for the phase transfer reactions of NO and NO_2 ((R13) and (R14)), were derived by fitting the experimental and calculated concentration–time curves using the commercial FACSIMILE software. For the fitting procedure we used the measured NO_3^- and NO_2^- concentrations and gas phase $NO_{x\,gas}$ concentrations. Since $NO_{x\,gas}$ was not directly measured, we calculated the gas phase concentration as the difference from the measured ($[NO_3^-]$, $[NO_2^-]$) to the initial NO_3^- and NO_2^- concentrations ($[NO_3^-]_0$, $[NO_2^-]_0$) in

Table 2
Reactions included in the mechanism for the photochemical transformation of NO_3^- and NO_2^- in snow

Reaction no.		Reaction rates[a]			Reference
		$T = -31\,°C$	$T = -20\,°C$	Summit[b]	
$OH + NO_2^- \rightarrow NO_2 + OH^-$	(R1)	$1 \times 10^{10}\,M^{-1}\,s^{-1}$	$1 \times 10^{10}\,M^{-1}\,s^{-1}$	$1 \times 10^{10}\,M^{-1}\,s^{-1}$	[41]
$(R2)NO_2^-(+H^+) \xrightarrow{h\nu} NO + OH$		$3 \times 10^{-3}\,s^{-1}$[c]	$8.4 \times 10^{-3}\,s^{-1}$[d]	$2.5 \times 10^{-5}\,s^{-1}$	This work
$2NO + O_2 \rightarrow 2NO_2$	(R3)	$360\,M^{-1}\,s^{-1}$[e]	$420\,M^{-1}\,s^{-1}$[e]	$420\,M^{-1}\,s^{-1}$[e]	[42]
$2NO_2 + H_2O \rightarrow NO_3^- + NO_2^- + 2H^+$	(R4)	$1 \times 10^{7}\,M^{-1}\,s^{-1}$	$1.4 \times 10^{7}\,M^{-1}\,s^{-1}$	$1.4 \times 10^{7}\,M^{-1}\,s^{-1}$	[43]
$NO_2 + OH \rightarrow H^+ + NO_3^-$	(R5)	$5 \times 10^{9}\,M^{-1}\,s^{-1}$	$5 \times 10^{9}\,M^{-1}\,s^{-1}$	$5 \times 10^{9}\,M^{-1}\,s^{-1}$	[44]
$(R6)NO_3^-(+H^+) \xrightarrow{h\nu} NO_2 + OH$		$1 \times 10^{-4}\,s^{-1}$[c]	$2.8 \times 10^{-4}\,s^{-1}$[d]	$8.3 \times 10^{-7}\,s^{-1}$	This work
$(R7)NO_3^- \xrightarrow{h\nu} NO_2^- + O$		$2 \times 10^{-5}\,s^{-1}$[c]	$5.6 \times 10^{-5}\,s^{-1}$[d]	$1.7 \times 10^{-7}\,s^{-1}$	This work
$O + O_2 \rightarrow O_3$	(R8)	$1.2 \times 10^{6}\,s^{-1}$[e]	$1.2 \times 10^{6}\,s^{-1}$[e]	$1.2 \times 10^{6}\,s^{-1}$[e]	[45]
$NO_3^- + O \rightarrow NO_2^- + O_2$	(R9)	$2 \times 10^{8}\,M^{-1}\,s^{-1}$	$2 \times 10^{8}\,M^{-1}\,s^{-1}$	$2 \times 10^{8}\,M^{-1}\,s^{-1}$	[19]
$NO + OH \rightarrow H^+ + NO_2^-$	(R10)	$2 \times 10^{10}\,M^{-1}\,s^{-1}$	$2 \times 10^{10}\,M^{-1}\,s^{-1}$	$2 \times 10^{10}\,M^{-1}\,s^{-1}$	[46]
$NO + NO_2 + H_2O \rightarrow 2NO_2^- + 2H^+$	(R11)	$3 \times 10^{8}\,M^{-1}\,s^{-1}$	$3 \times 10^{8}\,M^{-1}\,s^{-1}$	$3 \times 10^{8}\,M^{-1}\,s^{-1}$	[47]
$(R12)NO_2 \xrightarrow{h\nu} NO + O$		$1\,s^{-1}$	$2.8\,s^{-1}$	$8.3 \times 10^{-3}\,s^{-1}$	Estimated
$NO \rightarrow NO_{gas}$	(R13)	$45\,s^{-1}$[c]	$57\,s^{-1}$[d]	$57\,s^{-1}$	This work
$NO_2 \rightarrow NO_{2\,gas}$	(R14)	$3\,s^{-1}$[c]	$9.7\,s^{-1}$[d]	$9.7\,s^{-1}$	This work

[a] Reaction rates were taken from kinetic data determined in the aqueous liquid phase. If temperature-dependent rate constants were available, reaction rates were extrapolated to sub-freezing temperatures.
[b] Reaction rates estimated for conditions at GEO Summit in summer 2000.
[c] Reaction rates determined for experiments here, performed at −31 °C.
[d] Reaction rates determined for previously published experiments [27], performed at −20 °C.
[e] First- and second-order rate constants calculated with $[O_2] = 0.3\,\mu M$ [19].

the snow:

$$[NO_{x\,gas}] = [NO_3^-]_0 + [NO_2^-]_0 - ([NO_3^-] + [NO_2^-]) \quad (1)$$

Although the NO_x transfer rates k_{R13} and k_{R14} varied, we always used a fixed ratio of $k_{R13}/k_{R14} = 15$ since the extrapolated Henry's law constants of both compounds at $T = 31\,^{\circ}C$ differ by a factor of 15 [48]. This assumption is in agreement with previous laboratory experiments suggesting that NO_2 is more strongly bound than NO to the ice [26].

Several laboratory studies have provided evidence that the photolysis of nitrate and the subsequent reactions in ice and snow take place in a so-called quasi-liquid layer (QLL) on the surface of ice crystals [19,20,22,23]. Although the properties of the QLL are not well established, it is now well known that at temperatures close to the melting point and/or in the presence of impurities, the QLL shows a strongly enhanced disorder compared to the highly ordered interior of the ice crystal (e.g. [49–53]). Nevertheless, the QLL is always restricted to a limited number of layers of water molecules. If all reactions in the condensed phase take place in this much smaller volume, the calculations must be performed using significantly higher concentrations. Cho et al. [51] performed NMR spectroscopy to determine the fraction of water in the QLL φ_{H_2O} as a function of temperature T and the total solute concentration in the QLL C_T^0. They obtained the following equation (2):

$$\varphi_{H_2O}(T) = \frac{m_{H_2O} R T_f}{1000 H_f^0} \frac{T}{T - T_f} C_T^0 \quad (2)$$

Here, m_{H_2O} is the molecular weight of water, R the gas constant, H_f^0 the melting enthalpy of water, and T_f is the freezing temperature of water.

The concentration in the QLL is not directly available for our experiments since the analysis of the melted snow samples yields only the bulk snow concentrations. Nevertheless, these can be translated into the QLL concentrations if we assume that all impurities are located in the QLL. In that case, we can relate the bulk concentration C_{bulk} to the QLL concentrations C_T^0 by the following Eq. (3):

$$C_{bulk} = \varphi_{H_2O}(T) C_T^0 \quad (3)$$

Substituting this expression into Eq. (2), we find

$$\varphi_{H_2O}(T) = \sqrt{\frac{m_{H_2O} R T_f}{1000 H_f^0} \frac{T}{T - T_f} C_{bulk}} \quad (4)$$

The QLL fractions (φ_{H_2O} listed in Table 1 were obtained with Eq. (4) for the initial conditions of the four different snow batches. Applying Eq. (3), φ_{H_2O} was subsequently used to calculate QLL concentrations of NO_3^- and NO_2^- for the experiments performed with the four snow batches as shown in Table 1 for the initial concentrations. Fig. 3 shows the results of all four batches transformed into QLL concentration and also the gas phase NO_x concentrations as calculated from the differences between actual and initial NO_3^- and NO_2^- concentrations in the snow according to Eq. (1). For an easier comparison the $NO_{x\,gas}$ concentrations are also plotted in M units like the QLL concentrations.

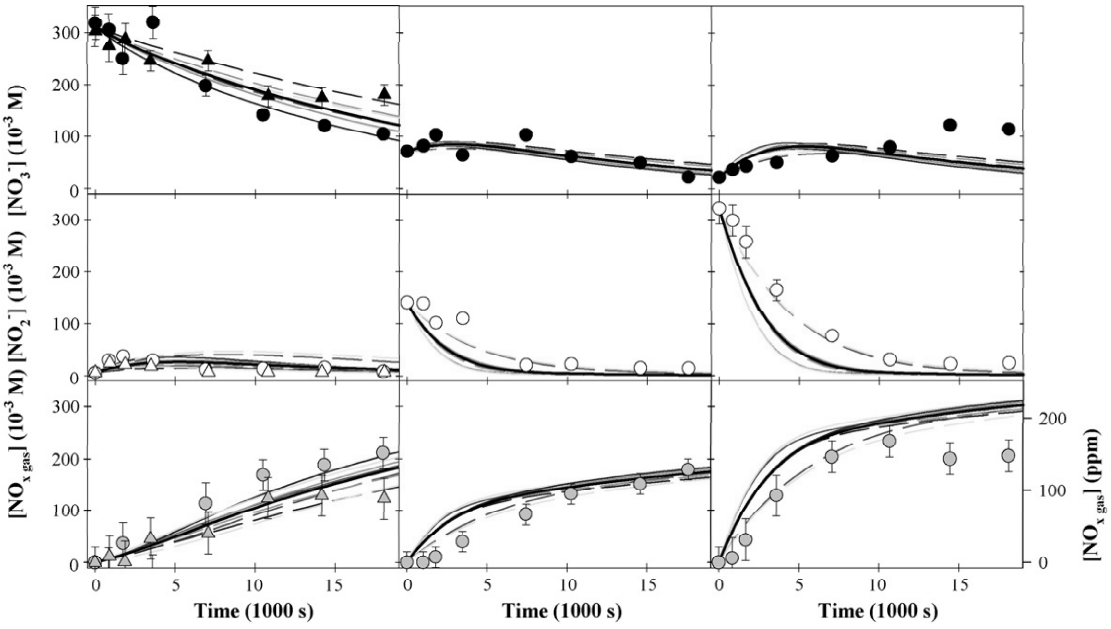

Fig. 3. Comparison of experimental and calculated concentration-time-profiles for NO_3^- (top) and NO_2^- concentrations (middle) in the QLL and $NO_{x\,gas}$ in the gas phase (bottom) for the snow batches 1 and 2 (left), batch 3 (middle), and batch 4 (right). On the left axis the NO_x concentration is shown in M as calculated according to Eq. (1) as the deficit of NO_3^- and NO_2^- in the snow samples. On the right axis the NO_x concentrations are transformed into gas phase mixing ratios taking into account the mass of the snow and the gas phase volume in the cell. The black line represents calculated profiles using the optimum rate constants (see text). Colored lines represent calculated profiles with single rate constants varying by +50% (full lines) and −50% (dashed lines) with variation of k_{R2}: red, k_{R7}: blue, k_{R6}: green, and k_{R13} and k_{R14}: yellow. Error bars for NO_3^- and NO_2^- represent analytical errors. The error of the gas phase NO_x is calculated from the analytical errors of NO_3^- and NO_2^- using error propagation. If no error bar is visible, the errors are smaller than the size of the symbols.

A common best-fit was determined using the QLL concentrations of all four batches of snow shown in Fig. 3. Best agreement between the experiments and the calculated concentration–time-profiles were found with the following rate constants for the photolytic reactions of NO_2^- and NO_3^-: $k_{R2} = 3 \times 10^{-3}\ s^{-1}$ $k_{R6} = 1 \times 10^{-4}\ s^{-1}$, and $k_{R7} = 2 \times 10^{-5}\ s^{-1}$. Thus, in our experiments the photolysis of NO_2^- occurred a factor of ~25 faster than the overall photolysis of NO_3^-. The two different reaction channels for the NO_3^- photolysis, generating NO_2 (R6) and NO_2^- (R7), contributed 83% and 17%, respectively, which is in reasonable agreement with previous studies in fluid and frozen media [19,21,22,33].

In addition, the optimum transfer rates for NO and NO_2 were determined to be on the order of $k_{R13} = 45\ s^{-1}$ and $k_{R14} = 3\ s^{-1}$, respectively. Fig. 3 shows a comparison of the time series of experimental and modeled QLL concentrations obtained with the optimum rate constants. The sensitivities of the calculated concentrations to changes in the rate constants were tested. The reaction rate constants k_{R2}, k_{R6}, and k_{R7} and the transfer constants k_{R13} and k_{R14} were separately changed by a factor of 2 (the ratio of k_{R13} to k_{R14} remained constant). The results of these sensitivity studies are also shown in Fig. 3.

In general, the calculated concentrations are in good agreement with the experimental data. The deviations between modeled and experimental data are in the same range as the variability of the results for the two different snow batches 1 and 2 with comparable initial concentrations. Applying the mechanism, we are able to reproduce the reduction in NO_3^- and NO_2^- if high initial concentrations of either compound were present in the snow. The mechanism also captures the transformation of NO_2^- to NO_3^- observed in the batches 3 and 4 (Fig. 3). The quick release of nitrogen oxides to the gas phase is also well reproduced by the model. However, the NO_2^- drop occurs somewhat faster in the model compared to the experiments performed with the batches 2 and 3. Better agreement is obtained if either the rate constant k_{R2} for the photolysis of NO_2^- (dashed red line) or the transfer rates k_{R13} and k_{R14} of NO and NO_2 (dashed yellow line) were reduced by 50% (Fig. 3). However, these higher rates would lead to a much worse agreement with the results of the batches 1 and 2 with small initial NO_2^- concentrations. Therefore, the proposed rate constants constitute a compromise for all four experiments. The gas phase NO_x concentrations are also sensitive to the rate constants k_{R2}, k_{R13}, and k_{R14}. Similar to NO_2^-, the agreement between modeled and measured NO_x becomes better with higher rate constants for the batches 3 and 4 and worse for the batches 1 and 2. In contrast, the calculated NO_3^- concentrations are most sensitive to the photolysis rate constants k_{R6} and k_{R7} of NO_3^-.

4.2. Comparison with previous laboratory data

Jacobi et al. [27] previously presented results of similar experiments regarding the photolytic decomposition of nitrate in snow. Here, we apply the newly developed reaction mechanism to reproduce the experimental data. However, due to the different experimental conditions the rate constants need to be adjusted. First, the distance between the reaction cell and the lamp was smaller in the previous experimental set-up (16 cm), compared to the current set-up (27 cm). These different distances caused higher radiation intensities per area by a factor of 2.8 since the intensity decreases with the square of the distances from the light source. Therefore, we increased all photolysis rates (k_{R2}, k_{R6}, k_{R7}, and k_{R12}) by a factor of 2.8 (Table 2). Second, the previous experiments were performed at a higher temperature of −20 °C [27]. We adjusted the rate constants k_{R3} and k_{R4} using the temperature dependencies of the rate constants reported in the literature [42,43]. However, the changes are smaller (≤40%) than the assumed error of the fitted photolysis rate constants (Table 2). Fig. 4 shows calculated concentration–time-profiles with the increased photolysis and reaction rates. Moreover, the temperature also influences the phase transfer. Using, again, Henry's law constants as a reference, we find that the con-

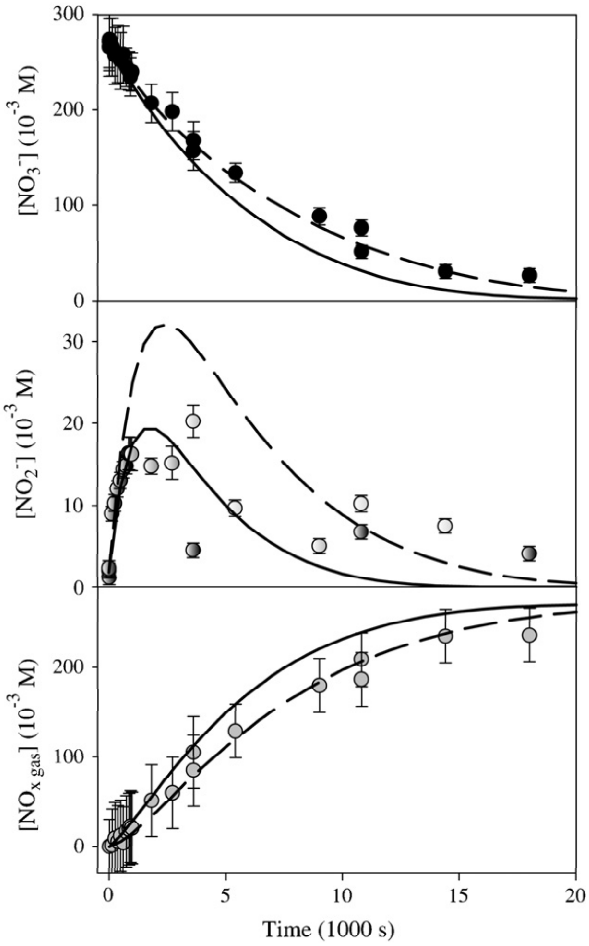

Fig. 4. Comparison of experimental and calculated concentration–time-profiles for NO_3^- (top) and NO_2^- concentrations (middle) in the QLL and NO_x in the gas phase (bottom) for previous experiments [27] performed at −20 °C. The NO_x concentrations are calculated according to Eq. (1). The dashed line represents calculated profiles with all photolysis rates multiplied by 2.8 (see text). The full lines represent calculated profiles with increased photolysis rates and increased transfer rates for NO and NO_2 as summarized in Table 2 (see text). Error bars for NO_3^- and NO_2^- represent analytical errors. The error of the gas phase NO_x is calculated from the analytical errors of NO_3^- and NO_2^- using error propagation.

stant for NO decreases from 5.6×10^{-3} M atm^{-1} at −31 °C to 4.4×10^{-3} M atm^{-1} at −20 °C [48]. The decrease is even more pronounced for NO_2 from 8.4×10^{-2} M atm^{-1} at −31 °C to 2.6×10^{-2} M atm^{-1} at −20 °C [48]. Therefore, we enhanced the transfer constants similarly (Table 2), reducing the ratio of k_{R13} to k_{R14} from 15 at −31 °C to smaller than 6 at −20 °C. Calculated concentration–time-profiles with the increased transfer rates are also shown in Fig. 4. The comparison with the experimental data shows that the agreement for NO_2^- is much improved with the higher transfer rates. With the lower transfer rates the maximum NO_2^- concentration is approximately 50% higher than the highest NO_2^- concentrations determined in any of the experiments. The higher transfer rates lead to maximum NO_2^- concentrations, which fall well in the range of the observed concentrations. On the other hand, the faster transfer leads to slightly overestimated values for the NO_x concentrations in the gas phase and slightly underestimated values for NO_3^-. The discrepancies become larger for experiments lasting longer than 5000 s (≈1.4 h) and might be due to the equilibrium of NO and NO_2 between the gas phase and the QLL. If the gas phase concentrations are sufficiently high a transfer back from the gas phase to the QLL becomes possible. This could explain the slightly lower gas phase and slightly higher NO_3^- concentrations observed in the experiments.

4.3. Comparison with field data: NO_x emissions

Having established a mechanism for the photochemical transformation of nitrogen containing compounds in snow, we can apply this mechanism to previous field observations. The most comprehensive data set, which provides the needed input information, is currently available from measurements performed at the Greenland environmental observatory summit (GEO Summit) on top of the Greenland ice sheet (72.6°N, 38.5°W, 3200 m elevation) in the summer of the year 2000. For example, nitrate photolysis rate coefficients were directly measured in the snow using chemical actinometry [10]. Average values for midday exposures were on the order of 10^{-6} s^{-1} at depths smaller than 5 cm. Therefore, we decreased the rate coefficients k_{R6} and k_{R7} so that the sum of both photolysis rates gives a value of 10^{-6} s^{-1} (Table 2). Accordingly, we also reduced the photolysis rates k_{R2} of NO_2^- and k_{R12} of NO_2 by the same factor, since this reaction will also be much slower under natural conditions. The reported snow temperatures for Summit varied between −4 °C at the surface and −21 °C at a depth of 15 cm for the period of the photolysis rate measurements [10]. Although the experimental temperature of −20 °C is close to the lower limit of the temperature in the natural snow, we did not attempt to adjust the rate constants further. NO_3^- in surface-snow at Summit shows considerable short-term variability [54]. We used an average concentration of 3 μM as reported by Dibb et al. [54] for the initial concentration in our calculations.

The rate constants and the initial calculated QLL concentration of NO_3^- are summarized in Tables 1 and 2. QLL concentrations and gas phase NO_x production rates simulated after reaction times of 2 and 4 h are shown in Table 3. Fig. 5 shows a concentration and flux diagram for conditions after reaction times of 2 h. The diagram shows the conversion of the nitrogen compounds in the QLL and the transfer to the gas phase.

For the applied conditions the model predicts that the photochemical transformation of NO_3^- occurs very slowly. For example, after a reaction time of 4 h the NO_3^- concentrations are apparently reduced by less than 1% compared to the initial NO_3^- concentration, although the observed photolysis rate suggests that in such a period almost 1.4% of the initial NO_3^- would have been photolyzed. Obviously, the recycling of NO_3^- via the oxidation of NO_2 contributes to the slower apparent NO_3^- decrease. Fig. 5 shows that after a reaction time of 2 h the total sink strength of NO_3^- via the photolysis reactions (R6) and (R7) and the reaction with the O atom (R9) assumes a value of 2.7×10^{-7} M s^{-1}. However, the net destruction of NO_3^- is reduced by more than 40% due to the oxidation of NO_2 to NO_3^- mainly via the reaction with OH (R5).

NO_2^- concentrations in the QLL increase quickly and reach maximum values of 5.9×10^{-9} M after just several seconds before they decrease slowly. Translating the QLL concentrations into bulk snow concentrations using the QLL fraction (Table 2) leads to extremely small NO_2^- concentrations of less than 2×10^{-13} M in the snow. Such concentrations are far beyond the detection limit of currently used chemical snow analysis methods (e.g. [55–57]). Nevertheless, NO_2^- concentrations up to 1.8×10^{-7} M in arctic snow samples were reported at depths of 25 cm, while the concentrations remained below 7×10^{-8} M at the surface [58]. A photochemical generation of such high NO_2^- concentrations is only possible with radiation intensities as high as in our laboratory experiments (Fig. 2). Since these intensities are orders of magnitudes higher than the intensity of the solar radiation at the Earth's surface [39], additional sources of NO_2^- must be invoked to explain the NO_2^- observations. Such sources could be the dry deposition of HONO or the precipitation of fresh snow with higher NO_2^- concentrations due to the scavenging of gas phase HONO. The destruction of NO_2^- is dominated by the reaction with OH (R1), while the photolysis is a negligible sink of NO_2^- under natural conditions. This

Table 3
Calculated QLL concentrations and gas phase NO_x production rates calculated for conditions at Summit observed in the summer of 2000

Time[a] (h)	$[NO_3^-]$ (M)	$[NO_2^-]$ ($\times 10^{-9}$ M)	$[NO_2]$ ($\times 10^{-8}$ M)	[NO] ($\times 10^{-12}$ M)	[OH] ($\times 10^{-9}$ M)	$P(NO_2)$[b] ($\times 10^{12}$ molecules s^{-1})	$P(NO)$[b] ($\times 10^{8}$ molecules s^{-1})
2	0.229	5.84	1.59	1.48	1.38	1.80	9.83
4	0.228	5.81	1.58	1.47	1.38	1.79	9.78

[a] Time after the initiation of the calculations.
[b] Production rates of gas phase NO_2 and NO calculated for 1 L of irradiated snow.

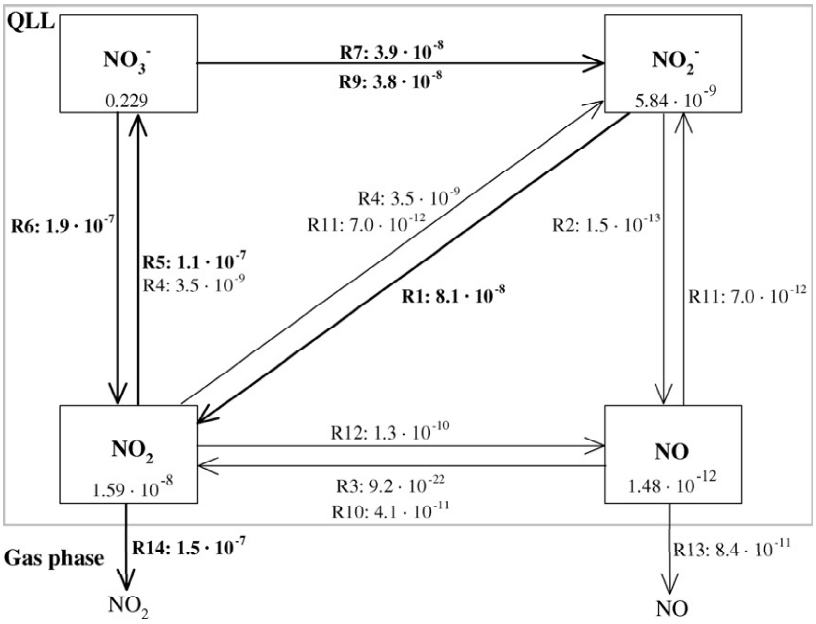

Fig. 5. Concentration and flux diagram for the photolysis of NO_3^- in the QLL of the surface snow calculated for typical conditions at Summit in the year 2000. The numbers are computed for $t = 2$ h after the initiation of the calculations. Concentrations are given in M, fluxes for single reactions (see Table 2 for reaction numbers) are given in M s^{-1}. For example, the flux of NO_2 to the gas phase of 1.5×10^{-7} M s^{-1} corresponds to an emission rate of 1.8×10^{12} molecules s^{-1} for 1 L of snow (see Table 3). Thick arrows represent dominant conversion pathways with fluxes larger than 3×10^{-8} M s^{-1}.

is in agreement with previous laboratory studies of the NO_3^- photolysis in the presence of radical scavengers. For example, Honrath et al. [18] observed a much smaller NO_2 production in the presence of OH scavengers. Similarly, Dubowski et al. [20] reported increased yields of NO_2^- if they added an OH radical scavenger like formate to their ice samples. Both observations indicate that the conversion of NO_2^- to NO_2 ceased if OH were significantly removed.

The model results demonstrate that the release of NO_x is dominated by NO_2 (Fig. 5). NO_2 is generated either directly by the photolysis of NO_3^- (R6) or via the formation of NO_2^- from NO_3^- by the reactions (R7) and (R9) and the subsequent reaction of NO_2^- with OH (R1). The main sinks of NO_2 are the oxidation to NO_3^- by the OH radical (R5) and the transfer to the gas phase (R14). Since both pathways are almost equal, a significant fraction of the NO_2 produced in the QLL undergoes chemical reactions prior to the release to the gas phase. This was also observed in previous laboratory experiments using thin ice films [25,26]. However, our model calculations indicate that for natural conditions the reaction with the OH radical (R5) is far more important than the hydrolysis of the NO_2 dimer (R4) as suggested for the laboratory experiments [25].

Compared to NO_2, NO concentrations as well as the NO transfer to the gas phase are orders of magnitude smaller. Therefore, NO in the QLL plays probably a negligible role for the photochemical transformation of nitrogen containing compounds as well as the release of NO_x to the firn air. The ratio of the NO_2 to NO fluxes to the gas phase assumes a value of approximately 1800 (Table 3) and remains constant for several hours in the simulations.

Similarly, previous studies of the NO_3^- photolysis using natural or artificial snow samples [3,5,18,21] or thin ice layers [23,26] have also indicated that the NO_x flux to the gas phase was dominated by NO_2, although in most cases the emission of NO was not negligible with ratios of the NO_2 to NO production rates between 2 and 8 in the snow experiments [5,18,21] and ratios between 10 and 23 in the experiments with the ice films [23,26]. However, the formation of NO possibly indicates further reactions in the gas phase like the photolysis of NO_2 and HONO, which can also lead to the formation of NO. At least in the snow experiments with long residence times of the sampled air in the illuminated zone on the order of minutes [5,18,21], these gas phase reactions must be considered as discussed by Cotter et al. [21].

The calculated NO_2 production rate amounts to 1.8×10^{12} molecules s^{-1} in 1 L of irradiated snow. Such a production rate translates into a NO_2 flux of 5.4×10^{12} molecules m^{-2} s^{-1} taking into account a snow layer with a depth of 1 cm and a density of 0.3 g cm^{-3}. This flux must be considered as representative for conditions at noon due to the selected photolysis rates for the model run. We can compare this value to NO_x fluxes measured above the snow surface at Summit in 2000. According to Honrath et al. [11], the NO_x emissions were correlated with the solar radiation intensities with two thirds of the NO_x fluxes observed around noon falling in a range between 2 and 11×10^{12} molecules m^{-2} s^{-1} [11]. The agreement between the modeled and observed NO_x fluxes is excellent if we assume that the NO_x release to the atmosphere is determined by the top 1 or 2 cm of the snow. However, it is very likely that a thicker snow layer contributes to the photochemical production of NO_x

since the penetration depth of the solar radiation into the snow is deeper than just a few centimeters. For example, in the UV and visible range Peterson et al. [59] found that in the same snowpack at Summit approximately 10% of the incident radiation at the snow surface is transmitted to a depth of 10 cm. Since the NO_x fluxes were measured above the snow surface, they represent only the fraction of NO_x, which actually escaped from the so-called firn air, which is the interstitial air of the surface snow. The NO_x production rates in the snow can be significantly higher if a large fraction is oxidized in the firn air and re-deposited to the snow before it is released to the atmosphere. An indication of high NO_x production rates is for example the extremely high NO_x concentration in the firn air also measured at Summit [14].

The modification of the reaction mechanism developed for the laboratory experiments to conditions in the natural snowpack is accompanied by rather high uncertainties. These mainly arise from the vastly different emission spectrum of the lamp compared to the spectrum of the solar radiation [27]. The irradiation emitted by the lamp shows a strong band in the UV range, which overlaps with the absorption spectrum of NO_3^-. However, such a band is absent in the solar radiation. Therefore, the ratio of the photolysis rates of NO_2^- and NO_3^- is probably larger in the natural snowpack compared to the laboratory experiments. To account for this effect, we performed additional model runs with fixed NO_3^- photolysis rates k_{R6} and k_{R7} determined by the rates measured at Summit as described above, but with a NO_2^- photolysis rate k_{R2} increased by a factor of 10 and 100, respectively. In both cases the effects on the calculated QLL concentrations are small. The largest effects are obtained for the modeled NO concentrations, which increase by less than 1% with k_{R2} multiplied by 10 and by less than 11% with k_{R2} multiplied by 100. The changes of all other concentrations are smaller than 1%. The reason for these small changes is the minor importance of the NO_2^- photolysis (R2) as displayed in Fig. 5. The production rate of NO by this reaction is almost three orders of magnitude smaller than by the photolysis of NO_2 (R12). Therefore, multiplying k_{R2} by a factor of 100 increases the total NO production rate only by a few percent. Such a small increase in the NO production has only a slight impact on the modeled NO concentrations and the ratio of the NO and NO_2 concentrations. Although additional experiments are needed to determine the exact photolysis rate constants for natural conditions, we do not expect drastic changes for instance in the ratio of the NO_2 to NO concentrations and fluxes to the gas phase.

4.4. HONO production in the surface snowpack

Besides the emission of NO_x, upward fluxes of HONO from the surface snow to the atmosphere have been reported for the Canadian Arctic [8] and Summit [11]. Although the gas phase HONO production is currently not incorporated into the mechanism, we can use the computed concentrations to determine if a sufficiently high production of HONO can occur in the QLL to explain the measured emissions. The HONO transfer to the gas phase depends on several parameters like the NO_2^- concentration in the QLL, the pH of the QLL, and the HONO phase transfer rate. Since we did not attempt to compute the proton concentrations directly, we will compare the ratio of the gas phase HONO to NO_2 production rates and discuss the impact of the pH on this ratio.

HONO is a moderately weak acid with a dissociation constant pK_a reported in the literature in the range from 2.3 to 5.2 [60]. Here, we use an extrapolated pK_a of 3.7 at a temperature of −20 °C [47]. Thus, 99% of the NO_2^- would be present at HONO in the QLL at a pH of 1.7. However, Table 3 demonstrates that the NO_2^- concentrations are always lower than the NO_2 concentrations by a factor of approximately 3. Even with a full conversion of NO_2^- to HONO at low pH values, the HONO concentrations will remain smaller than the NO_2 concentrations in the QLL. Nevertheless, the HONO flux to the gas phase could be comparable to the NO_2 flux if the lower concentration is compensated by a higher transfer rate. Similarly to the case of NO and NO_2, we calculate the phase transfer rate relative to the Henry's law constant. Due to the much higher solubility of HONO, the Henry's law constant is significantly higher compared to the values for the nitrogen oxides. Using temperature-dependent parameters [48], we obtain a value of 930 M atm^{-1} extrapolated to −20 °C for HONO. Since this number is a factor of 3.6×10^4 higher than the Henry's law constant of NO_2 at the same temperature, we assume that the phase transfer rate of HONO is significantly smaller compared to the transfer of NO_2. In combination with the lower transfer rate, we conclude that the HONO transfer from the QLL is orders of magnitude smaller than the parallel NO_x transfer. Thus, the NO_3^- photolysis in snow is a negligible direct source of HONO in contrast to previous suggestions (e.g. [37]). However, such small HONO production rates can explain neither the enhanced HONO concentrations measured in the firn air [14], nor the HONO emissions observed above the snowpack [8,11]. We suggest that HONO is produced in the firn air either by gas phase reactions (e.g. NO + OH) or by heterogeneous reactions of NO_2 or HO_2NO_2 at the snow crystal surfaces. Several studies have demonstrated that the heterogeneous hydrolysis of NO_2 yields gas phase HONO (e.g. [61]). More recently, George et al. [62] demonstrated that HONO was produced with a high efficiency by the heterogeneous reaction of NO_2 with light absorbing organic compounds. Since Grannas et al. [35] reported contributions of phenols and further aromatic compounds to the organic content of snow samples collected at Summit, the suggested mechanism might contribute to the HONO formation in the firn air. However, whether the firn air concentrations of NO_x, OH, and HO_2NO_2 are high enough to produce significant amounts of HONO remains unresolved as discussed by Cotter et al. [21].

It has been proposed that the HONO flux out of or into the snowpack depends on the pH value of the snow [17,36]. Our model calculations indicate that the pH value of the QLL does not impact the formation rate of HONO in the snow: the formation is always negligible due to the small NO_2^- concentrations obtained in the model calculations. However, the pH can obviously determine if the HONO produced in the firn air is absorbed by the QLL or rather released to the atmosphere above the snowpack. While pH values can enhance the dissociation of HONO into H^+ and NO_2^-, thus increasing the solubility of HONO in the QLL, this effect should be most obvious at pH values around

the pK_s of HONO. Varying the pH around the pK_s by ±1 means that either 90% or 10% of the HONO would be present in the not-dissociated form in the QLL. The measured snow pH represents an equilibrium value obtained from the melted snow sample. In other words, this is the pH of a solution containing all the electrolytes present in the snow sample. Recent laboratory experiments clearly demonstrated that the pH of the QLL can be significantly different compared to the melted ice [63]. At present it is not clear how the measured snow pH relates to the pH of the QLL. Further studies on natural snow samples are needed to investigate this value since it is the crucial parameter for the air–snow equilibrium of acidic and alkaline species.

Due to the small volume of the QLL, it still constitutes only a limited reservoir for HONO. However, as shown in Fig. 5, NO_2^- is unstable in the QLL, where it is destroyed with a rate of 9.5×10^{11} molecules L_{snow}^{-1} s^{-1} for typical conditions at Summit. We can compare this destruction rate with observed deposition fluxes of HONO to snow surfaces. For example, a HONO flux of up to 120 nmol m^{-2} h^{-1} was observed in the Apennine mountains in Italy in spring [36]. This value corresponds to a HONO flux of 2.0×10^{13} molecules m^{-2} s^{-1}. If we assume a typical snow density of 0.3 g cm^{-3}, the photochemical destruction in a snow layer with a depth of 7 cm is sufficient to destroy the deposited HONO completely. The conditions of the surface snow at Summit are probably significantly different compared to the springtime snow in the Apennines regarding the snow composition and temperature, the solar radiation intensities, and the pH of the snow. Nevertheless, the comparison indicates that the proposed photochemical mechanism for the surface snow is well able to explain the fate of the HONO deposited to the snow surface.

5. Summary and conclusions

We developed a comprehensive mechanism for the photochemical transformation of NO_3^- to NO_2^- in snow and further to more volatile nitrogen containing compounds like NO and NO_2. Applying this mechanism to data obtained in different laboratory experiments, we adjusted unknown photolysis rates of NO_3^- and NO_2^- in artificial snow for the experimental conditions. The rates were further verified using previously published laboratory experiments and field studies. These comparisons demonstrate that (i) the general mechanism is able to capture the main features of the photochemical transformation of nitrogen compounds in snow and (ii) the adjusted rates can be applied to a wide range of conditions.

We adjusted the photochemical mechanism to typical summer conditions for the Greenland ice sheet. These simulations showed that the NO_2^- concentrations in the snow remained extremely low. NO_2^- remains still an important intermediate for the formation of NO_2 in the snow although the NO_2 formation is dominated by the photolysis of NO_3^-. A large fraction of the produced NO_2 is oxidized back to NO_3^- reducing the net NO_3^- destruction rate by 40%. The model calculations indicate that for summer conditions in Greenland, out of five NO_3^- molecules initially photolyzed in the snow, approximately three are released to the firn air in the form of NO_2 and two molecules are re-oxidized back to NO_3^-. Comparisons of the modeled NO_2^- and NO_2 concentrations and the Henry's law constants of HONO and NO_2 further indicate that the HONO production within the snow is probably negligible. We suggest that HONO, which is readily emitted by the sun-lit snowpack, is formed in the firn air possibly by the heterogeneous reaction of NO_2 on the surface of the ice crystals.

The simulations with the photochemical mechanism further show that observed NO_x emissions are easily reconciled by the calculated NO_2 production in several centimeters of the surface snow. In addition, HONO deposition fluxes as observed onto more alkaline snow surfaces in lower latitudes are also in good agreement with the destruction rates for NO_2^- obtained with the model. In summary, we conclude that the proposed photochemical mechanism for the transformation of NO_3^- in snow represents a reasonable representation for the processes occurring in natural snow surfaces.

Nevertheless, further laboratory and field studies are needed to improve the mechanism and extend its applicability since several uncertainties remain. Although the mechanism is limited to nitrogen-containing compounds, the important role of other reactive species like the OH radical becomes already obvious. In agreement with previous experiments in the presence of radical scavengers [18,20], the model indicates that the reactions with OH radicals constitute important sinks for NO_2^- as well as for NO_2 (Fig. 5). Chu and Anastasio [64] concluded that the most important OH source in the snow is from the photolysis of H_2O_2, which is omnipresent in natural snow. This shows that the recommended photochemical mechanism cannot account for all processes known to occur in the natural snowpack. Besides the sources of OH radicals, this concerns also the processing of organic compounds in the snow. Further studies are needed to develop a full photochemical reaction mechanism for the snow.

Additional uncertainties arise from the limited knowledge of the properties of the QLL. Furthermore, less reactive impurities like sea-salt components may increase the liquid fraction and, thus, reduce the QLL concentrations of the reactive compounds. Further laboratory and modeling studies are needed to characterize the QLL so that it can be represented better in the model.

Acknowledgement

Financial support by the Deutsche Forschungsgemeinschaft (DFG) is gratefully acknowledged.

References

[1] F. Dominé, P.B. Shepson, Air–snow interactions and atmospheric chemistry, Science 297 (2002) 1506–1510.
[2] R.E. Honrath, M.C. Peterson, S. Guo, J.E. Dibb, P.B. Shepson, B. Campbell, Evidence of NO_x production within or upon ice particles in the Greenland snowpack, Geophys. Res. Lett. 26 (1999) 695–698.
[3] R.E. Honrath, M.C. Peterson, M.P. Dziobak, J.E. Dibb, M.A. Arsenault, S.A. Green, Release of NO_x from sunlight-irradiated midlatitude snow, Geophys. Res. Lett. 27 (2000) 2237–2240.
[4] B. Ridley, J. Walega, D. Montzka, F. Grahek, E. Atlas, F. Flocke, V. Stroud, J. Deary, A. Gallant, H. Boudries, J. Bottenheim, K. Anlauf, D. Worthy,

A.L. Sumner, B. Splawn, P. Shepson, Is the Arctic surface layer a source and sink of NO_x in winter/spring? J Atmos. Chem. 36 (2000) 1–22.
[5] A.E. Jones, R. Weller, E.W. Wolff, H.-W. Jacobi, Speciation and rate of photochemical NO and NO_2 production in Antarctic snow, Geophys. Res. Lett. 27 (2000) 345–348.
[6] A.E. Jones, R. Weller, P.S. Anderson, H.-W. Jacobi, E.W. Wolff, O. Schrems, H. Miller, Measurements of NO_x emissions from the Antarctic snowpack, Geophys. Res. Lett. 28 (2001) 1499–1502.
[7] D. Davis, J.B. Nowak, G. Chen, M. Buhr, R. Arimoto, A. Hogan, F. Eisele, L. Mauldin, D. Tanner, R. Shetter, B. Lefer, P. McMurry, Unexpected high levels of NO observed at South Pole, Geophys. Res. Lett. 28 (2001) 3625–3628.
[8] X. Zhou, H.J. Beine, R.E. Honrath, J.D. Fuentes, W. Simpson, P.B. Shepson, J.W. Bottenheim, Snowpack photochemical production of HONO: a major source of OH in the arctic boundary layer in springtime, Geophys. Res. Lett. 28 (2001) 4087–4090.
[9] J.E. Dibb, M. Arsenault, M.C. Peterson, R.E. Honrath, Fast nitrogen oxide photochemistry in Summit, Greenland snow, Atmos. Environ. 36 (2002) 2501–2511.
[10] R. Qiu, S.A. Green, R.E. Honrath, M.C. Peterson, Y. Lu, M. Dziobak, Measurements of $J_{NO_3^-}$ in snow by nitrate-based actinometry, Atmos. Environ. 36 (2002) 2563–2571.
[11] R.E. Honrath, Y. Lu, M.C. Peterson, J.E. Dibb, M.A. Arsenault, N.J. Cullen, K. Steffen, Vertical fluxes of NO_x, HONO, and HNO_3 above the snowpack at Summit, Greenland, Atmos. Environ. 36 (2002) 2629–2640.
[12] H.J. Beine, R.E. Honrath, F. Dominé, W.R. Simpson, J.D. Fuentes, NO_x during background and ozone depletion periods at Alert: fluxes above the snow surface, J. Geophys. Res. 107 (D21) (2002) 4584, doi:10.1029/2002JD002082.
[13] H.J. Beine, F. Dominé, A. Ianniello, M. Nardino, I. Allegrini, K. Teinilä, R. Hillamo, Fluxes of nitrate between snow surfaces and the atmosphere in the European high Arctic, Atmos. Chem. Phys. 3 (2003) 335–346.
[14] H.-W. Jacobi, R.C. Bales, R.E. Honrath, M.C. Peterson, J.E. Dibb, A.L. Swanson, M.R. Albert, Reactive trace gases measured in the interstitial air of surface snow at Summit, Greenland, Atmos. Environ. 38 (2004) 1687–1697.
[15] D. Davis, G. Chen, M. Buhr, J. Crawford, D. Lenschow, B. Lefer, R. Shetter, F. Eisele, L. Mauldin, A. Hogan, South Pole NO_x chemistry: an assessment of factors controlling variability and absolute levels, Atmos. Environ. 38 (2004) 5375–5388.
[16] J.E. Dibb, L.G. Huey, D.L. Slusher, D.J. Tanner, Soluble reactive nitrogen oxides at South Pole during ISCAT 2000, Atmos. Environ. 38 (2004) 5399–5409.
[17] A. Amoroso, H.J. Beine, R. Sparapani, M. Nardino, I. Allegrini, Observation of coinciding arctic boundary layer ozone depletion and snow surface emissions of nitrous acid, Atmos. Environ. 40 (2006) 1949–1956.
[18] R.E. Honrath, S. Guo, M.C. Peterson, M.P. Dziobak, J.E. Dibb, M.A. Arsenault, Photochemical production of gas phase NO_x from ice crystal NO_3^-, J. Geophys. Res. 105 (2000) 24183–24190.
[19] Y. Dubowski, A.J. Colussi, M.R. Hoffmann, Nitrogen dioxide release in the 302 nm band photolysis of spray-frozen aqueous nitrate solutions. Atmospheric implications, J. Phys. Chem. A 105 (2001) 4928–4932.
[20] Y. Dubowski, A.J. Colussi, C. Boxe, M.R. Hoffmann, Monotonic increase of nitrite yields in the photolysis of nitrate in ice and water between 238 and 294 K, J. Phys. Chem. A 106 (2002) 6967–6971.
[21] E.S.N. Cotter, A.E. Jones, E.W. Wolff, S.J.-B. Baugitte, What controls photochemical NO and NO_2 production from Antarctic snow? Laboratory investigation assessing the wavelength and temperature dependence, J. Geophys. Res. 108 (D4) (2003) 4147, doi:10.1029/2002JD002602.
[22] L. Chu, C. Anastasio, Quantum yields of hydroxyl radical and nitrogen dioxide from the photolysis of nitrate on ice, J. Phys. Chem. A 107 (2003) 9594–9602.
[23] C.S. Boxe, A.J. Colussi, M.R. Hoffmann, D. Tan, J. Mastromarino, A.T. Case, S.T. Sandholm, D.D. Davis, Multiscale ice fluidity in NO_x photodesorption from frozen nitrate solutions, J. Phys. Chem. A 107 (2003) 11409–11413.
[24] T. Blunier, G.L. Floch, H.-W. Jacobi, E. Quansah, Isotopic view on nitrate loss in Antarctic surface snow, Geophys. Res. Lett. 32 (2005) L13501.
[25] C.S. Boxe, A.J. Colussi, M.R. Hoffmann, J.G. Murphy, P.J. Wooldridge, T.H. Bertram, R.C. Cohen, Photochemical production and release of gaseous NO_2 from nitrate-doped water ice, J. Phys. Chem. A 109 (2005) 8520–8525.
[26] C.S. Boxe, A.J. Colussi, M.R. Hoffmann, I.M. Perez, J.G. Murphy, R.C. Cohen, Kinetics of NO and NO_2 evolution from illuminated frozen nitrate solutions, J. Phys. Chem. A 110 (2006) 3578–3583.
[27] H.-W. Jacobi, T. Annor, E. Quansah, Investigation of the photochemical decomposition of nitrate, hydrogen peroxide, and formaldehyde in artificial snow, J. Photochem. Photobiol. A 179 (2006) 330–338.
[28] G. Chen, D. Davis, J. Crawford, L.M. Hutterli, L.G. Huey, D. Slusher, L. Mauldin, F. Eisele, D. Tanner, J. Dibb, M. Buhr, J. McConnell, B. Lefer, R. Shetter, D. Blake, C.H. Song, K. Lombardi, J. Arnoldy, A reassessment of HO_x South Pole chemistry based on observations recorded during ISCAT 2000, Atmos. Environ. 38 (2004) 5451–5461.
[29] J. Yang, R.E. Honrath, M.C. Peterson, J.E. Dibb, A.L. Sumner, P.B. Shepson, M. Frey, H.-W. Jacobi, A. Swanson, N. Blake, Impacts of snowpack emissions on deduced levels of OH and peroxy radicals at Summit, Greenland, Atmos. Environ. 36 (2002) 2523–2534.
[30] M. Legrand, P. Mayewski, Glaciochemistry of polar ice cores: a review, Rev. Geophys. 35 (1997) 219–243.
[31] R. Röthlisberger, M.A. Hutterli, E.W. Wolff, R. Mulvaney, H. Fischer, M. Bigler, K. Goto-Azuma, M.E. Hansson, U. Ruth, M.-L. Siggaard-Andersen, J.P. Steffensen, Nitrate in Greenland and Antarctic ice cores: a detailed description of post-depositional processes, Ann. Glaciol. 35 (2002) 209–216.
[32] J.R. McCabe, C.S. Boxe, A.J. Colussi, M.R. Hoffmann, M.H. Thiemens, Oxygen isotopic fractionation in the photochemistry of nitrate in water and ice, J. Geophys. Res. 110 (2005) D15310, doi:10.1029/2004JD005484.
[33] J. Mack, J.R. Bolton, Photochemistry of nitrite and nitrate in aqueous solution: a review, J. Photochem. Photobiol. A 128 (1999) 1–13.
[34] A.L. Sumner, P.B. Shepson, Snowpack production of formaldehyde and its effect on the Arctic troposphere, Nature 398 (1999) 230–233.
[35] A.M. Grannas, P.B. Shepson, T.R. Filley, Photochemistry and nature of organic matter in Arctic and Antarctic snow, Global Biogeochem. Cycles 18 (GB1006) (2004), doi:10.1029/2003GB002133.
[36] H.J. Beine, A. Amoroso, G. Esposito, R. Sparapani, A. Ianniello, T. Georgiadis, M. Nardino, P. Bonasoni, P. Cristofanelli, F. Dominé, Deposition of atmospheric nitrous acid on alkaline snow surfaces, Geophys. Res. Lett. 32 (2005) L10808, doi:10.1029/2005GL022589.
[37] K.C. Clemitshaw, Coupling between the tropospheric photochemistry of nitrous acid (HONO) and nitric acid (HNO_3), Environ. Chem. 3 (2006) 31–34.
[38] W. Liao, A.T. Case, J. Mastromarino, D. Tan, J.E. Dibb, Observations of HONO by laser-induced fluorescence at the South Pole during ANTCI 2003, Geophys. Res. Lett. 33 (2006) L09810, doi:10.1029/2005GL025470.
[39] H.-W. Jacobi, B. Kwakye-Awuah, O. Schrems, Photochemical decomposition of hydrogen peroxide (H_2O_2) and formaldehyde (HCHO) in artificial snow, Ann. Glaciol. 39 (2004) 29–33.
[40] D. Zehavi, J. Rabani, Pulse radiolytic investigation of O_{aq}^- radical ions, J. Phys. Chem. 75 (1971) 1738–1744.
[41] G.C. Barker, P. Fowles, B. Stringer, Pulse radiolytic induced transient electrical conductance in liquid solutions. Part 2. Radiolysis of aqueous solutions of NO_3^-, NO_2^- and $Fe(CN)_6^{3-}$, Trans. Faraday Soc. 66 (1970) 1509–1519.
[42] H.H. Awad, D.M. Stanbury, Autoxidation of NO in aqueous solution, Int. J. Chem. Kinet. 25 (1993) 375–381.
[43] J.L. Cheung, Y.Q. Li, J. Boniface, Q. Shi, P. Davidovits, D.R. Worsnop, J.T. Jayne, C.E. Kolb, Heterogeneous interactions of NO_2 with aqueous surfaces, J. Phys. Chem. A 104 (2000) 2655–2662.
[44] T. Løgager, K. Sehested, Formation and decay of peroxynitrous acid: a pulse radiolysis study, J. Phys. Chem. 97 (1993) 6664–6669.
[45] U.K. Kläning, K. Sehested, T. Wolff, Ozone formation in laser flash photolysis of oxoacids and oxoanions of chlorine and bromine, J. Chem. Soc., Faraday Trans. 80 (1984) 2969–2979.

[46] H. Strehlow, I. Wagner, Flash photolysis in aqueous nitrite solutions, Z. Phys. Chem. NF 132 (1982) 151–160.
[47] J.-Y. Park, Y.-N. Lee, Solubility and decomposition kinetics of nitrous acid in aqueous solution, J. Phys. Chem. 92 (1988) 6294–6302.
[48] R. Sander, Compilation of Henry's Law Constants for Inorganic and Organic Species of Potential Importance in Environmental Chemistry, Version 3, 1999. http://dionysos.mpch-mainz.mpg.de/~sander/res/henry.html.
[49] C. Girardet, C. Toubin, Molecular atmospheric pollutant adsorption on ice: a theoretical survey, Surf. Sci. Rep. 44 (2001) 159–238.
[50] H. Bluhm, D.F. Ogletree, C.S. Fadley, Z. Hussain, M. Salmeron, The premelting of ice studied with photoelectron spectroscopy, J. Phys. Condens. Matter 14 (2002) L227–L233.
[51] H. Cho, P.B. Shepson, L.A. Barrie, J.P. Cowin, R. Zaveri, NMR investigation of the quasi-brine layer in ice/brine mixtures, J. Phys. Chem. B 106 (2002) 11226–11232.
[52] A. Döppenschmidt, H.-J. Butt, Measuring the thickness of the liquid-like layer on ice surfaces with atomic force microscopy, Langmuir 16 (2000) 6709–6714.
[53] X. Wei, P.B. Miranda, C. Zhang, Y.R. Shen, Sum-frequency spectroscopic studies of ice interfaces, Phys. Rev. B 66 (2002) 085401.
[54] J.E. Dibb, R.W. Talbot, J.W. Munger, D.J. Jacob, S.-M. Fao, Air-snow exchange of HNO_3 and NO_y at Summit, Greenland, J. Geophys. Res. 103 (1998) 3475–3486.
[55] P. Hoffmann, V.K. Karandashev, T. Sinner, H.M. Ortner, Chemical analysis of rain and snow samples from Chernogolovka/Russia by IC, TXRF and ICP-MS, Fresenius J. Anal. Chem. 357 (1997) 1142–1148.
[56] Y. Miura, H. Hamada, Ion chromatography of nitrite at the ppb level with photometric measurement of iodine formed by post-column reaction of nitrite with iodide, J. Chromatogr. A 850 (1999) 153–160.
[57] A. Fernandez-Gutierrez, C. Cruces-Blanco, S. Cortacero-Ramirez, A. Segura-Carretero, Sensitive determination of inorganic anions at trace levels in samples of snow water from Sierra Nevada (Granada, Spain) by capillary ion electrophoresis using Calix[4]arene as selective modifier, Chromatographia 52 (2000) 413–417.
[58] S.-M. Li, Particulate and snow nitrite in the spring arctic troposphere, Atmos. Environ. 27 (1993) 2959–2967.
[59] M. Peterson, D. Barber, S. Green, Monte Carlo modeling and measurements of actinic flux levels in Summit, Greenland snowpack, Atmos. Environ. 36 (2002) 2545–2551.
[60] E. Riordan, N. Minogue, D. Healy, P. O'Driscoll, J.R. Sodeau, Spectroscopic and optimization modling study of nitrous acid in aqueous solution, J. Phys. Chem. A 109 (2005) 779–786.
[61] B.J. Finlayson-Pitts, L.M. Wingen, A.L. Sumner, D. Syomin, K.A. Ramazan, The heterogeneous hydrolysis of NO_2 in laboratory systems and in outdoor and indoor atmospheres: an integrated mechanism, Phys. Chem. Chem. Phys. 5 (2003) 223–242.
[62] C. George, R.S. Strekowski, J. Kleffmann, K. Stemmler, M. Ammann, Photoenhanced uptake of gaseous NO_2 on solid organic compounds: a photochemical source of HONO? Faraday Disc. 130 (2005) 195–210.
[63] C. Robinson, C.S. Boxe, M.I. Guzmán, A.J. Colussi, M.R. Hoffmann, Acidity of frozen electrolyte solutions, J. Phys. Chem. B 110 (2006) 7613–7616.
[64] L. Chu, C. Anastasio, Formation of hydroxyl radical from the photolysis of frozen hydrogen peroxide, J. Phys. Chem. A 109 (2005) 6264–6271.

3.4 Role of sea ice formation in ozone depletion events

Publication 3.4.1

Jacobi, H.-W., M. Wolff, and O. Schrems,

Tropospheric ozone depletion events observed over the frozen Arctic Ocean,

in: C.S. Zerefos (ed.), Ozone, p. 358-359, Proceedings of the XX. Quadrennial Ozone Symposium, Vol. 1, Athens, Greece, 2004.

Tropospheric ozone depletion events observed over the frozen Arctic Ocean

H.-W. Jacobi, M. Wolff, and O. Schrems

Alfred Wegener Institute for Polar and Marine Research, Bremerhaven, Germany

Abstract. Surface ozone (O_3) measurements indicate that extended periods with depleted O_3 concentrations can exist during springtime in the boundary layer over the frozen Arctic Ocean. The longest observed ODE lasted for 11 days. 24-hr backward trajectories for this period cover roughly a triangle between the northern coasts of Greenland and Svalbard and the North Pole. The time series of O_3 and air temperature exhibited similar features. However, the air temperature remained above –20 °C during one third of the periods with depleted O_3 concentrations.

Introduction

Ozone depletion events (ODE) with concentrations below 10 ppb in the atmospheric boundary layer are regularly observed in springtime at stations in both polar regions [e.g. *Tarasick and Bottenheim*, 2002; *Wessel et al.*, 1998]. At arctic stations, ODEs are commonly encountered in air masses that were previously transported across the Arctic Ocean [*Wessel et al.*, 1998; *Bottenheim et al.*, 2002]. Moreover, recent model calculations demonstrated that ODEs are widespread phenomena in the Arctic and can cover up to 20 % of the northern high latitudes [*Zeng et al.*, 2003]. Nevertheless, the spatial and temporal extent of arctic ODEs is not well characterized. Therefore, we performed O_3 measurements aboard an icebreaker that operated in the ice-covered Arctic Ocean in spring 2003.

Methods and Instrumentation

O_3 measurements were performed aboard the RV *Polarstern* (ARK XIX/1). The cruise track started at Bremerhaven, Germany (54 °N) on 28 February 2003 and ended in Longyearbyen, Svalbard (79 °N) on 24 April 2003. The ship spent extended periods in two distinguished areas: in March in the Storfjord, the largest fjord in the Southeast of Svalbard, and in April in an area northwest of Svalbard. Except for the transit from Bremerhaven to the Storfjord and between the two working areas, the ship operated in ice-covered areas.

O_3 was measured continuously between 16 March and 23 April using an Ansyco GmbH model $O_3$41M, which is based on UV photometric detection at 254 nm with a limit of detection (LOD) of ~1.0 ppb. The inlet line consisted of approximately 5 m of 0.8 cm ID perfluoroalkoxy tubing The inlet line was mounted on the compass deck rail approximately 22 m above sea level.

Backward air parcel trajectories were simulated using the NOAA Hybrid Single-Particle Lagrangian Integrated Trajectory (HYSPLIT) model [*Draxler and Rolph*, 2003] driven by Final Run (FNL) reanalysis wind fields. The trajectories were initiated at the actual ship's positions with the starting height at ground level.

Results and discussion

The measured time series of surface O_3 concentrations is shown in Figure 1b. On several occasions the O_3 concentrations were depleted. The most pronounced ODE was encountered between 31 March and 11 April when O_3 concentrations were below the LOD for a period of 11 days only interrupted by three periods with detectable O_3 concentrations lasting between 11 and 34 hrs.

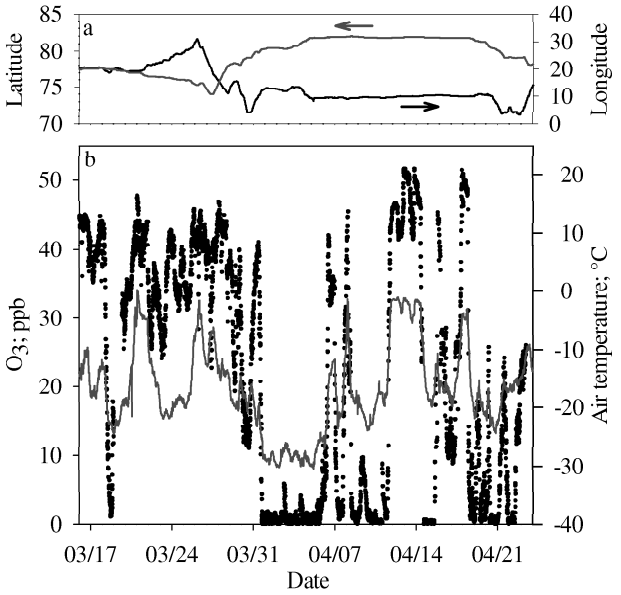

Figure 1. Time series of (a) the latitude (red line) and longitude (black line) of the ship's position and (b) 10-min averages of the O_3 concentrations (black dots) and air temperature (red line) measured aboard RV *Polarstern*.

This pronounced ODE was further analyzed using 24-hr backward trajectories since we assumed that the O_3 concentration remains relatively constant within this period. Therefore, the measured O_3 concentrations are regarded as representative for the entire area covered by the 24-hr trajectory.

The cruise track for the period 30 March until 12 April is shown in Figure 2 in different colors indicating measured surface O_3 concentrations. 24-hr backward trajectories every 12 hrs were calculated along the cruise track. The trajectories are shown in two different panels divided into high and low O_3 concentrations at the initial point. Trajectories corresponding to low O_3 concentrations covered a large area mainly between the northern coasts of either Greenland or Svalbard and the North Pole. On one occasion the trajectory originated from the Greenland Sea as far south as 78.2 °S. The covered area extended between 1100 km in north-south and 1800 km in west-east direction. None of the air masses with depleted O_3 concentrations were in contact with Greenland or Svalbard in the 24 hrs before they reached the ship's position. Moreover, charts of the sea ice extent for March / April 2003 (e.g. http://nsidc.org/data/seaice_index/ archives/) indicate that the air masses with depleted O_3 concentrations spent at least 24 hrs over the frozen Arctic Ocean with sea ice concentrations between 75 and 100 %.

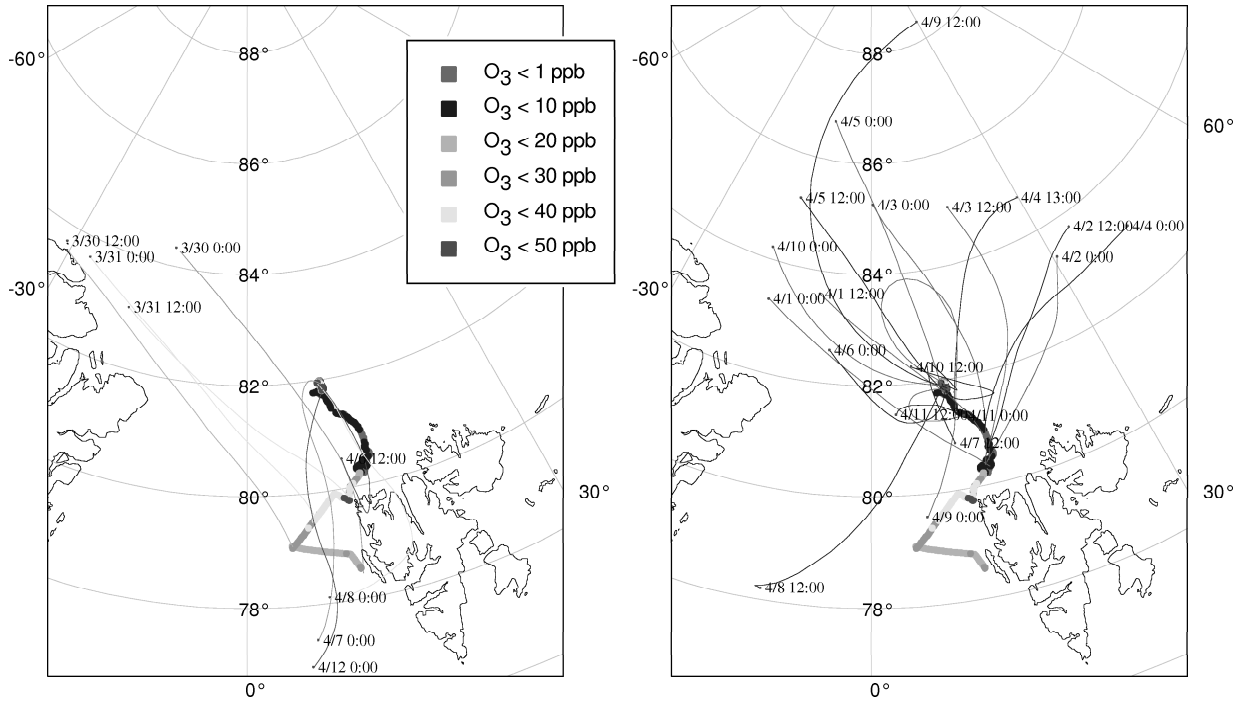

Figure 2. Cruise track (thick line) and 24-hr backward trajectories (thin lines) for the period between 30 March and 12 April. Surface O_3 concentrations measured along the cruise track are indicated by different colors. The same color code is used for the trajectories using the O_3 concentration measured at the initial point of each trajectory. Trajectories are calculated every 12 hrs. Dates and times of the initial time of the trajectories are plotted. The left panel shows all trajectories with high (>10 ppb), the right panel with depleted O_3 concentrations (<10 ppb).

The trajectories corresponding to higher O_3 concentrations can be divided into two different categories (Fig. 2). First, the O_3 peaks on 6, 7, and 8 April were observed in air masses, which reached the ship from southerly directions. The air masses had either contact with the landmass of Svalbard or with the open water along the west coast of Svalbard. The air mass finishing the ODE on 12 April also originated from the open water area west of Svalbard. The other category consists of trajectories covering the same area where later also the air masses with depleted O_3 originated. For example, the air masses encountered on 31 March, 12:00, and 1 April, 0:00, were 24 hrs earlier located at 83 °N, 18 °W and 83 °N, 16 °W, respectively. However, within these 12 hrs the measured O_3 concentration decreased from around 40 ppb to below the LOD (Fig. 1b).

A comparison of the air temperature and O_3 time series shows that ODEs are accompanied by low temperatures (Fig. 1b). Same patterns with simultaneous minima and maxima are observed. *Tarasick and Bottenheim* [2002] obtained a similar result. They concluded that a temperature of less than –20 °C is a prerequisite for an ODE. However, our results demonstrate that depleted O_3 concentrations (<10 ppb) were also observed at air temperatures up to –9.8 °C. In addition, almost one third of all depleted O_3 concentrations were observed at air temperatures above –20 °C.

Conclusions

Our measurements above the frozen Arctic Ocean indicate that ODEs are possibly more persistent and widespread than commonly observed at arctic stations. This is possibly due to the fact that ODEs are only registered if the air masses depleted in O_3 are transported to the stations from the Arctic Ocean, where the ODEs develop. Therefore, a better understanding of the temporal and spatial extent of ODEs can probably only be obtained by local measurements over the Arctic Ocean or remote sensing techniques.

Acknowledgments We thank S. Debatin, K. Buldt, and the crew of the RV *Polarstern* for their co-operation and technical assistance. The authors gratefully acknowledge the NOAA Air Resources Laboratory (ARL) for the provision of the HYSPLIT transport and dispersion model used in this publication.

References

Bottenheim, J.W., et al., Ozone in the Arctic lower troposphere during winter and spring 2000 (ALERT2000), *Atmos. Environ., 36*, 2535-2544, 2002.

Draxler, R.R., and G.D. Rolph, HYSPLIT (HYbrid Single-Particle Lagrangian Integrated Trajectory) Model access via NOAA ARL READY Website (http://www.arl.noaa.gov/ready/hysplit4.html), NOAA Air Resources Lab., Silver Spring, MD, 2003.

Tarasick, D.W., and J.W. Bottenheim, Surface ozone depletion episodes in the Arctic and Antarctic from historical ozonesonde records, *Atmos. Chem. Phys., 2*, 197-205, 2002.

Wessel, S., et al., Tropospheric ozone depletion in polar regions - A comparison of observations in the Arctic and Antarctic, *Tellus, 50B*, 34-50, 1998.

Zeng, T., et al., Widespread persistent near-surface ozone depletion at northern high latitudes in spring, *Geophys. Res. Lett., 30*, 2298, doi:10.1029/2003GL018587, 2003.

Publication 3.4.2

Kaleschke, L., A. Richter, J. Burrows, O. Afe, G. Heygster, J. Notholt, A.M. Rankin, H.K. Roscoe, J. Hollwedel, T. Wagner, and H.-W. Jacobi,

Frost flowers on sea ice as a source of sea salt and their influence on tropospheric halogen chemistry,

Geophys.Res.Lett. **31**, L16114, doi: 10.1029/2004GL020655, 2004.

Frost flowers on sea ice as a source of sea salt and their influence on tropospheric halogen chemistry

L. Kaleschke, A. Richter, J. Burrows, O. Afe, G. Heygster, and J. Notholt
Institute of Environmental Physics, University of Bremen, Germany

A. M. Rankin and H. K. Roscoe
British Antarctic Survey, Natural Environment Research Council, Cambridge, UK

J. Hollwedel and T. Wagner
Institute of Environmental Physics, University of Heidelberg, Germany

H.-W. Jacobi
Alfred Wegener Institute for Polar and Marine Research, Bremerhaven, Germany

Received 2 June 2004; revised 21 July 2004; accepted 2 August 2004; published 25 August 2004.

[1] Frost flowers grow on newly-formed sea ice from a saturated water vapour layer. They provide a large effective surface area and a reservoir of sea salt ions in the liquid phase with triple the ion concentration of sea water. Recently, frost flowers have been recognised as the dominant source of sea salt aerosol in the Antarctic, and it has been speculated that they could be involved in processes causing severe tropospheric ozone depletion events during the polar sunrise. These events can be explained by heterogeneous autocatalytic reactions taking place on salt-laden ice surfaces which exponentially increase the reactive gas phase bromine ("bromine explosion"). We analyzed tropospheric bromine monoxide (BrO) and the sea ice coverage both measured from satellite sensors. Our model based interpretation shows that young ice regions potentially covered with frost flowers seem to be the source of bromine found in bromine explosion events. *INDEX TERMS:* 0322 Atmospheric Composition and Structure: Constituent sources and sinks; 1640 Global Change: Remote sensing; 3309 Meteorology and Atmospheric Dynamics: Climatology (1620); 3339 Meteorology and Atmospheric Dynamics: Ocean/atmosphere interactions (0312, 4504); 3360 Meteorology and Atmospheric Dynamics: Remote sensing. **Citation:** Kaleschke, L., et al. (2004), Frost flowers on sea ice as a source of sea salt and their influence on tropospheric halogen chemistry, *Geophys. Res. Lett.*, *31*, L16114, doi:10.1029/2004GL020655.

1. Introduction

[2] The discovery of events of low ozone concentration in the atmospheric boundary layer at measurement stations located at high latitudes in the Northern Hemisphere has prompted much research into their origin. These events were found to be associated with enhanced amounts of inorganic bromine compounds [*Barrie et al.*, 1988; *McConnell et al.*, 1992; *Fan and Jacob*, 1992; *Foster et al.*, 2001]. Similar episodes have been observed in the Southern Hemisphere at high latitudes [*Wessel et al.*, 1998; *Frieß et al.*, 2004]. The advent of the measurement of tropospheric trace gases from space by the Global Ozone Monitoring Experiment, GOME, led to the discovery of enhanced amounts of BrO close to regions of sea ice in the Northern and the Southern Hemisphere [*Richter et al.*, 1998; *Wagner and Platt*, 1998]. GOME measures the light scattered from the atmosphere and reflected by the ground between 240 and 790 nm wavelength with a horizontal ground resolution of about 320 × 40 km^2 [*Burrows et al.*, 1999]. A retrieval algorithm, based on differential optical absorption spectroscopy (DOAS) and stratospheric BrO modeled by a three-dimensional radiative- dynamical-chemical model, yields the tropospheric fraction of the column density of BrO [*Richter et al.*, 1998; *Wagner and Platt*, 1998; *Chipperfield*, 1999]. Bromine destroys ozone very efficiently in two interlinked catalytic cycles which produce BrO and HOBr in the gas-phase [*Foster et al.*, 2001]. Gaseous HOBr reacts with Br ions in a slightly acidic sea salt solution and releases Br_2 and BrCl into the gas phase [*Fickert et al.*, 1999; *Adams et al.*, 2002]. The photolabile Br_2 molecule is subsequently photo-dissociated into atomic Br [*Foster et al.*, 2001]. Therefore, every Br atom of the HOBr molecule entering the liquid phase has the potential to release two Br atoms to the gas phase. The above gives a simplified description of the heterogeneous autocatalytic reaction that causes an exponential increase of gaseous Br radicals, the so-called bromine explosion. The main source of bromine over the open oceans in the marine boundary layer outside the polar regions was identified to be sea salt aerosol generated by breaking waves on the ocean surface [*Tang and McConnell*, 1996; *Vogt et al.*, 1996; *Sander et al.*, 2003]. The processes and sources unique to the polar ocean surfaces still remained unidentified, though the highest BrO amounts have been observed over the sea ice during the polar sunrise [*Ridley et al.*, 2003; *Zeng et al.*, 2003; *Frieß et al.*, 2004]. Recently, the potential role of frost flowers (Figure 1) in this processes has been raised [*Rankin et al.*, 2002]. Frost flowers are ice crystals which grow on frozen leads (linear breaks in the sea ice cover) and polynyas (openings between drift ice and fast ice or the coast). Frost flowers exhibit enhanced salinities and bromide ion concentrations of about three times of that of bulk seawater [*Perovich and Richter-Menge*, 1994; *Rankin et al.*, 2002].

0094-8276/04/2004GL020655$05.00

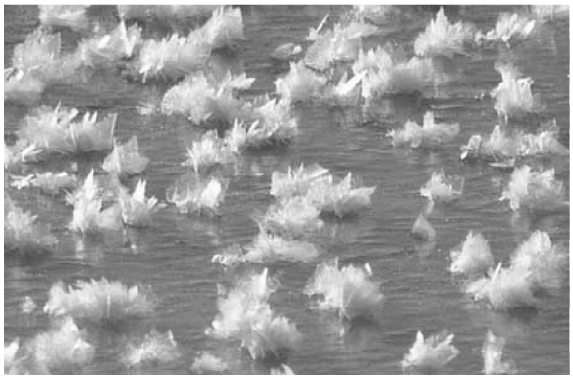

Figure 1. Frost flowers on sea ice covering a lead: Stellar dendrites of about 1 to 2 cm height on young sea ice (Courtesy of Stefan Kern, University of Hamburg). The photograph was taken at 75°58′N 25°34′E, 24 March 2003. The air temperature was about −18°C.

Frost flowers only last for a few days until they are blown away by strong winds or covered by drifting snow [*Perovich and Richter-Menge*, 1994]. The aerosol produced by frost flowers was identified in Antarctic ice cores and at coastal stations due to its depleted sulfate to sodium ratio compared to the aerosol originating from the open ocean [*Wagenbach et al.*, 1998; *Rankin et al.*, 2002; *Rankin and Wolff*, 2003].

2. Methods and Data Sets

[3] It is assumed, that the open water area (which is given by one minus the sea ice concentration) will be covered soon with thin new ice on which frost flowers can grow. The sea ice concentration is determined from analyses of the thermal microwave emission measured by the Special Sensor Microwave Imager (SSM/I) aboard the Defense Meteorological Satellite Program (DMSP) platform using the ASI algorithm [*Kaleschke et al.*, 2001; *Maslanik and Stroeve*, 2003]. Briefly this algorithm takes advantage of the higher polarisability of a specularly reflecting water surface compared to the more diffusely reflecting sea ice surface [*Kaleschke et al.*, 2001; *Kern et al.*, 2003].

[4] A one dimensional thermodynamic model has been developed to calculate the frost flower coverage (Figure 2). The model combines a frost flower growth parameterization obtained from laboratory experiments with the equations of sea ice heat balance which are described in more detail by *Martin et al.* [1996] and *Maykut* [1986]. We assume that the growth of frost flowers depends only on two basic prerequisites, the existence of new ice which is formed in leads or polynyas and of a strong negative temperature gradient above the ice surface. The two model input parameters, the surface air temperature T_a and the open water (OW) fraction, are taken from numerical weather prediction reanalysis data (NCEP/NCAR) and from satellite passive microwave measurements, respectively. The ice thickness $H = 1.33\Theta^{0.53}$ [cm] is calculated from the cumulative freezing days $\Theta = \int(T_f - T_a)dt$ with air temperature T_a and the freezing point of sea water $T_f = -1.9$°C. The sea ice surface temperature $T_0 = \frac{-15.96 + HT_a}{8.4 + H}$ is approximated for thin ice using an averaged heat transfer coefficient which describes both sensible and latent heat exchange [*Maykut*, 1986]. Assuming that the influence of a varying wind field and the insulating effect of frost flowers on the heat flux are negligible, then the frost flower growth rate $g = 0.000785e^{0.478(T_0 - T_a)}$ is readily calculated using coefficients from laboratory experiments [*Martin et al.*, 1996; *Maykut*, 1986]. The area coverage F_t is calculated using the recursive expression $F_t = F_{t\ \delta t} + g(1 - F_{t\ \delta t})\delta t$ for a time step δt. Because the growth rate decreases rapidly as the ice thickness increases, the model yields a maximum percentage area $F_{\max}(T_a)$ covered by frost flowers for a given surface air temperature. This is defined as the relative potential frost flower (PFF) area. The total PFF area is obtained by weighting the total area with the new ice fraction. The predicted relative PFF areas for different integration times and air temperatures are presented in Figure 2. The height and hence the volume of the frost flowers cannot be calculated as the parameterization of the growth rate was derived from video images which measured the area coverage. As there is currently insufficient microphysical understanding about the initial nucleation and growth of frost flowers as well as about the decay processes, a minimum frost flower area for a given set of conditions cannot be estimated [*Perovich and Richter-Menge*, 1994; *Martin et al.*, 1995, 1996]. The original aim of the above described method was to identify dates and regions worth to be analysed using costly very high resolution satellite images for the future development of a more direct frost flower retrieval algorithm [*Kaleschke and Heygster*, 2004].

3. Comparison of Model Results and BrO Data

[5] One typical example of the resulting PFF and the BrO data for the Antarctic is shown in Figure 3. The overall mechanism requires the release of bromine atom precursors, either directly on the frost flower surface or within its aerosol. We calculated forward air trajectories starting at regions with a high probability of frost flowers from the NCEP/NCAR Reanalysis surface wind field in order to account for the atmospheric transport of the aerosol or BrO. Some regions with a high probability of frost flower occurrence for example at the Ronne-Filchner Ice Shelf in the Weddell Sea show no corresponding BrO plumes

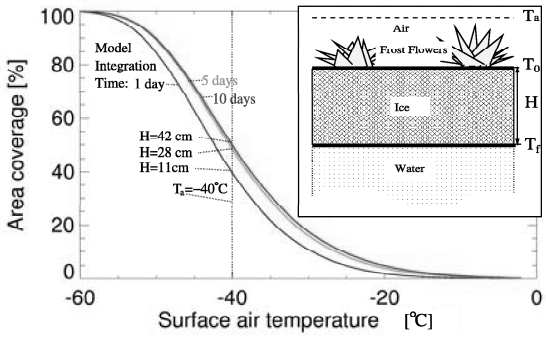

Figure 2. Frost flower model and frost flower coverage as a function of air temperature for different integration times. The three curves represent the integration times of one, five and ten days, respectively. The theoretical upper limit of frost flower coverage $F_{\max}(T_a)$ is approximately given by the upper curve.

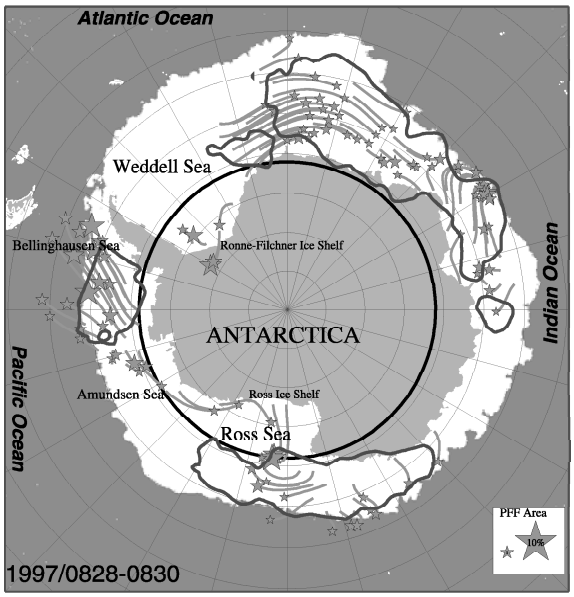

Figure 3. Comparison: Example total PFF coverage (green stars) and enhanced BrO amounts (red isolines) over the Antarctic ocean. The maximum values of two consecutive days are shown: from 28 to 29 and 29 to 30 August 1997 for PFF and BrO, respectively. The green stars mark the endpoints of 24h air trajectories starting at a frost flower area coverage of greater than 0.4%, sampled every 187 km. The PFF field was smoothed to 300 km spatial resolution to approximately match the GOME resolution. The total PFF coverage is proportional to the size of the stars. Two stars of 1% and 10% area coverage are shown in the lower right corner for comparison. The red isoline corresponds to enhanced BrO amounts of 3.6×10^{13} molec/cm^2 which is the mean (1.4) plus one standard deviation (2.2). The black circle indicates the almost dark latitudes (solar zenith angle > 80°). Sea ice covered regions are presented in white and the open ocean is coloured in blue.

because sunlight is needed for the photochemical reactions. The polynya at the Ross Ice Shelf that occurs frequently due to strong katabatic winds is shown to be a strong source of frost flower aerosol responsible for the enhanced BrO concentration farther north in the illuminated area. The trajectories are only a rough approximation as errors could occur in convective regions which are not well represented in the atmospheric boundary layer of the NCEP/NCAR model over sea ice [*Kaleschke et al.*, 2001]. Nevertheless, more than ninety percent of the trajectories hit the enhanced BrO areas in Figure 3. One key area of frequently occurring ozone depletion events in the Arctic is shown in Figure 4. This typical example shows the huge (almost 500×50 km^2) recurring shore polynya in the northwest of the Hudson Bay which is potentially covered with frost flowers. This polynya frequently appears under offshore wind conditions.

[6] We investigated the entire 1996 to 2002 dataset and found commonly more than two third of the PFF trajectories hitting the enhanced BrO areas for the Arctic and Antarctic during polar sunrise. Almost all cases of enhanced BrO amounts were associated with a high probability of frost flowers on the previous days. Occasionally enhanced PFF values appear without enhanced BrO amounts. However, this does not reject the hypothesis of frost flowers causing BrO production as the BrO retrieval could be hampered by clouds [*Richter et al.*, 1998; *Wagner and Platt*, 1998; *Frieß et al.*, 2004]. Furthermore, the PFF is a potential theoretical upper limit. Specific meteorological conditions could have prevented the actual growth of frost flowers. The influence of the wind is ambiguous: the dynamical opening of leads and polynyas is a wind driven effect and a prerequisite for thin ice production, but persisting strong winds could prevent the growth of frost flowers [*Perovich and Richter-Menge*, 1994]. Changing wind fields such as passing cyclones probably support the growth of frost flowers.

4. Conclusion

[7] It can be summarized that the sea salt and associated halogen flux from the ocean to the atmosphere is governed by different processes inside and outside the polar regions: Outside the polar regions, the sea salt is injected into the atmosphere by breaking waves on the ocean surface dominated by the wind [*Sander et al.*, 2003]. Whereas the process inside the sea ice covered regions is mainly modulated by the air temperature [*Zeng et al.*, 2003; *Frieß et al.*, 2004]. Previous work has been insufficient to localize the potential bromine sources [*Richter et al.*, 1998; *Wagner*

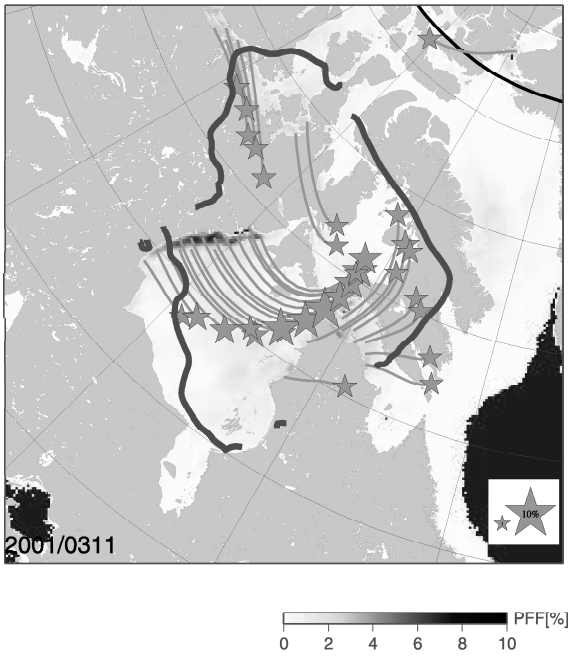

Figure 4. Example total PFF coverage (green stars) and enhanced BrO amounts (red isolines) over the Hudson Bay for 11 March 2001. Symbols and lines are similar to Figure 3, but the PFF coverage is displayed color coded. The 24h air trajectories start at PFF greater than 1% sampled every 62.5 km. The red isoline corresponds to enhanced BrO amounts of 8.8×10^{13} molec/cm^2 which is the mean (6.2) plus two standard deviations (1.3). The isoline is broken due to the data gaps of the GOME coverage.

and Platt, 1998; *Zeng et al.*, 2003; *Ridley et al.*, 2003; *Frieß et al.*, 2004]. We provided a method to localize the young ice regions potentially covered with frost flowers that seem to be a prerequisite for the bromine explosion. This provides a crucial step for a better understanding of the exchange processes between ocean, sea ice and atmosphere that are of great importance for the Earth's climate system [*Shepson et al.*, 2003].

[8] **Acknowledgments.** L. K. and HW. J. gratefully acknowledge the German Research Foundation (DFG) for funding. L. K. thanks Gunnar Spreen, Stefan Kern, Roland von Glasow, Eric W. Wolff, Mark Drinkwater, Robert Ezraty, Wolfgang Dierking, Christof Lüpkes, Thomas Busche and Christian Haas for discussions.

References

Adams, J. W., N. S. Holmes, and J. N. Crowley (2002), Uptake and reaction of HOBr on frozen and dry NaCl/NaBr surfaces between 253 and 233 K, *Atmos. Chem. Phys.*, *2*, 79–91.

Barrie, L. A., J. W. Bottenheim, R. C. Schnell, P. J. Crutzen, and R. A. Rasmussen (1988), Ozone destruction and photochemical reactions at polar sunrise in the lower Arctic atmosphere, *Nature*, *334*, 138–141.

Burrows, J. P., et al. (1999), The global ozone monitoring experiment (GOME): Mission concept and first scientific results, *J. Atmos. Sci.*, *56*(2), 151–175.

Chipperfield, M. P. (1999), Multiannual simulations with a three-dimensional chemical transport model, *J. Geophys. Res.*, *104*(D1), 1781–1805.

Fan, S. M., and D. J. Jacob (1992), Surface ozone depletion in Arctic spring sustained by bromine reactions on aerosols, *Nature*, *359*, 524–552.

Fickert, S., J. W. Adams, and J. N. Crowley (1999), Activation of Br-2 and BrCl via uptake of HOBr onto aqueous salt solutions, *J. Geophys. Res.*, *104*(D19), 23,719–23,727.

Foster, K. L., R. A. Plastridge, J. W. Bottenheim, P. B. Shepson, B. J. Finlayson-Pitts, and C. W. Spicer (2001), The role of Br-2 and BrCl in surface ozone destruction at polar sunrise, *Science*, *291*(5503), 471–474.

Frieß, U., J. Hollwedel, G. Konig-Langlo, T. Wagner, and U. Platt (2004), Dynamics and chemistry of tropospheric bromine explosion events in the Antarctic coastal region, *J. Geophys. Res.*, *109*(D6), D06305, doi:10.1029/2003JD004133.

Kaleschke, L., and G. Heygster (2004), Towards multisensor microwave remote sensing of frost flowers on sea ice, *Ann. Glaciol.*, in press.

Kaleschke, L., C. Lüpkes, T. Vihma, J. Haarpaintner, A. Bochert, J. Hartmann, and G. Heygster (2001), SSM/I sea ice remote sensing for mesoscale ocean-atmosphere interaction analysis, *Can. J. Remote Sens.*, *27*(5), 526–537.

Kern, S., L. Kaleschke, and D. A. Clausi (2003), A comparison of two 85 GHz SSM/I ice concentration algorithms with AVHRR and ERS-SAR, *IEEE Trans. Geosci. Remote Sens.*, *41*(10), 2294–2306.

Martin, S., R. Drucker, and M. Fort (1995), A laboratory study of frost flower growth on the surface of young sea ice, *J. Geophys. Res.*, *100*(C4), 7027–7036.

Martin, S., Y. Yu, and R. Drucker (1996), The temperature dependence of frost flower growth on laboratory sea ice and the effect of the flowers on infrared observations of the surface, *J. Geophys. Res.*, *101*(C5), 12,111–12,125.

Maslanik, J., and J. Stroeve (2003), DMSP SSM/I daily polar gridded brightness temperatures [CD-ROM], Natl. Snow and Ice Data Cent., Boulder, Colo.

Maykut, G. A. (1986), The surface heat and mass balance, in *The Geophysics of Sea Ice*, *NATO ASI B146*, edited by N. Untersteiner, pp. 395–463, Martinus Nijhoff, Zoetermeer, Netherlands.

McConnell, J. C., G. S. Henderson, L. A. Barrie, J. Bottenheim, H. Niki, C. H. Langford, and E. M. J. Templeton (1992), Photochemical bromine production implicated in Arctic boundary-layer ozone depletion, *Nature*, *355*, 150–152.

Perovich, D., and J. A. Richter-Menge (1994), Surface characteristics of lead ice, *J. Geophys. Res.*, *99*(C8), 16,341–16,350.

Rankin, A., and E. W. Wolff (2003), A year-long record of size segregated aerosol composition at Halley, Antarctica, *J. Geophys. Res.*, *108*(D24), 4775, doi:10.1029/2003JD003993.

Rankin, A. M., E. W. Wolff, and S. Martin (2002), Frost flowers: Implications for tropospheric chemistry and ice core interpretation, *J. Geophys. Res.*, *107*(D23), 4683, doi:10.1029/2002JD002492.

Richter, A., F. Wittrock, M. Eisinger, and J. P. Burrows (1998), GOME observations of tropospheric BrO in Northern Hemispheric spring and summer 1997, *Geophys. Res. Lett.*, *25*(4), 2683–2686.

Ridley, B. A., et al. (2003), Ozone depletion events observed in the high latitude surface layer during the TOPSE aircraft program, *J. Geophys. Res.*, *108*(D4), 8356, doi:10.1029/2001JD001507.

Sander, R., et al. (2003), Inorganic bromine in the marine boundary layer: A critical review, *Atmos. Chem. Phys.*, *3*, 1301–1336.

Shepson, P., P. Matrai, L. Barrie, and J. Bottenheim (2003), Ocean-atmosphere-sea ice snowpack interactions in the Arctic and global change, *Eos Trans. AGU*, *84*(36), 349–355.

Tang, T., and J. C. McConnell (1996), Autocatalytic release of bromine from Arctic snow pack during polar sunrise, *Geophys. Res. Lett.*, *23*(18), 2633–2636.

Vogt, R., P. J. Crutzen, and R. Sander (1996), A mechanism for halogen release from sea-salt aerosol in the remote marine boundary layer, *Nature*, *383*, 327–330.

Wagenbach, D., F. Ducroz, R. Mulvaney, L. Keck, A. Minikin, M. Legrand, J. S. Hall, and E. W. Wolff (1998), Sea-salt aerosol in coastal Antarctic regions, *J. Geophys. Res.*, *103*(D9), 10,961–10,974.

Wagner, T., and U. Platt (1998), Satellite mapping of enhanced BrO concentrations in the troposphere, *Nature*, *395*, 486–490.

Wessel, S., S. Aoki, P. Winkler, R. Weller, A. Herber, H. Gernandt, and O. Schrems (1998), Tropospheric ozone depletion in polar regions: A comparison of observations in the Arctic and Antarctic, *Tellus, Ser. B*, *50*(1), 34–50.

Zeng, T., Y. H. Wang, K. Chance, E. V. Browell, B. A. Ridley, and E. L. Atlas (2003), Widespread persistent near-surface ozone depletion at northern high latitudes in spring, *Geophys. Res. Lett.*, *30*(24), 2298, doi:10.1029/2003GL018587.

O. Afe, J. Burrows, G. Heygster, L. Kaleschke, J. Notholt, and A. Richter, Institute of Environmental Physics, P.O. Box 330440, D-28334 Bremen, Germany. (lkalesch@iup.physik.uni-bremen.de)

J. Hollwedel and T. Wagner, Institute of Environmental Physics, University of Heidelberg, Germany.

H.-W. Jacobi, Alfred Wegener Institute for Polar and Marine Research, Bremerhaven, Germany.

A. M. Rankin and H. K. Roscoe, British Antarctic Survey, Natural Environment Research Council, Cambridge, UK.

Publication 3.4.3

Jacobi, H.-W., L. Kaleschke, A. Richter, A. Rozanov, and J.P. Burrows,

Observation of a fast ozone loss in the marginal ice zone of the Arctic Ocean,

J.Geophys.Res. **111**, D15309, doi: 10.1029/2005JD006715, 2006.

JOURNAL OF GEOPHYSICAL RESEARCH, VOL. 111, D15309, doi:10.1029/2005JD006715, 2006

Observation of a fast ozone loss in the marginal ice zone of the Arctic Ocean

Hans-Werner Jacobi,[1] Lars Kaleschke,[2,3] Andreas Richter,[2] Alexei Rozanov,[2] and John P. Burrows[2]

Received 27 September 2005; revised 9 February 2006; accepted 24 April 2006; published 12 August 2006.

[1] In both polar regions tropospheric ozone regularly decreases during springtime to negligible concentrations in the atmospheric boundary layer. Here we report the observation of a dramatic ozone depletion event in the atmospheric boundary layer in the vicinity of new ice fields in the marginal ice zone (MIZ) of the Arctic Ocean monitored by instrumentation on board the icebreaker RV *Polarstern*. The ozone mixing ratio decreased from approximately 40 to below 1 ppbV in less than 7 hours. The analyses of backward trajectories and the synoptic conditions indicate that the observed decrease was not caused by the transport of ozone-free air, but that the ozone depletion occurred locally. Accordingly, bromine oxide, which is formed during the photochemical destruction of ozone in the presence of reactive bromine compounds, was significantly enhanced: Bromine oxide concentrations of approximately $1.8 \cdot 10^9$ molecules cm^{-3} are retrieved around the same location from SCIAMACHY satellite observations assuming a uniform vertical distribution within the boundary layer. The release of bromine in the MIZ where the new ice formation took place appears to be the most likely explanation for the activation of reactive bromine compounds and subsequent depletion of ozone. Since the conditions were favorable for the formation of frost flowers, we suggest that these are the most likely sources of the reactive bromine. However, contributions of heterogeneous reactions on other surfaces like the highly saline brine on the new ice, aerosols generated from frost flowers, and sea salt aerosols deposited on the snowpack on top of the sea ice cannot be ruled out.

Citation: Jacobi, H.-W., L. Kaleschke, A. Richter, A. Rozanov, and J. P. Burrows (2006), Observation of a fast ozone loss in the marginal ice zone of the Arctic Ocean, *J. Geophys. Res.*, *111*, D15309, doi:10.1029/2005JD006715.

1. Introduction

[2] The depletion of ozone (O_3) in the atmospheric boundary layer at high latitudes is a remarkable phenomenon, which was first reported almost 20 years ago [*Bottenheim et al.*, 1986; *Oltmans and Komhyr*, 1986; *Barrie et al.*, 1988]. Such O_3 depletion events (ODEs) having mixing ratios below 10 ppbV (parts per billion by volume) occur regularly in the atmospheric boundary layer at high latitude during springtime in the Arctic [e.g., *Tarasick and Bottenheim*, 2002] and the Antarctic [e.g., *Wessel et al.*, 1998]. Over the Arctic Ocean ODEs are widespread phenomena [*Ridley et al.*, 2003] covering up to 20% of the area of the northern high latitudes [*Zeng et al.*, 2003]. ODEs have been linked with high levels of filterable bromine [*Barrie et al.*, 1988], the presence of BrO clouds [*Wagner and Platt*, 1998], and the loss of gaseous elemental mercury from the atmosphere [*Schroeder et al.*, 1998].

[3] The O_3 destruction is driven and accompanied by high levels of halogen oxides. It proceeds via several catalytic reaction cycles. *Platt and Hönninger* [2003] described different catalytic reaction cycles involving halogen oxides, which can cause an efficient destruction of tropospheric O_3.

Catalytic cycle 1:

(R1) $2(X + O_3 \rightarrow XO + O_2)$

(R2) $XO + XO \rightarrow 2\,X + O_2$

(R3) $XO + XO \rightarrow X_2 + O_2$

(R4) $X_2 + h\nu \rightarrow 2\,X$

Net : $2\,O_3 \rightarrow 3\,O_2$

Catalytic cycle 2:

$X + O_3 \rightarrow XO + O_2$

(R5) $OH + O_3 \rightarrow HO_2 + O_2$

[1] Alfred Wegener Institute for Polar and Marine Research, Bremerhaven, Germany.
[2] Institute of Environmental Physics, University of Bremen, Bremen, Germany.
[3] Now at Institute of Oceanography, Center for Marine and Atmospheric Research, University of Hamburg, Hamburg, Germany.

0148-0227/06/2005JD006715$09.00

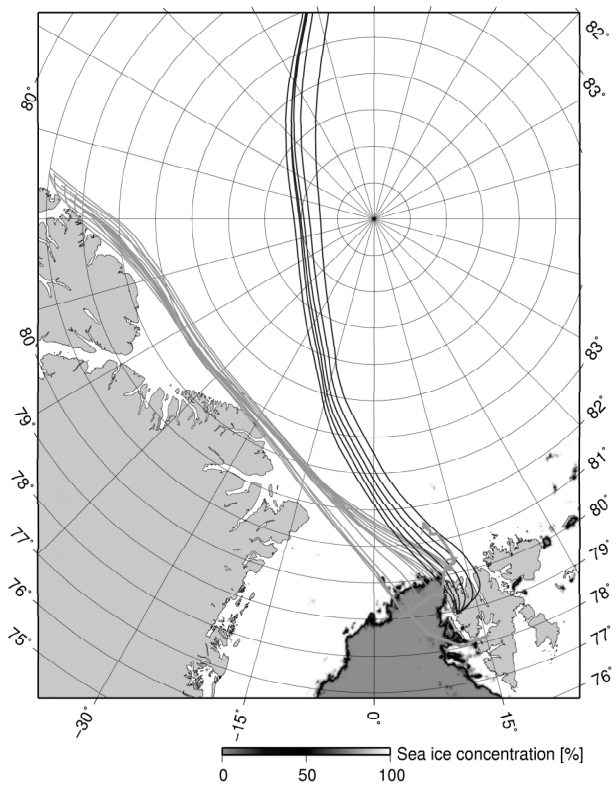

Figure 1. Sea ice concentration derived from AMSR-E 89 GHz data for 31 March. The thick green line indicates a part (29–31 March) of the cruise track of RV *Polarstern* west and northwest of Spitsbergen (ARK XIX/1). Green and blue lines indicate 72-hour backward trajectories for RV *Polarstern* and Zeppelin Station, Ny-Ålesund. Trajectories are shown for the period between 1200 UTC on 30 March and 1800 UTC on 31 March. Starting points of the trajectories are either the actual ship's positions or the Zeppelin station.

(R6) $HO_2 + XO \rightarrow HOX + O_2$

(R7) $HOX + h\nu \rightarrow OH + X$

Net : $2\ O_3 + h\nu \rightarrow 3\ O_2$

Catalytic cycle 3:

(R8) $XY + h\nu \rightarrow X + Y$

$X + O_3 \rightarrow XO + O_2$

(R9) $Y + O_3 \rightarrow YO + O_2$

(R10) $XO + YO \rightarrow X + YO_2$

(R11) $YO_2 + M \rightarrow Y + O_2 + M$

Net : $2\ O_3 + h\nu \rightarrow 3\ O_2$

[4] In these reactions X and Y represent Cl, Br, or I, X_2 represents Cl_2, Br_2, or I_2, HOX represents HOCl or HOBr, and XY represents BrCl, BrI, or ClI. As large amounts of bromine oxide (BrO) have been observed in ODEs and some evidence for a small activation of Cl exists, our current understanding is that X, X_2, HOX and XY in an ODE are primarily Br, Br_2, HOBr, and BrCl, respectively.

[5] At present, the source of the reactive halogens remains a matter of scientific debate. *Vogt et al.* [1996] proposed an autocatalytic production of photochemically active bromine including the heterogeneous production of molecular bromine (Br_2) on sea salt aerosols. The reactive bromine compounds (Br_2, BrCl) are released to the gas phase and photolyzed forming Br atoms. Interestingly, the gas phase reaction of BrO with HO_2 produces HOBr, which if absorbed into aerosols participates in the heterogeneous oxidation of bromide (Br^-), making the overall process autocatalytic. A similar cycle with reduced efficiency is feasible for ClO because of the significantly smaller photolysis frequency of HOCl compared to HOBr [*Sander et al.*, 2003] and the higher reactivity of Cl toward organics. At present it is not clear whether iodine and IO reactions are playing a significant role in ODEs.

[6] Assuming that the Br chemistry is dominating the ODE, then the chain length or effectiveness of the reaction cycles above depends on the photolysis frequencies of the bromine reservoirs and therefore on the actinic flux of radiation. The autocatalytic nature of the chain of reactions, coupled with the increase of the actinic radiation, implies a rapid growth of reactive bromine compounds after polar sunrise. This has been labeled the "bromine explosion" [e.g., *Wennberg*, 1999; *Platt and Hönninger*, 2003]. Since it appears unlikely that atmospheric aerosol can release sufficient bromine to explain this phenomenon [e.g., *Impey et al.*, 1997; *Lehrer et al.*, 2004], distinct surfaces with specific properties are more likely sources.

[7] Although ODEs are regularly observed at several Arctic stations [*Tarasick and Bottenheim*, 2002], the origin as well as the spatial and temporal extent of Arctic ODEs are not well characterized nor understood. The objective of this study was to identify the conditions necessary for the development of an ODE. Since previous measurements indicate that the Arctic Ocean is the origin of the ODEs, we used the extraordinary opportunity to perform measurements of O_3 on board an icebreaker, which operated in spring in the still ice-covered Arctic Ocean.

2. Methods

[8] Surface O_3 mixing ratios were measured continuously on board the icebreaker RV *Polarstern* during a cruise in the region west and northwest of the Spitsbergen archipelago (Expedition ARK XIX/1). The cruise track started at Bremerhaven, Germany (54°N) on 28 February 2003 and ended in Longyearbyen, Svalbard (78.2°N, 15.6°E) on 24 April 2003. The ship visited the port of Longyearbyen on 29 March and entered the Fram Strait late on the evening of the same day (Figure 1). O_3 was measured between 16 March and 23 April using a commercial detector ($O_3$41M, Ansyco GmbH, Karlsruhe, Germany), which is based on UV photometric detection at 254 nm. The

unheated inlet line consisted of approximately 5 m of 0.8 cm ID perfluoroalkoxy tubing and was mounted on the compass deck rail on the portside approximately 25 m above sea level. The concentrations were internally averaged and stored as 10-min averages resulting in a limit of detection of 1 ppbV.

[9] Standard meteorological data are routinely collected aboard the RV *Polarstern*. Information about the different sensors and their installation on board can be found at http://www.awi-bremerhaven.de/MET/Polarstern/poldatinfo.html. Retrieval of data from the data archive POLDAT is possible starting from http://www.awi-bremerhaven.de/MET/Polarstern/poldatquery.html. In addition, standard radiosondes were regularly launched from the helicopter deck of RV *Polarstern*.

[10] Further O_3 measurements in Spitsbergen are performed year-round at the Zeppelin mountain station (78°54′N, 11°53′E, 474 m above sea level) located on a mountain ridge south of the small research village at Ny-Ålesund (Figure 1). Ozone is monitored at the station by a commercial UV absorption instrument (API 400A # 612, Teledyne, San Diego, CA) with a lower detection limit of 0.6 ppbV. Zero and span checks are performed automatically every second week and a manual calibration is done once a year using a TEI 49 CPS #60955-329 as a reference. The air intake is through a 4.5 m FEP tube with an outer diameter of 0.635 cm and an inner diameter of 0.475 cm. The monitoring is part of the national, Norwegian monitoring program, EMEP (European Monitoring and Evaluation Programme) and GAW (Global Atmospheric Watch). A climatology of the low ozone episodes observed at the Zeppelin station was given by *Solberg et al.* [1996].

[11] Backward trajectories were calculated with the Hybrid Single-Particle Lagrangian Integrated Trajectory (HYSPLIT) Model (R. R. Draxler and G. D. Rolph, NOAA Air Resources Laboratory, Silver Spring, Maryland, model access via http://www.arl.noaa.gov/ready/hysplit4.html, 2003). The model was driven by Final Run reanalysis wind fields (FNL). The trajectories for the RV *Polarstern* cruise were initiated at the actual ship's positions with the starting height at the level of the O_3 measurements (25 m above the ground level). The trajectories for the Zeppelin station were initiated with the station position at an elevation of 475 m.

[12] BrO is one of the reactive halogen compounds, which are generated during the catalytic destruction of O_3. Clouds of elevated BrO can be identified using UV/visible remote sensing techniques from space and have been retrieved from measurements by the Global Ozone Monitoring Experiment (GOME) in both hemispheres [*Wagner and Platt*, 1998; *Richter et al.*, 1998]. In this study data from SCIAMACHY (SCanning Imaging Absorption spectroMeter for Atmospheric CHartographY) [*Bovensmann et al.*, 1999] are used, which has a somewhat improved spatial resolution as compared to GOME (240 km × 30 km compared to 320 km × 40 km for BrO in the region of interest). As the nadir measurements are sensitive to both stratospheric and tropospheric BrO, the stratospheric component must be accounted for before retrieval of the tropospheric amount. In this analysis the stratospheric BrO column over the region around Spitsbergen was determined by integrating the stratospheric BrO profiles deduced from SCIAMACHY limb measurements [*Rozanov et al.*, 2005] and averaging the results. On the basis of these data, the stratospheric column was approximated with $4 \cdot 10^{13}$ molecules cm^{-2} and subtracted from the total column observed in nadir. The resulting tropospheric slant columns were then converted to vertical columns assuming that BrO is well mixed in a 400 m thick boundary layer at a surface reflectivity of 90%. As both the stratospheric correction and the air mass factor have a large uncertainty, and a BrO background present in the free troposphere could also contribute to the signal, the error of the tropospheric columns is estimated to be of the order of 30%.

[13] The sea ice conditions surrounding the operational area of the vessel was analyzed using remote sensing data. Sea ice concentrations (Figure 1) were derived from 89 GHz AMSR-E data [*Kaleschke et al.*, 2001; G. Spreen et al., Sea ice remote sensing using AMSR-E 89 GHz channels, submitted to *Journal of Geophysical Research*, 2006]. In addition, a MODIS image for 31 March (1125 UTC) was used to investigate new ice formation in the marginal ice zone (MIZ) (Figure 2). Nilas is a type of new ice that forms in quite conditions. This thin elastic crust has a smooth surface and is up to 10 cm in thickness. Light nilas is more than 5 cm in thickness and commonly covered with frost flowers. It exhibits the highest emissivity at 89 GHz (ε_v = 0.955, ε_h = 0.925) as compared with other ice types [*Eppler et al.*, 1992]. Therefore light nilas can be detected with a simple threshold method using passive microwave data. The AMSR-E sensor measures the brightness temperature T_B with a spatial resolution of about 5 km, which is sufficient to detect larger leads. Here, we used a threshold of T_B(V-pol) > 230 K to detect the areas of light nilas.

3. Results and Discussion

[14] Figure 3 shows the O_3 measurements performed between 29 March and 6 April, when the ship traveled from the Isfjord through the Fram Strait to the Arctic Ocean. This part of the O_3 time series covers a period of more than 5 days, during which the O_3 concentrations almost exclusively remained close to or below the detection limit of 1 ppbV. The situation before and during the beginning of the ODE when the O_3 concentrations dropped from 39.7 to below 1 ppbV within less than 7 hours (31 March; 1130 until 1740 UTC) is analyzed in order to identify the specific conditions necessary for the O_3 depletion.

[15] The analysis of ODEs at Arctic stations is complicated by the transport of air masses with low O_3 concentrations to the stations across the Arctic Ocean [*Wessel et al.*, 1998; *Tarasick and Bottenheim*, 2002; *Bottenheim et al.*, 2002]. Only some events have been ascribed to local chemical processes [*Hopper et al.*, 1998; *Boudries and Bottenheim*, 2000]. For the ODE observed on 31 March, the origin of the O_3 decrease was investigated. The possibilities of the transport of O_3-poor air to the measurement location, of the transit of the ship into a region with low O_3 concentrations, and of the local chemical O_3 destruction taking place close to the ship's position were considered.

3.1. Long-Range Transport

[16] Long-range transport of air masses did not show any significant change during the period from 29 March to

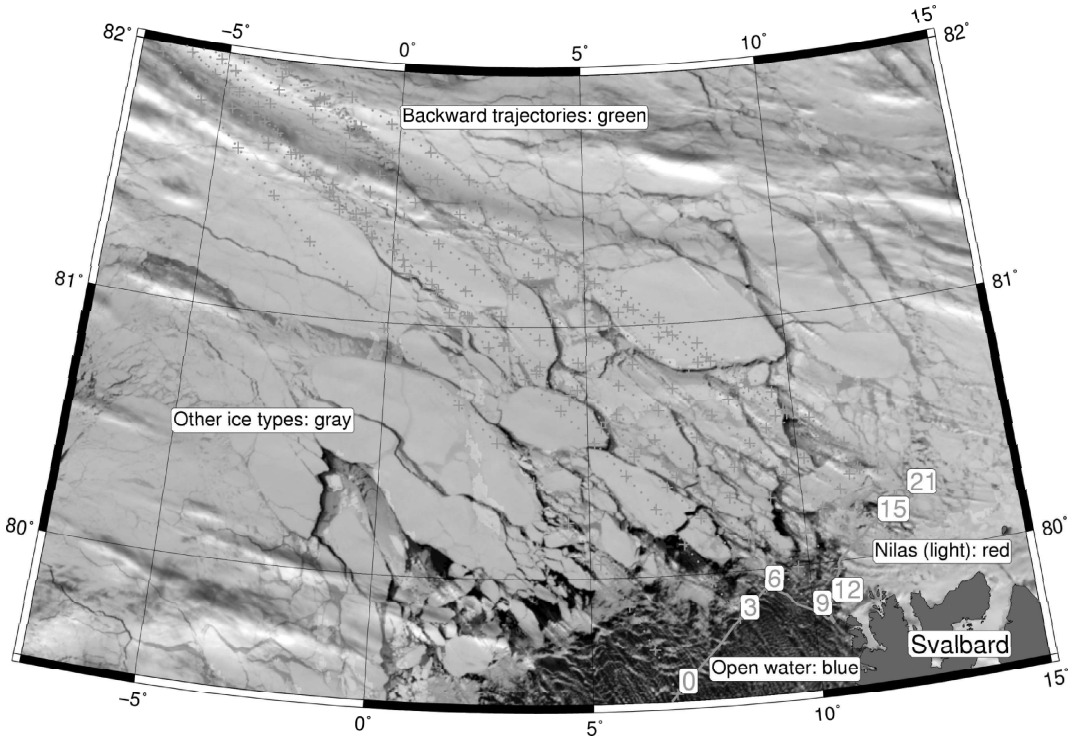

Figure 2. MODIS image (λ = 645 nm, 250 m resolution) for 31 March (1125 UTC) of the region northwest of Svalbard. The thick green line indicates a part of the cruise track of RV *Polarstern* and the corresponding hour of the day. Starting points of atmospheric back trajectories (dotted green line) are the actual ship's position. Crosses mark time steps of 1 hour along the trajectories. Open water (ice concentration <5%) is indicated in blue. Areas covered with light nilas (see text) are indicated in red.

1 April. The synoptic situation was dominated by a stationary high above northern Greenland. This high resulted in a constant meridional flow of air along the northern coast of Greenland into the Fram Strait and to the northwestern tip of Spitsbergen. 72-hour backward air parcel trajectories for the period from 29 March (0000 UTC) to 1 April (2300 UTC) were analyzed. They indicate a stable circulation pattern for the period before, during, and after the O_3 decrease. The trajectories followed similar pathways during the entire period investigated. Selected trajectories covering the period from 30 March (1200 UTC) to 31 March (1800 UTC) are shown as examples in the Figures 1 and 2. Accordingly, the meteorological parameters wind speed, relative humidity, radiation, and air pressure changed only gradually in agreement with the stable mesoscale meteorological conditions (Figure 4). Therefore it appears unlikely that the observed

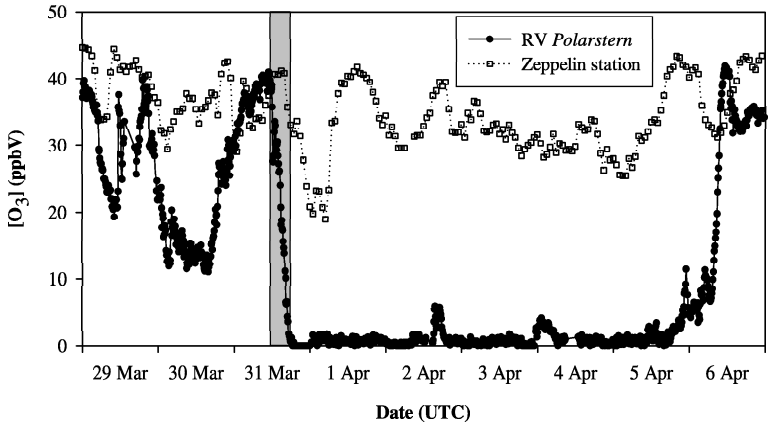

Figure 3. Time series of O_3 concentrations measured on board RV *Polarstern* (10-min averages) and at Zeppelin station (1-hour averages) at Ny-Alesund, Spitsbergen. The shaded area indicates the period when O_3 decreased from 39.7 ppbV (31 March, 1130 UTC) to less than 1 ppbV (31 March, 1740 UTC). Ticks mark midnight of each day.

O_3 decay is due to the change in the long-range transport of different air masses having either normal or low O_3 concentrations.

3.2. Spatial Versus Temporal O_3 Gradient

[17] As the ship was moving during the O_3 decrease, it is possible that the ODE developed earlier and the decreasing O_3 was caused by the transit from a region with normal O_3 into the center of the ODE where O_3 was destroyed earlier. However, the distance covered by the ship during the O_3 decrease was less than 62 km. The decrease from more than 15 to 1 ppbV occurred within a distance of 5 km, and the final decrease from more than 10 to 1 ppbV occurred while the ship traveled a distance of 1.3 km (Figure 5). This final O_3 drop while RV *Polarstern* remained almost immobile clearly indicates that the observed O_3 decrease was a temporal, not a spatial decline in the O_3 concentration.

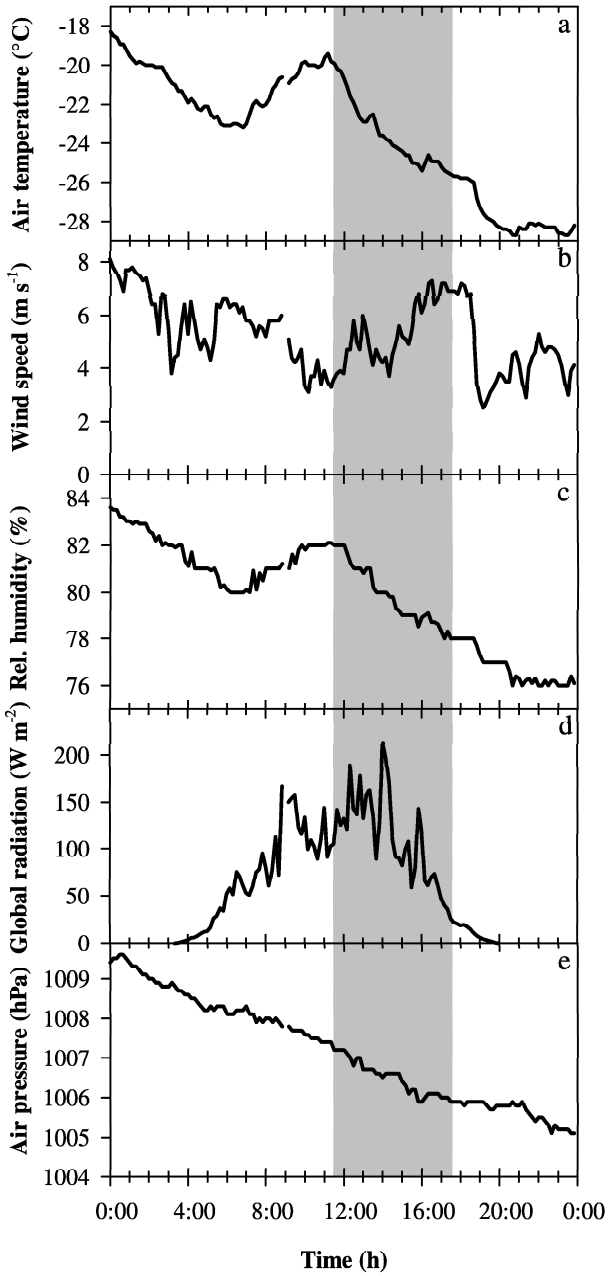

Figure 4. Ten-minute averages of meteorological parameters measured on board RV *Polarstern* on 31 March: (a) air temperature, (b) wind speed, (c) relative humidity, (d) global radiation, and (e) air pressure. The shaded area indicates the period between 1140 and 1730 UTC, when the rapid O_3 depletion occurred.

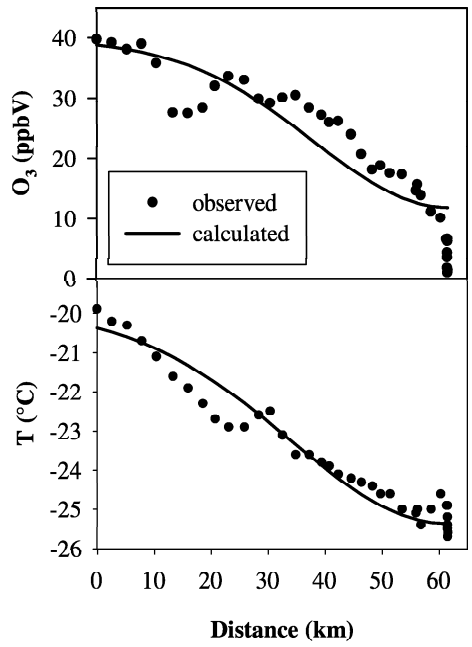

Figure 5. (top) O_3 concentration and (bottom) air temperature as a function of the traveled distance to the ship's location at 1130 UTC on 31 March (79.7629°N, 10.4216°E). The dots represent the measured values. The line shows the calculated transition described by a Gaussian curve according to atmospheric dispersion theory (see auxiliary material).

[18] In contrast, the air temperature measured during the same period demonstrates that regarding the meteorological conditions the ship covered a transition between two distinct regions. Figure 5 shows a plot of the observed air temperatures along the transit. In this case, a drop from −19.9°C to approximately −25°C was found. Such a profile can be analyzed using empirical atmospheric dispersion theory (see auxiliary material[1]). The calculated profiles for the air temperature and the O_3 concentration are also shown in Figure 5. These results suggest that the ship covered a transition between two regions with distinct different air temperatures entering an area with significantly lower values. The horizontal temperature profile between these two regions agrees well with the profile expected from atmospheric dispersion theory. Obviously, this is not the case for the observed horizontal O_3 concentration profile although low air temperatures as those found in the entered region are thought to be favorable for the occurrence of ODEs. The shape of the O_3 profile is distinctly different from the expected profile sug-

[1]Auxiliary materials are available in the HTML. doi:10.1029/2005JD006715.

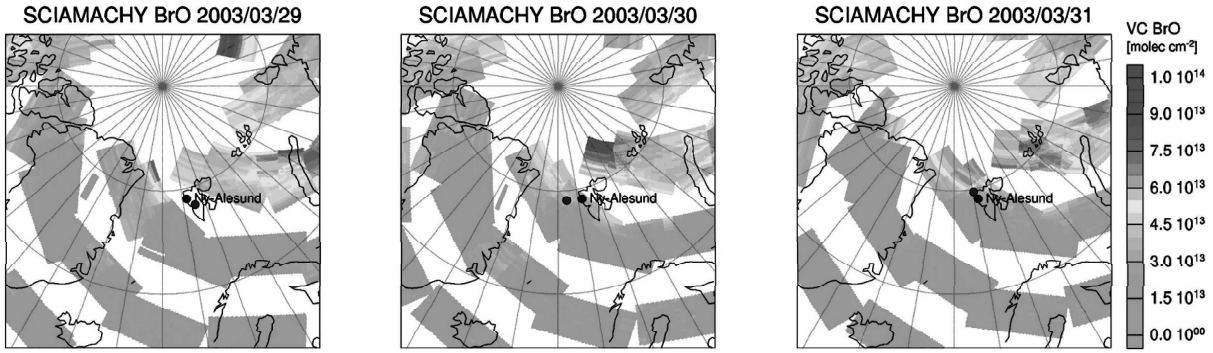

Figure 6. Tropospheric BrO columns as measured by SCIAMACHY. The graphs show daily composite maps, which at high latitudes are the average of up to three measurements. A constant stratospheric BrO column of $4 \cdot 10^{13}$ molecules cm^{-2} was assumed similar to the stratospheric profile measured in limb. Tropospheric columns were derived assuming a well-mixed boundary layer of 400 m and a surface reflectivity of 0.9, which is only appropriate over the ice-covered regions. The gaps result from the alternate limb and nadir scanning of SCIAMACHY. The blue dot indicates the ship position at the time of satellite overpass. However, as the measurements are taken sequentially, the data shown spread over a period of 24 hours.

gesting that the measured O_3 drop is not a spatial feature, but rather developed in time during the observations.

3.3. Bromine Oxide Concentrations

[19] Since the concentration of the BrO radical reaches high levels during the catalytic destruction of O_3 [e.g., *Tuckermann et al.*, 1997], observations of elevated BrO concentrations can support our conclusion. In Figure 6, daily tropospheric BrO columns from SCIAMACHY are shown between 29 and 31 March. A comparison with the map in Figure 2 reveals that BrO was enhanced on 31 March in the same area where the ODE was observed. In contrast, no indication for large BrO enhancements was found in this area on the previous days in the area probed by SCIAMACHY. On 29 March an area with enhanced BrO columns was also detected not far from the northeastern edge of Greenland. Air masses from this area were transported to the operational area of the icebreaker indicated by forward trajectories. However, the trajectories also demonstrate that these air masses were already sampled 24 hours later. In fact, the O_3 time series (Figure 3) exhibits concentrations below 20 ppbV for longer periods on 30 March, which in this case can obviously be attributed to the transport of air with reduced O_3 concentrations to the sampling site.

[20] Measurements of the BrO distribution in the troposphere inferred from multiple angle DOAS measurements at Alert in the Hudson Bay indicate that during the ODE the tropospheric BrO is mainly located in the boundary layer [*Hönninger and Platt*, 2002]. The height of the boundary layer was determined using data from regularly launched radiosondes. Profiles of the potential temperatures measured on 31 March and 1 April are shown in Figure 7. The profile on the morning of 31 March was measured in the open water area not far from the northwestern tip of Spitsbergen. It indicates neutral conditions in the boundary layer up to a height of approximately 380 m. On top of the boundary layer a strong inversion was observed. The profiles measured later in the evening of 31 March and in the morning of 1 April are representative for the conditions in the MIZ. Here temperatures in the boundary layer are several degrees lower, while temperatures at the height of 1000 m are similar above the open water and in the MIZ. In the MIZ the boundary layer was characterized by either neutral or stable conditions. The temperature inversions on top of the boundary layer were even stronger than in the open water area. The boundary layer heights varied between 220 and 380 m.

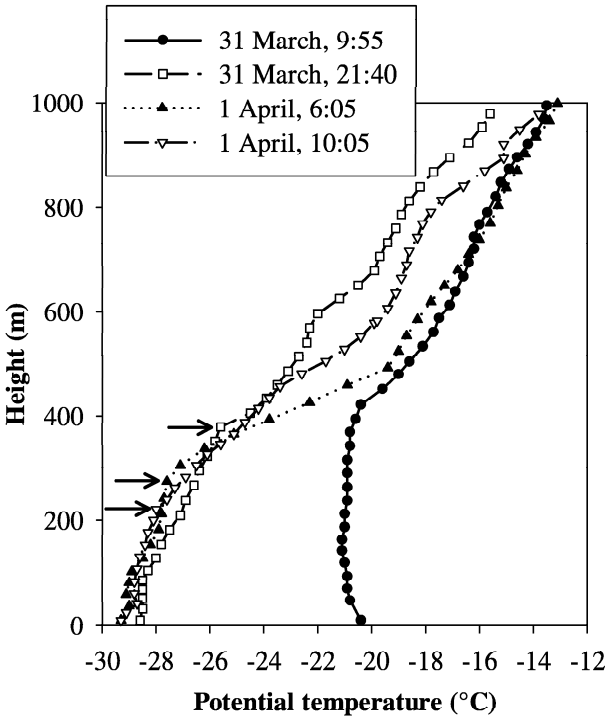

Figure 7. Profiles of the potential temperature measured on 31 March and 1 April. Arrows indicate the estimated heights of the boundary layer.

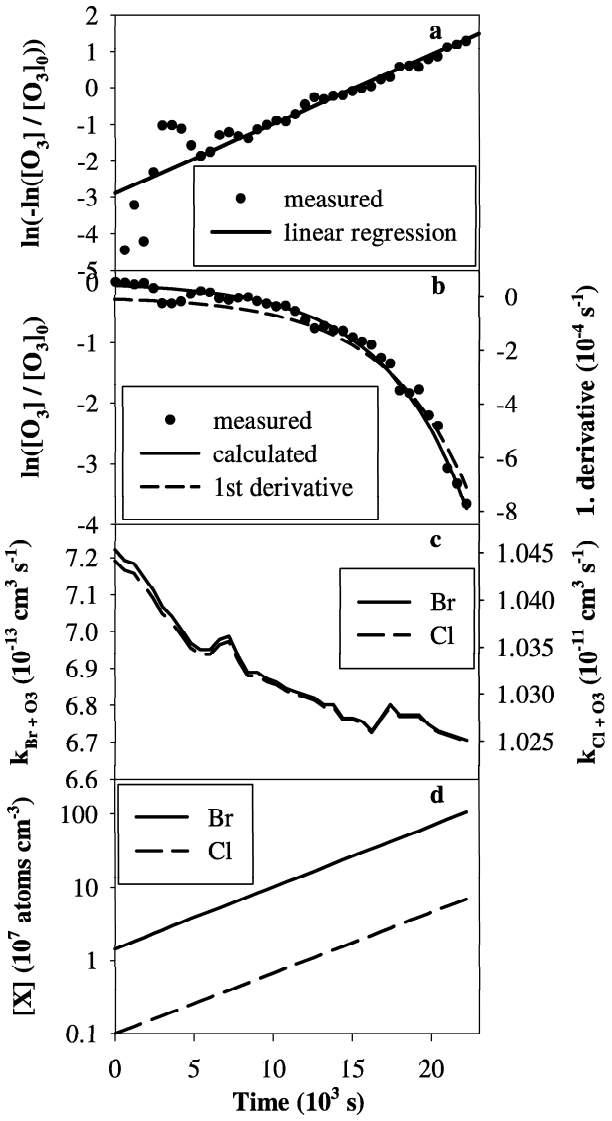

Figure 8. Analysis of the O_3 decay starting at 1130 UTC (31 March). (a) Plot of $\ln(-\ln([O_3]/[O_3]_0))$ versus time used to determine the coefficients a and b for equation (6); (b) logarithm of the relative O_3 concentrations versus time with the calculated fit according to equation (5) and calculated first derivative according to equation (7); (c) calculated temperature-dependent reaction rate coefficients for the reactions of Br and Cl with O_3; and (d) calculated halogen concentrations.

[21] The height of the boundary layer can be used to convert the BrO vertical column into mixing ratios. Assuming a mixing height of 380 m (Figure 7) and a BrO vertical column in the boundary layer of approximately $7 \cdot 10^{13}$ molecules cm^{-2} (Figure 6), a BrO concentration in the boundary layer of $1.8 \cdot 10^9$ molecules cm^{-3} results. This corresponds to a mixing ratio of 63 pptV in a well-mixed layer for the conditions on 31 March. These numbers are calculated assuming a uniform vertical BrO distribution in the boundary layer. However, the concentrations are possibly higher closer to the source of the reactive halogens. If this source was located at the surface it is likely hat a BrO concentration gradient was established with higher concentrations closer to the ground. Therefore the calculated BrO concentration has a rather high uncertainty on the order of approximately 50%. Nevertheless, The BrO mixing ratio was probably higher than the maximum values obtained from ground-based observations in the Arctic of ~30 pptV [*Tuckermann et al.*, 1997; *Martinez et al.*, 1999; *Hönninger and Platt*, 2002]. As a consequence there is sufficient reactive bromine present locally in the boundary layer to explain the extremely fast O_3 depletion observed.

3.4. O_3 Measurements at Zeppelin Station

[22] Another indication that the ODE, observed along the track of the RV *Polarstern*, was a local phenomenon is given by a comparison with the O_3 mixing ratios measured at the Zeppelin Station. Relevant O_3 data obtained at this station show no evidence for a simultaneous ODE at Zeppelin Station (Figure 3). The backward trajectories indicate that the air masses reaching the station between 0500 and 1300 UTC on 1 April passed over the area, where the ODE was observed (Figure 1). Nevertheless, at Zeppelin Station the O_3 concentrations remained between levels of approximately 20 to 40 ppbV. A closer look at the trajectories reveals that the air masses sampled at Zeppelin station traveled at an elevation higher than 500 m, i.e., above the boundary layer in the region with depleted O_3. Thus the O_3 depletion was confined to the boundary layer whereas normal O_3 levels existed above the temperature inversion.

3.5. Kinetic Analysis of the O_3 Decay

[23] Being convinced that the observed ODE can be ascribed to chemical processes, the chemical kinetics of the observed decay can be analyzed. Figure 8 shows the logarithm of the O_3 concentration during the decay. A linear decrease would indicate a constant first-order loss. In contrast, Figure 8 demonstrates that the O_3 loss begins relatively slowly and accelerates during the decay period. This behavior is in excellent agreement with the so-called bromine explosion, which causes accelerating O_3 losses due to exponentially increasing reactive Br concentrations [*Wennberg*, 1999; *Platt and Hönninger*, 2003].

[24] Assuming that the catalytic destruction is dominated by reactions (R1) to (R4), a first-order loss of O_3 can be expected because of the Br reaction (R1). *Tuckermann et al.* [1997] pointed out that the self-reactions of BrO (R2 and R3) could be rate-limiting steps leading to either a zero-order or second-order O_3 loss depending on the O_3 concentration. However, for the conditions observed during this cruise, we assume an unlimited bromine source, leading to a continuous supply of Br_2, which is immediately photolyzed to Br (R4) as the actinic radiation intensities were sufficiently high in the afternoon of 31 March (Figure 4).

[25] Therefore the O_3 decay was analyzed assuming a first-order loss due to reaction (R1) resulting in the following rate law (1):

$$\frac{d[O_3]}{dt} = -k_{1st} \cdot [O_3] \quad (1)$$

$$[O_3] = [O_3]_0 \quad \exp(k_{1st} \quad t) \quad (2)$$

$$\ln\frac{[O_3]}{[O_3]_0} = k_{1st} \quad t \tag{3}$$

[26] $[O_3]_0$ is the O_3 concentration at the beginning of the decay (1130 UTC) determined from the measured mixing ratio of 39.7 ppbV. The first-order rate constant k1st can be determined from the following equation:

$$\frac{d\left(\ln\left(\frac{[O_3]}{[O_3]_0}\right)\right)}{dt} = -k_{1st} \tag{4}$$

[27] The measured decrease of $\ln\left(\frac{[O_3]}{[O_3]_0}\right)$ versus time was fitted by a simple exponential equation:

$$\ln\left(\frac{[O_3]}{[O_3]_0}\right) = -\exp(b \cdot t + a) \tag{5}$$

$$\Leftrightarrow \ln\left(-\ln\left(\frac{[O_3]}{[O_3]_0}\right)\right) = b \cdot t + a \tag{6}$$

[28] The coefficients a and b are obtained from a linear regression of a plot of $\ln\left(-\ln\left(\frac{[O_3]}{[O_3]_0}\right)\right)$ versus time (Figure 8) resulting in values of $a = -(2.9 \pm 0.2)$ and $b = (1.9 \pm 0.1) \cdot 10^{-4}$ s^{-1} and a regression coefficient of $R^2 = 0.839$. Figure 8 shows the measured data together with the calculated curve according to equation (6) using the above mentioned values for a and b. The analytical solution of the first derivative of (6) finally gives the first-order rate constant k1st of the observed O_3 decay as a function of time:

$$\frac{d\left(\ln\left(\frac{[O_3]}{[O_3]_0}\right)\right)}{dt} = \quad b \cdot \exp(b \cdot t \mid a) = \quad k_{1st} \tag{7}$$

[29] Assuming that the first-order decay is dominated by the reaction of O_3 with the halogens Br or Cl, we are able to calculate the concentrations needed as a function of time according to equation (9):

$$k_{1st} = k_{X+O3} \cdot [X] \tag{8}$$

$$[X] = \frac{k_{1st}}{k_{X+O3}} \tag{9}$$

[30] The rate constants k_{Br+O3} and k_{Cl+O3} for the reactions of Br and Cl with O_3 exhibit temperature dependencies according to the equations (10) and (11) [*Sander et al.*, 2003].

$$k_{Br+O3} = 1.7 \cdot 10^{-11} \cdot \exp\left(-\frac{800}{T}\right) \tag{10}$$

$$k_{Cl+O3} - 2.3 \cdot 10^{-11} \cdot \exp\left(-\frac{200}{T}\right) \tag{11}$$

[31] The measured air temperature (Figure 4) was used to calculate rate constants for each measured O_3 concentration to derive the corresponding halogen concentration shown in Figure 8. Because of the different reactivities of O_3 toward the reactions with Br (slow) and Cl (fast), the halogen concentrations can serve as lower (Cl) and upper (Br) limits. The strong enhancement of the observed O_3 decay rates suggests that the halogen concentration also increase considerably. We find a good agreement if we assumed an exponential growth of the O_3 decay rate corresponding to an exponential increase of the halogen concentrations according to the so-called bromine explosion mechanism. If the Br reaction is solely responsible for the O_3 loss, the concentrations increase from $1.4 \cdot 10^7$ to almost $1.1 \cdot 10^9$ atoms cm^{-3} (corresponding to 37 pptV). On the other hand, the same loss can be caused by Cl concentrations increasing from $1 \cdot 10^6$ to $7 \cdot 10^7$ atoms cm^{-3}. However, these numbers necessarily exhibit large uncertainties for different reasons. The calculations only take into account the effect of the halogens separately as well as only the O_3 destruction by cycle 1. Therefore these values possibly represent only upper limits of the halogen concentrations. On the other hand, the numbers are calculated on the basis of the assumption that the halogens are homogenously distributed in the boundary layer. However, like in the case of BrO the possibility exists that a vertical gradient in the stable boundary layer can be established with higher concentrations closer to the source region, which might be the surface where the heterogeneous release of the halogens can take place. Taking this possibility into account the concentrations at the surface could be even higher than the calculated numbers. In summary, we estimate that the uncertainty of the calculated halogen concentrations is on the order of ±50%. Notwithstanding, the development of the halogen concentrations is consistent with the so-called bromine explosion mechanism.

[32] Even taking into account the large uncertainties the calculated halogen concentrations are surprisingly high. Previously reported halogen concentrations are based on the observation of the decay of different volatile organic compounds (VOC) [*Jobson et al.*, 1994; *Solberg et al.*, 1996; *Ariya et al.*, 1998; *Boudries and Bottenheim*, 2000]. The halogen concentrations depend linearly on the periods, in which halogen chemistry was active. Assuming reaction times between 1 and 20 days the derived Cl and Br concentrations varied between 0.39 to $10 \cdot 10^4$ atoms cm^{-3} and 0.30 to $10 \cdot 10^7$ atoms cm^{-3}. In the case of Cl the numbers are significantly smaller than our calculated value of more than 10^6 atoms cm^{-3}, which is unrealistically high. On the other hand, the agreement for the Br concentrations is better although the upper limit of the Br concentration obtained here is still high compared to the literature values. However, the difference might be due to the fact that the VOC method delivers a spatial and temporal (daily) average, whereas we calculated here a Br concentration more representative for a shorter period and for a stable boundary layer. It seems possible that under these circumstances the Br concentrations can be higher than previously reported.

[33] Previous modeling studies [e.g., *Fan and Jacob*, 1992; *Lehrer et al.*, 2004] clearly demonstrated that O_3 loss rates depend on the concentrations of reactive bromine compounds. While *Lehrer et al.* [2004] found that in the presence of 30 to 40 pptV of reactive bromine compounds the O_3 loss rate was in the order of 7.6 ppbV d^{-1}, *Fan and Jacob* [1992] calculated loss rates of approximately 40 ppbV d^{-1} in the presence of 100 pptV of reactive

bromine compounds. We observed an even higher average O_3 loss rate of 6.7 ppbV h^{-1} or 160 ppbV d^{-1} (Figure 3), which agrees well with the extremely high estimates of the Br mixing ratios with values of almost 40 pptV. Moreover, the observed rapid decay of O_3 is in agreement with the conclusions by *Hausmann and Platt* [1994]. On the basis of their measurements of BrO and O_3 in Alert, they argue that the O_3 depletion must be completed in less than one day to account for O_3 mixing ratios below 1 ppbV after the transport of the depleted air masses to the measuring site [*Hausmann and Platt*, 1994].

3.6. Influence of New Ice

[34] Having identified the ODE to be in the boundary layer and occurring close to the ship's position, other relevant and necessary conditions for the O_3 destruction were investigated. Figure 2 shows that the onset of the O_3 destruction occurred after the ship entered the MIZ, which was dominated by fields of new ice. The low air temperatures (Figure 4) measured in the MIZ make the formation of new sea ice very efficient. The trajectories (Figure 2) indicate that the air masses arriving at the ship during the O_3 decrease spent considerable time above the new ice fields in the MIZ suggesting that this is the region where the heterogeneous release of the reactive halogen compounds and the subsequent O_3 depletion took place. Unfortunately, areas with new sea ice are not characterized by a single sea salt containing surface, so that different types of surfaces can be considered for the heterogeneous release of the reactive halogens.

[35] For example, several investigations have demonstrated that temperatures below −20°C coupled with open water areas are conditions favorable for the formation of frost flowers (FF) [*Perovich and Richter-Menge*, 1994; *Rankin et al.*, 2002]. Since both requirements were fulfilled in the MIZ, the surface conditions were optimal for the formation of FF. Accordingly, FF were recorded several times in the notes of the visual sea ice observations made during the cruise. Although there is some debate about the size of the specific surface areas of FF [*Rankin et al.*, 2002; *Domine et al.*, 2005], FF surfaces provide optimal conditions for the release of halogens because they are characterized by high salinities [*Rankin et al.*, 2002]. Presumably the Br^- and Cl^- in the FF is converted in the presence of HOBr to Br_2 and/or BrCl by heterogeneous reactions on or in the surface of the FF and subsequently released to the atmosphere: the source of HOBr being the gas phase reaction between HO_2 and BrO and subsequent migration to the surface. As a result, *Kaleschke et al.* [2004] found excellent spatial agreement between the occurrence of FF and enhanced BrO concentrations detected from GOME in both hemispheres.

[36] Nevertheless, FF are always accompanied by the formation of a liquid and highly saline layer on top of the sea ice [e.g., *Rankin et al.*, 2002]. This layer also offers ideal conditions for the heterogeneous reactions necessary for the halogen activation. Aerosols generated from FF can also be regarded as ideal surfaces for the heterogeneous reactions. In this case the source of the halogens would not be restricted to the sea ice surface, but could occur within the entire boundary layer if the aerosols are well distributed within this layer. Finally, *Simpson et al.* [2005] proposed that sea-salt aerosols released from FF but deposited on the adjacent snowpack cold also contribute to the halogen activation. In that case the halogen release could occur over larger areas and not only over existing FF fields. Unfortunately, the current data set does not allow distinguishing between the roles of any of the described surfaces. Nevertheless, the conditions in the MIZ accompanied by the formation of new ice might be crucial parameters, which can possibly be used to estimate or model areas where the O_3 depletion in polar spring occurs.

[37] An alternative source of reactive bromine species is the photochemical conversion of halogenated organic or polyhalogenated compounds. These are produced in the Arctic Ocean by biological sources and subsequently released to the atmosphere [e.g., *Barrie et al.*, 1988; *Sturges et al.*, 1992] or stored under old sea ice. During this cruise, the biological activity was limited in the MIZ as indicated by the low concentrations of pelagic phytoplankton biomass and chlorophyll-a (J. N. Schwarz et al., manuscript in preparation, 2006). Both components showed higher concentrations farther south in the Fram Strait, where normal O_3 concentrations were observed. In summary, no evidence was found for the halogenated compounds being the source of the reactive bromine causing the observed ODE.

4. Conclusions

[38] Our observations show that during polar spring in the MIZ boundary layer O_3 can be completely removed within less than 7 hours. The observed removal was caused by local chemical processes as revealed by the analysis of air mass trajectories and further meteorological data. Simultaneously, a significant tropospheric column of BrO was retrieved from the measurements of SCIAMACHY. The efficient O_3 loss requires extremely high concentrations of reactive bromine, and is consistent with the BrO column retrieved from satellite data. Large fields of new ice characterized the MIZ during the observations. As a result of their properties and high bromide content, FF (or aerosols generated thereof either within the boundary layer or deposited on the snowpack) are well able to serve as the heterogeneous surface for the activation of such high levels of reactive bromine. However, contributions by reactions on other surfaces cannot be ruled out. Therefore further field studies in the MIZ and laboratory studies with FF are required to identify heterogeneous chemical processes occurring at the different kinds of surfaces. Nevertheless, the formation of new ice in combination with a stable atmospheric boundary layer possibly indicates a high probability of depleted surface O_3 concentrations. This has important implications for the determination of the extent of ODEs using remote sensing data.

[39] **Acknowledgments.** H.W.J. and L.K. thank the German Science Foundation (DFG) for financial support. We thank the crew of RV *Polarstern* for their assistance and cooperation and Sverre Solberg and Katrine Aspmo (NILU) for providing the O_3 data from Zeppelin station. SCIAMACHY radiances and irradiances were provided by ESA/DLR. Part of the retrieval was performed on HLRN (High-Performance Computer Center North). Services and support are gratefully acknowledged.

References

Ariya, P. A., B. T. Jobson, R. Sander, H. Niki, G. W. Harris, J. F. Hopper, and K. G. Anlauf (1998), Measurements of C_2-C_7 hydrocarbons during

the Polar Sunrise Experiment 1994: Further evidence for halogen chemistry in the troposphere, *J. Geophys. Res.*, *103*(D11), 13,169–13,180.
Barrie, L. A., J. W. Bottenheim, R. C. Schnell, P. J. Crutzen, and R. A. Rasmussen (1988), Ozone destruction and photochemical reactions at polar sunrise in the lower Arctic atmosphere, *Nature*, *334*, 138–141.
Bottenheim, J. W., A. J. Gallant, and K. A. Brice (1986), Measurements of NO_y species and O_3 at 82°N latitude, *Geophys. Res. Lett.*, *13*, 113–116.
Bottenheim, J. W., J. D. Fuentes, D. W. Tarasick, and K. G. Anlauf (2002), Ozone in the Arctic lower troposphere during winter and spring 2000 (ALERT2000), *Atmos. Environ.*, *36*(15/16), 2535–2544.
Boudries, H., and J. W. Bottenheim (2000), Cl and Br atom concentrations during a surface boundary layer ozone depletion event in the Canadian high Arctic, *Geophys. Res. Lett.*, *27*(4), 517–520.
Bovensmann, H., J. P. Burrows, M. Buchwitz, J. Frerick, S. Noël, V. V. Rozanov, K. V. Chance, and A. P. H. Goede (1999), SCIAMACHY—Mission objectives and measurement modes, *J. Atmos. Sci.*, *56*(2), 127–150.
Domine, F., A. S. Taillandier, W. R. Simpson, and K. Severin (2005), Specific surface area, density and microstructure of frost flowers, *Geophys. Res. Lett.*, *32*, L13502, doi:10.1029/2005GL023245.
Eppler, D., et al. (1992), Passive microwave signatures of sea ice, in *Microwave Remote Sensing of Sea Ice*, *Geophys. Monogr. Ser.*, vol. 68, edited by F. D. Carsey, pp. 47–71, AGU, Washington, D. C.
Fan, S.-M., and D. J. Jacob (1992), Surface ozone depletion in Arctic spring sustained by bromine reactions on aerosols, *Nature*, *359*, 522–524.
Hausmann, M., and U. Platt (1994), Spectroscopic measurement of bromine oxide and ozone in the high Arctic during Polar Sunrise Experiment 1992, *J. Geophys. Res.*, *99*, 25,399–25,414.
Hönninger, G., and U. Platt (2002), Observations of BrO and its vertical distribution during surface ozone depletion at Alert, *Atmos. Environ.*, *36*(15–16), 2481–2489.
Hopper, J. F., L. A. Barrie, A. Silis, W. Hart, A. J. Gallant, and H. Dryfhout (1998), Ozone and meteorology during the 1994 Polar Sunrise Experiment, *J. Geophys. Res.*, *103*(D1), 1481–1492.
Impey, G. A., P. B. Shepson, D. R. Hastie, L. A. Barrie, and K. G. Anlauf (1997), Measurements of photolyzable chlorine and bromine during the Polar Sunrise Experiment 1995, *J. Geophys. Res.*, *102*(D13), 16,005–16,010.
Jobson, B. T., H. Niki, Y. Yokouchi, J. Bottenheim, F. Hopper, and R. Leaitch (1994), Measurements of C_2-C_6 hydrocarbons during the Polar Sunrise 1992 Experiment: Evidence for Cl atom and Br atom chemistry, *J. Geophys. Res.*, *99*(D12), 25,355–25,368.
Kaleschke, L., C. Lüpkes, T. Vihma, J. Haarpaintner, A. Bochert, J. Hartmann, and G. Heygster (2001), SSM/I sea ice remote sensing for mesoscale ocean-atmosphere interaction analysis, *Can. J. Remote Sens.*, *27*(5), 526–537.
Kaleschke, L., et al. (2004), Frost flowers on sea ice as a source of sea salt and their influence on tropospheric halogen chemistry, *Geophys. Res. Lett.*, *31*, L16114, doi:10.1029/2004GL020655.
Lehrer, E., G. Hönninger, and U. Platt (2004), A one dimensional model study of the mechanism of halogen liberation and vertical transport in the polar troposphere, *Atmos. Chem. Phys.*, *4*, 2427–2440.
Martinez, M., T. Arnold, and D. Perner (1999), The role of bromine and chlorine chemistry for arctic ozone depletion events in Ny-Ålesund and comparison with model calculations, *Ann. Geophys.*, *17*(7), 941–956.
Oltmans, S. J., and W. D. Komhyr (1986), Surface ozone distributions and variations from 1973–1984 measurements at the NOAA Geophysical Monitoring for Climatic Change baseline observatories, *J. Geophys. Res.*, *91*(D4), 5229–5236.
Perovich, D. K., and J. A. Richter-Menge (1994), Surface characteristics of lead ice, *J. Geophys. Res.*, *99*(C8), 16,341–16,350.
Platt, U., and G. Hönninger (2003), The role of halogen species in the troposphere, *Chemosphere*, *52*, 325–338.
Rankin, A. M., E. W. Wolff, and S. Martin (2002), Frost flowers: Implications for tropospheric chemistry and ice core interpretation, *J. Geophys. Res.*, *107*(D23), 4683, doi:10.1029/2002JD002492.
Richter, A., F. Wittrock, M. Eisinger, and J. P. Burrows (1998), GOME observations of tropospheric BrO in Northern Hemispheric spring and summer 1997, *Geophys. Res. Lett.*, *25*, 2683–2686.
Ridley, B. A., et al. (2003), Ozone depletion events observed in the high latitude surface layer during the TOPSE aircraft program, *J. Geophys. Res.*, *108*(D4), 8356, doi:10.1029/2001JD001507.
Rozanov, A., H. Bovensmann, A. Bracher, S. Hrechanyy, V. Rozanov, M. Sinnhuber, F. Stroh, and J. P. Burrows (2005), NO_2 and BrO vertical profile retrieval from SCIAMACHY limb measurements: Sensitivity studies, *Adv. Space Res.*, *36*(5), 846–854.
Sander, S. P., et al. (2003), Chemical kinetics and photochemical data for use in atmospheric studies, evaluation 14, *JPL Publ. 02-25*, Jet Propul. Lab., Pasadena, Calif.
Schroeder, W. H., K. G. Anlauf, L. A. Barrie, J. Y. Lu, A. Steffen, D. R. Schneeberger, and T. Berg (1998), Arctic springtime depletion of mercury, *Nature*, *394*, 331–332.
Simpson, W. R., L. Alvarez-Aviles, T. A. Douglas, M. Sturm, and F. Domine (2005), Halogens in the coastal snow pack near Barrow, Alaska: Evidence for active bromine air-snow chemistry during springtime, *Geophys. Res. Lett.*, *32*, L04811, doi:10.1029/2004GL021748.
Solberg, S., N. Schmidbauer, A. Semb, F. Stordal, and Ø. Hov (1996), Boundary-layer ozone depletion as seen in the Norwegian Arctic in spring, *J. Atmos. Chem.*, *23*(3), 301–332.
Sturges, W. T., G. F. Cota, and P. T. Buckley (1992), Bromoform emission from Arctic ice algae, *Nature*, *358*, 660–662.
Tarasick, D. W., and J. W. Bottenheim (2002), Surface ozone depletion episodes in the Arctic and Antarctic from historical ozonesonde records, *Atmos. Chem. Phys.*, *2*(3), 197–205.
Tuckermann, M., R. Ackermann, C. Gölz, H. Lorenzen-Schmidt, T. Senne, J. Stutz, B. Trost, W. Unold, and U. Platt (1997), DOAS-observation of halogen radical-catalysed arctic boundary layer ozone destruction during the ARCTOC-campaigns 1995 and 1996 in Ny-Ålesund, Spitsbergen, *Tellus, Ser. B*, *49*(5), 533–555.
Vogt, R., P. J. Crutzen, and R. Sander (1996), A mechanism for halogen release from sea-salt aerosol in the remote marine boundary layer, *Nature*, *383*, 327–330.
Wagner, T., and U. Platt (1998), Satellite mapping of enhanced BrO concentrations in the troposphere, *Nature*, *395*, 486–490.
Wennberg, P. (1999), Bromine explosion, *Nature*, *397*, 299–301.
Wessel, S., S. Aoki, P. Winkler, R. Weller, A. Herber, H. Gernandt, and O. Schrems (1998), Tropospheric ozone depletion in polar regions—A comparison of observations in the Arctic and Antarctic, *Tellus, Ser. B*, *50*, 34–50.
Zeng, T., Y. Wang, K. Chance, E. V. Browell, B. A. Ridley, and E. L. Atlas (2003), Widespread persistent near-surface ozone depletion at northern high latitudes in spring, *Geophys. Res. Lett.*, *30*(24), 2298, doi:10.1029/2003GL018587.

J. P. Burrows, A. Richter, and A. Rozanov, Institute of Environmental Physics, University of Bremen, P.O. Box 330440, D-28334 Bremen, Germany.
H.-W. Jacobi, Alfred Wegener Institute for Polar and Marine Research, Am Handelshafen 12, D-27570 Bremerhaven, Germany. (hwjacobi@awi-bremerhaven.de)
L. Kaleschke, Institute of Oceanography, Center for Marine and Atmospheric Research, University of Hamburg, D-20146 Hamburg, Germany.

Die "Berichte zur Polar- und Meeresforschung" (ISSN 1618 - 3193) werden beginnend mit dem Heft Nr. 377 (2000) in Fortsetzung der früheren **"Berichte zur Polarforschung** (Heft 1-376, von 1982 bis 2000; ISSN 0176 - 5027) herausgegeben. Ein Verzeichnis aller Hefte beider Reihen befindet sich im Internet in der Ablage des electronic Information Center des AWI (**ePIC**) unter der Adresse http://epic.awi.de. Man wähle auf der rechten Seite des Fensters "Reports on Polar- and Marine Research". Dann kommt eine Liste der Publikationen und ihrer online-Verfügbarkeit in alphabetischer Reihenfolge (nach Autoren) innerhalb der absteigenden chronologischen Reihenfolge der Jahrgänge.

To generate a list of all 'Reports' past issues, use the following URL: http://epic.awi.de and select the right frame: Browse. Click on "Reports on Polar and Marine Research". A chronological list in declining order, author names alphabetical, will be produced. If available, pdf files will be shown for open access download.

Verzeichnis der zuletzt erschienenen Hefte:

Heft-Nr. 563/2007 — "Arctic Sea Ice Dynamics: Drift and Ridging in Numerical Models and Observations", by Torge Martin.

Heft-Nr. 564/2007 — "Charakterisierung der sommerlichen Schmelzperiode auf antarktischem Meereis durch Fernerkundung und Feldmessungen", von Sascha Willmes.

Heft-Nr. 565/2007 — "Geochemistry of the Ob and Yenisey Estuaries: A Comparative Study", by Viacheslav V. Gordeev, Bettina Beeskow, and Volker Rachold.

Heft-Nr. 566/2007 — "Russian-German Cooperation SYSTEM LAPTEV SEA: The Expedition LENA 2006", edited by Julia Boike, Dmitry Yu. Bolshiyanov, and Mikhail N. Grigoriev.

Heft-Nr. 567/2007 — "Effects of UV Radiation on Antarctic Benthic Algae - With Emphasis on Early Successional Stages and Communities", by Katharina Zacher.

Heft-Nr. 568/2007 — "The Expedition ANTARKTIS-XXIII/2 of the Research Vessel 'Polarstern' in 2005/2006", edited by Volker Strass.

Heft-Nr. 569/2008 — "The Expedition ANTARKTIS-XXIII/8 of the Research Vessel 'Polarstern' in 2006/20067", edited by Julian Gutt.

Heft-Nr. 570/2008 — "The Expedition ARKTIS-XXI/1 a and b of the Research Vessel 'Polarstern' in 2005", edited by Gereon Budéus, Eberhard Fahrbach and Peter Lemke.

Heft-Nr. 571/2008 — "The Antarctic ecosystem of Potter Cove, King-George Island (Isla 25 de Mayo). Synopsis of research performed 1999-2006 at the Dallmann Laboratory and Jubany Station", edited by Christian Wiencke, Gustavo A. Ferreyra, Doris Abele and Sergio Marenssi.

Heft-Nr. 572/2008 — "Climatic and hydrographic variability in the late Holocene Skagerrak as deduced from benthic foraminiferal proxies", by Sylvia Brückner.

Heft-Nr. 573/2008 — "Reactions on surfaces of frozen water: lQmportance of surface reactions for the distribution of reactive compounds int the atmosphere", by Hans-Werner Jacobi.